

ENHANCED POWER SYSTEM MONITORING AND ANALYSIS USING SYNCHROPHASOR TECHNOLOGY

Thesis

Submitted in partial fulfillment of the requirements for the degree of

DOCTOR OF PHILOSOPHY

by

TEENA JOHNSON



DEPARTMENT OF ELECTRICAL AND ELECTRONICS
ENGINEERING
NATIONAL INSTITUTE OF TECHNOLOGY KARNATAKA
SURATHKAL, MANGALORE - 575025

September 29, 2023

DECLARATION

By the Ph.D. Research Scholar

I hereby *declare* that the Research Thesis entitled “**ENHANCED POWER SYSTEM MONITORING AND ANALYSIS USING SYNCHROPHASOR TECHNOLOGY**” which is being submitted to the **National Institute of Technology Karnataka, Surathkal** for the award of the Degree of **Doctor of Philosophy in Department of Electrical and Electronics Engineering**, is a *bonafide report of the research work carried out by me*. The material contained in this Research Thesis has not been submitted to any University or Institution for the award of any Degree.



Teena Johnson, Reg. No. 177142177EE013,
Department of Electrical and Electronics Engineering

Place: NITK, Surathkal

Date: 03-10-2023

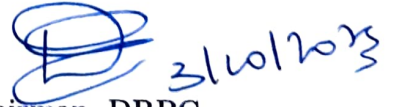
CERTIFICATE

This is to *certify* that the Research Thesis entitled “**ENHANCED POWER SYSTEM MONITORING AND ANALYSIS USING SYNCHROPHASOR TECHNOLOGY**” submitted by **TEENA JOHNSON**, Registration Number: **177142 177EE013** as the record of the research work carried out by her, is *accepted as the Research Thesis submission* in partial fulfilment of the requirements for the award of Doctor of Philosophy.



Dr. Tukaram Moger.

Research Guide
DR. TUKARAM MOGER B.E., M.Tech. (ITK), Ph.D. (IISc)
Assistant Professor
Department of Electrical & Electronics Engineering
National Institute of Technology Karnataka, Surathkal
P.O. Srinivasanagar, Mangalore-575025, Karnataka, INDIA.



Chairman, DRPC.

Dr. Dattatraya N Gaonkar.

ASSOC. PROFESSOR & HEAD
DEPT. OF ELECTRICAL & ELECTRONICS ENGINEERING
NATIONAL INSTITUTE OF TECHNOLOGY KARNATAKA
SURATHKAL SRINIVASANAGAR P.O., MANGALORE-575025

ACKNOWLEDGEMENTS

I would like to express my sincere gratitude to my guide **Dr. Tukaram Moger**, Department of Electrical and Electronics Engineering, for giving me an opportunity to work under his guidance which is invaluable. His keen insight into the subject has helped me in solving many problems during this work. His constant support, patience, suggestions, directions and feedbacks have helped in smooth progress of the project work. He has been a constant source of inspiration in all possible ways for successful completion of my project.

I ought to thank the HODs **Dr. B Venkatesa Perumal**, **Dr. K N Shubhanga**, **Dr. Gururaj S Punekar** and **Dr. Dattatraya N Gaonkar**, Department of Electrical and Electronics Engineering, NITK, Surathkal, for providing me with sufficient computational facilities to successfully complete the project work. I am grateful to the efforts put in by my RPAC panellists **Dr. Krishnan C M C** and **Dr. N. Gnanasekaran** for consistently monitoring my progress and giving important suggestions.

I am very thankful to National Load Dispatch Centre (NLDC)-Power System Operation Corporation Limited (POSOCO), India, for providing some real-time synchrophasor PMU data. This data has been helpful to carry out the analysis and make an insightful case study for one of the chapters in this thesis.

Special thanks to my caring husband **Deepak Manral** for the unconditional support and encouragement throughout my research work. I am so happy to thank my parents **M J Johnson** and **Lissy Johnson**, my grandparents **P T Joseph** and **Viji Joseph** and my parents-in-law **K S Manral** and **Usha Manral** for their constant support, motivation, prayers and love.

I owe a great deal of gratitude to **Sofia Banu**, **Sagar Dipesh Dahanuwala**, **Prathamesh Gachhi**, **Abhinandan M Pathak** and **Shantanu Arya** for carrying out some good collaborative research work. I wish to express my heartfelt thanks to **Vikas Singh**, **Rashmi**, **Dr. Roopa V Damodaran**, **Dr. Pavana Prabhu**, **Nisha K S**, **Asif Abdullah**, **Anvit Khare** and my other friends for their help, discussions, useful suggestions and keeping me motivated throughout my research work.

I am thankful to all the teaching and non-teaching staff of the Department of Electrical and Electronics Engineering for full co-operation and assistance. I also extend my thanks to the librarian, staff members from library, administration and academic sections. Finally, I thank all those who helped me directly or indirectly for the successful completion of this thesis.

TEENA JOHNSON

Abstract

Electric power system is the main source of energy for all major industrial applications and residential appliances. The power system has been rapidly evolving due to transformation from regulated to deregulated structure, increasing domestic and industrial consumers. A secure and reliable supply of electric power from such a complex system is a major challenge for the power engineers while carrying out the planning and operation. This calls for continuous real-time monitoring and control of the power system. This research work aims on exploring this research area dealing with setting up measurement system, dynamic state estimation and event detection in the power system using the latest synchrophasor technology.

Voltage stability analysis is considered important for secure power system operation. Many blackouts in India and abroad have been caused by voltage instability. So, the first step in the direction to solve this issue is voltage profile monitoring. A proper assessment is to be carried out so that the system operator can take preventive measures to keep the power system under stable conditions. Therefore, forecasting-aided state estimation (FASE) is performed for power systems having normal load variations. The estimation is carried out utilizing the measurements from the remote terminal units as well as the phasor measurement units. So far for the FASE studies, it is assumed that the changes in the system parameters, such as load variations are slow. Sudden changes in the power system states (namely voltage magnitude and angle) are therefore not considered. The effectiveness of the proposed algorithm Iterated Square-root Cubature Kalman filter (ISCKF) along with a state forecasting tool during normal load variations is evaluated with respect to already existing Kalman filter approaches. A state forecasting technique called Holt's Double exponential smoothing is utilized to forecast the states during the interval between two time instants of receiving the measurement sets from the field.

Research in the area of power system transient stability has recently shifted its focus on dynamic state estimation (DSE) involving PMU data with high reporting rate. Several mathematical models for induction motor and synchronous machine have been developed and various estimation approaches have been proposed in the literature for this purpose. In this work, the mathematical formulation of non-linear state space modeling and the principles of Kalman filter are utilized. Extended, Unscented and Cubature Kalman Filters (EKF, UKF and CKF) are the three non-linear estimation methods explored for dynamic state estimation in an induction motor for our preliminary studies. In the next stage, after presenting a thorough explanation about modeling of the synchronous machine, dynamic state estimation is applied on different power system case studies and the results of estimation methods are compared. Estimation studies are carried out in the

scenario of three phase fault at one of the buses in the power system. The improvised CKF called Iterated Square-root Cubature Kalman filter (ISCKF) is proposed for its application in DSE and its performance is compared with that of the EKF, UKF and CKF algorithms. The simulation results obtained show the great potential of the proposed estimation approach for accurately estimating the states of the machine as well as reducing the effect of noises.

With the deployment of PMUs for wide area monitoring system (WAMS), it is feasible to have an insight into the real-time events occurring in power systems based on measured data. Critical disturbances of the power system that may cause huge losses to the generation authority are noted as Events in this work. Initial studies are performed using analysis based on PMU data using various signal processing methods like Fast Fourier Transform, Yule-Walker Spectral Analysis, Matrix Pencil and Min-Max. That is, the events identifiable by two or more of these methods have been considered, to truly detect the occurrence of an Event based on the approach used by National Renewable Energy Laboratory. The results have been compiled on practical data from northern region of Indian power system during the Amphan cyclone. Then, a new major event detection method is proposed in this work, to detect the event efficiently using a data-driven approach and a dynamic thresholding technique.

For real time monitoring of the power system state variables, the measurement system needs to be properly set up. State of a system consists of a set of variables used to describe the behaviour of the system at a particular time. The optimal placement of measurement devices/sensors is essential for economic reasons and to maintain observability of the system. For measurement systems of electrical grid, supervisory control and data acquisition (SCADA) system was introduced around half a century ago to shoulder the operation and control of electric power system. As electric power system has been expanding in size due to advancements in the technologies and many new interconnections, the operation and monitoring of the power system has also become complex. Consequently, the measurement systems have been upgraded continuously. From the past three decades, synchrophasor technology has become one of the cutting edge advancement in the field of electrical power systems monitoring. But the devices of this technology are installed judiciously for economical reasons. But, the extent of installations of phasor measurement units (PMUs) is not full fledged so as to replace the SCADA. This is due to the high reliability of the SCADA systems and PMU installations are a costly affair. Further, PMU installations are being carried out in phases. But, the days are not far where certain applications such as state estimation, voltage stability monitoring, etc. could be carried with PMU data alone. This is the direction in which this research work has been carried out.

Contents

List Of Figures	v
List Of Tables	xi
List of Symbols and Abbreviations	xvii
1 Introduction	1
1.1 Historical Perspective on Synchrophasor Technology	1
1.1.1 Phasor Measurement Unit	5
1.1.2 IEEE Standards for Synchrophasor technology	6
1.1.3 Applications of Synchrophasor Technology	6
1.2 Power System State Estimation (PSSE)	7
1.2.1 Literature Survey on PSSE Methods	9
1.2.2 Comparison Studies of Power System State Estimation Methods	19
1.2.3 Forecasting-aided State Estimation for Voltage Profile Estimation in Power System	21
1.2.4 Dynamic State Estimation using Synchrophasor Technology	25
1.3 Event Detection in Power Systems	27
1.3.1 Categorization of Events	28
1.3.2 Review of Current Technologies for Event Detection	29
1.4 Need for Optimal Placement of PMUs in Power Systems	36
1.4.1 Overview of Synchrophasor Initiative in India	37
1.4.2 Various Methods for Solving Optimal Placement of PMUs	39
1.5 Motivation and Objectives	57
1.5.1 Motivation	57
1.5.2 Objectives	63
1.6 Organization of the Thesis	63
2 Forecasting-aided State Estimation in Power Systems during Normal Load Variations	67
2.1 Introduction	68

2.2	Objective and Contributions of this Chapter	71
2.3	Power System Modelling for Forecasting-aided State Estimation	71
2.4	Iterated Square-root Cubature Kalman Filter (ISCKF)	73
2.5	Case Studies on FASE for Test Systems	76
2.5.1	Data Generation and Simulation	76
2.5.2	Results and Discussion	78
2.6	Summary	84
3	Dynamic State Estimation in Power Systems	87
3.1	Introduction	88
3.2	Objective and Contributions of this Chapter	90
3.3	Introduction to Kalman Filters	91
3.3.1	Kalman Filter and its Comparison with Luenberger Observer	94
3.4	Preliminary DSE Studies: Dynamic State Estimation of Induction Motor	99
3.4.1	Induction Motor State Space Model	100
3.4.2	Simulation model of Induction Motor with Space Vector Modulation	103
3.4.3	Simulation Results	103
3.5	Power System Dynamic State Estimation (PSDSE)	109
3.5.1	Mathematical Description of the Synchronous Machine and the Classical Model	113
3.5.2	Simulation Results and Discussions for Power System DSE	117
3.6	Summary	137
4	A New Technique for Major Event Detection in Power Systems using PMU Data	139
4.1	Introduction	140
4.2	Objective and Contributions of this chapter	144
4.3	A New Technique for Major Event Detection in Power Systems using a Data-Driven and Dynamic Thresholding Approach	144
4.3.1	Windowing Schema for Abnormality Detection	145
4.3.2	Abnormality Detection	146
4.3.3	New Concept of Dynamic Thresholds	147
4.3.4	Effect of Type Number TN	148
4.3.5	Paralleling Abnormality Detection for Various Type Numbers	148
4.3.6	Thresholding Logic	149
4.3.7	Weighted Sum Abnormality	149
4.3.8	Post Processing Layer	150
4.4	Results and Observations	151
4.4.1	Data Definition and Data Processing	151

4.4.2	Recommended Hyper-Parameter Values	152
4.4.3	Inference from Substation A PMU Data Anaylsis	153
4.4.4	Inference from Substation B PMU Data Anaylsis	157
4.4.5	Inference from Substation C PMU Data Anaylsis	163
4.4.6	Variations in Hyper Parameters	169
4.5	Comparison with the existing NREL Methods	188
4.5.1	Simulation Results using Methods used by NREL for Detecting Events	188
4.5.2	False Positives and Increase in Number of Detections	196
4.5.3	Relative Intensity of Events	197
4.6	Summary	197
5	Optimal Placement of PMUs in Power Systems using Crow Search Algorithm	199
5.1	Introduction	200
5.2	Modeling of Problem Formulations and Methods for solving Optimal Placement of PMUs	200
5.2.1	Objective function	201
5.2.2	Constraints	205
5.3	Methodologies for Solving Optimal Placement of PMUs	219
5.4	Objective and Contributions of this chapter	223
5.5	New Proposed Method for OPP Studies: Crow search algorithm	223
5.5.1	Objective function	225
5.5.2	Constraints	226
5.5.3	Implementation of Crow search algorithm	226
5.6	Results and Discussions	234
5.6.1	Comparison studies for validating proposed method for OPP studies	236
5.6.2	Application of proposed CSA for various case studies	240
5.6.3	Limitations of the proposed method	264
5.7	Summary	264
6	Conclusion and Future Scope	267
6.1	Summary	267
6.2	Conclusions	269
6.3	Future Scope	270
	Appendix	271
	Bibliography	319
	Technical Publications	347

List of Figures

1.1	Block diagram of an energy management system	2
1.2	A SCADA system for the electrical power grid	3
1.3	Block diagram of a phasor measurement unit	6
1.4	Major research areas related to PMU technology during the years 2007-2022	7
1.5	Categorization of events	28
1.6	The geographical locations of PMUs installed in India (Corporation, 2013)	38
1.7	Review of Kalman filters used for FASE	58
1.8	Journals published until 2020 on PSSE	59
1.9	Problem statement of dynamic state estimation	60
2.1	The flowchart for the general flow of logic in forecasting-aided state estimation process using forecasting tool and Kalman filter	69
2.2	Single line diagram of the IEEE 30-bus system	77
2.3	Single line diagram of the NRPG 246-bus system	79
2.4	The estimated states and error plots at bus-7 in IEEE 30-bus system	81
2.5	The estimated states and error plots at bus-30 in NRPG 246-bus system	83
3.1	Time line showing priori and posteriori state estimation (Simon, 2006)	92
3.2	The ongoing discrete Kalman filter cycle (Welch and Bishop, 2006)	93
3.3	Luenberger observer	95
3.4	Estimation results of state x_1 with known initial condition	96
3.5	Estimation results of state x_1 with unknown initial condition	97
3.6	The estimated state x_1 estimation plots using measurements with added noises	97
3.7	System diagram of induction motor with space vector modulation	102
3.8	Simulink model of IM with SVM controller used for data generation	102
3.9	Estimated speed and error plots without considering noise in measurement data	104
3.10	Estimated Speed and error plots considering noise in the measurement data	105

3.11 Estimated speed and error plots with parameters $R_{s_{new}} = 0.8R_s$ and $R_{r_{new}} =$	
$0.8R_r$	107
3.12 Estimated speed and error plots with parameters $R_{s_{new}} = 1.2R_s$ and $R_{r_{new}} =$	
$1.2R_r$	108
3.13 Using PowerWorld simulator instead of real PMU to generate synchronized	
data for power system case studies	111
3.14 Problem statement of dynamic state estimation	112
3.15 Block Schematic of dynamic state estimation of synchronous machine	112
3.16 SMIB test system simulated in PowerWorld	117
3.17 IEEE 9-bus system simulated in PowerWorld	118
3.18 The error plots in estimated states at bus-4 for SMIB system under Case-1	119
3.19 The estimated rotor angle at bus-4 for SMIB using EKF, UKF and CKF	
with 100 and 1000 samples under Case-1	120
3.20 The estimated states for IEEE 9-bus system at bus-3 under Case-1	121
3.21 The error plots in estimated states for IEEE 9-bus system at bus-3 under	
Case-1	122
3.22 The error plots in estimated states at bus-4 for the SMIB under Case-2	124
3.23 Error plots in estimated states for IEEE 9-bus test system at bus-3 under	
Case-2	125
3.24 SMIB test system simulated in PowerWorld	127
3.25 The estimated rotor angle and error plots at main generator bus-4 for SMIB	128
3.26 The estimated speed deviation and error plots at bus-4 for SMIB	129
3.27 IEEE 9-bus system simulated in PowerWorld	131
3.28 The estimated rotor angle and absolute error plots at generator bus-2 for	
IEEE 9-bus system	132
3.29 The estimated speed deviation and absolute error plots at generator bus-2	
for IEEE 9-bus system	133
3.30 The rotor angle and error plots at generator bus-6 in 19-gen 42-bus test	
system	134
3.31 The estimated speed deviation and error plots at generator bus-6 in 19-gen	
42-bus test system	135
4.1 Flowchart of blocks inside event detection and processing of events	145
4.2 Abnormality detection for voltage and real power data at substation A	153
4.3 Abnormality detection for current & reactive power data at substation A	154
4.4 Weighted sum abnormality and 2 event indicators for voltage & real power	
data at substation A	155

4.5	Weighted sum abnormality and 2 event indicators based on data at sub-station A	156
4.6	Abnormality detection for voltage and real power data at substation B	158
4.7	Abnormality detection for current & reactive power data at substation B	159
4.8	Abnormality detection for voltage & real power data at substation B	160
4.9	Weighted sum abnormality and 2 event indicators for substation B	161
4.10	X-axis zoomed graph of <i>Major_faults</i> for substation B	162
4.11	Y-axis zoomed graph of <i>Major_faults</i> for substation B	162
4.12	Abnormality detection for voltage and real power data at substation C	164
4.13	Abnormality detection for current & reactive power data at substation C	165
4.14	Abnormality detection for voltage & real power data at substation C	166
4.15	Weighted sum abnormality and 2 event indicators for substation C	167
4.16	X-axis zoomed graph of <i>Major_faults</i> for substation C	168
4.17	Y-axis zoomed graph of <i>Major_faults</i> for substation C	168
4.18	Abnormality detection for voltage & real power data at substation A for reduced $W_{threshold}$ of 8500	170
4.19	Weighted sum abnormality and 2 event indicators for reduced $W_{threshold}$ of 8500 for substation A	171
4.20	Abnormality detection for voltage & real power data at substation B for reduced $W_{threshold}$ of 8500	172
4.21	Weighted sum abnormality and 2 event indicators for reduced $W_{threshold}$ of 8500 for substation B	173
4.22	X-axis zoomed graph of <i>Major_faults</i> for reduced $W_{threshold}$ of 8500 for substation B	174
4.23	Y-axis zoomed graph of <i>Major_faults</i> for reduced $W_{threshold}$ of 8500 for substation B	174
4.24	Abnormality detection for voltage & real power data at substation C for reduced $W_{threshold}$ of 8500	175
4.25	Weighted sum abnormality and 2 event indicators for reduced $W_{threshold}$ of 8500 for substation C	176
4.26	X-axis zoomed graph of <i>Major_faults</i> for reduced $W_{threshold}$ of 8500 for substation C	177
4.27	Y-axis zoomed graph of <i>Major_faults</i> for reduced $W_{threshold}$ of 8500 for substation C	177
4.28	Weighted sum abnormality and 2 event indicators for variation in TN for substation A	180
4.29	Weighted sum abnormality and 2 event indicators for variation in TN for substation A	181

4.30 Weighted sum abnormality and 2 event indicators for variation in TN for substation B	182
4.31 Weighted sum abnormality and 2 event indicators for variation in TN for substation B	183
4.32 X-axis zoomed graph of $Major_faults$ for variation in TN for substation B	184
4.33 Y-axis zoomed graph of $Major_faults$ for variation in TN for substation B	184
4.34 Weighted sum abnormality and 2 event indicators for variation in TN for substation C	185
4.35 Weighted sum abnormality and 2 event indicators for variation in TN for substation C	186
4.36 X-axis zoomed graph of $Major_faults$ for variation in TN for substation C	187
4.37 Y-axis zoomed graph of $Major_faults$ for variation in TN for substation C	187
4.38 Fault indication by multiple methods for PMU situated at substation A	190
4.39 Fault indication by multiple methods for PMU situated at substation B	191
4.40 Fault indication by multiple methods for PMU situated at substation C	192
4.41 Zoomed in plot for event detection using frequency at substation A	193
4.42 Zoomed in plot for event detection using frequency at substation B	193
4.43 Zoomed in plot for event detection using frequency at substation C	194
4.44 RPAD analysis for event detection between B and C	194
5.1 Number of conference and journal papers published on OPP in IEEE, ITEES, IET and Elsevier during the years 2003-2022	201
5.2 Optimal number of PMUs for a completely observable sample 6-bus system is 2.	202
5.3 Sample 6-bus system with 7 tie-lines	207
5.4 Effect of ZIB in power system observability	208
5.5 Sample 6-bus system during a single line contingency of line 2-5	210
5.6 Single line diagram of the IEEE 14-bus system	213
5.7 Single line diagram of the IEEE 14-bus system	215
5.8 Single line diagram of the IEEE 14-bus system split into two islands during a cascading fault	218
5.9 Classification of optimization techniques	220
5.10 Crow i 's next position can be to any position on the dashed line in Scenario 1	227
5.11 Parameter variation studies for IEEE 57-bus and practical 72-bus systems for different values of flight length (fl) and awareness probability (AP).	228
5.12 Case-1 PMU optimal placement solution - 17 PMUs for IEEE 57-bus when parameters are tuned to $fl=5$ and $AP=0.025$	229

5.13 Case-1 PMU optimal placement solution - 26 PMUs for practical 72-bus when parameters are tuned to $fl=5$ and $AP=0.025$	230
5.14 General flow of CSA used to solve optimal placement of PMU	233
5.15 System observability redundancy index (SORI) is (a) 8 (b) 6	237
5.16 Different locations of phasor measurement units (PMUs) in IEEE 30-bus system for Case 1 - topological observability obtained by using methods: (a) Crow search algorithm (CSA) (b) Particle swarm optimization (PSO) and (c) Binary integer linear programming (BILP). Optimal number of PMUs is 10 in all methods. Set of common/similar nodes in all methods is (10, 11, 12, 30). (Note: System observability redundancy index (SORI)) .	238
5.17 Multiple solutions for placement of phasor measurement units (PMUs) in IEEE 14-bus system for Case 1 using Crow search algorithm (CSA) method . Optimal number of PMUs is 4 in all the sub figures. Only common/similar node in all methods is 2. (Note: System observability redundancy index (SORI))	239
6.1 BILP logic using branch and bound algorithm	272
6.2 linearized and non-linear mean and covariance of 300 randomly generated points [9]	278
6.3 The comparison among exact, linearized, and unscented mean and covari- ance of 300 randomly generated points (Simon, 2006)	279
6.4 Finding N point DFT	285
6.5 Single line diagram of the IEEE 14-bus system	289
6.6 Single line diagram of the IEEE 30-bus system	292
6.7 Single line diagram of the IEEE 57-bus system	296
6.8 Online diagram of the Practical 72-bus test system	300
6.9 Geographical map of 72-bus equivalent system of Indian southern region power grid	301

List of Tables

1.1 Comparison of measurement system: SCADA vs. PMUs	4
1.2 Comparison of Static and Dynamic SE	9
1.3 Reviews of papers on event detection	32
1.4 Reviews Of papers on event detection	33
1.5 Reviews of papers on event detection (Contd.)	34
1.6 Reviews of papers on event detection (Contd.)	35
1.7 The details of the Synchrophasor Pilot Project in India	37
1.8 Main journals and conference articles on solving OPP using conventional methods - PART I	43
1.9 Main journals and conference articles on solving OPP using conventional methods - PART II	44
1.10 Main journals and conference articles on solving OPP using conventional methods - PART III	45
1.11 Main journals and conference articles on solving OPP using conventional methods - PART IV	46
1.12 Main journals and conference articles on solving OPP using conventional methods - PART V	47
1.13 Main journals and conference articles on solving OPP using conventional methods - PART VI	48
1.14 Main journals and conference articles on solving OPP using conventional methods - PART VII	49
1.15 Main journals and conference articles on solving OPP using heuristic methods - PART I	50
1.16 Main journals and conference articles on solving OPP using heuristic methods - PART II	51
1.17 Main journals and conference articles on solving OPP using meta-heuristic methods - PART I	52
1.18 Main journals and conference articles on solving OPP using meta-heuristic methods - PART II	53

1.19 Main journals and conference articles on solving OPP using meta-heuristic methods - PART III	54
1.20 Main journals and conference articles on solving OPP using hybrid methods - PART I	55
1.21 Main journals and conference articles on solving OPP using hybrid methods - PART II	56
1.22 Comparison of the different methods adopted for OPP studies	57
2.1 Mean of Absolute Errors (MAE) in the Estimated States using various KF algorithms for IEEE 30-bus test system	82
2.2 Mean of Absolute Errors (MAE) in the Estimated States using various Kalman filter (KF) based algorithms for NRPG 246-bus test system	82
2.3 Total computational time for estimation using one set of hybrid measurements and 49 PMU measurements	82
2.4 Absolute phase error percentage (APEP) and Absolute voltage error percentage (AVEP) comparison of proposed ISCKF with CKF methods for the two test systems	84
3.1 Mean of Absolute Errors (MAE) in the Estimated Speed of Induction motor considering noise in measurement data	103
3.2 Mean of Absolute Errors (MAE) in the Estimated Speed of Induction motor with new parameters	106
3.3 Mean of Absolute Errors (MAE) in the Estimated States at bus-4 for SMIB test system under Case-2	126
3.4 Mean of Absolute Errors (MAE) in the Estimated States at bus-3 for IEEE 9-bus test system under Case-2	126
3.5 Mean of Absolute Errors (MAE) in the Estimated States at bus-4 using SMIB test system	130
3.6 Mean of Absolute Errors (MAE) in the Estimated States at all generator buses in IEEE 9-bus system	131
3.7 Mean of Absolute Error (MAE) in the Estimated States of all generator buses of 42-bus test system (Measurement data: 1000 samples/s)	136
3.8 Mean of Absolute Error (MAE) in the Estimated States of all generator buses of 42-bus test system (Measurement data: 250 samples/s)	136
4.1 Threshold selected for precise Event Detections	153
4.2 Event Detection Latency in <i>Major_faults</i>	179
4.3 Events detected analyzing frequency signals (5 hours) during cyclone Amphan	195
4.4 Events detected analyzing RPAD signals (5 hours) during cyclone Amphan	195

4.5 Comparison of Events Detected (during 5 hours) by NREL and the proposed methods	196
5.1 Parameter settings for Crow search algorithm (CSA) and particle swarm optimization (PSO) methods ¹	227
5.2 Number of phasor measurement units (PMUs) with the location solutions for Cases 1 results using Crow search algorithm (CSA), particle swarm optimization (PSO) and Binary integer linear programming (BILP)	235
5.3 Optimized number of phasor measurement units (PMUs) obtained using the proposed Crow search algorithm method	240
5.4 Computational time (in seconds) for obtaining the global optimized number of phasor measurement units (PMUs) using the proposed Crow search algorithm method	241
5.5 Multiple PMU location solutions for Cases 1 and 2 results- PART I	244
5.6 Multiple PMU location solutions for Cases 1 and 2 results- PART II	245
5.7 Multiple PMU location solutions for Case 1 and 2 results considering ZIB- PART I	246
5.8 Multiple PMU location solutions for Case 1 and 2 results considering ZIB- PART II	247
5.9 Multiple PMU location solutions for Cases 1 and 2 results considering measurement channel limitation- PART I	248
5.10 Multiple PMU location solutions for Cases 1 and 2 results considering measurement channel limitation - PART II	249
5.11 Multiple PMU location solutions for Case 1 and 2 results considering measurement channel limitation (4 channels for each PMU) and ZIB- PART I	250
5.12 Multiple PMU location solutions for Case 1 and 2 results considering measurement channel limitation (4 channels for each PMU) and ZIB - PART II	251
5.13 Multiple PMU location solutions for Cases 1 and 2 results considering single PMU loss- PART I	252
5.14 Multiple PMU location solutions for Cases 1 and 2 results considering single PMU loss (SPL)- PART II	253
5.15 Multiple PMU location solutions for Cases 1 and 2 results considering single PMU loss- PART III	254
5.16 Multiple PMU location solutions for Cases 1 and 2 results considering single PMU loss- PART III (Contd.)	255

5.17 Multiple PMU location solutions for Case 1 and 2 results considering Single PMU loss and ZIB- PART I	256
5.18 Multiple PMU location solutions for Case 1 and 2 results considering Single PMU loss and ZIB- PART II	257
5.19 Multiple PMU location solutions for Case 1 and 2 results considering Single PMU loss and ZIB- PART II (Contd.)	258
5.20 Multiple PMU location solutions for Case 1 and 2 results considering Single PMU loss and ZIB- PART II (Contd.)	259
5.21 Multiple PMU location solutions for Cases 1 and 2 results considering single line contingency- PART I	260
5.22 Multiple PMU location solutions for Cases 1 and 2 results considering single line contingency- PART II	261
5.23 Multiple PMU location solutions for Cases 1 and 2 results considering single line contingency- PART II (Contd.)	262
5.24 Multiple PMU location solutions for Case 1 and 2 results considering Single line contingency and ZIB- PART I	262
5.25 Multiple PMU location solutions for Case 1 and 2 results considering Single line contingency and ZIB- PART II	263
6.1 System information of the IEEE 14-bus system	289
6.2 Line data of the IEEE 14-bus system	290
6.3 System information of the IEEE 30-bus system	291
6.4 Line data of the IEEE 30-bus system	293
6.5 System information of the IEEE 57-bus system	295
6.6 Line data of the IEEE 57-bus system	297
6.7 Line data of the IEEE 57-bus system(Contd.)	298
6.8 System information of the Practical 72-bus test system	299
6.9 Line data of the Practical 72-bus test system	302
6.10 Line data of the Practical 72-bus test system (Contd.)	303
6.11 Induction Motor parameters and initial simulation values	305
6.12 Main parameters of the simulated synchronous generator	307
6.13 Main parameters of the simulated synchronous generator models for IEEE 9-bus Test System	309
6.14 Bus data of the 19-generator 42-bus test system (Part I)	312
6.15 Bus data of the 19-generator 42-bus test system (Part II)	313
6.16 Line data of the 19-generator 42-bus test system	314
6.17 System information of the 19-generator 42-bus test system	315

6.18 Measurement types and corresponding standard uncertainties (Asprou et al.,	
2013; Sharma et al., 2014)	317

List of Symbols and Abbreviations

Symbols:

x_i or x_j	Decision variable for bus i or j respectively which take value 1 if bus i is equipped with a PMU) and 0 (otherwise).
o_i	Expression which accounts for the number of times bus i is observed.
N	Total count for buses in system.
F or F_i	Objective function for OPP
o_i^{allPMU}	Number of times a bus i is observed when all the buses have PMUs.
A	Node incidence matrix or binary connectivity matrix.
A_{ij}	Element of Node incidence matrix at position (i, j) .
X	Row vector of size $N \times 1$ with elements x_i .
O	Observability vector with elements o_i .
u	Row vector $N \times 1$ consisting of ones.
w_{ij}	Auxiliary binary variable between buses i and j equal to 1, if buses i and j are both connected to the same ZIB, otherwise 0.
W	Diagonal weight matrix
x_{pt}, x_{ct}, x_c	Actual cost of to be installed CT, PT or communication network establishments respectively
r	number of branches terminating at bus
x_{ad}	Accounts for additional costs.
q_i	Cost of PMU to be placed on bus i .
e_j	Probability of system state j .
h_j	Observability of power system state j .
$FVSI_{ij}$	Fast Voltage Stability Index for line $i - j$.
PO_i	Possibility of observability under single line outage.
A_{ij}^l	Modified node incidence matrix under influence of single line outage.
$E_{lsv,i}$	Error of the largest singular value.
s_{li}, s_{lm}	Largest singular values related to case that PMUs installed at all buses except bus i and to the case where PMUs are installed at all buses.
k	Count of PMU outages considered.
A_1	Modified Node incidence matrix corresponding to L line outages.
L	Total count of line outages considered.
u_1	Row vector of ones of size $2 \times L$.
P	Real power flow.
Q	Reactive power flow.
$P_{i,j}$	Real power flow from bus i to bus j .

$Q_{i,j}$	Reactive power flow from bus i to bus j .
e, \mathcal{E}	Each edge and set of all edges respectively.
w_e^t, w_e^u	Set to 1 if DULR is placed at lower end or at upper end respectively, else 0.
$v_{i,i}, v_{i,j}$	Vulnerability elements (i,i) and (i,j) in bias matrix.
o'_i	Observability constraints using Boolean algebra.
$\mathcal{N}()$	Open neighboring set of bus i , $\mathcal{N}() = j (i,j) \in \mathcal{E}$
ω_{ij}	Set to 1 if a PMU is installed at bus j and bus i can be observed by the current measurement on line $(i-j)$ or 0, otherwise.
\mathcal{P}	Observability propagations.
\mathcal{Z}	Set to 1 if ZIB else 0.
\mathcal{Y}	Observability propagation variables of ZIBs.
ν	Observability propagation variables of conventional measurements.
o''_i	Modified observability function which includes ZIB effect.
Z_i	Observability function of bus i , which is a zero-injection bus or adjacent to a ZIB.
b_{ij}	Binary auxiliary variable, 1 indicates calculation of voltage phasor of bus $i - U_i$ is assigned to resulting equation from the zero injection j .
N_z	Set containing indices of zero injection buses.
N_c	Set containing indices of zero-injection buses and their adjacent buses.
ζ_i	ZIB set of ZIB i .
V_i	Voltage at bus i .
V_j	Voltage at bus j .
$I_{i,j}$	Current flowing from bus i to bus j through the branch.
$y_{i,j}$	Admittance of the branch connecting bus i to bus j .
d_j	Binary variable equal to 1 if j^{th} bus has flow measurement device, else 0.
f_{ij}	Auxiliary binary variable of buses i and j , that decides which bus should be made observable by flow measurement devices.
q, m	Cost vectors of PMUs and flow measurement devices respectively.
G_i	Observability constraint related to joint placement of PMU and flow devices.
$z_{i,j}$	Flow placement binary variable between buses i and j .
a, t, f	Variables.
d_j^{FMt}	Updated d_j during contingency of flow measurement device.
f_{ij}^{FMt}	Updated f_{ij} during contingency of flow measurement device.
R_k	Number of rows for each bus.
N_k	Count of bus positions with ones in row R_k in connectivity matrix A except the diagonal element
${}^{N_k}C_l$	l combinations of N_k
l	Fixed number of channels considered for the PMU
B	New decision matrix by modifying A Node incidence matrix for considering measurement channel limit.
S	Sum of R_k 's; N is number of buses.
p_i	The elements p_i that correspond to rows of B corresponding to different combinations for a particular bus are assigned with the same x_i decision variable as that of the particular bus.
H_1	Sub-matrix of measurement Jacobian matrix for PMU at bus 1.
H'	The matrix that incorporates the vulnerability of the bus/branch into O
V	Voltage magnitude.

I	Current magnitude.
$V_{1,r}$	Real part of the bus 1 voltage phasor
$V_{1,x}$	Imaginary part of the bus 1 voltage phasor
$I_{1-2,r}$	Real part of the current phasor flowing from buses 1 to 2.
$I_{1-2,x}$	Imaginary part of the current phasor flowing from buses 1 to 2.
$I_{1-5,r}$	Real part of the current phasor flowing from buses 1 to 5.
$I_{1-5,x}$	Imaginary part of the current phasor flowing from buses 1 to 5.
H_i	Sub-matrix of measurement Jacobian matrix for PMU at bus i .
C_1	Jacobian matrix related to zero-injection measurements at bus-1.
c_1	Total count of buses connected to ZIB-1.
D	A coefficient matrix.
n	Number of states in the system.
g_i	Non-linear topological observability constraints.
ad_i	Set of adjacent buses to bus i .
$g_{inj,2}$	Zero injection formulation with non-linear constraints for bus 2.
A_{ij}^{CI}	Binary entry in connectivity matrix for post-islanding network.
PO_i	Probability of observability associated with bus i .
P'_{ij}	Constant value representing the probability of observability of bus i because of PMU t bus j .
N^{hor}	Set of buses for the horizon year.
x_i^{hor}	PMU Placement variables for the horizon year.
PO_i^{hor}	Probabilistic observability for the horizon year.
$PO_i^{hor,min}$	Minimum probability of observability required for bus i .
f	frequency.
v_i^k	current velocity of the particle i at iteration k .
v_i^{k+1}	modified velocity of particle i .
$rand()$	function which generates random number between 0 and 1.
x_i^k	current position of particle i at iteration k .
$pbest_i$	personal best position of particle i .
$gbest_i$	global best position in the previous iteration among all the particles in the population.
w_i	weight function for the velocity of particle i .
c_i	weight coefficient of each term.
$Y(\cdot)$	Power spectrum density.
y_{pre_event}	RPAD before event occurred.
y_{post_event}	RPAD after event occurred.
t_{max}	Time instant at which ROCOF was maximum.
t_{min}	Time instant at which ROCOF was minimum.
M	Number of PMUs considered for event detection study.
$W_{threshold}$	Window for calculating the dynamic threshold for an electrical parameter.
W_{Lbase}	Window for calculating nominal magnitude for an electrical parameter.
pos	Present data position of analysis.
W_{cw}	Current/present window.
K	Number of data points in W_{cw} .
$W_{cwincrement}$	Increment in W_{cw} .
W_{max}	Window of recommended number of 30 data points
K	Number of data points in W_{max} .
W_1	The moving window having length same as W_{max} .

W_2	Smaller window within W_1 taking value from W_{cu}
f	frequency.
$Y(\cdot)$	Power spectrum density.
y_{pre_event}	RPAD before event occurred.
y_{post_event}	RPAD after event occurred.
t_{max}	Time instant at which ROCOF was maximum.
t_{min}	Time instant at which ROCOF was minimum.
M	Number of PMUs considered for event detection study.
$W_{threshold}$	Window for calculating the dynamic thresholds for an electrical parameter.
W_{Lbase}	Window for calculating nominal magnitude for an electrical parameter.
$L_{magnitude}$	Magnitude of any electrical parameter at a particular data point.
L_{base}	Root mean square of any electrical parameter in window W_{Lbase} .
$L_{basemat}$	Matrix having dimensions of $L_{magnitude}$ and value L_{base} .
D	Matrix consisting of deviations of data points in window W_2
with	respect to $L_{basemat}$.
$FE(n)$	Fault Energy given by root mean square of D about their n^{th} column over the window W_2 .
FE_{pos}	FE data points associated with every data position pos .
FE_{mat}	Matrix consisting of FE data points for window $W_{threshold}$.
FE_{posT}	Total number of FE data points used for calculation of thresholds, i.e., $FE_{pos} \times T$.
σ	Standard deviation.
TN	Type number.
$FE_{threshold}$	Threshold calculated using mean of FE_{mat} and product of TN and standard deviation of FE_{mat} .
$FE_{matdiff}$	Matrix with differences in FE for W_2 and FE for $W_2 - 1$.
$FE_{matdiffthreshold}$	Threshold calculated using mean of $FE_{matdiff}$ and product of TN and standard deviation of $FE_{matdiff}$.
TN_{min}	Minimum limit for varying type number TN .
TN_{max}	Maximum limit for varying type number TN .
$D_{binaryFE}$	Matrix consisting ones when FE values overshoot $FE_{threshold}$, 0 otherwise.
$D_{binaryFEdiff}$	Matrix consisting ones when $FE_{matdiff}$ elements overshoot $FE_{diffthreshold}$, 0 otherwise.
$D_{binaryProduct}$	Hadamard product of $D_{binaryFE}$ and $D_{binaryFEdiff}$.
F_{fault}	Matrix with $D_{binaryProduct}$ for all 4 electrical parameters and for multiple pos .
$F_{faultDist}$	2D matrix consisting of summation of products of TN varying from TN_{min} to TN_{max} and F_{fault} .
$V_{faultDist}$	$F_{faultDist}$ with respect to voltage parameter.
$Q_{faultDist}$	$F_{faultDist}$ with respect to reactive power parameter.
$P_{faultDist}$	$F_{faultDist}$ with respect to real power parameter.
$I_{faultDist}$	$F_{faultDist}$ with respect to current parameter.
V_Q_faults	Hadamard product of $V_{faultDist}$ and $Q_{faultDist}$.
P_I_faults	Hadamard product of $P_{faultDist}$ and $I_{faultDist}$.
$Major_faults$	Hadamard product of V_Q_faults and P_I_faults .
$Weighted_faults$	Sum of V_Q_faults , P_I_faults and twice $Major_faults$.

Abbreviations:

ABSO	Artificial bee swarm optimization
AC	Alternating current
ADC	Analog-to-Digital converter
APEP	Absolute phase error percentage
AVEP	Absolute voltage error percentage
BILP	Binary integer linear programming
BOI	Bus observability index
BPSO	Binary particle swarm optimization
CE	Cummulative Energy
CGA	Constant gain algorithm
CLA	Cellular learning automata
CSA	Crow search algorithm
CT	Current transformer
DBMS	Database management system
DCS	Distributed control system
DE	Differential evolution
DFT	Discrete Fourier transform
DLR	Dynamic line rating
DSE	Dynamic state estimation
DSSE	Distributed system state estimation
DULR	Dual-use line relay
EDA	Estimation of distribution algorithm
EILP	Equivalent integer linear programming
EKF	Extended Kalman filter
EMS	Energy management system
EPSOWP	Enhanced particle swarm optimizer incorporating a weighted particle
ESN	Echo state network
FACTS	Flexible AC transmission systems
FASKO	Fuzzy augmented state Kalman observer
FDS	Fast decoupled state
FDSE	Fast decoupled state estimation
FE	Fault Energy
FESOS	Fast exact second order state
FIR	Finite impulse response
FVSI	Fast voltage stability index
GA	Genetic algorithm
GOSC	General optimal substation coverage
GPS	Global positioning system
HV	High voltage
HVDC	High voltage direct current
IEEE	Institute of Electrical and Electronics Engineers
IED	Intelligent electronic devices
IET	Institution of Engineering and Technology
ILP	Integer linear programming
ISO	Independent system operator

ITEES	International Transactions on Electrical Energy Systems
KFSCA	Kalman-filter-based sine cosine algorithm
LAN	Local area network
LAV	Least absolute variance
LDC	Load dispatch centre
LMCS	Lattice Monte Carlo simulation
LQP	Line stability index
LP	Linear programming
LHS	Left hand side
MCC	Main control centre
MLCL	Maximum load loss coefficient limit
MO	Multi-objective
MVEE	Minimum Volume Enclosing Ellipsoid
NASPI	North American synchro phasor initiative
NLP	Non-linear Programming
NLDC	National load dispatch centre
NDS	Non-dominated sorting
NREL	National Renewable Energy Laboratory
NSGA	Nondominated sorting genetic algorithm
OLTC	On-load tap changer
ONS	Brazilian electric system national operator
OPP	Optimal placement of PMUs
OSI	Open system interconnection
OSRI	over system reliability index
PDC	Phasor data concentrator
PMU	Phasor measurement unit
POSOCCO	Power System Operation Corporation Limited
PPS	Pulse per second
PSO	particle swarm optimization
PSE	Phasor-only state estimator
PSSE	Power system state estimation
PSWV	Particle swarm optimization without velocity
PT	Potential transformer
RLDC	Regional load dispatch centre
RMS	Root mean square.
ROCOF	Rate of change of frequency
RPAD	Relative Phase Angle Difference
RTDS	Real-time digital simulator
RTS	Reliability Test System
RTU	Remote terminal unit
SA	Simulated annealing
SAARC	South Asian Association for Regional Cooperation
SCA	Sine cosine algorithm
SCADA	Supervisory control and data acquisition
SE	State estimator/estimation
SKF	Simulated Kalman filter
SLDC	State load dispatch centre

SLRG	State Level Regional power Grid
SMDG	Single sub-matrix of a decoupled gain matrix
SMDJ	Single sub-matrix of a decoupled Jacobian matrix
SORI	System observability redundancy index
SQP	Sequential quadratic programming
SSFD	Strongest Signal First Detection
TCP/IP	Transmission control protocol/ internet protocol
TS	Tabu search
TPMU	Traditional phasor measurement unit
UKF	Unscented Kalman filter
VAr	voltage ampere reactive
VSLI	Voltage stability load index
WAMS	Wide area monitoring systems
WLS	Weighted least squares
ZI	Zero injection
ZIB	Zero injection bus

Chapter 1

Introduction

This chapter briefly reviews some aspects of power system monitoring and operation. An overview on synchrophasor technology, synchrophasor initiative in India, challenges in optimal placement of phasor measurement units in power systems, power system state estimation methods, voltage profile monitoring and event detection methods are briefly explained. An outline of the contributions made in this thesis and its organization are presented.

1.1 Historical Perspective on Synchrophasor Technology

The difficulties in power system operation are swelling multifold day by day. These are as a consequence of an expanding system size, quick capacity enlargement, bulk power flows between areas/regions far apart, multiple players, rise in competition in the power market, environmental change, extensive augmentation of renewable resources in certain areas and rising customer demands. Hence, situational awareness of the wide area network becomes extremely important. This is completely dependent on the real-time measurement system and monitoring. Especially, visualizations on the dashboard at main control centre (MCC) play an inevitable role in assisting system operator to make better decisions.

¹Based on the literature survey on optimal placement of PMUs presented in this chapter, a review journal paper entitled *A critical review of methods for optimal placement of phasor measurement units* has been published in *International Transactions on Electrical Energy Systems*, 2020.

²A conference paper entitled *Latest Trends in Electromechanical Dynamic State Estimation for Electric Power Grid* has been published in IEEE 2022 International Conference of Emerging Technologies (INCET), pp. 1-6, May 2022.

³A conference paper entitled *Review of Advancements in Forecasting-aided State Estimation based on Kalman Filter Approach for Voltage Profile of Power Systems* has been published in 2nd IEEE International Conference on Emerging Frontiers in Electrical and Electronic Technologies (ICEFEET- 2022), pp. 1-6, June 2022.

⁴A conference paper entitled *Latest Trends in Event Detection Techniques in Power Systems* has been published in 7th Students' Conference on Engineering and Systems, July 2022.

As electric power system has expanded, Supervisory Control and Data Acquisition-Energy management system (SCADA-EMS) (introduced half a century ago) has also become large-scale. SCADA provides real-time data exchange between a control center (master) and field devices (slaves) (Marihart, 2001). In this Master-Slave architecture, the master and a machine with SCADA software configured, requests data from the field devices at regular intervals and updates the operator with the latest status provided by them. This gives a holistic overview of the state of the system to the operator. In addition, SCADA allows the operator to take control actions by sending commands to field devices. The master logs and records all events in a file and generates automatic reports and notifications in case of critical situations. It also provides visual and audio alarms in case a certain measurement from a field device has violated the threshold limits set by the operator. The SCADA/ EMS achieved a revolution by implementing an information processing systems (Kokai et al., 1998).

Conventionally, SCADA data are measured at substation level. And this information is forwarded to load dispatch centre (LDC) through SCADA. At every 4-10 seconds, the information is transmitted and revised at the respective LDC. Phasor angle difference between buses or coherent groups of generators directly corresponds to the stress in the grid. The load phase angle is estimated either from available SCADA data or phase difference between any two substations derived during post-analysis. Both ways have their obstructions due to delay in data transfer, skewdness and inaccuracy inherent in SCADA/EMS. Synchrophasor technology along with wideband communication facility compensates for the above drawbacks.

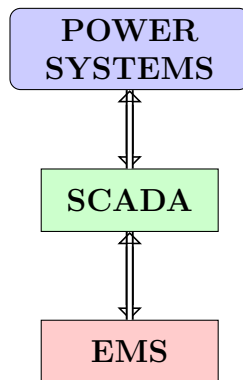


Figure 1.1: Block diagram of an energy management system

Fig. 1.1 shows the block diagram of EMS. Power Systems contain generators, transformers, transmission lines, different loads to industry and consumers. SCADA consists mostly of hardware components, which measure the quantities (Voltage, current, power, etc.) from various meters. SCADA consists of collection of information from meters distributed throughout the area through Remote Terminal Units (RTUs). Embedded systems are commonly used at the lower level in SCADA systems (Naess, 2004). SCADA

systems are a typical example of a system of systems architecture where each computer system is a part of a hierarchical infrastructure. As illustrated by Fig. 1.2, electrical substations in the power grid are essentially smaller decentralized embedded systems spread out over a wide geographical area. The Distributed Control System (DCS) controller gathers data from the Intelligent Electronic Devices (IED) that further communicates with low level smart transducers such as sensors and actuators. Embedded systems in electrical substations are an important part of the data collection in a distributed control system for the electrical power grid.

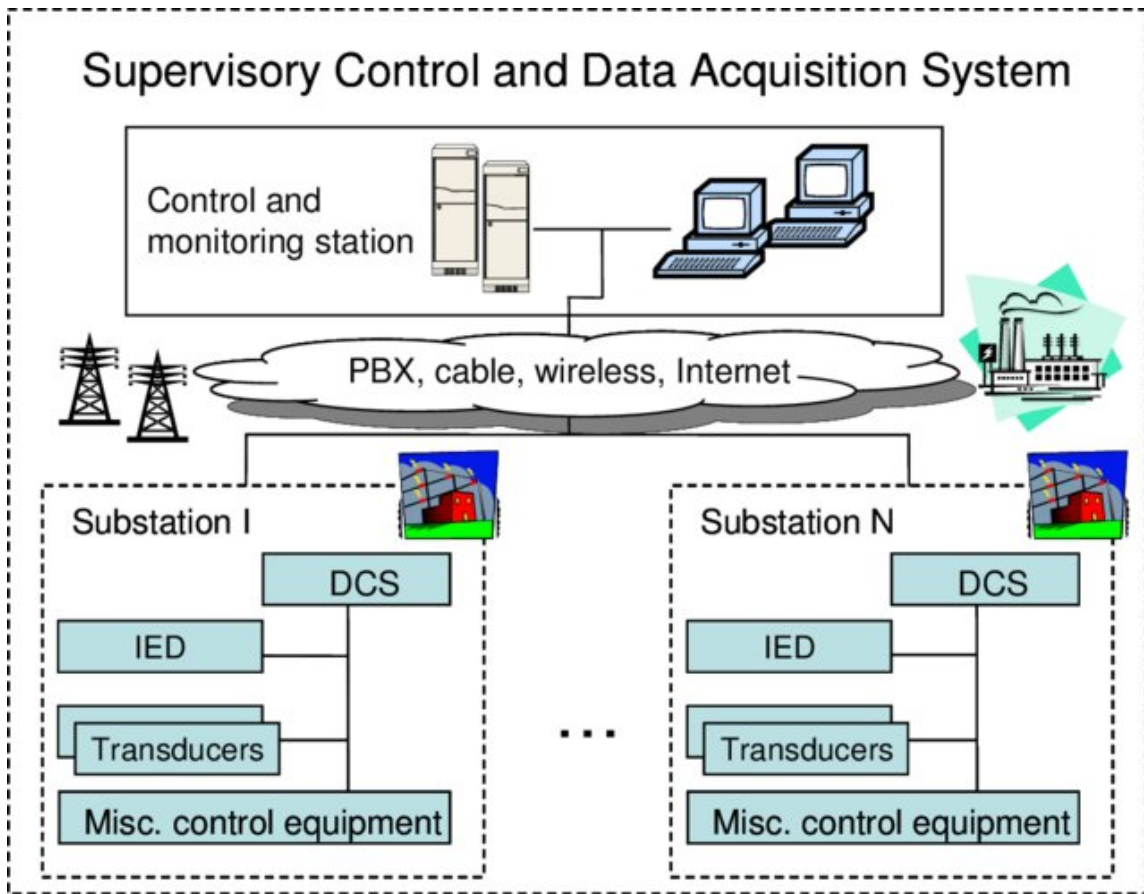


Figure 1.2: A SCADA system for the electrical power grid

In the conventional SCADA-EMS system, the voltage magnitude, frequency, MW, MVA_r and the circuit breaker status are available at the control centre through direct measurements (using transducers) while the load angle of the buses are estimated (by the State Estimator). Alternatively, the angular separation between adjacent nodes could be derived from the power flow on the line connecting them, impedance of the line and the voltage magnitude at the two ends. These angular separations could be algebraically added up along the path to obtain the angular separation between any coherent groups of generators/ pair of nodes. It is established that the angular separation between different

nodes in the grid is an indicator of the stress in the grid and the need for monitoring it in real-time is felt (Corporation, 2013). Analysis revealed the plot of the angular separation could be used for detecting major grid events within the same region or in neighboring regions; detecting islands and tagging exceptional grid operating conditions such as load crash. However, since the direct measurement of phase angles is not available through SCADA fundamentally, the state of power system can be determined if one has the voltage and angle of every bus in the interconnected power system. These measurements are carried out and used in check synchronization relays at substation level. However, the visibility of phase angle measurements at control centre is constrained due to limitations in communication and SCADA/EMS technology. Besides, there are other issues in utility of phase angle data from SCADA/EMS. The state estimator (SE) runs periodically or on change of circuit breaker status. In a rapidly growing power system, the SE results are often inaccurate and unreliable due to limited network observability and bad data.

Table 1.1: Comparison of measurement system: SCADA vs. PMUs

SCADA	PMU
The SCADA system receives data from RTU located across different substations & generating stations.	PMU measures phasor values (both magnitude and angle) of voltages at a bus.
Quantities like P, Q, voltage, system frequency, switch & circuit breaker position: reported by reception or scanned periodically.	Magnitude and angle of three-phase voltage/current, frequency, rate of change of frequency (ROCOF) and angular separation can be evaluated with ease.
The rms values of current & voltage measured by RTU and transmitted to SE at MCC.	Measurements are sent to MCC with GPS time-stamping to ensure synchronism between PMUs at all buses for better state estimation.
SCADA data are transmitted and revised at the respective load dispatch center at every 4-10 seconds.	Visualization of quantities possible at every 40 ms in LDC.

Recent breakthrough - the synchrophasor technology has overcome the limitations with respect to state measurement and its telemetry at the control centre. This is due to the advantages of its reporting rate and other features as listed in Table 1.1. Synchrophasors are precise measurements of the state of the system available from Phasor Measurement Units (PMUs). PMUs are microcontroller based devices that computes phasor values of voltage and current from current transformer (CT) and potential transformer (PT)

measurements respectively. Operation of PMUs are controlled by pulse per second (PPS) sent by GPS satellites. Hence, PMU is a monitoring device that generates real-time snapshot of wide area monitoring system (WAMS). The measurements are usually referred as synchrophasors, which means both magnitude and phasor measurements are done at the same time. PMUs provide synchrophasor and frequency measurements of one or more of 3-phase alternating current (AC) voltage and/or current waveforms. Another important feature of synchrophasors is that they are all time stamped integrated with global positioning system (GPS) signal. All the measurements are made in time intervals as small as 20 ms. Voltage and current are parameters characterizing the delivery of electric power from generation plants to end-user loads, while frequency is the key indicator of the balance between electric load and generation. Thus, frequency that does not deviate very much from 50Hz or 60Hz is key to ensuring the proper operation of the power system and its reliability. Thus, these parameters represent the “heart-beat” and health of the power system. At present, PMUs are the most accurate and time-synchronized technology for power engineers and system operators for wide area monitoring systems.

It is only during the past three decades when the synchrophasor technology began to emerge as a powerful tool for power system monitoring. This technology is developed near the end of the 1980s and first product came into market in 1990s. The installations of PMUs have been sluggish due to the inherent costs involved. Though the PMU installations have been very slow, the benefits from these few installations have been proved to be tremendously notable. Hence, the installations have been carried out in multistages ever since. At present, PMUs are the most accurate and time-synchronized technology for power engineers and system operators for wide area monitoring systems.

1.1.1 Phasor Measurement Unit

The PMU consists of the components anti-aliasing filters, GPS receiver, phase-locked oscillator, analog-digital converter (ADC), phasor micro-processor and modem (shown in Fig. 1.3).

The functionality of each of the blocks are given below:

- Anti-aliasing filters restricts the bandwidth of analog input signal to approximately satisfy the sampling theorem.
- The filtered output signal is converted to digital values using ADCs.
- Phase-locked oscillator ensures synchronization of sampling with reference signal from GPS.
- ADC output is fed to phasor microprocessor, where the phasor values are estimated using discrete Fourier transform (DFT).

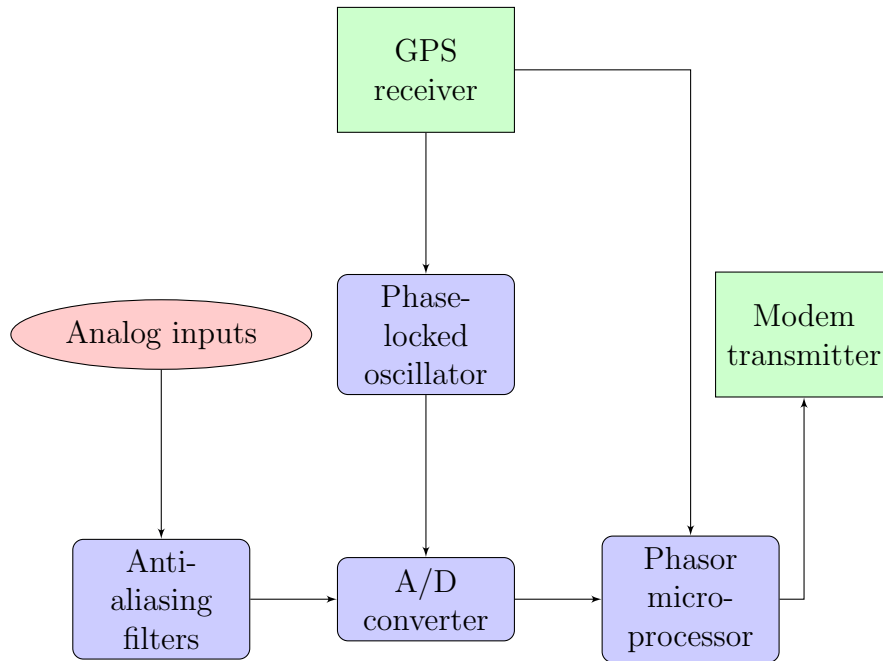


Figure 1.3: Block diagram of a phasor measurement unit

- The computed phasor values are assembled in message stream and sent via communication network to the WAMS by the modem.

1.1.2 IEEE Standards for Synchrophasor technology

IEEE standard 1344-1995 establishes connection to the universal time clock (UTC), and details regarding time accuracy, signal sampling requirements. It is followed by IEEE standard C37.118-2005 which further includes measurement related requirements and data hierarchy. But a major developmental progress happened when a joint project is started between IEEE and IEC for synchronising radio transmission (RT) communication specified in C37.118 with IEC 61850 communication and resulted in C37.118-2011 (Committee et al., 2011). Under this, C37.118.1-2011 standard (Martin et al., 2014; Martin, 2015) deals with measurement and performance of synchrophasors under dynamic systems conditions. IEEE Standard C37.118.2-2011 Synchrophasor Data Transfer for Power Systems. IEEE standards C37.242-2013, C37.244-2013 and C37.247-2013 are guide for synchronisation, guide to operation of phasor data concentrator (PDC) and PDC standard respectively (Martin, 2013).

1.1.3 Applications of Synchrophasor Technology

The research areas associated with synchrophasors can be classified into voltage stability studies, event detection, bad data analysis, optimal placement of PMUs, adaptive

protection and control, model parameter estimation and state estimation. The pie-chart representation indicates the weightage given to each of the areas with reference to the research articles published (Refer Fig. 1.4). It is observed that state estimation, voltage stability and OPP are the most explored with highest percentages in their respective publications count. The following are the applications which are most critical to industry while can be implemented with limited/low number of PMUs:

1. State estimation and protection of power system
2. Voltage stability monitoring
3. Angle/frequency monitoring
4. Compliance monitoring - Post Mortem analysis
5. Power system restoration

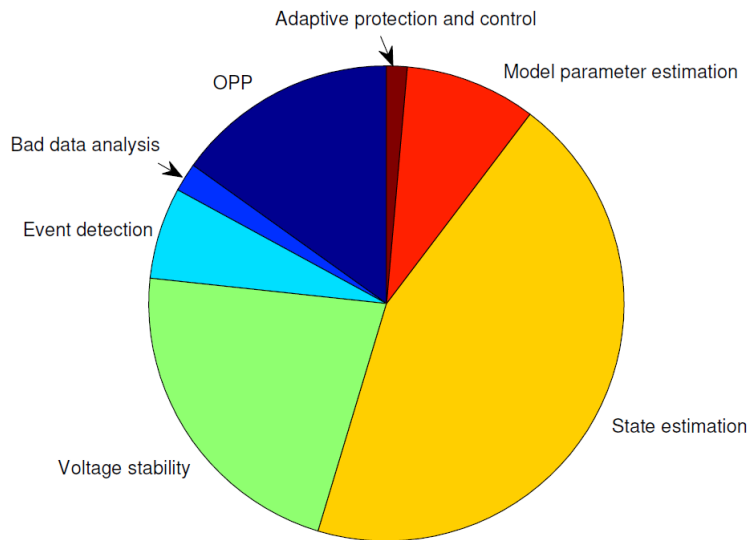


Figure 1.4: Major research areas related to PMU technology during the years 2007-2022

1.2 Power System State Estimation (PSSE)

Power system monitoring and control for power system is very much important for stable system operation. This is due to the fact that the system are being operated very close to the stability limits. State estimation (SE) provides static estimates of the system states using line active, reactive power flow measurements and phasor measurements. The load flow analysis has been conditioned such that the count of unknown quantities to be found and the count of measurements are exactly equal. This type of a system is

called a completely determined system. But if the number of measurements exceed the number of unknown variables then such a system is called an over-determined system. In this scenario the state estimation comes into picture. The idea is to utilize the data received from the measuring devices and estimate the values of the states of the system like voltage magnitude and angles at the buses. Some of them are measured and remaining are calculated. Although real-time measurements are available from Supervisory control and data acquisition (SCADA) and phasor measurement unit (PMU), calculations are necessary:

- To find node voltage angles
- For economical measurement, communication systems.
- To secure against loss of measurement and bad data.
- To carry out contingency analysis.

Power flows at both ends of every line and at LV winding of transformers are gathered as measurements. State estimation is also used to filter noise or to remove errors from measurements.

State estimation (SE) is classified into two types:

1. **DC / Linear state estimation:** In this type of estimation, only the phase angles of the buses are estimated. All the voltage magnitudes of the buses are taken as 1.0 p.u.. All the reactive power injections and flows are taken as zero. Here, only real power flows and injections used for estimation.
2. **AC / Non-linear state estimation:** Here, the voltage magnitudes and phase angles of the buses are estimated. Both real and reactive power flows and injections are used for estimation.

For power systems, generally the system is considered to be AC by modeling the DC components as constant or dynamic loads. So, at large, the system can be considered as AC system. There are three criteria considered for state estimation: (a) maximum likelihood criterion, (b) weighted least square criterion and (c) minimum variance criterion.

Table [1.2](#) lists the differences between static and dynamic SEs with reference to measuring time interval, time stamping, reliability, mathematical approach used and data acquisition rate. The construction and the overall software structure of a static state estimator is described in literature ([Lo et al., 1983](#)). The process of estimation and bad data suppression is outlined. A fast decoupled method is used in the estimating procedure. The method's initial estimates are much closer to the final true solution than the unmodified methodology, which is an important feature.

Table 1.2: Comparison of Static and Dynamic SE

Static SE	Dynamic SE
No time stamping possible	Time stamping possible
Phase measurements calculated from SCADA data causing delay	Phase measurements directly from PMUs
Data acquisition at slower rate (sampling frequency lower) Measured at an interval of 4-6 seconds.	Data acquisition at faster rate (sampling frequency higher) Measured at an interval of 0.001-0.01 second typically.
WLS approach most common	Kalman filter approach most common

Modern power system regulation relies heavily on optimal state estimates (Simon, 2006). The primary aim of state estimation (SE) is to offer precise information of one or more of a system's states, which may then help in operation or control. In general, sensing devices cannot be used to measure every state variable of the electric grid, due to either high capital and maintenance costs or impracticability. Speed measurement devices for all the generators and motors, for instance, can not be economical. Similarly, placing a sensor to measure the flux of the windings is infeasible. As a result, an optimum SE provides the benefits such as:

- a) knowledge on a system's immeasurable states.
- b) more precise details regarding measurable states by decreasing the influence of errors in the sensing devices.

For linear and non-linear systems, the Kalman Filter is a strong and popular SE technique. The basis of this computational technique is focused on reducing the mean squared error between actual and estimated variables (Welch and Bishop, 2006). Understanding how the average and covariance of variables propagate across linear and non-linear models is the fundamental basis of the Kalman Filter.

1.2.1 Literature Survey on PSSE Methods

Static and Dynamic State Estimation

SCADA system data sampled at refresh rate of few seconds is fed into traditional state estimators. Static state estimation for node voltage magnitude and angles is performed using the SCADA data and a load flow model. Because the power flow model ignores the dynamic transitions, only the static variables of the power grid are estimated, i.e., only a few snapshots of the system states are made at fixed intervals, and the dynamic variation

in between the snapshots isn't taken into account..

The rotor angle and speed of a dynamic power system are the smallest set of variables that may be used to assess the system's condition. Useful insights can be drawn from a dynamic model with precise states. In this way, dynamic state estimation (DSE) enables real-time dynamic simulation, dynamic contingency studies, and wide-area management. DSE is made possible by the availability of high quality PMU data and increasing computational capabilities. PMU data with refresh rate of 30 or 60 samples/s, is synced with global positioning system (GPS) and can consistently record a power system's dynamics under normal and abnormal situations; thus it can enable dynamic state estimation. The difficult task is to incorporate PMU data into a dynamic model for estimating dynamic states and to undertake real-time analysis using latest computing techniques. Many studies in literature have investigated DSE in electrical network using various estimating techniques. (Huang et al., 2007; Ghahremani and Kamwa, 2011a; Gao and Wang, 2010; Wang et al., 2011); Kalman and particle filters are two of the most often utilised methodologies. The variables under concern for network monitoring and control are: (Dopazo et al., 1970, 1972):

- Node voltages, node power injections.
- Line power flows.

The challenge is how to assimilate PMU data into a dynamic model for estimating dynamic states and how to utilize advanced computing technologies to perform analysis in real time. Many researchers have used various estimation approaches to investigate dynamic state estimation in power systems. Kalman and particle filters (Huang et al., 2007; Ghahremani and Kamwa, 2011a; Gao and Wang, 2010; Wang et al., 2011) are among the most referred estimation approaches (Atkinson et al., 1991). The major classification of the methods explored in literature are briefly described below:

1. Conventional methods:

State vector is determined using Least Square Estimator (Dopazo et al., 1972). Feasibility of estimating states when number of measurements and pseudo measurements are less than, equal to or more than the unknowns has been discussed. The state vector is determined using Newton's method and square root method. State estimation solution time is reduced by later method compared to direct application of former method. Estimator processes imperfect information available and produces best possible estimate of true state of system (Larson et al., 1970). Least square state estimation applied to power network under assumed static conditions. State estimation is done using linear power flow model. If measured variables are nonlinear functions of state variables, a commonly used approach is to linearize the measurement equations about a nominal value. If there is a priori estimate of state variables that is sufficiently close to actual values, then this

approach is satisfactory.

2. Fast Decoupled State Estimation

A fast decoupled static state-estimator is used for electric power systems (Horisberger et al., 1976). It solves the static, time-invariant weighted least-square state-estimation problem for large-scale electric power systems. The solution is obtained through P- θ (real power and bus voltage angle) and Q-V (reactive power and bus voltage magnitude) decoupling and alternately iterating the active and reactive equations using fixed, simplified submatrices of the information matrix. Thus, a much faster algorithm is obtained yielding the exact solution and requiring little computer storage. The new method is compared with the basic WLS and the *Line-Only* algorithms on a practical HV network.

A variable step size decoupled state estimator is a static SE based on minimization of weighted least squares of the residuals (Rao and Tripathy, 1979). The basic idea of P- θ , Q-V decoupling of the fast decoupled load flow for node injections is extended to line flows. The solution is obtained alternately iterating the real and reactive power equations using constant submatrices of the information matrix. Since no approximation is made in mismatch functions, the final solution is as accurate as the exact solution. This algorithm is compared with a constant gain algorithm (CGA) using a full size gain matrix derived in terms of the Jacobian which is evaluated only at the first iteration. The decoupled state estimator requires considerably less storage and solution time but more iterations. However, by varying the step size during iterations, the convergence behavior of DSE approaches that of the CGA.

A fast-decoupled state estimator which uses decoupled detection and identification of bad data has been presented (Garcia et al., 1979). Bad data is eliminated by pseudo-measurement generation. This procedure avoids gain-matrix retriangulations or the use of modification techniques like Woodbury formula. In the identification process, the diagonal of the covariance matrix of the measurement residuals is calculated using the sparse inverse matrix method. Two main types of fast-decoupled estimators are tested: algorithm-decoupled and model-decoupled.

To reduce inherent difficulties and metering inaccuracies, modern online control schemes use some form of state estimation. The operation and control of power systems depends on adequate metering. An economic design of metering pattern to improve the metering performance is has been presented (Mafaakher et al., 1979). This method is based on a fast-decoupled estimator that can be used to design new systems or improve existing ones. The paper includes some practical results of designing and improving existing metering system.

New methods are introduced for the stabilization of the power system during violent swings after major disturbances (Zaborszky et al., 1981). These techniques utilize existing

or attainable measurements, computer facilities, and devices such as short rating resistors, capacitors, or fast valving. Components of this state space associated with individual buses can be computed locally from local conventional measurements. The origin is always the stable system equilibrium-the target of the control. Further, methods are introduced to track this target by purely local feedback. No telemetering is involved in either the state estimation or the control. Stability of the control in a global domain is proven. Excellent performance is demonstrated by simulation on a 118 bus system with a consistent, up to ten-fold, increase in the critical clearing times.

A new steady-state estimator based on the Cartesian coordinate formulation of nodal and line flow equations and minimization of WLS of the residuals has been developed (Rao and Roy, 1983). The fact that the rectangular coordinate version of network performance equations is completely expressible in a Taylor series and contains terms up to the second order derivatives only which results in a Fast Exact Second Order State (FESOS) estimator. In this estimator, the Jacobian and information matrices are constant, and hence need to be computed once only. The size of the mathematical model for the new estimator is the same as that of the widely used fast decoupled state (FDS) estimator, and hence characterized by comparable computational requirements (storage and time per iteration). It is found that the exactness of the FESOS algorithm provides an accurate solution during all modes of system operation, and assures convergence to the right solution in spite of network ill-conditioning. In particular, the convergence behaviour and accuracy of solution of the FESOS estimator approach are same as those of the FDS estimator for lightly loaded and well-conditioned power systems during normal modes of operation, but are vastly superior during unusual modes of system operation or in relation to ill-conditioned networks.

Zhuang and Balasubramanian (1985) presented a new decoupled power system state estimator. The decoupling is achieved via simple linear transformations on power measurements in contrast with the fast decoupled state (FDS) estimators, which assume decoupling by direct negligence of the off-diagonal blocks of the Jacobian of the observation functions. A method that combines internal state estimation and external network modeling is developed in literature (Monticelli and Wu, 1985). The external system is represented by an unreduced load flow model. A single state estimation covering both the internal system and the external system is used. The external system operating data on power injections and bus voltages are entered as pseudo-measurements. At each iteration, a set of active pseudo-measurements are selected to conform with the specified variables in a load flow program. Because such a set of non-redundant measurements is used, the internal state estimation is not affected by the external system pseudo-measurements. The method can easily be implemented by modifying an existing state estimation program. It has been implemented in a fast model-decoupled estimation program. Because of the

dormant measurement technique, the constant gain matrix evaluated at flat voltage is used in every iteration. The number of iterations for the method to converge is usually the same as the regular state estimation runs.

[Monticelli \(1999\)](#) presented a new framework for fast decoupled state estimators. Decoupling is seen not as zeroing coupling submatrices in the problem Jacobian, but as a two-step procedure to solve full-Newton equations without major approximations. In addition to presenting a sound derivation of the standard version of the fast decoupled state estimator, the authors showcase a new version which presents better performance when applied to systems with critical R/X ratios.

Two different state estimation decoupling techniques using node voltages in rectangular co-ordinates: the exact-decoupled technique and the modified fast-decoupled technique are discussed in literature ([Habiballah and Quintana, 1991](#)). The proposed techniques decouple the Jacobian matrix into real- and reactive-power submatrices, which are evaluated only once at the beginning of the process. Efficient data structure management algorithms are discussed to improve the computational process required in calculating the nonzero elements of the Jacobian matrix, and the elements of the mismatching vector, which are essential to any state estimation problem.

[Sinha et al. \(1994\)](#) presented a new framework for decoupled state estimation of AC-DC power systems. Here, decoupling is not done by zeroing the off-diagonal submatrices of the Jacobian and gain matrices but as a two-step procedure. The mathematical model involves both the first and second order derivatives of the performance equations. Only diagonal blocks of the gain matrix are required to be factorized, and they remain constant in the iterative solution scheme. Their size and structure are similar to those in the fast decoupled state estimator which is based on the linearised version of the Taylor series equations. This method performs satisfactorily and its computational requirements are comparable with those of the fast decoupled state estimator.

A three-phase fast decoupled state estimation method is presented for distribution systems in ([Lin and Teng, 1996](#)). The WLS approach is used. A current-based formulation is discussed first and then the decoupled version. The proposed method produces a constant symmetric gain matrix which can be decoupled into two identical sub-gain matrices. The method offers good performance in handling the distribution system and is many times faster than other formulations, especially for large systems.

A new method is developed and presented in ([Roy and Mohammed, 1997](#)) to solve the state estimation problem of power systems. The method involves application of a rotational operator to the state and measurement functions resulting in an automatic decoupling of the Jacobian and gain matrices. The elements of these matrices are different from those in the existing decoupled state estimators. A solution is obtained through alternately iterating the active and reactive equations using the constant gain matrix and

avoiding the approximation due to the decoupling of the Jacobian matrix. Digital simulation studies on a variety of systems indicate that the new estimator is comparable to the best available version of the fast decoupled state estimator in terms of core size, solution time, mathematical structure, convergence behavior, accuracy, robustness, reliability and versatility. Systems with low and high r/x ratio lines, heavy loading, ill-conditioning, and low/high reference bus voltage are tested.

A scenario with most transmission systems being fully observable by only PMU measurements is distant in future. Because the PMU measurement equations are linear, it will enable quicker and simpler non-iterative SE solution. But, it can be further advantageous as these equations reveal more potential for simplification and hence, provide an enhanced performance of SE using only PMU inputs (Göl and Abur, 2015a). In particular, another decoupled approach is developed that minimises the size of the SE problem, improves computing speed, and retains excellent estimation precision. Within the established decoupled formulation, both SE and bad data handling may be performed efficiently. Fast decoupled SE for distribution grids is presented with rapid convergence and increased efficiency (Ju et al., 2018). Conventionally, branch current magnitude measurements cannot be incorporated into FDSE models; however, here, branch ampere measurements are reformulated as active and reactive branch loss measurements and directly formulated in the FDSE model. Using the complex per unit normalization technique and special chosen state variables, the performance of this FDSE can be guaranteed when it is applied to distribution networks. Numerical tests on seven different distribution networks show that this method outperforms Newton type solutions and is a promising method for practical application.

3. Linear programming method:

A fast and efficient technique for solving the power system state estimation problem using linear programming (LP) (El-Ela, 1992). It is based on the exact linearisation of the Cartesian co-ordinate formulation of nodal load flow equations. The LP technique is used to solve the state estimation problem without any approximation for the load flow equations. In this technique, the Jacobian and Hessian matrices are kept constant, and hence need to be computed only once, at the beginning of the solution, and then stored in the computer memory using the sparsity storage procedure. Because, in this technique the active and reactive power problems are attempted to be solved simultaneously, not sequentially, there is no need to use decomposition into two sub-problems, namely P- θ and Q-V. This formulation improves the solution time significantly.

Three algorithms namely polar co-ordinate formulations of the full and fast-decoupled weighted least squares (WLS) and the Cartesian co-ordinate WLS are explored for PSSE in (Keyhani and Abur, 1985). A detailed study of the convergence characteristics and an

assessment of the performance of three algorithms.

On the basis of observations and forecasts, DSE applied to electric grid using PMU data would estimate the actual states. In DSE, the confidence levels of projected and measured data, that are inversely related to the associated variances, influence their relevance. During hourly demand variations, component failures or line trips, state variables can fluctuate dramatically. The use of predicted data might worsen the DSE results in such scenarios. When abrupt variations in the states are sensed, a mixed-integer programming model of DSE can be used to voluntarily ignore predicted data (Aminifar et al., 2014b). This implementation improves DSE analysis and eliminates the need for repetitive iterations.

4. Artificial intelligence (AI) based algorithms:

These are powerful tools for solving non-linear set of equations and for a complicated search space. This is because, unlike classical methods that need derivative information, they just require a fitness function to direct the search. DSSE with zero-injection restrictions is performed (Lin and Teng, 1995; Guo et al., 2013).

Particle swarm optimization (PSO) is implemented to estimate system states of IEEE 6-bus system by minimizing all measurement errors in (Tungadio et al., 2015). This method has been established to be the best among AI algorithms, as it provides high-quality estimates in lesser computational time and stable convergence curve. The measurements used here are simulated SCADA measurements, that is, power injection, power flow and voltage measurements. The measurements are simulated by adding random errors (noise) in actual measurements obtained from NR load flow method. This paper compares the the results of PSO with that of genetic algorithm (GA) toolbox using MATLAB respectively. Two objective functions are formulated as: weighted least square (WLS) and weighted least absolute value (WLAV) methods. Constraints of this problem are fixed upper and lower bounds for each state variable such as voltage magnitude and angle at each bus of network. Comparison of estimates obtained from test cases show that PSO method's accuracy for estimating voltage magnitude is slightly better than that of GA for WLS-based objective function. While there exists contradicting behavior in case of WLAV formulation, the accuracy of PSO method is better than that of GA method. But GA method's accuracy is better than that of PSO in case of estimation of voltage angle for WLAV formulation.

Modern technologies are required for management and control in real-time for PSSE (Tungadio et al., 2016). Particle swarm optimization with velocity (PSWV) and advanced particle swarm optimization with weighted particle (EPSOWP) are the two hybrid approaches using PSO which was utilized. Personal best and global best positions are linearly combined to form PSWV, i.e., flying between their own best and global best.

EPSOWP can instruct the swarm to better path to find the best solution. The PSO variant models have better estimation capability than the original PSO, ABSO, and GA models.

5. Distributed State Estimation or Multi-area State Estimation:

[Zhao and Abur \(2005\)](#) performed the distributed/multi-area SE using synchronized PMU data. Each area may apply a unique estimating method. In a similar context, one PMU provides angle measurement in every subsystem which is a vital component of local SE. A distinguishing step is re-evaluating SE results of only the border buses and vulnerable inner buses. [Jiang et al. \(2007\)](#) adopted this kind of distributed state estimation approach.

A new and efficient diakoptical static state estimation algorithm is presented in [Ahmed and Brameller, \(1991\)](#). The main objective of developing this algorithm is to obtain an estimator with an improved performance in terms of robustness, accuracy, online CPU time, core memory occupation, inter-computer data transfer, scope for sparsity exploitation, and localization of bad data effect. In the developed method, a system has been divided into a number of subsystems to take advantage of low dimensionality, sparsity, fast decoupled estimation and parallel processing. The co-ordination among the subsystem level estimators is carried out in each iteration.

The need for higher frequency in state estimation execution covering larger supervised networks has led to the investigation of faster and numerically more stable state estimation algorithms. However, technical developments in distributed Energy Management Systems, based on fast data communication networks, open up the possibility of parallel or distributed state estimation implementation. This possibility is exploited [\(Falcao et al., 1995\)](#) to derive a solution methodology based on conventional state estimation algorithms and a coupling constraints optimization technique .

In electrical network, a completely distributed SE technique is used for wide-area management [\(Xie et al., 2012\)](#). Through iterative information exchange with designated neighboring control areas, all the balancing authorities (control areas) can achieve an unbiased estimate of the entire power system's state. In comparison with existing hierarchical or distributed state estimation methods, the novelty of the presented approach lies in that: 1) the assumption of local observability of all the control areas is no longer needed; 2) the communication topology can be different than the physical topology of the power interconnection; and 3) for DC state estimation, no coordinator is required for each local control area to achieve provable convergence of the entire power system's states to those of the centralized estimation.

A robust decentralised DSE of the electric grid has been implemented using multiple hypothesis testing [\(Zhao and Mili, 2018\)](#). It can discover, recognise and discard three kinds of outliers. It is able to detect, identify and suppress three types of outliers, namely

observation, innovation and structural outliers. Observation outliers refer to the received PMU measurements providing unreliable metered values due to gross errors or cyber attacks; innovation outliers are typically caused by impulsive system process noise, whereas structural outliers are induced by incorrect parameters of the generators or its associated controllers, such as exciters and speed governors. To enable the fast estimation of generator states of large-scale power systems in a decentralized manner, two model decoupling approaches are presented and compared.

6. Kalman filter based state estimation:

Configuration of an on-line state estimator is described in (Gomez-Exposito and Abur, 2004). Generally, in some parts of network there are redundant measurements, while in other parts of network there are no measurements at all. An elementary introduction on Kalman filtering, starting from the simplest of all estimation problems, namely that of estimating a time independent scalar quantity from a number of noisy measurements, is presented in in (Hargrave, 1989). Then a case is considered where the quantity to be estimated is a function of time, and a generalized results are obtained for the estimation of a time dependent vector. Finally, the resulting Kalman Filter equations are applied to an elementary but nevertheless real problem in navigation.

For Kalman filter-based data fusion in sensor networks, based on the weighted least squares (WLS) method, two distributed measurement fusion Kalman filtering algorithms are presented in terms of the average weighted measurements and the average inverse-covariance matrices (Ran and Deng, 2008), where the second algorithm is equivalent to the micro-Kalman filter derived from the centralized Kalman filter in sensor networks. Using the information filter, it is proved that they are functionally equivalent to the centralized fusion Kalman filtering algorithm. They not only have the global optimality, but also can reduce the computational burden.

Two distributed measurement fusion Kalman filtering algorithms based on WLS method are presented for Kalman filter (KF)-based data fusion in sensor networks (Ran and Deng, 2008). Here, the second algorithm is equivalent to the micro-KF obtained based on the centrally controlled KF in sensor networks. It is demonstrated using data filter that they function like the centralised fusion Kalman filtering technique. They are not only global optimum, but they can also lower the computational effort. A form of generator model state and parameter estimate approach using PMU data is discussed (Fan, 2015). At every sampling interval, the KF algorithm provides an estimation.

7. Hybrid measurements State Estimation:

Hybrid state estimation estimates system states utilizing both SCADA and PMU data. An estimation fusion method (Costa et al., 2013): handling each type of data separately

helps to retain the estimation structure of the conventional estimator. Execution times are significantly less in comparison with those taken by hybrid simultaneous schemes. SCADA-based estimates are further integrated with output of Phasor-only state estimation block which are unaffected by bad data.

Branch-current based distribution system state estimation is presented which allows PMU data to be included (Pau et al., 2013). It helps to extend state model, so the knowledge of voltage profile is significantly improved. A hybrid state estimator that effectively does the state estimation incorporating limited number of PMUs (Göl and Abur, 2015b). This improves state monitoring precision and speed, which is especially critical in rapidly varying system conditions when quick control response is needed. Control action may depend on the start of voltage instability as a result of an unforeseen disturbance. Due to lower sampling rates in the range of seconds, SE using SCADA data may be too sluggish in tracking such changes in the states. While PMU data give millisecond sampling rate, although they may not provide complete network observability. To address the lack of observability caused by PMU data while ensuring rapid tracking and robustness against measurement inaccuracies, the hybrid SE is suggested.

With amplitude and phase information, time-synchronized measured phasor data of bus voltages and line currents can be used to calculate, without iterations, the voltage phasor on neighbouring buses. In some PMUs, it has been observed that the voltage and current phasors exhibit phase biases, which can corrupt the conventional state estimator solution if it is augmented with such biased phasor data. A new approach for synchronized phasor measurement-based state estimation is proposed (Vanfretti et al., 2011), which can perform phasor angle bias correction given measurement redundancy. In this approach, polar coordinates are used as the state variables, because the magnitude and phase are largely independent measurements. The state estimation is formulated as an iterative least-squares problem.

A decentralized methodology for hybrid SE is presented to enhance computing capability with minimum inaccuracies (Göl, 2018). Here, a sensitivity matrix links the measurement errors to state estimates to generate isolated bus groups and observable sub-islands. This approach is employed in least absolute value (LAV) estimator, which is resistant to bad data. The decentralisation approach reduces the computing overhead of the LAV estimation relative to the traditional WLS estimation.

8. Phasor-only state estimation (PSE):

Conventional static state estimators use measurements of line flows and injections to estimate the positive sequence voltage phasors. Static state estimators incorporating direct measurements which enhances estimation is presented in (Thorp et al., 1985). Until 1985, many utilities regularly use state estimation to monitor their HV (greater than 132 kV)

network. If lower voltage levels are to be used in the online security system, direct state measurement looks appealing. A measurement vector made up of all voltage magnitudes and angles with no flows or injections is conceivable. Here, relation between measurement data and the states is linear. When angle measurements replace flow measurements, data volume reduces. Total number of measurements decrease as number of buses with phase angle measurements increase. For instance, here it is observed that base case has 490 measurements while the number reduced to 250 measurements with the help of this method.

9. Hybrid methods for PSSE:

A novel stochastic search strategy is integrated with scenario approach (Nejati et al., 2012) for dynamic state estimation of power systems. Incorporating elements of both differential evolution and bacterial foraging, a novel stochastic search approach is developed providing a large search capacity. With the previously available state estimators (for instance, WLS), SE can only be performed only when the electric grid is observable. For both observable and unobservable electrical network, a DSE approach has been presented that can address the estimation problem reasonably precision. Also, precise, accurate, and up-to-date data on rotor angle and speed can improve power system integrity and stability. The non-linear approaches Extended Kalman Filter (EKF) and Unscented Kalman Filter (UKF) are used to predict the states of a power system utilising PMU data (Tebianian and Jeyasurya, 2013). When it comes to solving the challenges in DSE of non-linear stochastic time varying system, an approach that relies on fuzzy augmented state kalman observer has been developed (Maalej et al., 2014). Kalman filter theory is used in combination with fuzzy Takagi Sugeno dynamic process. Kalman filter formulas are employed in the local linear models within the fuzzy logic.

10. Forecasting aided state estimation:

Another approach proposed makes use of forecast aided measurements data synchronization in robust power system state estimation (Khosravi et al., 2016). Robustness of this presented method is guaranteed as outliers (huge amplitude error) are filtered by using conventional measurements data and utilising robust Kalman filter. This estimator also follows system dynamics a lot faster than existing approaches.

1.2.2 Comparison Studies of Power System State Estimation Methods

A decoupled orthogonal row processing algorithm for power system state estimation (Wang and Quintana, 1984) employs a single sub-matrix of a decoupled Jacobian ma-

trix (SMDJ) instead of using a Single sub-matrix of a decoupled gain matrix (SMDG). Then, Givens transformations have been used to solve a PSSE WLS problem. Thus, the algorithm has the advantages of both decoupling and orthogonal transformations. Tested on IEEE 30-bus test power system, this algorithm is found to be considerably superior to the conventional normal equation algorithm and other decoupling algorithms after comparison of results.

SE has been considered as one of the security monitoring technique (Wu, 1988). There are five major SE methods (Holten et al., 1988) which are used for state estimation calculation until 1988. Tests are carried out with low and high redundancy factors with zero injection measurement at some or all buses. Comparative study in terms of numerical stability, computational efficiency and implementation complexity is done on the following:

- Normal equations method
- Orthogonal transformation method
- Hybrid method
- Normal equations with constraints
- Hachtel's augmented matrix method

A comparison of algorithms for least absolute value state estimation electric power networks is presented in (Bagchi et al., 1994). The performance of three methods, that is, two primal and one dual interior point techniques, are compared for solving a nonlinear programming formulation of the WLAV estimation problem. Here, least squares state estimation is used as a benchmark.

(Charalampidis and Papavassilopoulos (2009) have compared traditional and modified recursive SE approaches for non-linear systems. A novel set of sigma-points for the unscented Kalman filter, and also a method to replace a nonlinear response with a linear version, are described. The relevance of the state function while developing the state estimator is demonstrated. Simulations are used to compare all of the described approaches against the conventional EKF, UKF, and particle filter considering different sampling rates. The findings reveal that in some instances, there is a significant decrease in estimation error using modified approach.

Comparison of WLS electric grid SE in polar and rectangular forms is considered in (Okon and Wilkosz, 2010). The influence of a coordinate system, power system stress, and data redundancy on SE factors like count of iterations, condition number of the gain matrix, and parameters describing calculation precision and estimate dependability are studied. An introduction and study of several strategies used to handle the SE for

nonlinear power systems is presented (Kazempour and Poshtkouhi, 2012). To approach the problem, conventional Newton, Quasi-Newton, Sequential Quadratic Programming (SQP), and Linear Programming (LP) methods are studied and applied. The computational effort, accuracy, and reliability of these different approaches are compared. The LP approach minimizes the norm-1 objective function and has the feature of eliminating bad data or topological inaccuracies. If further equality and inequality criteria must be satisfied, the SQP approach is the best way to address the problem. To link the state variables to measurements, a methodology for transient SE is created utilising approximation methods for derivatives (Molina-Moreno et al., 2018). To define the pre-fault operating conditions, no information of the steady state is required. To achieve full observability, the strategy employs an efficient monitoring system based on topological analysis. To evaluate the performance of the instruments placed, a saving index is designed. To estimate the fault position, a transient index is used. The transient SE may be produced with cost saving in the number of measurement devices placed and improved computational efficiency.

1.2.3 Forecasting-aided State Estimation for Voltage Profile Estimation in Power System

The well-known procedure for Forecasting-aided state estimation (FASE) algorithm briefly consists of following stages:

1. System state model identification
2. State forecasting/prediction
3. State filtering

The term ‘dynamic’, when applied to a quasi-steady state operation may be misleading but has been used in literature more commonly even for smooth load variations. Therefore, under this scenario the developed estimators are called FASE (Zhao et al., 2019).

Literature Survey of Recent Advances in FASE

Rousseaux et al. (1988) proposed a combination of dynamic state forecasting and hierarchical filtering for electric grid state estimation. It consists of a multi-level extended Kalman filter whose prediction stage uses the dynamic load forecasting approach, and whose filtering stage uses the hierarchical approach. This paper precisely highlights the problems with respect to dynamic state estimation: (a) dimensionality, due to computationally involved EKF and multi-dimensional real systems. (b) modeling, that is to attain a proper trade-off between mimicking the real dynamic systems and also being

simple enough to implement easily. Dynamic of focus is the trend component of load changes, that is, low frequency changes. The prediction step of EKF is crucial since load forecasting depends on the previous estimates of injections which is based on this prediction state vector. Therefore DSE and load forecasting are interdependent and compliment each other. IEEE 118-bus system: Maximum accuracy obtained by this method are observed to Mean std. deviation in voltage magnitude p.u. is 1.55×10^{-3} and voltage angle (deg) is 0.08. Computational time for 2-level DHSE: Parallel local estimation: 18.09s and Sequential local estimation: 52.26s. Computational time for 2-level DHSE: Parallel local estimation: 11.76s and Sequential local estimation: 42.97s.

In another attempt to estimate both fundamental and harmonic components of voltage magnitude and angles of a power system, Kalman filter was used successfully (Beides and Heydt, 1991). The effect of load variation on harmonics of power system is presented. Input to estimator is simulated by harmonic load flow program. They are tested on modified IEEE 14-bus system with 1% to 10% standard deviation errors in measurement data. Estimated and actual values of different harmonic voltage magnitude and phase angles are very close and the filters are very effective.

Under certain circumstances such as large load changes, the DSE using EKF may degrade the filter performance. Therefore, an effort to incorporate non-linearity in measurement function is carried out by two proposed schemes/algorithms (Mandal et al., 1995). First scheme is linearised EKF with local iteration being executed at each time sample. Thus providing better reference trajectory and consequently better estimation becomes possible. Second scheme considers complete Taylor series, which implies that there is no need to calculate Jacobian or gain matrices for local iterations in filtering step. The second scheme has only 2^{nd} order term calculation in each local iteration, while in first scheme both K and H needs to be calculated in each of the local calculation. Consequently, computational time and efforts are reduced in scheme 2 than 1. Also, it was observed that for sudden load/generation change scheme 1 and 2 are better than EKF model. Computational time for EKF is the least while for scheme 2 it slightly higher due to calculation of 2^{nd} order terms and more iterations. While scheme 1 takes 2-3 times the time of EKF model due to calculation of gain and Jacobian matrices and more iterations. Therefore, the paper concludes that the proposed schemes need to be used only when sudden load/generation change condition is detected. In normal conditions the linearized EKF model is sufficient. Scheme 2 is more viable for real time applications when compared to scheme 1.

Because of fast response and efficient learning, an Artificial neural network (ANN) based short-term load forecasting is used for prediction step in dynamic state estimation (Sinha and Mondal, 1999). The ANN based model provided better prediction and better state estimates when compared to conventional prediction model based DSE. Compu-

tational time is almost same as conventional DSE scheme. In another work, non-linear autoregressive ANN is applied with multivariate external input (Buitrago and Asfour, 2017) achieved a mean absolute percent errors in the forecast in the order of 1%. Alternatively, very short term load forecasting was carried out using recurrent neural network for distribution substations (de Andrade et al., 2014). Here, the load time series measured at five-minute intervals were analyzed. A comprehensive review have been presented on the electric load forecasting techniques (Hammad et al., 2020; Munoz et al., 2010).

To improve the performance degradation due to anomaly conditions, the weighted least square method based state estimation technique is modified. Further, a robust algorithm with exponential weighting function as error-reduction tool is implemented (Shih and Huang, 2002). The average percentage errors with respect to true states for IEEE 30-bus system at the filtering stage was 0.38 for both EKF and proposed method.

The fuzzy logic based dynamic state estimation provided a feasible solution as it was able to manage uncertain events better, since it was based on human knowledge and experience. But, the way of system modeling required for fuzzy control system design was time consuming. So, dynamic state estimation with fuzzy logic controller enhanced using sliding surface concept is explored to solve uncertainty of state estimation (Lin et al., 2003). Here, the error and rate of error is embedded into the scheme as an integrated input variable. This further reduces the count of fuzzy rules significantly. For sudden load changes, the proposed method showed good filtering performance with least maximum absolute error in estimated state and performance index. While under normal condition, all three methods under comparison showed similar performances but proving feasibility of the proposed method.

Kalman filter based algorithms seem to dominate the DSE in power systems, while for the state prediction step ANN, fuzzy logic, auto-regression, Box and Jenkins methods are explored in literature. Non-linearity of measurement function is addressed by Mandal et al. (1995) but one disadvantage of this approach is that the measurement covariance matrix is not sparse and consequently computationally demanding. Square root KF is more stable but algebraically equivalent to KF (Wang et al., 2015b). When compared to the KF, the square-root filter minimizes random errors in field measurements, saves time and computer memory. Also, square-root of the covariance matrices are used instead of covariance matrices. This helps in better numerical conditioning and product of two square-root matrices can not be singular. Linear exponential smoothing technique is used for prediction step. Kalman filter based filtering have a drawback that their perform poorly in case of outliers in the measurements. To overcome this, m-estimation concept is used which assumes that complex bus voltage is determined not only by the preceding voltage value, but also by the most recently accessed voltage variation.

Phasor measurements in state estimation is observed to be advantageous it helps to

help in active power measurement estimation. With the help of high accuracy angle measurement increases the convergence speed. If only phasor measurements are considered used state estimation is simple due to linear equations. But angle measurement errors affect state estimation results than errors in power measurements. PMU measurements with higher weightage (around 100 to 200) when compared to normal measurements, is preferred for improving accuracy. Holt's double exponential smoothing is used for prediction of state vector. EKF is used for filtering step. An Adaptive EKF (AEKF) is explored for dynamic state estimation under normal, bad data and sudden load changes scenarios (Li and Li, 2009). When compared to traditional EKF and REKF, the filtering performance index of AEKF is the best by reducing the estimation errors. But the computational time is slightly higher. To address the DSE even in case of missing of measurement data due to communication failure, an approach of load forecasting based on time-forward Kriging model is used (Gu and Jirutitijaroen, 2015). It predicts the absent load data by employing the accessible measurements. Load forecast is then converted to state forecast by using power flow analysis. Further, EKF is used for filtering step by combining forecast state. Here, 5 minute time interval load data is used. It is observed that DSE using the method proposed has smaller estimation error compared to WLS state estimation under missing measurements for any duration between 5 minutes to 48 hours. Even if one load bus measurement is available for the system, DSE can be carried out when utilizing Kriging method. But, in similar scenario WLS estimator will not perform as system becomes unobservable.

Unscented KF being a simpler and derivative free implementation is applied for dynamic state estimation (Valverde and Terzija, 2010). Its results were compared to EKF and static WLS estimator. Under all scenarios the performance index of UKF is best among the three. Due to its simplicity and absence of linearisation steps, it is possible to implement higher order dynamic models of generators or loads for DSE. Projected UKF (Yang et al., 2014) was proposed for dynamic state estimation using UT and zero injection constraints being considered by estimate-projection. It performed better in state prediction and measurement filtering when compared to EKF and UKF.

Regression analysis based state transition matrix D is proposed for improving DSE (Hassanzadeh and Evrenosoglu, 2011). The method is developed which updates the state transition after a specified time periods. The matrix D is taken as block diagonal when compared to the general assumption of diagonal. Results are compared based on mean squared error. It is observed that there is good improvement in the accuracy of voltage magnitude and angle due to block diagonal state transition matrix and its calculation after fixed intervals of time.

Hyndman et al. (2002) implemented the state space framework pushing exponential smoothing into the same category as ARIMA models in terms of being broadly applicable

and having a solid stochastic mechanism underpinning the forecasts.

Another approach proposed makes use of forecast aided measurements data synchronization in robust power system state estimation (Khosravi et al., 2016). Robustness of this presented method is ensured by excluding outliers by forecasting conventional measurements data and using the Kalman filter's ability to filter noisy data. Moreover, this estimator accurately determines the dynamic behaviour of system way quicker than the conventional techniques.

Its also relevant to mention that forecasting-aided state estimation has been applied to distribution systems as well wherein smart meter measurements are used as input. A recent work (Huang et al., 2022) highlights the use of deep learning technique for the state forecasting step in FASE. It helped in making the state estimation process feasible as the smart meter measurements have low reporting rate. And deep learning technique utilizing historian data predicted measurements between smart meter measurements.

1.2.4 Dynamic State Estimation using Synchrophasor Technology

State Estimation is a process that enables the system operator make better decisions about how to keep the power system secure when there are concerns due to disturbance events which might lead to loss of generators or transmission lines. One of the very first positive impacts of using a PMU is that the accuracy of the SE of the power network improves (Antonova et al., 2011). SE solution diverges generally during evolving faults. This is when a good state estimation is most vital. The industry is always coming up with new ways to make SE more accurate. Dynamic state estimation based monitoring applications firstly focuses on monitoring electromechanical dynamics (Zhao et al., 2020). The DSE derives the generator and its controller states during faults with respect to time. Among these, the synchronous machine rotor speed and angle are extensively utilized to detect oscillations in power system. Interestingly, it has been observed that if the rotor speeds are accessible, all node frequencies are determinant. The fact that buses outnumber machines minimises the need for PMU placements for node frequency measurement. Historically, the stability of an interconnected power system was attributed to synchronous machine dynamics, i.e., transient rotor angle stability (El-Shimy, 2015). For a power system to be stable, mainly the quantities rotor angle, frequency and voltage need to be monitored and studied. Voltage stability is the capacity of an electrical grid to maintain appropriate steady state voltages among all buses (in the allowed limits) even when a disturbance occurs (Kundur et al., 2004). PMU data gathered by PDCs are utilised in control centres for real-time situational awareness applications, such as real-time stability studies (Pourramezan et al., 2017).

Current Practices for Dynamic State Estimation

Some initial studies have been carried out to explore the feasibility of the dynamic state estimation. Researchers have explored with DSE in electrical networks using a variety of estimation methods and case studies. The feasibility of adopting the II-order model of the synchronous machine to employ the Extended Kalman Filter (EKF) to the IEEE 9-bus system is studied (Huang et al., 2007). SMIB serves as a case study for assessing an EKF method for DSE in the absence of field voltage (Ghahremani and Kamwa, 2011a). Although EKF remains KF's elegant and computationally efficient recursive update form, it only functions well in a mild nonlinear environment, due to its first-order Taylor series approximation of non-linear function. It is unsatisfactory and can potentially give diverging results. Furthermore, the linearization can only be applied if the Jacobian matrix exists. While Jacobian matrices can be complicated and error-prone.

The unscented transformation (UT) was meant to solve linearization's drawbacks by converting mean and covariance information directly. Ghahremani and Kamwa (2011c) applied this approach to design Unscented Kalman Filter (UKF) which is an estimator for SMIB system utilising a PMU placed on the generator node. Both of these papers utilised the synchronous machine's 2-axis fourth order state space model. Implementation of UKF for DSE was carried out on several test systems utilising a II order synchronous machine model (Wang et al., 2011; Gao and Wang, 2010). Here, inputs were the machine's speed and electrical output. A divide-by-difference-filter driven technique is used for DSE of the machine rotor angle in a large scale network (Tripathy et al., 2009). Zhou et al. (2013) elaborate the findings of DSE for an SMIB utilising an extended particle filter. However UKF built by the sigma-point set, the mean is highly significant as it carries more weight which is usually negative for high-dimensional systems. Therefore the UKF may encounter numerical instability troubles when used in high-dimensional problems.

Arasaratnam and Haykin (2009) proposed the Cubature Kalman Filter (CKF) method which uses a more accurate cubature technique to compute mathematically Gaussian-weighted integrals. This method has been utilized to determine the states of an electric grid (Sharma et al., 2014). CKF requires the error covariance matrix to maintain its positive definiteness in each update which can stop the CKF from running continuously. Wang et al. (2015a) used a modified Iterated Square-root Cubature Kalman filter (IS-CKF) is proposed for non-cooperative space target tracking problem in space surveillance systems, where it is demonstrated that the ISCKF outperforms the conventional filters.

1.3 Event Detection in Power Systems

There is a strong relation between advancement of a civilization and the amount of energy it controls. With an increase in energy demand there comes an inherent need to control and properly distribute this energy through power grids. As the energy demand increases, the complexity and scale of power grids also increase. This leads to a need for efficient and robust power system fault detection algorithms. These algorithms are aimed at increasing reliability of very complex and large power grids. To judge the grid operating conditions there is an inherent need to measure the state variables of the system. These state variables are measured by using a Phasor Measurement Unit (PMU) in the present days. Due to its ability to collect time synchronized data with a high sampling rate, it provides a deeper insight into the operations of the power system.

Electrical power networks are subjected to a variety of disturbances. The magnitudes of these disturbances may however be a deciding factor for them to be critical or not. In the scope of this paper, disturbances that might cause interruption or damage to the power system have been classified as Events. These Events have to be addressed as soon as possible as they could bring huge losses to Power Generation organizations. The terminology event used in this paper refers to large disturbances in network and quick variations in renewable energy generation output (Allen et al., 2013). The former not only consists of short circuits on transmission lines; protective relay operations functioning to clear events, such as line trip and reclosing operations; or a huge and abrupt loss of generator or load.

Disturbances in a grid can be of varying magnitudes from small disturbances to large disturbances. Some disturbances can also be caused due to normal operation of the grid. The recorded data from the PMU consists in it a component of real world noise with the actual signal. The real world noise recorded by each PMU changes from one PMU to another. This variation depends on many factors including geographical location, environmental factors, grid topology and connectivity. To make things worse small to medium magnitude disturbances have comparable magnitudes to normal operational disturbances. It is difficult but not impossible to separate the dynamically changing real world noise from the actual true signal in order to avoid false positives and/or false negatives.

Synchrophasor data and wide area monitoring enables grid operators to visualize the whole electric power system spread through an entire interconnection, interpret grid conditions in online, and analyse and take action to solve emerging problems (Nuthalapati, 2019). Wide area monitoring system provides a better visibility, and the employing the advanced detection techniques to alarm the system operators regarding the possible system instability, can prevent the occurrence of blackouts.

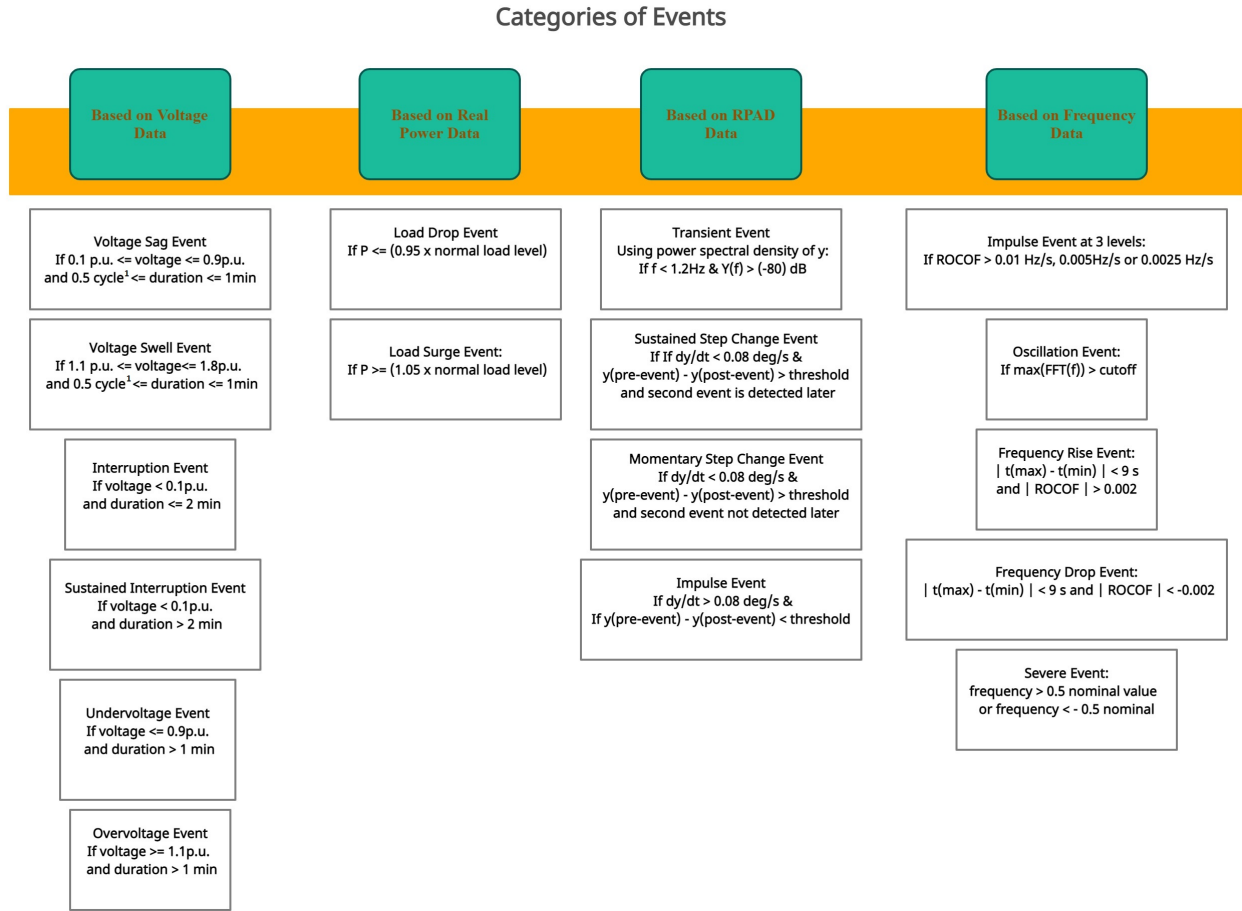


Figure 1.5: Categorization of events

1.3.1 Categorization of Events

The general structure of power system is formed by interconnection between smaller power systems using tie-lines at transmission level voltage. This includes several generating units. Although this interconnected structure provides a high degree of reliability, a major tie-line fault or a loss of large generation/load can cause instability and may lead to cascading events and blackouts. Alternatively, failures may also be brought due to natural calamities putting the system operate in stressed conditions and beyond its stability limits. Therefore, detecting any such disturbance event at the earliest is very important.

In literature, it is observed that, mostly fixed thresholds are defined for defining the different events based on the historian knowledge and experience of the power engineers and operators at control centers. For practical implementation of event detection in Texas Synchrophasor Network, National Renewable Energy Laboratory gathered data from 120 V voltage level (Allen et al., 2013). At this voltage level, only data provided are voltage magnitude, angle, and frequency. And events are identified based on Relative Phase Angle

Difference (RPAD) and frequency data. On the other hand, event categorization based on real power and voltage have been studied in (Ge et al., 2015).

The categorization of events maybe either based on

- RPAD Data.
- Frequency Data.
- Voltage Data.
- Real Power Data

Based on visual analysis of the signals and a screening algorithm, categorization of events is given as shown in Fig. 1.5.

1.3.2 Review of Current Technologies for Event Detection

A literature survey is carried for the research articles published in the past decade (Refer Tables 1.3, 1.4, 1.5 and 1.6).

- The NREL report (Allen et al., 2014) suggests to use multiple algorithms to detect a fault and if more than 2 algorithms detect a fault at a particular data location then that location can be deemed as an actual event. They are based on either relative phase angle difference or frequency as input signals.
- A method of ellipsoids for auto detection of events is employed (Gajjar and Soman, 2014). To detect major events, perform the principal component analysis and error ellipsoid methods for frequency samples of duration of 5 s, 10 s and 20 s. Magnitude of error variances is compared to fixed threshold to identify event. Frequency data is used as input.
- Recent advances of deep learning is used to build a convolutional neural network model to detect events (Wang et al., 2020). Here, the rate of change of frequency and the relative angle shift are as the inputs.
- Patent US8457910B2 (Muthu-Manivannan et al., 2013) uses an electronic computing device and identifies power system event when one or more of the criteria are satisfied. If an RMS current in one or more phases is greater than a predetermined threshold level, a fault current is flowing. The selection criteria is based on computing resource constraints, or on the existence of known patterns or features in the data that are more likely to be power system events. This is for distribution system only. There is no mention of dynamic thresholds for the quantities. Only pre-determined thresholds are used based on historian data and fault patterns. Since data signal

is directly taken from CT, PT and converted to digital using ADC, identification might not be fast.

- Patent US10324132B2 (Saarinen et al., 2019) focuses mainly on line event detection from measured value (mainly fault current) from a power line signal. System has intelligent electronic device (IED) connected to the power line and a processor linked to IED.
- In patent US8738191B2 power transmission line monitoring is performed by using devices: Dynamic line rating (DLR) devices and additional phasor measurement units. Here the input signals are: (a) Voltage and current via at least one PMU located along at least one of said power transmission lines to be monitored in grid. (b) physical line data corresponding to thermal line limits via DLR devices. Park's transformation is applied on the transient data extracted. Further, Spectral analysis is performed on the current signal. The zone (adjacent and/or upstream monitoring zone) of occurrence of event is identified using two fixed thresholds.
- Patent US20160320435A1 applies event detection logic based on at least one element selected from group. The group consists of limits, sensitivities, margins, deviations, aggregations and rate of change for one or more measurements from data streams across the wide area, the derived dynamic stability metrics including frequency instability, voltages, power flows, phase angles, damping and oscillation modes. The metrics associated with the detected events comprise time of event, event location, type of event, magnitude of event, root cause of event. All types of events are detected.
- Patent CA2508965A1 (Roger, 2005) is used for monitoring parameters in an electric power distribution system. This is carried out based on the input signals: voltage, current, total harmonic distortion in voltage, flicker and frequency. It defines two thresholds: first dynamic threshold which is three times the standard deviation and second dynamic threshold, that is, six times the standard deviation. The method generates a caution signal when measured value greater than or equal to first dynamic threshold. While an alarm is raised and an action is suggested when measured value greater than or equal to second threshold. Since the parameters are calculated from the measurements from CT, PT and not PMU device, it might involve some inherent delay. The dynamic threshold is generally based on weekly average till yearly average is obtained.
- Event detection and classification algorithm using frequency data from Wide Area Measurement Systems device frequency disturbance recorder (Okumus and Nuroglu,

[2018]. The algorithm scans each sample of the data and compares the frequency variation with a specified threshold. When the variation value is above the threshold the event is detected.

Table 1.3: Reviews of papers on event detection

Paper	Topic	Input signal	Algorithm	Summary
Dahal et al. (2013)	Comprehensive Clustering of Disturbance Events Recorded by PMU	Features extracted from disturbance file obtained from PDC	1. MVEE (Minimum Volume Enclosing Ellipsoid) method is used to extract features. 2. Agglomerative Hierarchical Clustering Method to make clusters	This paper is able to classify all the disturbance file into 19 clusters. Each cluster representing one class of fault. (Not all faults are known , hence every clustered is not named yet).
Dahal and Brahma (2012)	Preliminary Work to Classify the Disturbance Events Recorded by Phasor Measurement Units	Voltage, frequency, and power flow recorded by PMUs during a disturbance are considered as input parameters for our classification method	1. MVEE method is used to extract features 2. The decision tree approach is proposed to classify the disturbance events	1. Each disturbance file is 3-minutes long with a total of 5400 samples for each waveform. A total of 62 sets of data are recorded in each disturbance file 2. A total of 58 features as described in are collected from each of the disturbance events to construct a features vector. 3. A decision tree algorithm is used to classify faults.
Rasmussen and Jorgensen (2006)	Synchronised Phasor measurement of power system event	Data measured using PMU , i.e positive sequence voltage , frequency, etc	The voltage and current are sampled at rate of 36KHz, Then synchronised phasors are calculated using these values every 20ms using GPS .This paper demonstrates that direct observation of inter area oscillation modes using phasor measurements is more convenient than computation of eigenvalues using a detailed model of a specific system configuration.	This paper presents one of the first Nordic applications of synchronized phasor measurements in monitoring power system oscillations during a tie-line switching.

Table 1.4: Reviews Of papers on event detection

Paper	Topic	Input signal	Algorithm	Summary
Xie et al. (2014)	Dimensionality Reduction of Synchrophasor Data for Early Event Detection: Linearized Analysis	Various parameters such as Voltage, Current, Angle, Frequency measurements recorded by the PMUs across the Grid can be considered as valid input.	Early Event Detection algorithm, Principal Component Analysis for Dimensionality Reduction	In this paper, by exploring the dimensionality reduction of the PMU data, proposed an early event detection algorithm, along with theoretical justifications, to detect power system events at an early stage.
Singh et al. (2019)	Storage and Analysis of Synchrophasor Data for Event Detection in Indian Power System Using Hadoop Ecosystem	Data Recorded from PMUs is given as input.	The models that can identify disturbance directly from the change in frequency range are designed by Gaussian distribution method .A few approaches to identify events by using some mathematical models are proposed to apply convex optimization method known as ellipsoid model well known as MVEE	The experiments conducted depict the efficacy of the proposed methodology. PMU data storage more reliably in a decentralized fashion with security by using low-cost commodity hardware units (i.e., Hadoop clusters and Hadoop Distributed File System). This method is coefficient than current vertical scalable high-end server systems providing more faster processing. This paper focuses to improve the visualization of computed data point and further analysis and storage and is necessary at load dispatch centers rather than data point and reading of PMUs.
Biswal et al. (2016)	Supervisory Protection and Automated Event Diagnosis using PMU data	Voltage and frequency signals	SSFD (Strongest signal selection and fault detection) with concepts of CE (Cumulative Energy) and FE (Fault Energy). Time Frequency analysis using Fast Variant of discrete S transform and special feature selection	Event detection and its characterization is done using feature maps created from the frequency transforms(Time-frequency transforms) . It also provides a clear picture on what characteristics is expected from a system when abnormalities have occurred. And at the end by using an Extreme Learning Machine the classification of faults takes place.

Table 1.5: Reviews of papers on event detection (Contd.)

Paper	Topic	Input signal	Algorithm	Summary
Shi et al. (2020)	Online Event Detection in Synchrophasor Data with Graph Signal Processing	Streaming PMU Data, Voltage Signal, Frequency of the system	Discrete Fourier Transform, Graph Fourier Transform, Graph Signal Processing	In addition to being extremely scalable, this paper proposed an algorithm that can accurately capture and leverage the spatio-temporal correlations of the streaming PMU data. This paper also develops a general technique to decouple spatial and temporal correlations in multiple time series. Finally, This paper developed a unique framework to construct a weighted adjacency matrix and graph Laplacian for product graph.
Samuelsson et al. (2006)	Monitoring of Power system at transmission and distribution level	Data measured using PMU i.e., positive sequence voltage, frequency, etc.	It is just monitoring and analysing of the data , no algorithm is encountered	It is able to show the relation between fault at transmission and distribution level. Lower voltage levels are used to identify power transmission dynamics.
Wang et al. (2014)	Multiple Event Detection and Recognition through Sparse Unmixing for High Resolution Situational Awareness in power grid.	Real Time frequency Recorded data by the PMUs in Power Grid acts as input	Nonnegative sparse event unmixing algorithm for multiple event separation and temporal localization and Linear Unmixing Concept	Experimental results with both simulated and real event cases demonstrated the effectiveness of the proposed algorithm. The experimental results demonstrate that the framework is reliable to detect and recognize multiple cascading events as well as their time of occurrence with high accuracy.

Table 1.6: Reviews of papers on event detection (Contd.)

Paper	Topic	Input signal	Algorithm	Summary
Ge et al. (2015)	Power System Real-Time Event Detection and Associated Data Archival Reduction Based on Synchrophasors	Voltage Signal, Current Signal	Principal Component Analysis, Curve Fitting Algorithms like OLS. This paper consisted of a lot of statistical algorithms where mean median, maxima and minima is calculated and used for the benefit of event detection.	Present methods on real-time event detection and data archival reduction based on synchrophasor data produced by phasor measurement unit (PMU).Event detection is performed with principal component analysis and a second order difference method with a hierarchical framework for the event notification strategy on a small-scale microgrid.
Negi et al. (2017)	Event Detection and it's Signal Characterization in PMU Data Stream	Phase Angle signal, Voltage signal, Frequency of the system	An improved kernel principal component analysis combined with support vector machine is used for event diagnosis. Use of short-time Fourier transform is applied for analyzing voltage signal event. Auto Regressive Moving Average	Event detection scheme uses computation of spectral kurtosis on sum of intrinsic mode functions. The algorithm is capable of detecting the event in phasor measurement units (PMU) data by comparing the maximum energy and root-mean square of energy content of present analysis segment with respect to previous segment.

The methods used for event detection in the literature can be classified into:

1. Time-frequency transform methods
 - Principal component analysis,
 - Fourier spectrum analysis, short time Fourier transform, graph Fourier transform,
 - Based on cumulative energy and fault energy: using fast variant of s-transform.
2. Statistical Analysis:
 - Minimum volume enclosing ellipsoid method,
 - Auto regressive moving average method,
3. Pattern Analysis:
 - Non-negative sparse event unmixing method,
 - deep learning method,
 - K-means algorithm

1.4 Need for Optimal Placement of PMUs in Power Systems

The phase angle difference is an indicator of stress in the grid and the urge to observe it online is highlighted in literature (Corporation, 2013). Also, the plot of the angle difference is a key indicator to detect major events in an area or in adjacent areas; detection of islands and marking abnormal conditions like load collapse. The direct measurement of phase angle is possible only with the breakthrough in wide area monitoring system (WAMS). It is the synchronization technology which helped in overcoming the limitations of state measurement and its telemetering at main control center. This telemetry gives more precise measurements by using the device called phasor measurement units (PMUs). The technology is developed near the end of 1980s and the first product came into market in 1990s. Table 1.1 summarizes the differences between SCADA and PMU measurement systems and why PMUs are gaining more importance.

Several large-scale deployment projects are being carried out worldwide including NASPI (North American Synchro Phasor Initiative) led by NERC, the WAMS in the Western Grid of the North America (Phadke and Tianshu, 2018), Brazilian phasor measurement system led by ONS (the Brazilian ISO), the WAMS in China, various developments in Europe, etc. Installations of PMUs have been sluggish due to the inherent

costs involved. But, the benefits from these few installations have been proved to be tremendously notable in monitoring of system. This is due to the enabling of visualization of magnitude and angle of three-phase voltage/current, frequency, rate of change of frequency (ROCOF) and angular separation at every few millisecond interval (40 ms) in LDC. Hence, PMUs are presently the most accurate measurement technology with GPS time stamping providing information to power engineers and system operators for WAMS. But each PMU costs from \$1260-\$10,000. So, it is very crucial to find the minimum number of such PMUs required for implementation in a given power system network. This is a rigorous research area since the past 3 decades.

1.4.1 Overview of Synchrophasor Initiative in India

The functioning of power grid in India is being coordinated by State, Regional and National Load Dispatch Centre (SLDCs/RLDCs/NLDCs). It is mandatory for the LDCs to exercise supervisory and control on transmission system and ensuring integrated operation within their scope.

Table 1.7: The details of the Synchrophasor Pilot Project in India

Description	ER	NER	NR	SR	WR	NLDC
No. of PMUs installed	8	6	8	6	11	18
PDC locations	ERLDC, Kolkata; Binaguri substation; Biharshariff substation; Rourkela substation; Sasaram substation;	NERLDC, Shillong	NRLDC, New Delhi	SRLDC, Bengaluru	WRLDC, Mumbai	NLDC, New Delhi

The synchrophasor projects were undertaken in India since May 2010 (Corporation, 2013). There were 14 PMUs commissioned by end of May 2012. The PMU placement for the pilot/demo project was done in two phases. Synchrophasor technology at inter-state level was first introduced in India in 2010-11 in northern region. In northern region, the PMUs have been placed at nine 400kV substations which are Vindhyanchal (HVDC back-to-back), Kanpur, Dadri (HVDC terminal), Moga, Kishenpur, Agra, Bassi, Hisar and Karcham Wangtoo. In western region, PMUs have been placed at two 400kV substations namely Raipur and Bhadravati. In southern region, three substations Salem, Hyderabad

and Bengaluru have PMUs installed. Three phasor data concentrators (PDC) established at respective RLDCs at New Delhi, Mumbai and Bengaluru. Later on, the eastern region is further divided into eastern and north-eastern regions and the updated details of the project (as of 2013) are as shown in Table 1.7. Location of the PMUs (Corporation, 2013) on the map of India are indicated in Fig. 1.6.



Figure 1.6: The geographical locations of PMUs installed in India (Corporation, 2013)

Criteria for Locaton of PMU Installations: The primary objective of the pilot/demo projects is to comprehend the synchrophasor technology and its applications for power system operation. A heuristic approach is adopted for finding locations to implement the PMUs. The broad procedure for selection of PMU locations is given below:

- locations separated by large geographical distance.
- locations with large phase angle separation estimated from steady state load flow studies for different anticipated scenario.
- locations near large generation complex.
- locations having broadband communication link with the PDC.
- locations perceived to be critical based on operator experience.

Though PMUs are situated only at few locations in the Indian power grid as furnished above, it strikingly raised visualization and level of perception of power system at the control centre within few months of their deployments. Evidently, gestation and payback period of investment in synchrophasors is very small compared to its advantages. This is especially due to the enhanced situational awareness in real-time. Offline PMU data helped in better forensic analysis of faults/grid incidents, post-dispatch analysis of grid operation and oscillation detection-monitoring in system. It is reported that the philosophy for placement of PMUs-strategic/optimal is one of the major challenges faced during the pilot project. There is a demand for developing customized applications to realize the potential of the technology particularly in view of its utility for large-scale integration of renewable energy sources and reliable operation of large synchronous pan India/SAARC (South Asian Association for Regional Cooperation) grid.

1.4.2 Various Methods for Solving Optimal Placement of PMUs

In optimal placement of PMUs (OPP) studies, finding the exact global solver that solves in a reasonable duration of time is a challenge. Each of the techniques/methods evolved with time have its own particular mathematical and computational characteristics (Yuill et al., 2011; Manousakis et al., 2012; Gupta and Pandey, 2014; Aminifar et al., 2014a; Nazari-Heris and Mohammadi-Ivatloo, 2015; Mohanta et al., 2016; Chouhan and Jaiswal, 2016) . The classification of the methods discussed in literature are discussed in further sub-sections.

A. Conventional methods

Initial work related to research for OPP is done around 1988 (Wu, 1988) for achieving complete observability using combinational approach, graph theoretic approach or factorization-based approach. In many of the earlier literature on OPP, the conventional *Integer linear programming* (ILP) approach has been utilized (Gou, 2008a; Dua et al., 2008; Gou, 2008b) considering with and without zero-injection and flow measurements. Further, the scenarios with critical contingencies are considered in (Sodhi et al., 2009).

ILP method is used to check how the solutions when two grids are evaluated separately and interconnected (Gopakumar et al., 2013). And topology transformation method merges zero injection bus (ZIB) and one of its neighbors (Rahman and Zobaa, 2016). Tables 1.8-1.14 make critical remarks on the use of conventional methods for solving OPP. The formulation and algorithm is non-linear and hence size of computation increases with increased number of complex buses considered (Jelodar and Fini, 2016). Some infeasible results are reported in some cases (Aminifar et al., 2010b). Another recent work carried out an outer approximation scheme based on BILP (Korres et al., 2015) which has improved speed and efficiency. Also, the method lead to lesser number of PMUs than existing techniques.

B. Heuristic methods

Heuristic method is an experience-based technique for solving optimization problems, in which optimal point is not obtainable in finite time. Heuristics contain in their underlying principles some specialized operators (Nazari-Heris and Mohammadi-Ivatloo, 2015) that could enable wider exploration of the space of the solutions. The solution of OPP is derived for incomplete observability using the novel concept - depth of unobservability (Nuqui and Phadke, 2005). Here, spanning trees of power system graph and a *tree search* technique is used.

Binary search algorithm, an exhaustive algorithm is used to solve OPP problem (Chakrabarti and Kyriakides, 2008). Lexicographic algorithm helps in giving fast formulations of combinations that can be used by the binary search one at a time. OPP considering measurement channel failure based on a *modified binary search* is accounted (Albuquerque and Paucar, 2013). This is in the view that failure of measurement channels is more common than failure of the PMU itself.

An *information-theoretic* approach for OPP solution is dependent on mutual information between PMU data and system states (Li et al., 2013). A *greedy PMU placement* algorithm based on the covariance matrix installs PMUs in stages. Single line outage detection would be a trivial problem if there are PMUs at each of the buses in the system. But the challenge is maximizing the ability to detect any single line outages in the system by placing only a limited PMUs (Kim and Wright, 2018). This is done by *Multinomial Logistic Regression Model* (MLR), a machine-learning approach based on observation vectors which has voltage phasor differences as its elements. Computationally intensive although the method gives the global optimal point (Chakrabarti and Kyriakides, 2008). The Tables 1.15 and 5.1 shows the features of the works reporting heuristic methods.

C. Meta-heuristic methods

Meta-heuristics are problem-independent methods. These methods act like black boxes and are not dependent on the uniqueness of the particular problem. Generally, they even consider a temporary degraded solution, which helps the algorithm to search more explicitly the search space and thus to get a hopefully better solution.

As noted in the literature while implementing a meta-heuristic approach, it is absolutely necessary to perform some refining of its intrinsic parameter values so as to readjust the method to solve the problem at hand. In fact, a meta-heuristic is also a heuristic, but is more effective due to its inherent nature to avoid being trapped in a local optimum. Further, the meta-heuristic is an advanced application of heuristic method by escorting them through the search space, to use its best capabilities obtaining improved results. These techniques generate new solutions by recombination of one or more good solutions.

Genetic algorithm (GA) is used for finding minimum number of PMUs required wherein the number of current measures for topological observability is also taken into account (Marin et al., 2003). A fault observability rule using basic theories of power system observability is introduced (Golshan et al., 2018). Network expansion plan is considered as a constraint in the OPP problem for a multi-year time-frame instead of a one-year period (Asgari and Firouzjah, 2018) solved using GA.

The *Simulated annealing* formulation is extended for solving pragmatic phased installation of PMUs recognizing the limitations in availability of communication facilities. The applicability of immunity genetic algorithm for OPP problem is explored (Aminifar et al., 2009b). Incorporation of immune operator in canonical genetic algorithm (GA) with an intention of preserving GA's advantages is possible. This is performed utilizing some characteristics and knowledge of problems for prevention of degenerative phenomena during evolution, thus improving efficiency of algorithm.

In order to cope with the continuous changes in the power system's topology, Al-Mohammed et al. (2011) formulated the optimization problem considering not only the new PMUs to be installed but also the existing ones to be retained or relocated. And this is done with the help of a meta-heuristic method called *Differential Evolution* (DE). In addition, a single PMU loss case is considered (Venkateswaran and Kala, 2012). An analytical framework based on cost/benefit analysis is presented (Aminifar et al., 2013a).

The main aim of the authors in (Zhao et al., 2015) is to improve robustness when dealing large systems. An improved GA based on serial number coding is used to prevent infeasible results and improve the algorithm's performance. Topological constraint analysis reduces computation cost. Full observability with maximum redundant measurements for buses identified as critical, with the same count of PMUs as under normal conditions, is achieved with *Lyapunov exponent-based approach* (Rashidi and Farjah, 2016b,a).

General optimal substation coverage (GOSC) algorithm (Pal et al., 2017) considers the

practical constraints such as redundancy in critical measurements of the system and calculating tap ratios of transformers present. The optimal measurement system incorporating communication infrastructure constraints is reported (Singh and Singh, 2017; Almasabi and Mitra, 2018). Case studies with contingencies are also carried out to ensure reliable solution for system.

There has been multi-stage OPP wherein the PMUs are installed in stages. This is done by determining placement scheme with a given certain level of unobservability in association with subsequent stages. The OPP problem is tackled in single- or multi-stages by using probabilistic approaches taking element outages probability into consideration. One terminal algorithms utilize only measurements at one end of the transmission lines for fault location, thus required number of PMUs would be lesser than two-end algorithm (Sun et al., 2018).

The literature which appeared after Cho et al. (2001); Mishra et al. (2016) revealed that solutions obtained are not the optimum values even for small systems. GA takes higher convergence time than the conventional method BILP (Kumar et al., 2018). The meta-heuristic methods can not be applied on any power system without tuning the values of the certain parameters it is dependent on. Major works done using Meta-heuristic methods been noted in Tables 1.17, 1.18 and 1.19.

D. Hybrid methods

Earlier studies has not been done on reduction of number of PMUs to implement fault location algorithms based on single terminal data. In a similar context, the objective considered (Milosevic and Begovic, 2003) is of achieving simultaneous optimization of two conflicting objectives, that is, minimizing the number of PMUs and maximizing the measurement redundancy. The *non-dominated sorting genetic algorithm* (NSGA) is used to solve and get the pareto-optimal solutions, that is, a set of best trade-offs between competing objectives.

A four-staged optimization technique consisting of sequential elimination method, sequential addition method, binary integer programming and a heuristic algorithm is presented (Rakpenthai et al., 2007). Some of the hybrid methods requires complex computations (Milosevic and Begovic, 2003), therefore dependent on network size. Zhao et al. (2015) described a hybrid method that does not guarantee optimality nor does it inform how good their sub-optimal solutions are with respect to the optimal one. Similar shortcomings have been noted in remarks column of Table 1.20 and 1.21.

Table 1.8: Main journals and conference articles on solving OPP using conventional methods - PART I

Reference	Technique	Constraints	Test system	Year	Advantages/Shortcomings
Xu and Abur (2004); Gou (2008a), Dua et al. (2008); Gou (2008b), Chen and Abur (2008), Ahmed and Imran (2019), Abdelkader et al. (2019)	Simple/binary Integer linear programming approach used as it is and extended, generalized to satisfy different needs.	A, B, C, F,G	IEEE 14, IEEE 30, IEEE 57, IEEE 118 bus systems	2004, 2008, 2019	(Gou 2008a) ZIBs concerned constraints are not incorporated. (Dua et al. 2008) It lacked in considering complete power system observability under any contingency. (Gou 2008b) Numerical observability are not embedded in OPP studies, for a stable decentralized SE. (Chen and Abur 2008): The technique increases the cost as improvement is made by strategically placing few extra measurements. (Ahmed and Imran 2019): $N-1$ contingency constraints increases reliability of system. (Abdelkader et al. 2019): SE errors decreased by OPP solution.

A: Complete system observability, B: Depth of one unobservability, C: Measurement redundancy, D: Single PMU loss, E: Other contingencies, F: ZIB consideration, G: Depth of two unobservability, H: Measurement channels, I: Communication infrastructure

Table 1.9: Main journals and conference articles on solving OPP using conventional methods - PART II

Reference	Technique	Constraints	Test system	Year	Advantages/Shortcomings
Sodhi et al. (2009), Abbasy and Ismail (2009), Emami and Abur (2010), Emami and Abur (2010), Sodhi et al. (2011), Kavasseri and Srinivasan (2010, 2011),	Sodhi et al. (2009), Emami and Abur (2010), Sodhi et al. (2011), Kavasseri and Srinivasan (2011, 2010): Integer linear programming;	A, E, F, H	IEEE 14, IEEE 30, IEEE 57, IEEE 118 bus system, New England 39 bus system, Northern region power grid, 246-bus Indian system, a large 2383-bus Polish system, Iranian national grid, 2746-bus Polish grid, Polish 3375-bus test system	2009 2010 2011 2012 2013	(Sodhi et al. 2009): Contingency conditions, i.e., line outages and loss of measurements are not considered separately nor simultaneously for solving OPP. Zero-injection measurements and communication constraints as measurement limitations are not included in the model. (Abbasy and Ismail 2009): Line outage contingencies are not considered there. Zero-injection buses & channel limits are not considered. (Sodhi et al. 2011): The optimal PMU locations is obtained for the last stage and places these PMUs in stages; hence the problem is not formulated as a whole. Here, all buses are considered equally; although, in real systems, few selected nodes are more critical. (Kavasseri and Srinivasan 2010): The linear model is formed at the cost of additional constraints and variables. This method is applicable only for utilities ready to re-locate their existing traditional flow measurements along with installation of new PMUs to limit overall observability cost. (Kavasseri and Srinivasan 2011): The constraint for flow measurements is a non-linear constraint, which takes longer execution time to get the global optimal solution of the problem because of mixed integer linear programming problem formulation.

A: Complete system observability, B: Depth of one unobservability, C: Measurement redundancy, D: Single PMU loss, E: Other contingencies, F: ZIB consideration, G: Depth of two unobservability, H: Measurement channels, I: Communication infrastructure

Table 1.10: Main journals and conference articles on solving OPP using conventional methods - PART III

Reference	Technique	Constraints	Test system	Year	Advantages/Shortcomings
Korkali and Abur (2010), Aminifar et al. (2010a), Azizi et al. (2012), Aminifar et al. (2013b)	Abbasy and Ismail (2009): BILP with Multi-criteria decision-making approach; Korkali and Abur (2010); Aminifar et al. (2010a), Aminifar et al. (2013b), Karimi et al. (2019): Mixed integer linear programming; Azizi et al. (2012): Equivalent integer linear programming	A, E, F, H	IEEE 14, IEEE 30, IEEE 57, IEEE 118 bus system, New England 39 bus system, Northern region power grid, 246-bus Indian system, a large 2383-bus Polish system, Iranian national grid, 2746-bus Polish grid, Polish 3375-bus test system	2009, 2010, 2011, 2012, 2013	(Korkali and Abur 2010): For the first time the number of channels present in the selected model of PMU is accounted for. This is found to be significantly influential in deciding the locations for PMU placement. Installation cost is directly proportional to how dense the system is connected, by applying developed technique. (Aminifar et al. 2013b): Takes into account the effect of DC lines on network observability. (Azizi et al. 2012): Not suitable for large-scale systems with huge search space.
A: Complete system observability, B: Depth of one unobservability, C: Measurement redundancy, D: Single PMU loss, E: Other contingencies, F: ZIB consideration, G: Depth of two unobservability, H: Measurement channels, I: Communication infrastructure					

Table 1.11: Main journals and conference articles on solving OPP using conventional methods - PART IV

Reference	Technique	Constraints	Test system	Year	Advantage/disadvantage
Azizi et al. (2014)	Boolean algebra, Integer linear programming	A, F	IEEE 14, IEEE 30, IEEE 39, IEEE 118 and IEEE 300 buses test systems	2012	A unified model for optimal multi-stage placement of PMUs is successfully implemented by using ILP equivalents for Boolean expressions.
Chakrabarti et al. (2009) , Lu et al. (2017)	Integer/Binary quadratic programming	A, C, D, E	IEEE 9, IEEE 14, IEEE 30, IEEE 39, IEEE 57, IEEE 118 & IEEE 145 bus systems	2009, 2018	Chakrabarti et al. (2009) : Transfer of uncertainty in PMU data along the transmission lines, and further into the estimated states is not looked into yet.
Kekatos et al. (2012)	Gradient projection algorithm	A, E, I, J	IEEE 14, IEEE 30 and IEEE 57 bus systems	2012	Bypasses combinatorial search with convex relaxed OPP problem formulation for guaranteed numerical optimality.

A: Topological observability, B: Depth of one unobservability, C: Measurement redundancy, D: Single PMU loss, E: Other contingencies, F: ZIB consideration, G: Depth of two unobservability, H: Measurement channels, I: Communication infrastructure, J: Numerical observability

Table 1.12: Main journals and conference articles on solving OPP using conventional methods - PART V

Reference	Technique	Constraints	Test system	Year	Advantage/disadvantage
Gopakumar et al. (2013), Azizi et al. (2013), Biswal and Mathur (2015), Rahman and Zobaa (2016)	Integer Linear Programming	A, B, F	Southern region Indian states, IEEE 14, IEEE 24, IEEE 30, IEEE 57, IEEE 118 bus systems, New England 39 bus system	2013 2015 2016	(Gopakumar et al. 2013): Analyzed the solutions when two grids are evaluated separately and interconnected. Also, ILP failed in obtaining satisfactory results as it failed in observing bus number 105 in Kerala SLRG as shown in (Suresh 2016). (Biswal and Mathur 2015): In this study, each substation is represented as a simple bus although in real networks they are complex types. Complex buses are represented by two distinct buses under many circumstances. So, the observability may be incomplete if placing of PMU devices is considering only simple buses. (Rahman and Zobaa 2016): This method generally results in a single solution while many optimal solutions might be possible.

A: Topological observability, B: Depth of one unobservability, C: Measurement redundancy, D: Single PMU loss, E: Other contingencies, F: ZIB consideration, G: Depth of two unobservability, H: Measurement channels, I: Communication infrastructure, J: Numerical observability

Table 1.13: Main journals and conference articles on solving OPP using conventional methods - PART VI

Reference	Technique	Constraints	Test system	Year	Advantage/disadvantage
Theodorakatos et al. (2015)	Sequential quadratic programming	A, D, F, H	IEEE 14, IEEE 24, IEEE 30, NE 39-bus, IEEE 57, IEEE 118 test systems	2014	This method gave same optimal number solution as BILP with different placement sets.
Korres et al. (2015) , Manousakis and Korres (2019)	Binary semi-definite programming	A, J, C, D, E, J	IEEE standard test systems, a large-scale system with 3120 buses	2015 2019	(Korres et al. 2015) : The ZI buses have been utilized to modify the constraints to obtain reduced requirement of PMU devices. With unknown tap ratios, if all ZI buses are treated equally it can result in instances where topological and numerical observabilities differ. (Manousakis and Korres 2019) : Unlike earlier works, numerical observability is considered.
Jelodar and Fini (2016)	Modified PMU placement algorithm, Probabilistic PMU placement algorithm	A	IEEE 14 bus with different type of buses	2016	The formulation is non-linear and the size of problem becomes large if complex buses in the system increases. Hence, it is very difficult to solve the problem for large networks.
Nikkhah et al. (2017)	Equivalent single-level mixed-integer programming	A, C, E, F	Modified 7-bus test network, IEEE 118 and 2383-bus IEEE test networks	2018	Since this method involves a non-linear model, it gets complicated to apply in cases where there are other measurements or when many ZIBs are present in the system.

Table 1.14: Main journals and conference articles on solving OPP using conventional methods - PART VII

Reference	Technique	Constraints	Test system	Year	Advantage/disadvantage
Lu et al. (2018)	Integer Linear Programming	A, F, H	IEEE 14, IEEE 30, IEEE 39, IEEE 57, IEEE 118 & IEEE 300 bus systems, Polish 2383-bus test system and practical power system in China	2018	Test network is studied during expanded time horizon.
Almunif and Fan (2020)	Mixed integer linear programming (MILP), Non-linear programming (NLP)	A, D, E, F, H, I	IEEE 14, IEEE 57, IEEE 118, IEEE 300 test systems and a large 2383- bus Polish system	2019	MILP and NLP gave same optimal number results. MILP takes lesser CPU time to obtain a single global optimal solution. While NLP gives several alternative local optimal solutions.

A: Topological observability, B: Depth of one unobservability, C: Measurement redundancy, D: Single PMU loss, E: Other contingencies, F: ZIB consideration, G: Depth of two unobservability, H: Measurement channels, I: Communication infrastructure, J: Numerical observability

Table 1.15: Main journals and conference articles on solving OPP using heuristic methods - PART I

Reference	Technique	Constraints	Test system	Year	Advantages/Shortcomings
Nuqui and Phadke (2005)	Spanning tree search	A, B	Two electric utility systems, IEEE 14, IEEE 30, IEEE 57 bus systems	2005	The novel concept - depth of unobservability explored.
Peng et al. (2006) , Koutsoukis et al. (2013)	Tabu search, Recursive Tabu search	A, C, J	IEEE 14, IEEE 30, IEEE 57, IEEE 118 bus systems, New England 39 bus system, 2383-bus power system	2006 2013	(Peng et al. 2006) Contingency conditions are not explored. (Koutsoukis et al. 2013) : First time numerical observability analysis method is combined with a meta-heuristic technique to solve the OPP problem. But, there is no focus on obtaining multiple optimal solutions which could help decide on selecting the one solution among them which gives maximum redundancy. This kind of solution would have lead to more precise SE & higher robustness against element outages. Transmission and PMU outages are not taken into consideration.

A: Topological observability, B: Depth of one unobservability, C: Measurement redundancy, D: Single PMU loss, E: Other contingencies, F: ZIB consideration, G: Depth of two unobservability, H: Measurement channels, I: Communication infrastructure, J: Numerical observability

Table 1.16: Main journals and conference articles on solving OPP using heuristic methods - PART II

Reference	Technique	Constraints	Test system	Year	Advantages/Shortcomings
Chakrabarti and Kyriakides (2008), Albuquerque and Paucar (2013)	Binary search algorithm, Modified binary search	A, E	IEEE 14, IEEE 24, IEEE 30, IEEE 39 & IEEE 118 bus systems, New England 39 bus test system	2008	(Chakrabarti and Kyriakides 2008): Lexicographic algorithm helps in giving fast formulations of combinations used by the binary search one at a time. It achieves the global optimal solution to OPP problem, it gets computationally involved for bigger systems. (Albuquerque and Paucar 2013): OPP considering measurement channel failure is accounted, under observation that outage of channels of PMU is more common than failure of the PMU itself.
Li et al. (2013)	Greedy PMU placement using information-theoretic approach	A	IEEE 14, IEEE 30, IEEE 57, RTS 96 bus systems	2013	Mutual information between PMU data and system states and covariance matrix are used by the algorithm in installation of PMUs in stages. But, important parameters such as transmission line admittances are neglected by only considering binary connectivity graph
Kim and Wright (2018)	Group-sparse heuristic, Greedy heuristic	E	IEEE 14, IEEE 30, IEEE 57, IEEE 118 bus systems	2018	The performance of model used is shown to be inferior to neural network for classification of outages for wider range of electricity demands. This is because the PMU signatures of each outage is more widely dispersed and thus harder to classify.

A: Topological observability, B: Depth of one unobservability, C: Measurement redundancy, D: Single PMU loss, E: Other contingencies, F: ZIB consideration, G: Depth of two unobservability, H: Measurement channels, I: Communication infrastructure, J: Numerical observability

Table 1.17: Main journals and conference articles on solving OPP using meta-heuristic methods - PART I

Reference	Technique	Constraints	Test system	Year	Advantages/Shortcomings
Cho et al. (2001), Mallikarjuna et al. (2016)	Simulated Annealing	A	Regional grids of India	2001 2016	(Cho et al. 2001) As reported in the literature after this paper reported that its results are not the optimum values even for small systems. (Mallikarjuna et al. 2016): Solves pragmatic phased deployment of PMUs recognizing the scarcity of communication infrastructures.
Marin et al. (2003), Kumar et al. (2018), Rashidi and Farjah (2016b a), Golshan et al. (2018), Müller and Castro (2016), Asgari and Firouzjah (2018)	Genetic algorithm	A, E, C, H	IEEE 14, IEEE 30, IEEE 39, IEEE 57, IEEE 118 bus systems, Eastern region Indian power grid 90 bus real system, New England 39 bus test system	2003 2016 2018	(Marin et al. 2003) Clarity is lacking about the fixed number of current measurement channels considered for each PMU. Directly results are plotted. (Kumar et al. 2018) GA has higher convergence time than BILP. (Rashidi and Farjah 2016b a): Full observability with maximum redundant measurements for buses identified as critical with the same count of PMUs as under normal conditions is achieved with Lyapunov exponent based approach to improve GA. (Golshan et al. 2018) A fault observability rule is introduced ignoring loss of PMU. (Müller and Castro 2016) Effect of ZIB, single branch outage and PMU channel limitation are not considered in the OPP. The network is studied with expanded time horizon. (Asgari and Firouzjah 2018): Network expansion plan is incorporated as a constraint for OPP.

A: Topological observability, B: Depth of one unobservability, C: Measurement redundancy, D: Single PMU loss, E: Other contingencies, F: ZIB consideration, G: Depth of two unobservability, H: Measurement channels, I: Communication infrastructure, J: Voltage Stability Index

Table 1.18: Main journals and conference articles on solving OPP using meta-heuristic methods - PART II

Reference	Technique	Constraints	Test system	Year	Advantages/Shortcomings
Aminifar et al. (2009b)	Immunity genetic algorithm	A	IEEE systems, a realistic large-scale power system	2009	Incorporates immune operator in the canonical genetic algorithm to prevent degeneration during evolution, thus improving performance.
Al-Mohammed et al. (2011) , Venkateswaran and Kala (2012) , Ghafarzadeh et al. (2015) , Tarif et al. (2019)	Differential Evolution(DE), Adaptive DE, Pareto archive DE	A, D, E, F	IEEE 14, IEEE 24, IEEE 30, IEEE 39, IEEE 57, IEEE 118 bus systems, 6-bus test system	2011, 2012, 2014, 2019	This method can not be applied on any power system without tuning the values of the certain parameters it is extremely dependent on the crossover factor and scaling factor. Ghafarzadeh et al. (2015) Incorporates weight and reduction factors improving convergence and applicability for large-scale problem. Based on PMU data, from the OPP solution, fault location strategy implemented.
Mishra et al. (2016) , Rather et al. (2016) , Saleh et al. (2017)	Binary particle swarm optimization. And its improved version.	A, I	IEEE 14, IEEE 30 and IEEE 118 bus systems, a large-scale network of Dominion Virginia power system	2016, 2017	Mishra et al. (2016) BPSO does not always achieve the global optimum point. Rather et al. (2016) Realistic constraints such as availability of CT, PT and communication network to satisfy topological observability.

A: Topological observability, B: Depth of one unobservability, C: Measurement redundancy, D: Single PMU loss, E: Other contingencies, F: ZIB consideration, G: Depth of two unobservability, H: Measurement channels, I: Communication infrastructure, J: Voltage Stability Index

Table 1.19: Main journals and conference articles on solving OPP using meta-heuristic methods - PART III

Reference	Technique	Constraints	Test system	Year	Advantages/Shortcomings
Parpaei et al. (2017)	Rational random walk (RRW)	A, E	Real life systems in Iran networks 2383-bus Polish test system	2017	It is independent of tuning parameters and simple structure compared to other meta-heuristic methods. RRW superimposes on other optimization algorithm enhances convergence speed.
Zhang et al. (2017)	Spectral clustering	A	IEEE 118-test system, New England 39 bus system	2017	To improve the monitoring of the power system in terms of reliability, some critical and tie-line buses are monitored more precisely.
Dubey et al. (2018)	Multi-objective differential evolution	A, D, E, F	IEEE 30 bus system	2018	Comparison studies of this method is carried out with binary imperialistic competition algorithm and genetic algorithm results.
Almasabi and Mitra (2018) , Almasabi and Mitra (2019)	An opposition-based elitist binary genetic algorithm	A, I	IEEE 14, IEEE 30 and IEEE 118 bus system	2018	Considers both communication infrastructure and installation cost. Primary objective minimizes cost and secondary objective is to maximize observability with vulnerability analysis.
Manoharan et al. (2018)	Ant lion optimization	A, I, J	IEEE 14, IEEE 30 and IEEE 57 bus systems, 2383 bus Polish system	2018	It is capable of solving optimization with escaping from local optima and performing a robust search of a solution space.

A: Topological observability, B: Depth of one unobservability, C: Measurement redundancy, D: Single PMU loss, E: Other contingencies, F: ZIB consideration, G: Depth of two unobservability, H: Measurement channels, I: Communication infrastructure, J: Voltage Stability Index

Table 1.20: Main journals and conference articles on solving OPP using hybrid methods - PART I

Reference	Technique	Constraints	Test system	Year	Advantages/Shortcomings
Nimbalkar and Joshi (2019)	Ant colony optimization	A	IEEE 14-bus system	2019	OPP solution is expected in a finite time set initially even for larger systems.
Milosevic and Begovic (2003)	Non-dominated sorting genetic algorithm method	A, C	IEEE 39, IEEE 118 bus systems	2003	Solve to obtain pareto-optimal solutions for satisfying competing objectives. But, becomes complex and computationally intensive for large power systems.
Nuqui and Phadke (2005)	Spanning trees method & Simulated annealing	A, B	IEEE 14, IEEE 30, IEEE 57 bus systems. Two electric utility systems	2005	None of the contingencies are considered for finding the solution of OPP.
Rakpenthai et al. (2007)	Four-staged algorithm: Sequential elimination, Sequential addition, binary integer programming and a heuristic method	A, F	IEEE 14, IEEE 30, IEEE 39, IEEE 57 bus systems,	2007	The carrying forward of uncertainty in PMU data along the transmission lines, and their further influence on the estimated states are not looked into so far.
Mazhari et al. (2013)	Cellular Learning Automata	A, E,	IEEE standard systems, Iranian 230- & 400-kV transmission grids	2013	An appropriate integrated model to consider ZIBs and conventional measurements is not utilized to consider contingencies effects (Khajeh et al. (2017)).

A: Topological observability, B: Depth of one unobservability, C: Measurement redundancy, D: Single PMU loss, E: Other contingencies, F: ZIB consideration, G: Depth of two unobservability, H: Measurement channels, I: Communication infrastructure

Table 1.21: Main journals and conference articles on solving OPP using hybrid methods - PART II

Reference	Technique	Constraints	System	Year	Advantages/Shortcomings
Zhao et al. (2015)	New algorithm based on combination of graph theory and genetic algorithm	A, F	IEEE 30, IEEE 57, IEEE 118 bus systems	2015	Although this method provides multiple solutions, contingencies are not considered.
Prasad and Kumar (2018b)	Interior point method is hybridized with estimation of distribution algorithm	E	IEEE 69-bus system, Indian 85-bus system	2018	It does not provide optimality assurance nor does it inform how good their sub-optimal solutions are with respect to the optimal one.
Wu et al. (2018)	Mixed-integer linear programming & genetic algorithm	A,E	IEEE 33-bus test system, 69-bus test system	2018	OPP with Dual-use line relays and traditional PMUs, considering observability & maximum load loss coefficient limit after single branch outage.
Prasad and Kumar (2018a)	Hybrid particle swarm optimization- Krill Herd algorithm	A	IEEE 69-bus system	2018	Robust meter placement for active distribution state estimation is carried out successfully.
Sun et al. (2018)	Hybrid approach based on global search algorithm	A, C	IEEE 30 bus system	2018	The formulation is developed for steady-state robust estimations only, hence, it is applicable only to static power systems.
Laouid et al. (2019)	Hybrid approach based on PSO and Gravitation search algorithm	A, C, D, E, F	IEEE 14, IEEE 30, IEEE 57 bus systems	2019	OPP results while improving measurement redundancy is obtained equal to less than those obtained in recent papers.

A: Topological observability, B: Depth of one unobservability, C: Measurement redundancy, D: Single PMU loss, E: Other contingencies, F: ZIB consideration, G: Depth of two unobservability, H: Measurement channels, I: Communication infrastructure

Table 1.22: Comparison of the different methods adopted for OPP studies

Type of Method	Advantages	Shortcomings
Conventional	The computational time is very less. And gives an optimal solution for every system considered.	All the discussed ILP methods yields only one optimum solution for an OPP problem.
Heuristic	They are problem-oriented methods. That is, they are readjusted to the problem at hand, taking full favour of its particularities. And therefore, these methods are computationally intensive.	Due to their greedy nature, they tend to be trapped in local optimum and thus being unsuccessful in reaching the global optimum. Clearly, heuristics exclusively perform best on a particular type of problems.
Meta-heuristic	Meta-heuristics gather the information all along the search to drive the search process. They are equipped with operators to rescue from being caught in a local optima.	There is no guarantee of reaching the global optimum solution without sufficient number of trials with varying parameter values.
Hybrid	The best features of two methods used in combination leads to better results.	Due to computational complexity in cases where heuristics or meta-heuristics are used as part of the hybrid method, the time consumed might be high with increasing size of the problem.

1.5 Motivation and Objectives

1.5.1 Motivation

Prediction and control of power system operations to prevent blackouts is one of the key research areas, so to ensure better stabilization of the network. Situational awareness of the wide area network becomes extremely important for carrying out planning and monitoring of the modern power systems. This is completely dependent on the real-time measurement system and monitoring. Especially, visualizations on the dashboard at main control centre play an inevitable role in assisting system operator to make better deci-

sions. PMUs are the fastest measurement technology available presently. But, initially the integration of synchrophasor measurements to the already existing reliable technology SCADA system (Data reporting is at every 2-4 seconds typically) is expected due to the difference in their data reporting rates. The synchrophasor technology provides good basis for tracking dynamics in network responses for better monitoring and control (bin Mohd Nasir et al., 2019). Phasor measurements based state estimation and hybrid measurement based state estimation showed significantly improved performances when compared to classical state estimation. The classical state estimation is based on SCADA measurements alone and therefore fails to capture all the critical dynamics of the power systems.

For voltage profile monitoring, the dynamic state estimation based on the voltage magnitude and voltage angle as state variables is focused first. This is also inline with the fact that state estimation does not have a unique state vector and different set of state variables can be chosen for a study. In literature, an approach proposed makes use of forecast aided measurements data synchronization in robust power system state estimation (Khosravi et al., 2016). Robustness of this presented method is guaranteed by rejecting outlier by forecasting conventional measurements data and using robustness property of the Kalman filter against noise in data. Hybrid state estimation determines the states of systems monitored both by conventional SCADA measurements and PMUs. As shown in Fig. 1.7, Kalman filter based algorithms seem to dominate the FASE in power systems (Shivakumar and Jain, 2008). An estimation fusion method (Costa et al.,

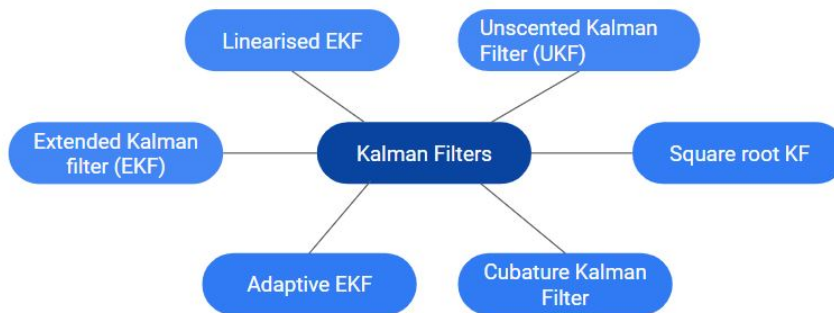


Figure 1.7: Review of Kalman filters used for FASE

2013) is utilized for processing of conventional and phasor measurements separately which helps to retain the estimation structure of the conventional estimator. Also, processing data obtained from different measuring channels and gathered at very distinct sampling rates would be easier. Execution times tend to be significantly less than those required by hybrid simultaneous schemes. SCADA-based estimates which are later fused with results of DSE module are free from influence of bad data. Phasor-only state estimation

on the other hand will enable faster and numerically easier state estimation solution which will be non-iterative due to the linearity of the PMU measurement equations. However, the benefits do not end there and a closer look at these equations reveals that further possibilities of simplification and thereby improved performances are achievable with state estimators that use only PMU measurements (Göl and Abur, 2015a). Based on the literature survey, the motivation for further research in FASE is to improve a Kalman filter based estimator's accuracy and robustness against noise.

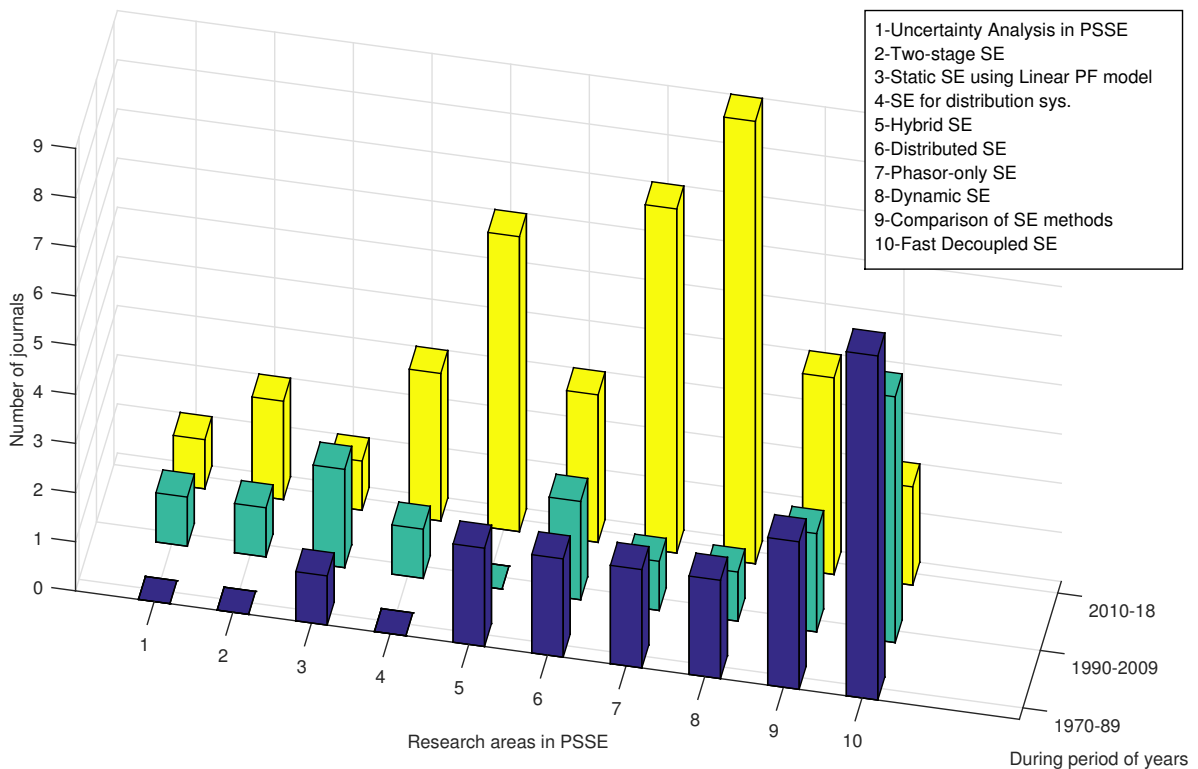


Figure 1.8: Journals published until 2020 on PSSE

Secondly, the monitoring of system in a holistic way is possible based on the system states. The states needs to be estimated using the state estimation methods. The 3-D plot for journals published until 2020 sorted decade-wise, related to power system state estimation (PSSE) with different research areas specified, is shown in Fig. 1.8. It is clearly seen that the research areas such as hybrid SE, phasor-only SE and dynamic SE are the hot topics in recent years. Now, dynamic state estimation (Refer Fig. 1.9) could be utilized to estimate the machine parameters (i.e., rotor angle and rotor speeds) or voltage profile as system states. States are the minimum set of variables that can determine the status of a dynamic system for a time scale of interest. Many approaches including Kalman filter, neural networks, fuzzy logic, etc. have been explored in literature. There is rigorous research taking place in these research areas. To emphasize on the importance

of dynamic state estimation, we looked into some of the ongoing works related to dynamic security assessment (DSA).

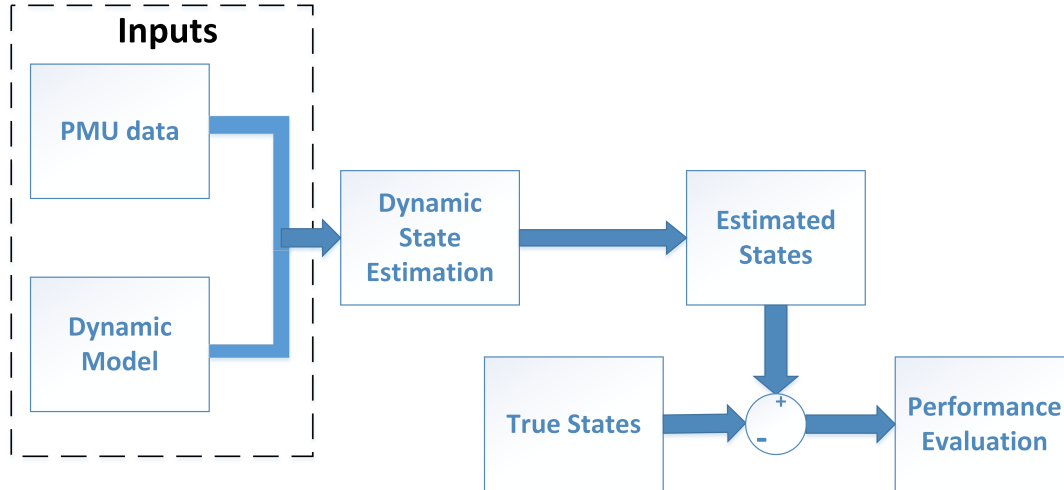


Figure 1.9: Problem statement of dynamic state estimation

Dynamic security assessment is responsible for prevention of scenarios like blackouts. Generally, if a power system is stable at a frequency 60Hz (or 50Hz), static state estimation (SSE) is sufficient to initialize the differential equations, as performed for DSA in today's energy management system (Zhao et al., 2020). When the system is unstable, that is, not operating at 60Hz (or 50Hz), SSE results cannot be utilized for differential equations initialization. Evidently in future power systems with high penetration of distributed renewable resources, the variables will vary frequently and more rigorously, for which SSE proves to be sluggish to provide DSA tools with a precise snapshot of the system states. But it is during this time period that DSA would be extremely significant for power system operation. For instance, 2003 Northeast blackout in US and Canada caused power outage wherein the system frequency deviated from 60Hz for 2-4 hours. In such scenarios, DSA would help to guide operator's restorative actions. For the electromechanical machine dynamics, the time scale is at a level between 100 milliseconds and 1 second. The machine dynamic states can be used to enhance the rotor angle stability of a power system by enabling dynamic contingency analysis and state prediction. Depending on the requirement of an application, the states can be estimated for past, current and future time. A smoothing method estimates the states of past time and can be used to reproduce past events for forensic studies. A filtering method estimates the states at the current time and can be used to drive control signals to improve system stability and to guide proactive remedial actions. The ultimate goal of this study is to enhance power system stability in real time, and therefore the focus is placed on the filtering method. In literature, various Kalman filter based approaches have been explored for DSE. In a recent work, the Cubature Kalman Filter (CKF) proposed in (Arasaratnam

and Haykin, 2009) which uses a more accurate cubature technique to compute mathematically Gaussian-weighted integrals has been used to determine the states of an electric grid (Sharma et al., 2017). But, CKF requires the error covariance matrix to maintain its positive definiteness in each update which can stop the CKF from running continuously. This research gap was identified in the DSE studies in our work.

In the event detection scenario, the need for real time implementation for prevention of blackouts is still the main focus of power engineers. And in efforts to improve system reliability, synchrophasor data based approaches are leading the way out to tackle event cascading and blackouts. Some of the drawbacks/deficiencies of these available solutions for event detection problem are identified as follows:

1. The already existing method (Allen et al., 2014) use fixed thresholds, with a Strongest Signal First Detection (SSFD) mechanism. Multiple fault detections are observed throughout the time period suggesting that the algorithms are not well optimized for avoiding false detections. This algorithm has a low precision of 10 s.
2. One drawback of ellipsoid method (Gajjar and Soman, 2014) is that it gives a coarse duration with range of 20s the major event could have occurred any time within that period. Event instance is identified later using Kalman filtered df/dt (rate of change of frequency) data. But even this event detection has a precision of only 1 s.
3. Patent CA2508965A1 (Roger, 2005) have the dynamic threshold calculations but it captures any deviation from normal. While EP3173799B1 does anomaly monitoring based feature generation from frequency, voltage and current data. But both type of detections would not be able to differentiate between major from minor events.
4. Patent CN109787979B describes a power network event and intrusion detection method using K-means algorithm. But, this method has disadvantages such as: (a) it is required to specify the number of clusters in advance, (b) It can not handle noisy data and outliers.
5. For all machine learning techniques:
 - (a) Huge amount of training dataset need to be provided for high precision (Wang et al., 2020; Gholami and Srivastava, 2021). But, there is less quantity of classified/labeled information available for the training.
 - (b) Event signatures can also dynamically change and vary during daily system operation.
 - (c) Requirement of human involvement based on experience with system operations for tuning of the methodology.
 - (d) It does not directly include operational conditions, such as real power and reactive power as inputs. This is influential as these operational conditions can impact the actual frequency and relative angle shift.

Based on the survey, research work was taken up in an aim to provide a comprehensive approach considering operational conditions such as voltage, current, real power and reactive power as inputs. And the aim is to develop a data driven approach to yield the event instance location with increased precision and reduced latency.

The efficient and intelligent placement of phasor measurement units in the power system is the initiative to be taken up. Various approaches have been explored in the literature. Still there is lot of scope for improvement based on various aspects which can be studied. Based on the expository survey carried out, the following challenges in the field of optimal placement of PMUs (OPP) are to be considered:

1. The method adopted for solving OPP should be able to give a feasible global optimal solution for the system considered.
2. System observability constraint considered in OPP studies in the literature can be either topological, numerical or both. Most of the literature on OPP studies takes into account only topological observability. But it is observed that in some cases though rare, the topological observability may not assure the numerical observability. And for a successful execution of state estimation, numerical observability is necessary. Hence, it is recommended that numerical or combined observability is considered for finding OPP solution.
3. The presence of ZIBs should be exploited for minimizing the count of PMUs significantly for getting an observable system.
4. It is necessary to consider single PMU failure constraint as it is common for any device to fail in the long run. Under such circumstances as well, the measurement system should be in a position to observe all the buses in the system and carry out state estimation. Thus, reliability of the OPP solution shall be ensured.
5. Measurement channel limitation is also an obvious condition which needs to be taken into account while carrying out OPP studies.
6. A method which solves large-sized optimization problem including thousands of design variables corresponding to network buses with reasonably less computational burden is preferable. This would be helpful for OPP analysis on large interconnected power systems.
7. Basically, OPP solution is used for the planning stage, therefore, computational time is not the main concern. The focus can hence, be on obtaining different alternative solutions giving different locations combinations to help maintain security of the system.

1.5.2 Objectives

1. Forecasting-aided State Estimation for monitoring voltage profile during normal load variations.
2. An improved Cubature Kalman Filter for dynamic state estimation during a three-phase fault.
3. Event detection based on practical synchrophasor signals gathered by PMUs using an efficient and system-independent technique.
4. Implementation of a new meta-heuristic approach called Crow search algorithm for Optimal placement of PMUs problem in power networks.

1.6 Organization of the Thesis

The thesis has been divided into the following chapters:

Chapter 1 gives an overview of the existing technologies/methodologies in the concerned research areas for power system monitoring and analysis using Synchrophasor Technology. A review of the methodologies for estimation of bus voltage angles and magnitudes is carried out. Further, the dynamic state estimation literature study for estimating rotor angle and rotor speed of machines in the power system is taken up. The event detection methods being used in literature are surveyed to identify the challenges and scope for improvement. The measurement system setup related research called the optimization of phasor measurement unit placement is explored. Consequently, the motivation for the research work carried out in the thesis is described. And the research objectives are coined.

In the next chapter the first objective of state estimation for voltage profile of power system during normal load variations has been studied. Here, the aim is to ensure state estimation before the arrival of next measurement set and with improved accuracy.

Chapter 2 presents forecasting-aided state estimation carried out for monitoring voltage profile during normal load variations. Forecasting aided State estimation is a type of dynamic state estimation, wherein the aim is to utilize all available measurements (from both RTU and PMU) and ensure state estimation before the arrival of next measurement set. Thus overcoming the drawback of the traditional static SE which does not consider the most recent measurements received from the RTUs during its execution, and its results always fall behind the actual system states in time. Voltage profile monitoring under normal load variations is essential for ensuring secure and reliable electric supply in the

system. Since, the pattern of normal load variation could be predicted with the help of a forecasting tool, it is called as forecasting-aided state estimation. The parameters for the forecasting tool is determined before the start of actual FASE process. The Iterated Square-root Cubature Kalman Filter (ISCKF) along with Holt's double exponential smoothing tool is employed and found to be effective in improved estimation accuracy for two different sized test systems in comparison to that of the cubature Kalman filter. The online real-time application feasibility is illustrated. Test systems considered for the study are IEEE 30-bus and Northern Region Power Grid (NRPG) 246-bus systems.

In the next chapter, the second objective of state estimation for synchronous machine states of power system during three-phase fault condition has been studied using the same ISCKF method explored in this chapter. The DSE is aimed to provide accurate estimates of the rotor angle and rotor speed deviation of synchronous machines in the system with the available measurements. Thus, both FASE and DSE help in better situational awareness of the power grid.

Chapter 3 utilizes an ISCKF for dynamic state estimation during a three-phase fault. For better monitoring of the machines in the power system, accurate dynamic state estimation is necessary. Preliminary studies are done with existing Kalman filters on induction motors. Further, the possibility of employing an improved version of cubature Kalman filter called the ISCKF for this dynamic state estimation for synchronous machines is studied and a comparison is made with extended Kalman filter, unscented Kalman filter and cubature Kalman filter. The power system DSE studies are carried out on test systems such as single machine infinite bus (SMIB), IEEE 9-Bus and 19-Generator 42-Bus test systems.

In the next chapter, the third objective of event detection based on practical synchrophasor signals gathered by PMUs using an efficient and system-independent technique has been studied. This would consequently help in taking better protection and control measures for maintaining a resilient, secure and stable system.

Chapter 4 presents event detection studies based on practical synchrophasor signals gathered by PMUs using a data-driven approach and a dynamic thresholding technique. A new comprehensive method based on abnormality detection, weighted sum abnormality and custom feature maps is designed for the purpose. Case studies are carried out on the practical PMU data of Northern region of India during cyclone Amphan, obtained from National Load Dispatch Center (NLDC), India. For comparison studies, some signal processing methods used by National Renewable Energy Laboratory power system engineers are utilized.

In the next chapter the last objective of Optimal placement of PMUs in power networks is studied in detail with more focus on literature survey and implementation of a relatively new meta-heuristic method. The measurement system using PMU device is essential for the modern power system monitoring and analysis.

Chapter 5 presents an implementation of a new meta-heuristic approach called Crow search algorithm for optimal placement of PMUs problem in power networks. This is mainly a combinatorial problem with binary decision variables. In literature, there are four major types of methods, used for finding locations for placement of phasor measurement units in power systems, namely conventional, heuristic, meta-heuristic and hybrid methods. In this chapter, the performance of a relatively new nature-inspired algorithm called the Crow search algorithm is evaluated for its best use in optimal placement problem. The results are compared with binary integer linear programming (BILP) and a meta-heuristic method particle swarm optimization method. BILP is the dominant method in this optimization problem to get the global optimal value. Test systems considered are of varied sizes such as IEEE 14-bus, IEEE 30-bus, IEEE 57-bus and 72-bus practical equivalent system of Indian southern region power grid.

Chapter 6 presents the conclusions drawn based on the research studies carried out in the concerned fields and future scope of research are also suggested.

This is followed by appendices, bibliography and author's publications. The appendices provide the details of the different test systems used for carrying out the case studies and the different existing methodologies used for comparison studies.

Chapter 2

Forecasting-aided State Estimation in Power Systems during Normal Load Variations

Forecasting-aided state estimation (FASE) is performed for power system to help in monitoring and control of the system. The estimation is carried out employing the data from remote terminal units along with that from phasor measurement units. FASE is a type of dynamic state estimation, wherein the aim is to utilize all the available measurements (from both SCADA and PMU) and ensure state estimation before the arrival of next measurement set. It is observed that the static state estimator results always fall behind the actual system states in time due to high execution time that the RTU scan rate. So far for FASE, it is assumed in the literature that the variations in the system variables, for instance load demand variations at a bus are slow. Quick variations in the states of an electric grid are hence not included for the study. To predict the states at a time instant in between receiving the two measurement datasets from the measurement system, a state forecasting approach is being used. The filtering step is carried out with the help of a Kalman filter approach.

The utilization of an iterated square-root cubature Kalman filter (ISCKF) for power system forecasting-aided state estimation (FASE) is being studied during normal load variations. The estimation is carried out utilizing hybrid measurements from remote terminal units and phasor measurement units. The effectiveness of the proposed algorithm ISCKF during normal load variations is evaluated with respect to already existing Kalman filter approaches. The state vector is forecasted using the proposed method in the interval period between two measurement arrivals from the devices. This aids in the estimation of power

¹Based on the contribution of this chapter, a journal paper entitled *Dynamic State Estimation of Synchronous Machines using Iterated Square-root Cubature Kalman Filter and Synchrophasor Measurements* has been communicated to Journal of Electronics and Electrical Engineering.

system states during periods when field data are unavailable. The efficacy of the proposed algorithm to FASE is evaluated for IEEE 30-bus system and Northern Region Power Grid (NRPG) 246-bus system. The algorithm could achieve better accuracy and is observed to be robust against noise. Feasibility of online real-time application is discussed as well.

2.1 Introduction

State estimating process for power network has been traditionally described as a static estimate issue, solved using weighted least square (WLS) technique. With the advent of wide area measurement systems, hybrid state estimation algorithms are created by adapting the traditional WLS technique to include phasor measurement units (PMU) measurements (Valverde et al., 2010; Asprou et al., 2013; Sodhi et al., 2010; Lixia et al., 2012; Pau et al., 2013). The PMU and remote terminal unit (RTU) measurements are combined to generate the augmented measurement set (Valverde et al., 2010; Asprou et al., 2013). As a result, the Jacobian matrix is changed in order to run the WLS-based static state estimation (SE). The WLS approach is utilized only for RTU data, and later the PMU data and the SE results are used together to perform the linear SE (Sodhi et al., 2010). PMU current measurements are used to run the hybrid state estimation (Pau et al., 2013). In the literature, a few different versions of the WLS technique, such as recursive WLS (Kusljevic and Poljak, 2011), have been used for SE. The Jacobian matrix grows in size as the PMU measurements are included in the hybrid state estimation execution. As a result, the SE's execution time increases. Furthermore, the current SSE technique does not allow for the use of all relevant metrics in predicting states. As a result, a quick SE technique is needed, one that can use both RTU and PMU data to estimate states before the next set of measurement data arrives.

The main steps involved in the implementation for Forecasting-aided state estimation (FASE) methodology consist of following:

1. System state model identification
2. State prediction using a forecasting tool
3. State filtering

Although it is deceptive to refer to a quasi-steady state operation as "dynamic", the phrase is frequently in literature even for smooth load fluctuations. As a result, in this case, the constructed estimators are referred to as FASE (Zhao et al., 2019). An extended multi-stage Kalman filter with a hierarchical filtering step (Rousseaux et al., 1988) and a dynamic load prediction approach is used to estimate the condition of the power system. This work clearly identifies the issues in estimation such as (i) computation demand when

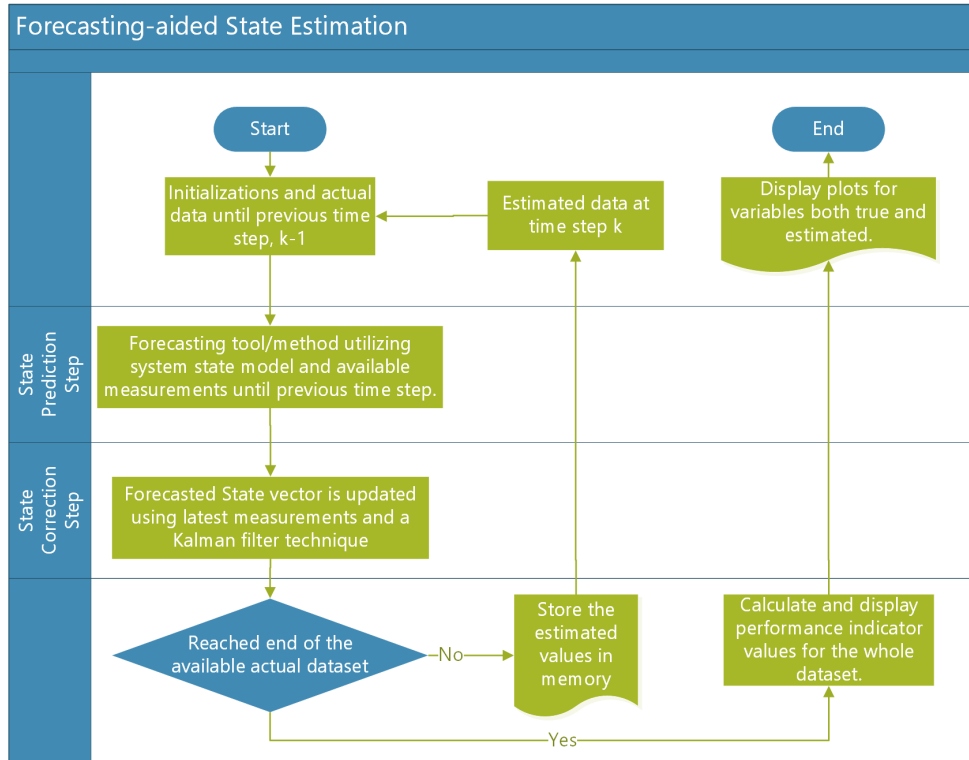


Figure 2.1: The flowchart for the general flow of logic in forecasting-aided state estimation process using forecasting tool and Kalman filter

dealing with multi-dimensional practical systems and (ii) modelling with balance between accuracy and ease of implementation. It has been noted that load forecasting and DSE are complimentary.

The prediction stage in DSE (Sinha and Mondal, 1999) uses an Artificial Neural Network (ANN) based short-term load forecasting due to its quick reaction and effective learning. When compared to estimations based on traditional prediction models, the ANN-based approach offered improved state estimations while taking similar execution time. Similarly deep learning has been explored for distribution system FASE (Huang et al., 2022). DSE with fuzzy logic controller has been explored in literature to solve uncertainty of state estimation (Lin et al., 2003).

According to a survey (Shivakumar and Jain, 2008), Kalman filter (KF) based approaches appear to predominate in the DSE for electric grids, and along with that for the state prediction stage ANN, fuzzy logic, auto-regression approaches have all been investigated. Mandal et al. (1995) addressed the non-linearity of the measurement function, but the method has non-sparse measurement covariance matrix and hence requires large computational time. To overcome this shortcoming, Bahgat et al. (1989) proposed to utilize a two-level estimation. KF is algebraically equivalent to its square root version (Ferreira and Barbosa, 1994). The square root version is more stable. Square root KF reduces

uncertainty in measured data, saving time and computational memory when compared to KF. In addition, square-root of covariance matrices are employed rather than covariance matrices. Thus, improving numerical conditioning and preventing singularity by taking the product of two square-root matrices.

Phasor data from wide area monitoring system devices are advantageous in state estimation (Jain and Shivakumar, 2008) as they provide high accuracy angle measurements, convergence speed increases. For the state prediction stage, Holt's double exponential smoothing is employed and EKF is used for the filtering step. Under typical bad data and rapid load shifts conditions, an adaptive EKF is investigated for DSE (Li and Li, 2009). The filtering efficiency of adaptive EKF is superior to original EKF. However, the computation time is a little longer. A method of load forecasting based on time-forward Kriging model is utilised to solve the DSE even at times of lacking field data owing to communication failure (Gu and Jirutitijaroen, 2015). Unscented KF is used for DSE because it has easier and derivative-free implementation (Valverde and Terzija, 2010). Under all scenarios the performance index of unscented Kalman filter (UKF) is best among EKF and static WLS estimator. Compared to EKF and UKF, Projected UKF (Yang et al., 2014) fared better in FASE. A state transition matrix based on regression analysis is presented for enhancing the DSE (Hassanzadeh and Evrenosoglu, 2011). The block diagonal state transition matrix and its computation periodically are seen to have a positive impact on the accuracy of complex voltage estimation. In the filtering procedure, a hybrid strategy that combines differential evolution and bacteria foraging is employed (Nejati et al., 2012). In contrast, the forecasting stage makes use of an unique stochastic search strategy and the Lattice Monte Carlo method. There is an insufficiency in the number of real-time measurements in distribution systems for carrying out FASE (Huang et al., 2022). Despite the fact that many smart metres are placed, they have poor sampling rate when compared to RTU or PMU data and is impossible to predict within the desired execution time.

Sharma et al. (2017) utilized the Cubature Kalman Filter (CKF) (Refer Appendix A5) originally proposed in (Arasaratnam and Haykin, 2009) which "employs a more precise cubature process for numerically computing Gaussian-weighted integrals is used for estimating the states in power system". CKF mandates that the error covariance matrix to be positive definite in every update, which can terminate the CKF from carrying out further execution of the program. Wang et al. (2015a) proposed a modified Iterated Square-root Cubature Kalman filter (ISCKF) for space target tracking problem in space surveillance systems, where it is demonstrated that the ISCKF operates better than traditional filters.

2.2 Objective and Contributions of this Chapter

Objective: Forecasting-aided State Estimation for monitoring voltage profile during normal load variations.

This chapter focuses on forecasting-aided state estimation of the power system states; voltage magnitudes and voltage phase angles at all buses for normal load variations. The aim is to do the same with improved accuracy and in real time. So, it will be feasible for implementation for practical systems. One of the advantages associated with FASE is the predicted states help in security and control operations. The power systems considered for case studies are IEEE 30-bus system and NRPG 246-bus system. The test systems under consideration are considered to have varying loads by $\pm 15\%$ to simulate the real time practical system scenario. Further, the estimation of states is attempted using an improved Cubature Kalman filter based approach called Iterated Square-root Cubature Kalman Filter (ISCKF). The accuracy of its results is compared with that of the earlier Kalman filter techniques such as EKF, UKF and CKF. The computational speed of the estimation algorithm is evaluated to check whether it will provide a feasible practical solution. Contributions of this chapter are briefed as follows:

1. The ISCKF is designed for its best use in FASE in power systems. Here, the estimation of voltage magnitude and phase angle at all buses is carried out.
2. Performance of proposed ISCKF method is compared with the existing CKF in terms of estimation error and computation time by the simulation studies. Feasibility of online real-time application is studied.
3. The efficiency of the ISCKF application for the FASE is tested using two test systems.

2.3 Power System Modelling for Forecasting-aided State Estimation

The linear state transition model for power system and measurements is represented as discrete time functions using difference equations:

$$\mathbf{x}_k = \mathbf{f}(\mathbf{x}_{k-1}) + \mathbf{w}_{k-1} \quad (2.1)$$

$$\mathbf{z}_k = \mathbf{h}(\mathbf{x}_k) + \mathbf{v}_k \quad (2.2)$$

$$\mathbf{w}_{k-1} = N(0, \mathbf{\Omega}_{k-1})$$

$$\mathbf{v}_k = N(0, \mathbf{R}_k)$$

where x_k is the state vector at the k^{th} instance, z_k is the measurement vector, w_{k-1} is a Gaussian process noise with zero mean and Ω_{k-1} covariance, v_k is a Gaussian measurement noise with zero mean and R_k covariance, and $f(\cdot)$ and $h(\cdot)$ are the non-linear functions for the state space and the measurement space, respectively. Various measurement types and their standard uncertainties, used in this study, are given in Table 6.18 in Appendix J. These standard uncertainty values for various types of measurements, are utilized to randomly generate the measurement values, which are used in the simulation of the proposed approach.

For the FASE formulation, the RTU as well as the PMU measurements are considered. The state vector x_k consists of the voltage (V_k) and the angle (θ_k) state sub-vectors. The measurement vector z_k comprises of the sub-vectors of voltage magnitude measurements (V_{mk}), real power injection measurements (P_{mk}), reactive power injection measurements (Q_{mk}), real power flow measurements (PF_{mk}), reactive power flow measurements (QF_{mk}), and voltage angle measurements (θ_{mk}) at k^{th} instant expressed as follows:

$$x_k = \left[V_k | \theta_k \right]^T \quad (2.3)$$

$$z_k = \left[V_{mk} | P_{mk} | Q_{mk} | PF_{mk} | QF_{mk} | \theta_{mk} \right]^T \quad (2.4)$$

where the subscript m indicates the measured quantities.

While formulating the dynamic model of the power system for the FASE, it is assumed that the changes in the system parameters, such as load variations, are slow. Sudden changes in the power system states are therefore not considered in the present problem. Under the above assumption, it is possible to use some state forecasting tool (Da Silva et al., 1983; Durgaprasad and Thakur, 1998) to model the state transition function and accommodate the variations in the states from one time-step to the next time-step. The error in the state forecasting from one simulation step to another step can be modelled with the process noise w .

$$f(x_k) = a_{k-1} + b_{k-1} \quad (2.5)$$

where

$$\mathbf{a}_{k-1} = \alpha_{k-1} \mathbf{x}_{k-1} + (1 - \alpha_{k-1}) \mathbf{x}_{k-1}^- \quad (2.6)$$

$$\mathbf{b}_{k-1} = \beta_{k-1} (\mathbf{a}_{k-1} - \mathbf{a}_{k-2}) + (1 - \beta_{k-1}) \mathbf{b}_{k-2} \quad (2.7)$$

The α_{k-1} and β_{k-1} are the parameters at $(k-1)^{th}$ instant containing values between

0 and 1, x_{k-1} is the predicted state vector, and a_{k-1} and b_{k-1} are the vectors defined by (2.6) and (2.7) at $(k-1)^{th}$ instant. While executing the state prediction step (time update) of the Kalman filtering approach, the state forecasting function (2.5) is used in (2.1) to predict the state vector in advance.

To define the measurement function $h(\cdot)$ for the power system, the standard real and reactive power balance and line flow equations are used, which are given by (Abur and Exposito, 2004)

$$P_i = \sum_{j=1}^N |V_i||V_j| (G_{ij} \cos \theta_{ij} + B_{ij} \sin \theta_{ij}) \quad (2.8)$$

$$Q_i = \sum_{j=1}^N |V_i||V_j| (G_{ij} \sin \theta_{ij} - B_{ij} \cos \theta_{ij}) \quad (2.9)$$

$$P_{ij} = V_i^2 (G_{si} + G_{ij}) - |V_i||V_j| (G_{ij} \cos \theta_{ij} + B_{ij} \sin \theta_{ij}) \quad (2.10)$$

$$Q_{ij} = -V_i^2 (B_{si} + B_{ij}) - |V_i||V_j| (G_{ij} \sin \theta_{ij} - B_{ij} \cos \theta_{ij}) \quad (2.11)$$

where P_i is the real power injection at bus i , Q_i is the reactive power injection at bus i , P_{ij} is the real power flow between buses i and j , Q_{ij} is the reactive power flow between buses i and j , $|V_i|$ is the voltage magnitude at bus i , G_{ij} is the conductance of the line between buses i and j , B_{ij} is the susceptance of the line between buses i and j , G_s is the conductance of the shunt at bus i , and B_{si} is the susceptance of the shunt at bus i .

Using this power system model the proposed approach is simulated to estimate the states, the voltage magnitude and phase angles at all the buses for the test systems.

2.4 Iterated Square-root Cubature Kalman Filter (ISCKF)

The ISCKF technique is expected to have an increased filtering capability in terms of accuracy and numerical stability, This is due to the fact that its implementation involves "Newton-Gauss iterative method (Yang et al., 2007) being embedded into the square-root cubature Kalman filter (SCKF)". This has been incorporated within the filtering step by using the N_{iter} iterations to derive the filtered state vector. Steps to implement ISCKF algorithm for FASE are described below:

Forecasting Step

At this step, the state vector given in (2.3) is forecasted based on the estimated state vector from the previous iteration and using the forecasting tool: Holt's double exponential

method (Da Silva et al., 1983) as described in (2.5).

1. Assuming initial flat start voltage profile and initial state covariance matrix is considered as $1 \times 10^{-3} \times I$.
2. The cubature points are calculated for state vector as follows:

$$X_{i,k-1|k-1} = \hat{S}_{k-1|k-1} \xi_i + \hat{x}_{k-1|k-1} \quad i = 1, 2, \dots, m$$

where, $m = 2n$ and when $k = 1$

$$S_{0|0} = \text{sqrt}(P_0)$$

3. Evaluate propagated cubature points ($i = 1, 2, \dots, m$)

$$X_{i,k-1|k-1}^* = f(X_{i,k-1|k-1})$$

where $f(X)$ is given in (2.5)

4. Estimate predicted state

$$\hat{x}_{k|k-1} = \frac{1}{m} \sum_{i=1}^m X_{i,k|k-1}^*$$

5. Now, computing the square-root of the predicted error covariance

$$\hat{S}_{k|k-1} = \text{Tri}a([x_{k|k-1}^*, S_{Q,k-1}])$$

where $S_{Q,k-1}$ denotes a square-root factor of Q_{k-1} , such that $Q = S_{Q,k-1} S_{Q,k-1}^T$, and $x_{k|k-1}^*$ defined as

$$x_{k|k-1}^* = \frac{1}{\sqrt{m}} [X_{1,k|k-1}^* - \hat{x}_{k|k-1}, X_{2,k|k-1}^* - \hat{x}_{k|k-1}, \dots, X_{m,k|k-1}^* - \hat{x}_{k|k-1}]$$

Filtering Step

Here, based on the measurements for time instant k and the forecasted state vector, the Kalman gain is calculated and filtered state vector is derived. This is done recursively for iterations $j = 0, 1, \dots, N_{iter}$ where $N_{iter}=2$ in our study, to get even better filtering effect.

6. Evaluate cubature points ($i = 1, 2, \dots, m$) for filtering step,

$$X_{i,k|k-1}^{(j)} = \hat{S}_{k|k-1}^{(j)} \zeta_i + \hat{x}_{k|k-1}^{(j)}$$

where internal iteration count $j = 0, 1, \dots, N_{iter}$ for the filtering step $j = 0$, $\hat{S}_{k|k-1}^{(0)} = \hat{S}_{k|k-1}$ and $\hat{x}_{k|k-1}^{(0)} = \hat{x}_{k|k-1}$

7. Evaluate propagate cubature points ($i = 1, 2, \dots, m$)

$$Z_{i,k|k-1}^{(j)} = h(X_{i,k|k-1}^{(j)})$$

8. Estimate the predicted measurement

$$\hat{z}_{k|k-1}(j) = \frac{1}{m} \sum_{i=1}^m Z_{i,k|k-1}^{(j)}$$

9. Estimate the square-root of the innovation covariance matrix

$$\hat{S}_{zz,k|k-1}^{(j)} = \text{Tri}a([Z_{k|k-1}^{(j)}, S_{R,k}^{(j)}])$$

where $S_{R,k}^{(j)}$ denotes a square-root factor of $R_k^{(j)}$ such that $R_k^{(j)} = S_{R,k}^{(j)}(S_{R,k}^{(j)})^T$ and $Z_{k|k-1}^{(j)}$ is defined as

$$Z_{k|k-1}^{(j)} = \frac{1}{\sqrt{m}} [Z_{1,k|k-1}^{(j)} - \hat{z}_{k|k-1}^{(j)}, Z_{2,k|k-1}^{(j)} - \hat{z}_{k|k-1}^{(j)}, \dots, Z_{m,k|k-1}^{(j)} - \hat{z}_{k|k-1}^{(j)}]$$

10. Estimate the cross-covariance matrix

$$P_{xz,k|k-1}^{(j)} = X_{k|k-1}(Z_{k|k-1}^{(j)})^T$$

where $X_{k|k-1}$ is defined as

$$x_{k|k-1}^{(j)} = \frac{1}{\sqrt{m}} [X_{1,k|k-1}^{(j)} - \hat{x}_{k|k-1}^{(j)}, X_{2,k|k-1}^{(j)} - \hat{x}_{k|k-1}^{(j)}, \dots, X_{m,k|k-1}^{(j)} - \hat{x}_{k|k-1}^{(j)}]$$

11. Estimate the Kalman gain

$$P_{zz,k|k-1}^{(j)} = \hat{S}_{zz,k|k-1}^{(j)} (\hat{S}_{zz,k|k-1}^{(j)})^T \quad (2.12)$$

$$W_k^{(j)} = \frac{P_{xz,k|k-1}^{(j)}}{(P_{zz,k|k-1}^{(j)} + R_k^{(j)})} \quad (2.13)$$

12. Estimate the updated state

$$\hat{x}_{k|k}^{(j)} = \hat{x}_{k-1|k}^{(j)} + W_k^{(j)} (z_k^{(j)} - \hat{z}_{k|k-1}^{(j)})$$

13. Estimate the square-root factor of the corresponding error covariance

$$\hat{S}_{k|k}^{(j)} = \text{Tria} \left(\left[\chi_{k|k-1}^{(j)} - W_k^{(j)} Z_{k|k-1}^{(j)}, W_k^{(j)} S_{R,k}^{(j)} \right] \right)$$

14. Make $\hat{x}_{k|k-1}^{(j+1)} = \hat{x}_{k|k}^{(j)}$, $\hat{S}_{k|k-1}^{(j+1)} = \hat{S}_{k|k}^{(j)}$ and $j = j + 1$.

Return to Step 6 and end for $j = N_{iter}$.

2.5 Case Studies on FASE for Test Systems

2.5.1 Data Generation and Simulation

To execute the ISCKF-based FASE approach, the measurements from the PMUs as well as from the RTUs are considered. It is assumed that, for a 50-Hz system, the PMU measurements are refreshed at every 40 ms (25 frames/s), and the RTU measurements are refreshed at every 2 s. A refresh rate of 25 frames/s is commonly used for the PMUs installed in 50-Hz power systems worldwide. In India, the PMUs deployed in the actual power system network are configured to provide measurements at the rate of 25 frames/s. Hence, in this study, the PMU refresh rate is considered as 25 frames/s.

To simulate the RTU and PMU measurements for the FASE execution, the actual values of the system states at various time instants are obtained by running the load-flow repeatedly for various loading conditions, simulated by varying the loads randomly. The maximum and the minimum limit on the load changes during the simulation period are set as +30% and -30% of their nominal base case values, respectively. The loads are changed gradually in each time step by limiting maximum variations of $\pm 5\%$ from their previous values during the simulation period. All the loads are varied randomly to simulate a realistic load profile. The measurement values are then extracted randomly around the actual values of the system states at various instants, from the probability distribution defined according to the standard uncertainty values of the various types of measurements, shown in Table 6.18 in Appendix J.

The FASE on the test systems are run using 100 simulations of the hybrid measurements under various loading conditions using MATLAB R2020a platform. Between two consecutive RTU measurements, 49 PMU measurements (first set of PMU measurements is processed with the RTU measurements) are also processed. Therefore, a total of 4951 ($100 + 49 \times 99$) simulations are utilized in executing the proposed approach.

The values of α and β used in the load forecasting process, are estimated using 20,000 Monte Carlo (MC) simulations (Sharma et al., 2017). In this process, the generated random samples of the measurements are processed to estimate the mean values of α and β . The MC simulation is utilized only as an offline process to estimate the values of α

and β . The values of α and β for the IEEE 30 bus system are estimated only once before the FASE simulation. Subsequently, the above obtained values of α and β are utilized in the execution of the proposed ISCKF-based FASE approaches.

The following are the test systems considered for the analysis:

1. IEEE 30 Bus System

Single line diagram of the IEEE 30-bus system is shown in Fig. 2.2 (Refer Appendix C for more details). The estimated values of α and β for the IEEE 30 bus system are obtained as 0.76 and 0.53, respectively (Sharma et al., 2017). For this system, 3 PMUs are considered at buses 6, 9, and 12. Other buses are considered to be having RTUs for the measurement data reporting.

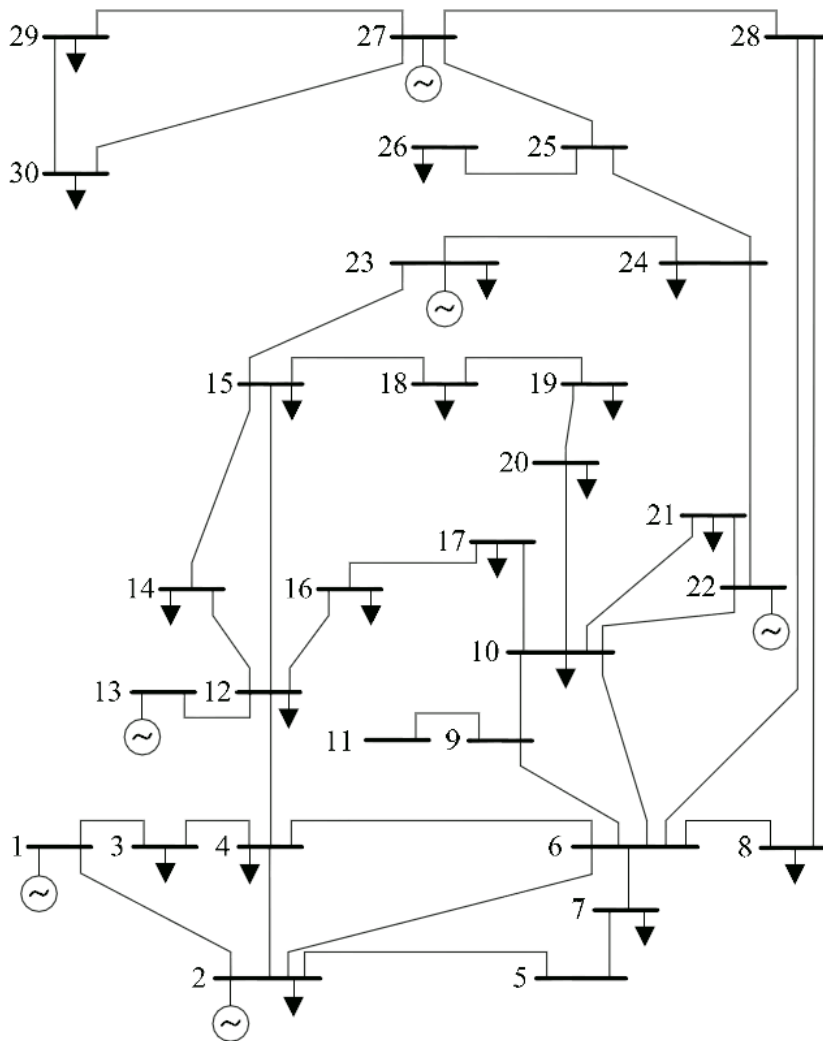


Figure 2.2: Single line diagram of the IEEE 30-bus system

2. Northern Region Power Grid (NRPG) 246-bus test system

The estimated values of α and β for the NRPG 246-bus system (See Fig. 2.3) are obtained as 0.83 and 0.64, respectively (Sharma et al., 2017). For this system, 30 PMUs are considered at the large generator buses (Refer (IITK, 2020) for system details). Other buses are considered to be having RTUs for the measurement data reporting.

2.5.2 Results and Discussion

The ISCKF based FASE is implemented using 100 hybrid (PMU and RTU) measurements with 49 PMU measurements between each successive RTU measurements. Suppose the proposed FASE begins, at the time step $T = 0$, by estimating the states with the help of immediately accessible hybrid measurements. Further, utilizing the state estimation outcome for the measurements at $T = 0$, at the time instant $T = 1$ (i.e., at 40 ms), the estimate results are forecasted. Now, the combination of these forecasted states as pseudo data along with the PMU data accessible at $T = 1$, derives estimated state variables at $T = 1$. These steps are carried out for every PMU measurement set received in the interval between the time steps $T = 0$ and $T = 50$. At $T = 50$ (i.e., at 2 s), when the second batch of RTU data comes, the state is recalculated using the hybrid measurements. The simulation studies are performed using Intel Core-i7 3.4 GHz computer having 32 GB RAM and Windows 10 OS.

For the test systems in the study, the measurement data is simulated by adding noises to the actual data with the standard measurement uncertainty of the devices (See Appendix J) at each iteration, to ensure that the simulation findings are consistent. The voltage phasors are added with White Gaussian noises randomly, while Cauchy noises are added to the power measurements. Subsequently, the mean of absolute errors (MAE) for state estimates in each iteration are noted down. By estimating the voltage magnitude and phase angle at all buses in the test systems, the mean of the absolute errors at all buses are compared in the Tables 2.1 and 2.2. The speed of an algorithm can be measured by the capability of an algorithm to keep up with the speed of inflowing data. The execution times have been noted down in Table 2.3 for the systems using CKF and ISCKF for immediate comparison.

Some important inferences from the results are discussed below:

IEEE 30-bus system (See Fig. 2.2):

1. For the comparison of ISCKF and CKF estimation results, actual data and estimation results consisting of voltage magnitude and voltage phase angle plots and their corresponding error plots at bus-7 are shown in Fig. 2.4. From Fig. 2.4b and Fig. 2.4d, it is observed that the error in estimation using ISCKF is significantly less

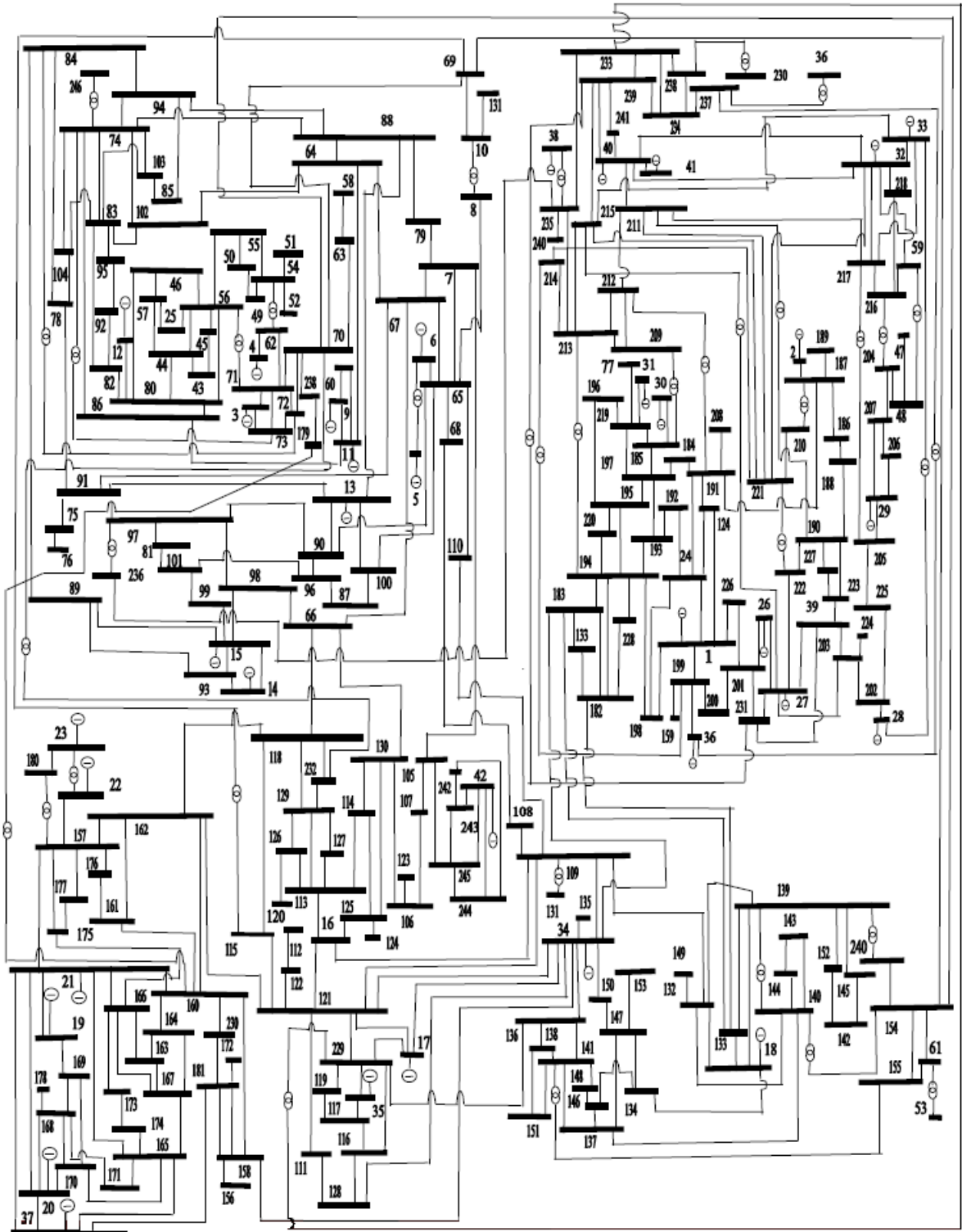


Figure 2.3: Single line diagram of the NRPG 246-bus system

than that of using CKF.

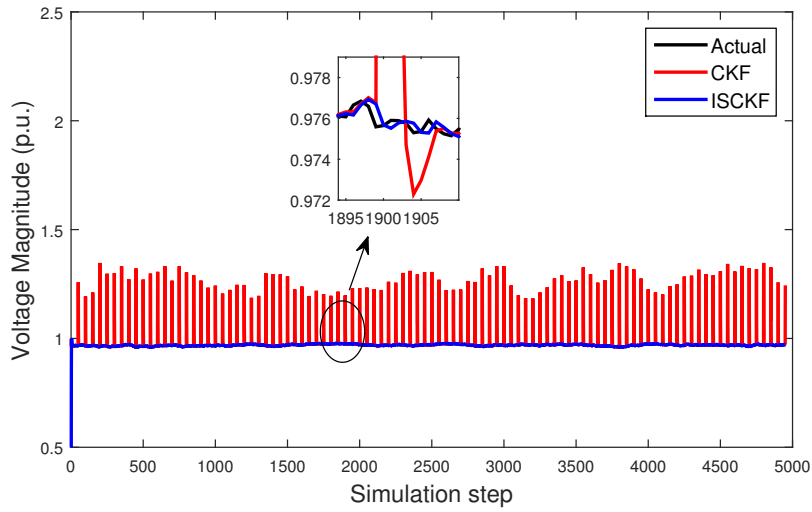
2. Estimation Error studies:

- Mean of absolute error: It is observed in Table 2.1 that using ISCKF the Mean absolute error in the voltage magnitude estimation is decreased to 1/5th the error that obtained using CKF. That is, the accuracy in the voltage magnitude estimation by ISCKF has increased by 78% when compared to that of CKF. And for voltage phase angle, the mean of absolute errors using ISCKF is decreased to half that of using CKF. Alternatively, it can be said that the accuracy in the voltage phase angle estimation by ISCKF has increased by 48% than that of CKF.
- Performance indices such as Absolute phase error percentage (APEP) and Absolute voltage error percentage (AVEP) (Gu and Jirutitijaroen, 2015) at a time instant are calculated as follows:

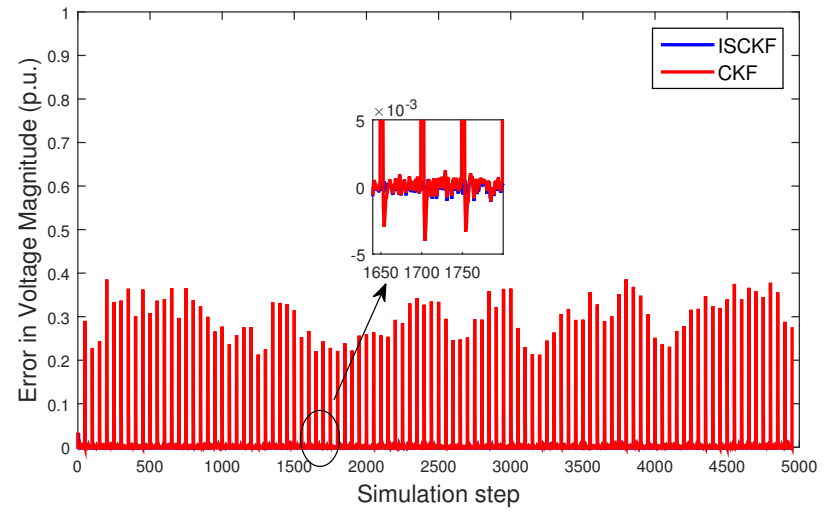
$$APEP = \frac{100}{n_b - 1} \sum_{i=2}^{n_b} \frac{\hat{\theta}_i - \theta_i}{\theta_i} \quad (2.14)$$

$$AVEP = \frac{100}{n_b} \sum_{i=1}^{n_b} \frac{\hat{V}_i - V_i}{V_i} \quad (2.15)$$

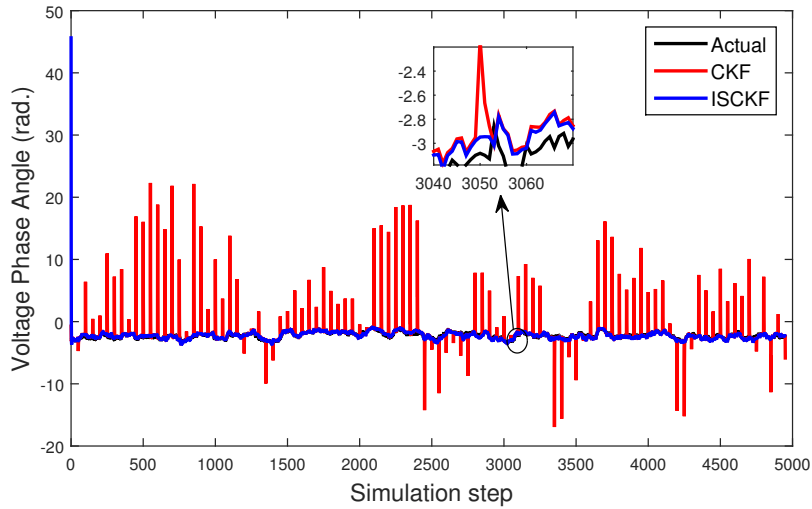
where n_b is count of buses in the system, $\hat{\theta}_i$, \hat{V}_i are forecasted phase angle and voltage at the bus respectively, θ_i , V_i are actual phase angle and voltage magnitude at the bus. It is also verified (from Table 2.4) with all the parameters mean, maximum and standard deviation of absolute phase error percentage (APEP) (Gu and Jirutitijaroen, 2015) and absolute voltage error percentage (AVEP) using ISCKF are less than that of CKF for IEEE 30-bus system.



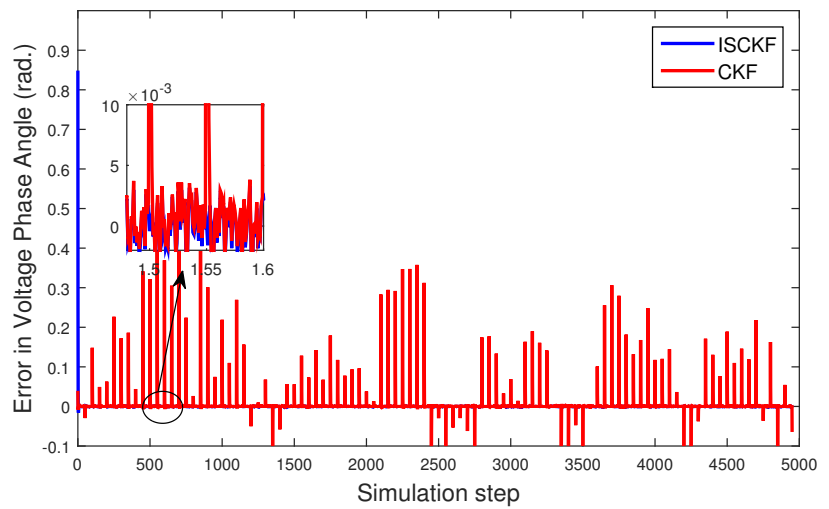
(a) Voltage magnitude plot at bus-7



(b) Plot for error in voltage magnitude estimation at bus-7



(c) Voltage phase angle at bus-7



(d) Plot for error in voltage phase angle estimation at bus-7

Figure 2.4: The estimated states and error plots at bus-7 in IEEE 30-bus system

3. Execution time: It can be observed from the Table 2.3 that the ISCKF takes 15.93 ms whereas the CKF takes 7.43 ms. for execution of one hybrid data and 49 PMU data. It is evident that ISCKF is slightly slower than the CKF. However the data reporting time for hybrid measurement is 2 s, so ISCKF is able to give results before the next set of hybrid data arrives, which is expected from an estimation algorithm.

Table 2.1: Mean of Absolute Errors (MAE) in the Estimated States using various KF algorithms for IEEE 30-bus test system

Filter type	MAE in V Magnitude (p.u.)	MAE in V angle (rad.)
ISCKF	0.854×10^{-3}	1.7×10^{-3}
CKF (Sharma et al., 2017)	3.9×10^{-3}	3.3×10^{-3}
UKF (Sharma et al., 2017)	4.2×10^{-3}	4.9×10^{-3}
EKF (Sharma et al., 2017)	4.4×10^{-3}	4.7×10^{-3}

NRPG 246-bus system (See Fig. 2.3):

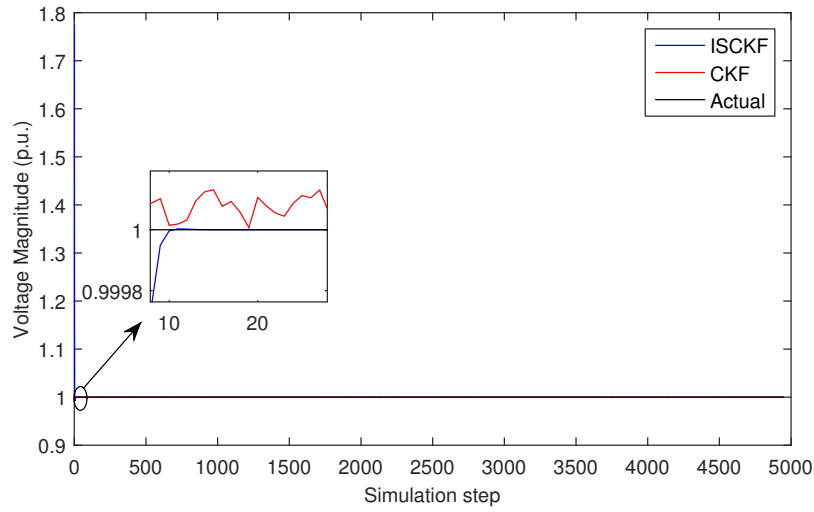
1. For the comparison of ISCKF and CKF estimation results, actual data and estimation results consisting of voltage magnitude and voltage phase angle plots and their corresponding error plots at bus-30 are plotted in Fig. 2.5. From Fig. 2.5b and Fig. 2.5d, it is observed that the error in estimation using ISCKF is significantly less than that of using CKF.

Table 2.2: Mean of Absolute Errors (MAE) in the Estimated States using various Kalman filter (KF) based algorithms for NRPG 246-bus test system

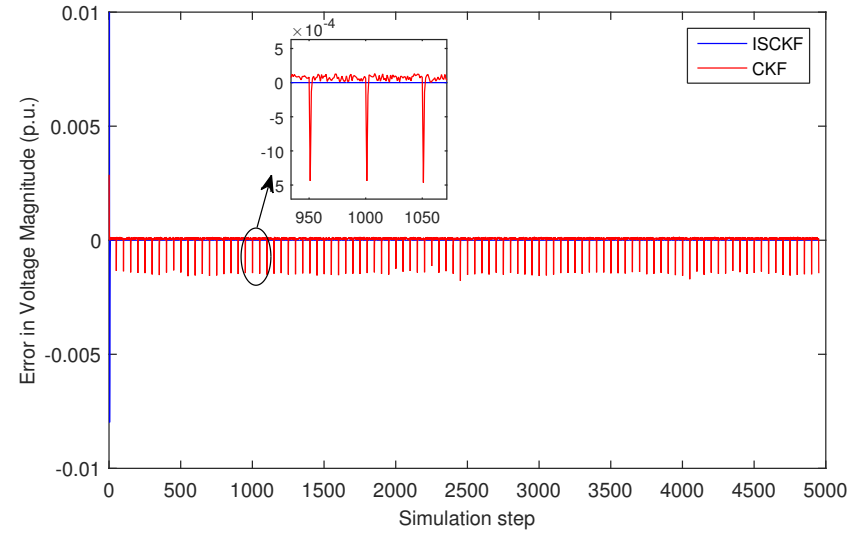
Filter type	MAE in V Magnitude (p.u.)	MAE in V angle (rad.)
ISCKF	1.8×10^{-4}	2.0×10^{-4}
CKF (Sharma et al., 2017)	2.8×10^{-3}	2.1×10^{-3}
UKF (Sharma et al., 2017)	4.8×10^{-3}	3.9×10^{-3}
EKF (Sharma et al., 2017)	5.8×10^{-3}	6.2×10^{-3}

Table 2.3: Total computational time for estimation using one set of hybrid measurements and 49 PMU measurements

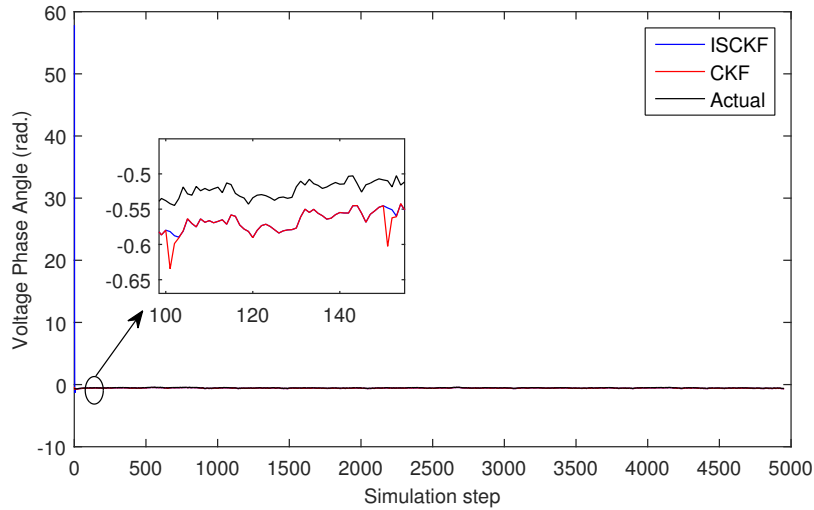
	Estimation Time IEEE 30-bus system	Estimation Time NRPG 246-bus system
CKF	7.43 ms	0.84 s
ISCKF	15.93 ms	1.36 s



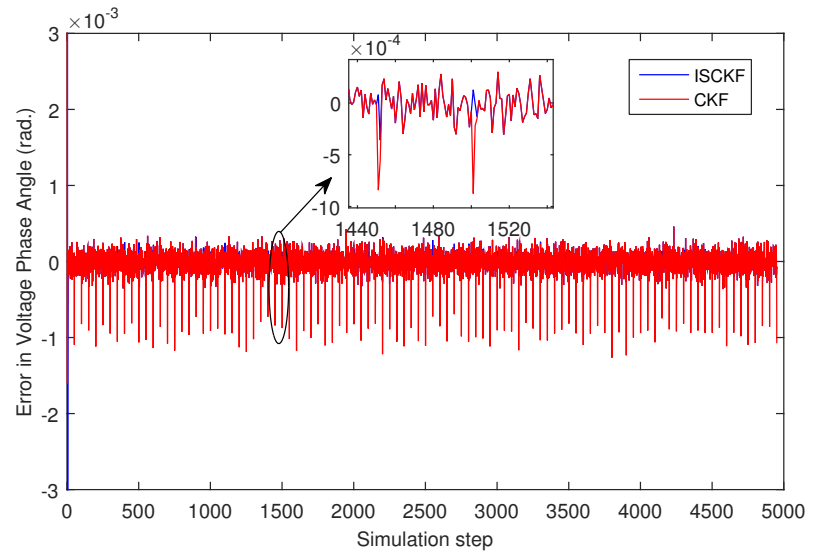
(a) Voltage magnitude plot at bus-30



(b) Plot for error in voltage magnitude estimation at bus-30



(c) Voltage phase angle plot at bus-30



(d) Plot for error in voltage phase angle estimation at bus-30

Figure 2.5: The estimated states and error plots at bus-30 in NRPG 246-bus system

Table 2.4: Absolute phase error percentage (APEP) and Absolute voltage error percentage (AVEP) comparison of proposed ISCKF with CKF methods for the two test systems

IEEE 30-bus system						
	APEP			AVEP		
Filter Type	Mean	Max.	SD	Mean	Max.	SD
ISCKF	0.32	91.27	2.01	0.21	38.73	1.17
CKF	0.35	101.24	2.14	0.96	80.77	5.05
NRPG 246-bus test system						
	APEP			AVEP		
Filter Type	Mean	Max	SD	Mean	Max	SD
ISCKF	0.01	1.33	0.03	0.02	33.22	0.97
CKF	0.03	1.78	0.08	0.80	66.28	4.53

□

2. Error in estimation:

- It is observed (Refer Table 2.2) that the mean of absolute error in voltage magnitudes at all buses is reduced to 1/16th that obtained using CKF. The accuracy in the voltage magnitude estimations by ISCKF is increased by approximately 94% than that of CKF. And the mean of absolute errors of voltage phase angle using ISCKF is decreased to 1/11th that of using CKF. Alternatively, it can be said that the accuracy in the voltage phase angle estimation by ISCKF has increased by 90% than that of CKF.
 - It is verified (from Table 2.4) with all the parameters mean, maximum and standard deviation of APEP and AVEP using ISCKF are less than that of CKF.
3. Execution time: It can be observed from the Table 2.3 that the ISCKF takes 1.36s whereas the CKF takes 0.84s for execution of one hybrid data and 49 PMU data. It is evident that ISCKF is slower than the CKF. However the data reporting time for hybrid measurement is 2 s. So, ISCKF will be able to give results before the next set of hybrid data arrives (expected from an estimation algorithm). Therefore, the proposed estimation algorithm is applicable for real-time practical application, with respect to large power systems as well.

2.6 Summary

This chapter demonstrates the application of iterated square-root cubature Kalman filter for forecasting-aided state estimation during normal load variations. It is performed

utilizing the hybrid measurements from both field devices: RTUs and PMUs. The IS-CKF method has the Newton-Gauss iterative method embedded into square-root CKF to improve its performance and stability. Consequently, ISCKF removes the risk of losing positive definiteness of the error covariance matrix in each update, which can cause the CKF to cease operating. The simulation results show that the proposed ISCKF outperforms the CKF by significant improvement in accuracy of forecasting-aided state estimation. This is evaluated with the help of mean of absolute errors, absolute phase error percentage and absolute voltage error percentage. The online real-time application feasibility is demonstrated with respect to the two different sized test systems IEEE 30-bus and NRPG 246-bus systems.

Chapter 3

Dynamic State Estimation in Power Systems

Research in the area of power system transient stability has recently shifted its focus on dynamic state estimation (DSE) involving PMU data with high reporting rate. Several mathematical models for induction motor and synchronous machine have been developed and, various estimation approaches have been proposed in the literature for this purpose. In this work, the mathematical formulation of non-linear state space modeling and the principles of Kalman filter are utilized. Extended, Unscented and Cubature Kalman Filters (EKF, UKF and CKF) are the three non-linear estimation methods explored for dynamic state estimation in an induction motor for preliminary studies. In the next stage, after presenting a thorough explanation about modeling of the synchronous machine, dynamic state estimation is applied on different power system case studies and the results of estimation methods are compared. The improvised CKF called Iterated Square-root Cubature Kalman filter (ISCKF) is proposed for its application in DSE and its performance is compared with that of the EKF, UKF and CKF algorithms. Estimation studies are carried out in the scenario of three phase fault at one of the buses in the power system. The simulation results obtained show the great potential of the proposed estimation approach for accurately estimating the states of the machine as well as reducing the effect of noises.

¹Based on the contribution of this chapter, a journal paper entitled *Dynamic State Estimation of Synchronous Machines using Iterated Square-root Cubature Kalman Filter and Synchrophasor Measurements* has been published in Journal of Electronics and Electrical Engineering, pp.8-8, June 2023.

²Based on the preliminary studies presented in this chapter, a paper entitled *A Comparative Analysis of Speed Estimation of Induction Motor Drive using Non-linear Kalman Filters* has been published in Proceedings of IEEE 31st Australian Universities Power Engineering Conference, 2021.

³Based on the preliminary studies presented in this chapter, a paper entitled *A Comparative Study of Bayesian based filters for Dynamic State Estimation in Power Systems* has been published to 2021 IEEE International Power and Renewable Energy Conference (IPRECON).

3.1 Introduction

Nowadays our daily lives depend heavily on smart supervision and reliable performance of the important infrastructures, like electric power systems, telecommunication networks, and water distribution systems, etc. Because of the continuous increase in their size, network complexity, inherent uncertainty, random nature of changing loads, and mutual interactions, it has become a demanding task to design, monitor, and control such systems (Chakrabarti et al., 2008). In terms of power systems, the safe and dependable operation has become a difficult task due to the daily-increasing demand for electric power. The ever-increasing number of the power system interconnections, higher penetration percentage of the various forms of renewable energies and new regulations of the power market are the main motivations for power companies all around the world to invest in a real-time Wide Area Monitoring, Protection, and Control (WAMPAC) system. Synchronized measurement technology can be considered as the central supporting part of this system (Chakrabarti et al., 2008).

Synchrophasors are essentially accurate power grid measurements provided by PMUs installed all over a large scale power system. The measurements are taken at high rate compared to the conventional technologies and are synchronized using a common time reference signal. The synchronized data provided by PMUs helps to better detect stresses on a power grid and improve the accuracy of the corrective decisions to maintain stability of the power system. In 1986, phasor measurement has been introduced as a new measurement approach in power systems (Martin and Carroll, 2008).

Based on the measurements available, a state estimator holds a central function in power grid operations as it generates critical inputs for other operational tools, such as contingency analysis, automatic generation control, and optimal power flow (Abur and Exposito, 2004; Monticelli, 2000). Any inaccuracy or deficiency introduced in the state estimation process will be propagated and possibly exaggerated through these tools and greatly affect system operation efficiency. Therefore, the method used for dynamic state estimation needs to be as accurate as possible. And the detailed literature survey carried out points to the fact that there is still scope for further improvement in the estimators.

In power systems, electromechanical dynamic models are commonly used to investigate transient and small signal stability issues. A dynamic model with proper known states can accurately show system responses and, can be used to predict system behaviour and enhance power system stability. Power system dynamic state estimation (PSDSE) estimates the dynamic states (e.g., rotor speeds and angles) by using synchronized phasor measurement unit (PMU) measurements.

Researchers have used various estimation approaches and case studies to investigate dynamic state estimation in power systems. Extended Kalman Filter (EKF) has been

applied to PSDSE using second order model of the synchronous generator (Huang et al., 2013b). Evaluation of an EKF based estimator for power system considering lack of field voltage has been explored (Ghahremani and Kamwa, 2011b). Dynamic state estimation (DSE) of synchronous machines in power system has been carried out with the help of EKF (Pan et al., 2018). The generator swings are observed for the three-phase fault case and load variation. This provided further scope for identification of coherent group of generators in the system with the PMU measurements and help in adaptive protection of the system. Although EKF is an elegant and computationally efficient recursive update form of Kalman filter, it only functions well in a mild non-linear environment, due to its first-order Taylor series approximation of non-linear function (Zhou et al., 2014). It is found to be unsatisfactory and can easily lead to divergence when used for non-linear situations. While Jacobian matrix determination can be complicated and error-prone, the linearization is possible only if the Jacobian matrix exists. When the system is highly non-linear, EKF tends to have very poor performance in precise estimation as it is based on first order Taylor approximation. While Unscented Kalman Filter (UKF) can achieve second or third order Taylor approximation for a non-linear system. The unscented transformation has been designed to overcome EKF's linearization difficulty, by offering a more direct and clear mechanism for transforming mean and covariance information. UKF has been designed for PSDSE with PMU installed on generator bus (Ghahremani and Kamwa, 2011c). A two-axis fourth order state space model of the synchronous machine has been used in this study. UKF has been applied to different power system case studies using second order synchronous generator model while considering speed and electrical output power of the machine as available measurements (Wang et al., 2011; Gao and Wang, 2010). However, since UKF is built by the sigma-point set, the mean is highly significant as it carries more weight which is usually disadvantageous for high-dimensional systems. Therefore, UKF may encounter numerical instability troubles when used in high-dimensional problems.

A divide-by-difference-filter based algorithm has been proposed for dynamic estimation of the generator rotor angle in a large power system (Tripathy et al., 2009). The results of state estimation in a single machine infinite bus (SMIB) system using extended particle filter considering non-Gaussian noise is compared with that of particle filter, EKF and UKF (Zhou et al., 2013). Data-driven DSE based on artificial neural networks (Del Angel et al., 2007) and operator theory (Netto and Mili, 2018) have been explored in literature. A hybrid-learning dynamic state estimator has been used for estimating the states of power system (Tian et al., 2020). Three-phase line trip faults have been considered during the study. The hybrid-learning DSE is a data-driven approach using a power system model and by training neuroestimators with real time data. Pros and cons of this approach when compared to EKF and square-root UKF are presented. Zhao et al. (2020) highlighted the

applications and implementation details of DSE with respect to modelling, monitoring and operation of power system. The DSE for synchronous machines and converter-based resources have been explored (Liu et al., 2021). Further, comparison studies are carried out for Kalman filter based approaches and observers for DSE based control and protection.

Cubature Kalman Filter (CKF) (Arasaratnam and Haykin, 2009) employs a more precise cubature process for numerically computing Gaussian-weighted integrals, which is used for estimating the states in power system (Sharma et al., 2017). CKF requires error covariance matrix to maintain its positive definiteness in each update, otherwise it can stop the CKF from running continuously. A robust CKF has been proposed for handling unknown noise characteristics in the measurement data (Li et al., 2019). In this work, Huber's M-estimation theory is incorporated into the original CKF approach. Comparison studies are carried for different types of noises. The estimated plots of rotor angle and speeds using robust CKF is found to be closer and overlapping with the actual/true plots when compared to CKF.

A modified version of CKF called an Iterated Square-root Cubature Kalman filter (ISCKF) has been proposed for non-cooperative space target tracking problem in space surveillance systems (Wang et al., 2015a), where it is demonstrated that ISCKF outperforms the conventional filters. Here, square-root CKF (Ferreira and Barbosa, 1994) approach differs from CKF approach, as the square-root of error covariance matrix is determined by QR decomposition instead of Cholesky decomposition. Thereby, ISCKF eliminates the hazardous situation of the loss of positive definiteness of error covariance matrix in each update step, which could stop the UKF and CKF from running continuously. Newton-Gauss iterative method has been incorporated into the measurement update step of the square-root CKF for implementing the proposed ISCKF approach. Thus, improving the estimation accuracy.

3.2 Objective and Contributions of this Chapter

Objective: An improved Cubature Kalman Filter for dynamic state estimation during a three-phase fault.

In this chapter, the mathematical background of the state space modelling and dynamic state estimation using Kalman filters are addressed in detail. Kalman filter principles are compared with the Luenberg observer to identify its distinct advantages using a first-order linear differential equation example. Further, the dynamic state estimation using Kalman filter approach is applied to speed estimation of induction motor as preliminary study. Then, the classical model of the synchronous machine is utilized for its dynamic state estimation using an improvised and more robust filtering algorithm called iterated square-root cubature Kalman filter is proposed. Further, ISCKF is designed for

its best use in PSDSE. The performance evaluation is carried out by implementing this filter to estimate the rotor speeds and angles of synchronous generators in SMIB, IEEE 9-bus and 19-generator 42-bus test systems. The simulation results are compared with that obtained using the existing DSE algorithms such as EKF, UKF and CKF.

3.3 Introduction to Kalman Filters

The Kalman filter is the most widely used Bayesian-based data assimilation method (Kalman et al., 1960). Assuming Gaussian noise, the Kalman filter provides minimum-variance estimates of states through a recursive approach. The major difference among different non-linear Kalman-filter methods is their approach for propagating the mean and covariance of the dynamic states. “The Kalman filter in its various forms is clearly established as a fundamental tool for analysing and solving a broad class of estimation problems” (McGee and Schmidt, 1985). This estimation method operates by propagating the mean and covariance of the states of a system through time. To derive the equations that govern the discrete-time Kalman Filter, assume a linear discrete-time system given as follows (Simon, 2006):

$$x_k = F_{k-1}x_{k-1} + G_{k-1}u_{k-1} + w_{k-1} \quad (3.1)$$

$$y_k = H_k x_k + v_k \quad (3.2)$$

w_k and v_k are process and measurement noises of the system which determine covariance matrices. The process and measurement noises are essentially considered as white, zero-mean and uncorrelated with the covariance matrices Q_k and R_k , respectively.

$$\begin{aligned} w_k &\sim N(0, Q_k) \\ v_k &\sim N(0, R_k) \\ E[w_k w_j^T] &= Q_k \delta_{k-j} \\ E[v_k v_j^T] &= R_k \delta_{k-j} \\ E[v_k w_j^T] &= 0 \end{aligned} \quad (3.3)$$

In (1.31), δ_{k-j} is the Kronecker delta function in which $\delta_{k-j} = 1$ if $k = j$ and $\delta_{k-j} = 0$ if $k \neq j$ (Simon, 2006). The main target here is to estimate the states of the system x_k , using the available noisy measurements y_k and knowledge about the dynamic response which is accessible from the differential equations of the system (Simon, 2006). In this regard, different kinds of estimation can be defined. If all of the measurements up to and including time k are available for the estimate of x_k , then a posteriori estimate can be calculated which is normally represented by \hat{x}_k^+ . The “+” superscript implies that a posteriori estimate is formed. The following equation shows the way to portray

the posteriori estimate of x_k using the expected value of x_k conditioned on all of the measurements up to and including time k (Simon, 2006):

$$\hat{x}_k^+ = E[x_k | y_1, y_2, y_3, \dots, y_k] \quad (3.4)$$

A priori estimate denoted by \hat{x}_k^- can be formed if all of the measurements before and not including time k are available for the estimation purpose. The following equation explains how a priori estimate is calculated (Simon, 2006):

$$\hat{x}_k^- = E[x_k | y_1, y_2, y_3, \dots, y_{k-1}] \quad (3.5)$$

Although \hat{x}_k^- and \hat{x}_k^+ are both estimates of the same quantity, the difference between a priori and a posteriori estimate is that \hat{x}_k^- is the estimate of x_k before the measurement y_k is taken into account, and \hat{x}_k^+ is the estimate of x_k after the measurement y_k has been considered (Simon, 2006). The intuitive expectation here is that \hat{x}_k^+ would be a better estimation than \hat{x}_k^- , because more information is used for its computation. The first measurement is taken at time $k = 1$. Due to the lack of available knowledge from previous measurements at this moment, \hat{x}_0^+ is considered as the expected value of the initial state x_0 .

$$\hat{x}_0^+ = E(x_0) \quad (3.6)$$

The term P_k is used to denote the covariance of the estimation error (Welch and Bishop, 2006). Consequently, P_k^- represents the covariance of the estimation error of \hat{x}_k^- , and P_k^+ represents the covariance of the estimation error of \hat{x}_k^+ . These error covariance matrices are defined as follows:

$$P_k^- = E[(x_k - \hat{x}_k^-)(x_k - \hat{x}_k^-)^T] \quad (3.7)$$

$$P_k^+ = E[(x_k - \hat{x}_k^+)(x_k - \hat{x}_k^+)^T] \quad (3.8)$$

The following time line in Fig. 3.1 depicts the relationship between a priori and a posteriori state and error covariance estimation.

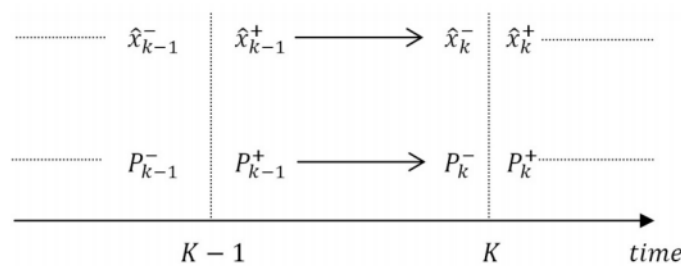


Figure 3.1: Time line showing priori and posteriori state estimation (Simon, 2006)

Now, it is possible to write an update equation for the new estimate (a posteriori estimate), by combining the previous estimate (a priori estimate) as follows:

$$\hat{x}_k^+ = \hat{x}_k^- + K_k(y_k - H_k\hat{x}_k^-) \quad (3.9)$$

The matrix K_k in the above equation is called the Kalman gain and the term $y_k - H_k\hat{x}_k^-$ is known as the innovation or measurement residual (Welch and Bishop, 2006). This matrix is chosen such that the a posteriori error covariance (P_k^+) is minimized. The minimization is carried out by substituting (3.9) into (3.8) which is the definition for P_k^+ . Then, the indicated expectation is performed and the derivative of the trace of the result with respect to K is calculated. By setting the result equal to zero and then solving for K , the final expression for the Kalman gain K can be given as,

$$K_k = P_k^- H_k^T (H_k P_k^- H_k^T + R_k)^{-1} \quad (3.10)$$

Considering the dynamic system presented in (3.1) and (3.2), the discrete-time Kalman filter is summarized here as a recursive algorithm (Simon, 2006)

1. The filter is initialized as follows:

$$\begin{aligned} \hat{x}_0^+ &= E(x_0) \\ P_0^+ &= E \left[(x_0 - \hat{x}_0^+) (x_0 - \hat{x}_0^+)^T \right] \end{aligned} \quad (3.11)$$

2. The prediction step or time update is accomplished as:

$$\begin{aligned} P_k^- &= F_{k-1} P_{k-1}^+ F_{k-1}^T + Q_{k-1} \\ K_k &= P_k^- H_k^T (H_k P_k^- H_k^T + R_k)^{-1} \\ \hat{x}_k^- &= F_{k-1} \hat{x}_{k-1}^+ + G_{k-1} u_{k-1} = a \end{aligned} \quad (3.12)$$

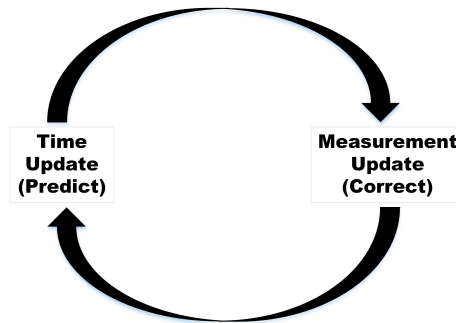


Figure 3.2: The ongoing discrete Kalman filter cycle (Welch and Bishop, 2006)

3. The correction step or measurement update is completed by the following equations:

$$\begin{aligned}\hat{x}_k^+ &= \hat{x}_k^- + K_k(y_k - H_k\hat{x}_k) \\ P_k^+ &= (1 - K_k H_k)P_k^-\end{aligned}\tag{3.13}$$

The ongoing discrete Kalman filter cycle is presented in the Fig. [3.2](#)

3.3.1 Kalman Filter and its Comparison with Luenberger Observer

To understand the KF, it is important to understand the state observer and how they work. State observers are used to measure the internal states of the system using the available measurements. To justify the selection of KF in this work, the performance of the KF is compared with the state observer. Luenberger Observer possesses a relatively simple design that makes it an attractive general design technique ([Bhattacharyya, 1978](#)).

Luenberger Observer

This design is based on eigenvalue assignment (or pole placement), and is known as the Luenberger observer. It is named after David Gilbert Luenberger. To understand the observer design, consider a real system as,

$$x(k+1) = Ax(k) + Bu(k)\tag{3.14}$$

$$y(k) = Cx(k) + Du(k)\tag{3.15}$$

The copy of the system, which is a numerical simulator reproducing the behaviour of the real system,

$$\hat{x}(k+1) = A\hat{x}(k) + Bu(k)\tag{3.16}$$

$$\hat{y}(k) = C\hat{x}(k) + Du(k)\tag{3.17}$$

where x is the true state, y is true output of the system. \hat{x} is the estimated state and \hat{y} is the estimated output. The Luenberger observer design is explained in the following Fig. [3.3](#)

The dynamics of state estimation error are given as follows,

$$\tilde{x}(k+1) = x(k+1) - \hat{x}(k+1)\tag{3.18}$$

$$\tilde{x}(k+1) = Ax(k) + Bu(k) - A\hat{x}(k) - Bu(k) - L(y(k) - C\hat{y}(k))\tag{3.19}$$

$$\tilde{x}(k+1) = (A - LC)\tilde{x}(k)\tag{3.20}$$

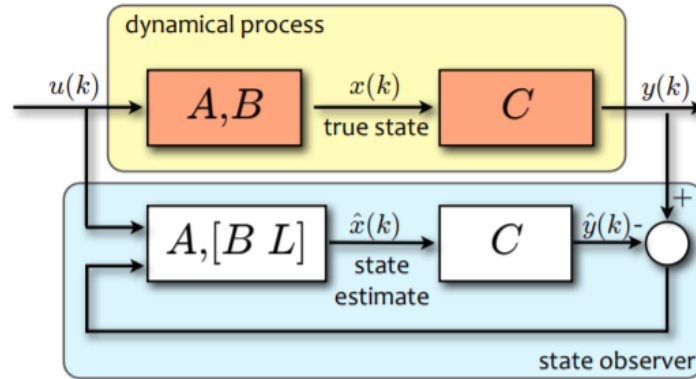


Figure 3.3: Luenberger observer

Where L is observer gain and is chosen such that the matrix $(A - LC)$ has its eigen values inside unit circle.

The performance of this observer to estimate the state of a system is compared with that obtained using the Kalman Filter.

State Estimation using Observer and Kalman Filter

Consider a discrete time system called as a Logistic Curve (Luenberger, 1979). The standard first-order linear differential equation defining exponential growth is often modified to reflect the fact that, due to crowding, limited resources, or a variety of other reasons, growth cannot continue indefinitely. There are invariably restraining factors whose influence eventually dominates. So, for one such example logistic curve, the mathematical formulation can be given as follows:

$$x(k + 1) = Ax(k) + Bu(k) \tag{3.21}$$

$$y(k) = Cx(k) + Du(k) \tag{3.22}$$

Where

$$A = \begin{bmatrix} 1.8097 & -0.8187 \\ 1 & 0 \end{bmatrix}, \quad B = \begin{bmatrix} 0.5 \\ 0 \end{bmatrix}, \\ C = \begin{bmatrix} 0.1810 & -0.1810 \end{bmatrix}, \quad D = 0$$

With initial state $x_0 = [1, 1]^T$ and input $u(k)$ is a step input with magnitude 0.1. The states of the system are estimated using Observer and Kalman Filter under different scenarios and the estimation results of the two are compared.

Estimation results with known and unknown initial conditions

Firstly, it is assumed that the initial condition of the system is known, that is, $x_0 = [1, 1]^T$. The Fig. 3.4 shows that the estimated state x_1 using both Observer and KF converge to the actual value and they both show similar performance. However, in practical,

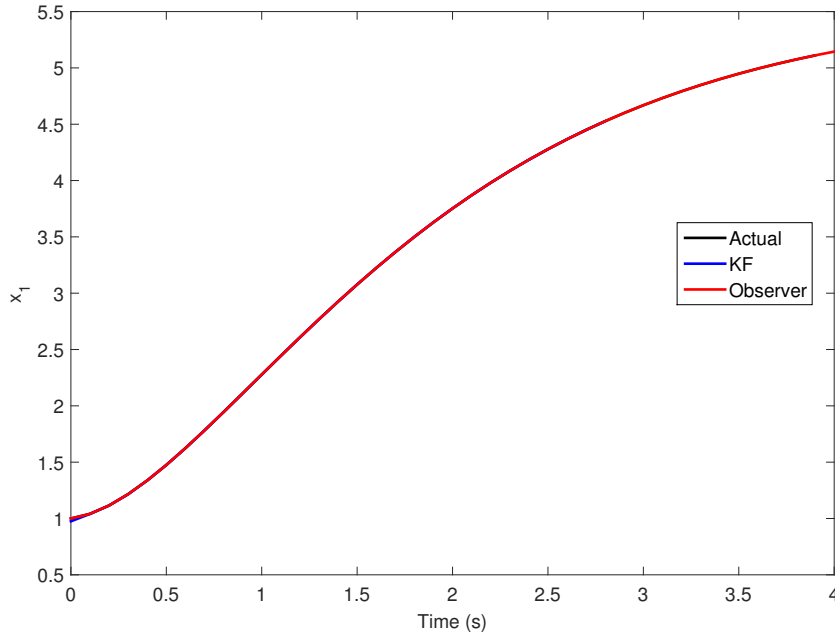


Figure 3.4: Estimation results of state x_1 with known initial condition

knowing the initial conditions of a real world system is not possible. So, an assumption of the initial condition is made and then the states of such a system are estimated. Assuming that the initial state of the system given in (3.21) and (3.22) is not known, we assume the initial state to be $x_0 = [0; 0]$. Then, the states are estimated using Observer and KF and the results are shown in Fig. 3.5. Under unknown initial condition, the estimation results from Fig. 3.5 can be seen that Observer is taking more time to converge to the actual value as compared to KF making Kalman filters more efficient in estimating the states of a practical system.

Estimation results with system uncertainties

The mathematical model that is used for state estimation is only an approximation of real system and it is subject to uncertainties. To account for these uncertainties, it is tried to model them as process noise w and measurement noise v which are random variables.

Although these random variables do not follow a pattern, using probability theory their average properties can be derived. For example, w and v are considered to be white

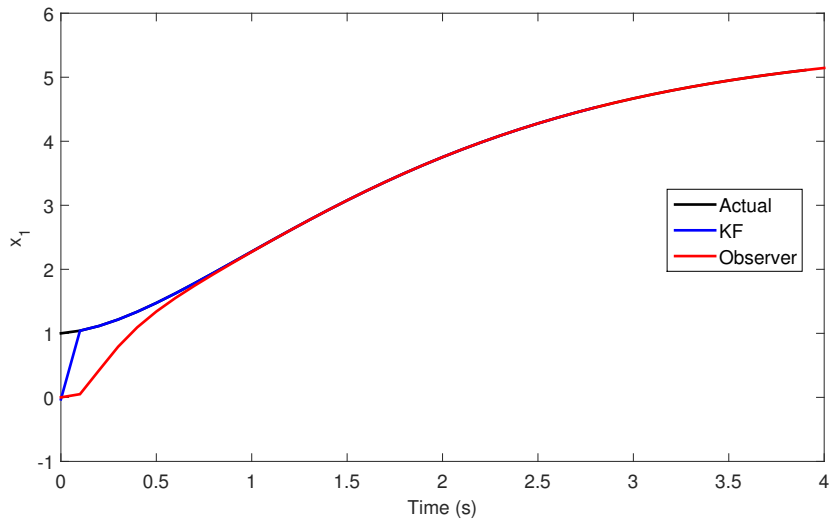
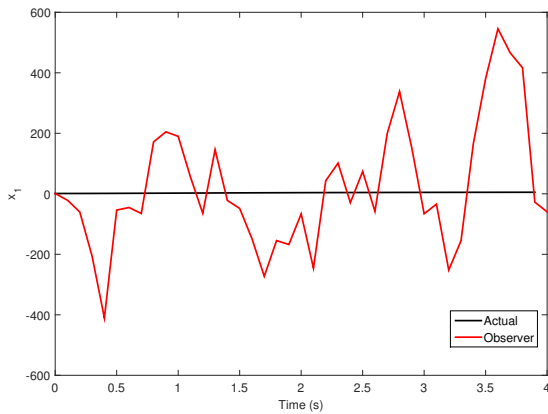
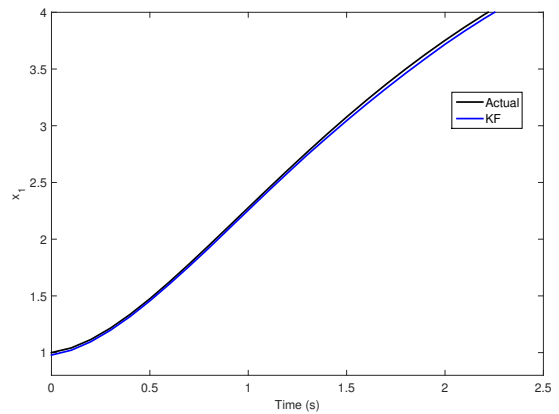


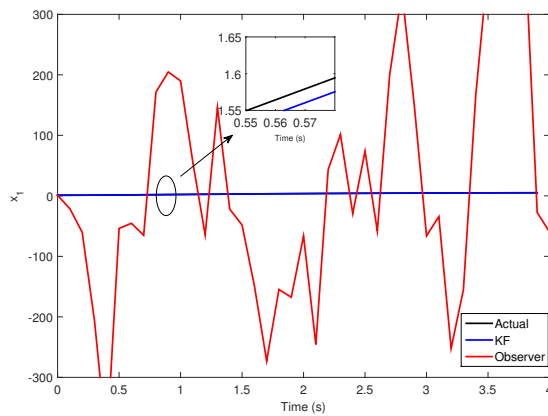
Figure 3.5: Estimation results of state x_1 with unknown initial condition



(a) Plot of estimated state x_1 using Observer



(b) Plot of estimated state x_1 using KF



(c) Comparison of Observer and KF estimations

Figure 3.6: The estimated state x_1 estimation plots using measurements with added noises

noises with zero mean and standard deviations of $q = 2.3$ and $r = 0.5$ respectively for the system given in (3.21) and (3.22). Under these conditions, the state estimation results using Observer and KF are as shown in the Fig. 3.6c. It can be observed from Fig. 3.6b that the estimated state using KF is converging to the actual value and is robust to the process and measurement noise. Fig. 3.6a shows that the Observer is diverging.

Comparing Observer and Kalman Filter

The strengths and weaknesses relative to each functionality are presented based on the technical, theoretical capabilities and simulation results.

Feasibility: Using observers, the state estimates are guaranteed to converge if the solution to matrix inequality exists. In contrast, the KF methods do not require that.

Unknown initial conditions: Most observers are independent on the knowledge of initial conditions of the system. However, if the initial conditions for the system state is chosen reasonably, then KF gives faster convergence to actual value compared to observers.

Numerical stability: Observers do not have numerical stability problems while some KF techniques (UKF) can encounter numerical instability because the P matrix is not always guaranteed to be positive definite.

Tolerance to process and measurement noise: The observers shows poor performance in presence of noises. By design, the KF techniques are developed to deal with such noise.

Hence it could be argued that the Kalman filter is a good estimator against a wide range of disturbances.

Features of Existing Kalman Filters

The following features of the CKF compared to the EKF and UKF are the reason for the increased accuracy and robustness of the algorithm,

- In comparison to EKF and similar to UKF, CKF is also derivative free and simpler to apply.
- CKF, like UKF, approximates the Gaussian distribution with a weighted collection of symmetric points. However, since there is no stem at the centre of the cubature-point range, it does not suffer from the numerical instability issues that UKF does.
- UKF considers the calculation of posterior statistics and the derivation of the sigma-point collection for the prior density to be two separate problems. CKF, on the other hand, extracts the cubature-point collection directly in order to precisely calculate

the first two-order moments of a non-linear transformation, thus increasing the precision of numerical estimates for moment integrals.

- EKF, UKF, and CKF are all suboptimal Bayesian filters with some model uncertainty robustness. The ability to effectively deal with non-linear transformations determines the degree of robustness. Due to a first-order Taylor series approximation of the non-linear functions, the EKF is the least robust form, while the CKF is the most robust since it uses a more accurate cubature approach.

3.4 Preliminary DSE Studies: Dynamic State Estimation of Induction Motor

The discussion in the previous sections has been dedicated to linear systems; however, real systems are eventually non-linear. Even a simple relationship between current and voltage of a resistor is not linear for all values and Ohm's Law is only an approximation over a certain linear range (Simon, 2006). This linear function can describe the behaviour of a resistor until the voltage does not exceed a certain threshold. Although many systems are close enough to linear under certain conditions so as to provide satisfactory results with linear estimation methods. But in many others cases, this is not true and some systems are not even linear over a small range of operation. Therefore, the use of non-linear estimators is inevitable.

Non-linear estimation is not yet fully developed and there is still a lot of space for research in this field. Extended Kalman Filter (EKF), Unscented Kalman Filter (UKF), Cubature Kalman Filter (CKF) and particle filter are among the most popular and widespread non-linear estimation approaches developed until now. Speed estimation in Induction Motors (IMs) has been an interesting area of research. Estimation of the speed of the machine results in elimination of mechanical speed sensors (e.g. tachometer).

Electric induction motors are an essential part of modern industrial applications. In most speed and torque controlled motor drive systems, closed loop control is based on the measurement of speed or position of the motor using a shaft encoder. However, in some cases, it is difficult or extremely expensive to use sensors for speed measurement of induction motor (IM). Estimation of speed of the machine results in elimination of mechanical speed sensors(e.g. tachometer). This is accompanied by advantages like low costs, reduced maintenance requirements, reliable system and better robustness against noises (Zaky et al., 2008). The evaluation of speed estimation algorithms for IM needs to be done considering effect of measurement noise and parameter changes during running conditions.

To implement estimation of speed of IM, spectrum analysis based on harmonics in

rotor slots has been taken up ([Ilas et al., 1994; Holtz, 2002; Staines et al., 2006]). This is a time consuming procedure and reduces the range of speed control. Yet another set of technique is to send high frequency probe signals to stator terminals to derive the rotor flux ([Hinkkanen et al., 2005]). But, this sometimes would lead to injecting ripples in the speed. Therefore, KF approaches are adopted to avoid these drawbacks. KF a unique type of observer that enables efficient filtering of the device and system noises, if covariance matrices associated with these noises are known. EKF and UKF are the most referred estimation methods for this purpose due to the recursive nature, making them suitable for implementation on digital platforms. Using a reduced order EKF yielded reduced computational efforts ([Peng and Fan, 2007; Leite et al., 2004]). Small range of speed and load torque changes can be estimated by using EKF. A full order EKF is deployed as a more powerful observer for estimating speed as a parameter with small variation ([Velázquez et al., 2004; Shi et al., 2002]). The main drawback of the EKF based estimator is that it is not able to follow the states of the system in transient time. Equation of motion is added to the state space model to make it more appropriate for dynamic state estimation ([Peng and Fan, 2007; Leite et al., 2004; Velázquez et al., 2004; Shi et al., 2002; Mohanty and Patra, 2005]). An EKF based estimator is designed which is capable of estimating parameters of the motor along with its main states ([Atkinson et al., 1991; Barut et al., 2005, 2007; Bogosyan et al., 2007]). EKF is able to approximate the mean and covariance of the states of a non-linear transformation upto the first order. Thus, UKF is used for state estimation in an IM to overcome this drawback and capture better the non-linearity of the system ([Jafarzadeh et al., 2011]). In a more precise manner, the covariance and posterior mean is thus captured by the UKF upto third order for any non-linearity when these sample states are used in the exact non-linear system equations for estimation ([Barut et al., 2007]). Despite having several advantages UKF runs with some major flaws like filter instability, numerical inaccuracy. Consequently, a new variety of Kalman filter called Cubature Kalman Filter (CKF) for highly non-linear system is proposed which employs a more precise cubature process for numerically computing Gaussian-weighted integrals ([Jafarzadeh et al., 2011]).

EKF, UKF and CKF are selected for this study and explained in brief in the Appendices A3, A4 and A5 respectively. For the better understanding of these algorithms, in this section these algorithms are simulated for the speed estimation of IM and the simulation results are presented.

3.4.1 Induction Motor State Space Model

The state space model of an IM is composed of four independent state variables, namely rotor flux components (ψ_{qr}, ψ_{dr}) , stator-current components (i_{qs}, i_{ds}) , which are the q and

d axis components obtained by Park transformation. The two inputs for this model are stator-voltage components v_{qs} and v_{ds} . By considering the dynamic motion equation of an IM, the state vector can also be extended to w_m , angular velocity.

$$\begin{bmatrix} i'_{ds} \\ i'_{qs} \\ \Psi'_{dr} \\ \Psi'_{qr} \\ \omega'_m \end{bmatrix} = \begin{bmatrix} -\left(\frac{R_s}{L_\delta} + \frac{R'_r L_m^2}{L_r'^2 L_\delta}\right) & 0 & \frac{R'_r L_m}{L_r'^2 L_\delta} & \frac{L_m}{L_\delta L_r'^2} P_p \omega_m & 0 \\ 0 & -\left(\frac{R_s}{L_\delta} + \frac{R'_r L_m^2}{L_r'^2 L_\delta}\right) & -\frac{L_m}{L_\delta L_r'^2} P_p \omega_m & \frac{R'_r L_m}{L_r'^2 L_\delta} & 0 \\ \frac{R'_r}{L_r' L_m} & 0 & -\frac{R'_r}{L_r'} & -P_p \omega_m & 0 \\ 0 & \frac{R'_r L_m}{L_r'} & P_p \omega_m & -\frac{R'_r}{L_r'} & 0 \\ 0 & 0 & 0 & 0 & 0 \end{bmatrix} \begin{bmatrix} i_{ds} \\ i_{qs} \\ \Psi_{dr} \\ \Psi_{qr} \\ \omega_m \end{bmatrix} + \begin{bmatrix} \frac{1}{L_\delta} & 0 \\ 0 & \frac{1}{L_\delta} \\ 0 & 0 \\ 0 & 0 \\ 0 & 0 \end{bmatrix} \begin{bmatrix} v_{ds} \\ v_{qs} \end{bmatrix} + W_t \quad (3.23)$$

where $K_r = R_s + \frac{L_m^2 R'_r}{L_r'^2}$ and $\tau_r = \frac{L_r'}{R'_r}$, R_s -stator resistance; R_r -rotor resistance; P_p -pole pairs; $L_\delta = \delta L_s$ -stator transient inductance; leakage/coupling factor $\delta = 1 - (L_m^2/L_s L_r')$; L_m - mutual inductance; $L_s = L_{ls} + L_m$ and $L_r' = L'_{lr} + L_m$ - inductances of stator and rotor; and L_{ls} and L'_{lr} -leakage inductances of stator and rotor. There are two inputs for the model, stator-voltage components (v_{ds}, v_{qs}) (Barut et al., 2007; Bogosyan et al., 2007). The stator current components are the output signals of this model.

$$\begin{bmatrix} i_{ds} \\ i_{qs} \end{bmatrix}_y = \begin{bmatrix} 1 & 0 & 0 & 0 \\ 0 & 1 & 0 & 0 \end{bmatrix}_C \begin{bmatrix} i_{ds} \\ i_{qs} \\ \psi_{dr} \\ \psi_{qr} \end{bmatrix}_x + v_t \quad (3.24)$$

This IM model is used as an estimation model for speed estimation using the different non-linear kalman filters. The system diagram of Speed estimation in Space vector modulation based Induction motor drive is shown in Fig. 3.7.

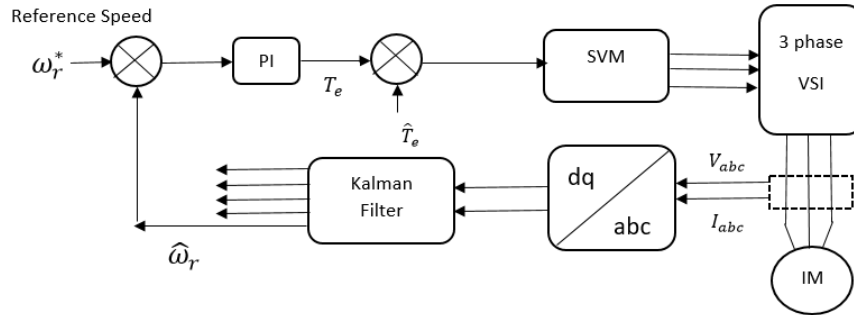


Figure 3.7: System diagram of induction motor with space vector modulation

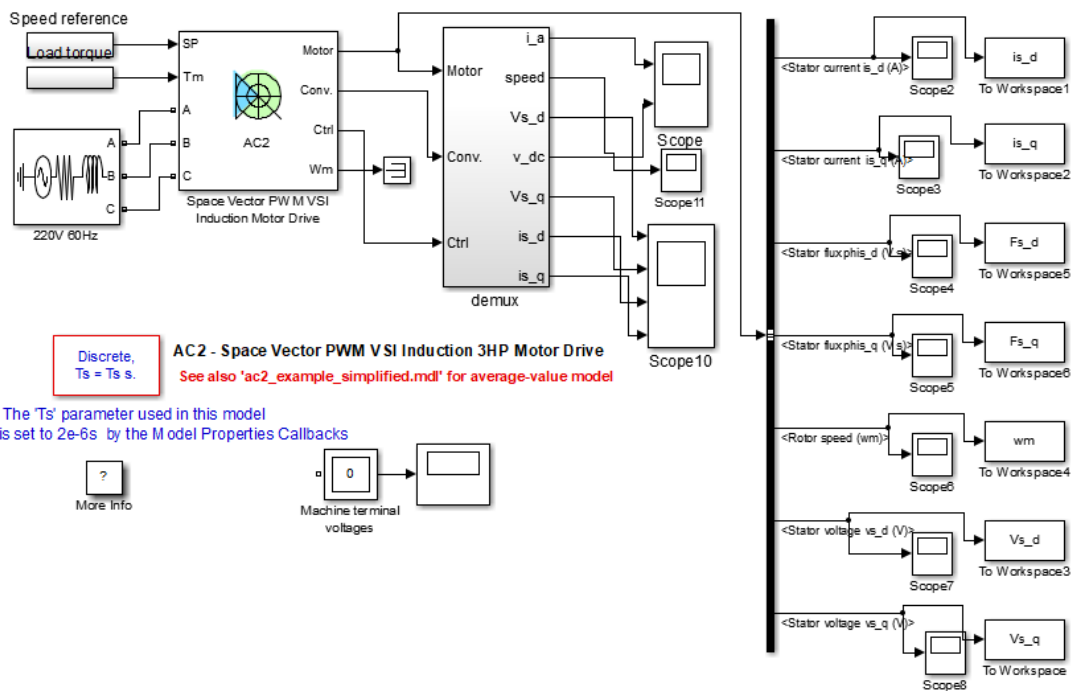


Figure 3.8: Simulink model of IM with SVM controller used for data generation

3.4.2 Simulation model of Induction Motor with Space Vector Modulation

In this section, to generate the actual data for speed estimation of IM, an IM model is simulated in Matlab/Simulink (MATLAB© R2013a) with Space Vector Modulation (SVM) drive. The model as shown in Fig. 3.8 is used to generate data with $T_s = 2 \times 10^{-6}$ second sampling time. The induction motor parameters and initial value of x , P , Q and R as well as other considerations used for the simulation are listed in Appendix F.

The IM is driven with 1000 rpm reference speed and after a transient time, at $t=1.0$ second, the speed reference is increased to 1500 rpm. The speed of the IM is estimated using (3.23) and (3.24).

3.4.3 Simulation Results

To demonstrate effectiveness of the existing filters for speed estimation of IM, EKF, UKF and CKF algorithms are implemented by developing script code in MATLAB© R2013a. For all algorithms, initial states are set as $\hat{x} = 0$ and initial covariance $P_0=10^{-3} \times I$. Here, I is identity matrix with ones on the diagonal. Measurement and process noise covariance are $R = 0.001 \times I$ and $Q = 10^{-6} \times I$ respectively.

Fig. 3.9a gives the speed plots estimated using EKF, UKF and CKF and the corresponding error plots are given in Fig. 3.9b, it can be noticed that all these methods are able to estimate the speed equally efficiently with least error possible. The error in the estimated speed compared to the simulated using the actual data.

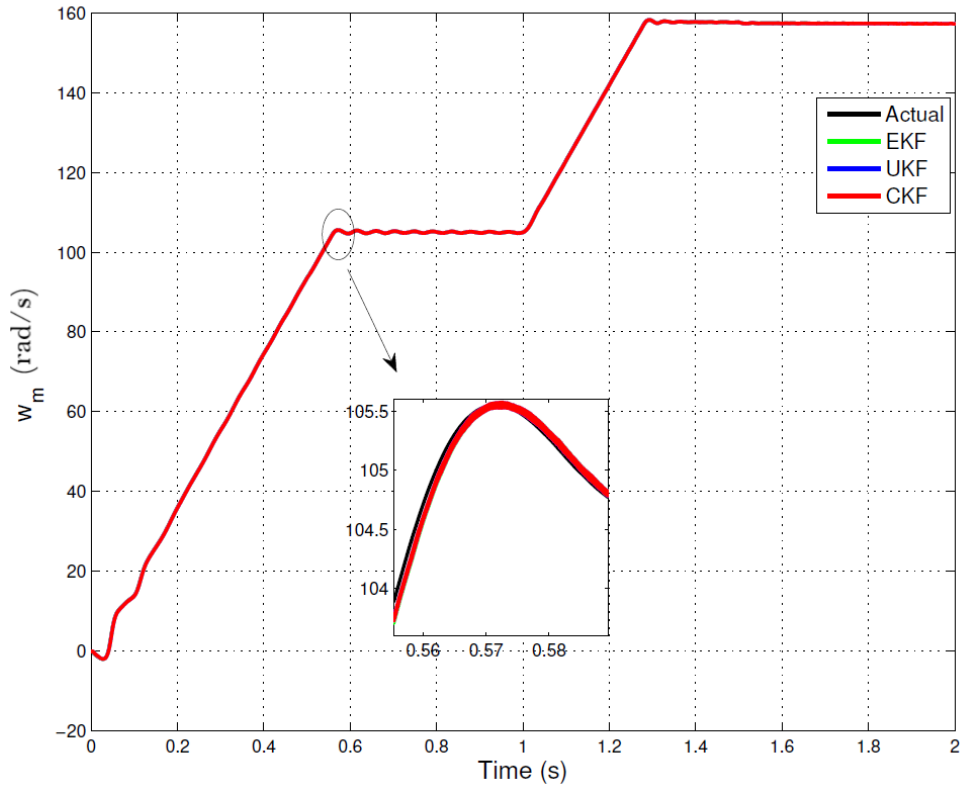
Effect of measurement noise

To account for the measurement device errors, white noises are added to the actual data to simulate measurement data. Accordingly, a random noise of variance 5% is added to the voltage and current phasors. To evaluate the noise rejection capability, the estimated speed plots and error plots with added noise are compared in Fig. 3.10. The mean of absolute error in the estimated speed using EKF, UKF and CKF are shown in Table 4.3.

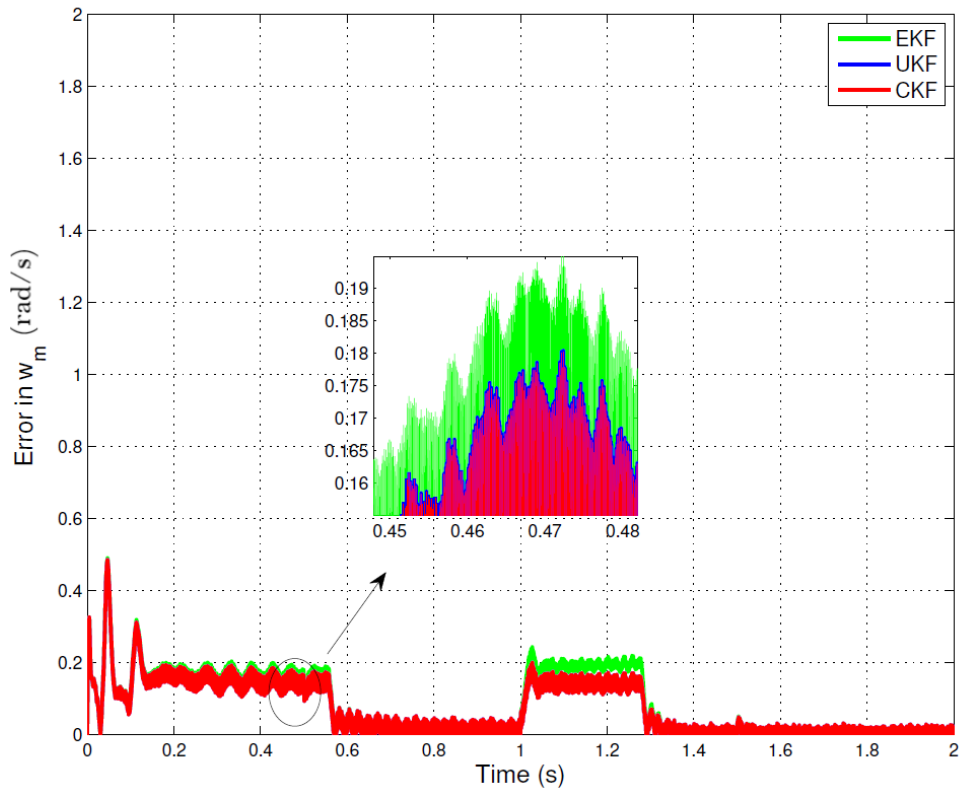
Table 3.1: Mean of Absolute Errors (MAE) in the Estimated Speed of Induction motor considering noise in measurement data

	MAE in rotor speed (rad/s)
CKF	0.0973
UKF	0.0974
EKF	0.1129

From Fig.4(b) it is observed that all methods are able to estimate the speed accurately

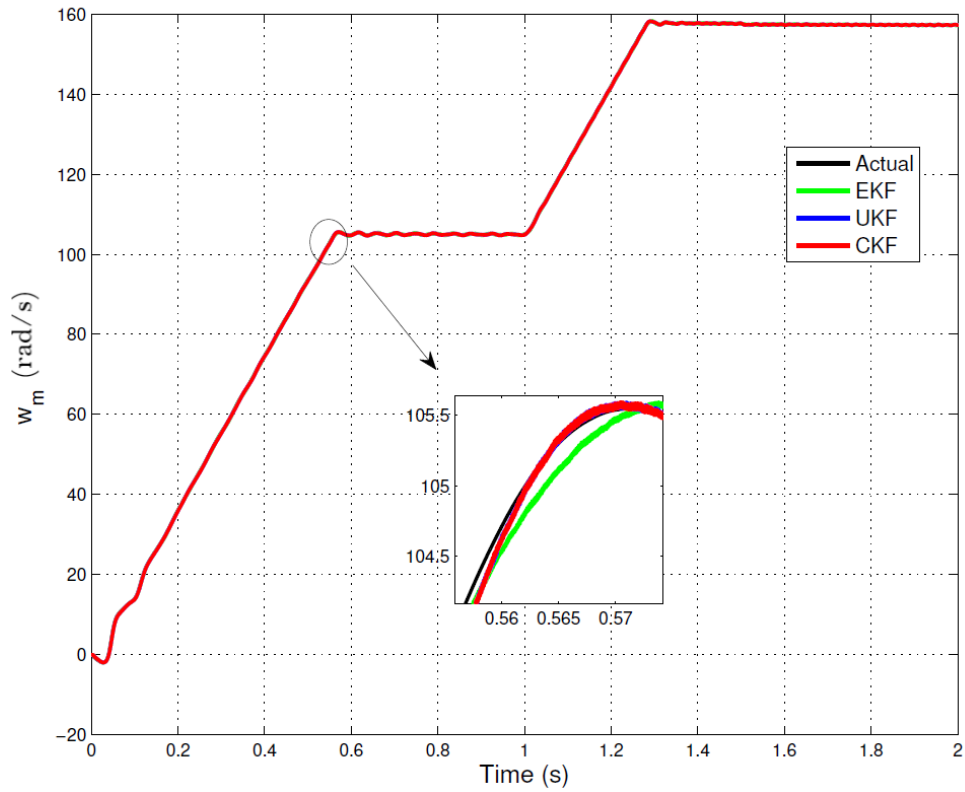


(a) Rotor speed

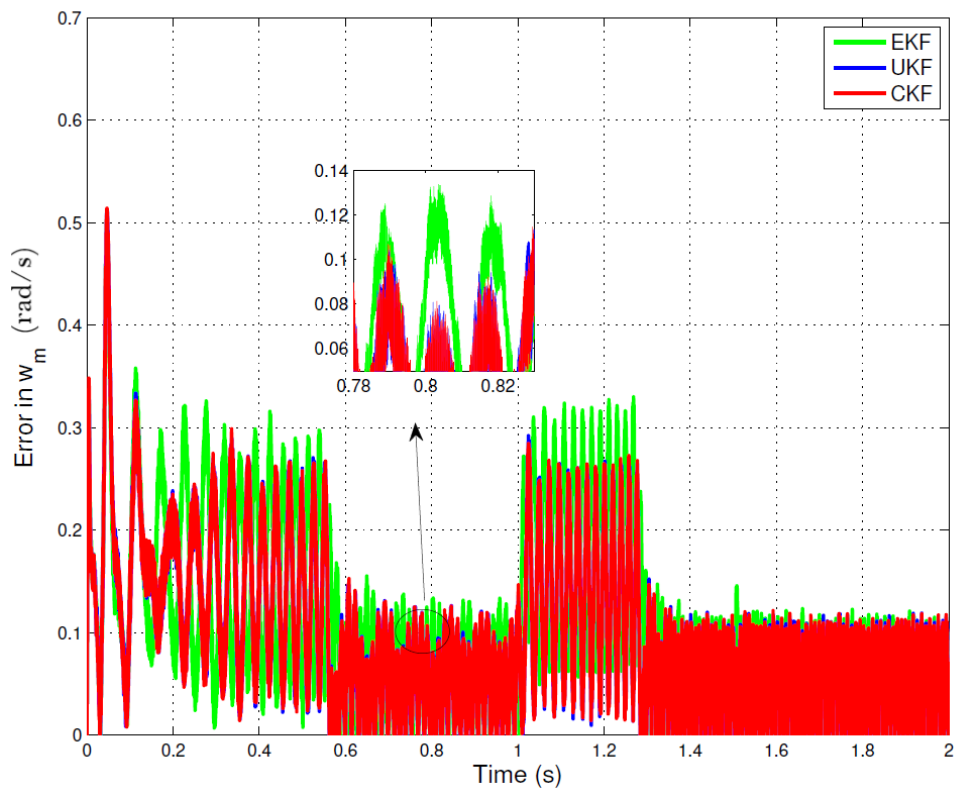


(b) Error in rotor speed

Figure 3.9: Estimated speed and error plots without considering noise in measurement data



(a) Rotor speed



(b) Error in rotor speed

Figure 3.10: Estimated Speed and error plots considering noise in the measurement data

in the presence of noise, but the error plot in the estimated speed using CKF is below the other two algorithms (EKF and UKF). As noted in Table 4.3, the mean of absolute error (MAE) in estimated speed obtained by using CKF and UKF are 0.0973 rad/s and 0.0974 rad/s respectively. This indicates CKF is slightly more robust to the measurement noise than the UKF. Whereas using EKF the mean of absolute error is 0.1129 rad/s which is 0.1603 times and 0.1591 times more than that of CKF and UKF respectively.

Effect of parameter changes

In induction motor, the rotor and stator resistances are not constant parameters and start changing with variation in motor temperature and speed. In this section, the estimation results when stator and rotor resistances are changed to 0.8 and 1.2 times the initial values respectively are shown Fig. 3.11 and Fig. 3.12.

The mean of absolute errors (MAE) in the estimated speed of induction motor considering the changes in stator and rotor resistances estimated using EKF, UKF and CKF are compared in Table 4.4. From the plot given in Fig.5(b), the error plots with $R_{s_{new}} = 0.8R_s$

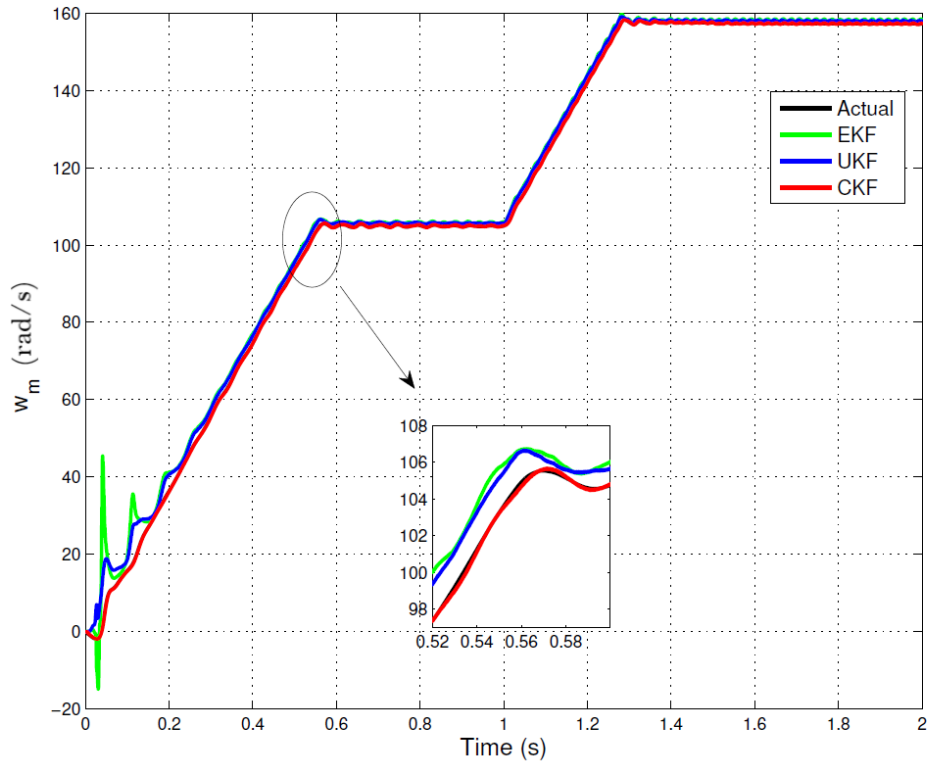
Table 3.2: Mean of Absolute Errors (MAE) in the Estimated Speed of Induction motor with new parameters

MAE in Rotor speed (rad/s)		
	$R_{s_{new}} = 0.8R_s$ and $R_{r_{new}} = 0.8R_r$	$R_{s_{new}} = 1.2R_s$ and $R_{r_{new}} = 1.2R_r$
CKF	0.1161	0.2384
UKF	1.4424	1.5856
EKF	1.7607	1.5939

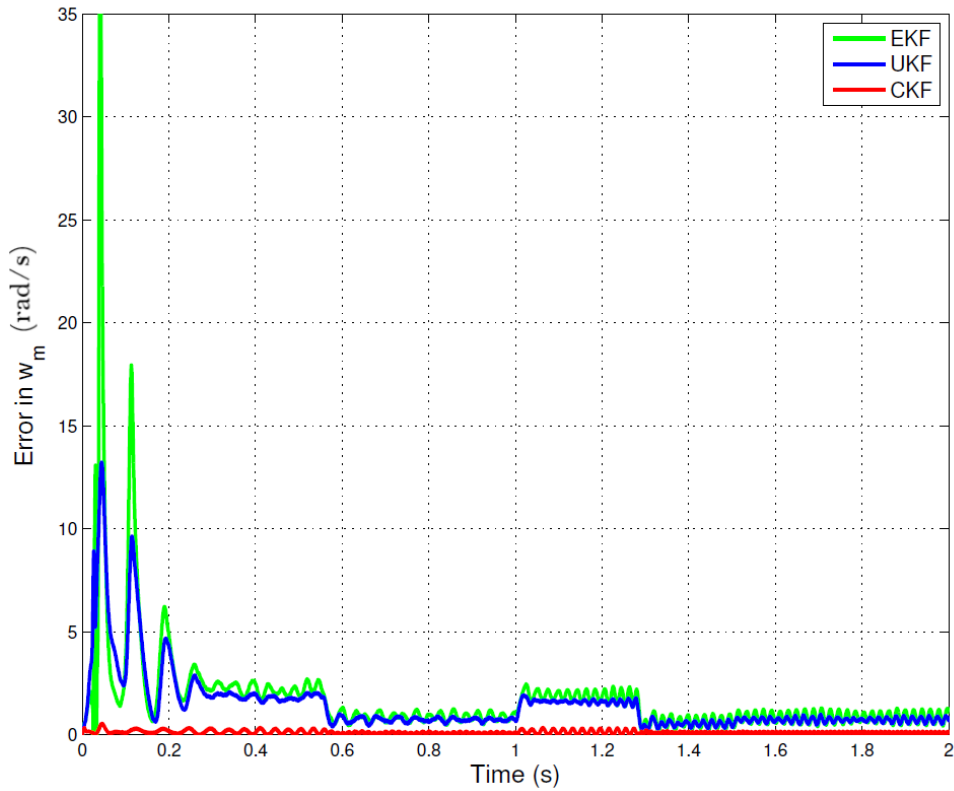
and $R_{r_{new}} = 0.8R_r$, it is observed that CKF has the least error than the other two filters. And it can be seen from Fig.6(b) that, the error plots with $R_{s_{new}} = 1.2R_s$ and $R_{r_{new}} = 1.2R_r$, CKF is again showing more accurate estimation results than EKF and UKF. As shown in Table 4.4, the mean of absolute error using CKF when $R_{s_{new}} = 0.8R_s$ and $R_{r_{new}} = 0.8R_r$, is 0.1161 rad/s which is approximately 92% and 93% less than that of UKF and EKF respectively. And when $R_{s_{new}} = 1.2R_s$ and $R_{r_{new}} = 1.2R_r$, the MAE using CKF is 0.2384 rad/s which is approximately 85% less than that of both UKF and EKF respectively. Hence it can be argued that the parameter variation in induction motor does not significantly affect the accuracy of the speed estimation using CKF.

Conclusions from speed estimation studies of IM

The non-linear kalman filters: EKF, UKF and CKF are designed to estimate the rotor speed of an induction motor with space vector modulation drive (SVM). Estimation

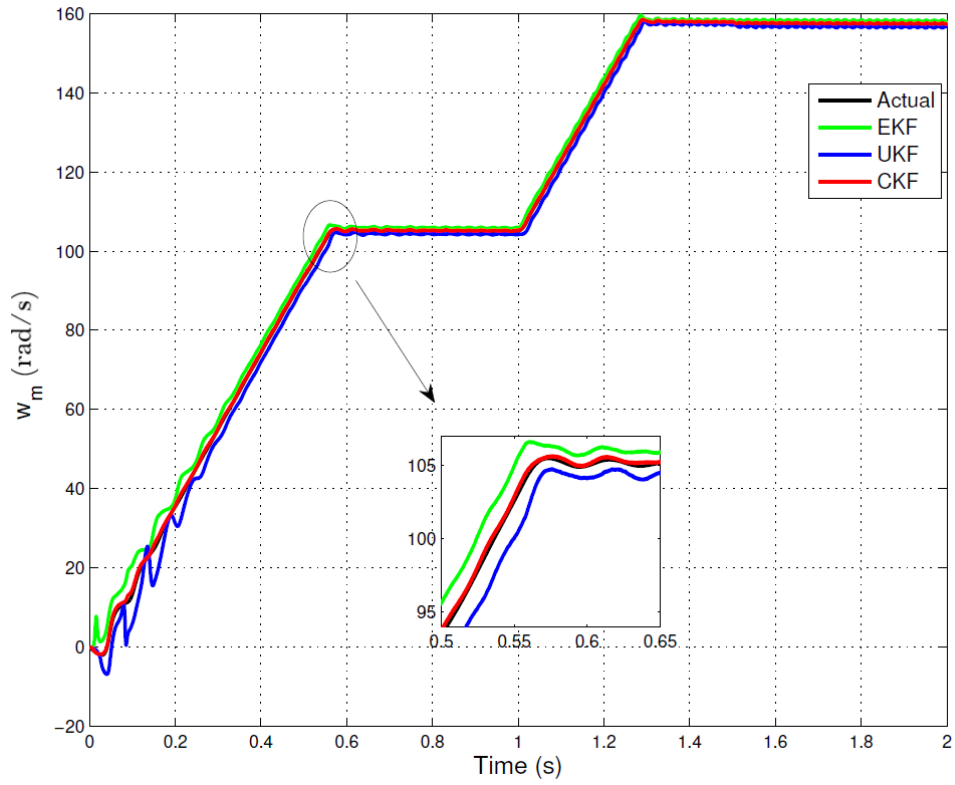


(a) Rotor speed

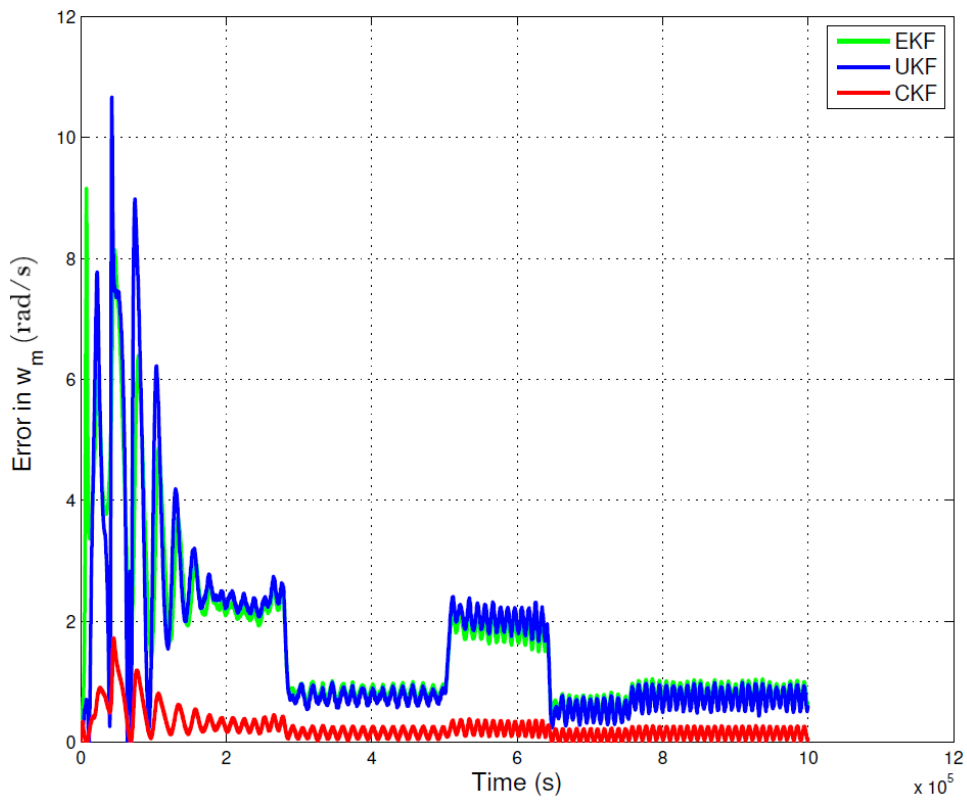


(b) Error in rotor speed

Figure 3.11: Estimated speed and error plots with parameters $R_{s_{new}} = 0.8R_s$ and $R_{r_{new}} = 0.8R_r$



(a) Rotor speed



(b) Error in rotor speed

Figure 3.12: Estimated speed and error plots with parameters $R_{s_{new}} = 1.2R_s$ and $R_{r_{new}} = 1.2R_r$

results show that all these filters are capable of estimating the speed of IM efficiently. However, it is observed that cubature Kalman filter (CKF) is the most accurate when compared to EKF and UKF. Effects of measurement noise and parameter variations are also investigated. The simulation results show that the CKF has good noise rejection and is insensitive to variations in the machine parameters.

3.5 Power System Dynamic State Estimation (PS-DSE)

The major advantage of using synchronized measurement technology in power systems are that measurements from widely spread spots can be synchronized with a signal received by the Global Positioning System (GPS) clock. The direct measurement of the voltage phase angles allow the realization of a precise and dramatically rapid dynamic state estimation (Chakrabarti et al., 2008). Based on the ability of wide area monitoring system to capture dynamic state information, the state estimators can generate dynamic states of major components of the power system. For example, for the synchronous generator, the rotor angle and speed can be estimated instead of the static values of the voltage magnitudes and phase angles (Ghahremani and Kamwa, 2011b,c).

At the present time, phasor estimation has been essentially performed using steady state measurements. Phasor systems are typically faster than the dynamics of most power systems; therefore, this kind of estimation has been rational and sufficient. Nevertheless, power systems are changing daily and more accurate methods might be needed for difficult operational situations (Martin and Carroll, 2008). Data communication systems have also evolved dramatically in recent years. Most of the utilities are equipped with a broadband at 1MB/s or higher for their data communication and the remaining ones at least have plans to do so (Martin and Carroll, 2008). LAN and WAN supporting equipments are prevalent and easy to install these days. This progress has been a stimulus to change minimal data sets to more complete data packages. Based on all these reasons, many institutes all around the world are doing research on dynamic measurement of the power systems. Particularly, an IEEE working group has recently been revising C37.118 to add dynamic performance requirements while paying attention to not invalidating current ones (Martin and Carroll, 2008). Recent experiences have proved that synchronized wide area system history of the dynamic events are key in the analysis and understanding of the system performance, behaviour, and the types of control decisions made for large scale power system contingencies (Terzija et al., 2010). It is a time consuming effort to analyse and determine the main reason of major contingencies in a power system without the time-stamped PMU data or the related PDC.

Dynamic state estimation in a power system provides accurate and synchronized information about the main states of the generating unit which are working in an interconnected large power system. In addition to the noise elimination on measurement signals provided by PMUs, dynamic state estimation provides high rate information of the immeasurable states of the synchronous generators which are advantageous in better control of the power stations; real-time angle, voltage, and frequency transient stability analysis of the power system; improved damping property for the inter-area oscillations; and better rush hour power management.

In the subsequent sections, the high rate data provided by PMU is simulated and used for dynamic state estimation in different power system case studies. As practical PMU data is not accessible for this study, PowerWorld Simulator (powerWorld ver22, 2021) and PST tool in MATLAB© R2015a are used for this purpose. Since, these simulators are able to simulate transient stability of the power systems with predetermined faults and desired resolutions. It is assumed to mimic the outputs of the PMUs installed on the buses of a system. The sampling rate of the present commercialized PMUs are near 25 to 50 samples per second. Therefore, different sampling rates are considered in the simulation procedure to evaluate the effect of this factor on the accuracy of the estimation results, and also to examine whether the whole idea of the dynamic state estimation in power systems using existing PMU technology is realizable. The diagram presented in Fig. 3.13 clearly shows the idea being used in this study to generate accurate data using PowerWorld Simulator for modelling, validation and dynamic state estimation. This diagram shows that by designing a desired power system case study in PowerWorld and providing information about steady state active and reactive power of the generators; transient parameters of the generators; parameters and characteristics of the transmission lines; fault location, moment, duration, and resolutions; simulation time and sampling frequency; and states of the systems to be sampled during the simulation procedure; synchronized high rate information about the power system can be generated. This data is then used to validate the classical model developed for the synchronous generator. The validated model is then used for dynamic state estimation in different power system case studies. The measurement data simulated are further added with a white Gaussian noise to mimic to the real time practical data.

A dynamic state estimation problem in context of power system consists of the available input, the expected outcome of dynamic state estimation and evaluation criteria. The structure of the problem statement is illustrated by Fig. 3.14 which is used to develop and evaluate potential solutions.

To estimate the current dynamic states, only the data and models that are available up to the current time can be used as the inputs of a filtering method. All the PMU data available up to the current time can be used. Studies shall be carried out with proper considerations of the practical constraints of models and data discussed as follows:

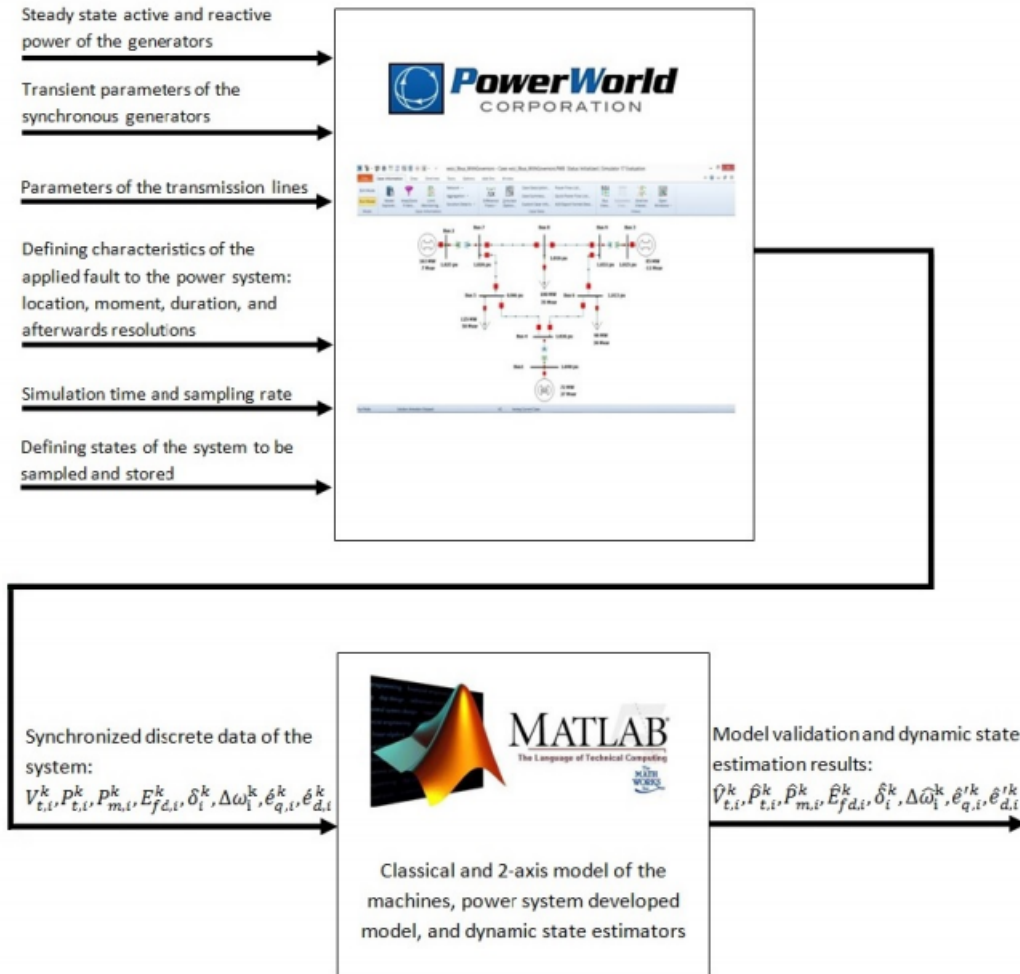


Figure 3.13: Using PowerWorld simulator instead of real PMU to generate synchronized data for power system case studies

- PMU data: PMU data have measurement noise. The measurement noises are defined as total vector errors (TVEs). For a PMU that follows Institute of Electrical and Electronics Engineers (IEEE) Standard C37.118, the PMU device error shall be smaller than 1% (Martin, 2008). In addition, a noise is often introduced by current transformers (CT) and potential transformers (PT) as well.
- Dynamic models: Dynamic models are often available to describe the dynamic features of a power system. The dynamic models are only an approximate description of a power system. Therefore, the system responses and model responses to a stimulation are often different at various levels. The response difference reveals the modelling noises and deficiencies and must be considered for a real application.

The goal of dynamic state estimation is to estimate the dynamic states of a power system. Dynamic states are the minimum set of variables that can determine the status of a dynamic system (DeRusso et al., 1997) for a time scale of interest. For the electrome-

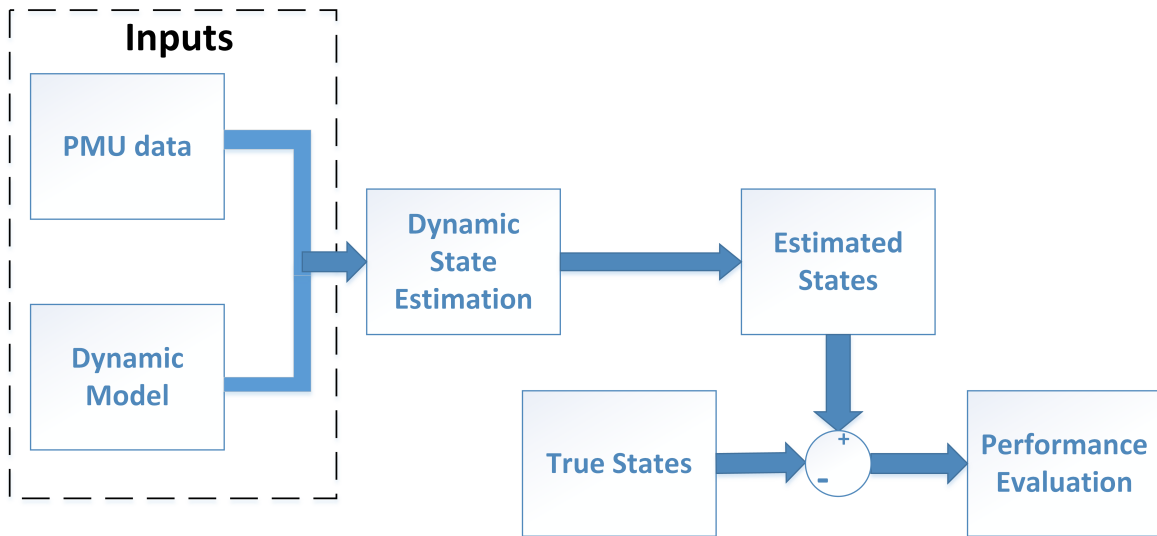


Figure 3.14: Problem statement of dynamic state estimation

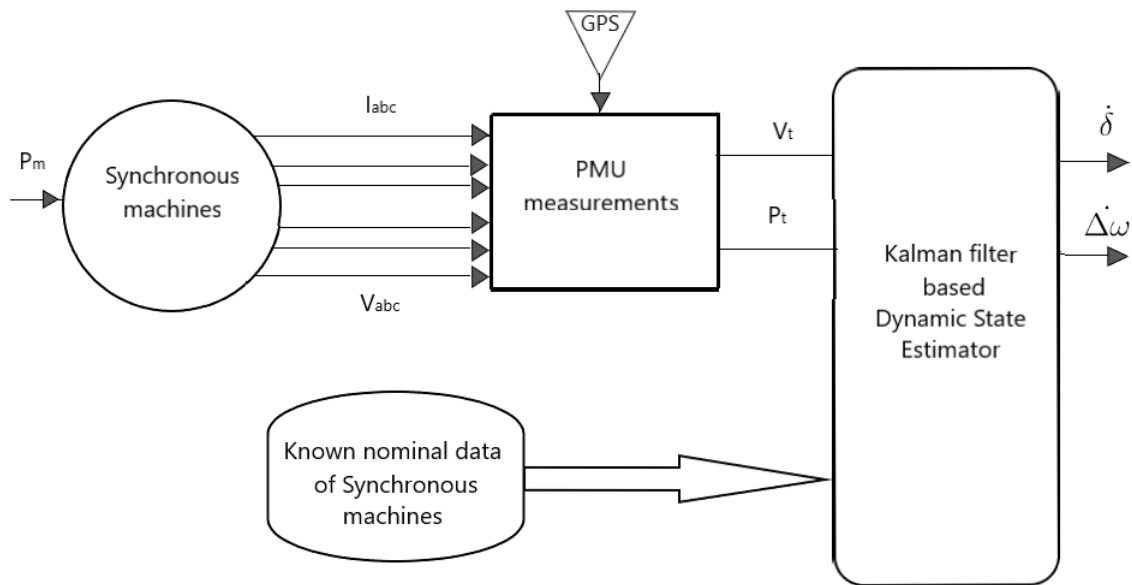


Figure 3.15: Block Schematic of dynamic state estimation of synchronous machine

mechanical dynamics, the time scale is at a level between 100 milliseconds and 1 second. The block schematic of the dynamic state estimation used to estimate rotor angle and rotor speed deviation for the synchronous machines is shown in Fig. 3.15. The dynamic states can be used to enhance the rotor angle stability of a power system by enabling dynamic contingency analysis and state prediction. Depending on the requirement of an application, the states can be estimated for past, current and future time. A smoothing method estimates the states of past time and can be used to reproduce past events for forensic studies. A filtering method estimates the states at the current time and can be

used to drive control signals to improve system stability. A prediction method estimates the states of future time and can be used to guide proactive remedial actions. The ultimate goal of this study is to enhance power system stability in real time, and therefore the focus is placed on the filtering method.

Evaluation Criteria

There are many algorithms for estimating dynamic states of a power system. Evaluation criteria are needed to evaluate and compare the estimation performance to select a proper estimation algorithm. The following quantities are evaluated to quantify the performance of a dynamic state estimation algorithm under a statistical framework.

1. **Accuracy:** Accuracy is defined as the difference between estimated states and true states. In this work, a Mean Absolute Error in the estimated states is used to evaluate the accuracy of the algorithms.
2. **Robustness against modelling errors and measurement errors:** The robustness of an algorithm can be measured by its tolerance of noise in a model and data. In practice, the robustness of an algorithm is evaluated by the maximum modelling errors or measurement errors under which the algorithm can still achieve the required state estimation accuracy.
3. **Speed of computation:** The speed of an algorithm can be measured by the capability of an algorithm to keep up with the speed of inflowing data. Ideally, the results are available before the next set of data arrives.
4. **Scalability:** Scalability of an algorithm refers its effectiveness when it is applied to a larger system. A robust, numerically stable algorithm may be able to solve larger problems than one that is computationally more efficient but numerically unstable. Scalability at all levels is critical because methods that work for small problems may fall apart when applied to large real-world problems.

3.5.1 Mathematical Description of the Synchronous Machine and the Classical Model

Based on Newton's second law, the rotor motion of a synchronous generator can be expressed by the following (Glover and Sarma, 2011),

$$J\alpha_m(t) = T_m(t) - T_e(t) \quad (3.25)$$

J is the total moment of inertia of the rotor and the other rotating parts in $Kg - m^2$; α_m is the rotor angular acceleration in rad/s^2 ; T_m is the mechanical torque provided by the prime mover excluding the retarding torque of mechanical losses in $N - m$; and T_e is the electrical torque whose per-unit value is equal to the total per-unit three-phase output electrical power of the generator including electrical losses (Glover and Sarma, 2011). $\alpha_m(t)$ is also defined as

$$\alpha_m(t) = \frac{d\omega_m(t)}{dt} = \frac{d^2\theta_m(t)}{dt^2} \quad (3.26)$$

$\omega_m(t)$ is the angular velocity in rad/s and θ_m is the angular position with respect to a stationary axis (stator) in rad . T_m and T_e are normally equal in steady state, resulting in zero rotor acceleration and a constant rotor speed known as synchronous speed. As the generator inductances are functions of θ_m . For more convenience and reduced complexity of the equation, the rotor angular position is defined with respect to a synchronously rotating reference frame as follows (Glover and Sarma, 2011):

$$\theta_m(t) = \omega_{m0}t + \delta_m(t) \quad (3.27)$$

Where ω_{m0} is the synchronous angular velocity of the rotor in rad/s , and $\delta_m(t)$ is the angular position of the rotor compared to this new defined reference frame. (3.26) and (3.27) are inserted into (3.25) to obtain,

$$J \frac{d^2\theta_m(t)}{dt^2} = J \frac{d^2\delta_m(t)}{dt^2} = T_m(t) - T_e(t) \quad (3.28)$$

(3.28) is multiplied by $\omega_m(t)$ and divided by apparent power S_{rated} which results in

$$\frac{J\omega_m(t)}{S_{rated}} \frac{d^2\delta_m(t)}{dt^2} = \frac{\omega_m(t)T_m(t) - \omega_m(t)T_e(t)}{S_{rated}} \quad (3.29)$$

$$= \frac{P_m(t) - P_e(t)}{S_{rated}} = P_m(t) - P_e(t) \quad p.u \quad (3.30)$$

where P_m is mechanical power supplied by the prime mover minus mechanical losses in per unit and P_e is electrical power output of the generator plus electrical losses in per unit. Finally, the normalized inertia constant H is defined for more simplicity as follows:

$$H = \frac{\frac{1}{2}J\omega_{m0}^2}{S_{rated}} \quad \frac{joules}{VA} \quad (3.31)$$

The H constant is normally a value between 1 and 10 p.u. While S and J varies widely with different generators physical characteristics (Glover and Sarma, 2011). Using (3.29),

(3.28) can be written as follows:

$$2H \frac{\omega_m(t)}{\omega_{m0}^2} \frac{d^2 \delta_m(t)}{dt^2} = P_m(t) - P_e(t) \quad p.u \quad (3.32)$$

The per-unit rotor angular velocity is defined as follows:

$$\omega_{p.u.}(t) = \frac{\omega_m(t)}{\omega_{m0}} \quad p.u \quad (3.33)$$

Therefore, (3.32) becomes

$$\frac{2H}{\omega_{m0}} \omega_{p.u.}(t) \frac{d^2 \delta_m(t)}{dt^2} = P_m(t) - P_e(t) \quad p.u \quad (3.34)$$

The electrical angular acceleration, electrical radian frequency, power angle, and synchronous electrical radian frequency for a synchronous generator with P number of poles are defined as follows (Glover and Sarma, 2011):

$$\begin{aligned} \alpha(t) &= \frac{P}{2} \alpha_m(t) \\ \omega(t) &= \frac{P}{2} \omega_m(t) \\ \delta(t) &= \frac{P}{2} \delta_m(t) \\ \omega_0 &= \frac{P}{2} \omega_{m0} \end{aligned} \quad (3.35)$$

The per-unit electrical frequency is also expressed as follows:

$$\omega_{p.u.}(t) = \frac{\frac{2}{P} \omega(t)}{\frac{2}{P} \omega_0} = \frac{\omega_m(t)}{\omega_{m0}} \quad (3.36)$$

(3.36) is then modified by adding an extra term that represents a damping torque anytime the generator deviates from its synchronous speed, with its value proportional to the speed deviation,

$$\frac{2H}{\omega_0} \omega_{p.u.}(t) \frac{d^2 \delta(t)}{dt^2} = P_m(t) - P_e(t) - \frac{D}{\omega_0} \frac{d\delta(t)}{dt} \quad (3.37)$$

Considering (3.36) and (3.37) as two first order equations, the classical model of the synchronous generator is

$$\begin{aligned} \frac{d\delta(t)}{dt} &= \omega_m(t) - \omega_0 \\ 2H\omega_{p.u.}(t) \frac{d\Delta\omega(t)}{dt} &= P_m(t) - P_e(t) - \frac{D}{\omega_0} \frac{d\delta(t)}{dt} \end{aligned} \quad (3.38)$$

D is the damping factor which is normally a small positive value between 0 and 2 (Glover and Sarma, 2011). Also, $\omega_{p.u.}$ is approximated to 1 as in practical rotor speed does not significantly vary from synchronous speed. From now on, for more simplicity, the variable t is eliminated from all functions while keeping in mind that all variables and functions defined up to the present are functions of time ' t '. It is more convenient to develop the model based on the speed deviation from synchronous speed in per unit

$$\begin{aligned}\Delta\omega &= \omega_{p.u.} - 1 \\ \omega_0\Delta\omega &= \omega_m(t) - \omega_0\end{aligned}\quad (3.39)$$

Therefore, the classical dynamic model of the synchronous machine only in terms of only state variables and constants is as follows:

$$\begin{aligned}\frac{d\delta}{dt} &= \omega_0\Delta\omega \\ \frac{d\Delta\omega}{dt} &= \frac{1}{2H}(P_m - P_e - D\Delta\omega)\end{aligned}\quad (3.40)$$

Since all of the parameters are in per unit, $p.u.$ subscript is also eliminated from the equations of the model for more simplicity.

The classical model of the synchronous machine is used in the state estimation process, the model for the estimator used, can be written as,

$$\begin{aligned}\dot{\delta} &= \omega_0\Delta\omega \\ \dot{\Delta\omega} &= \frac{1}{2H}(P_m - P_e - D\Delta\omega)\end{aligned}\quad (3.41)$$

where δ is the rotor angle in radian; $\Delta\omega$ is the rotor speed deviation, P_m is the mechanical power and P_e is the electric air gap power. The angular frequency's rated value is denoted as ω_0 ; inertia constant as H ; and the damping factor as D . To facilitate the generalized notation, (3.41) is transformed into a general state space model (3.42) and (3.43),

$$\dot{x} = f_c(x, u) + w_c \quad (3.42)$$

$$y = h_c(x, u) + v_c \quad (3.43)$$

$$E[w_c w_c^T] = Q \quad (3.44)$$

$$E[v_c v_c^T] = R \quad (3.45)$$

$$x = [\delta, \Delta\omega]^T \quad (3.46)$$

$$u = [P_m]^T \quad (3.47)$$

$$y = [P_t]^T \quad (3.48)$$

In (3.42) and (3.43), x is state vector, u is input vector, and y is output vector. The state

transformation and output functions, respectively, are $f_c(*)$ and $h_c(*)$. The continuous time model is indicated by the subscript "c". The process and output noise are represented by the vectors w_c and v_c respectively. They are represented as Gaussian white noise with covariance matrices defined by (3.44) and (3.45) as Q and R . $E[*]$ represents statistical expectation. All the model expressions discussed are discretized using modified Euler's method (Schinkel et al., 2003) as measurements used for estimation are discrete (Zhou et al., 2013).

All filtering algorithms use state estimation models, which are introduced in this section. We know that the simulation model may be different from the estimation model, simulation model is for mimicking system behaviours while an estimation model is for estimating states.

3.5.2 Simulation Results and Discussions for Power System DSE

Simulation Data for Preliminary Studies with Existing KF methods

PowerWorld Simulator (powerWorld ver22, 2021) is chosen to produce simulation data in order to simulate the responses of a real system. The Single machine infinite bus (SMIB) test system is shown in Fig. 3.16 and IEEE 9-bus Test System is shown in Fig. 3.17, are used to produce the dynamic responses of the system for the three-phase fault.

In SMIB test system, a fault occurs at bus-3 at a time instant of 1 s and the fault is cleared by removing the line 1-3 and line 2-3 at 1.3 s. In IEEE 9-bus test system, a fault occurs at bus-8 at a time instant of 1 s and the fault is cleared by removing line 7-8 and line 8-9 at 1.3s. The simulation time step is set to 0.001 s to capture the dynamics and minimise integration errors. The main parameters of the simulated generators in SMIB and IEEE 9-bus test systems are tabulated as Table 6.12 and Table 6.13 in Appendices G and H.

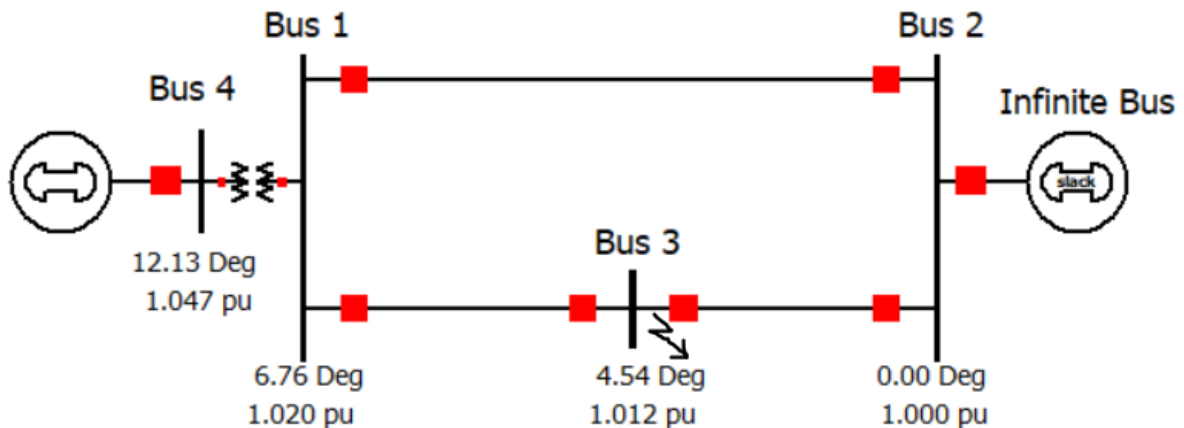


Figure 3.16: SMIB test system simulated in PowerWorld

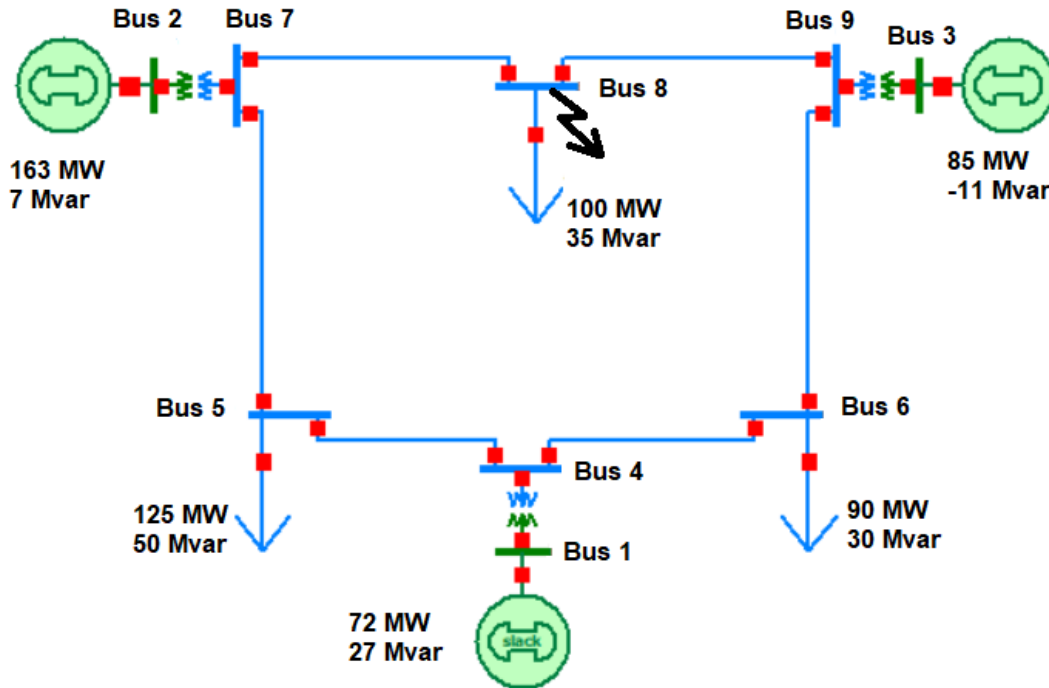


Figure 3.17: IEEE 9-bus system simulated in PowerWorld

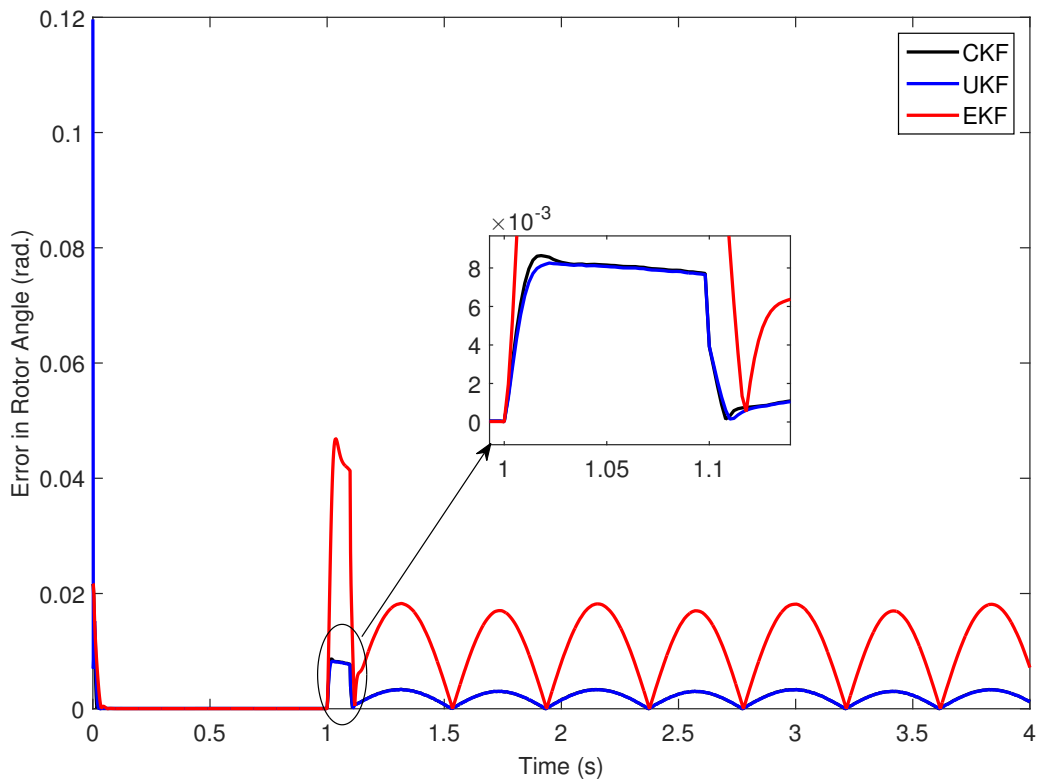
Assume that all of the buses have PMUs to calculate the voltage and current phasors. The machine responses are down-sampled to a rate of 25 samples per second to replicate the measurements from PMUs. White noises are applied to the device responses to imitate measurement noise, according to IEEE Standard C37.118-2005 (Martin, 2008). Algorithms based on Kalman filter approaches are coded for performing the estimation of dynamic states of generator.

Case Studies Using Existing KF based Methods

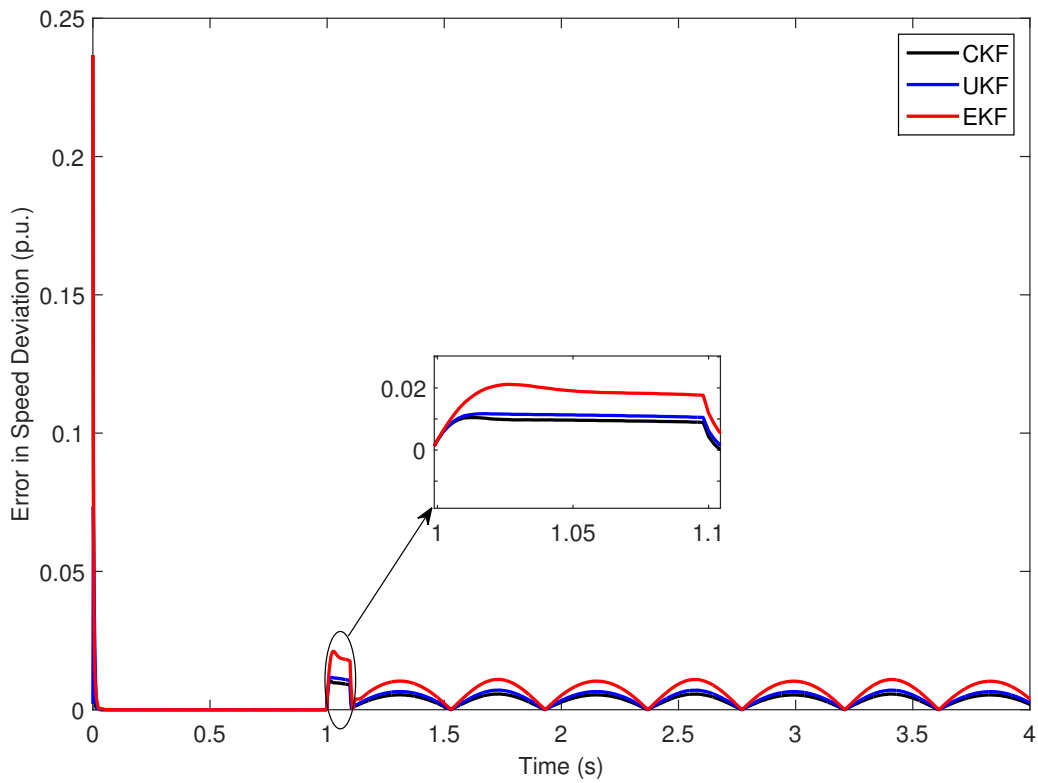
Dynamic simulation studies are performed in this section to compare the performances of the EKF, UKF, and CKF to estimate the dynamic states of a power system.

Case-1

A basic scenario is set up for comparison. For all the algorithms, the initial states are set as $\hat{x} = 0$ in (3.42). Initial covariance P_0 is set to be $10^{-3} \times I$. Measurement and process noise covariance are considered as $R = 0.001 \times I$ and $Q = 0.01 \times I$, respectively for this study. To evaluate the influence of the measurement sampling rate on estimation accuracy of all these algorithms, 100 and 1000 samples/s have been used for testing these algorithms.

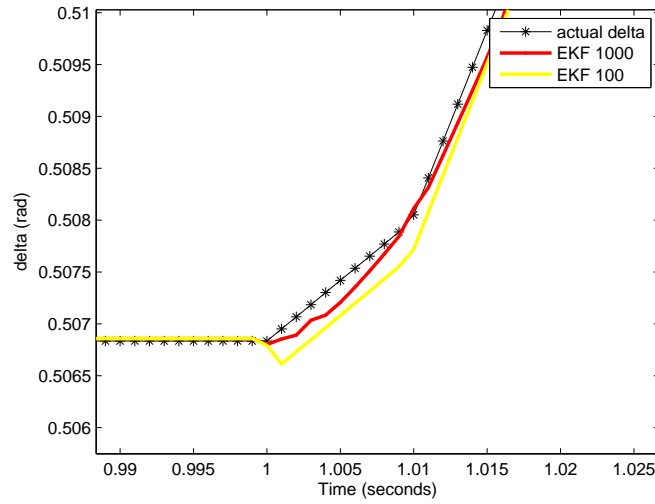


(a) Error in rotor angle

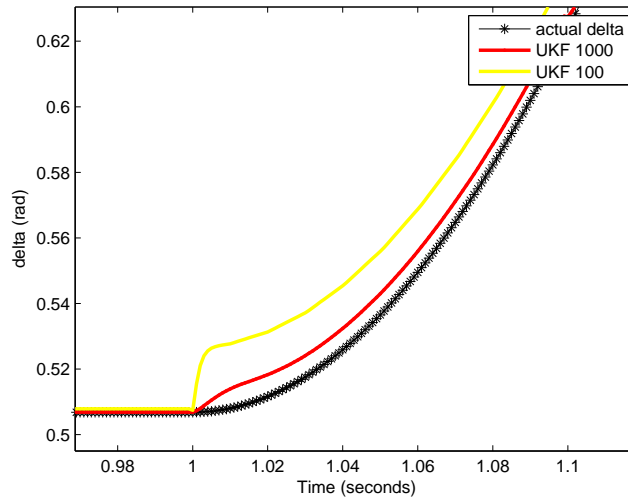


(b) Error in speed deviation

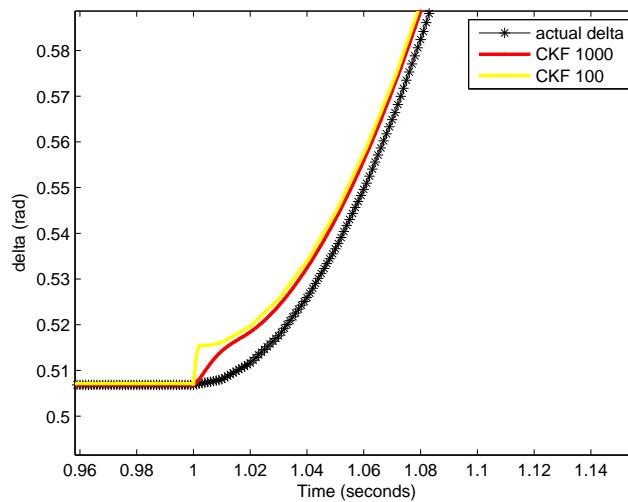
Figure 3.18: The error plots in estimated states at bus-4 for SMIB system under Case-1



(a) Rotor angle plots with EKF

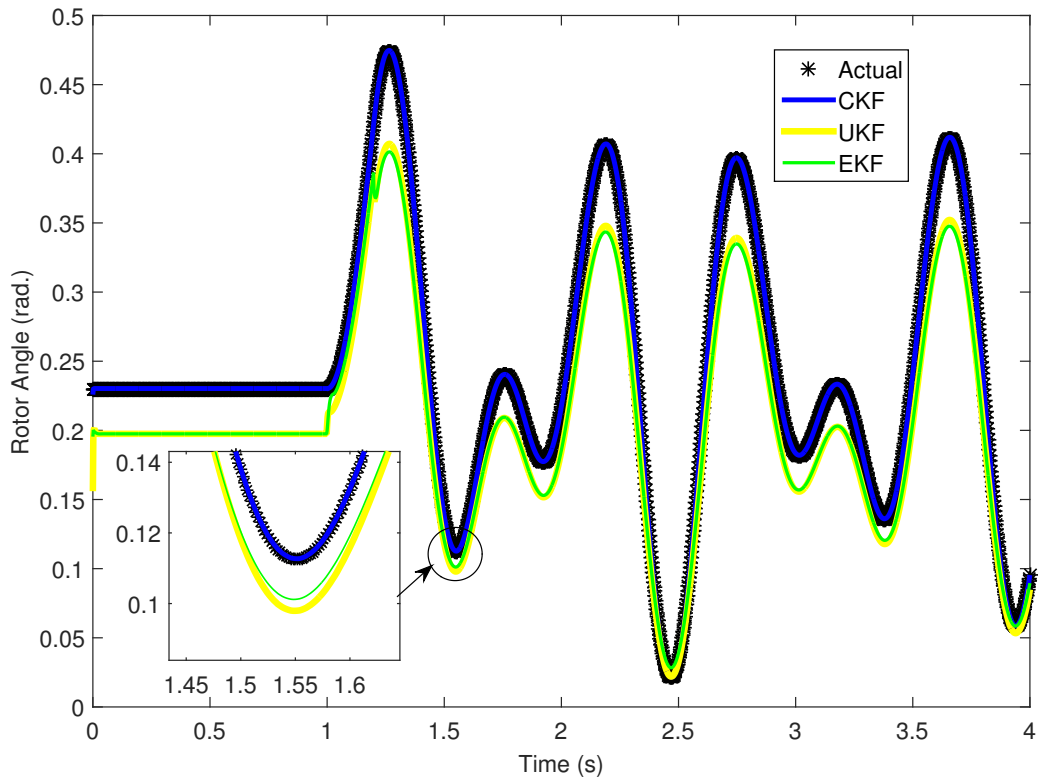


(b) Rotor angle plots with UKF

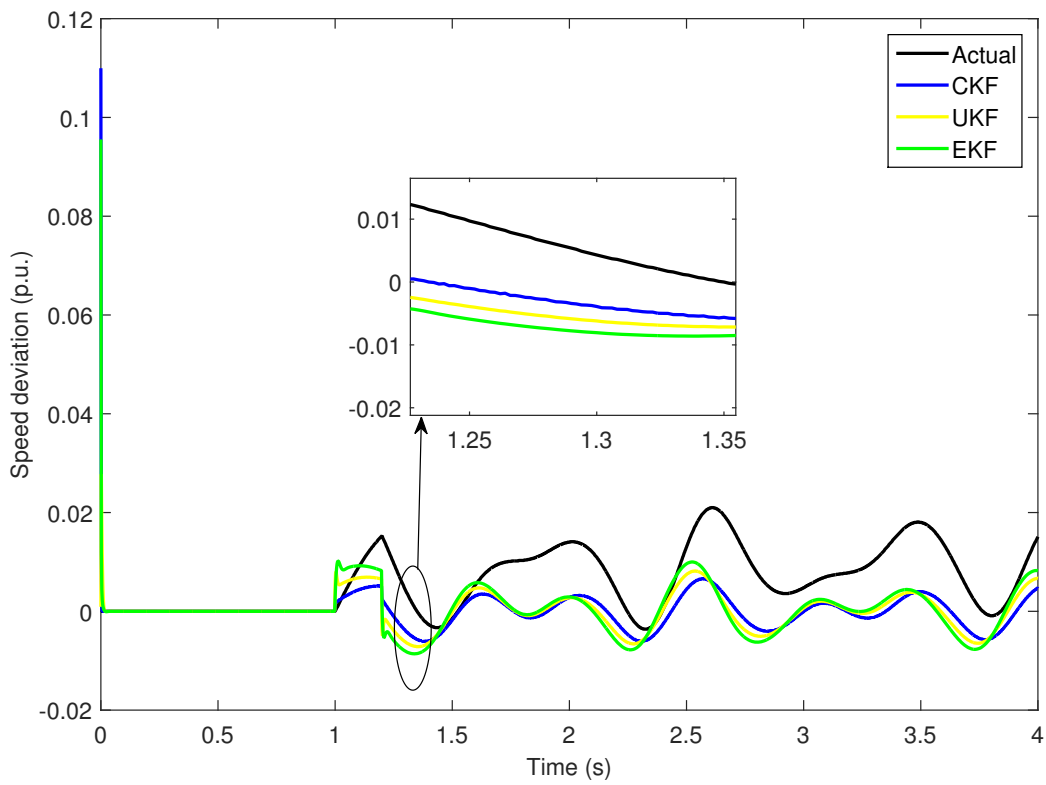


(c) Rotor angle plots with CKF

Figure 3.19: The estimated rotor angle at bus-4 for SMIB using EKF, UKF and CKF with 100 and 1000 samples under Case-1

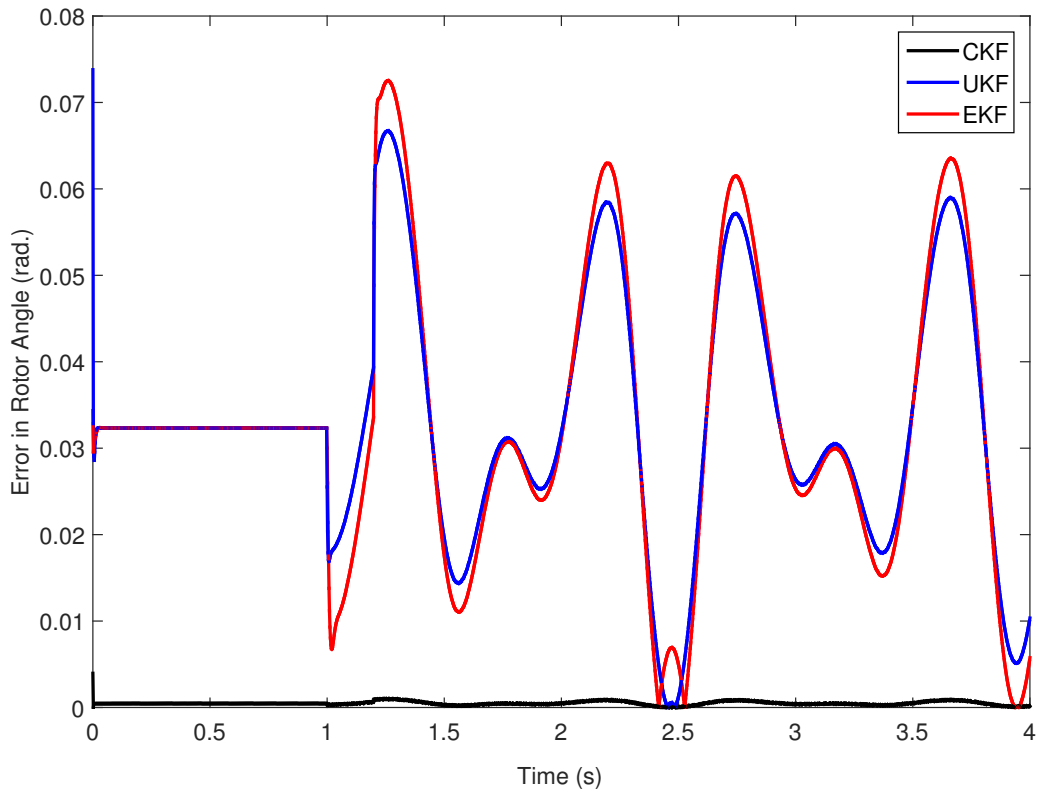


(a) Rotor angle

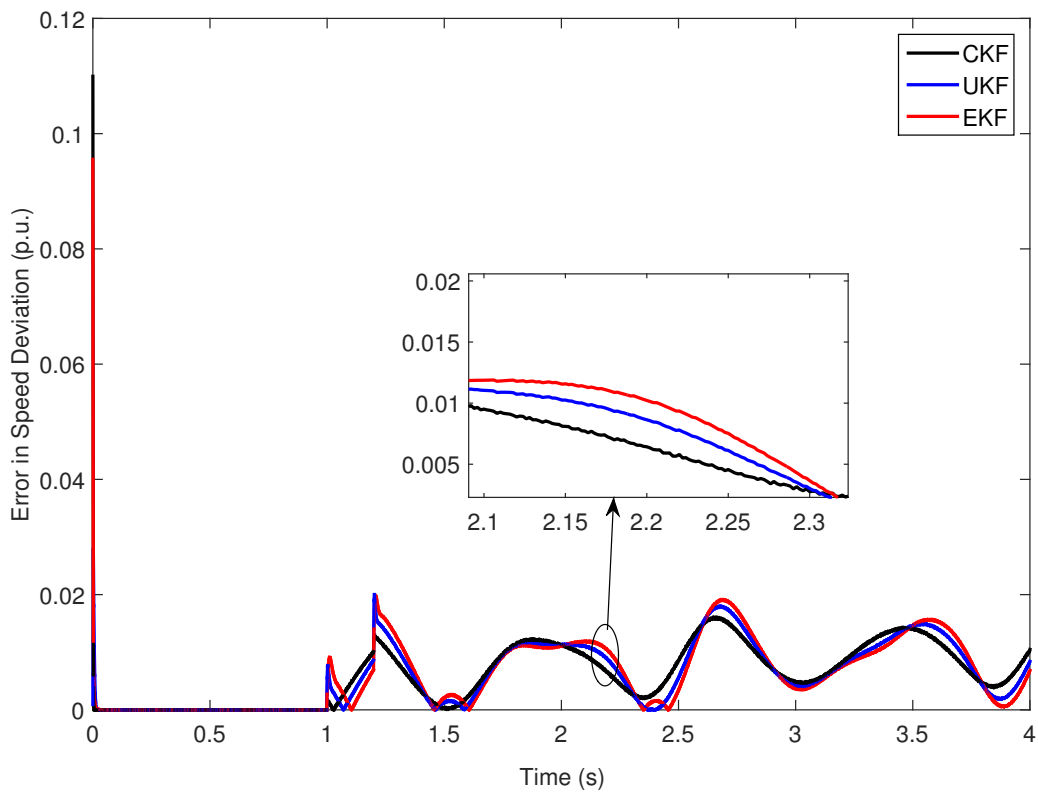


(b) Speed deviation

Figure 3.20: The estimated states for IEEE 9-bus system at bus-3 under Case-1



(a) Error in rotor angle



(b) Error in speed deviation

Figure 3.21: The error plots in estimated states for IEEE 9-bus system at bus-3 under Case-1

In the Fig. 3.19, it can be shown that with a higher measurement sampling rate, the filtering algorithms produce more accurate results. As a result, adding further measurements boosts the efficient sampling rate thus lowering linearisation errors. By using linear interpolation to incorporate additional pseudo measurements for every two measurement points, the sampling rate is increased from 25 to 500 samples per second. As a consequence of the interpolation, the sampling time interval t is reduced from 40ms to 2ms. The process noise covariance Q is then reduced to 1/20 of its original value. The R remains the same. The simulation results for the main states, the error plots in rotor angle and speed deviation of the generator are presented in Fig. 3.18 for the SMIB system. It can be observed that the estimated states using CKF converges to the actual values with the least errors as compared to the EKF and UKF.

The main states of synchronous generator at the bus-3 (See Fig. 3.17) of the IEEE 9-bus test system are shown in Fig. 3.20 and the corresponding error plots are shown in Fig. 3.21. It is observed from the result plots that the CKF is more accurate.

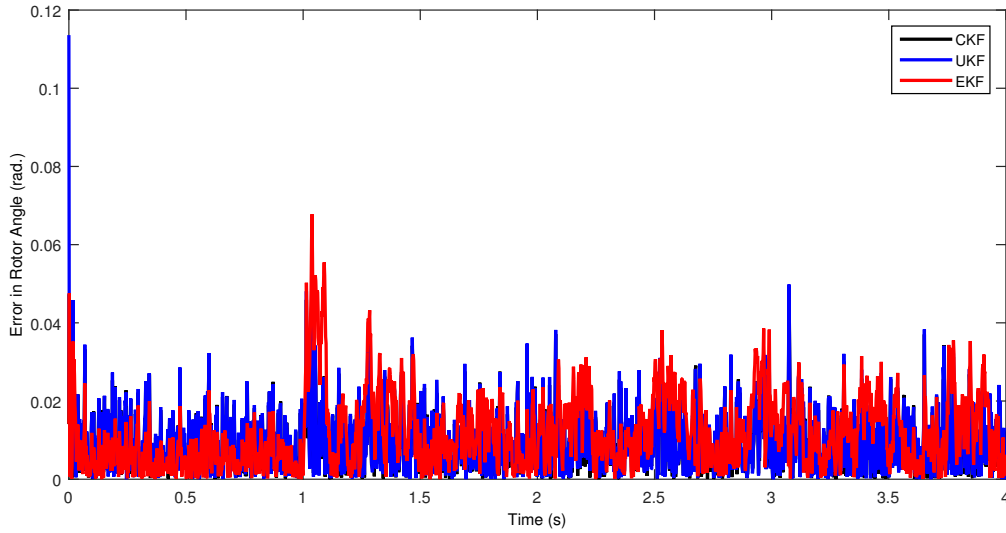
Case-2

The aim is to simulate the more practical situation, in which a readily available model is often a simplified representation of a real system. To account for transformer noise, measurement noise has been introduced. For the PMU measurements, The voltage and current phasor measurements are simulated by adding 5% measurement noise to their actual values. Additional noise has been applied to account for measurement noise introduced by current and potential transformers. The rest of the setup for all of the algorithms is identical to Section 3.5.2.

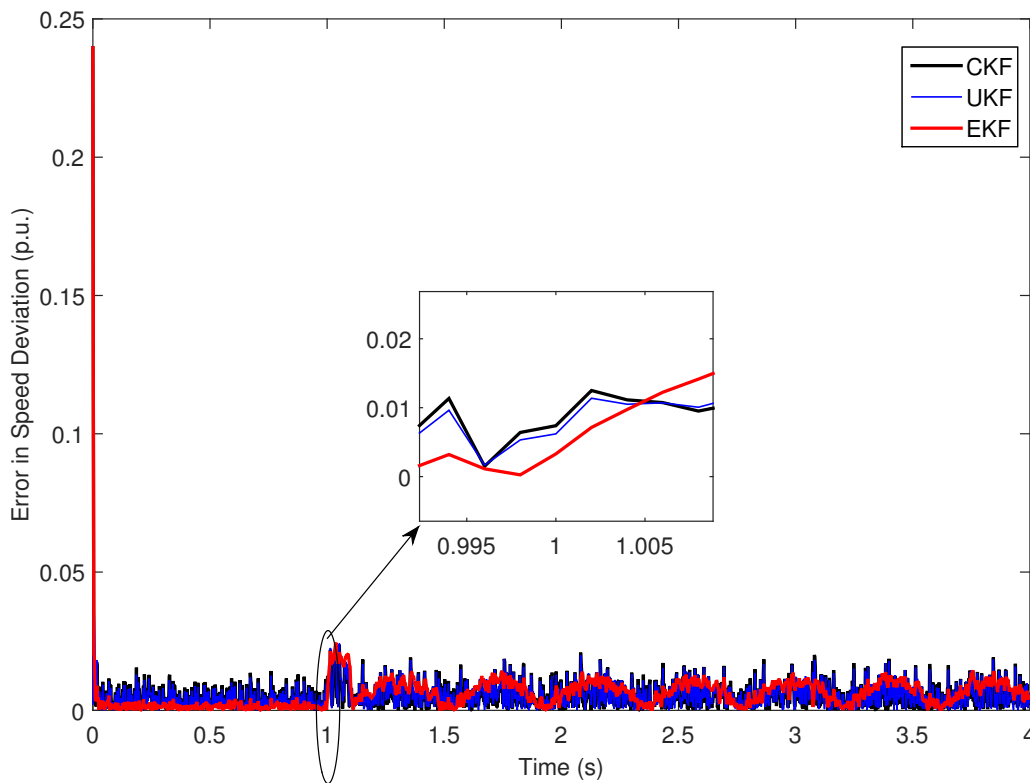
The estimation errors for SMIB system using EKF, UKF and CKF are shown in Fig. 3.22. Under Case-2 with the explicitly added measurement noise as discussed in section 3.5.2, the error plots in the estimated states of generator at bus-4 (See Fig. 3.16) for SMIB test system are shown in Fig. 3.22a and Fig. 3.22b. The mean of absolute errors in estimated rotor angle and speed deviation using CKF, UKF and EKF are shown in Table 4.3. From this table, it can be observed that the MAE in rotor angle is 0.0091 rad. which is 2.15% less than that of using UKF and 22.22% less than that of using EKF, and the MAE in speed deviation using CKF is 0.0055 p.u. which is 3.50% less than that of using UKF and 9.83% less than that of using EKF.

The estimation errors for IEEE 9-bus system using EKF, UKF and CKF are shown in Fig. 3.23. The MAE in estimations obtained using CKF, UKF and EKF are tabulated in Table 4.4. From this table, it is observed that MAE in rotor angle using CKF is 0.0074 rad. which is 77.57% less than that of using UKF and 77.64% less than that of using EKF. The MAE in speed deviation using CKF is 0.0069 p.u. which is 54.3% and 58.43% less than that of using UKF and EKF algorithms respectively. The results shows that

the CKF is more robust to the measurement noises in the model than EKF and UKF algorithms.

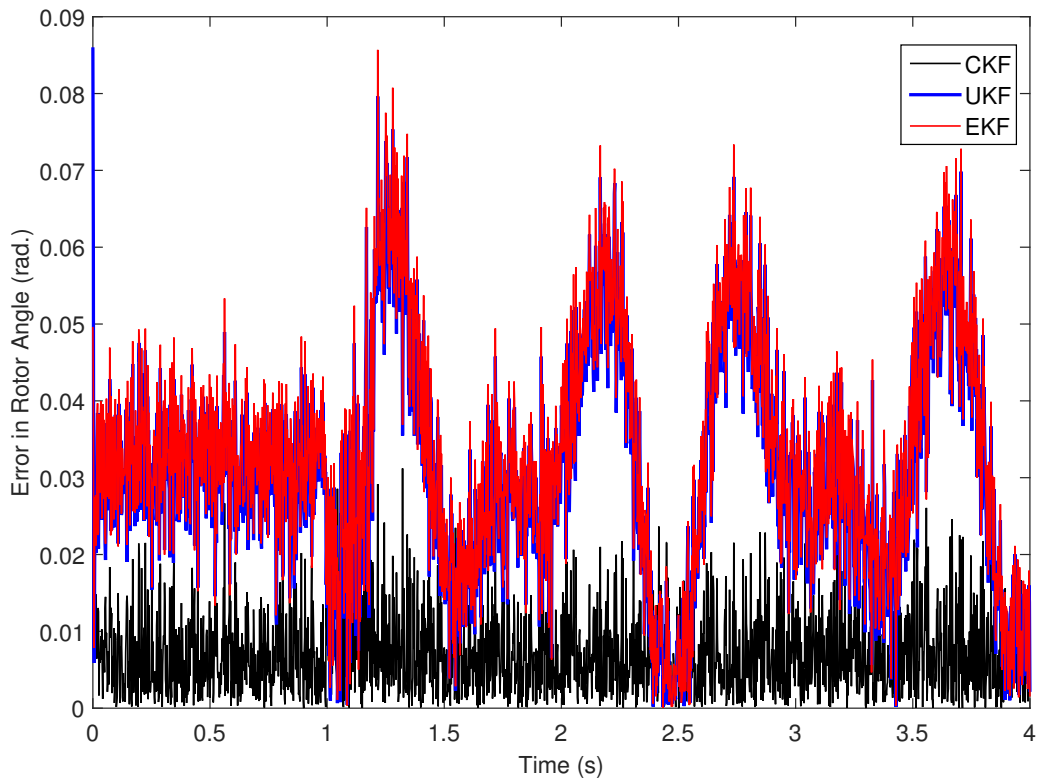


(a) Error in rotor angle at bus-4

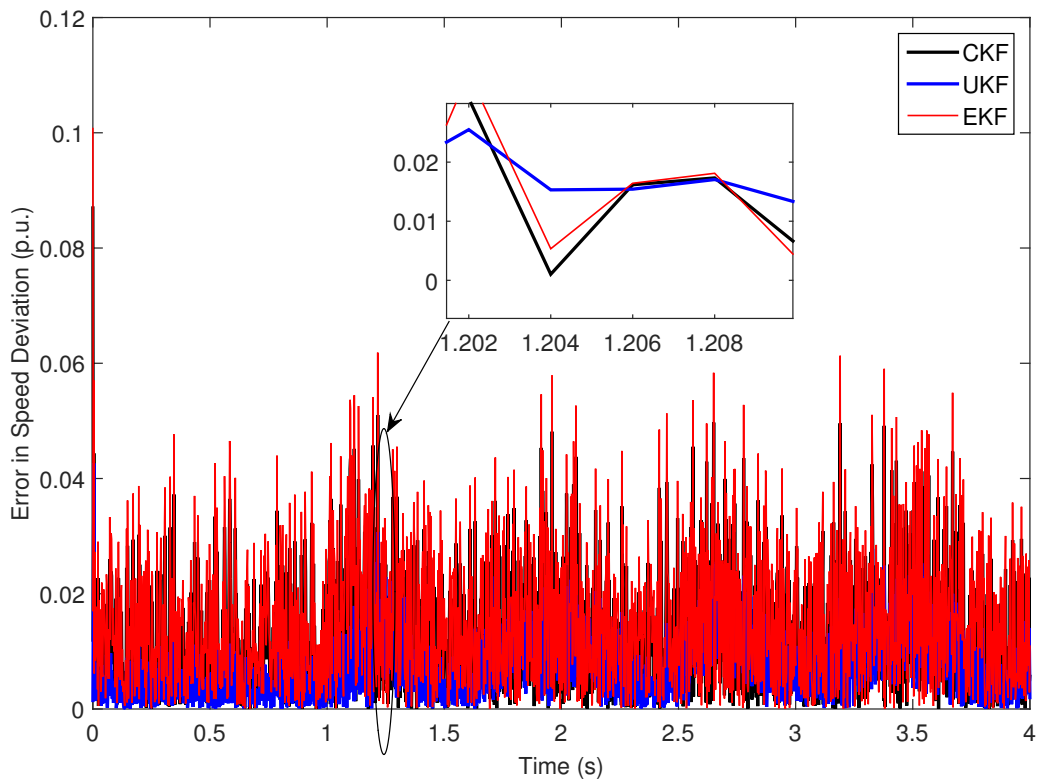


(b) Error in speed deviation at bus-4

Figure 3.22: The error plots in estimated states at bus-4 for the SMIB under Case-2



(a) Error in rotor angle at bus-3



(b) Error in speed deviation at bus-3

Figure 3.23: Error plots in estimated states for IEEE 9-bus test system at bus-3 under Case-2

Table 3.3: Mean of Absolute Errors (MAE) in the Estimated States at bus-4 for SMIB test system under Case-2

	MAE in Rotor Angle (rad.)	MAE in Speed Deviation (p.u.)
CKF	0.0091	0.0055
UKF	0.0093	0.0057
EKF	0.0117	0.0061

Table 3.4: Mean of Absolute Errors (MAE) in the Estimated States at bus-3 for IEEE 9-bus test system under Case-2

	MAE in Rotor Angle (rad.)	MAE in Speed Deviation (p.u.)
CKF	0.0074	0.0069
UKF	0.0330	0.0151
EKF	0.0331	0.0166

Conclusions for the Preliminary Studies with Existing KF-based methods EKF, UKF and CKF

The different Bayesian-based DSE methods are discussed by providing an overview of EKF, UKF, and CKF. On a SMIB and IEEE 9-bus test system, the proposed methods have been thoroughly tested. The CKF has the highest precision and is more resistant to practical measurement noise levels in the model, as shown. The strengths and limitations of EKF, UKF, and CKF estimation algorithms for power system DSE are summarised based on theoretical capabilities and simulation performance.

Case Studies Using Proposed ISCKF Method

To demonstrate the validity and reliability of the proposed algorithm, in this section ISCKF is proposed to be used for DSE for the test systems considered in the subsequent subsections. The estimator algorithm ISCKF is coded in MATLAB© R2015a platform and run on Windows 10 with Intel core i5 with 8GB RAM.

Some initial parameters are defined as follows: the covariance of state process noise Q is a diagonal matrix $[10^{-6}, 10^{-2}]$, the covariance of the measurement noise $R = 0.001$, the initial states $\hat{x} = 0$, initial covariance $P_0 = 10^{-3} \times I$. Here I is the identity matrix of size $n_x \times n_x$. The internal iteration number N for ISCKF is set as 5. All the simulation data for state estimation is generated at 25 samples/s to mimic the PMU sampling rate. Adding further measurements boosts the efficient sampling rate thus lowering linearisation errors

(Akhlaghi et al., 2016). By using linear interpolation to incorporate additional pseudo measurements for every two measurement points, the sampling rate is increased from 25 to 1000 samples per second. As a consequence of the interpolation, the sampling time interval Δt is reduced from 40 ms to 1 ms. To simulate the more practical situation, a measurement noise is added to the simulated data. For the PMU measurements, 5 % of measurement noise is added to the voltage and current phasors. The measurement noise includes the noises introduced by PMU device, current transformers and potential transformers.

SMIB

A simplified equivalent model of a general power system which is a single generator connected through a transformer and parallel transmission lines to an infinite bus is simulated in PowerWorld Simulator (powerWorld ver22, 2021). The PowerWorld schematic of SMIB is given in Fig. 3.24. The main parameters of the system are provided in Table 6.12 of Appendix G with $P_{base} = 100$ MVA.

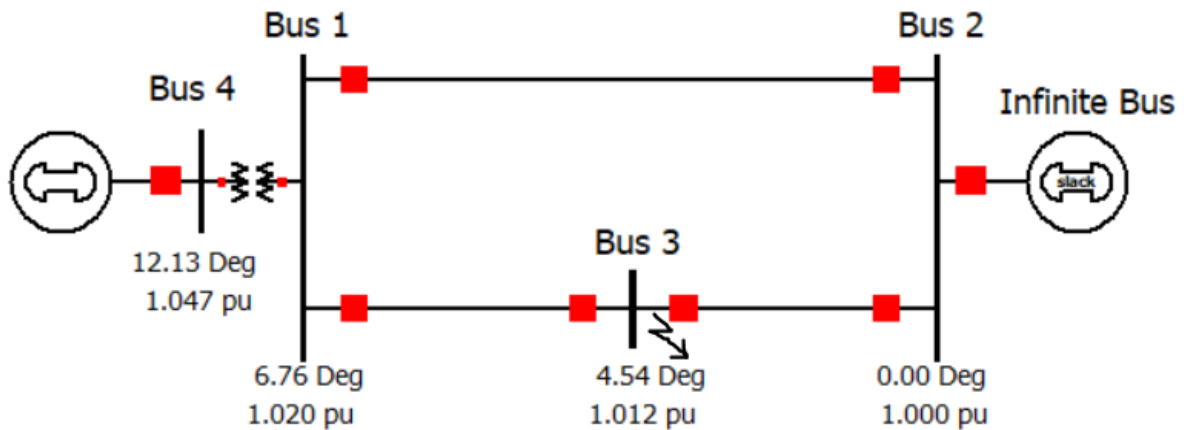
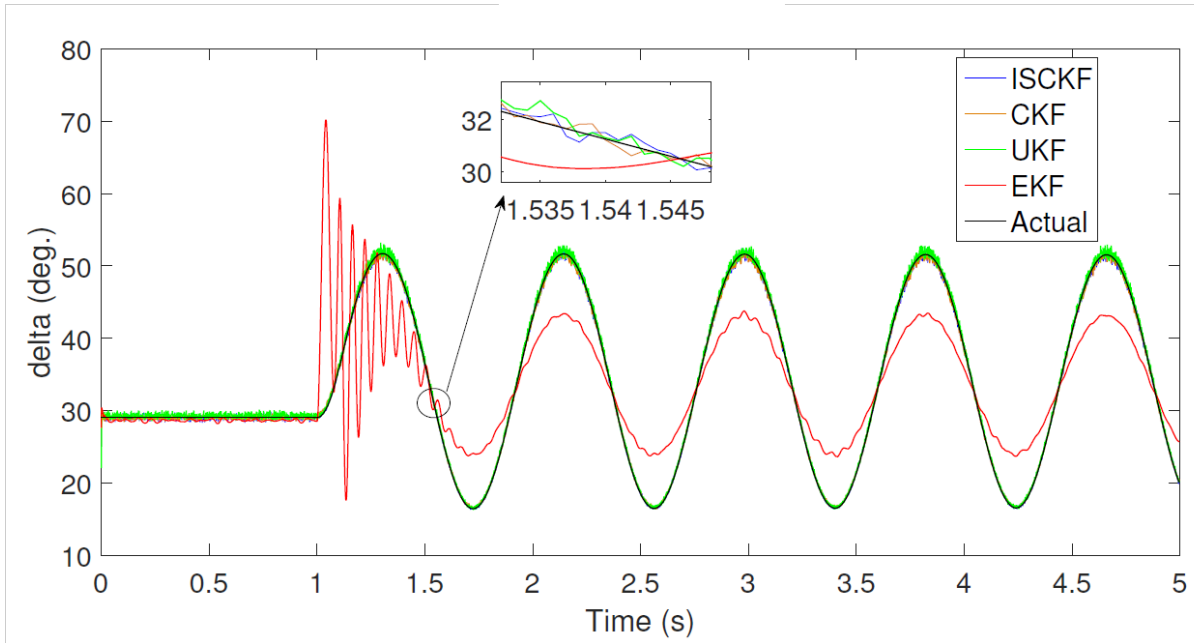


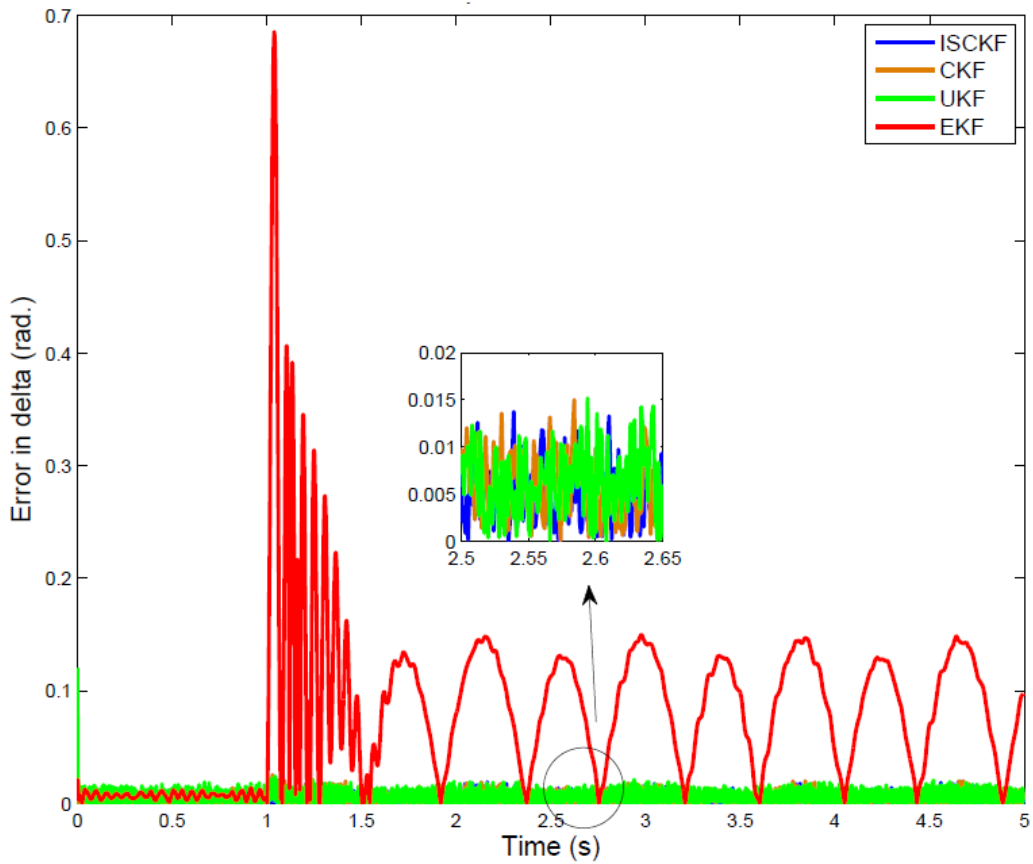
Figure 3.24: SMIB test system simulated in PowerWorld

The simulation scenario is a symmetrical permanent three-phase-to-ground bolted short circuit fault added to bus-3 at 1 s and cleared by removing the line 1-3 and line 2-3 at 1.3 s. Assuming the PMU is placed at the main generator. The simulation data of the main generator and bus is taken from the PowerWorld Simulator (powerWorld ver22, 2021). The simulation results for the main states, rotor angle and rotor speed deviation of the main generator estimated using ISCKF are compared with EKF, UKF and CKF are presented in Fig. 3.25 and Fig. 3.26 respectively.

From the Fig. 3.25b and 3.26b, ISCKF is giving least error. The mean of absolute errors in the states and the estimation time per iteration are listed in the Table 3.5. From these results, it is observed that by using ISCKF, the accuracy in rotor angle estimation

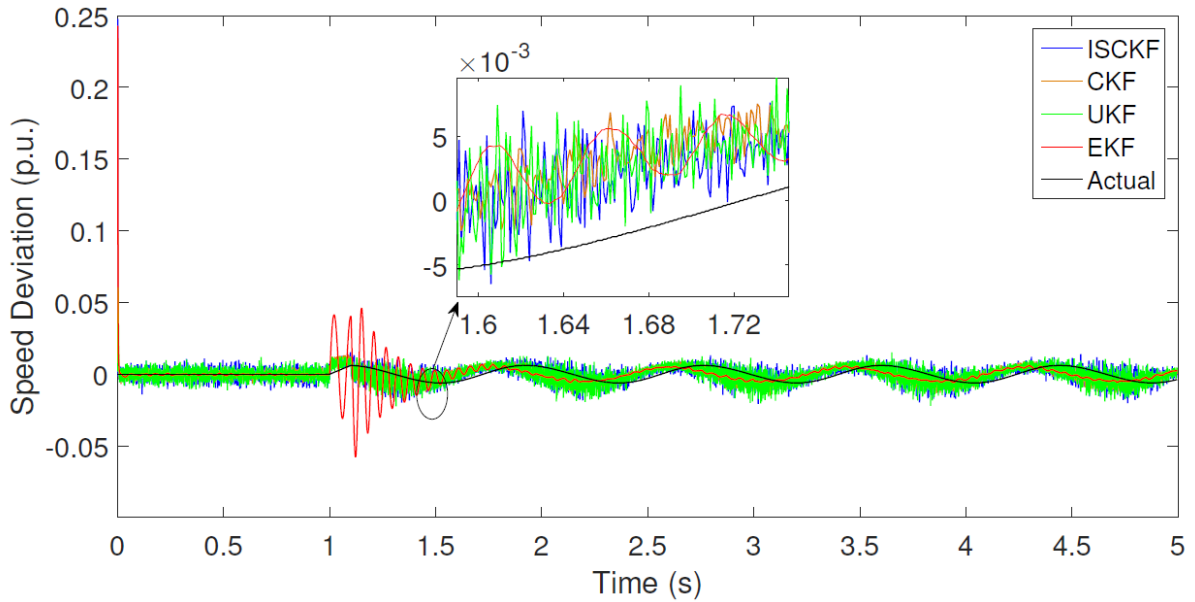


(a) Rotor angle plots

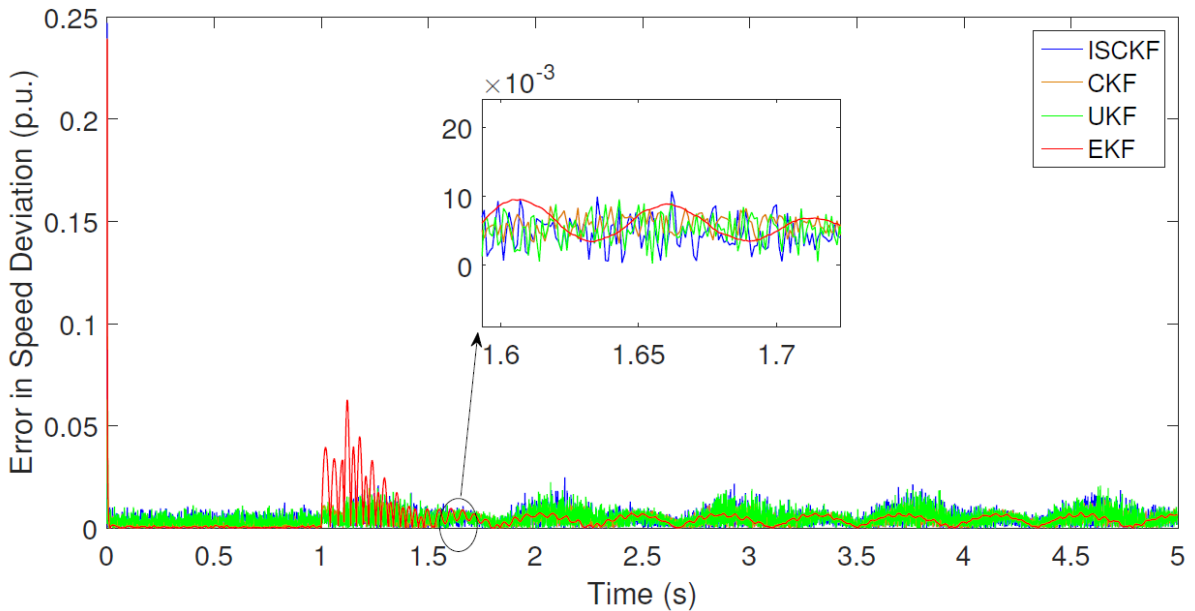


(b) Error in rotor angle

Figure 3.25: The estimated rotor angle and error plots at main generator bus-4 for SMIB



(a) Speed deviation plots



(b) Error in speed deviation

Figure 3.26: The estimated speed deviation and error plots at bus-4 for SMIB

Table 3.5: Mean of Absolute Errors (MAE) in the Estimated States at bus-4 using SMIB test system

	MAE in Rotor Angle (rad.)	MAE in Speed Deviation (p.u.)	Estimation time per iteration (ms)
ISCKF	0.0041	0.0043	0.30
CKF	0.0044	0.0045	0.08
UKF	0.0060	0.0046	0.09
EKF	0.0801	0.0048	0.03

has increased by 6.82% and in speed deviation the estimation accuracy has increased by 4.44% that of CKF. The percentage increase in accuracy is calculated as follows:

$$\frac{\text{MAE}_{ISCKF} - \text{MAE}_{CKF}}{\text{MAE}_{CKF}} \times 100 \quad (3.49)$$

Here, MAE (mean of absolute errors) is either with respect to rotor angle or rotor speed deviation of all the generators. And the estimation time per iteration is within the time next set of measurements arrive, that is 1 ms for all the 4 types of estimators.

IEEE 9-bus System

The case study is carried out on IEEE 9-bus system shown in Fig. 3.27. All generators are represented by the classical model of the synchronous generator as explained in Section 5.2. The first step for transient stability analysis of a multi-machine system is to find the initial conditions of the generators and buses. The steady state voltages and angles of the buses can be easily obtained by power flow solution. These steady state values are taken as initial conditions along with the main parameters of the generators (Refer Appendix H) for the simulation in Power World simulator.

The fault scenario considered for this case is a balanced three-phase to ground fault on Bus-8 at $t=1$ s which is cleared at $t=1.1$ s by removing the lines 7-8 and line 9-8 . The PMU sampling rate of 25 samples per second is used in simulation data and linear interpolation is used to increase the effective sampling rate to 1000 samples per second.

For comparison of the ISCKF with EKF, UKF and CKF the estimation results of rotor angle, speed deviation and the corresponding error plots at generator bus-2 are given in Fig. 3.28 and Fig. 3.29. The mean of absolute errors in the estimated states and the estimation time per iteration and the estimation time per iteration are listed in Table 3.6.

From the results and the mean of absolute errors, it can be observed that the MAE in rotor angle estimation using ISCKF is 0.0019 rad., which is 13.64% less than that of

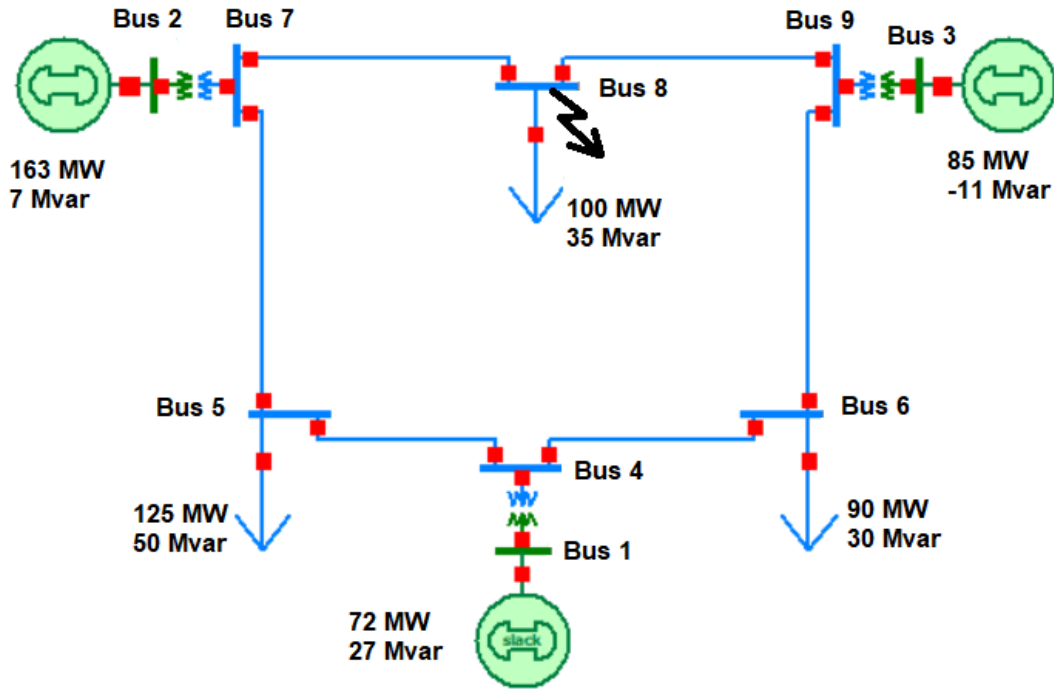
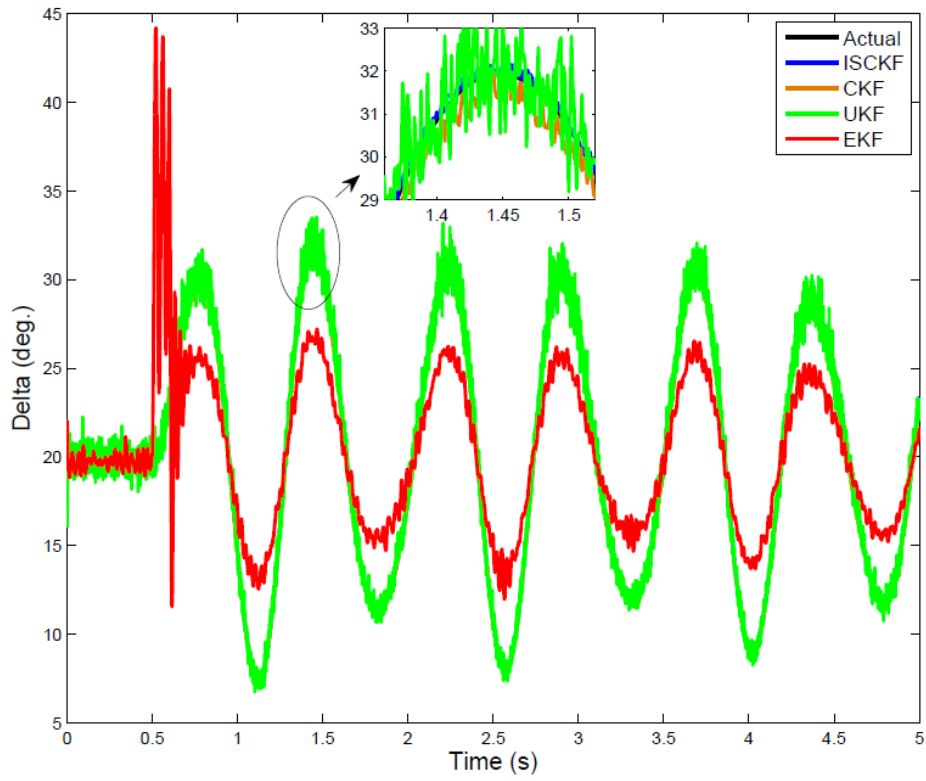


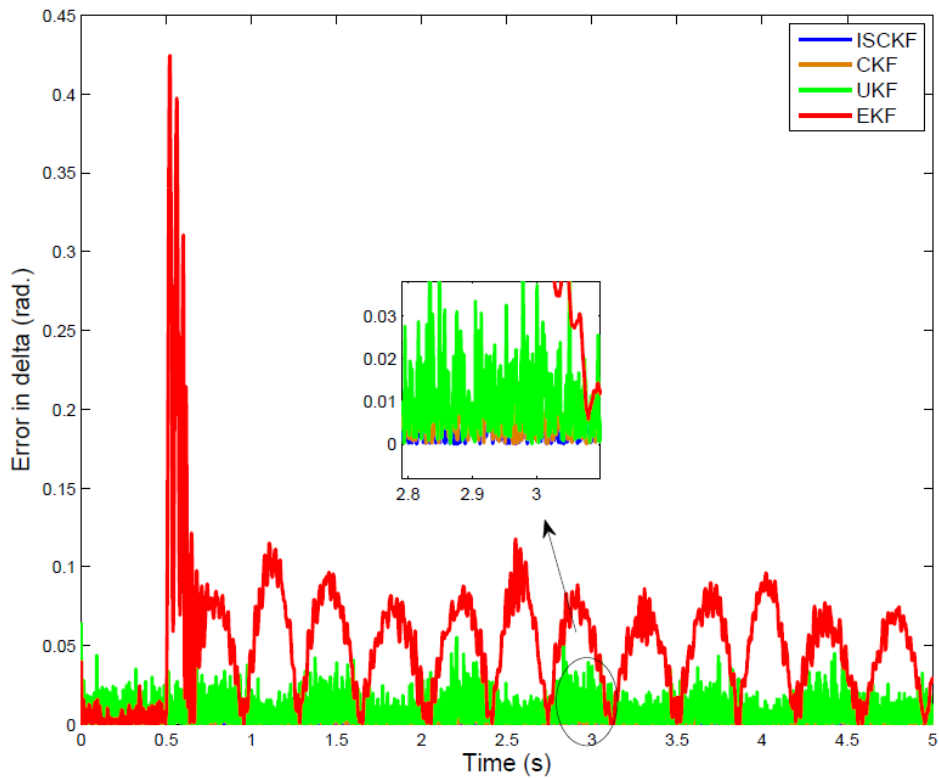
Figure 3.27: IEEE 9-bus system simulated in PowerWorld

Table 3.6: Mean of Absolute Errors (MAE) in the Estimated States at all generator buses in IEEE 9-bus system

	MAE in Rotor Angle (rad.)	MAE in Speed Deviation (p.u.)	Estimation time per iteration (ms)
ISCKF	0.0019	0.0088	0.80
CKF	0.0022	0.0097	0.30
UKF	0.0026	0.0098	0.20
EKF	0.0025	0.0102	0.06

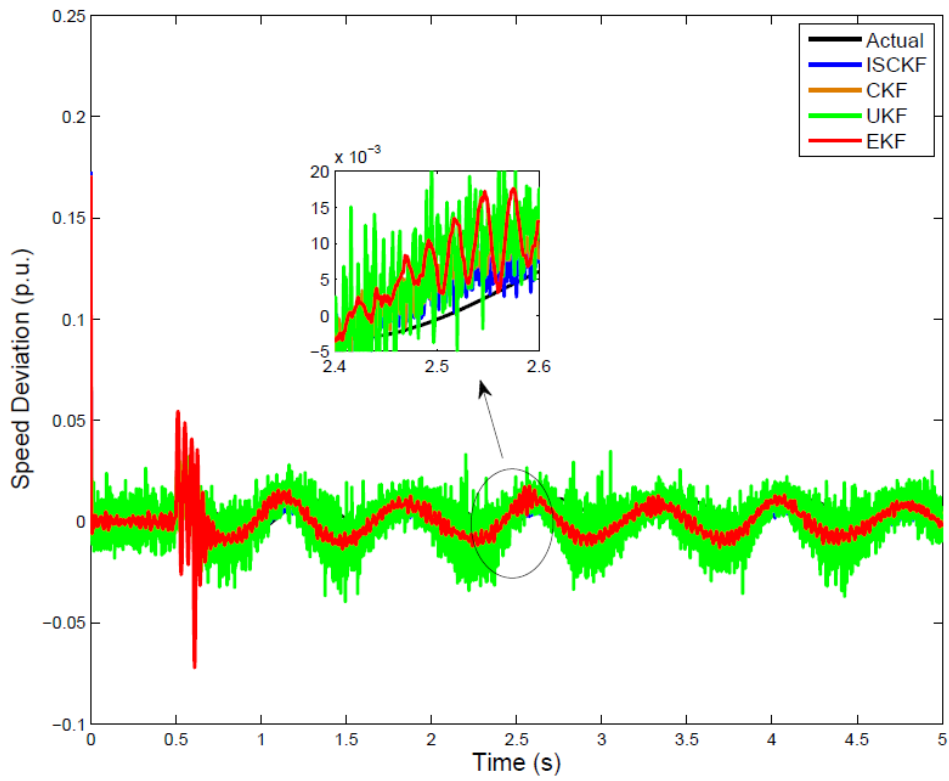


(a) Rotor angle

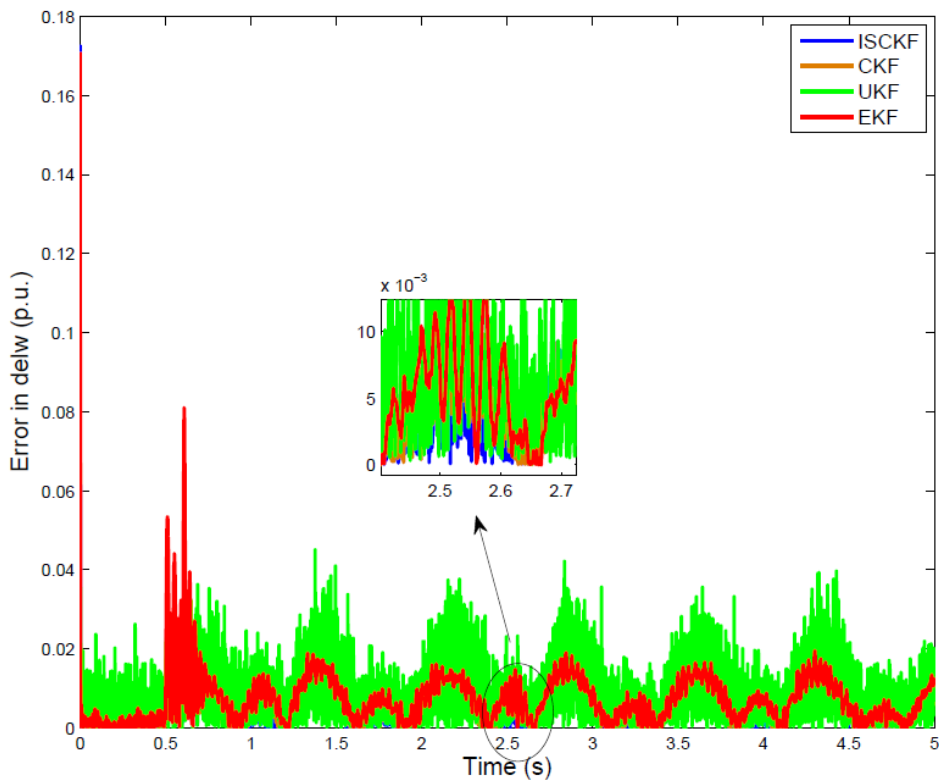


(b) Error in rotor angle

Figure 3.28: The estimated rotor angle and absolute error plots at generator bus-2 for IEEE 9-bus system



(a) Speed deviation



(b) Error in speed deviation

Figure 3.29: The estimated speed deviation and absolute error plots at generator bus-2 for IEEE 9-bus system

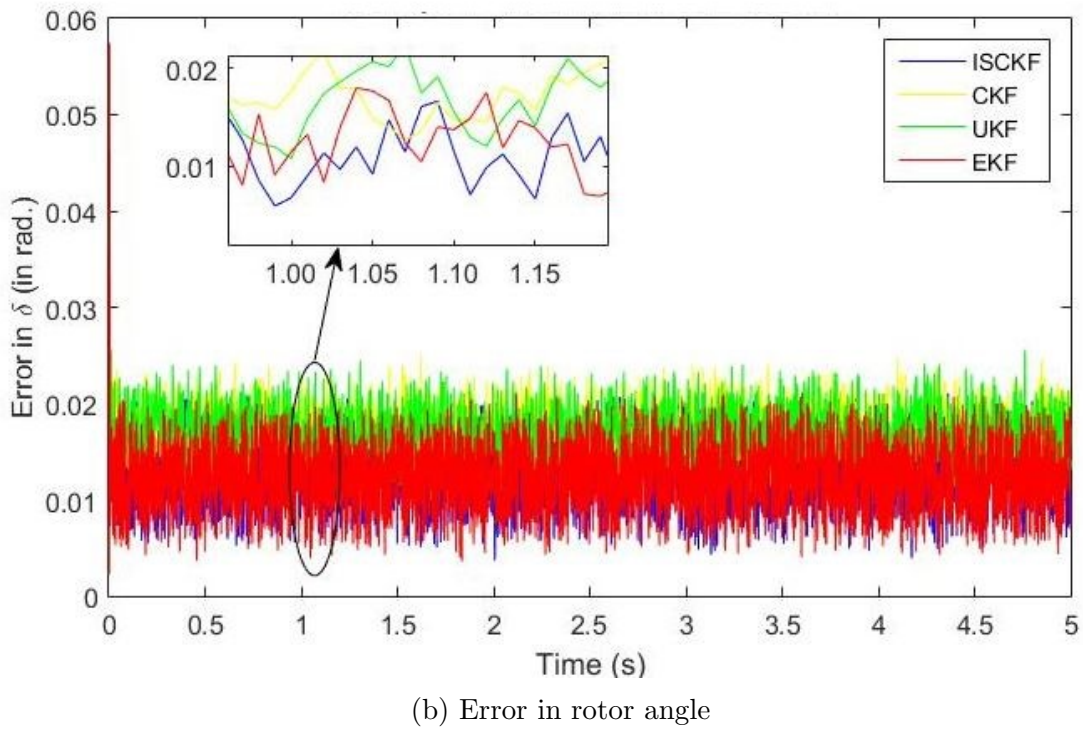
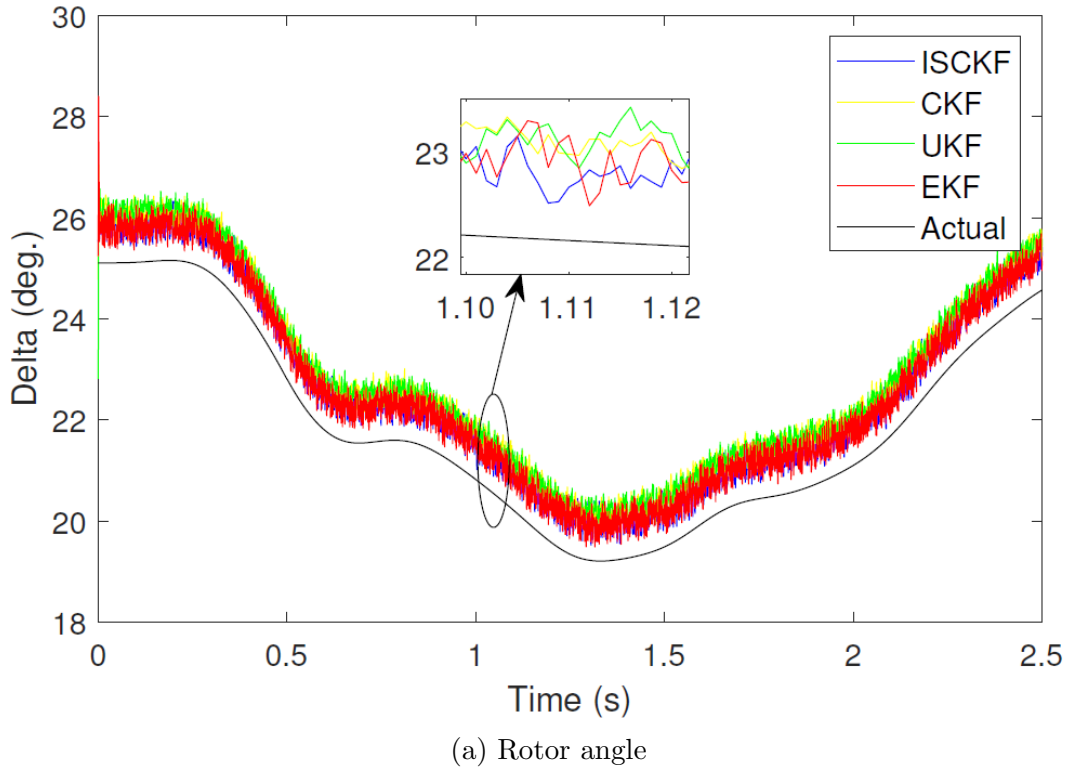
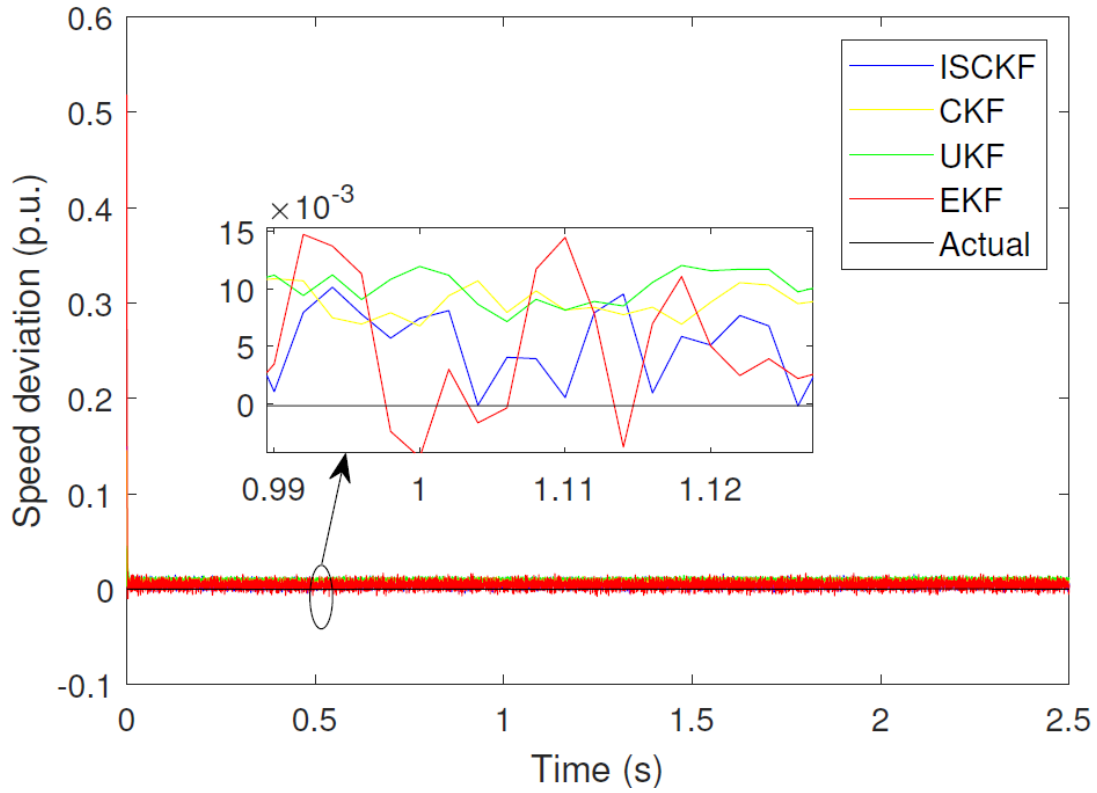
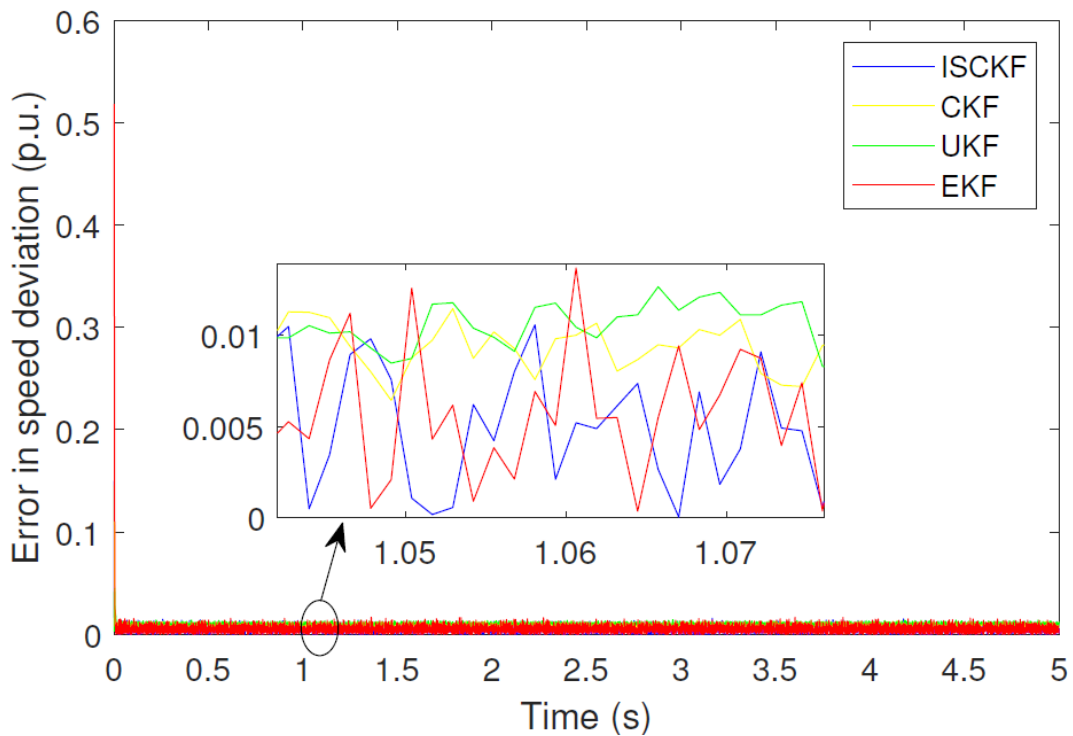


Figure 3.30: The rotor angle and error plots at generator bus-6 in 19-gen 42-bus test system



(a) Speed deviation



(b) Error in speed deviation

Figure 3.31: The estimated speed deviation and error plots at generator bus-6 in 19-gen 42-bus test system

using CKF. The MAE in speed deviation is 0.0088 p.u, which is 9.28% less than that of using CKF. ISCKF is proved to be more accurate for the state estimation in the multi-machine system as well. And the estimation time per iteration is within the time next set of measurements arrive, that is 1 ms for all the 4 types of estimators.

19-Generator 42-Bus Test System

The 19-generator 42-bus test system data is generated using the existing script files "case19l" and "s_simu" in *psdat* and *pstv2* folders of Power System toolbox version 2 (Sauer et al., 2017). MATLAB© R2015a platform is used to run and generate the data for state estimation. The system details utilized from "case19l" script file are provided in Appendix I. The simulation scenario is a three-phase fault applies at bus-30 at 1.0 s and is cleared by removing the line at 1.1 s. For simulation, the sampling time is taken as

Table 3.7: Mean of Absolute Error (MAE) in the Estimated States of all generator buses of 42-bus test system (Measurement data: 1000 samples/s)

	MAE in Rotor Angle (rad.)	MAE in Speed Deviation (p.u.)	Estimation time per iteration (ms)
ISCKF	0.0036	0.0047	3.1
CKF	0.0051	0.0061	1.8
UKF	0.0050	0.0070	1.8
EKF	0.1845	0.0052	0.5

Table 3.8: Mean of Absolute Error (MAE) in the Estimated States of all generator buses of 42-bus test system (Measurement data: 250 samples/s)

	MAE in Rotor Angle (rad.)	MAE in Speed Deviation (p.u.)	Estimation time per iteration (ms)
ISCKF	0.0033	0.0045	3.7
CKF	0.0052	0.0063	1.6
UKF	0.0051	0.0070	1.7
EKF	0.1525	0.0108	0.5

typical PMU reporting rate 25 samples per second linearly interpolated to 1000 samples per second as considered in previous system simulations. As a consequence of the interpolation, the sampling time interval Δt for the input and measurement data is reduced from 40 ms to 1 ms. From the tabulated errors in the Table 3.7, it is observed that by using ISCKF, the accuracy in the rotor angle estimations is increased by 29.41% and the accuracy in the speed deviation estimation has increased by 22.95% than that obtained by CKF. But, it has been observed that the estimation time per iteration is exceeding 1

ms for ISCKF, CKF and UKF estimators (See Table 3.7). That is, the estimation is not being performed before the arrival of next set of measurements. For this larger system, as the estimation process involves large number of variables, a trade-off has to be made between the samples per second of measurement data and the number of variables in the estimation process. The only part which can be modified is samples per second of measurement data, by using down-sampling technique. Hence, 250 samples per second is chosen, to make the estimation process feasible within the arrival time of next set of measurement, by interpolating 25 samples per second to 250 samples per second. Also, the number of internal iterations count N of ISCKF has been reduced to 3 instead of 5 (which has been used in smaller systems discussed in previous sub-sections). Now, the results after these changes are noted in Table 3.8 showing that the estimation time per iteration is within 4 ms for all types of estimators. Thus, can be implemented for real-time online DSE. Further if the measurement data are considered at the rate 250 samples per second (See Table 3.8), the accuracy of state estimations by ISCKF is the best among all. The accuracy in the rotor angle estimations by ISCKF is increased by 36.54% than that of CKF. While the accuracy in the speed deviation estimation by ISCKF has increased by 28.57% than that of CKF. The estimation results obtained at generator bus-6 with 250 samples per second input and measurement data is shown in Fig. 3.30 and Fig. 3.31. The mean of the absolute errors in estimation of states at all the generator buses using different filters is tabulated in the Table 3.8.

When the results of Tables 3.5, 3.6 and 3.7 are compared, it can be observed that with increase in number of generator buses from 1 to 19 in the system, though the computational time increases almost linearly, the MAE is almost the same and hence estimation accuracy is consistently good.

Since the proposed method has repetitive iterations within the state update step, the computational time is higher than the other methods as observed in Tables 3.5, 3.6 and 3.7. But the accuracy is improved significantly and hence is advantageous. The increase in estimation time for the first two test system SMIB system and IEEE 9-bus system is well within the arrival time of next set of data and hence does not adversely affect the estimator performance.

3.6 Summary

Dynamic system modelling and state estimation is necessary for optimal control of complicated systems. Beside the noise rejection capability, an estimator uses the state space model of a system to provide information about the states of the system which are in some cases immeasurable. In this study, the mathematical state space modelling is utilized for dynamic state estimation using non-linear Kalman Filters. Preliminary studies are car-

ried out for speed estimation process of an induction motor using the existing Extended, Unscented and Cubature Kalman filter versions. The simulation results of this section shows the capability of the proposed approaches to estimate the speed optimally even with the added noisy measurements. Further, classical model of the synchronous generator are used to model single machine infinite bus system and then large multi-machine power systems (such as IEEE 9-bus and 19-generator 42-bus test systems). Iterated square-root cubature Kalman filter (ISCKF) based state observer design is proposed for the dynamic state estimation of rotor angle and speed of synchronous machines in power systems. Theoretically, ISCKF approach eliminates the hazardous situation of the loss of positive definiteness of error covariance matrix in each update step which can stop the UKF and CKF from running continuously. Through the simulation studies carried out during a three-phase short circuit fault, the performance comparison of ISCKF is carried out with the existing methods such as EKF, UKF and CKF. It is clearly evident that the accuracy of state estimations is improved greatly when compared to that of EKF, UKF and CKF. At the measurement data rate of 250 samples per second, the estimation time per iteration is within the time 4 ms, i.e., before the next set of measurements arrives. Therefore, it can be implemented for online dynamic state estimation for synchronous machines in a power system. For smaller systems such as SMIB and IEEE 9-bus systems, higher sampling rate of 1000 samples per second for measurement data, further improves the accuracy of estimation.

Chapter 4

A New Technique for Major Event Detection in Power Systems using PMU Data

This chapter presents a robust and efficient framework for the detection and localization of events in large power systems using the real time measurements from phasor measurement units (PMUs). In contrast to the already existing methods proposing fixed thresholds with a Strongest Signal First Detection (SSFD) mechanism, the proposed approach analyses PMU data from multiple locations and breaks down the data into multiple custom feature maps. These feature maps aid in parallel computing hence paving a way for higher computational efficiency in detection. Using these custom feature maps, the algorithm calculates various thresholds, limits and other parameters of the system by itself and dynamically varies them as it learns from the data. The algorithm involves 3 layers to event detection in order to avoid false positives even if the hyper parameters are set incorrectly by an operator. This in turn leads to a robust algorithm which can work well for a large variety of systems. The effectiveness of the proposed method is exhaustively verified using the data provided by National Load Dispatch Center (NLDC) and compared with results obtained by methods used by National Renewable Energy Laboratory (NREL). On proper selection of hyper parameters, the detections occur within 40 ms. Detection of major events are exact without any false positives or false negatives.

¹Based on the contribution work presented in this chapter, an Indian patent entitled *Method and System for Major Event Detection in a Power System* has been granted. (29th September 2022)

²Based on the preliminary case studies carried out in this chapter, a paper entitled *Case Studies of Event Detection for Indian Power System using Signal Processing Methods* has been published in Proceedings of IEEE 31st Australian Universities Power Engineering Conference, 2021

4.1 Introduction

Modern power system handles a massive amount of energy with the increasing demands of an ever-expanding grid. There have been rigorous research and developments to improve the system reliability to supply the consumers with quality power having no or minimal interruptions. So it is an implicit requirement to make the system reliable and resilient to system faults. A powerful and quick fault detection technique would help the protection system and the operators to take necessary remedial actions as early as possible.

The faults in the power network can be varied categories and sizes. Some disturbances may be caused by normal operating conditions, and some noises in the equipment and measurement devices. These should not be considered as they do not cause significant losses to the generation authorities. On the other hand, major fault disturbances such as line trips, generation, load losses, etc., must be identified immediately. Then proper corrective actions need to be taken to avoid cascading failures and extreme case of a blackout.

To set up a fault event detection system, an efficient measurement system should be in place to gather the data from different locations. The advanced synchrophasor technology comes to the rescue by providing GPS time-stamped electrical data. The challenge of analyzing data streams from PMUs is taken up. It is known that the PMU easily captures the system events due to its high reporting rates, typically 25 samples per second when compared to the SCADA measurement system, which recorded data only every 2-4 seconds. Detection of events from the signals is not the only parameter to be considered, but along with that it is crucial to understand the information contained in detection and how the detection contributes towards situational awareness of the grid. Instead of detecting based on Strongest signal first detection principle (SSFD) (Biswal et al., 2016), it is essential to gather an idea of operating characteristics of all the PMUs in relation to the PMU which detects the fault. To judge the grid operating conditions, there is an inherent need to measure the state variables of the system. The state variables such as voltage, current, real and reactive powers can be directly measured with the help of PMUs in recent times. Due to its ability to collect time-synchronized data with a high sampling rate, it provides a deeper insight into the operations of the power system.

A case study on Texas Synchronous network is discussed based on relative phase angle difference (RPAD) and frequency signals from 6 substation PMUs (Allen et al., 2013, 2014). Multiple graph signal processing methods such as fast fourier transform, Yule Walker, Min-Max, Matrix Pencil methods are used for event detection as discussed in the National Renewable Energy Laboratory (NREL) report (Allen et al., 2014). And strongest signal first detection (SSFD) mechanism is used. When two or more methods detect event based on their corresponding fixed threshold comparisons, it is classified as

event. But, precision of event detected is only in the range of 10 seconds. Suppose an event is detected at 500 seconds, this implies actual event between 490 and 510 seconds.

The first category of techniques explored in the literature for event detection is time-frequency transform methods. [Dahal and Brahma \(2012\)](#); [Dahal et al. \(2013\)](#) carried out early event detection techniques based on principal component analysis. [Dahal et al. \(2013\)](#) explored the comprehensive clustering of disturbance events recorded by PMU. Here, the features are extracted from disturbance file obtained from PDC. MVEE (Minimum Volume Enclosing Ellipsoid) method is used to extract features. Further, Agglomerative hierarchical clustering method is used to make clusters which is able to classify all the disturbance file into 19 clusters. Each cluster representing one class of fault. (Not all faults are known, hence every clustered is not named yet).

The second category of event detection techniques is based on statistical analysis. An ellipsoid method [\(Gajjar and Soman, 2014\)](#) is used for analysing frequency signal. A method of ellipsoids for auto detection of events is employed [\(Gajjar and Soman, 2014\)](#). To detect major events, perform the principal component analysis and error ellipsoid methods for frequency samples of duration of 5 s, 10 s and 20 s. Magnitude of error variances is compared to fixed threshold to identify event. Length of the minor axis of error ellipsoid when overshoots a fixed threshold helps identify as an event location. For small fault, just the 5 s batch detects event. While for major fault, all the three batches are triggered. Further, the event instance is identified later with 1 s precision using rate of change of frequency (ROCOF) data. ROCOF data is derived from f data by passing it through a finite impulse response (FIR) filter to remove noise. Then, Kalman filter is used to estimate the ROCOF data. The filtered ROCOF data is compared to a maximum of 0.005 or 10% of highest value of variance in data window already identified.

Data storage more reliably in a decentralized fashion with security using low-cost commodity hardware units (i.e., Hadoop clusters and Hadoop distributed file system) [\(Singh et al., 2019\)](#). Min-max method used - window frame is 300 samples - crossing a fixed threshold. Faults identified in the coarse duration with precision of ± 12 s (25 samples/s PMU data rate).

[Xie et al. \(2014\)](#) utilized various parameters such as Voltage, Current, Angle, Frequency measurements recorded by the PMUs across the Grid as valid input. Here, by exploring the dimensionality reduction of the PMU data, authors propose an early event detection algorithm, along with theoretical justifications, to detect power system events at an early stage.

[Negi et al. \(2017\)](#) utilizes phase angle, voltage and frequency signals of the system using PMU devices for event diagnosis. An improved kernel principal component analysis combined with support vector machine is used. Event detection scheme uses computation of spectral kurtosis on sum of intrinsic mode functions. The algorithm is capable of

detecting the event in PMU data by comparing the maximum energy and root-mean square of energy content of present analysis segment with respect to previous segment.

Event detection and its characterization is carried out using feature maps created from the frequency transforms (Time-frequency transforms) [Biswal et al. \(2016\)](#). SSFD (Strongest signal selection and fault detection) based on Voltage and Frequency signals from PMU data are given as input for analysis. Cumulative energy (CE) is calculated as summation of squared deviations from nominal base voltage for n samples after an event triggers. Highest CE valued signal is identified as SSFD. Further fault energy (FE) is determined as RMS value of negative deviations of n samples. FE value compared with fixed threshold is checked for a fault analysis window, which is incremented till maximum window is reached. Faults are identified within a maximum of 8 samples or 0.1333 s (for PMU refresh rate of 60 samples/s). At the end, a clear picture on what characteristics is expected from a system when abnormalities have occurred by using an Extreme Learning Machine the classification of faults takes place.

The third category of techniques explored is pattern recognition based. [Wang et al. \(2014\)](#) carried out the analysis with a nonnegative sparse event unmixing algorithm. Deep learning-based convolutional neural network technique ([Wang et al. 2020](#)) which works on the inputs rate of change of frequency and relative angle shift has been explored. Patent CN109787979B implements event detection using K-means algorithm. But these methods require a lot of training to perform well.

[Shi et al. \(2020\)](#) proposed an algorithm that can accurately capture and leverage the spatio-temporal correlations of the streaming PMU data. Streaming PMU Data consists of voltage and frequency of the system. This work also develops a general technique to decouple spatial and temporal correlations in multiple time series. Finally, a unique framework is developed to construct a weighted adjacency matrix and graph Laplacian for product graph.

Recent advances of deep learning is used to build a convolutional neural network model to detect events ([Wang et al. 2020](#)). Here, the rate of change of frequency and the relative angle shift are the inputs. This approach needs large amount of training data to work efficiently.

Apart from these categories, some literature works directly detect events from the PMU data signals. [Rasmussen and Jorgensen \(2006\)](#) presents one of the first Nordic applications of synchronized phasor measurements in monitoring power system oscillations during a tie-line switching. Here, the data from eastern Denmark power system are measured using PMU, that is, positive sequence voltage, frequency, etc. The synchronised voltage and current phasors are obtained every 20ms using Global Positioning Satellite (GPS) system. The case study demonstrates that direct observation of inter area oscillation modes using phasor measurements is more convenient than computation

of eigenvalues using a detailed model of a specific system configuration.

[Samuelsson et al. \(2006\)](#) is able to show the relation between fault at transmission and distribution level of power system. Lower voltage levels are used to identify power transmission dynamics. The data measured using PMU i.e., positive sequence voltage, frequency, etc. is directly used for identification with use of no algorithm.

Frequency disturbance recorder has been used to detect events from frequency variation with a specific limit ([Okumus and Nuroglu, 2018](#)). Frequency variation of every data sample between max and min > specified threshold - event is detected. The event type is classified using the correlation method.

Most of the works in literature do not explicitly consider the operating characteristics (P or Q) as inputs. This is influential as whenever there is event, each parameter exhibits different characteristics. That would lead to better event detections.

Patent US8457910B2 ([Muthu-Manivannan et al., 2013](#)) uses an electronic computing device and identifies power system event when one or more of the selection criteria based on some fixed thresholds are fulfilled. The selection criteria is based on computing resource constraints or based on known patterns or features. This method is for distribution system only and there is no mention of dynamic thresholds for the quantities. Since the data signal is directly taken from CT, PT and converted to digital using ADC, event identification might not be fast.

Patents US10324132B2 ([Saarinen et al., 2019](#)) and US8738191B2 focuses on line event detection. First method utilizes measured value (mainly fault current) from a power line with the help of intelligent electronic device (IED) connected to the power line and a processor linked to IED. While the second method uses Dynamic line rating (DLR) devices and additional phasor measurement units. Physical line data corresponding to thermal line limits is provided by DLR devices. The zone (adjacent and/or upstream monitoring zone) of occurrence of event is identified using two fixed thresholds.

Patent CA2508965A1 ([Roger, 2005](#)) is used for monitoring parameters in an electric power distribution system. This is carried out based on the input signals: voltage, current, total harmonic distortion in voltage, flicker and frequency. It defines two thresholds: first dynamic threshold which is three times the standard deviation and second dynamic threshold, that is, six times the standard deviation. The method generates a caution signal when measured value greater than or equal to first dynamic threshold. While an alarm is raised and an action is suggested when measured value greater than or equal to second threshold. Since the parameters are calculated from the measurements from CT, PT and not PMU device, it might involve some inherent delay. The dynamic threshold is generally based on weekly average till yearly average is obtained.

4.2 Objective and Contributions of this chapter

Objective: Event detection based on practical synchrophasor signals gathered by PMUs using an efficient and system-independent technique.

After carrying out the literature survey as elaborated in Section 1.3, this chapter presents a new technique for major event detection in power systems using dynamic thresholds and weighted sum abnormality. This helps in detection and localization of major events in large power systems using the real time measurements from PMUs. In contrast to the already existing methods which propose fixed thresholds with a Strongest Signal First Detection (SSFD) mechanism, the proposed approach analysis PMU data from multiple sources and breaks down the data into multiple custom feature maps. These feature maps aid in parallel computing hence paving a way for higher computational efficiency in detection. Using these custom feature maps the algorithm calculates various thresholds, limits and other parameters of the system by itself and dynamically varies them as it leans from the data. The algorithm also proposes 3 layers to event detection in order to avoid false positives even if the hyper parameters are set incorrectly by an operator. This in-turn leads to a robust algorithm which can work well for a large variety of systems. The proposed method is exhaustively verified using the PMU data provided by NLDC during "Amphan" cyclone recorded on 20th May 2022 (Allen et al., 2021).

4.3 A New Technique for Major Event Detection in Power Systems using a Data-Driven and Dynamic Thresholding Approach

There is a strong relation between advancement of a civilization and the amount of energy it controls. With an increase in energy demand, there comes an inherent need to control and properly distribute this energy through power grids. As the energy demand increases. the complexity and scale of power grids also increase. This leads to a need for efficient and robust power system fault detection algorithms. These algorithms are aimed at increasing reliability of very complex and large power grids.

To judge the grid operating conditions, there is an inherent need to measure the state variables of the system. These state variables are measured by using a Phasor Measurement Unit (PMU) in the present days. Due to its ability to collect time synchronized data with a high sampling rate, it provides a deeper insight into the operations of the power system.

Disturbances in a grid can be of varying magnitudes from small disturbances to large disturbances. Some disturbances can also be caused due to normal operation of the grid.

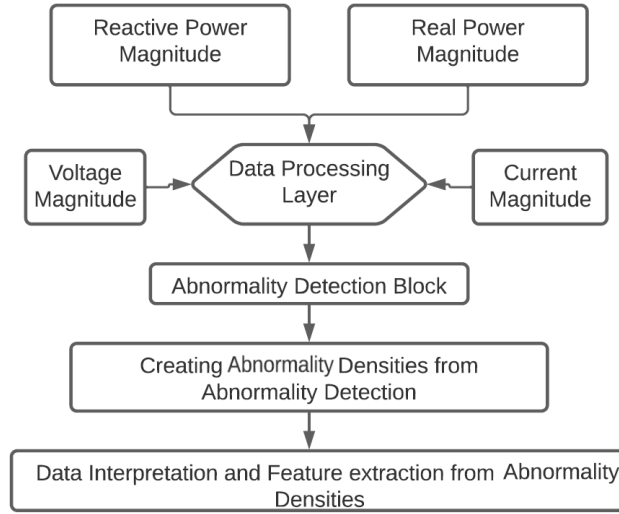


Figure 4.1: Flowchart of blocks inside event detection and processing of events

The recorded data from the PMU contains noise with the actual signal mainly due to environmental conditions during Amphan cyclone. The noise recorded by each PMU changes from one PMU to another. This variation depends on many factors including geographical location, environmental factors, grid topology and connectivity. It is difficult but not impossible to separate the dynamically changing noise from the actual true signal in order to avoid false positives and/or false negatives.

Detection of events is not the only parameter to be considered, rather it is important to understand the information content in detection and how the detection contributes towards situational awareness of the grid. Instead of detecting based on Strongest signal first detection principle (SSFD), it is important to gather an idea of operating characteristics of all the PMUs in relation to the PMU which detects the fault.

To overcome all these challenges, a robust and efficient schema is proposed, consisting of 3 levels in detection and refinement as shown below:

1. Abnormality Detection.
2. Generation of Weighted Sum Abnormality.
3. Post Processing layer for Weighted Sum Abnormality

A basic flowchart of the algorithm is shown in Fig. [4.1](#)

4.3.1 Windowing Schema for Abnormality Detection

Let there be M PMUs in a system, hence in a matrix there would be M columns. Let each column have N data points, hence the data matrix A would be of size $N \times M$.

A window $W_{threshold}$ is used for calculating the dynamic thresholds of Voltage, Current, Real Power and Reactive Power magnitudes while a window length of W_{Lbase} is used for calculating nominal magnitudes of the same. As the windows shift, new values of the thresholds and nominal magnitudes are calculated in order to dynamically learn the system behaviour. Let the $W_{threshold}$ be set to T data points and let W_{Lbase} be set to U data points.

The region of influence of windows $W_{threshold}$ and W_{Lbase} only depends on pos where pos denotes the present data position of analysis. The value of pos increments by one during every iteration. If pos is a multiple of T then the new region is assigned to $W_{threshold}$ is bounded by $pos - T$ to pos . Similarly when pos is a multiple of U the new region assigned to W_{Lbase} becomes $pos - U$ to pos .

The updation strategy for two more windows W_1 and W_2 are as shown below: Suppose a new data point has come from each of the M PMUs totalling $(N + 1)$ data points for M PMUs. Assuming a W_{max} as K , set the pos at $(N + 1)$ and lock the data-points from $(N + 1 - K)$ to $(N + 1)$ into W_1 . Initially setting for W_{cw} is 2. Define another smaller window W_2 inside the window W_1 , which has a size of W_{cw} taking the last element of W_1 as the pivot. Hence if $W_{cw}=2$ then W_2 will have data-points from $(N + 1 - W_{cw})$ to $(N + 1)$. Analyzing the data inside W_2 , on completion of analysis there can be increase in W_{cw} by $W_{cwincrement}$. Updating W_2 to a new window size of $(N + 1 - W_{cw} - W_{cwincrement})$ to $(N + 1)$, analyze this new window and repeat . Do the calculations until size of W_2 is less than W_1 , when size of W_2 becomes greater than W_1 , increase pos by 1 and repeat.

4.3.2 Abnormality Detection

An abnormality is any deviation from normal grid operation which may or may not be due to occurrence of an event. Different electrical quantities like Voltage, Current, Real Power and Reactive Power magnitudes will be at their normal operating conditions but whenever there is an abnormality or an event, each parameter exhibits different characteristics. The algorithm has been tested for all of the parameter variations and accounts for their different characteristics.

Taking the deviation from the mean gives a general idea of the variation in a particular parameter with respect to its nominal operating magnitude. For example, when there is an open circuit fault in a line, the voltage of the line rises while during a short circuit fault the voltage drops. Hence, both these variations can be captured if both $+ve$ or $-ve$ deviations are considered. The 4 different quantities to be judged for grid abnormalities are:

1. Voltage Magnitude (V)
2. Current Magnitude (I)

3. Real Power (P)

4. Reactive Power (Q)

In the discussion which follows, L can indicate in general for any of the quantities I , P , Q or V . $L_{magnitude}$ is the magnitude of anyone of these at a particular data point. The root mean square of the parameter in the window W_{Lbase} defined by L_{base} is as follows :

$$L_{base} = \frac{1}{W_{Lbase}} \sqrt{\sum_{k=1}^{W_{Lbase}} (L_{magnitude}(k))^2}$$

In further calculations, $L_{magnitude}$ refers to $L_{magnitude}$ values in the form of a matrix (size $W_2 \times M$) consisting of the data points within the window W_2 hence:

Suppose $J_{W_2 \times M}$ be a matrix consisting of ones with size $W_2 \times M$. Define a matrix $L_{basemat}$ having dimensions of $L_{magnitude}$ (that is, $W_2 \times M$) as follows :

$$L_{basemat} = L_{base} \times J_{W_2 \times M}$$

The deviation matrix D (size $W_2 \times M$) consisting of deviations of the data points in the window W_2 with respect to $L_{basemat}$ is calculated as follows :

$$D = |L_{magnitude} - L_{basemat}|$$

Root mean square of these deviations about their columns over the window W_2 is named as Fault Energy (FE) (matrix size $1 \times 4 \times M$):

$$FE(n) = \frac{1}{W_2} \sqrt{\sum_{k=1}^{W_2} (D(n, k))^2}$$

As FE are the RMS values, they are inherently normalized for any window length W_2 .

4.3.3 New Concept of Dynamic Thresholds

Let the number of FE data points associated with every data position pos be FE_{pos} .

$$FE_{pos} = \frac{(W_{max} - 2)}{W_{cwincrement}}$$

Store the FE that are obtained after every increment of pos , for a length of $W_{threshold}$ data-points, into a matrix FE_{mat} . Then use these values to find the thresholds. These thresholds are to be calculated whenever the region of the window $W_{threshold}$ changes according to the update rule defined in Section [4.3.1](#).

Hence, the total number of FE data points used for the calculation of thresholds is $FE_{pos} \times T$. Let this be denoted by FE_{posT} with matrix size $FE_{posT} \times M$. The FE data in itself contains the deviations of L . The normal deviation of FE with respect to its mean gives the expected deviation in FE .

Hence, using a simple thresholding technique leads to elimination of the noise components in FE. This is done by taking into consideration only those FE data which lie beyond a certain number of standard deviations from the mean. The number of standard deviations depends on a type number denoted by TN .

$$FE_{threshold} = mean(FE_{mat}) + TN \times \sigma(FE_{mat})$$

The mean and σ are taken about the columns hence both would have same matrix size $1 \times 4 \times M$.

There is a secondary layer of thresholds called the "Difference Thresholds". This secondary layer helps to check whether a particular FE of window length W_2 in consideration for abnormality has erratically changed from the previous FE of window length $W_2 - 1$. This is done by calculating the normal variations expected in the differences between FE of W_2 and FE of $W_2 - 1$ and comparing the calculated difference thresholds with the difference in FE for a particular data point.

For calculating the difference thresholds store the values of the differences in FE for W_2 and FE for $W_2 - 1$ in a matrix $FE_{matdiff}$ (size $FE_{posT} \times M$).

Using the same concept of mean and standard deviation we get $FE_{matdiffthreshold}$ (size $1 \times M$):

$$FE_{matdiffthreshold} = mean(FE_{matdiff}) + TN \times \sigma(FE_{matdiff})$$

4.3.4 Effect of Type Number TN

It can be observed that there is a great dependency for the detection of abnormalities on type-number. Wrongly choosing the type number TN of high value for a system can result in detection of major faults while ignoring the small and medium intensity faults. Whereas choosing a very low value of TN can result in false positives. To reduce the rate of false positives and false negatives there is a need for analysis of various values of type numbers.

Let the type number in consideration go from TN_{min} to TN_{max} . If the TN_{min} number is chosen too low there will be a high number of abnormality detection but these detections will include a lot of false positives. If the TN_{max} number is chosen too high then it will increase computation time as well as it will lead to increased chances of only highlighting major events.

4.3.5 Paralleling Abnormality Detection for Various Type Numbers

The basic concept is to eliminate additional loops in calculation of faults for varying values of type number TN . Hence, making it possible to get the abnormalities of 15 to

30 different types in one go with minimum impact on RAM utilization or CPU time.

The dimensions of matrices discussed in Section 4.3.2 will be changed as following:

$$D : size(W_2) \times M \times size(TN_{max} - TN_{min} + 1)$$

$$FE : size(TN_{max} - TN_{min} + 1) \times M$$

$$FE_{threshold} : size(TN_{max} - TN_{min} + 1) \times M$$

$$FE_{matdiffthreshold} : size(TN_{max} - TN_{min} + 1) \times M$$

4.3.6 Thresholding Logic

For each and every window W_2 , FE is calculated and compared to $FE_{threshold}$ of various types. Those FE values which overshoot $FE_{threshold}$ will be evaluated to 1 while others will be evaluated to 0, this is then stored in a matrix namely $D_{binaryFE}$ containing 1's and 0's. Now the difference between FE of window W_2 and FE of window $W_2 - 1$ is compared to $FE_{diffthreshold}$ and the values overshooting $FE_{diffthreshold}$ will be evaluated to 1 and the others are evaluated to 0. The same is stored in $D_{binaryFE_{diff}}$. Now a hadamard product of $D_{binaryFE}$ and $D_{binaryFE_{diff}}$ is calculated and stored in $D_{binaryProduct}$ containing 0's and 1's.

In $D_{binaryProduct}$ the positions having a one denotes an abnormality detection for that particular type and for that particular data point. The dimensions of this $D_{binaryProduct}$ will be $(TN_{max} - TN_{min} + 1) \times W_{cw}$.

The $D_{binaryProduct}$ consists of abnormality detection for each type for a particular position pos and for a particular input parameter. Storing these $D_{binaryProduct}$ for all 4 parameters and for multiple pos is required for efficient computation, this is stored in a F_{fault} with matrix size $Num_datapoints_considered \times (4 * M) \times (TN_{max} - TN_{min} + 1)$.

4.3.7 Weighted Sum Abnormality

There is a requirement to condense the information of abnormality detection into a graph which clearly shows regions in the data which have higher level of detection of an event. To do this, weights are assigned to detections corresponding to each TN . Using these weights a formulation of weighted sum abnormality graphs are created. These graphs show the intensity of an abnormality at a particular position. A lower TN has the highest number of detected abnormalities (which may or may not be true abnormalities) whereas when moving towards a higher TN , the number of detected abnormalities decreases (For higher TN , strong correlation is there between detected abnormalities and true abnormalities). Hence appropriately weighing these different types is essential. Major events have their presence in both lower as well as higher TN whereas minor events

have their presence only in the lower TN . Hence weights for the corresponding TN are considered to be linear and stored in *weights_of_type* matrix. That is lower weight for lower level and higher weight for higher levels.

Let this graph be plotted from a matrix namely $F_{faultDist}$ with size $Num_datapoints_considered \times (4 * M)$.

$$F_{faultDist}(i, j) = \sum_{k=TN_{min}}^{TN_{max}} (weights_of_type(k) * F_{fault}(i, j, k))$$

4.3.8 Post Processing Layer

$F_{faultDist}$ matrix contains the data for weighted sum abnormality for all parameters namely magnitudes of voltage (V), current (I), real power (P) and reactive power (Q). In order to not allow loss of information, all the 0 values in $F_{faultDist}$ is made 1. This helps to give a wider view during post processing as intersections of various level of detections are taken into account. Once this is done, normalize the $F_{faultDist}$ matrix by dividing it by the maximum value in the whole matrix (including all parameters V, I, P and Q). This type of normalization can be done due to the fact that while converting the various parameters to $F_{faultDist}$, there is an inherent projection of all the various parameters to the subspace. This is due to the fact that each parameter had its own dynamically varying threshold hence detection of abnormalities is performed on their corresponding thresholds.

$$F_{faultDist} = (F_{faultDist} / \max(\max(F_{faultDist})))$$

Hence all the data points would be between 0 and 1 with none of them being 0. From $F_{faultDist}$, extract the different level of detection: $V_{faultDist}$, $Q_{faultDist}$, $P_{faultDist}$ and $I_{faultDist}$.

With the normalized abnormality densities, find multiple fault parameters as shown below :

$$V_Q_faults = (V_{faultDist} \times Q_{faultDist})$$

$$P_I_faults = (P_{faultDist} \times I_{faultDist})$$

$$Major_faults = (V_Q_faults \times P_I_faults)$$

$$Weighted_faults = (2 \times Major_faults + V_Q_faults + P_I_faults)$$

Once the calculations for the different fault parameters are obtained, normalize them with respect to their highest value. This will help determine the region in which the fault occurs so that one can find the geographical location (closest substation) of the fault. This also forms the basis to get relative fault intensities between PMUs. Hence forming a rigid framework to understand which region in a large system has the largest, 2nd largest, 3rd largest, ..., nth largest fault using probabilistic model.

$$V_Q_faults = V_Q_faults./max(max(V_Q_faults))$$

$$P_I_faults = P_I_faults./max(max(P_I_faults))$$

$$Major_faults = Major_faults./max(max(Major_faults))$$

$$Weighted_faults = Weighted_faults./max(max(Weighted_faults))$$

This forms the final stage to display the precise event locations while avoiding false positives and false negatives.

4.4 Results and Observations

4.4.1 Data Definition and Data Processing

An extensive time series PMU dataset that is analyzed consists of a 5-hour PMU data during cyclone 'Amphan' (on 20th May 2020) provided by National Load Dispatch Centre (NLDC)-Power System Operation Corporation Limited (POSOCO), India. Amphan had hit the Eastern Coast of India, that is, in the states of West Bengal and Odisha during May 2020 but affected the power systems in many regions of India including the Northern region. The data under the case studies of this chapter consists of PMU data gathered from three substations A, B and C belonging to northern region of India. The data is recorded by PMU at each substation with a refresh rate of 50 samples per second each. The data set has 0.9 million data points for each parameter of each PMU. A total of 3 substations A, B and C are analysed for the effectiveness of the algorithm. The Grid disturbance report (Allen et al., 2021) of NLDC records that a major line trip event occurs at around 3182s of the duration of the data provided for analysis. Each substation records data for parameters like Voltage Phase Magnitude, Voltage Phase Angle, Current Phase Angle, Current Phase Magnitude, Real Power, Reactive Power and Frequency at 50 samples per second for a duration of 5 hours. The Frequency and RPAD parameters have been considered for all the signal processing methods generally used by NREL for comparison studies in further Section 4.5.1.

It is observed that each substation shows 3 distinct conditions of operation of the grid and noise levels in the data as follows:

- Substation A: Fault absent and high noise in data
- Substation B: Fault present and low noise in data
- Substation C: Fault present and high noise in data

From NLDC Grid events table in 2020 (Allen et al., 2021). An event of line tripping is recorded on 20th May 2020 at 15:53 in Uttar Pradesh on 2 Lines as follows,

- 400KV Azamgargh-Mau(UP) Ckt-1
- 400KV Mau(UP)-Baliala(PG) Ckt-1

The data provided by NLDC is from 15:00 onwards. The fault on 20th May 2020 has occurred at 15:53 from (Allen et al., 2021). Hence the fault should be seen at the 53rd minute mark. From the data provided, a change in operating conditions is observed exactly at 53 minutes 2 seconds and 700 milli-second. At 50 samples per second this would mean an event at $(53 \times 60 \times 50) + (2.7 \times 50)$ sample or 1,59,136th data point.

Each Substation PMU records 4 parameters namely voltage magnitude, real power magnitude, current magnitude and reactive power magnitude. Let all the data be stored in a matrix *Data*. A min-max normalization scheme is adopted to limit the amplitudes between 0 and 1. The window for normalization is the previous 5 hour data. This $Data_n$ is the normalized data which is used for the results.

$$Data_n = \frac{Data - Data_{min}}{Data_{max} - Data_{min}}$$

4.4.2 Recommended Hyper-Parameter Values

The following selection is based on careful consideration of the trade-off between computational time and effective detection:

1. $TN_{min} = 3$
2. $TN_{max} = 30$
3. $W_{max} = 30$ data points
4. $W_{cwincrement} = 6$ data points
5. $W_{threshold} = 65000$ data points

It is recommended to set $W_{threshold}$ to at least 20 minutes at a PMU sampling rate of 50 samples per second. W_{Lbase} is initially set to 2000 data points but this changes to $10 \times W_{max}$ as the algorithm progresses. The thresholds chosen for the identification of events are specified in Table 4.1 and also the number of major events identified by *Major_faults* at each of the 3 substations are noted down in this table.

Table 4.1: Threshold selected for precise Event Detections

Number of Detections				
	Threshold	Substation A	Substation B	Substation C
V_Q_faults	0.5	0	1	1
P_I_faults	0.35	0	1	1
$Major_faults$	0.1	0	1	1

4.4.3 Inference from Substation A PMU Data Analysis

The plots associated with Substation A are from Fig. 4.2 to 4.5. From the normalized input data, as shown in Figs. 4.2a, 4.2b, 4.3a and 4.3b it is observed that the noise in the data is high compared to the data plots of Substation B and Substation C. These are the variations due to normal operating conditions due to environmental factors and not the actual event.

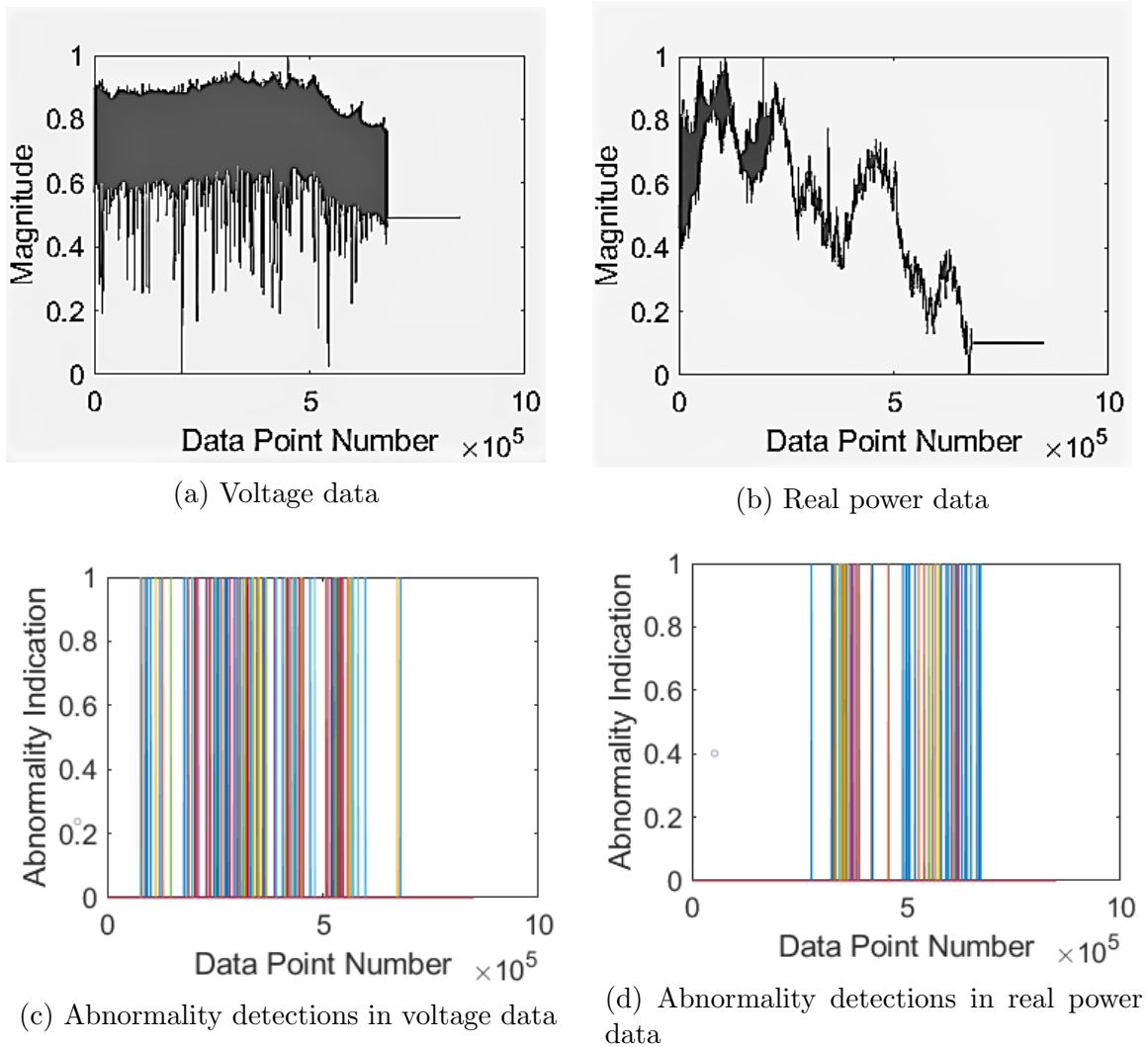
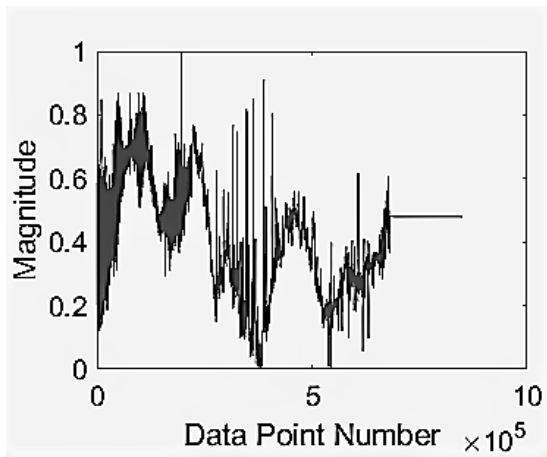
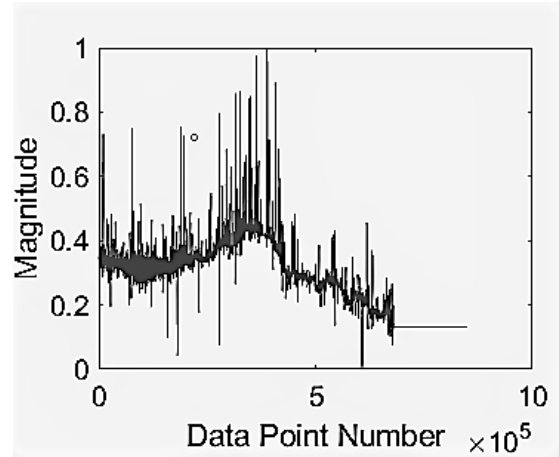


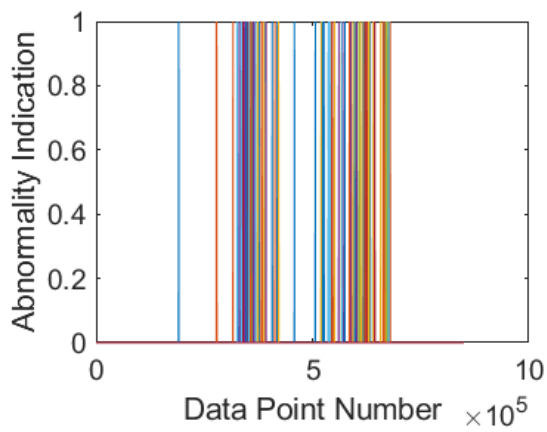
Figure 4.2: Abnormality detection for voltage and real power data at substation A



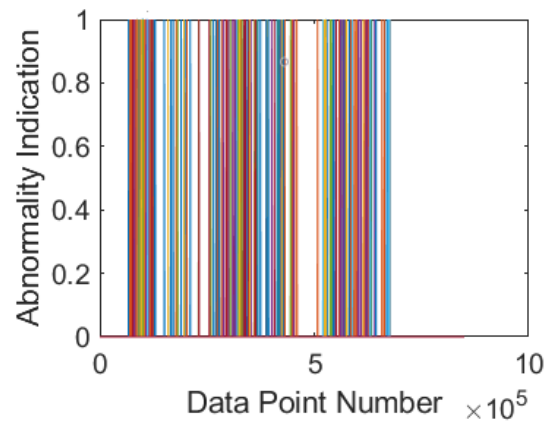
(a) Current data



(b) Reactive power data

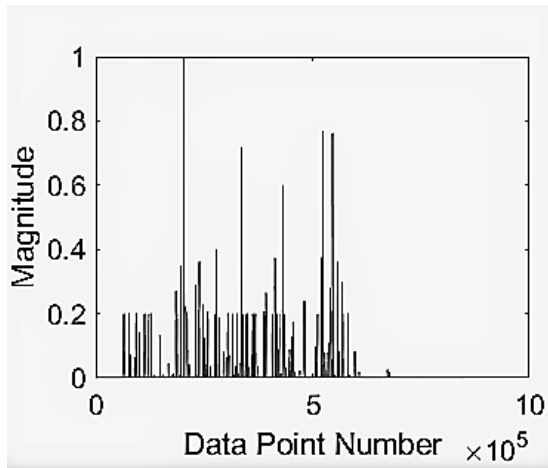


(c) Abnormality detections in current data

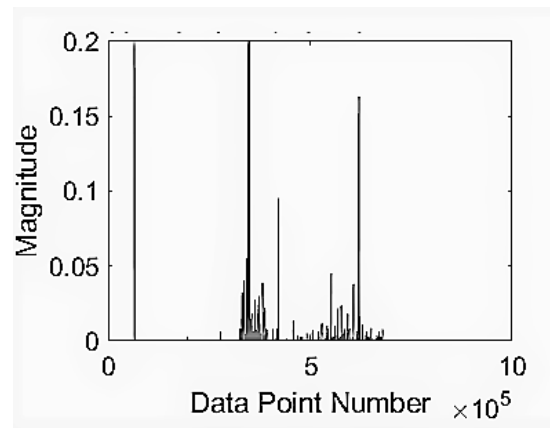


(d) Abnormality detections in reactive power data

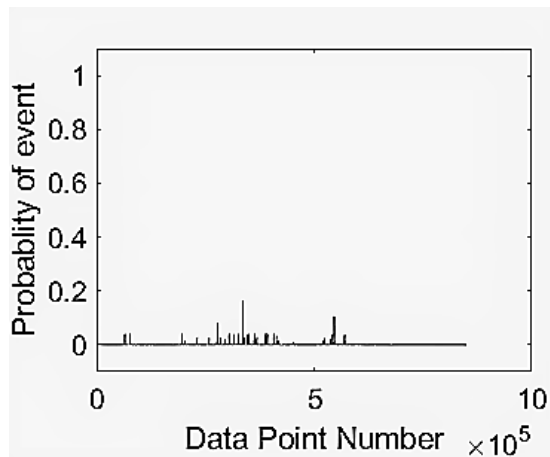
Figure 4.3: Abnormality detection for current & reactive power data at substation A



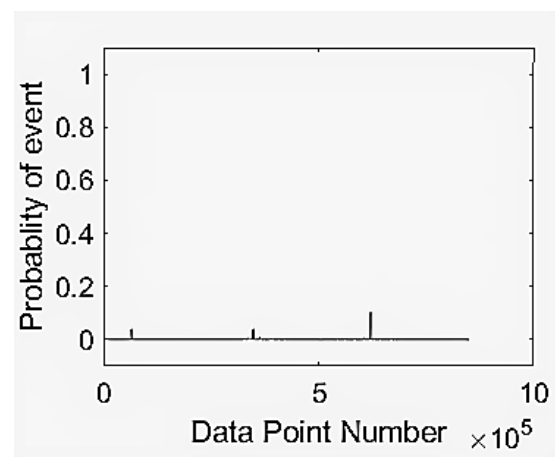
(a) Weighted sum abnormality plot for voltage



(b) Weighted sum abnormality plot for real power

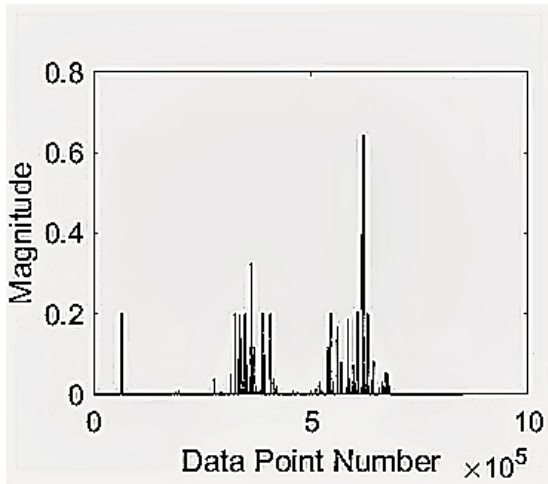


(c) Event indicators based on V and Q

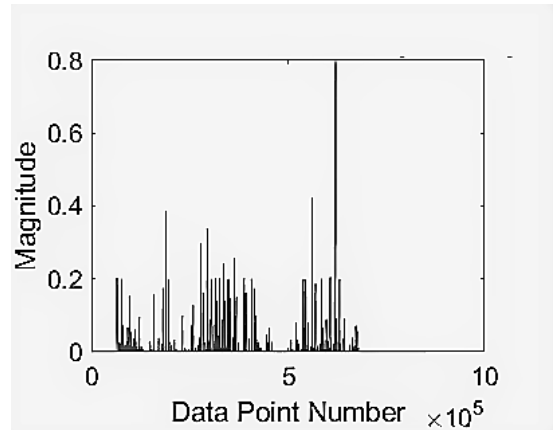


(d) Event indicators based on P and I

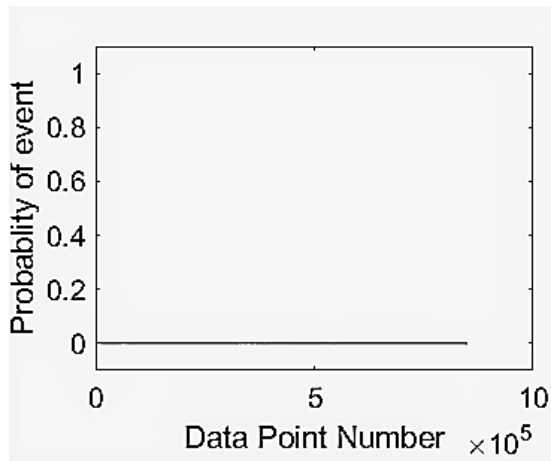
Figure 4.4: Weighted sum abnormality and 2 event indicators for voltage & real power data at substation A



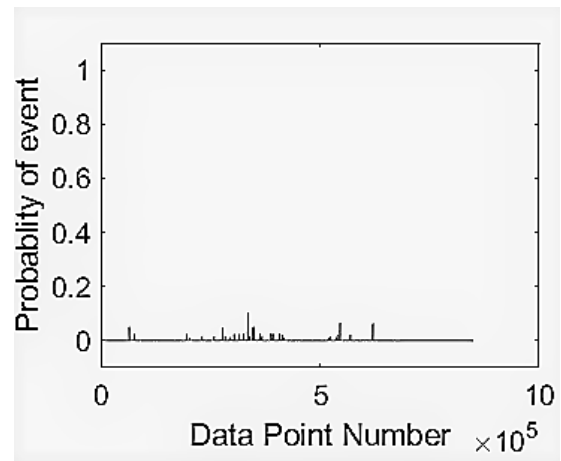
(a) Weighted sum abnormality plot for current



(b) Weighted sum abnormality plot for reactive power



(c) Major event indicators based on V-Q and P-I events



(d) Weighted event indicators based on V-Q and P-I events

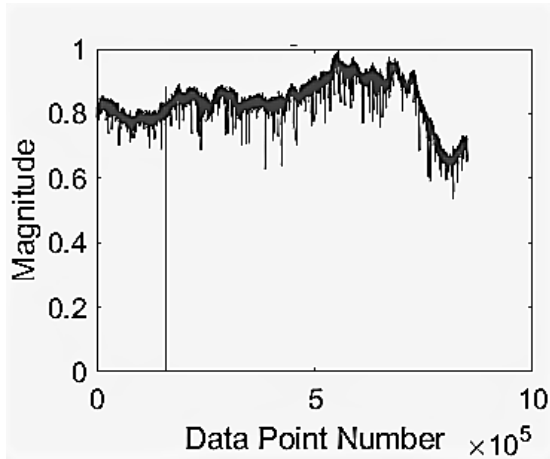
Figure 4.5: Weighted sum abnormality and 2 event indicators based on data at substation A

Figs. 4.4c, 4.4d, 4.5c and 4.5d consists of the plots after post processing. The *V-Q_faults*, *P-I_faults*, *Major_faults* and *Weighted_faults* plots shows no significant fault. The relative intensities of faults is very low to nil as the level of detection of event for all the plots is very low. There are no major events detected. This becomes clearer from the fact that Substation A is very far away from the line trip event.

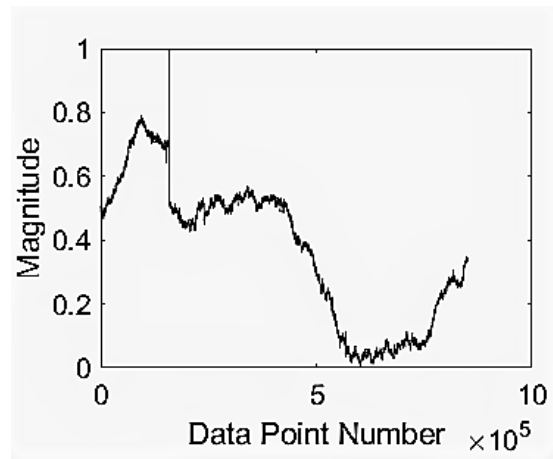
4.4.4 Inference from Substation B PMU Data Analysis

The normalized input data ($Data_n$) for Substation B are shown in Figs. 4.6a, 4.6b, 4.7a and 4.7b which are utilized to get the corresponding abnormality detections for various types is shown in Figs. 4.6c, 4.6d, 4.7c and 4.7d. These results come from the F_{fault} as described in Section 4.3.6. The Abnormality Detection plot consists of multiple colors, each color representing a detection for a particular TN for that particular parameter. The density of detections increases for higher as well as lower TN in regions of high grade abnormality. The secondary level of abstraction is performed by the weighted sum abnormality block as discussed in Section 4.3.7. The weighted sum abnormality plots are shown in Figs. 4.8a, 4.8b, 4.9a and 4.9b. It is seen that the largest magnitude of detection in these abnormality density is near 1,59,000 which is the actual location of the event. The Reactive Power Abnormality Density plot in Fig. 4.9b shows four high magnitude detections having a magnitude one. The first detection is of the actual major event in the system. The second detection is due to an abnormal upward trend observed in Reactive Power Data plot. The 3rd and 4th detections are due to sudden abrupt changes in the operating conditions of the system. These Abnormality Density plots are extracted from the Abnormality Detections shown in Figs. 4.6c, 4.6d, 4.7c and 4.7d respectively.

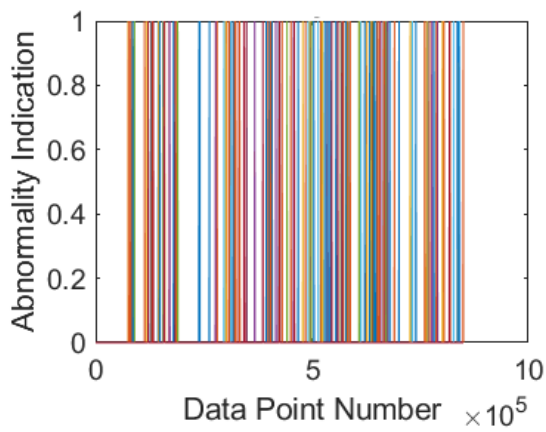
Figs. 4.8c, 4.8d, 4.9c and 4.9d consists of the results obtained after the Post Processing as discussed in Section 4.3.8. The figures show *V-Q_faults*, *P-I_faults*, *Major_faults*, *Weighted_faults* associated with Substation B. Very Few *V-Q_faults* detections have a probability greater than 0.35 and only one detection for probability greater than 0.5. Only one event has a probability greater than 0.1 in *P-I_faults*. *Major_faults* graph shows just 1 detection with a high probability while all the other small and medium grade events have a probability lower than 0.0005. Fig. 4.11 shows the Y-axis zoomed version of the *Major_faults* events graph. It can be seen that there are 2 data points whose probability of event detection cross 0.0005. These data-points are 65,000 and 1,59,100 respectively. As the $W_{threshold}$ is set to 65,000, the first detection at 65,000 is not a detection rather it is an indication that the algorithm has learnt successfully from the first 65,000 data-points and has begun the detection schema. Hence the only detection to be considered are after 65,000 data-point. Therefore the only detection by the algorithm which crosses a probability of 0.0005 is the one near 1,59,100. Hence 0.0005 can be called the minimum threshold $Threshold_{min}$



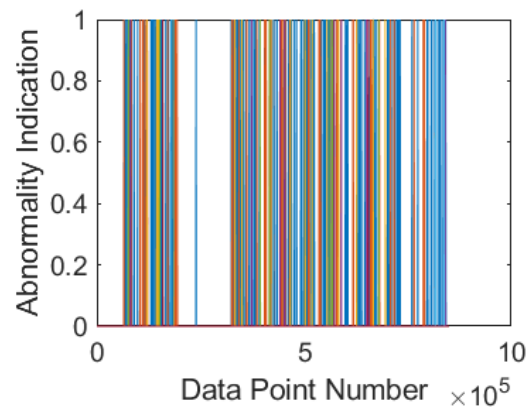
(a) Voltage data



(b) Real power data

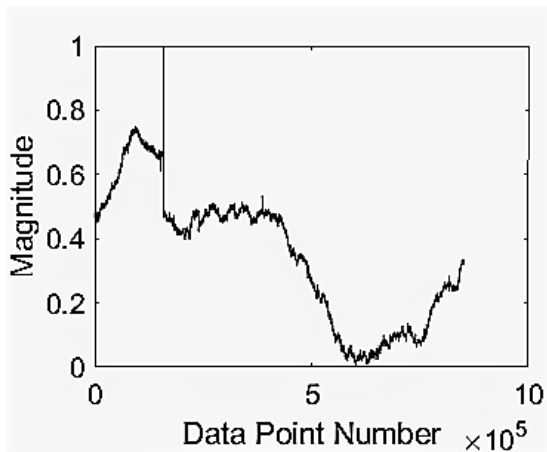


(c) Abnormality detections in voltage data

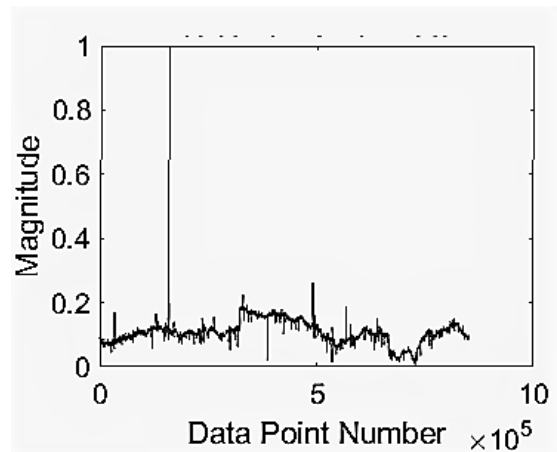


(d) Abnormality detections in real power data

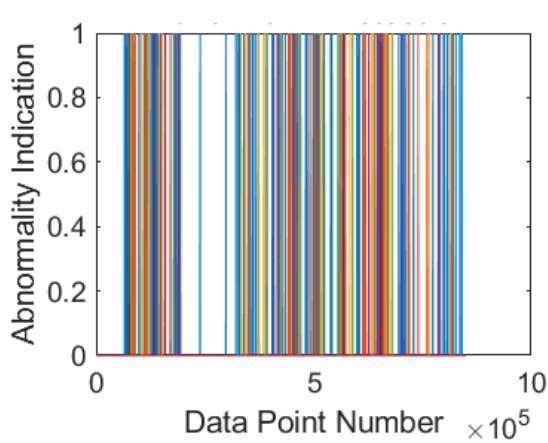
Figure 4.6: Abnormality detection for voltage and real power data at substation B



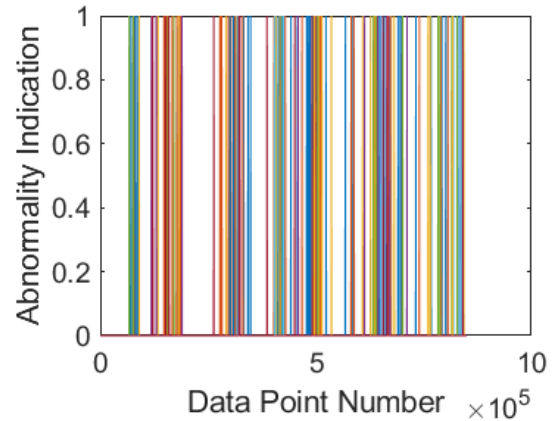
(a) Current data



(b) Reactive power data

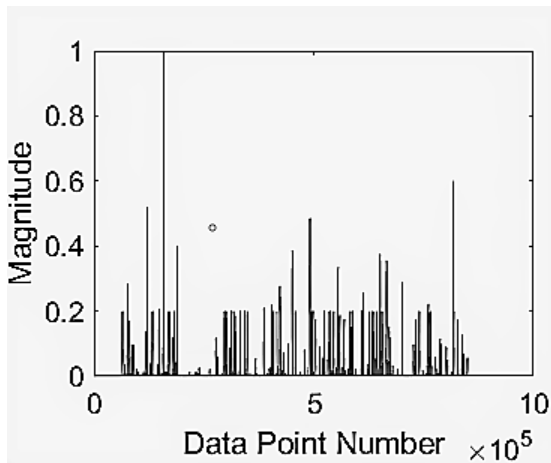


(c) Abnormality detections in Current data

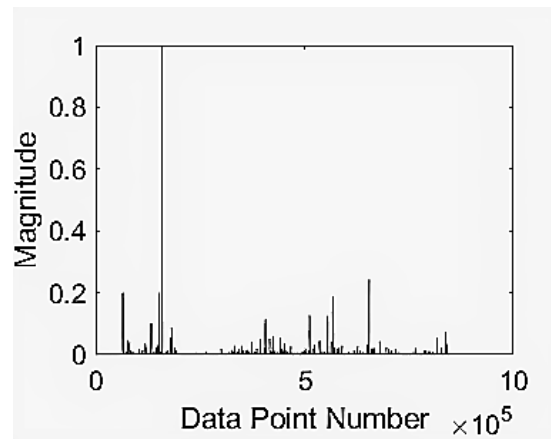


(d) Abnormality detections in reactive power data

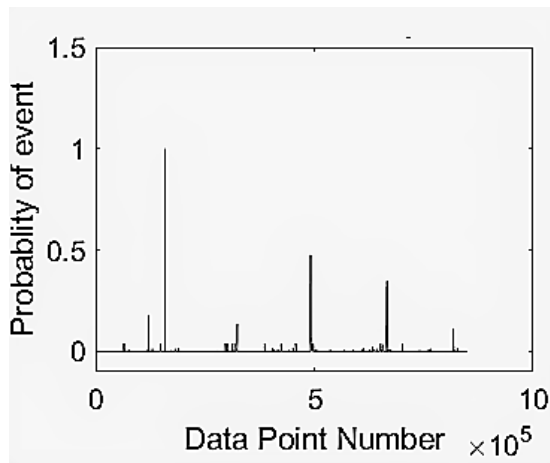
Figure 4.7: Abnormality detection for current & reactive power data at substation B



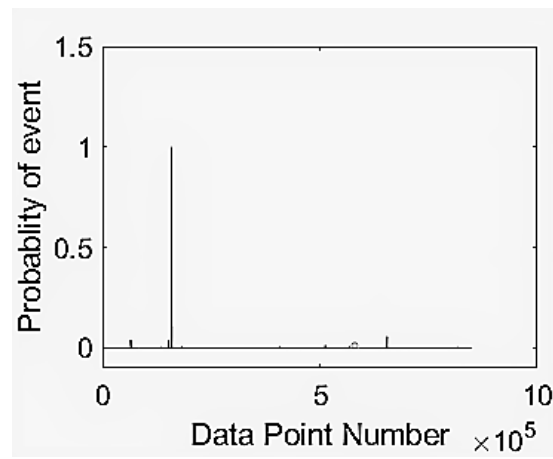
(a) Weighted sum abnormality plot for voltage



(b) Weighted sum abnormality plot for real power

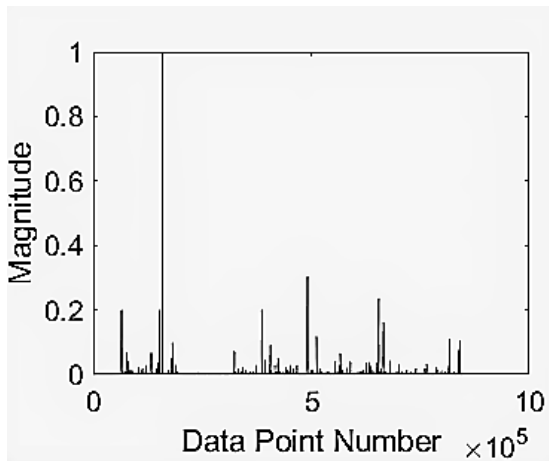


(c) Event indicators based on V and Q

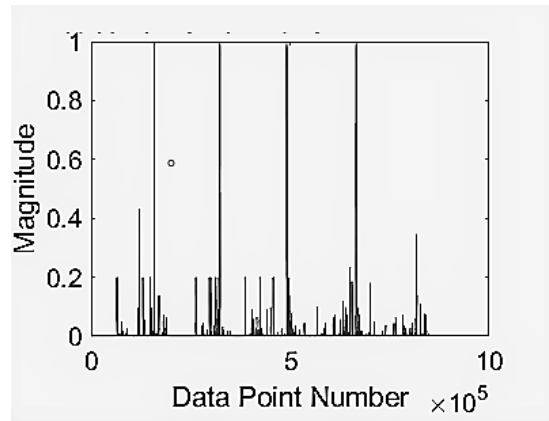


(d) Event indicators based on P and I

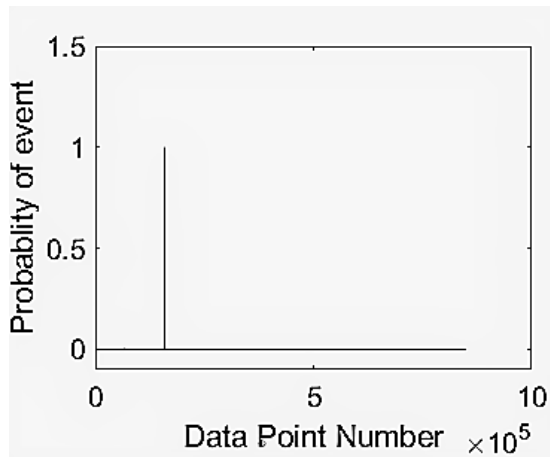
Figure 4.8: Abnormality detection for voltage & real power data at substation B



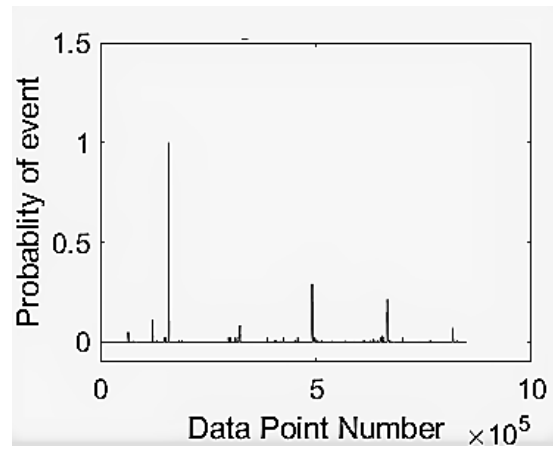
(a) Weighted sum abnormality plot for current



(b) Weighted sum abnormality plot for reactive power



(c) Weighted sum abnormality plot in current data



(d) Abnormality detections in reactive power data

Figure 4.9: Weighted sum abnormality and 2 event indicators for substation B

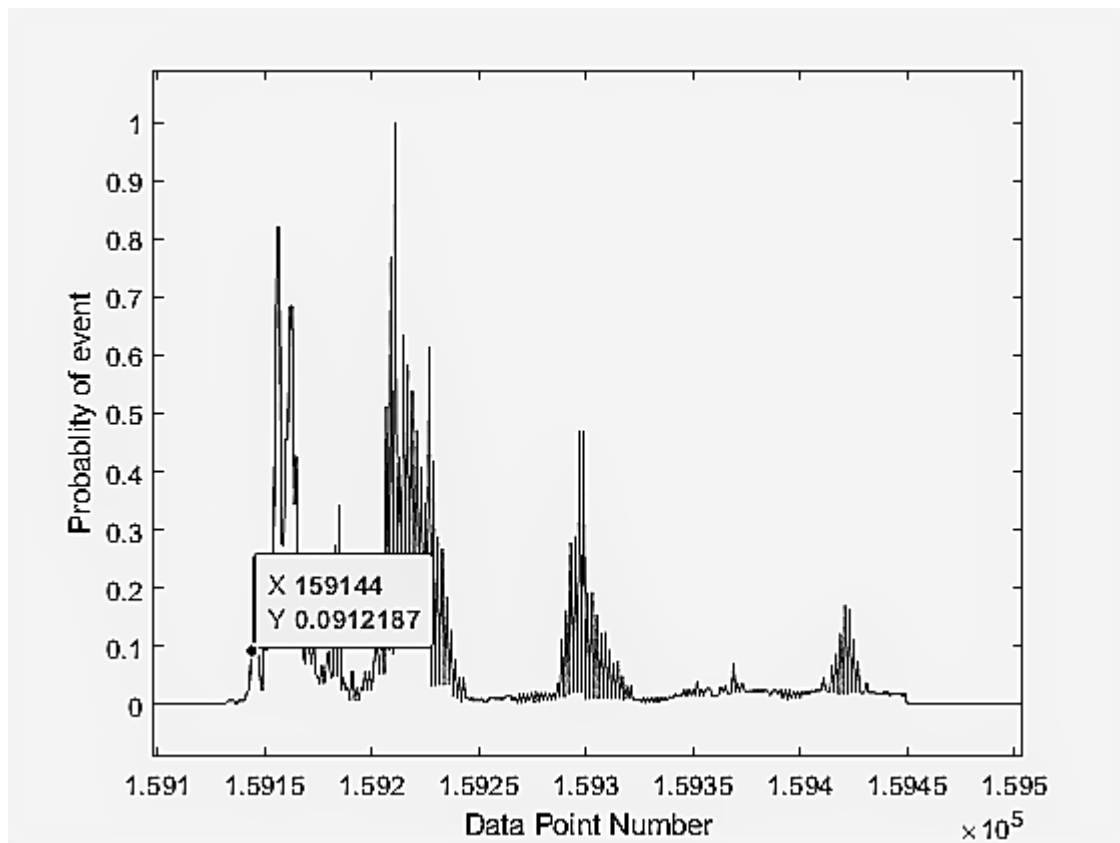


Figure 4.10: X-axis zoomed graph of *Major_faults* for substation B

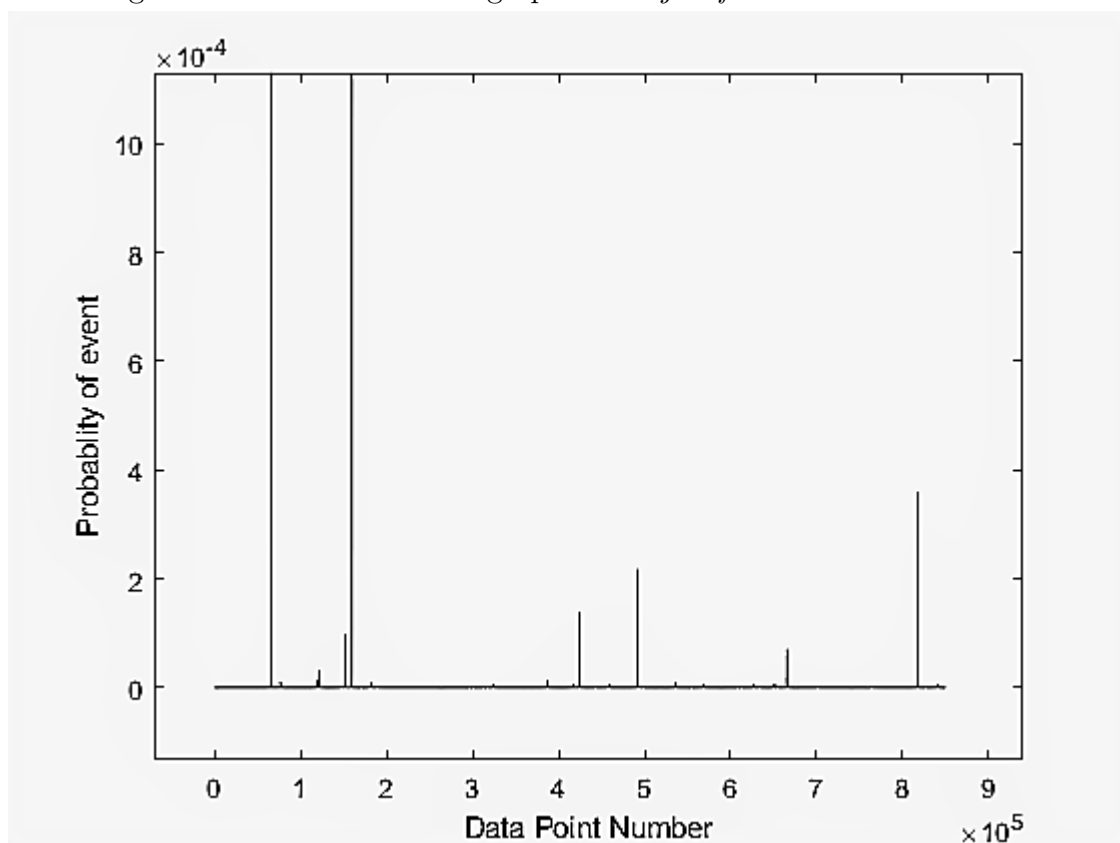


Figure 4.11: Y-axis zoomed graph of *Major_faults* for substation B

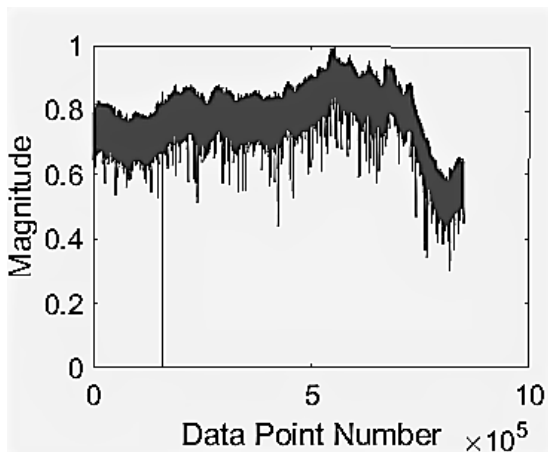
for the correct classification of an event as a major event. Assuming safety factors of 10 and 180 for robustness, set $Threshold_{10 \times Min}$ and $Threshold_{180 \times Min}$ as :

$$\begin{aligned} Threshold_{10 \times Min} &= 10 \times Threshold_{min} = 0.005 \\ Threshold_{180 \times Min} &= 180 \times Threshold_{min} = 0.09 \end{aligned}$$

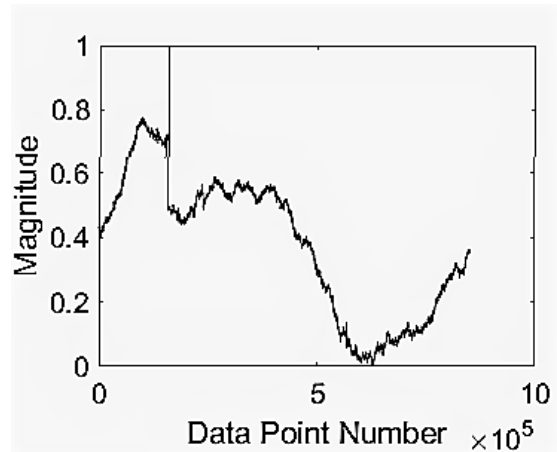
An x-axis zoom between data points 1,59,100 and 1,59,500 of the *Major_faults* graph for Substation B is shown in Fig. 4.10. It is seen that the first detection using $Threshold_{180 \times Min}$ has occurred at data point 1,59,144 which is just 8 data-points or 0.16 seconds after the occurrence of event. If the threshold for the probability of event detection is lowered to $Threshold_{10 \times Min}$ then the first detection is observed at 1,59,138 which is just 2 data-points or 40 milliseconds after the occurrence of event.

4.4.5 Inference from Substation C PMU Data Analysis

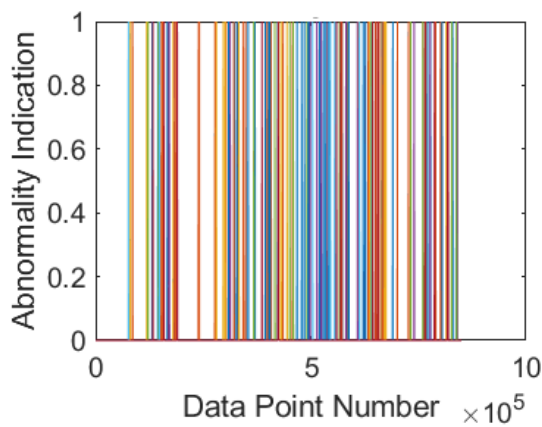
The plots for Substation C are shown in Figs. 4.12 to 4.17. From the input data in the Figs. 4.12a, 4.12b, 4.13a and 4.13b, it is seen that the noise in the data is high compared to the data of Substation B, particularly the V data. The plots of interest are in the secondary level of abstraction which are in the Figs. 4.14a, 4.14b and 4.15b. In the Voltage Abnormality Density graph, it is observed that the magnitudes of other detections has increased considerably. Even though the real event at 159136 has the highest magnitude, there are other events detected near the 4,00,000, 6,00,000 and 8,00,000 data point. These detections are due to the sudden abnormal dips in voltages at or near those data points as seen in V Data plot. The inference made on Q Abnormality Density B plot in Section 4.4.4 also applies to Q Abnormality Density C 4.13. Figs. 4.14c, 4.14d, 4.15 and 4.15d consists of V_Q_faults , P_I_faults , $Major_faults$ and $Weighted_faults$ plots showing only one event at 1,59,145. The Maximum Probability of event in *Major_faults* at substation C (See Fig. 4.15c) is 0.8, while the highest peak reached by *Major_faults* at substation B (See Fig. 4.9c) is 1. This shows a relative intensity of fault between Substation B and Substation C. This relative probability of events can also be inferred from the fact that Substation C is further away from the actual grid event when compared to Substation B. This means that the intensity of disturbance caused by the actual fault is lower at Substation C as compared to Substation B. An x-axis zoom between data points 1,59,100 and 1,59,500 of the *Major_faults* graph for Substation C is shown in Fig. 4.17. It is seen that the first detection using $Threshold_{180 \times Min}$ has occurred at data point 1,59,145 which is just 9 data-points or 0.4 s after the occurrence of event. If the threshold for the probability of event detection is lowered to $Threshold_{10 \times Min}$ then the first detection is observed at 1,59,138 which is just 2 data-points or 40 ms after the occurrence of event.



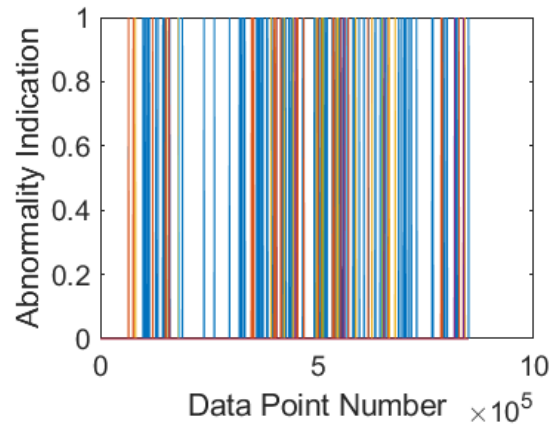
(a) Voltage data



(b) Real power data

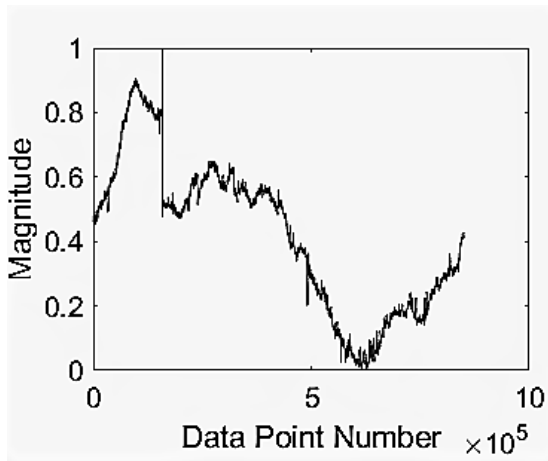


(c) Abnormality detections in Voltage data

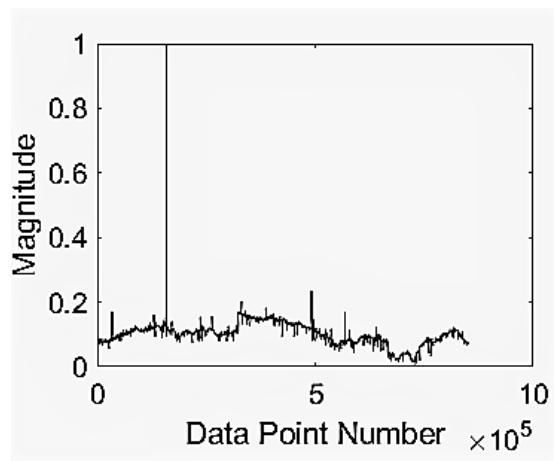


(d) Abnormality detections in Real power data

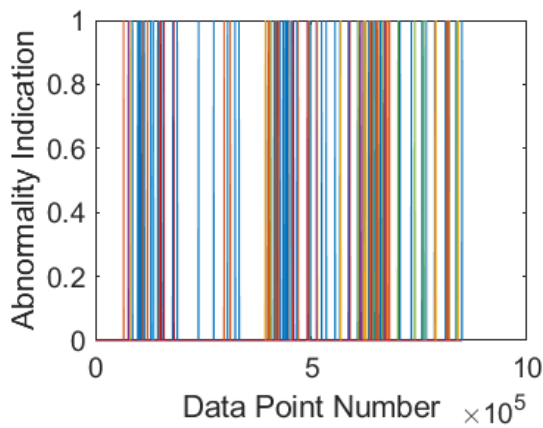
Figure 4.12: Abnormality detection for voltage and real power data at substation C



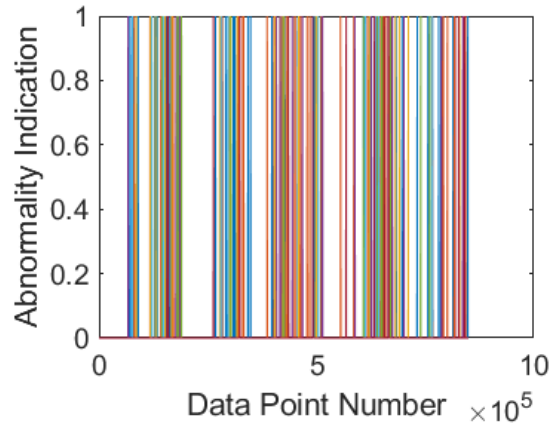
(a) Current data



(b) Reactive power data

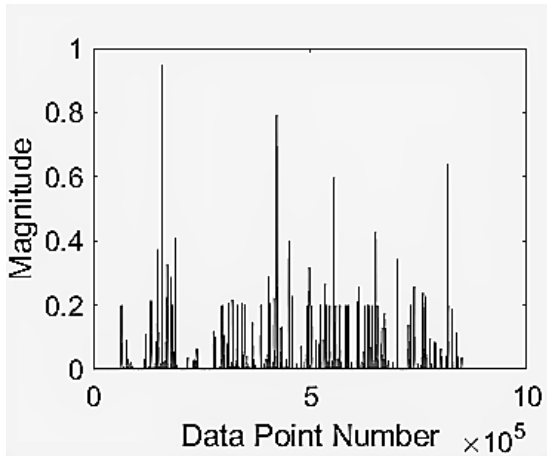


(c) Abnormality detections in current data

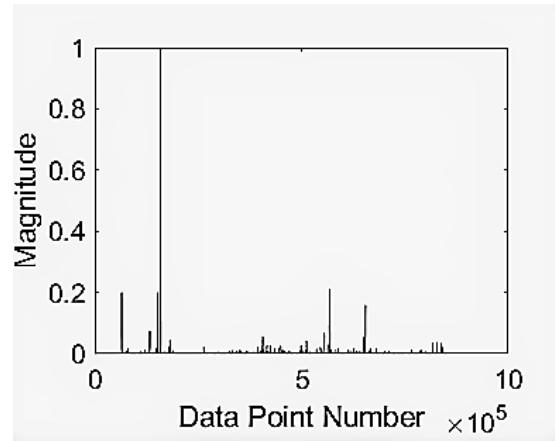


(d) Abnormality detections in reactive power data

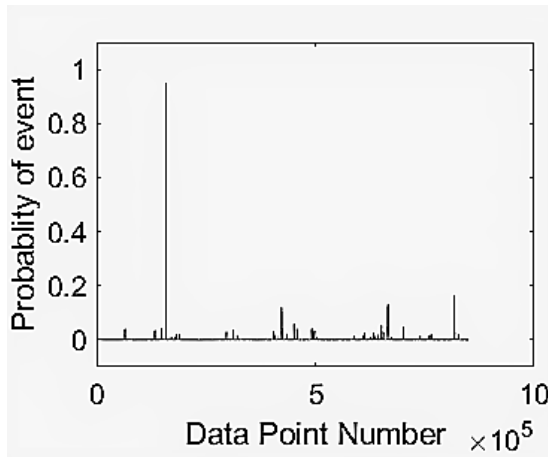
Figure 4.13: Abnormality detection for current & reactive power data at substation C



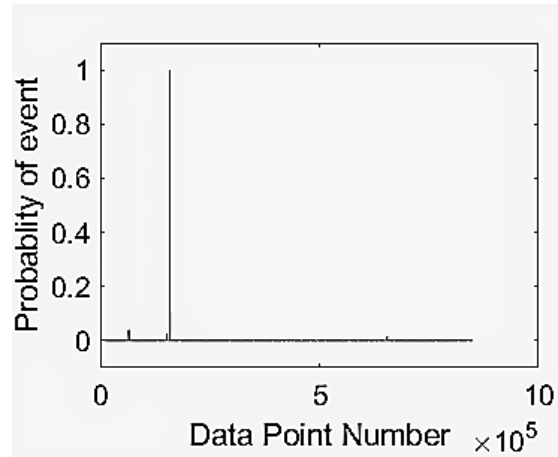
(a) Weighted sum abnormality plot for voltage



(b) Weighted sum abnormality plot for real power

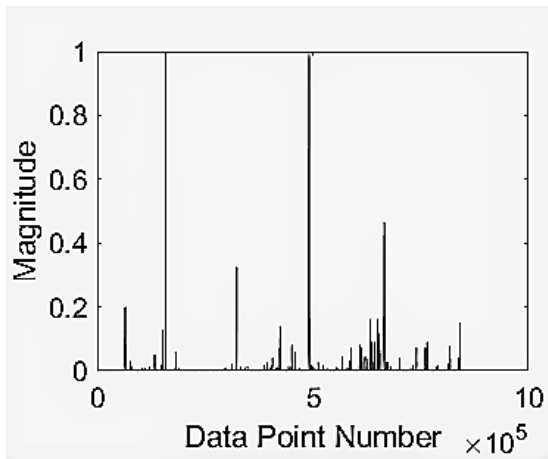


(c) Event indicators based on V and Q

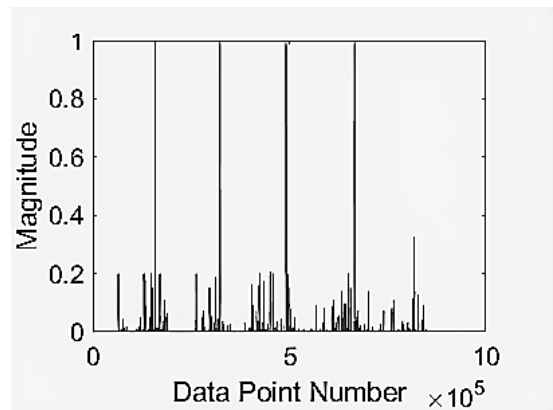


(d) Event indicators based on P and I

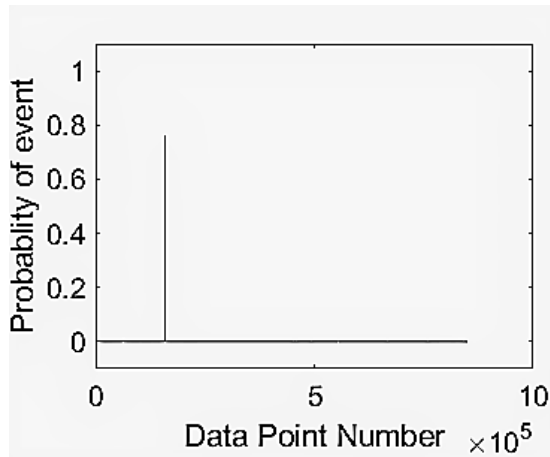
Figure 4.14: Abnormality detection for voltage & real power data at substation C



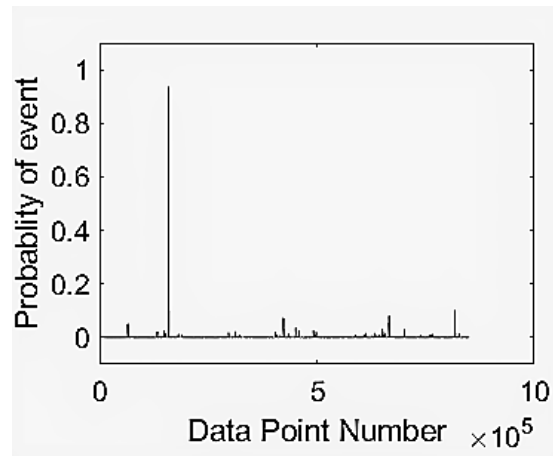
(a) Weighted sum abnormality plot for current



(b) Weighted sum abnormality plot for reactive power



(c) Major event indicators based on V-Q and P-I events



(d) Weighted event indicators based on V-Q and P-I events

Figure 4.15: Weighted sum abnormality and 2 event indicators for substation C

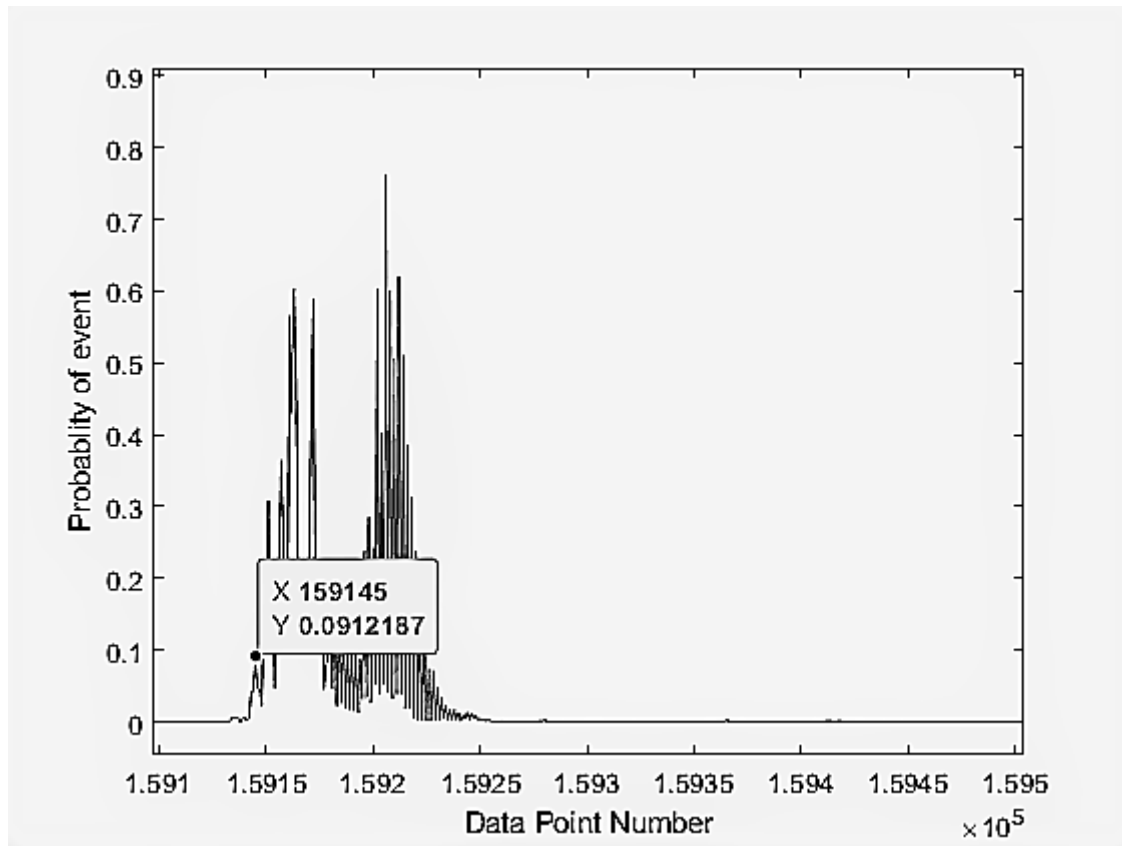


Figure 4.16: X-axis zoomed graph of *Major_faults* for substation C

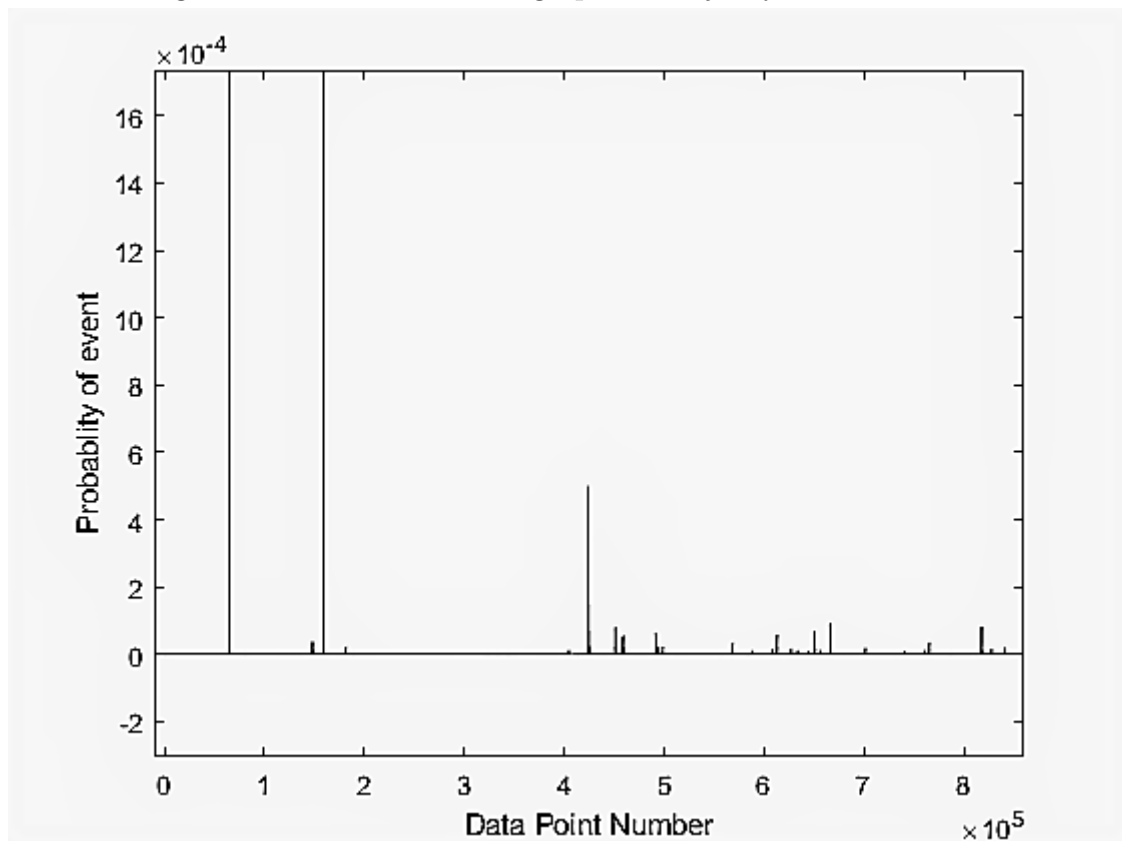


Figure 4.17: Y-axis zoomed graph of *Major_faults* for substation C

4.4.6 Variations in Hyper Parameters

Variation in $W_{threshold}$

As mentioned in Section 4.4.2, the optimal window for thresholding must be minimum of 20 minutes in order to get optimal results. Decreasing the window length from 65,000 (21.667 minutes at 50 samples/second) to 8500 (2.833 minutes at 50 samples/second) leads to distortion of results for intermediate layers while the final result remains similar.

With the decrease in Window length to 2.833 minutes, the Voltage Abnormality Density sees an increase in number of high detection magnitude detections. Figs. 4.18a, 4.18b, 4.19a, 4.19b, 4.20a, 4.20b, 4.21a, 4.21b, 4.24a, 4.24b, 4.25a and 4.25b show a clear trend of increased detections for Voltage Abnormality Density and Current Abnormality Density plots. This is due to the fact that the algorithm has not got an inner insight of the nominal variations of the recorded data. Hence multiple data points cross the dynamically learned thresholds even though those data points would not contain huge abnormality.

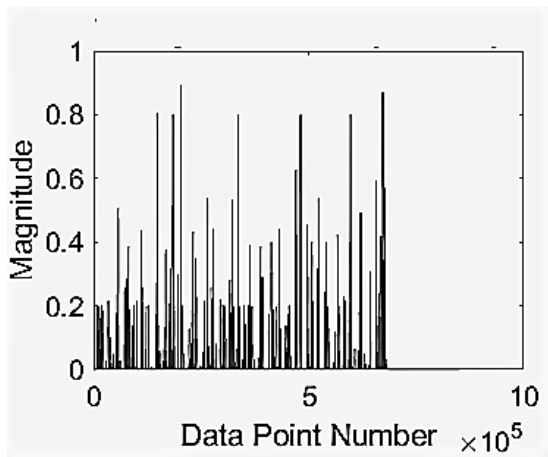
The post processing layer is placed in order to not allow such absurd setting of hyper parameters to affect the final result. Hence the plots of concern are in Row 2 of the same Figures. The V_Q_faults and P_I_faults show 2 high intensity detections for both Substation B and Substation C. While the $Major_faults$ plot just has one detection. From the Y-axis zoomed image of Fig. 4.23 it can be seen that only 2 detections cross a probability of 0.005. One of the detection is at 8500 which is just an indication for the correct start of algorithm as mentioned in Section 4.4. Hence the only real detection to take into consideration is the one near 1,59,000. The x-axis zoomed plot between 1,59,100 and 159500 data point is shows in Fig. 4.22. It can be seen that there are 2 detections indicated at data points 159142 and 159144 having probability of events of 0.0277 and 0.11.

As the only detection by the algorithm which crosses a probability of 0.005 is the one near 1,59,100. Hence 0.005 can be called the minimum threshold $Threshold_{min}$ for the correct classification of an event as a major event. Assuming a safety factors of 4 and 20 for robustness set $Threshold_{4 \times Min}$ and $Threshold_{20 \times Min}$ as :

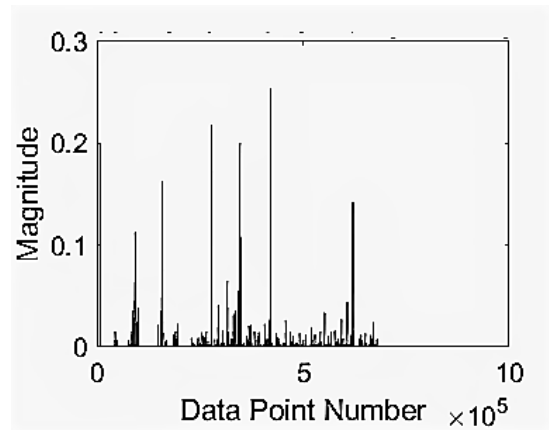
$$Threshold_{4 \times Min} = 5 \times Threshold_{min} = 0.02$$

$$Threshold_{20 \times Min} = 20 \times Threshold_{min} = 0.1$$

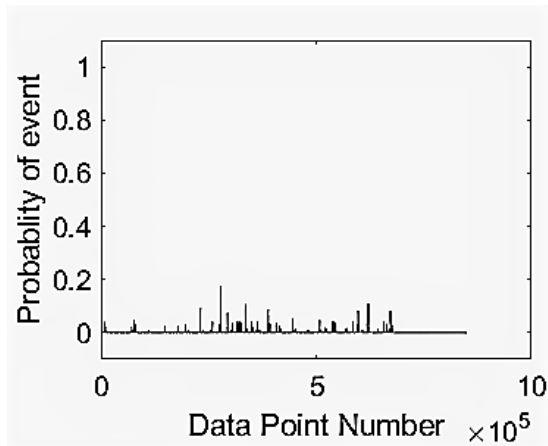
It is seen that the first detection using $Threshold_{20 \times Min}$ has occurred at data point 1,59,144 which is just 8 data-points or 0.16 seconds after the occurrence of event. If the threshold for the probability of event detection is lowered to $Threshold_{4 \times Min}$ then the first detection is observed at 159142 which is just 6 data-points or 0.12 seconds after the occurrence of event. Similar results are obtained for Substation C (See Figs. 4.26 and 4.27). Hence the effective speed of detection of major events has reduced a little.



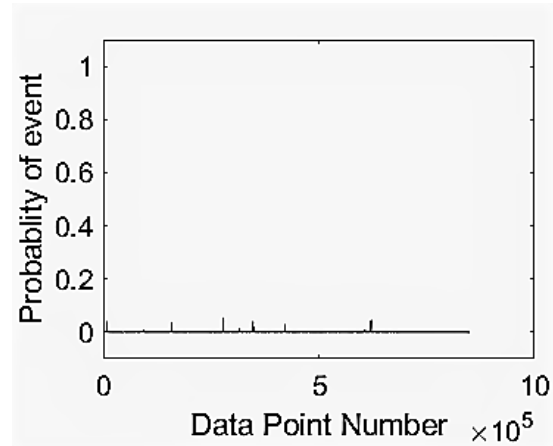
(a) Weighted sum abnormality plot for voltage



(b) Weighted sum abnormality plot for real power

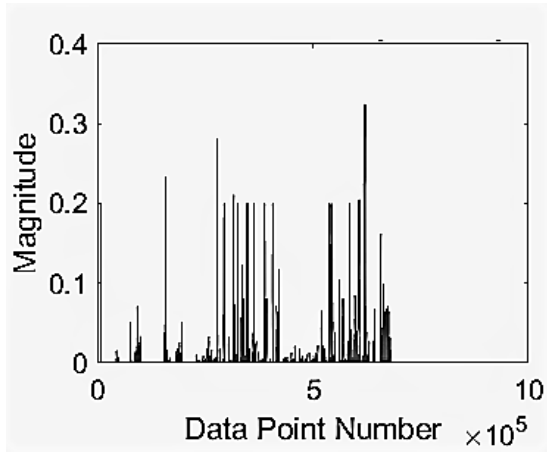


(c) Event indicators based on V and Q

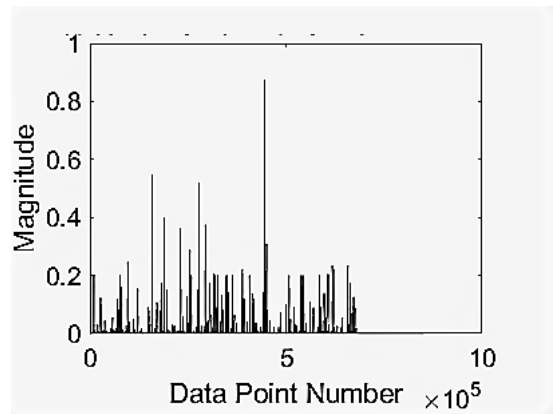


(d) Event indicators based on P and I

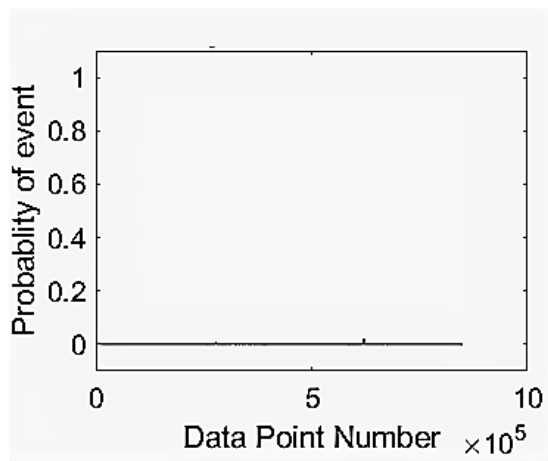
Figure 4.18: Abnormality detection for voltage & real power data at substation A for reduced $W_{threshold}$ of 8500



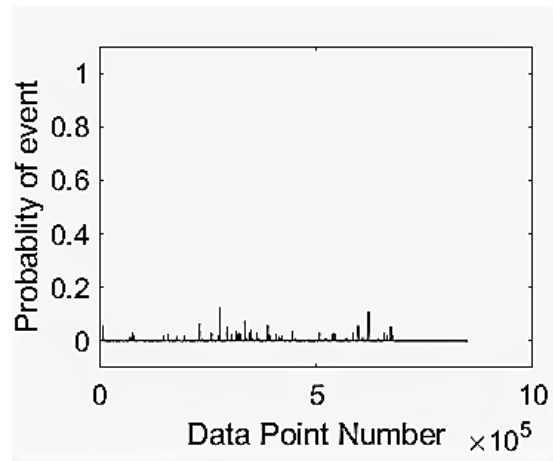
(a) Weighted sum abnormality plot for current



(b) Weighted sum abnormality plot for reactive power

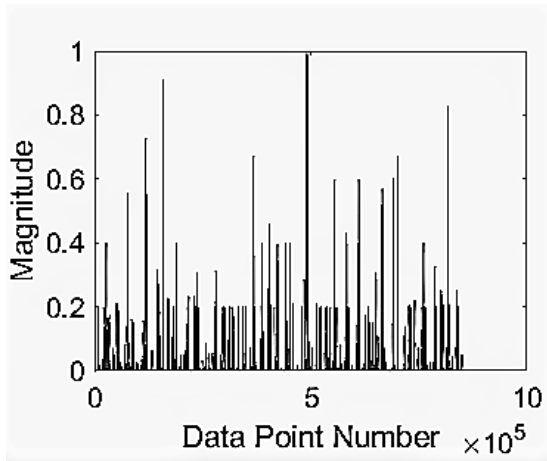


(c) Major event indicators based on V-Q and P-I events

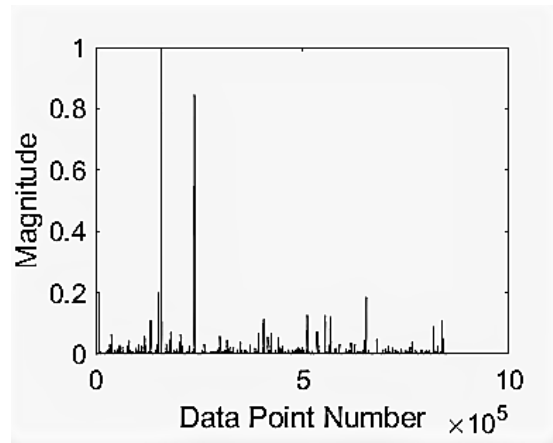


(d) Weighted event indicators based on V-Q and P-I events

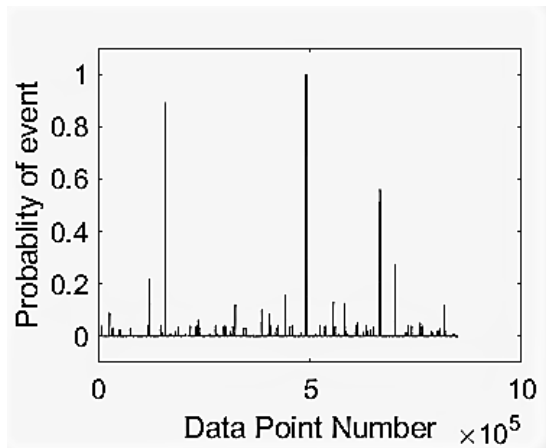
Figure 4.19: Weighted sum abnormality and 2 event indicators for reduced $W_{threshold}$ of 8500 for substation A



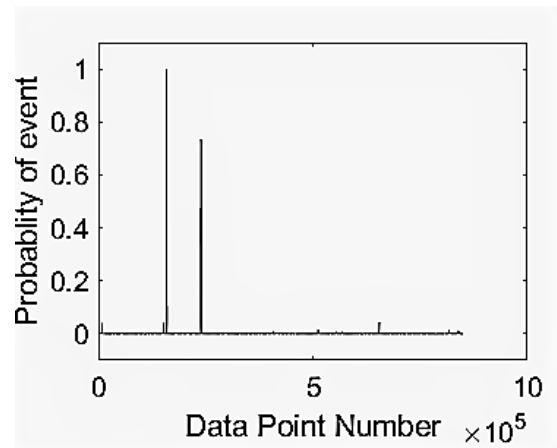
(a) Weighted sum abnormality plot for voltage



(b) Weighted sum abnormality plot for real power

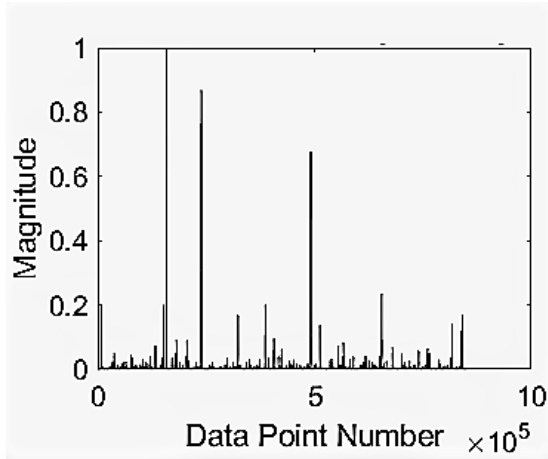


(c) Event indicators based on V and Q

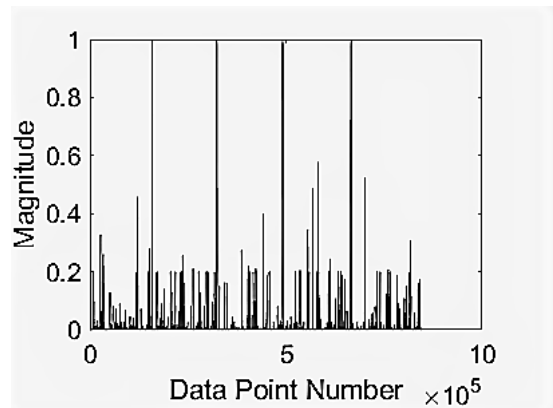


(d) Event indicators based on P and I

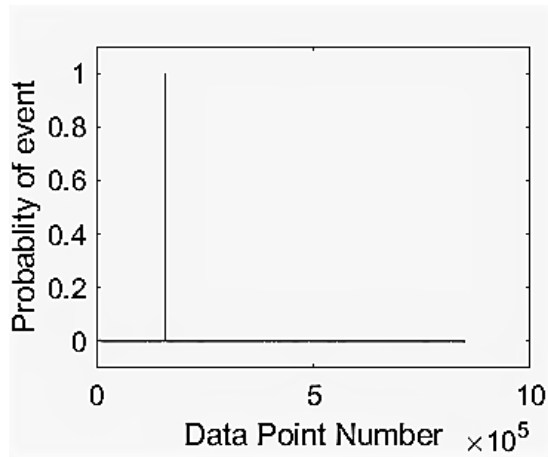
Figure 4.20: Abnormality detection for voltage & real power data at substation B for reduced $W_{threshold}$ of 8500



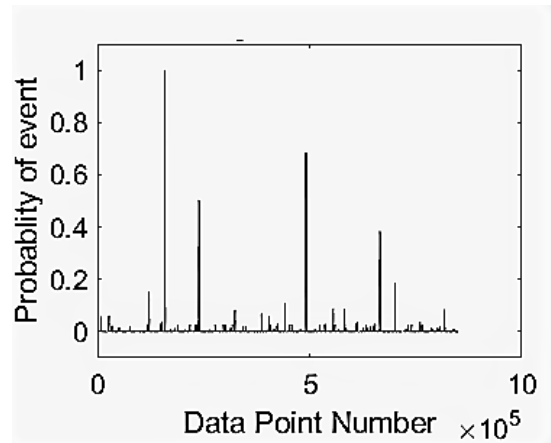
(a) Weighted sum abnormality plot for current



(b) Weighted sum abnormality plot for reactive power



(c) Major event indicators based on V-Q and P-I events



(d) Weighted event indicators based on V-Q and P-I events

Figure 4.21: Weighted sum abnormality and 2 event indicators for reduced $W_{threshold}$ of 8500 for substation B

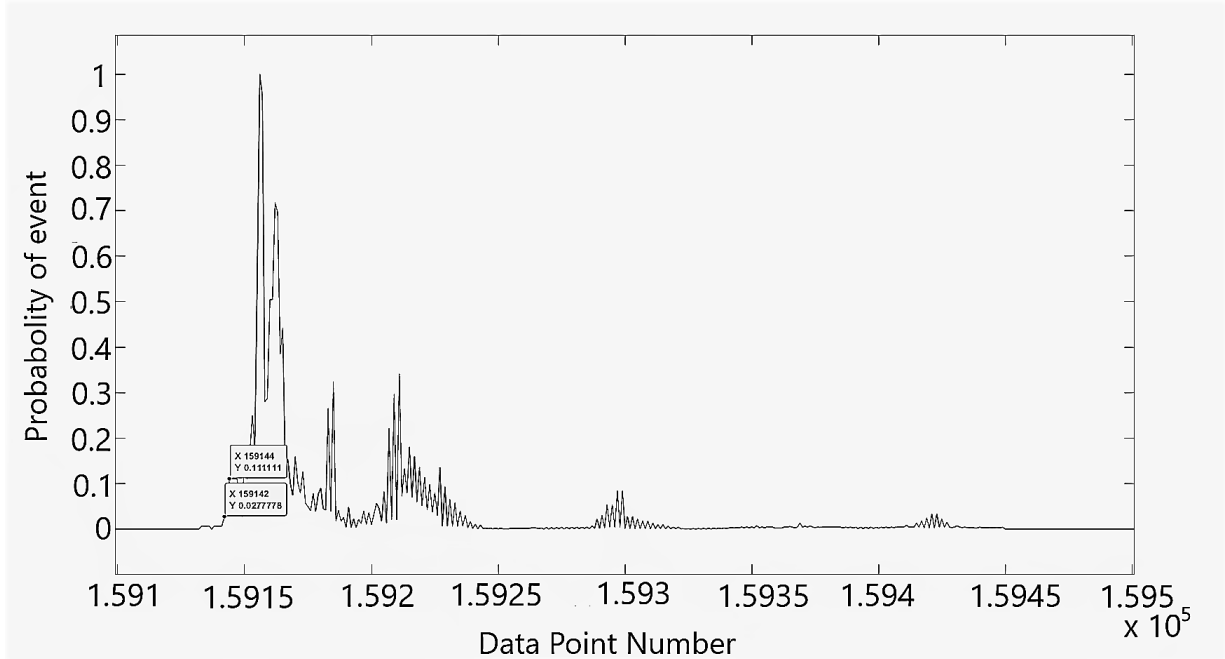


Figure 4.22: X-axis zoomed graph of *Major_faults* for reduced $W_{threshold}$ of 8500 for substation B

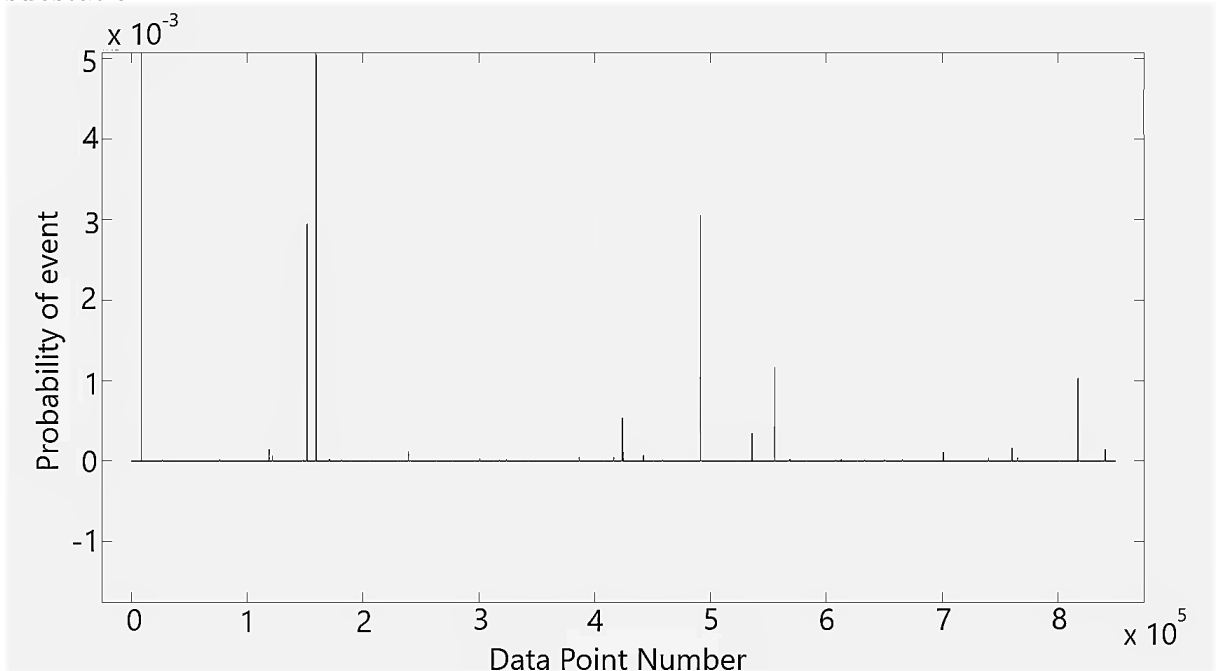
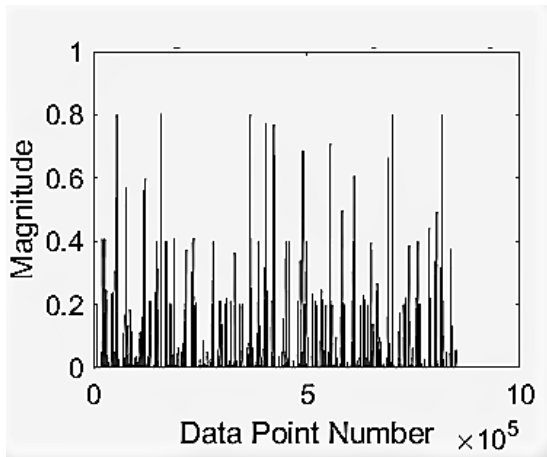
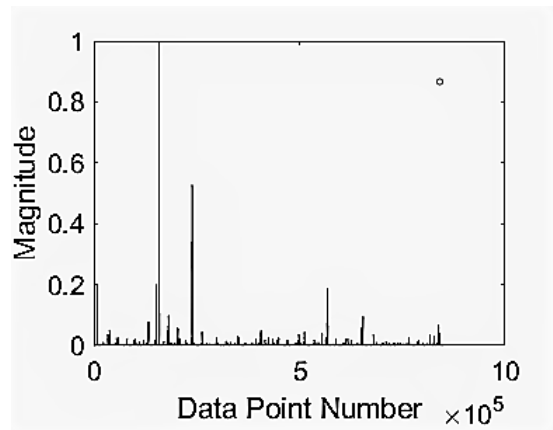


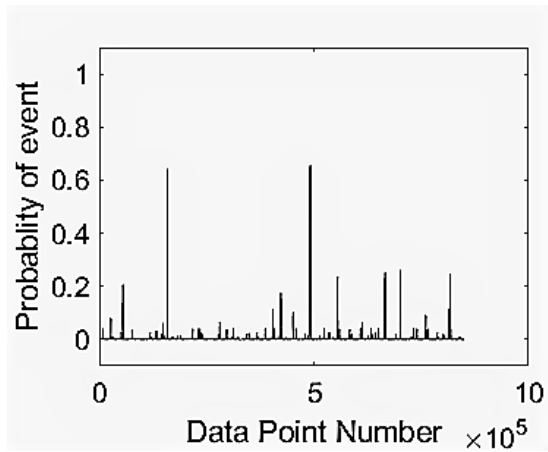
Figure 4.23: Y-axis zoomed graph of *Major_faults* for reduced $W_{threshold}$ of 8500 for substation B



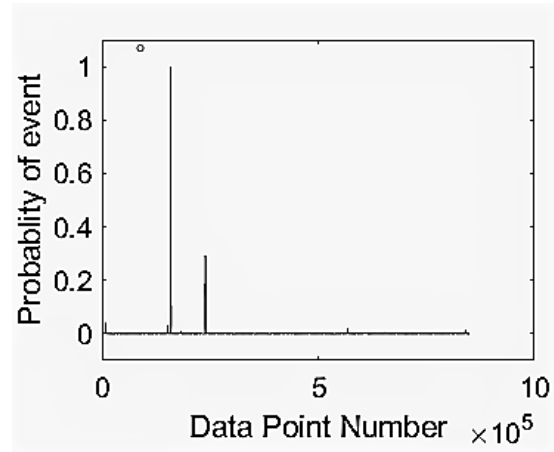
(a) Weighted sum abnormality plot for voltage



(b) Weighted sum abnormality plot for real power

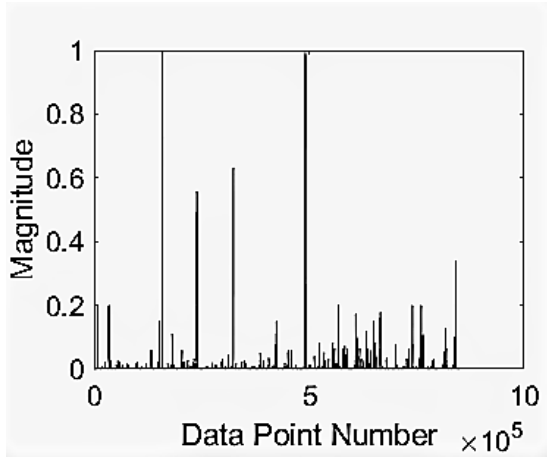


(c) Event indicators based on V and Q

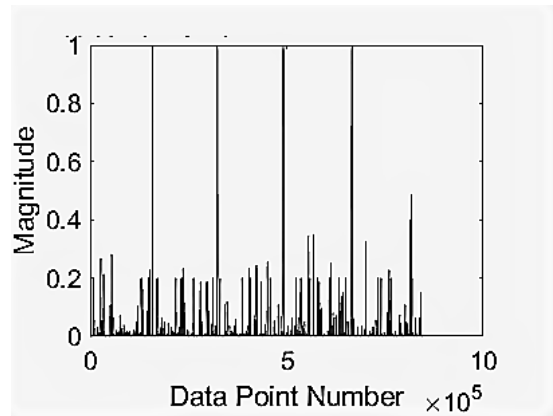


(d) Event indicators based on P and I

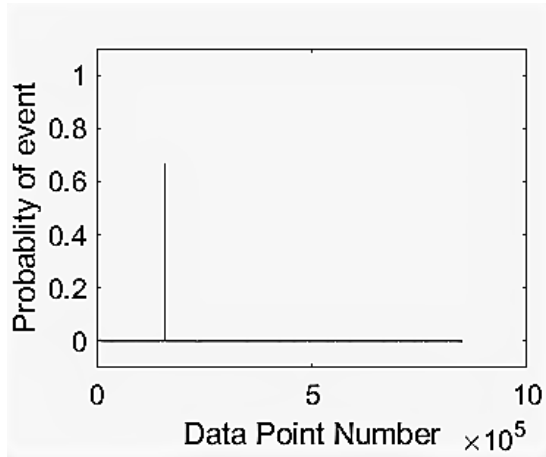
Figure 4.24: Abnormality detection for voltage & real power data at substation C for reduced $W_{threshold}$ of 8500



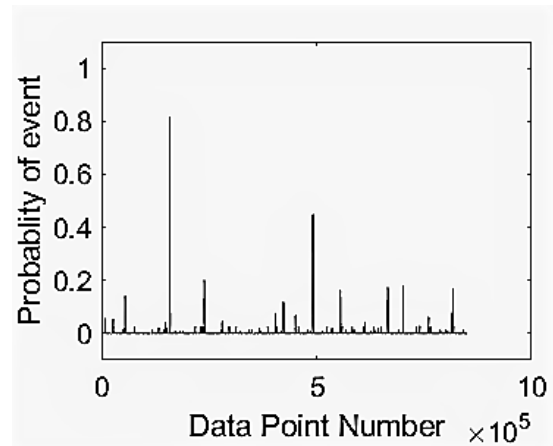
(a) Weighted sum abnormality plot for current



(b) Weighted sum abnormality plot for reactive power



(c) Major event indicators based on V-Q and P-I events



(d) Weighted event indicators based on V-Q and P-I events

Figure 4.25: Weighted sum abnormality and 2 event indicators for reduced $W_{threshold}$ of 8500 for substation C

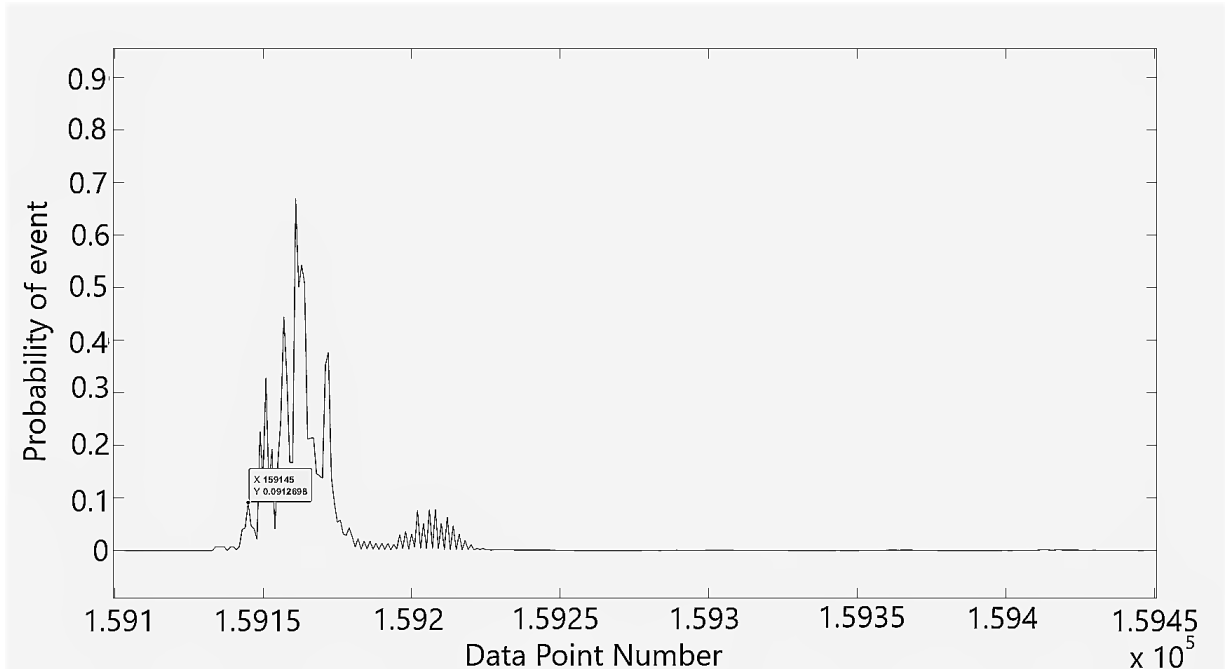


Figure 4.26: X-axis zoomed graph of *Major_faults* for reduced $W_{threshold}$ of 8500 for substation C

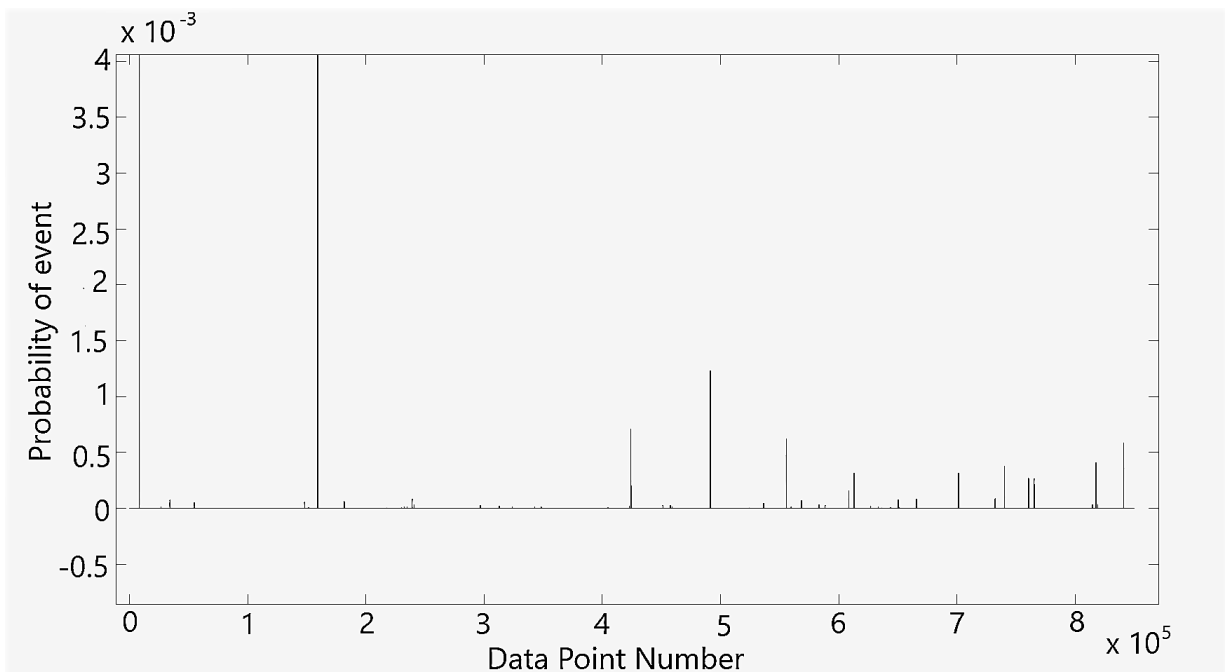


Figure 4.27: Y-axis zoomed graph of *Major_faults* for reduced $W_{threshold}$ of 8500 for substation C

However robustness is maintained as there are no false detections. Only the events which can be considered as a major abnormality are reported. For Substation A, no detection of high intensity is present, which clearly shows the robustness of the algorithm in avoiding false positives. Hence, even if the window length is not set to the recommended value, the algorithm is very effective in detecting events with high level of certainty. But this absurd setting of window length can affect magnitudes it assigns for the intensity of an event in relation to another one as seen for *V_Q_faults* and *P_I_faults*. Hence to avoid such a dilemma the *Weighted_faults* graph must be seen to get a clear picture of the important events. Algorithm will still be very precise at differentiating big events from small events in *V_Q_faults*, *P_I_faults* detection and also be very precise to include only the major events in the *Major_faults* plot.

Variation range of Type Number TN

The nominal value of TN_{min} and TN_{max} recommended for the algorithm is 3 and 30 respectively. It has already been discussed in Section 4.3.2 regarding the effect of variation in type number range would affect the results but having a look of the practical results gives a better insight. Keeping the window length for thresholding at 65,000 data points, set new values of $TN_{min}=2$ and $TN_{max}=15$. Differentiation between the major and minor events will become very subtle this is because clear distinctions between major events and sub major events (events which are neither minor nor major) can be achieved only if a TN_{max} is assigned a higher value. From Figs. 4.28a, 4.28b, 4.29a, 4.29b, 4.30a, 4.30b, 4.31a, 4.31b, 4.34a, 4.34b, 4.35a and 4.35b, it is seen that the abnormality detection and weighted sum abnormality graphs show many abnormalities densities of high magnitudes. It is also clear that the actual main event at 1,59,136 is having a high magnitude but not high enough to make a distinction from other sub normal events.

The *V_Q_faults* and *P_I_faults* (Figs. 4.30c, 4.30d, 4.34c and 4.34d) of substations 1 and 2 show multiple detections of high magnitudes. This clearly shows that the decrease in the range of TN significantly affects the learning process of thresholds yielding incorrect magnitude assignment and relative level of detections to these events. While major event detection remains unaltered with a very distinct localization of the event.

As seen in Figs. 4.33 and 4.37, the magnitude of Probability of event is low of the order of 0.005 for most events except for the one near 1,59,000. The x-axis zoomed plot between 1,59,100 and 1,59,500 shown in Figs. 4.32 and 4.36. It can be seen that the detections marked at data points 1,59,142 and 1,59,153 for Substation B have an intensity of 0.01 and 0.09 respectively. Similarly the detections marked at data points 1,59,145 and 1,59,151 for Substation C have an intensity of 0.04 and 0.1369 respectively. As the only detection by the algorithm for the reduced range of TN which crosses a probability of 0.005 is the one near 1,59,100 in *Major_faults*. Hence 0.005 can be called the minimum threshold

Table 4.2: Event Detection Latency in *Major_faults*

	Substation B	Substation C
$Threshold_{10 \times Min}$	0.04 s	0.04 s
$Threshold_{180 \times Min}$	0.16 s	0.16 s
Variation in $W_{threshold}$		
$Threshold_{4 \times Min}$	0.12 s	0.12 s
$Threshold_{20 \times Min}$	0.16 s	0.16 s
Variation in TN		
$Threshold_{4 \times Min}$	0.12 s	0.18 s
$Threshold_{20 \times Min}$	0.34 s	0.3 s

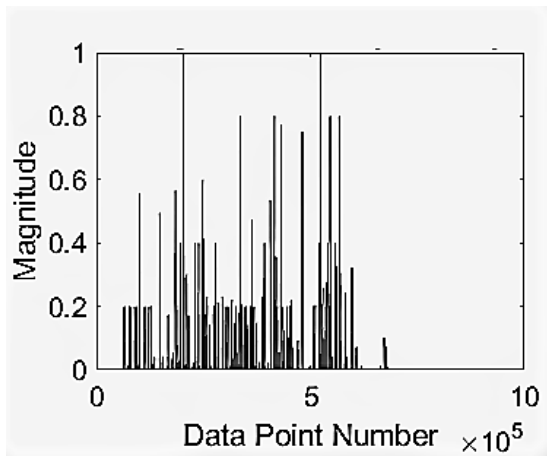
$Threshold_{min}$ for the correct classification of an event as a major event. Assuming a safety factors of 4 and 20 for robustness set $Threshold_{4 \times Min}$ and $Threshold_{20 \times Min}$ as :

$$Threshold_{4 \times Min} = 4 \times Threshold_{min} = 0.02$$

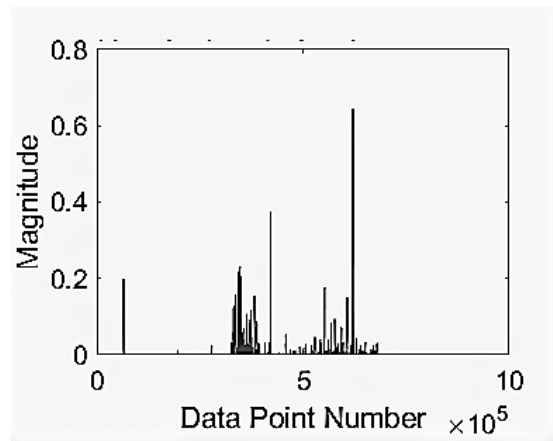
$$Threshold_{20 \times Min} = 20 \times Threshold_{min} = 0.1$$

From Figs. [4.32](#), [4.33](#), [4.36](#) and [4.37](#). It is seen that the first detection using $Threshold_{20 \times Min}$ has occurred at data point 1,59,153 which is just 17 data-points or 0.34 seconds after the occurrence of event. If the threshold for the probability of event detection is lowered to $Threshold_{4 \times Min}$ then the first detection is observed at 159142 which is just 6 data-points or 0.12 seconds after the occurrence of event. Similar results are obtained for Substation C. Hence the effective speed of detection of major events has reduced considerably. The detection of Major events has still been quite robust while detections made by V_Q_faults and P_I_faults are inaccurate. Hence, even if the TN_{min} and TN_{max} are not set to the recommended value the algorithm is effective in detecting Major events. But this absurd setting of TN_{min} and TN_{max} has affected magnitudes it assigns for the intensity of an event in relation to another one as seen for V_Q_faults and P_I_faults . Hence to avoid such a dilemma the *Weighted_faults* graph must be seen to get a clear picture of the important events. Algorithm will still be very precise at differentiating big events from small events in *Major_faults* plot.

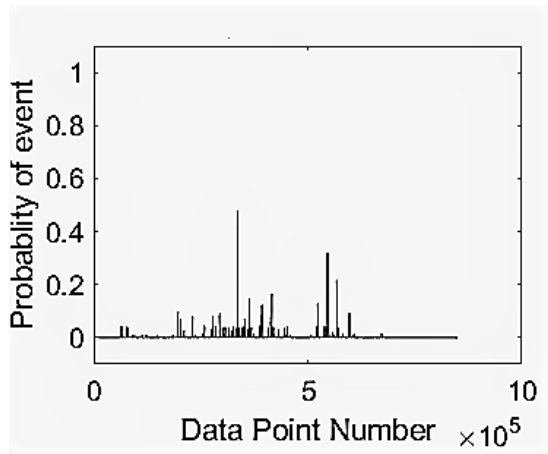
The summary of detection latency while selecting different $Threshold_{Min}$ with respect to recommended hyper parameters and while studying variations in hyper parameters are noted down carefully in Table [4.2](#). Therefore, proposed new technique for major event detection has a detection delay in the range of 40-160 ms when recommended hyper parameters are adopted.



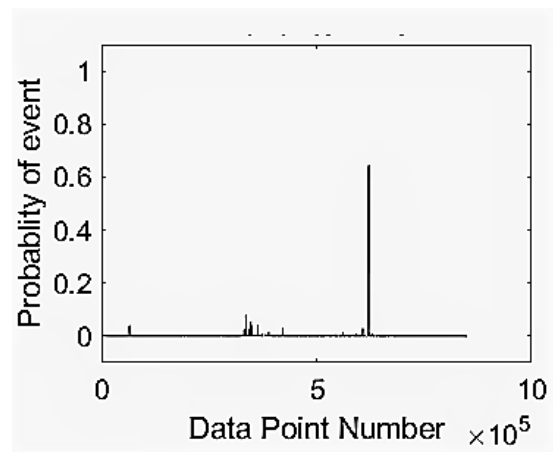
(a) Weighted sum abnormality plot for voltage



(b) Weighted sum abnormality plot for real power

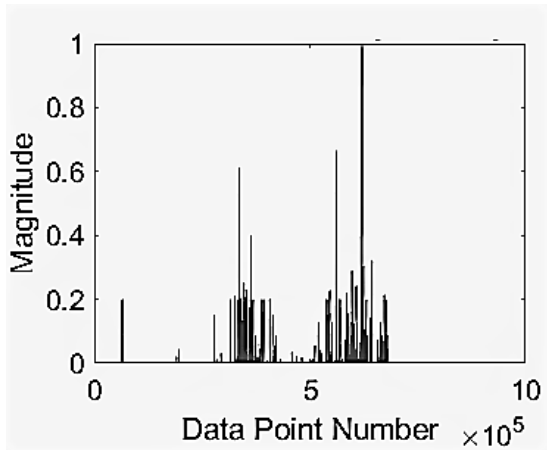


(c) Event indicators based on V and Q

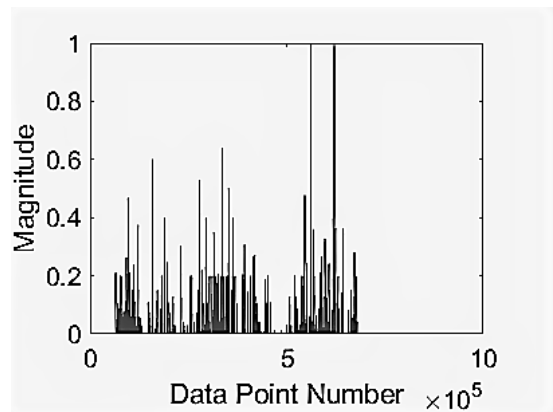


(d) Event indicators based on P and I

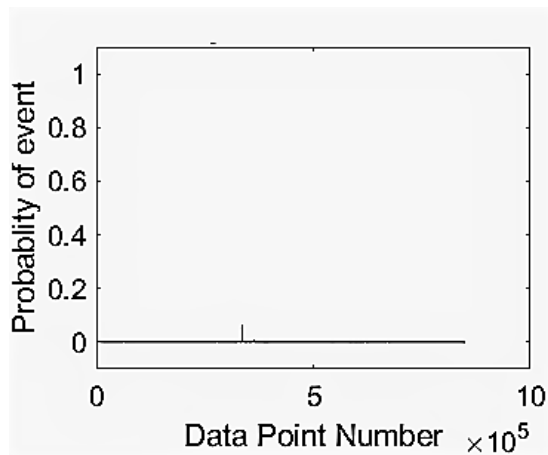
Figure 4.28: Weighted sum abnormality and 2 event indicators for variation in TN for substation A



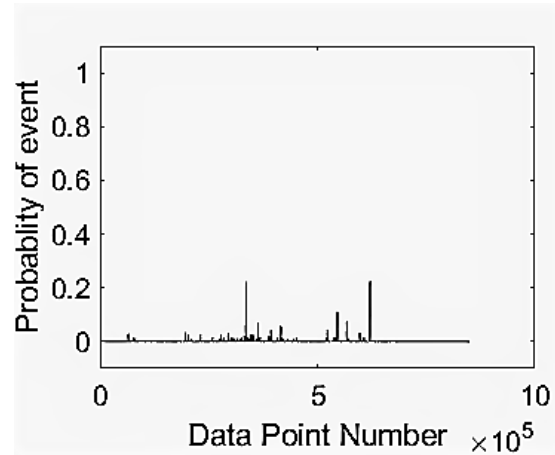
(a) Weighted sum abnormality plot for current



(b) Weighted sum abnormality plot for reactive power

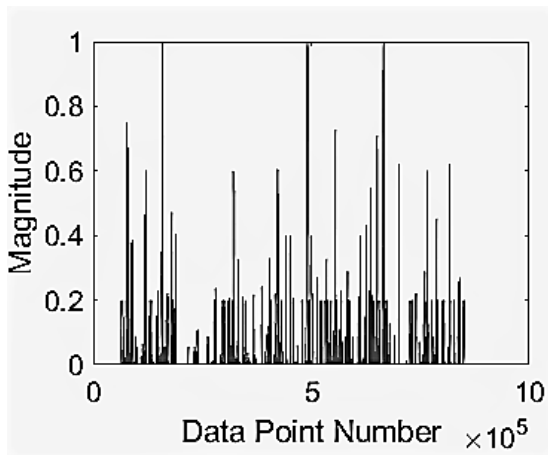


(c) Major event indicators based on V-Q and P-I events

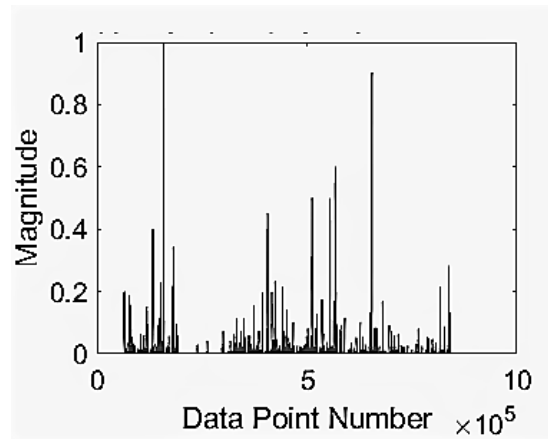


(d) Weighted event indicators based on V-Q and P-I events

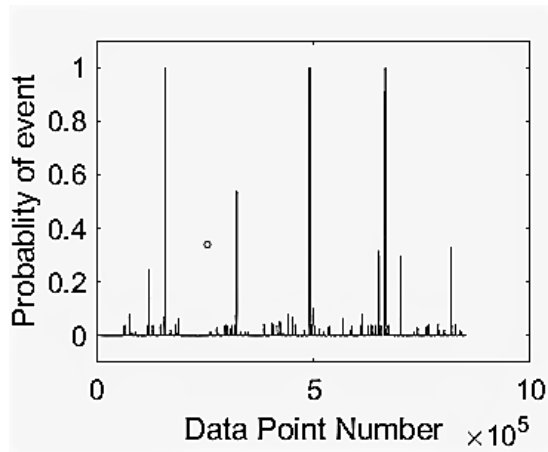
Figure 4.29: Weighted sum abnormality and 2 event indicators for variation in TN for substation A



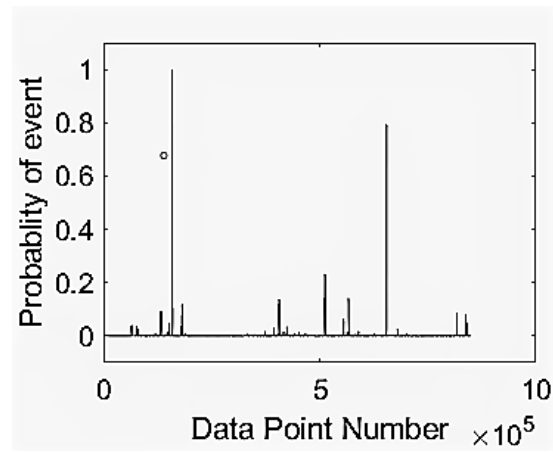
(a) Weighted sum abnormality plot for voltage



(b) Weighted sum abnormality plot for real power

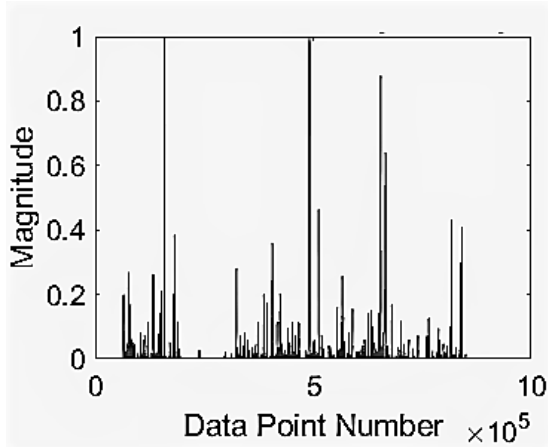


(c) Event indicators based on V and Q

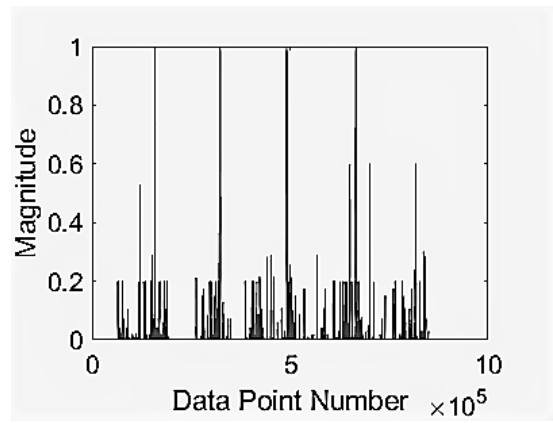


(d) Event indicators based on P and I

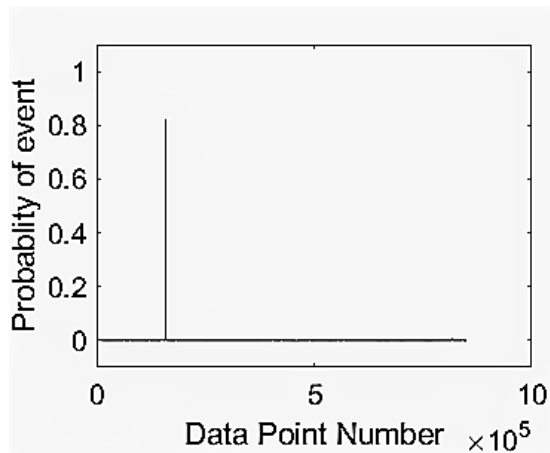
Figure 4.30: Weighted sum abnormality and 2 event indicators for variation in TN for substation B



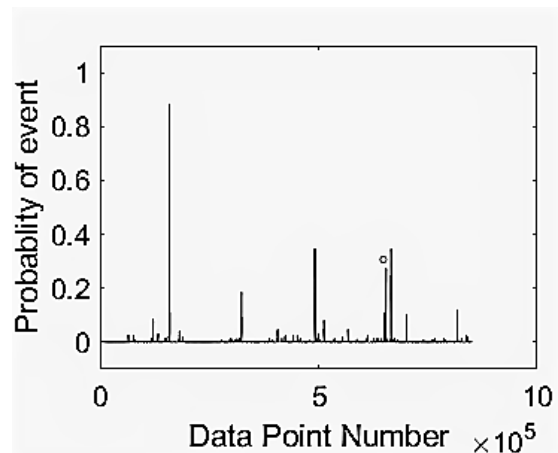
(a) Weighted sum abnormality plot for current



(b) Weighted sum abnormality plot for reactive power



(c) Major event indicators based on V-Q and P-I events



(d) Weighted event indicators based on V-Q and P-I events

Figure 4.31: Weighted sum abnormality and 2 event indicators for variation in TN for substation B

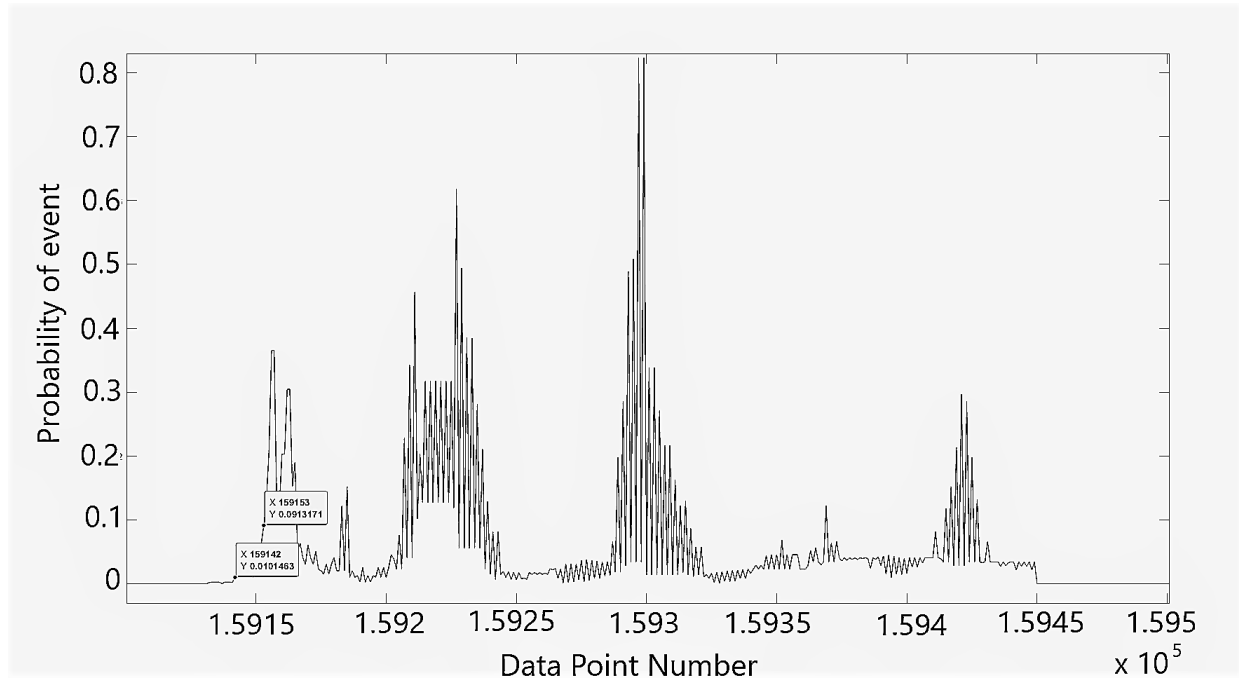


Figure 4.32: X-axis zoomed graph of *Major_faults* for variation in *TN* for substation B

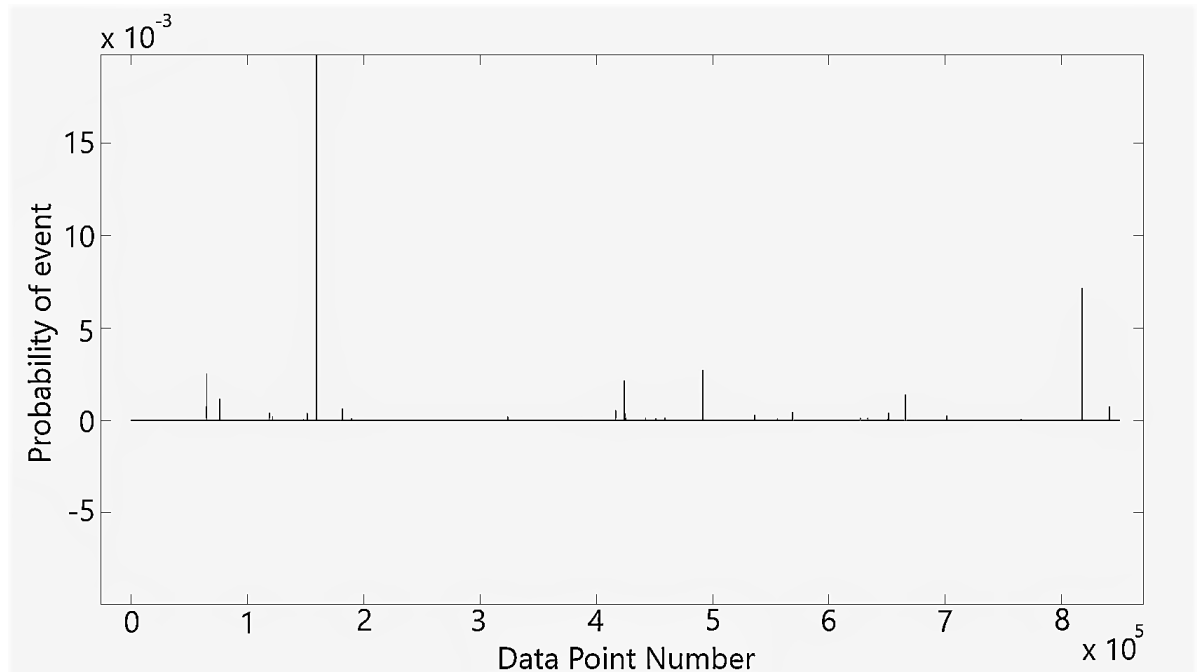
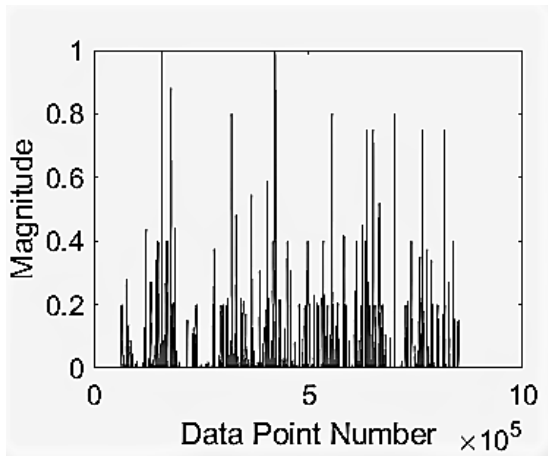
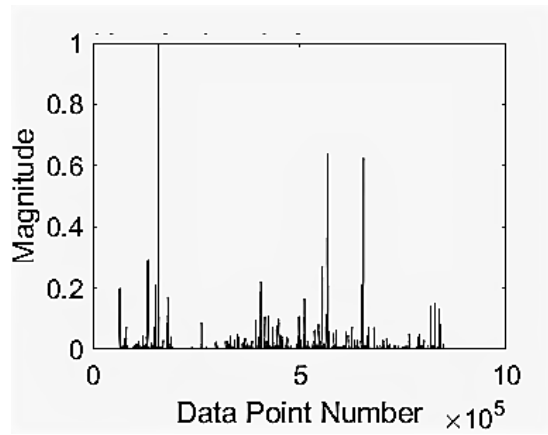


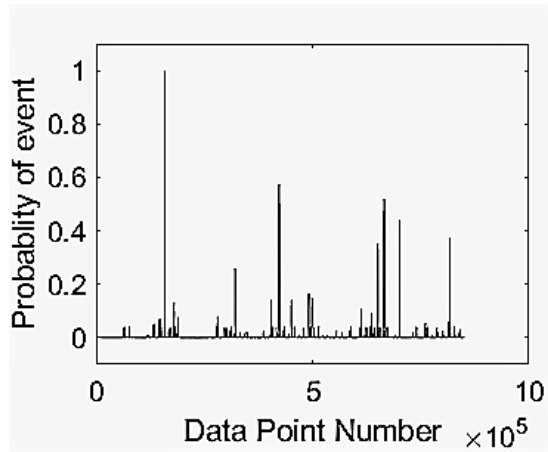
Figure 4.33: Y-axis zoomed graph of *Major_faults* for variation in *TN* for substation B



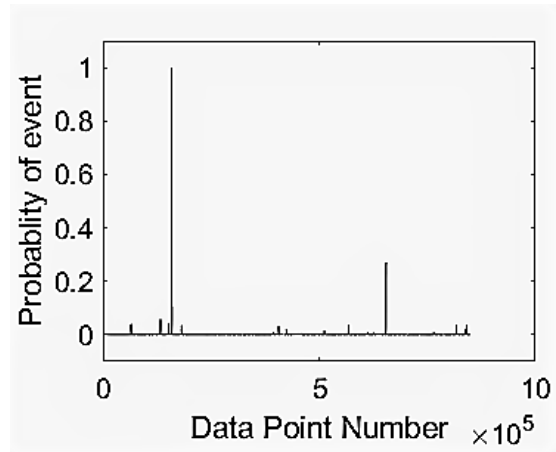
(a) Weighted sum abnormality plot for voltage



(b) Weighted sum abnormality plot for real power

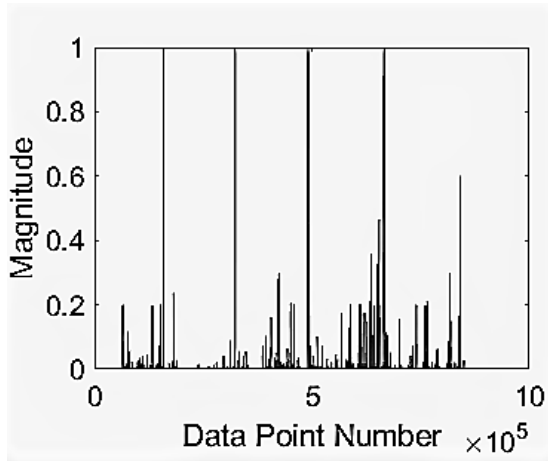


(c) Event indicators based on V and Q

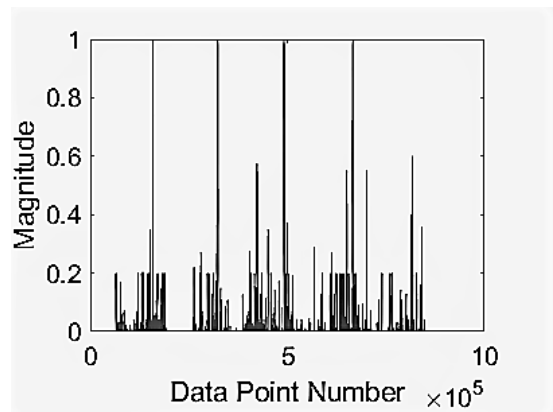


(d) Event indicators based on P and I

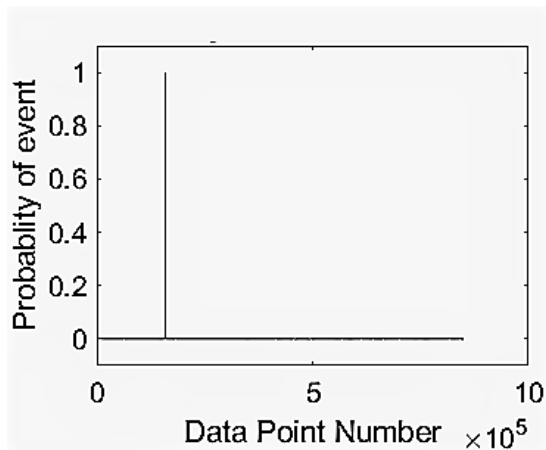
Figure 4.34: Weighted sum abnormality and 2 event indicators for variation in TN for substation C



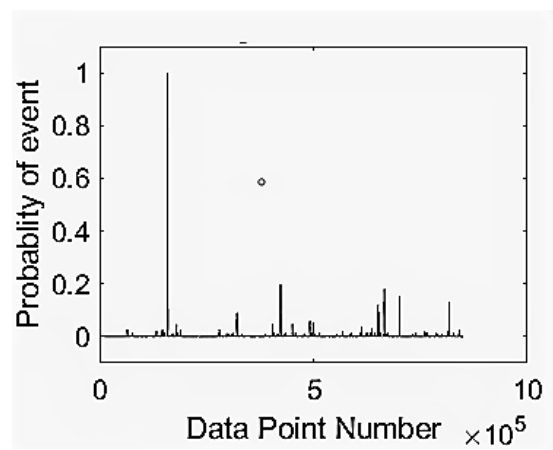
(a) Weighted sum abnormality plot for current



(b) Weighted sum abnormality plot for reactive power



(c) Major event indicators based on V-Q and P-I events



(d) Weighted event indicators based on V-Q and P-I events

Figure 4.35: Weighted sum abnormality and 2 event indicators for variation in TN for substation C

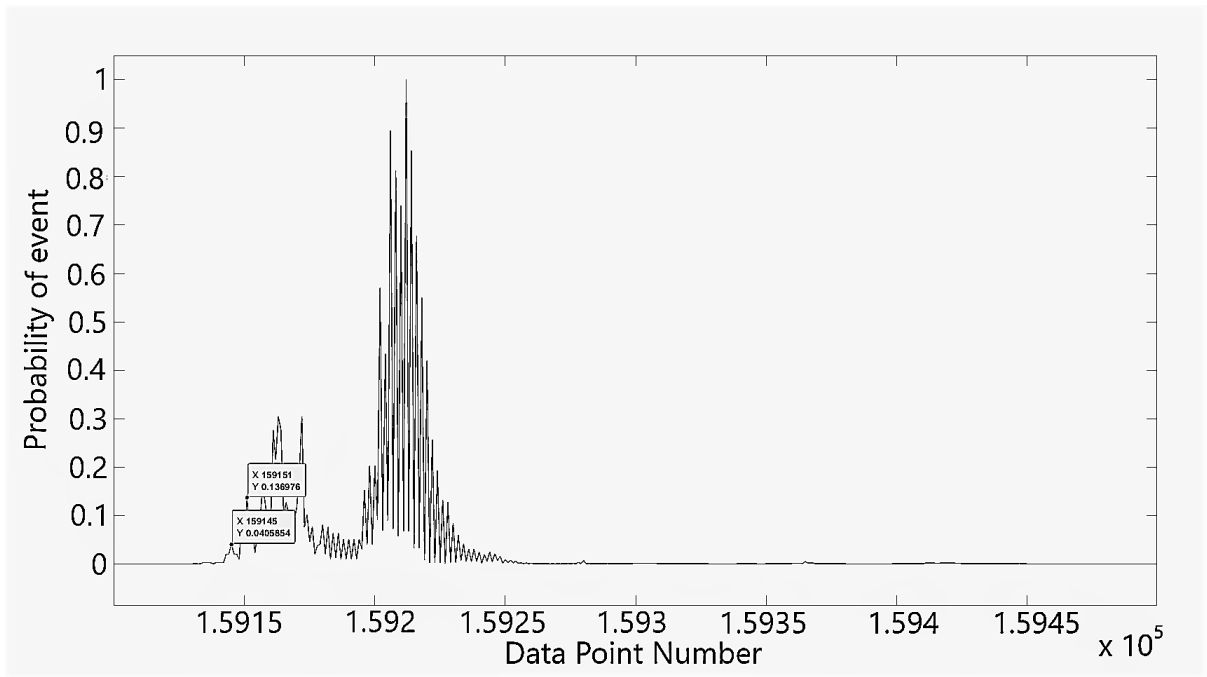


Figure 4.36: X-axis zoomed graph of *Major_faults* for variation in *TN* for substation C

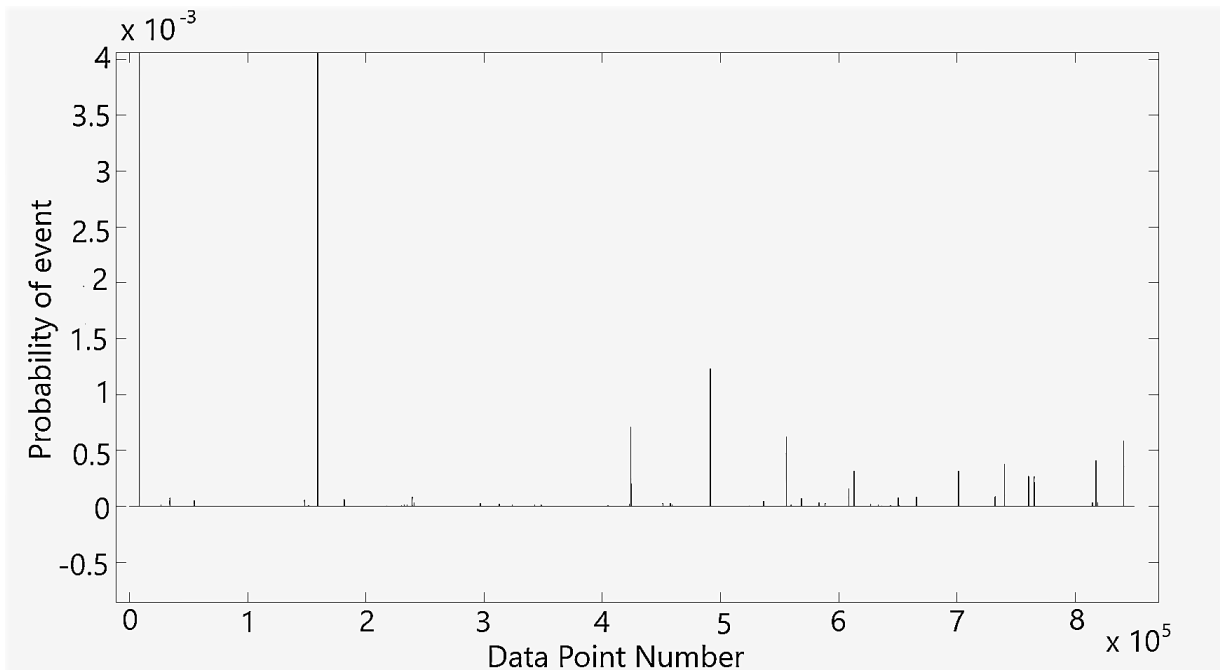


Figure 4.37: Y-axis zoomed graph of *Major_faults* for variation in *TN* for substation C

4.5 Comparison with the existing NREL Methods

4.5.1 Simulation Results using Methods used by NREL for Detecting Events

The National Renewable Energy Laboratory (NREL) in its 2014 report (Allen et al., 2013) used multiple algorithms to detect a fault and if more than 2 algorithms detect a fault at a particular data location then that location can be deemed as an actual event. The overlapping of detections made by two or more algorithms among the four algorithms Fast Fourier Transform, Yule Walker Method, Min-Max Method and Matrix pencil Method (Refer Appendices A.6 to A.9) is considered as an event in the NREL report. The power system event detections by NREL method are based on basically two signals: (a) the difference in phase angle between two PMUs called the relative phase angle difference (RPAD) and (b) frequency which is directly measured by each PMU. Each of the signal data is analysed for every 10 seconds, that is, 250 samples. That is, the window size for analysis is chosen as 10 seconds. On every sliding window, the signal processing methods have been applied and the potential events that have been captured by the algorithms have been stored. Further, these data points are classified as events whenever these data points cross the threshold of 3 standard deviations from the mean. The signal processing methods generally used by NREL have been applied to detect events for the datasets to carry out the analysis. Earlier, NREL (Allen et al., 2013, 2014) had analyzed the Texas Synchronphasor Network dataset consisting of six PMU substations namely: Austin, Harris, McDonald's, UT-3Phase, UT-PanAm and WACO. As there exists three signals (Voltage Magnitude, Voltage Phase Angle and Frequency) for every PMU substation, precisely 324,000 data points are generated each hour. The Synchronized Phasor and Frequency Measurements are stored discretely at a rate of 30 samples/s. In this case, only low-frequency oscillations, that is, below 15 Hz are analyzed as the data has a sampling frequency of 30Hz. Capacitor bank switching producing oscillations of the range of a few hundred Hz to 1.5 kHz can not be picked up and hence are observed in the PMU dataset.

Results and Discussion for NREL Methods Application on NLDC PMU data

Results are displayed in the form of plots having subplots: one showing the signal (frequency/RPAD) and the second showing the events detected by the methods. And the intersection time instants of two or more methods' results are encircled to make a conclusive decision of occurrence of events.

Dataset analysis for Northern region of Indian power system based on PMU data (frequency and RPAD signals) from 3 substations:

Various events can be seen to be detected by two or more methods, however, their magnitude might vary depending on their severity (Refer Table 4.3). The algorithms are run on all the 3 substations A, B and C. Since, it is already known that a major line trip fault occurs at approximately 3182 s according to the Grid Disturbance Report of NLDC, only the results obtained for first 4000s are shown in the plots (Refer Figs. 4.41, 4.42, 4.43 and 4.44). This zoomed view of the first 4000s would enhance the visualisation and understanding of the events detected with respect to the report. In Figs. 4.41, 4.42, 4.43 and 4.44, two or more methods have been successful in detecting the major line trip fault occurring approximately at 3182s. A sharp spike is observed at around 14824 s and 14855 s respectively in the RPAD signals of substations A-B and A-C. However, these spikes are found to be created during the data pre-processing stage of filling in for the missing values in substation A, and must not be considered as an event. Except 2-3 events being detected around these time instants, no other events are detected by any of the methods (Refer Table 4.4). Hence, the plots have not been included in this report. This could be considered as a limitation of the methods, that they are sensitive to missing data.

Events are detected and recorded in the Indian Power System for the Northern region of India during "Amphan" cyclone. To make the conclusion, intersection of events detected by two or more methods have been classified as an event. And their corresponding timestamps are noted as well. This approach is used to detect large faults in power systems. The analysis successfully detects the major line trip fault in the first dataset and the oscillation fault in the second dataset as shown in the plots and tables. It can be suspected that since a window length of 10 seconds is used for all the implementation of the methods, the time at which a fault is detected might have an error margin of ± 10 seconds. Another limitation observed is the methods are sensitive to data pre-processing of RPAD signal calculated from PMU data in some cases.

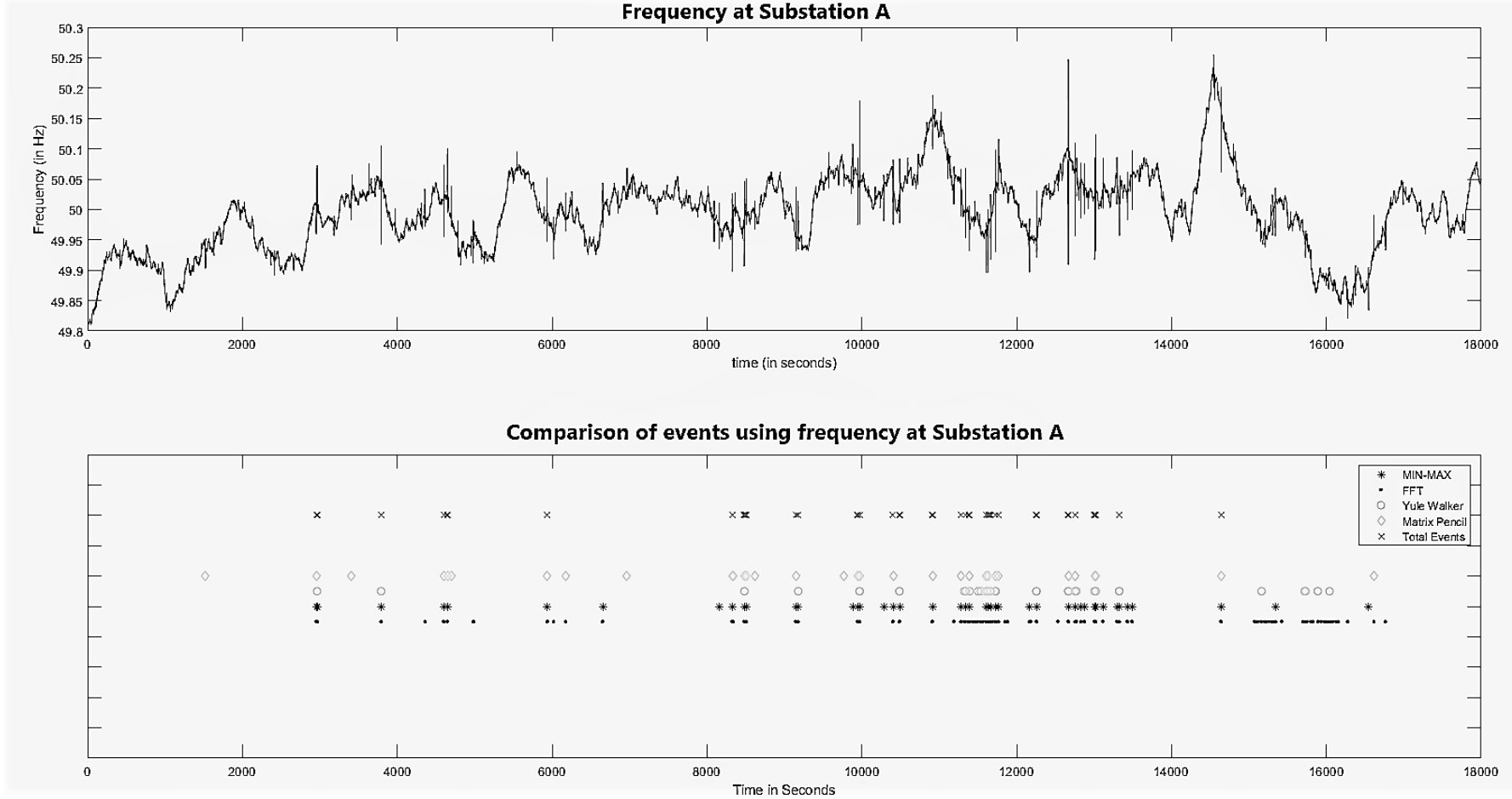


Figure 4.38: Fault indication by multiple methods for PMU situated at substation A

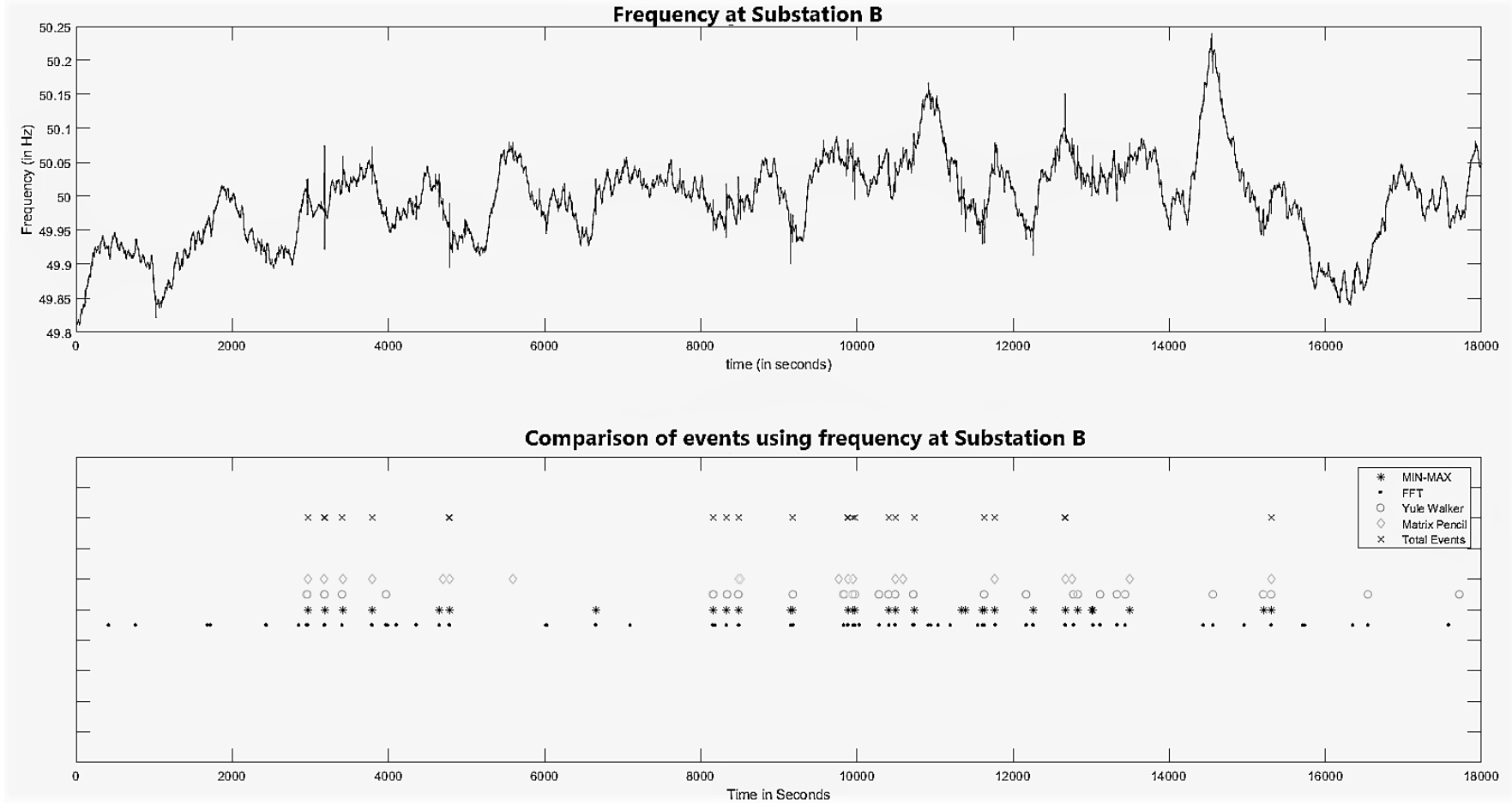


Figure 4.39: Fault indication by multiple methods for PMU situated at substation B

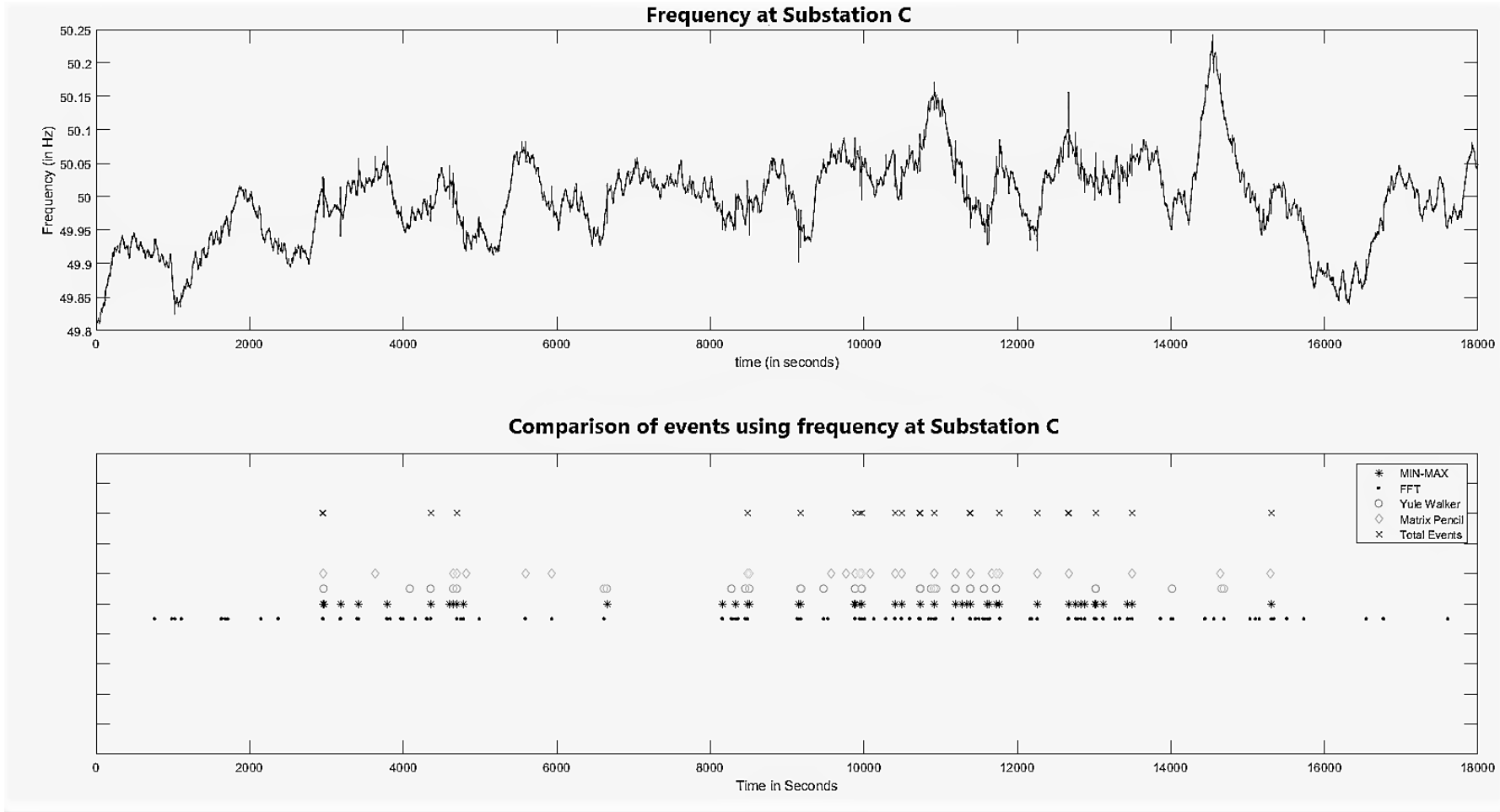


Figure 4.40: Fault indication by multiple methods for PMU situated at substation C

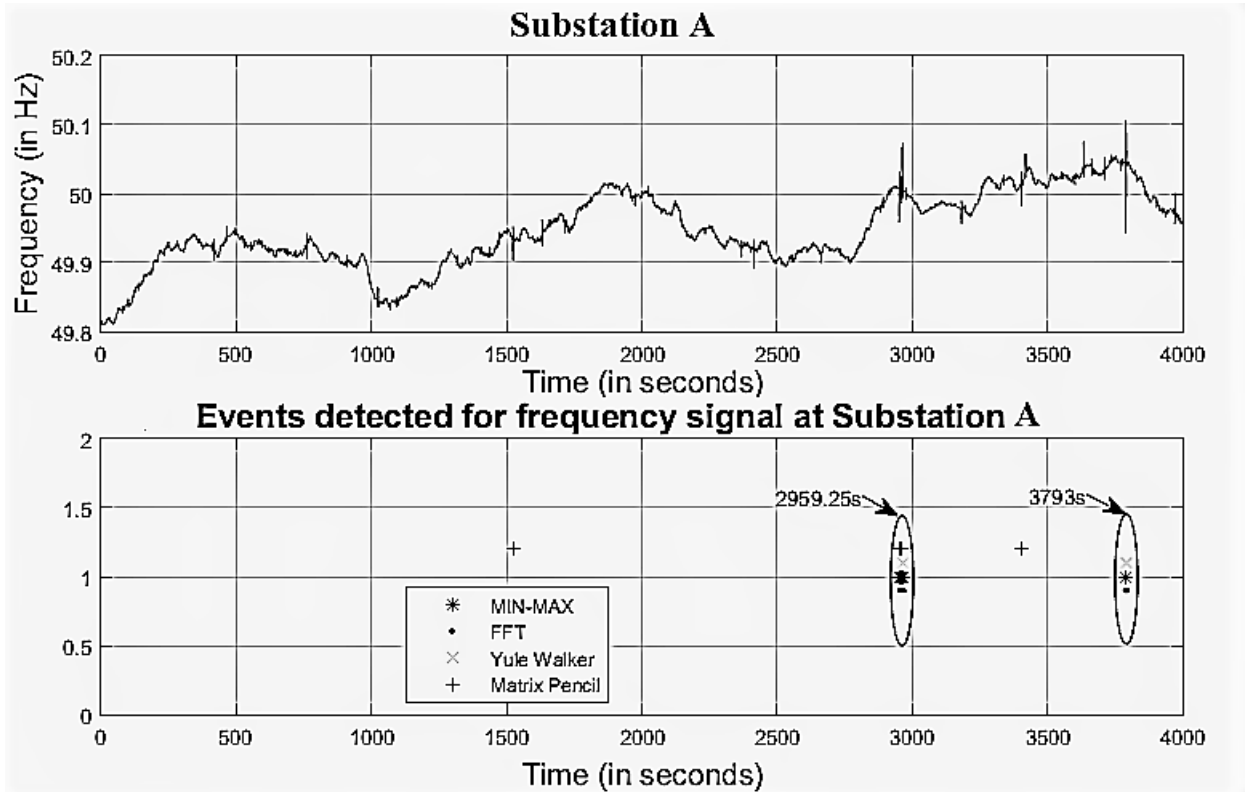


Figure 4.41: Zoomed in plot for event detection using frequency at substation A

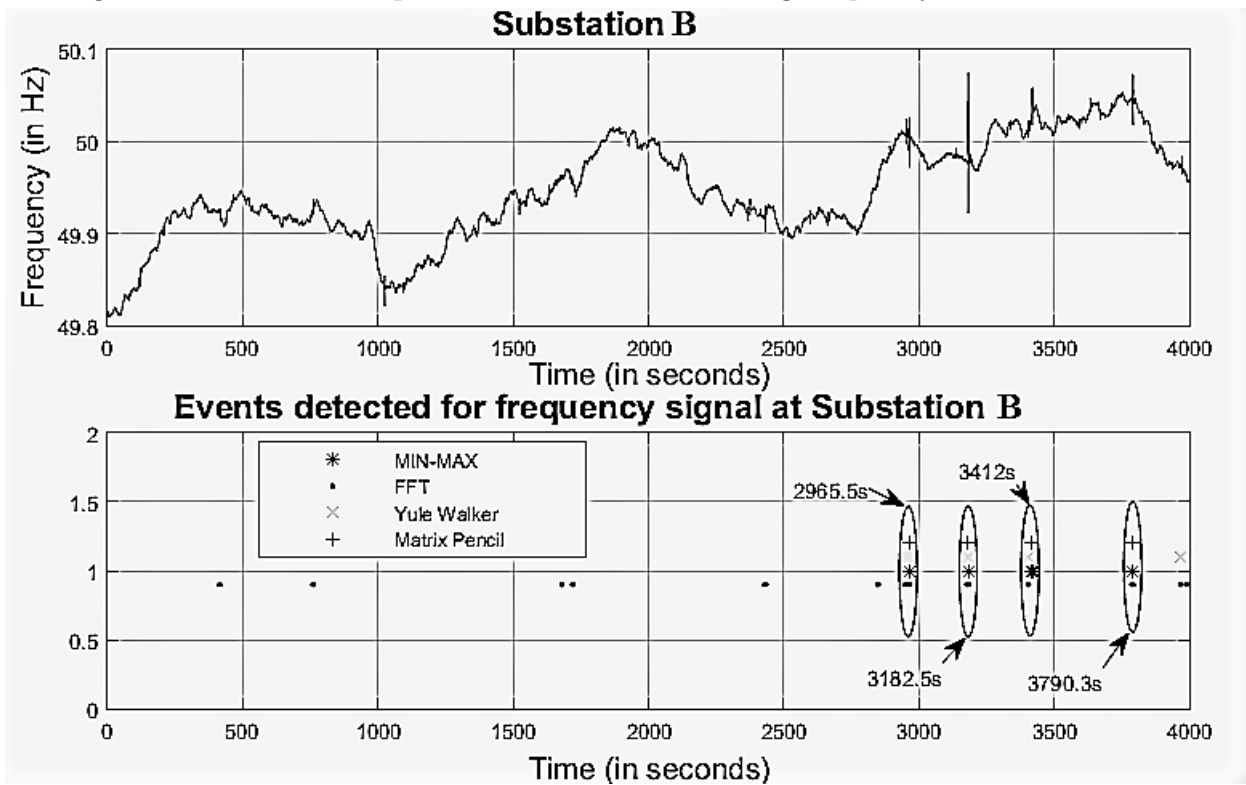


Figure 4.42: Zoomed in plot for event detection using frequency at substation B

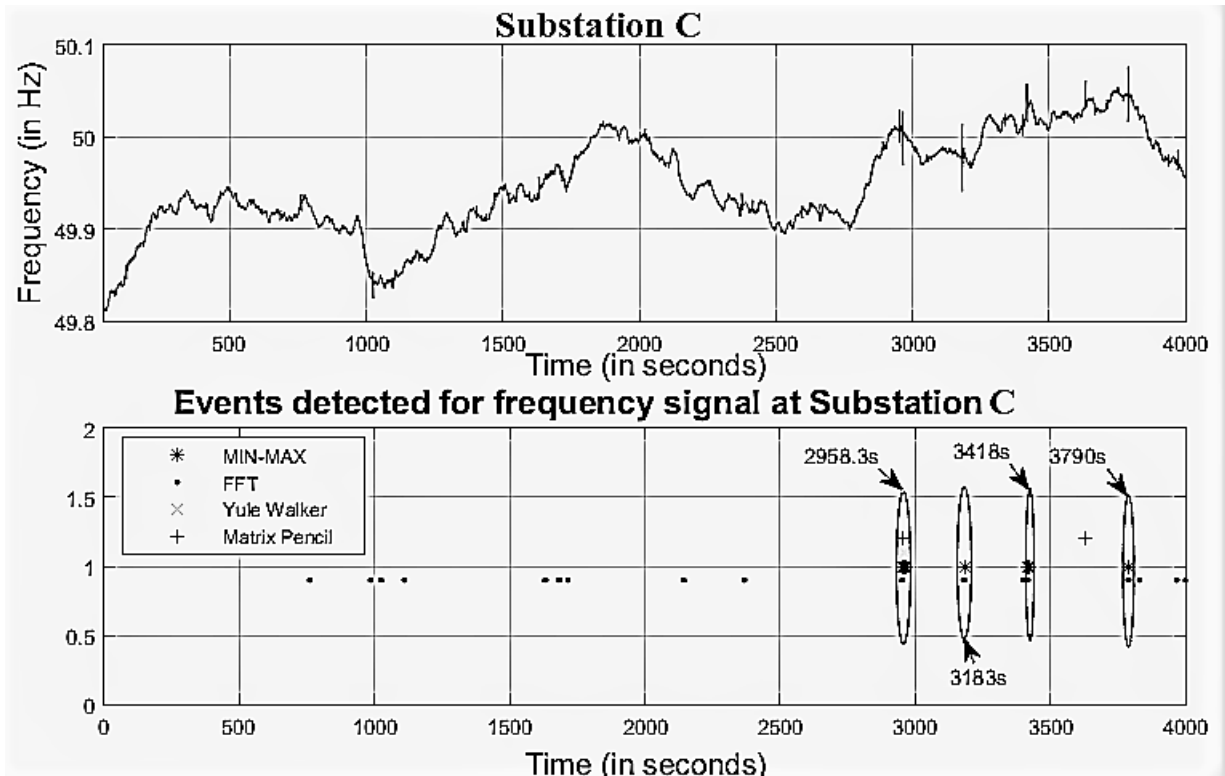


Figure 4.43: Zoomed in plot for event detection using frequency at substation C

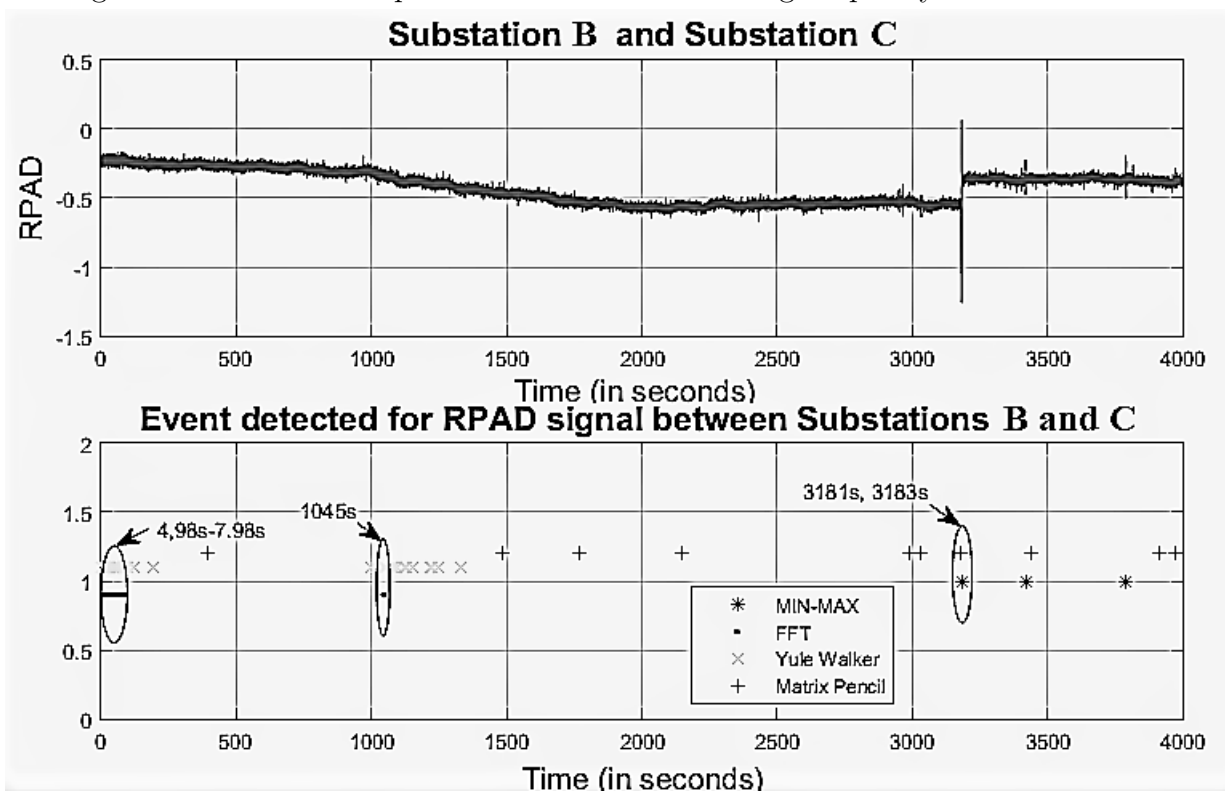


Figure 4.44: RPAD analysis for event detection between B and C

Table 4.3: Events detected analyzing frequency signals (5 hours) during cyclone Amphan

Method used	PMU substation		
	Substation A	Substation B	Substation C
FFT Method	172	80	131
Yule Walker Method	41	40	34
Min-Max Method	91	63	89
Matrix Pencil Method	33	19	29
Events	31	14	16

Table 4.4: Events detected analyzing RPAD signals (5 hours) during cyclone Amphan

Method used	Between PMU substations		
	C and A	B and C	A and B
FFT Method	2	30	2
Yule Walker Method	11	69	16
Min-Max Method	2	64	2
Matrix Pencil Method	3	61	3
Events	2	26	3

Inferences from the Comparative Studies

The effectiveness of the new algorithm supersedes most of the currently existing algorithm. The results obtained by using the methods utilized by National Renewable Energy Laboratory(NREL) (Allen et al., 2014) are compared with that of the proposed method. The NREL report suggests to use multiple algorithms to detect a fault and two or more algorithms detect a fault at a particular data location then that location can be deemed as an actual event. Figs. 4.38, 4.39 and 4.40 show the detections for all 0.9 million data points. Each method is shown with its unique legend and event detection is shown with another legend.

The x-axis represents time in seconds considering a sampling rate of 50 samples per second, it is known that the major event has occurred at 1,59,137 data point hence at 3182.74 seconds. However, multiple fault detections are observed throughout the time period which suggests that the algorithms are not well optimized for avoiding false detections. These algorithm has a precision of 10 seconds. Suppose an event is detected at 500 seconds then the actual event can be in between 490 and 510 seconds. Hence, the maximum deviation in identification of event is 10 seconds. This in itself makes the new proposed algorithm a lot better than the already existing algorithm suggested by NREL (Allen et al., 2014). With the proposed method, the *V-Q-faults*, *P-I-faults*, *Major-faults* and *Weighted-faults* plot shows only one event and that is at 1,59,144 data

point. An x-axis zoom between data points 1, 59, 100 and 1, 59, 500 of the *Major_faults* graph for Substation C is shown in Fig. 4.17. It is seen that the first detection using $Threshold_{180 \times Min}$ has occurred at data point 1,59,145 which is just 9 data-points or 0.4 seconds after the occurrence of event. If the threshold for the probability of event detection is lowered to $Threshold_{10 \times Min}$ then the first detection is observed at 1, 59, 138 which is just 2 data-points or 40 milliseconds after the occurrence of event.

4.5.2 False Positives and Increase in Number of Detections

In Figs. 4.39, 4.40 and 4.38 there are multiple events detected as shown by the total events legend. This is also observed alternatively in the Table 4.5. Since, there is no distinction between major and minor events detected by the NREL method (intersection of the 4 Methods), it is extremely difficult to distinguish important/major events which causes huge losses to the generating authority from the normal operating condition disturbances. Therefore, we may say that false positive alarms are more in case of NREL method event detection. The information provided by each of these detections is negligible. While using the proposed major event detection technique, the information density in detection is also reduced considerably and only the exact and precise major event location is highlighted.

Table 4.5: Comparison of Events Detected (during 5 hours) by NREL and the proposed methods

Method Used	Substation B	Substation C	Substation A
FFT	172	80	131
Yule Walker	41	40	34
Min-Max	91	63	89
Matrix Pencil	33	19	29
Events Detected by NREL: Intersection of Methods	31	14	16
Events Detected by Proposed Method	1	1	0

From Figs. 4.38 and 4.40 the number of false positives have increased when compared to Fig. 4.39, implying that the increase in detections is because of the random noise in the system. Most algorithms have this characteristics that the number of detections is directly proportional to the noise in data. This implies the lack of robustness of the method as the detection should depend on events occurring in the system and not the amount of noise in the system. Hence, if there is a thunderstorm in a particular area then

the algorithm will continuously detect events in the grid even though the grid is operating properly. But with the proposed method the *V-Q_faults*, *P-I_faults*, *Major_faults* and *Weighted_faults* plot shows only one event and that is approximately at 1,59,145 data point.

4.5.3 Relative Intensity of Events

Relative intensity of an event provided by the *Weighted_faults* plot at each substation will give an idea as to which substation is closest to the occurrence of fault. Also, relative intensity of a fault at one location with respect to another location gives a general idea of fault propagation and helps to localize the area where the fault will propagate to. But, in the existing method used by NREL, there is no framework present to distinguish the intensity of an event in one location with respect to another location. This leads to lower information content in detection and also does not contribute to the situational awareness of the grid.

With the proposed method, the *V-Q_faults*, *P-I_faults*, *Major_faults* and *Weighted_faults* plot shows only one event and that is at 1,59,144 data point. At that time instant, it is observed that the maximum probability of event in *Weighted_faults* at substation C (See [4.15](#)) is 0.8, while the highest peak reached by *Weighted_faults* at substation B (See Fig. [4.9](#)) is 1. This shows a relative intensity of fault between Substation B and Substation C. This relative probability of events can also be inferred from the fact that Substation C is farther away from the actual grid event when compared to Substation B. This means that the intensity of disturbance caused by the actual fault is lower at Substation C as compared to that at Substation B.

4.6 Summary

The proposed new technique for major event detection is proven to be efficient. On proper selection of hyper parameters, the detections occur within 40 ms, the method has been elaborately presented. The main features of the proposed technique are listed below:

- Precise and fast detection of major events with data point location. Hence forming a sensitive yet accurate event instance identifier.
- Framework presented incorporates differing thresholds for each substation depending on nominal operating characteristics of that particular Substation.
- Framework to understand which region in a large system has the largest, 2nd largest, 3rd largest, ... n^{th} largest fault using probabilistic model.

- Probabilistic framework is useful for identifying the major events and ignore the minor events.
- Framework constantly learns nominal system noise hence eliminating False positives even in a very high noise environment.
- Multiple layers of refinement is carried out for obtaining high level of abstraction.
- Robust Detection even on selection of absurd hyper-parameter values.
- Avoids repetitive fault detection for the same fault, instead the framework gives the exact time instance with an associated probability of event for the detection which in turn improves the information content in detection.
- Weighted detection which gives a weighted probabilistic intensity of an event compared to other events occurring in the system hence giving a better insight of the system stability.

Further, comparison studies are carried using the event detection method generally used by NREL in a power system based on Synchrophasor data (frequency and RPAD signals). Many events are detected and recorded for the datasets of the Northern region of Indian Power System during cyclone Amphan. But, there is no way to identify if the events are major or minor events. Some of them might be false positive events due to the noise content in the PMU data. In contrast, the proposed new technique for major event detection has an inbuilt robustness to filter high noise data in order to detect actual events with a labelling of intensity of the event. Whatsoever, the analysis successfully detects the major line trip fault in the dataset as shown in the plots and tables. Since a window length of 10 seconds is used for all the implementation of the methods, the time at which a fault is detected might have an error margin of ± 10 seconds. Another limitation observed is the NREL method is that it is sensitive to data pre-processing of RPAD signal calculated from PMU data in some cases.

Chapter 5

Optimal Placement of PMUs in Power Systems using Crow Search Algorithm

Situational awareness of the electric power system is the need of the hour. This is in the wake of recent blackouts in various parts of the world. These blackouts could have been prevented with better telemetry and real-time monitoring of power system states. For precise power system monitoring, a major focus is on involvement of the latest technology based on phasor measurement units (PMUs). As the sole system monitor, state estimator plays an important role in the security of power system operations. Optimal placement of PMUs (OPP) with numerical observability ensures reliable state estimation. For economical and efficient utilization, there is a need to optimize the placement of PMUs in the power system network. This optimal placement of PMUs (OPP) problem is a binary/boolean optimization problem which is combinatorial in nature. A new approach called Crow Search Algorithm (CSA) has been implemented for solving optimal placement problem. The new approach is compared to the binary integer linear programming method which is the dominant method for an optimization problem providing global optimum point. The major constraints such as topological, numerical observability conditions with and without zero-injection buses (ZIBs) are considered. Contingencies and limitation of measurement channels in a PMU device are also incorporated as constraints. The main advantage of using the CSA is that it provides multiple solution sets. This becomes advantageous in planning stage for power engineers for placing PMUs depending on the concern more significant for a particular power system. The results obtained are compared with that of the dominant binary integer linear programming method. Test systems are

¹Based on the contribution work presented in this chapter, a journal paper entitled *Security-Constrained Study of Optimal Placement of PMUs using Crow Search Algorithm* has been published in *Journal of Applied Soft Computing*, Elsevier, 2022

of varied sizes such as: IEEE 14-bus, IEEE 30-bus, IEEE 57-bus and 72-bus practical equivalent system of Indian southern region power grid.

5.1 Introduction

The difficulties in power system operation are swelling multifold day by day. These are as a consequence of an expanding system size, quick capacity enlargement, bulk power flows between areas/regions far apart, multiple players, rise in competition in the power market, environmental change, extensive augmentation of renewable resources in certain areas and rising customer demands. Hence, situational awareness of the wide area network becomes extremely important. This is completely dependent on the real-time measurement system and monitoring. Especially, visualizations on the dashboard at main control centre (MCC) play an inevitable role in assisting system operator to make better decisions. On 14th Aug 2003, one of the largest blackouts brought down 263 power plants in USA & Canada and affected 8 states, 3 regions, 61800 MW load. In India, largest blackout affected loads of 48000 MW. Recently, on August 2019, the UK experienced one of the worst blackouts in a decade, resulting in 1.1 million electricity customers losing power, major disruption to parts of the rail network and impacts to other critical facilities including a hospital and airport. Although power outages on this scale are rare, the incident served as a reminder of the importance of ensuring security of supply and raised important questions across the industry.

PMUs are microcontroller based devices that computes phasor values of voltages and currents from voltage transformer (PT) and current transformer (CT) measurements respectively. Operation of PMUs are controlled by pulse per second (PPS) sent by GPS satellites, enabling the real-time visualization of WAMS. Time-stamping and highest accuracy compared to other existing measuring systems makes it stand out as the best option for WAMS. Several large-scale deployment projects are being carried out worldwide including NASPI (North American Synchro Phasor Initiative) led by North American Electric Reliability Corporation (NERC), the WAMS in the Western Grid of the North America (Phadke and Tianshu, 2018), Brazilian phasor measurement system, the WAMS in China, various developments in Europe, etc.

5.2 Modeling of Problem Formulations and Methods for solving Optimal Placement of PMUs

PMUs are presently the most accurate measurement technology with GPS time stamping providing information to power engineers and system operators for WAMS. But each

PMU costs from \$1260-\$10,000 depending on the number of channels it provides for measurement. So, it is very crucial to find the minimum number of such PMUs required for implementation in a given power system network. This is a rigorous research area and a number of conference and journal papers have been published on OPP in IEEE, ITEES, IET and Elsevier during years 2003-2020 (Refer Fig. 5.1).

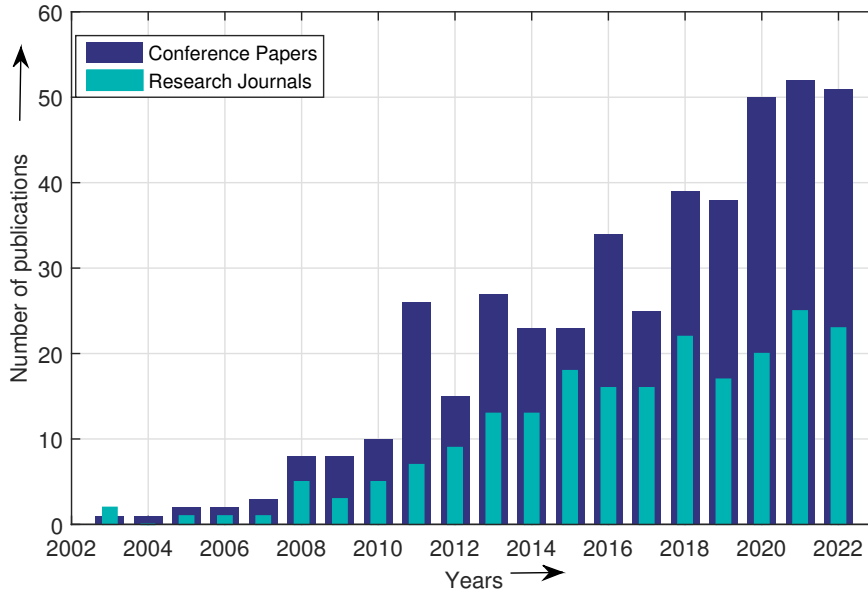


Figure 5.1: Number of conference and journal papers published on OPP in IEEE, ITEES, IET and Elsevier during the years 2003-2022

OPP is a binary optimization problem. Based on objective function and constraints, the OPP problem could be formulated with variables and equations that are partially discrete, partially continuous, non-differentiable and non-linear. Two components of OPP problem formulation: objective function and constraints are briefly presented as follows.

5.2.1 Objective function

The objective function model may be to cut down the possible cost comprising of variable and fixed PMU installation cost. Other possible objectives may be to maximize measurement redundancy or maximizing selection of more significant buses with respect to small signal stability assessment. Another viable model uses a multi-objective model as the aim of OPP formulation.

The objective functions considered in OPP problems found in the literature until now are mainly for minimization of number of PMUs (5.1), maximization of redundancy (5.2) or both (5.3) as a multi-objective function.

$$Min F_1 = \sum_{i=1}^N x_i \tag{5.1}$$

where x_i is a decision variable taking value 1 (if bus i is equipped with a PMU) and 0 (otherwise). For example, in Fig. 5.2 for a sample 6-bus network, there are many possible PMU locations for the optimal number of PMUs to achieve complete observability constraint. Complete observability means every bus is either having a PMU device installed on it or is connected to a bus with PMU device. Consider the two possible cases of PMU placements as shown in Fig. 5.2 (a) and (b). Any of these two solutions may be obtained when the objective is minimization of PMUs as described by (5.1), as the cost for both these solutions will be same ($F_1 = 2$). And the constraint of complete observability of the system cannot be obtained with just one PMU ($F_1 = 1$). Ideally if there are no constraints and only objective function is to minimize cost, 0 PMUs will be the solution. Hence, for any optimization problem, along with the objective function some constraints are also considered as discussed in the next section 5.2.2

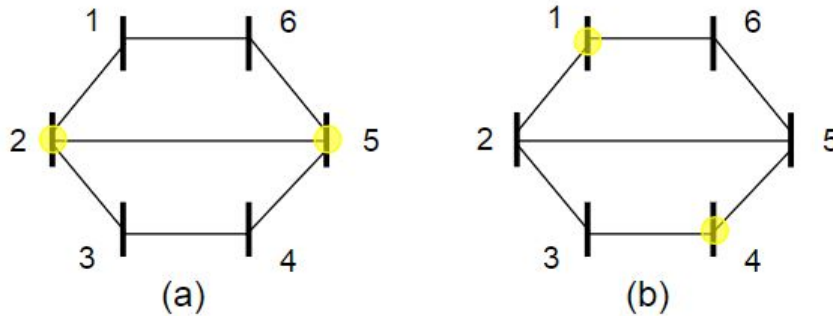


Figure 5.2: Optimal number of PMUs for a completely observable sample 6-bus system is 2.

The following is the Objective function for maximization of redundancy:

$$Max F_2 = \sum_{i=1}^N o_i \quad (5.2)$$

where o_i is the expression which accounts for the number of times bus i is observed; N is the total count of buses in the power system; F_1 and F_2 are the objective functions for number of PMUs and redundancy respectively as shown in (5.1) and (5.2). For the same example of 6-bus network, the placement locations shown in Fig. 5.2. If the objective is maximization of redundancy as described in (5.2). Among the two possibilities shown in Fig. 5.2, (b) is a better solution, since for (a) $F_2 = 1+2+1+1+2+1 = 8$ (b) $F_2 = 1+1+1+1+1+1 = 6$. But, maximum value for this objective function will be obtained when PMUs are placed on all the buses, which is not feasible due to economical reasons. Hence, for any optimization problem, along with the objective function some constraints are also considered as discussed in the next section 5.2.2

Combining both objectives is possible by changing second function into minimization problem. Thus, by changing the sign of second function into negative and aggregate the

problem as follows:

$$\text{Min } F = \sum_{i=1}^N x_i - \frac{1}{N \times \max(o_i^{\text{allPMU}} + 1)} \sum_{i=1}^N o_i \quad (5.3)$$

where o_i^{allPMU} is the number of times that bus i is observed when all the buses are having PMUs. The coefficient in the second term of (5.3) makes sure that F_1 has higher importance than F_2 in the OPP. In majority of the works, only (5.1) considering F_1 is taken to be the objective function for the OPP.

A non-linear programming (NLP) formulation (Almunif and Fan, 2020) is a non-convex optimization solved by sequential quadratic programming (SQP). This can lead to several local minimum optimal points. The corresponding objective function is as follows:

$$\text{Min } F_3 = X^T W X = \sum_{i=1}^N w_i x_i^2 \quad (5.4)$$

where W is the diagonal weight matrix.

Some realistic constraints like CT, PT or communication network availability is incorporated in the objective function (Rather et al., 2014):

$$\text{Min } F_4 = \sum_{i \in N} x_i$$

where

$$x_i = x_{pmu} + x_{pt} + (r - 1) \times x_{ct} + x_{shd} + x_c + x_{ad}$$

$$x_{pt} = \begin{cases} 0; \text{ if PT is available for PMU use.} \\ \text{Actual cost of PT; if new PT is to be installed} \end{cases}$$

$$x_{ct} = \begin{cases} 0; \text{ if CT is available for PMU use.} \\ \text{Actual cost of CT; if new CT is to be installed} \end{cases}$$

$$x_c = \begin{cases} 0; \text{ if feasible communication network is available for PMU use.} \\ \text{Actual cost; Otherwise} \end{cases}$$

r is number of branches terminating at bus; x_{ad} accounts for additional costs.

A multi-objective model (Manoharan et al., 2018) which provides full topological ob-

servability, monitoring voltage stability and minimizes communication channel cost is formulated as follows:

$$\text{Min } F_5 = \left(\min \sum_{i=1}^N q_i x_i (1 - \sum_{j=1}^n e_j h_j), \min \sum_{i=1}^N \sum_{j=1}^N FVSI_{ij} x_j \right) \quad (5.5)$$

where q_i is cost of PMU to be placed on bus i ; e_j probability of system state j ; h_j observability of power system state j ; $FVSI_{ij}$ is Fast Voltage Stability Index for line $i - j$.

Another multi-objective model (Huang et al., 2019) considers the objective functions: one same as in (5.1) and another is F_6 , average possibility of unobservability:

$$\text{Min } F_6 = 1 - APO = 1 - \frac{1}{N} \sum_{i=1}^N PO_i$$

here APO stands for average possibility of observability as defined above. And PO_i given by,

$$PO_i = 1 - \prod_{j=1}^N (1 - x_j A_{ij}^l) \quad \forall i = 1, 2, \dots, N$$

where PO_i is the possibility of observability under single line outage; A_{ij}^l Modified node incidence matrix under influence of single line outage.

Small signal stability assessment based OPP objective (Arpanahi et al., 2019) is defined as,

$$\text{Max } F_7 = \sum_{i=1}^N E_{lsv,i} x_i$$

where $E_{lsv,i}$ is the error of the largest singular value defined as,

$$E_{lsv,i} = |s_{li} - s_{lm}|$$

where s_{li} and s_{lm} are the largest singular values related to case that PMUs install at all buses except bus i and to the case where PMUs are installed at all buses.

Another application based OPP has been carried out with the strategy to employ PMUs in close proximity of higher probability contingencies (Almasabi and Mitra, 2019). Thus, increasing the likelihood of more effective remedial actions, both preventive and corrective. The multi objectives in this case with higher level objective being cost and

lower level being the observability are:

$$\text{Min } F_8 = \sum_{i=1}^N (a_i + b_i + k(i)x_i) + PDC \quad (5.6)$$

$$\text{Max } F_9 = \sum_{i=1}^N O'_i \quad (5.7)$$

where

a_i is unit cost for PMU at substation i

b_i is cost for installing additional channels at substation i

$k(i)$ is cost function for the communication network infrastructure at substation i

PDC cost of phasor data concentrator.

$$O' = H' \times X$$

$$H'_{ij} = \begin{cases} 1 + v_{i,i}, & \text{if a PMU is installed at bus } i \\ 1 + v_{i,j}, & \text{if there is a branch connecting bus } i \text{ to bus } j \\ 0, & \text{Otherwise} \end{cases}$$

where $v_{i,i}$ is the vulnerability element (i,i) in bias matrix (Almasabi and Mitra, 2019) and $v_{i,j}$ is the vulnerability element (i,j) in bias matrix.

In an attempt to include DULR (dual-use line relay) placement as well in OPP formulation (Rosalina et al., 2019) for a better economic study of power system, the following objective function is used,

$$\text{Min } F_{10} = \sum_{i=1}^N q_i x_i + \Delta \sum_{e \in \mathcal{E}} \{w_e^u + w_e^t\}$$

Here, for each edge e , there are binary valued variables, w_e^t (set to 1 if DULR is placed at lower end) and w_e^u (set to 1 if DULR is placed at upper end); \mathcal{E} is set of all edges.

5.2.2 Constraints

Conventional constraints are just observability of the network by making sure that each bus is observable while maintaining a certain measurement redundancy. Majority of the research papers on OPP have considered only topological, but few papers emphasize on the need for numerical observability for successful state estimation. And recent works deal with constraints based on critical contingency conditions, loss of conventional measurements, PMU measurements, communication infrastructure, reliability and fault observability. A brief description of different constraints reported in the literature are

presented in following subsections.

A. Complete topological observability of the network under normal conditions (Dubey et al., 2018)

Let O be the observability vector consisting of observability expressions consisting of o_i 's each standing for i^{th} observability constraint. Then, for complete topological observability the following inequality should be satisfied,

$$O = AX \tag{5.8}$$

$$O \geq u \tag{5.9}$$

where, A is the Node incidence matrix or binary connectivity matrix, whose size is $N \times N$ and is of the form:

$$A = \begin{bmatrix} 1 & 0 & \dots & 1 \\ 1 & 1 & \dots & 0 \\ \vdots & \vdots & \vdots & \vdots \\ 1 & 0 & \dots & 1 \end{bmatrix}$$

whose elements are given by,

$$A_{ij} = \begin{cases} 1 & ; \text{ if either } i = j \text{ or } i \text{ and } j \text{ buses are joined by a branch;} \\ 0 & ; \text{ Otherwise .} \end{cases}$$

X is row vector having size $N \times 1$ with elements $x_i, i=1,2,\dots,N$ as follows

$$X = [x_1, x_2, \dots, x_N]^T$$

u is a row vector $N \times 1$ consisting of ones, representing that a bus is observable by atleast one PMU is given by

$$u = [1, 1, \dots, 1]^T$$

In another approach, that is, by using Boolean algebra (Azizi et al., 2014), the observability of bus i as a function of PMU locations is as follows:

$$o'_i = \vee_{i \in N} A_{ij} x_i \tag{5.10}$$

where “ \vee ” is the Boolean “OR” symbol.

For example, let us consider a 6-bus system with network connectivity as shown in Fig. 5.3. The complete topological observability constraint (5.8) for achieving the goal of

every bus to be observable by atleast one PMU device will be as follows:

$$\begin{array}{c}
 x_1 \\
 x_2 \\
 x_3 \\
 x_4 \\
 x_5 \\
 x_6
 \end{array}
 \begin{bmatrix}
 1 & 1 & 0 & 0 & 0 & 1 \\
 1 & 1 & 1 & 0 & 1 & 0 \\
 0 & 1 & 1 & 1 & 0 & 0 \\
 0 & 0 & 1 & 1 & 1 & 0 \\
 0 & 1 & 0 & 1 & 1 & 1 \\
 1 & 0 & 0 & 0 & 1 & 1
 \end{bmatrix}
 \begin{bmatrix}
 x_1 \\
 x_2 \\
 x_3 \\
 x_4 \\
 x_5 \\
 x_6
 \end{bmatrix}
 \geq
 \begin{bmatrix}
 1 \\
 1 \\
 1 \\
 1 \\
 1 \\
 1
 \end{bmatrix}$$

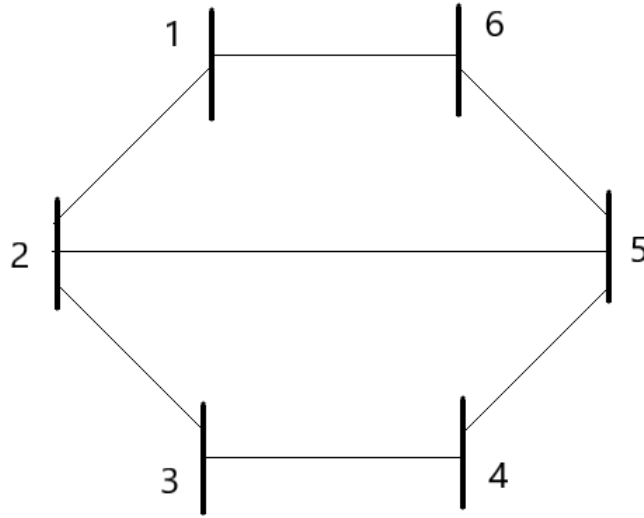


Figure 5.3: Sample 6-bus system with 7 tie-lines

B. Effect of zero-injection buses (ZIB) on topological observability of the network (Gou, 2008a; Xu and Abur, 2004)

To illustrate this concept, an example of a simple 3-bus system (Babu et al., 2020) is considered as shown in Fig. 5.4. For instance, if a PMU placed on bus 1, while bus 2 being a ZIB and bus 3 is a load bus. Bus 1 is directly observable while bus 2 is connected to the PMU bus and is also indirectly observable by Ohm’s law considering the voltage drop. As bus 2 is a ZIB, the current flowing over lines 1–2 and 2–3 are equal. By knowing the voltage at bus 2 and the current phasor on line 2–3, the voltage on bus 3 can be computed using Ohm’s law. As a result, buses 1, 2, and 3 are all observable when bus 2 appears to be a ZIB. Therefore, consideration of ZIB minimizes the number of PMUs required to make the power network completely observable.

Now, this effect of ZIB on topological observability can be implemented in two ways as follows:

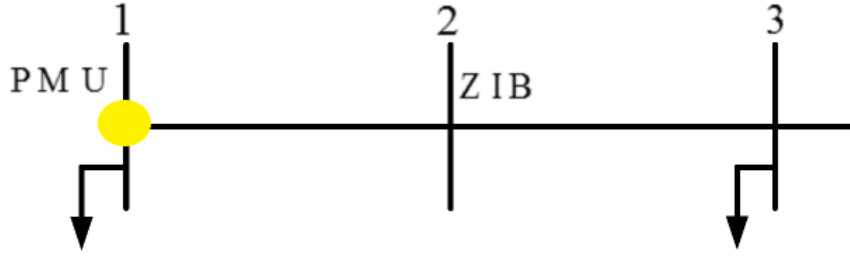


Figure 5.4: Effect of ZIB in power system observability

1. Auxiliary variable technique: The topological observability constraint of each of the buses connected to a zero-injection bus (ZIB) is updated by introducing virtual connections to every other non-ZIB bus connected to that same ZIB. The observability function (5.8) is modified to become:

$$o_i = \sum_{j=1}^N A_{ij}x_j + \sum_{j=1}^N w_{ij}x_j \quad \forall i = 1, 2, \dots, N \quad (5.11)$$

$$O \geq u$$

where, w_{ij} is an auxiliary binary variable equal to 1, if buses i and j are both connected to the same ZIB, otherwise 0.

Another approach to solving zero-injections would be by augmenting product terms into the constraints associated with the neighboring buses (Xu and Abur, 2004).

A Boolean algebra approach (Azizi et al., 2014) is used for forming the observability function as follows:

$$o_i'' = o_i' \vee Z_i$$

where o_i' is as expressed in (5.10) and Z_i is observability function of bus i , which is a zero-injection bus or adjacent to a ZIB, given by,

$$Z_i = \vee_{j \in N_z} A_{ij}b_{ij}, \forall i \in N_c$$

where b_{ij} is a binary auxiliary variable, whose value 1 indicates calculation of voltage phasor of bus i , is assigned to resulting equation from the zero injection j ; N_z is set containing indices of zero injection buses; N_c is set containing indices of zero-injection buses and their adjacent buses. An enhanced OPP formulation is developed incorporating observability propagation depth and this involves an iterative

approach (Guo et al., 2020). The initial condition is given as,

$$o_i[1] = x_i + \sum_{j \in \mathcal{N}(\cdot)} \omega_{ij}$$

where $\mathcal{N}(\cdot)$ are open neighboring set of bus i , $\mathcal{N}(\cdot) = j | (i, j) \in \mathcal{E}$; ω_{ij} , is 1 if a PMU is installed at bus j and bus i can be observed by the current measurement on line $(i - j)$ or 0, otherwise. Next iterative refinement of observability function is given by,

$$o_i[\mathcal{P} + 1] = o_i[\mathcal{P}] + \sum_{j \in \mathcal{N}_c} (\mathcal{Z}_j \mathcal{Y}_{ij}[\mathcal{P}] \nu_j) \quad \forall i = 1, 2, \dots, N$$

where \mathcal{P} is observability propagations; \mathcal{Z} is set to 1 if ZIB else 0; \mathcal{Y} is observability propagation variables of ZIBs; ν is observability propagation variables of conventional measurements.

2. Aggregating each zero-injection bus set (ZIB bus and its adjacent buses) as a single constraint. In this technique along with the constraint (5.8), the following constraints are included:

$$\begin{aligned} \sum_{j \in \zeta_i} o_j &\geq |\zeta_i| - 1 \forall N_z \\ o_i &\geq 1 \forall i \notin \zeta_j (j \in N_z) \end{aligned}$$

where ζ_i is the ZIB set of ZIB i .

C. Complete topological observability with single PMU loss or N-k security criterion (Nikkhah et al., 2017; Chakrabarti et al., 2009)

For both single PMU loss or N-k security cases, the LHS of the observability inequality constraints will remain the same as (5.8), that is,

$$O = AX$$

But, the right hand side of the inequality is modified as follows for single PMU loss,

$$O \geq 2 \times u \tag{5.12}$$

The security criterion $N-k$ considers all possibilities of PMU outages (upto k PMUs), which is incorporated into the OPP formulation as,

$$O \geq (k + 1) \times u$$

D. Complete topological observability with single line outage (Chakrabarti et al., 2009)

Outage of line leads to higher number of PMUs needed for achieving observability of the system. Single line outage is incorporated into the OPP formulation by adding some additional constraints apart from the constraints mentioned in (5.8). There will be two additional constraint inequalities added for every line outage by removing the connectivity between corresponding buses. Single line outage considers all line outages, but each line is made out of service one by one. Let the set of row vectors which need to be modified due to the line outages, one at a time, be denoted by A_1 . The set of these additional constraints are given as,

$$A_1 X \geq u_1$$

where u_1 is row vector of ones of size $2 \times L$ considered and L is a total count of line outages considered.

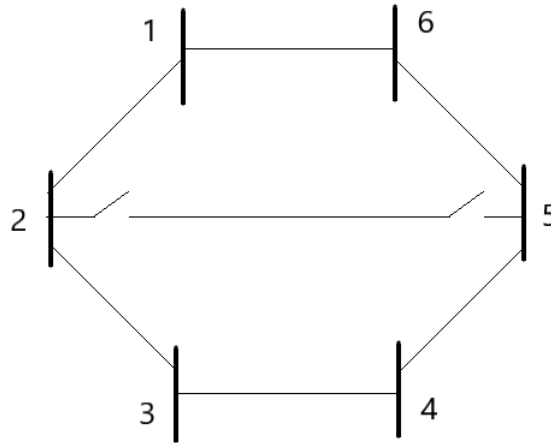


Figure 5.5: Sample 6-bus system during a single line contingency of line 2-5

Now for example, the additional constraints for the 6-bus system for a single line outage of line 2-5 (See Fig. 5.5) will be as follows :

$$\begin{matrix} & x_1 & x_2 & x_3 & x_4 & x_5 & x_6 \\ x_2 & \begin{bmatrix} 1 & 1 & 1 & 0 & 1 & 0 \end{bmatrix} \\ x_5 & \begin{bmatrix} 0 & 1 & 0 & 1 & 1 & 1 \end{bmatrix} \end{matrix} \begin{bmatrix} x_2 \\ x_5 \end{bmatrix} \geq \begin{bmatrix} 1 \\ 1 \end{bmatrix}$$

Similarly, 2 additional constraints for each of the single line contingencies will be added.

E. Complete topological observability with simultaneous occurrence of single PMU failure and line outage (Aminifar et al., 2009a)

Simultaneous contingencies can be considered, that is, to say that if there are both single PMU loss and single line outages. This scenario can be incorporated by combining the formulations given in (5.12) and (5.13) and is given by,

$$A_1 \geq 2 \times u_1$$

F. Complete topological observability when including conventional devices

Conventional devices are both power flow and injection measuring devices. But only flow measurement devices are considered here (Dubey et al., 2018). The power which flows in branch between buses i to j at i side is given by,

$$P_{i,j} - jQ_{i,j} = V_i I_{i,j} = V_i(V_i - V_j)y_{i,j} \quad (5.13)$$

where $y_{i,j}$ is primitive admittance of the branch connecting bus i to bus j .

Given voltage measurement on either of the buses i or j at which device is placed, the voltage at the other bus can be calculated by using (5.13). Therefore, by placing flow measurement device too that bus becomes observable. The topological observability function incorporating flow measurement device is given as,

$$o_i = \sum_{j \in N} A_{ij} x_j + \sum_{j \in N} A_{ij} d_j f_{ij}$$

where, d_j is a binary variable equal to 1 if j^{th} bus has flow measurement device, otherwise 0; f_{ij} is auxiliary binary variable of buses i and j , which is responsible to make decision of which bus should be observed by the flow measurement devices.

In an earlier work, the flow measurement is incorporated by combining the constraints of the two terminal buses into one (Xu and Abur, 2004). While the injection measurements are taken care by augmenting product terms to the constraints of their neighboring buses.

Combined optimal placement of PMUs and power-flow measurements can reduce the overall number of PMUs for system observability (Kavasseri and Srinivasan, 2010). This problem formulation termed as Joint Placement Problem considered both flow measurements locations (Y on lines) and PMU locations (X on buses) as free binary variables. The formulation as follows:

$$\begin{aligned} & \text{Min} \quad q^t X + m^t Y \\ & \text{s.t.} \quad G_i \geq 1, i = 1, 2, 3, \dots, N \end{aligned}$$

where q and m are cost vectors of PMUs and flow measurement devices respectively. The constraints G_i (Kavasseri and Srinivasan, 2010) are given as,

$$G_i = o_i + \sum_{j \in ad_i} z_{i,j} o_j \geq 1$$

where ad_i is set of neighboring buses for bus i and $z_{i,j}$ is the flow placement binary variable between buses i and j . Here, if any two terms are of the form $zo + o$ then it is taken equivalent to o , thereby reducing the number of non-linear terms. The remaining non-linear terms of the product form $t \times f$ are further resolved using an additional variable a as follows:

$$\begin{aligned} a - t - f &\geq -1 \\ t - a &\geq 0 \\ f - a &\geq 0 \end{aligned}$$

However, this resolution leads to linearity by additional number of constraints and variables. The results shows that this model provides a better economical solution to system observability compared to those with only PMUs. This is applicable to utilities that are willing to re-locate the traditional measurements and install PMUs to reduce overall cost of observability.

Line, PMU and flow measurement device contingencies also can be considered for better OPP problem formulations. The observability function considering flow measurement device contingency is as follows,

$$o_i = \sum_{j \in N} A_{ij} x_j + \sum_{j \in N} A_{ij} d_j^{FMt} f_{ij}^{FMt}$$

where d_j^{FMt} , f_{ij}^{FMt} are parameters accounting outage of flow measurement device.

G. Complete topological observability with Measurement channel limitation (Korkali and Abur, 2009)

A PMU has capability to measure only a defined number of quantities simultaneously due to its limited measurement channels. To consider this effect a new decision matrix B is employed using A (5.8) matrix, whose number of rows for each bus is given by,

$$R_k = \begin{cases} N_k C_l & ; \text{if } l \leq N_k \\ 1 & ; \text{Otherwise.} \end{cases} \quad (5.14)$$

where, N_k is the number of bus positions with ones in row R_k in the connectivity matrix A except the diagonal element; l is the fixed number of channels considered for the PMU.

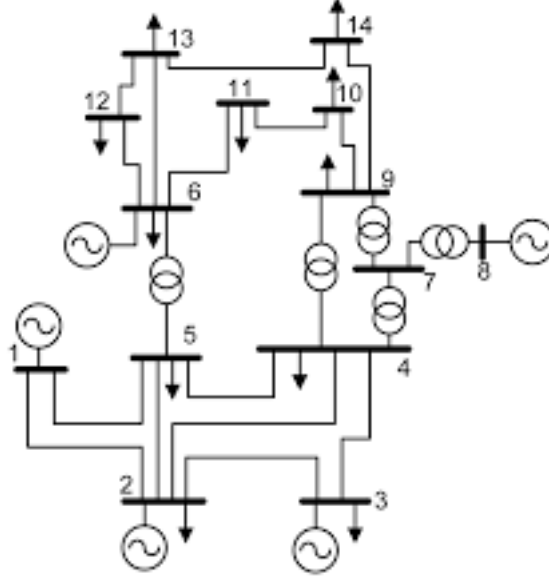


Figure 5.6: Single line diagram of the IEEE 14-bus system

For example, consider for a IEEE 14-bus system (See Fig. 5.6) with PMUs having only 2 channels. The bus-2 which is connected to the buses 1, 3, 4 and 5; it's corresponding rows in B matrix would be 2-combinations of this set and each row will place one corresponding to bus 2. The rows of new decision matrix B corresponding to bus-2 will become as follows:

$$B = \begin{matrix} \text{Bus-1:} \\ \text{Bus-2:} \\ \text{Bus-3:} \\ \vdots \\ \text{Bus-14:} \end{matrix} \begin{bmatrix} 1 & 1 & 1 & 0 & 0 & 0 & \dots & 0 \\ 1 & 1 & 0 & 1 & 0 & 0 & \dots & 0 \\ 1 & 1 & 0 & 0 & 1 & 0 & \dots & 0 \\ 1 & 1 & 1 & 1 & 0 & 0 & \dots & 0 \\ 0 & 1 & 1 & 0 & 1 & 0 & \dots & 0 \\ 0 & 1 & 0 & 1 & 1 & 0 & \dots & 0 \\ \dots & \dots & \dots & \dots & \dots & \dots & \dots & \dots \\ \vdots & \vdots & \vdots & \vdots & \vdots & \vdots & \vdots & \vdots \\ 0 & \dots & 0 & 1 & 0 & 0 & 0 & 1 & 1 \end{bmatrix}$$

$$o_i = \sum_{i \in S} \sum_{j \in N} B_{ij}^T p_i \forall i = 1, 2, \dots, N \quad (5.15)$$

where, S is the sum of R_k 's; N is total count for buses in system; the elements p_i that

correspond to rows of B corresponding to different combinations for a particular bus are assigned with the same x_i decision variable as that of the particular bus.

An unique observation is that independent of the system size, using PMUs having greater than four channels does not provide any lower objective function value (Korkali and Abur, 2009). Few more works with respect to fixed channel capacity of PMUs for OPP studies are reported (Korkali and Abur, 2010; Miljanić et al., 2012).

H. Complete topological observability considering DC lines in the network (Aminifar et al., 2013b)

For consideration of effect of DC lines on the network topological observability, the connectivity matrix elements are modified as follows:

$$A_{ij} = \begin{cases} 1 & ;\text{if } i = j \\ 1 & ;\text{if buses } i \text{ and } j \text{ are connected by an AC line} \\ 0 & ;\text{Otherwise.} \end{cases}$$

I. Numerical observability of the network with and without considering zero-injection measurements (Kekatos et al., 2012; Korres et al., 2015; Koutsoukis et al., 2013; Manousakis and Korres, 2019)

Although in most of the research publications related to OPP studies, the focus has been on topological observability of the system using PMUs. But, numerical observability is very essential in further analysis of the system such as state estimation. This is all the more important since in few cases where topologically observable system may not be numerically observable due to singularity of gain matrix. Although rare, these cases can occur in practice (Monticelli, 2000; Monticelli et al., 1992).

It is known that a PMU can measure the voltage phasor at the bus where it is placed/installed and current phasors in the branches connected to it. Therefore, a branch to bus incidence matrix (Murty, 2017) is required to form the measurement Jacobian matrix. And the AC measurement Jacobian matrix with respect to voltage phasors as state variables is formed. The voltage phasor needs to be considered in rectangular form to prevent Gain matrix ill-conditioning. It is noted that the system observability is independent of the line parameters or the operating condition of the system. Thus, for simplicity of observability analysis, all line impedances are assumed as $j1.0$ p.u. and all bus voltages are assumed as 1.0 p.u. The sub-matrix H_1 with regard to a PMU placed on bus-1 in an IEEE 14-bus system (See Fig. 5.7) would be as follows:

$H_1 =$

$$\begin{matrix}
 & V_{1,r} & V_{2,r} & V_{3,r} & V_{4,r} & V_{5,r} & V_{6,r} & \dots & V_{14,r} & V_{1,x} & V_{2,x} & V_{3,x} & V_{4,x} & V_{5,x} & V_{6,x} & \dots & V_{14,x} \\
 \begin{matrix} V_{1,r} \\ V_{1,x} \\ I_{1-2,r} \\ I_{1-5,r} \\ I_{1-2,x} \\ I_{1-5,x} \end{matrix} & \begin{bmatrix} 1 & 0 & 0 & 0 & 0 & 0 & \dots & 0 & 1 & 0 & 0 & 0 & 0 & 0 & 0 & \dots & 0 \\ 0 & 0 & 0 & 0 & 0 & 0 & \dots & 0 & 1 & 0 & 0 & 0 & 0 & 0 & 0 & \dots & 0 \\ 1 & -1 & 0 & 0 & 0 & 0 & \dots & 0 & 1 & -1 & 0 & 0 & 0 & 0 & 0 & \dots & 0 \\ 1 & 0 & 0 & 0 & -1 & 0 & \dots & 0 & 1 & 0 & 0 & 0 & -1 & 0 & \dots & 0 \\ 1 & -1 & 0 & 0 & 0 & 0 & \dots & 0 & 1 & -1 & 0 & 0 & 0 & 0 & \dots & 0 \\ 1 & 0 & 0 & 0 & -1 & 0 & \dots & 0 & 1 & 0 & 0 & 0 & -1 & 0 & \dots & 0 \end{bmatrix}
 \end{matrix}$$

where $V_{1,r}, V_{1,x}$ are the real and imaginary parts of the bus 1 voltage phasor respectively; $I_{1-2,r}, I_{1-2,x}$ are the real and imaginary parts of the current phasor flowing from buses 1 to 2 respectively; $I_{1-5,x}$ are the real and imaginary part of the current phasor flowing from buses 1 to 5 respectively. Similarly, H_i matrices are calculated for all buses where PMUs

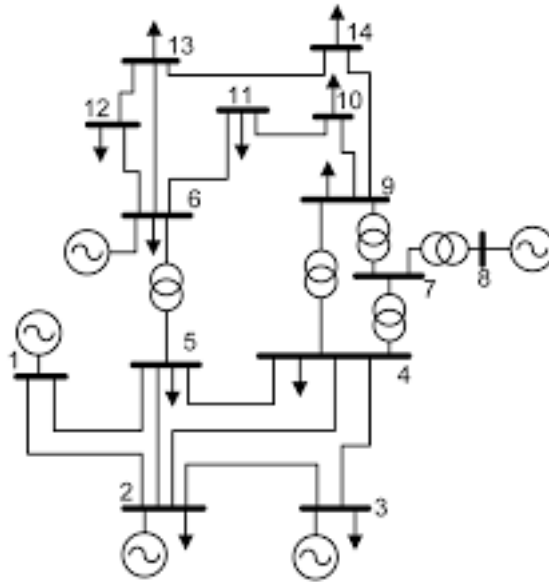


Figure 5.7: Single line diagram of the IEEE 14-bus system

are installed and concatenated to form the H matrix. The rank of H matrix should be full for numerical observability of the system without considering zero-injections (Kekatos et al., 2012).

Further, if zero-injection measurements are available, then Jacobian matrix related to the these measurements is formed (Korres and Manousakis, 2012). Below is an example of how this matrix looks when zero injection at bus-1 is measured:

$C_1 =$

$$\begin{matrix}
 & V_{1,r} & V_{2,r} & V_{3,r} & V_{4,r} & V_{5,r} & V_{6,r} & \dots & V_{14,r} & V_{1,x} & V_{2,x} & V_{3,x} & V_{4,x} & V_{5,x} & V_{6,x} & \dots & V_{14,x} \\
 \begin{matrix} I_{1,r} \\ I_{1,x} \end{matrix} & \begin{bmatrix} c_1 & -1 & 0 & 0 & -1 & 0 & \dots & 0 & -c_1 & 1 & 0 & 0 & 1 & 0 & \dots & 0 \\ c_1 & -1 & 0 & 0 & -1 & 0 & \dots & 0 & -c_1 & 1 & 0 & 0 & 1 & 0 & \dots & 0 \end{bmatrix}
 \end{matrix}$$

where, c_1 is the total count of buses connected to ZIB-1.

The system is numerically observable only if the coefficient matrix D has full rank as

shown below:

$$\text{rank } D = \text{rank} \begin{pmatrix} H^T H & C^T \\ C & 0 \end{pmatrix} = \text{rank} \begin{pmatrix} H \\ C \end{pmatrix} = n$$

where, n is the number of states in the system, that is, two times the total count of buses in case of phasor only state estimation.

[Manousakis and Korres \(2019\)](#) carried out optimal allocation of PMUs based on full numerical observability.

J. Non-linear programming constraints for OPP ([Almunif and Fan, 2020](#))

The objective function for NLP formulation is given in [\(5.4\)](#) and is subjected following non-linear topological observability constraints (Here, ad_i is set of adjacent buses to bus i):

$$g_i = (1 - x_i) \prod_{j \in ad_i} (1 - x_j) = 0$$

$$0 \leq x_i \leq 1, \forall i \in N$$

The zero-injection formulation can be illustrated with an example ([Almunif and Fan, 2020](#)). Suppose, bus 2 of a six-bus system has a zero-injection and its adjacent buses are buses 1, 3 and 5. The set of constraints would be as follows:

$$g_{inj,2} = \{g_1g_2 = 0, g_1g_3 = 0, g_1g_5 = 0, g_2g_3 = 0, g_2g_5 = 0, g_3g_5 = 0\}$$

$$g_4 = (1 - x_3)(1 - x_4) = 0$$

$$g_6 = (1 - x_1)(1 - x_3)(1 - x_6) = 0$$

K. Probabilistic and Stochastic observabilities ([Aminifar et al., 2010a](#); [Arpanahi et al., 2019](#))

In the sense of deterministic assessment of observability, a network bus is observable when its corresponding probabilistic observability for the horizon year PO_i^H is positive. The probability of observability associated with bus i is given by,

$$PO_i = 1 - \prod_{j \in N} (1 - x_j P'_{ij}) \quad \forall i$$

where P'_{ij} is a constant value representing the probability of observability of bus i because of PMU t bus j .

The problem formulation for a horizon year is given as follows:

$$\begin{aligned} \text{Min} \quad & F^{hor} = \sum_{i \in N^{hor}} x_i^{hor} + (1 - APO^{hor}) \\ \text{subject to,} \quad & PO_i^{hor} \geq PO_i^{hor, min} \quad \forall i \in N^{hor} \end{aligned}$$

where hor refers to the horizon year.

Stochastic observability model (Mandich et al., 2019) is proposed as:

$$o_i = \sum_{j \in N} A_{ij} \eta_{ij} x_i + \sum_{j \in N} A_{ij} \eta_{ij} d_j f_{ij}$$

where, d_j is a binary variable equal to 1 if j^{th} bus has flow measurement device, otherwise 0; f_{ij} is auxiliary binary variable of buses i and j , which is responsible to make decision of which bus should be observed by the flow measurement devices.

L. OPP considering controlled islanding of power system (Huang et al., 2013a)

The observability constraints given in (5.9) are modified as follows:

$$o_i = \sum_{j=1}^N A_{ij}^{CI} x_j \geq 1 \quad \forall i = 1, 2, \dots, n$$

where A_{ij}^{CI} is the binary entry in connectivity matrix for post-islanding network defined as,

$$A_{ij}^{CI} = \begin{cases} 0 & ; \text{if line } i - j \text{ is opened during controlled islanding process} \\ a_{i,j} & ; \text{Otherwise.} \end{cases} \quad (5.16)$$

These constraints can keep the power network completely observable both for normal and controlled islanding conditions. The OPP with controlled islanding and contingencies are also discussed (Huang et al., 2013a).

For example, during a cascading fault in the IEEE 14-bus system (See Fig. 5.8) the system is split into 2 islands by opening several connecting tie-lines and the node incidence matrix A_{ij} will be modified to A_{ij}^{CI} according to (5.16).

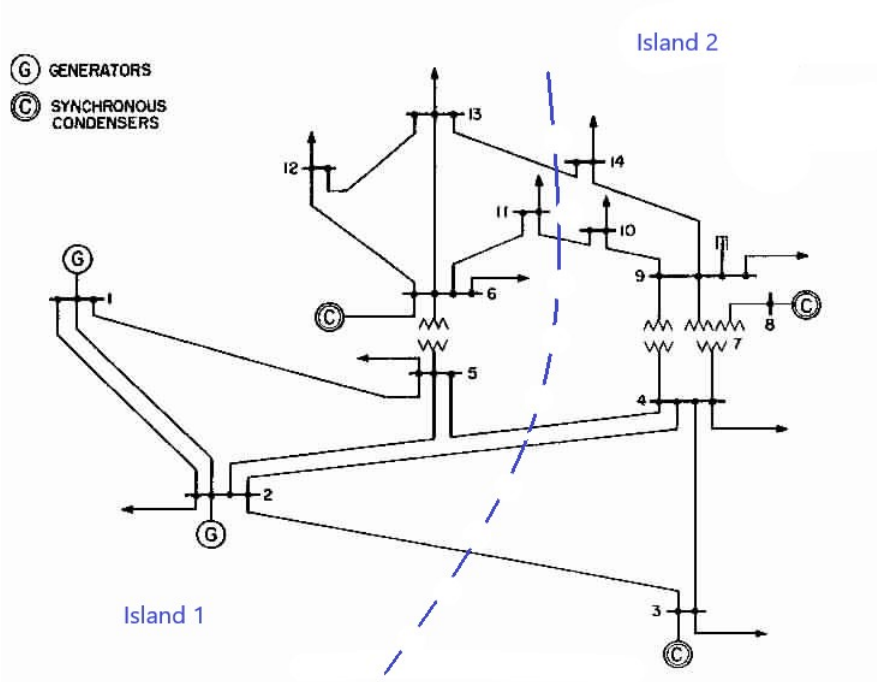


Figure 5.8: Single line diagram of the IEEE 14-bus system split into two islands during a cascading fault

M. Voltage stability consideration (Manoharan et al., 2018)

The multi-objective function described in (5.5) is subjected to the following constraints:

$$\sum_{i=1}^N A_{ij}x_i + \sum_{a=1}^v A_{j,Z_{i'}}K_{j,Z_{i'}} \geq 1$$

$$1 \leq BOI_i \leq (\text{maximum connectivity of bus } i)$$

$$2 \leq WBOI_t \leq (\text{number of branches connected to weak bus } t + 1)$$

where WBOI is weak bus observability index; $K_{j,Z_{i'}}$ Binary variable whose value 1, if i' is ZIB and 0, otherwise.

N. Small signal stability monitoring and control based OPP (Sharma and Tyagi, 2015; Tarif et al., 2019)

According to this control scheme, critical buses are identified and bus topological observability criteria is considered. Critical buses are generator buses to which controller is attached or feedback signal are taken or tie-line buses to monitor tie-line performance. In such cases, PMUs are placed at these preferred buses in initial stages and rest of buses are made observable in later stages.

O. OPP using Fault-Tolerance based approach (Almasabi and Mitra, 2019)

The objective function described in (5.6) is subjected to $F_8 \leq \text{Budget cost}$. While the lower objective (5.7) is subjected to the constraints:

$$\frac{O'}{O} \geq \gamma \quad (5.17)$$

$$O \geq u \quad (5.18)$$

where $O' = A' \times X$

$O = A \times X$

γ is priority index.

$$H'_{ij} = \begin{cases} 1 + v_{ii} & ;\text{if } i = j \\ 1 - v_{ij} & ;\text{if buses } i \text{ and } j \text{ are connected by an AC line} \\ 0 & ;\text{Otherwise.} \end{cases}$$

$v_{ij} = V_k$, if a component c_k is connected between buses i and j

V_k is vulnerability of index of component k which calculated using cumulative distribution function for normal function and failure probability of the component c_k

$$v_{ii} = \sum_{j=1}^{j=N} (1 + v_{i,j}) - \sum_{j=1}^{j=N} A_{i,j}$$

5.3 Methodologies for Solving Optimal Placement of PMUs

In OPP studies, finding the exact global solver that solves in a reasonable duration of time is a challenge. Each of the techniques/methods evolved with time have its own particular mathematical and computational characteristics (Yuill et al., 2011; Manousakis et al., 2012; Gupta and Pandey, 2014; Aminifar et al., 2014a; Nazari-Heris and Mohammadi-Ivatloo, 2015; Mohanta et al., 2016; Chouhan and Jaiswal, 2016). The major classification of the methods explored in literature are shown in Fig. 5.9. The detailed features, comparison and shortcomings of these methods have been discussed in section 1.4.2 in the introduction Chapter 1. The classification of the methods in literature are discussed briefly in further sub-sections.

A. Conventional methods

Initial work related to research for OPP is performed around 1988 for achieving complete observability using combinational approach, graph theoretic approach or factorization-based approach (Wu, 1988). In many of the earlier literature on OPP, the conventional

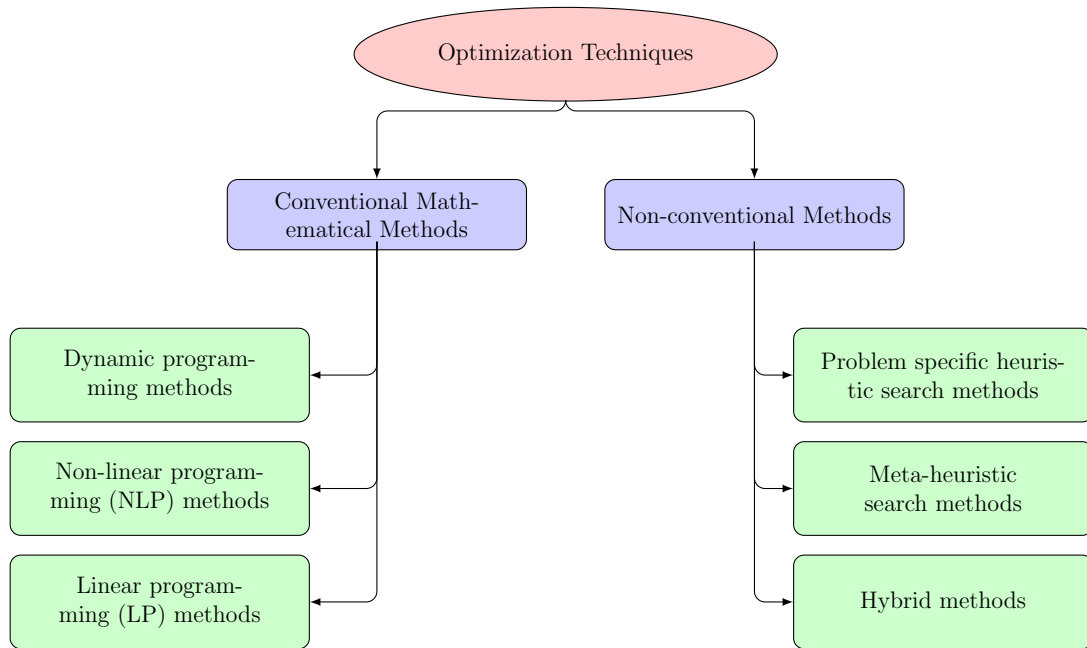


Figure 5.9: Classification of optimization techniques

Integer linear programming (ILP) approach has been utilized (Gou, 2008a; Dua et al., 2008; Gou, 2008b) considering with and without zero-injection and flow measurements. Further, the scenarios with critical contingencies are considered (Sodhi et al., 2009). ILP method is used to check how the solutions when two grids are evaluated separately and interconnected (Gopakumar et al., 2013). And topology transformation method merges zero injection bus (ZIB) and one of its neighbors (Rahman and Zobaa, 2016). The formulation and algorithm is non-linear and hence size of computation increases with increased number of complex buses considered (Jelodar and Fini, 2016). Some infeasible results are reported in some cases (Aminifar et al., 2010b). Another recent work carried out an outer approximation scheme based on BILP (Korres et al., 2015) which had improved speed and efficiency. Also, the method lead to lesser number of PMUs than existing techniques.

B. Heuristic methods

Heuristic method is an experience-based technique for solving optimization problems, in which optimal point is not obtainable in finite time. Heuristics contain in their underlying principles some specialized operators (Nazari-Heris and Mohammadi-Ivatloo, 2015) that could enable wider exploration of the space of the solutions. The solution of OPP is derived for incomplete observability using the novel concept - depth of unobservability (Nuqui and Phadke, 2005). Here, spanning trees of power system graph and a *tree search* technique is used.

Binary search algorithm, an exhaustive algorithm is used to solve OPP problem (Chakrabarti and Kyriakides, 2008). Lexicographic algorithm helps in giving fast formulations of combinations that can be used by the binary search one at a time. OPP

considering measurement channel failure based on a *modified binary search* has been performed (Albuquerque and Paucar, 2013). This is in the view that failure of measurement channels is more common than failure of the PMU itself.

An *information-theoretic* approach for OPP solution is dependent on mutual information between PMU data and system states (Li et al., 2013). A *greedy PMU placement* algorithm based on the covariance matrix installs PMUs in stages. Single line outage detection would be a trivial problem if there are PMUs at each of the buses in the system. But the challenge is maximizing the ability to detect any single line outages in the system by placing only a limited PMUs (Kim and Wright, 2018). This is done by *Multinomial Logistic Regression Model* (MLR), a machine-learning approach based on observation vectors which has voltage phasor differences as its elements. Computationally intensive although the method gives the global optimal point (Chakrabarti and Kyriakides, 2008).

C. Meta-heuristic methods

Meta-heuristics are problem-independent methods. These methods act like black boxes and are not dependent on the uniqueness of the particular problem. Generally, they even consider a temporary degraded solution, which helps the algorithm to search more explicitly the search space and thus to get a hopefully better solution.

As noted in the literature while implementing a meta-heuristic, it is absolutely necessary to perform some refining of its intrinsic parameter values so as to readjust the method to solve the problem at hand. In fact, a meta-heuristic is also a heuristic, but is more effective due to its inherent nature to avoid being trapped in a local optimum. Further, the meta-heuristic is an advanced application of heuristic method by escorting them through the search space, to use its best capabilities obtaining improved results. These techniques generate new solutions by recombination of one or more good solutions.

Genetic algorithm (GA) is used for finding minimum number of PMUs required wherein the number of current measures for topological observability is also taken into account (Marin et al., 2003). A fault observability rule using basic theories of power system observability is introduced (Golshan et al., 2018). Network expansion plan is considered as a constraint in the OPP problem for a multi-year time-frame instead of a one-year period solved using GA (Asgari and Firouzjahi, 2018).

The *Simulated annealing* formulation is extended for solving pragmatic phased installation of PMUs recognizing the limitations in availability of communication facilities. The applicability of immunity genetic algorithm for OPP problem is explored (Aminifar et al., 2009b). Incorporation of immune operator in canonical genetic algorithm (GA) with an intention of preserving GA's advantages is possible. This is performed utilizing some characteristics and knowledge of problems for prevention of degenerative phenomena during evolution, thus improving efficiency of algorithm.

In order to cope with the continuous changes in the power system's topology, [Al-Mohammed et al. \(2011\)](#) formulated the optimization problem considering not only the new PMUs to be installed but also the existing ones to be retained or relocated. And this is done with the help of a meta-heuristic method called *Differential Evolution* (DE). In addition, a single PMU loss case is considered ([Venkateswaran and Kala, 2012](#)). [Aminifar et al. \(2013a\)](#) discusses an analytical framework based on cost/benefit analysis.

[Zhao et al. \(2015\)](#) aimed to improve robustness when dealing large systems. An improved GA based on serial number coding is used to prevent infeasible results and improve the algorithm's performance. Topological constraint analysis reduces computation cost. Full observability with maximum redundant measurements for buses identified as critical with the same count of PMUs as under normal conditions is achieved with *Lyapunov exponent-based approach* ([Rashidi and Farjah, 2016b,a](#)).

General optimal substation coverage (GOSC) algorithm ([Pal et al., 2017](#)) considers the practical constraints such as redundancy in critical measurements of the system and calculating tap ratios of transformers present. [Singh and Singh \(2017\)](#); [Almasabi and Mitra \(2018\)](#) incorporated communication infrastructure constraints in the optimal measurement system. Case studies with contingencies are also carried out to ensure reliable solution for system.

There has been multi-stage OPP wherein the PMUs are installed in stages. This is done by determining placement scheme with a given certain level of unobservability in association with subsequent stages. The OPP problem is tackled in single- or multi-stages by using probabilistic approaches taking element outages probability into consideration. One terminal algorithms utilize only measurements at one end of the transmission lines for fault location, thus required number of PMUs would be lesser than two-end algorithm ([Sun et al., 2018](#)).

The literature which appeared after ([Cho et al., 2001](#); [Mishra et al., 2016](#)) revealed that solutions obtained are not the optimum values even for small systems. GA takes higher convergence time than the conventional method BILP ([Kumar et al., 2018](#)). The meta-heuristic methods can not be applied on any power system without tuning the values of the certain parameters it is dependent on.

D. Hybrid methods

Earlier studies had not been done on reduction of number of PMUs to implement fault location algorithms based on single terminal data. In a similar context, the objective of achieving simultaneous optimization of two conflicting objectives, that is, minimizing the number of PMUs and maximizing the measurement redundancy ([Milosevic and Begovic, 2003](#)). The *non-dominated sorting genetic algorithm* (NSGA) is used to solve and get the pareto-optimal solutions, that is, a set of best trade-offs between competing objectives.

(Rakpenthai et al., 2007) discusses a four-staged optimization technique consisting of sequential elimination method, sequential addition method, binary integer programming and a heuristic algorithm. Some of the hybrid methods requires complex computations (Milosevic and Begovic, 2003), therefore dependent on network size. A hybrid method does not guarantee optimality nor does it inform how good their sub-optimal solutions are with respect to the optimal one (Zhao et al., 2015).

5.4 Objective and Contributions of this chapter

Objective: Implementation of a new meta-heuristic approach called Crow search algorithm for Optimal placement of PMUs problem in power networks.

For precise power system monitoring, a major focus is on involvement of the latest technology based on phasor measurement units (PMUs). As the sole system monitor, state estimator plays an important role in the security of power system operations. Optimal placement of PMUs (OPP) with numerical observability ensures reliable state estimation. For economical and efficient utilization, there is a need to optimize the placement of PMUs in the power system network. A new approach called Crow Search Algorithm (CSA) devised by others, has been used to solve an OPP problem. The performance of this new approach is compared to the dominant method for an optimization problem - binary integer linear programming (BILP). Comparison studies have also been carried out with particle swarm optimization (PSO) method. The major constraints such as topological, numerical observability conditions with and without zero-injection buses (ZIBs) are considered. Contingencies and limitation of measurement channels in a PMU device are also incorporated as constraints. The main advantage of using the CSA is that it provides multiple location sets for same optimal number of PMUs (optimal number same as obtained by BILP). While BILP method provides only one set of locations for the optimal number of PMUs obtained. This becomes advantageous in planning stage for power engineers for placing PMUs. Test systems considered for the case studies are of varied sizes such as IEEE 14-bus, IEEE 30-bus, IEEE 57-bus and 72-bus practical equivalent system of Indian southern region power grid.

5.5 New Proposed Method for OPP Studies: Crow search algorithm

Engineering problems have elaborate objective functions, a large number of decision variables, and a large number of constraints, all of which contribute to the complexity of an already difficult optimization problem. Traditional optimization strategies are constrained

by the aforementioned features. As a result of the search for an alternate strategy, a new field of study was launched in the late 1980s called swarm intelligence (Beni and Wang, 1993).

A heuristic is another approach that is specifically applied to address a certain problem. While heuristic approaches have proven to be effective in solving problems that are otherwise difficult to solve, but they still have some flaws. Heuristics, like other traditional techniques, are typically built by taking into account certain specific features of the problem at hand, consequently it becomes hard to apply them to other problems without altering them partially or the whole of their structure (Fausto et al., 2020).

Many academics have recently become interested in developing procedures that might potentially handle a wide range of problems in a generic manner, resulting in the development of metaheuristics, a special type of "intelligent" optimization techniques (Yang and Press, 2010). These techniques use a set of generic techniques and abstract concepts to iteratively improve a set of possible solutions. As a result, metaheuristics are frequently commended for their capacity to arrive at optimum solutions for majority of problems, regardless of their design or features. To implement a metaheuristic algorithm effectively, the parameters of the algorithm must be adjusted. On the other hand, setting parameters is a time-consuming process. As a result, in a range of optimization scenarios, algorithms with a small number of parameters are easier to implement.

The optimal placement of PMUs in power system for both topological and numerical observability with some additional constraints is a combinatorial optimization problem. Combinatorial optimization aims to seek best possible solution from a set of possibilities and the set of feasible solutions is discrete. Crow search algorithm (CSA) is a newly developed nature-inspired algorithm (Bozorg-Haddad and Omid, 2018). It is a meta-heuristic method developed for providing solutions to constrained engineering optimization problems (Askarzadeh, 2016). It is a population-based technique using the idea of how a flock of crows keep their excess food in hiding places and retrieve it when food is needed. Now the context why the Crow search algorithm is visualized as better than other population based meta-heuristic algorithms is discussed here: (a) Inherent feature: Crow is the most intelligent among birds due the large brain relative to their body size. They have self identification ability in mirror and tool-making skills. Crow is known to watch other crows, and their food hiding place and steal when the owner leaves. If a crow has committed a theft, it will become even more alert by moving hiding places to prevent becoming a future victim. Hence, the intelligence incorporated in the bio-inspired technique introduces better way of diversification of results. (b) Advantage with respect to its parameter setting: Only two parameters namely flight length (fl) and awareness probability (AP) need to be tuned compared to most other popular metaheuristic methods. Promising results are obtained and revealed during simulation results obtained for solving constrained en-

gineering optimization problems using CSA when compared with various other methods (Askarzadeh, 2016).

On a set of benchmark functions, it is observed that CSA outperformed among all the population-based algorithms. The justifications as to why the CSA method was preferred as an alternative for the existing methods are discussed below:

1. World's most intelligent species with an encephalization quotient/intelligence quotient equal to that of many non-human primates (Rincon, 2005). As a group, crows show remarkable examples of intelligence and often score very highly on intelligence tests.
2. It is able to give global optimal solution as compared with the BILP algorithm. CSA utilizes a population of crows to search within the search space. This ensures that sequences of trial points generated by the method always converges to the global solution point.
3. Compared to PSO, CSA is not greedy algorithm because even if a crow produces a new position that is not better than its present position, it shall take the new position. Thus, increases the diversity of generated solutions.
4. In CSA, only two parameters needs to be tuned. Tuning of parameters has been the major shortcoming of optimization techniques due to the fact that it is a time-consuming task. Therefore, techniques with lesser parameters to tune are preferred for easier deployment (Askarzadeh, 2016). While in PSO, HS and GA have 4, 3 and 6 tunable parameters respectively.
5. This method provides multiple alternative solutions, which help planning engineers to design a better monitoring system.

5.5.1 Objective function

The objective function model may be to cut down the possible cost comprising of variable and fixed PMU installation cost. Other possible objectives may be maximize measurement redundancy. Another viable model uses a multi-objective (MO) model as the goal of OPP formulation.

The objective functions considered here is (5.1) given by

$$\text{Min } F1 = \sum_{i=1}^N x_i$$

where x_i is a decision variable which take value 1 (if PMU is placed) and 0 (otherwise); N is the count of buses in the power system; $F1$ is the objective function for number of

PMUs.

5.5.2 Constraints

The different constraints that have been considered in OPP studies using CSA are discussed below.

- Case 1: Complete topological observability of the network under normal conditions Refer section 5.2.2.A.
- Case 1 along with consideration of zero-injection buses effect on observability. Refer section 5.2.2.B.
- Case 1 along with single PMU loss. Refer section 5.2.2.C.
- Case 1 along with single line outage. Refer section 5.2.2.D.
- Case 1 with measurement channel limitation. Refer section 5.2.2.G.
- Case 2: Numerical observability of the network Refer section 5.2.2.I.

5.5.3 Implementation of Crow search algorithm

Crow is the most intelligent among birds due the large brain relative to their body size. They have self identification ability in mirror and tool-making skills. Crow is known to watch other crows, and their food hiding place and steal when the owner leaves. If a crow has committed a theft, it will become even more alert by moving hiding places to prevent becoming a future victim. CSA is built upon the following principles (a) crows live in form of a flock, (b) crows memorize the position of their hiding places, (c) crows follow each other to do thievery, and (d) crows protect their caches from being pilfered by a probability.

Logic used for finding set of PMU locations using the CSA algorithm

Suppose at an iteration $iter$, crow j wishes to retrieve food from its hiding place (from memory), $m^{j,iter}$. At the same time, crow i decides to follow crow j . At this stage, two possible scenarios are as follows:

Scenario 1- Crow j is unaware about crow i following it. As a result, crow i will go over to the hiding place of crow j ;

Scenario 2- Crow j is aware that crow i is following it. Therefore, to protect its hiding place from being noticed, crow j will mislead crow i by moving to some random position of the search space.

The two scenarios can be summarized as :

$$x^{i,iter+1} = \begin{cases} x^{i,iter} + r_j \times fl \times (m^{j,iter} - x^{i,iter}); & \text{if } r_j \geq AP^{j,iter} \\ \text{a random position} & ; \text{ Otherwise .} \end{cases} \quad (5.19)$$

where fl is the flight length; r_j is a randomly generated number between 0 and 1 and $AP^{j,iter}$ represents the awareness probability of crow j at iteration $iter$. Fig. 5.10 shows the schematic of scenario 1. Large values of fl results in global search (far from $x^{i,iter}$).

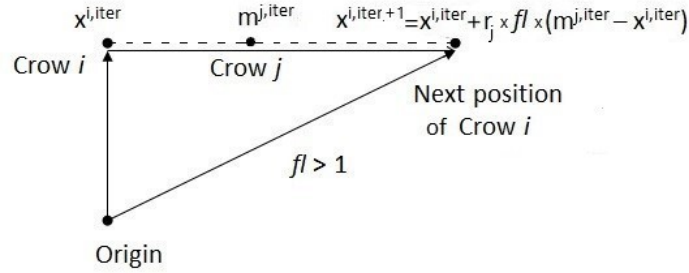


Figure 5.10: Crow i 's next position can be to any position on the dashed line in Scenario 1

If the value of fl is selected more than 1, the next position of crow i is on the dashed line which may exceed $m^{i,iter}$ (See Fig. 5.10).

Parameter Settings used for CSA and PSO

The two tuning parameters used are flight length - fl and awareness probability of crow j - AP . In general, the range of the two tuning parameters of CSA for obtaining global optimal value are as follows:

- (a) flight length fl is taken more than 1 so as
- (b) awareness probability AP is taken lower value than or equal to 0.1.

Table 5.1: Parameter settings for Crow search algorithm (CSA) and particle swarm optimization (PSO) methods ¹

Parameters for CSA Method	Parameters for PSO Method (Del Valle et al., 2008)
$fl = 5$; $AP = 0.025$.	$\omega = 0.4$ to 0.9 ; $v_{max} = 4$; $A_1 = 2$; $A_2 = 2$;

¹ fl : flight length of the i^{th} crow individual at the i^{th} iteration; AP : Awareness probability of the i^{th} crow at i^{th} iteration; ω : inertia weight; v_{max} : maximum value of velocity; A_1, A_2 : cognitive and social parameters respectively.

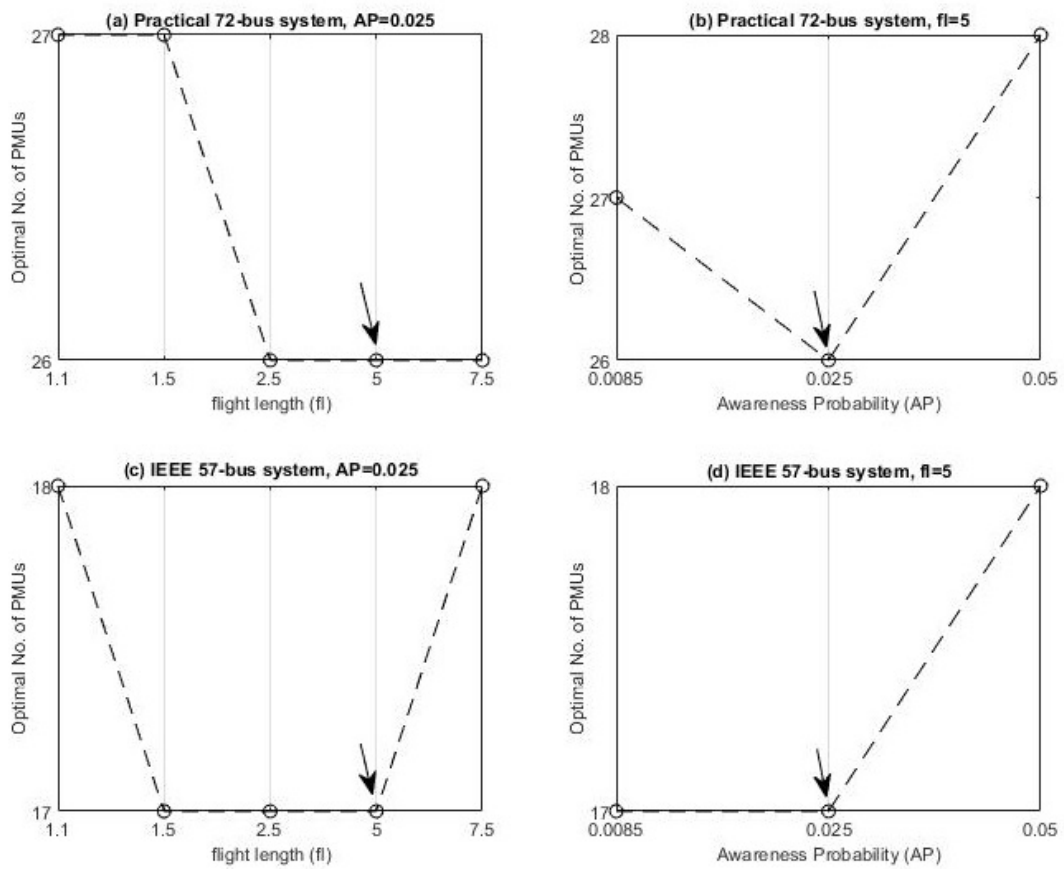


Figure 5.11: Parameter variation studies for IEEE 57-bus and practical 72-bus systems for different values of flight length (fl) and awareness probability (AP).

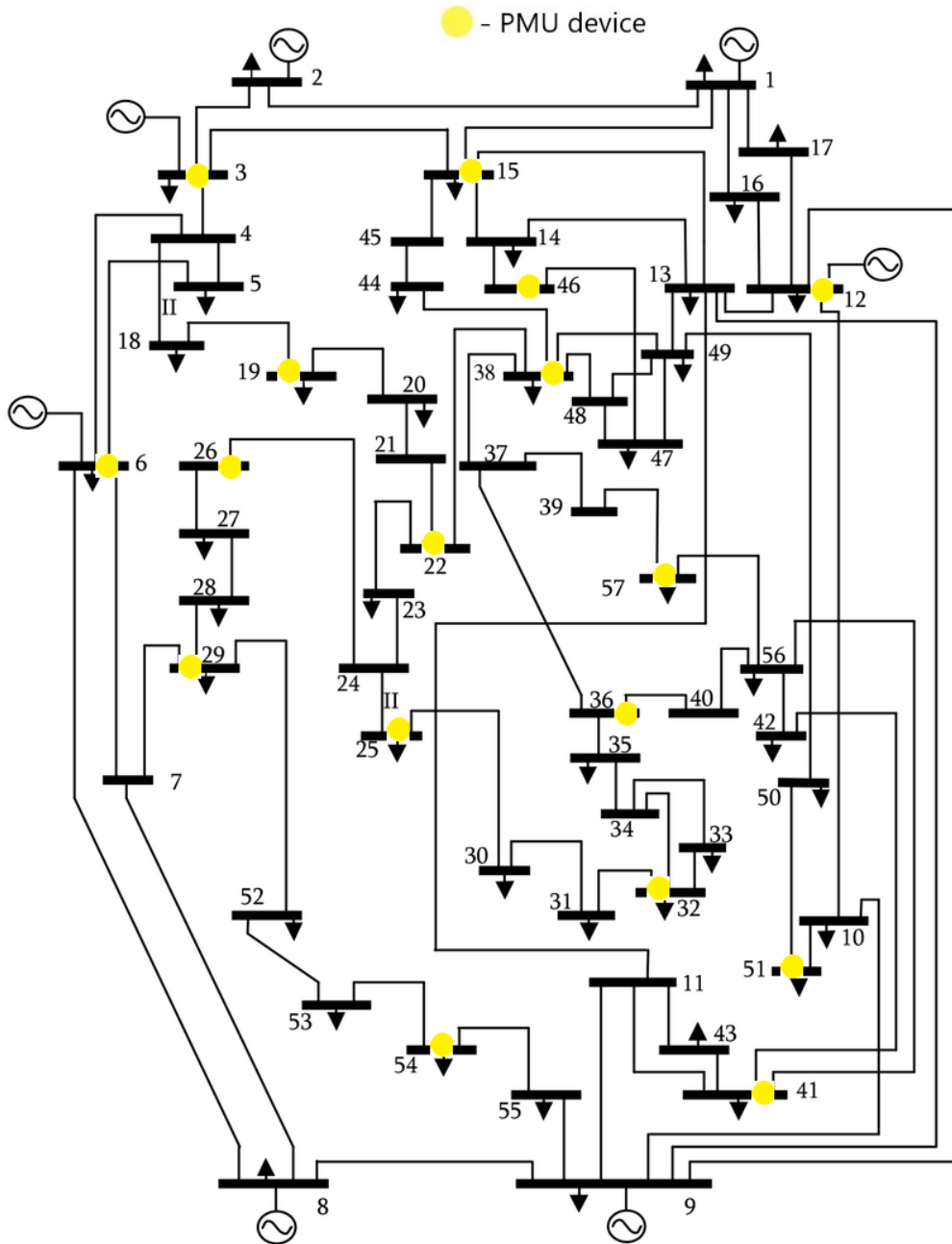


Figure 5.12: Case-1 PMU optimal placement solution - 17 PMUs for IEEE 57-bus when parameters are tuned to $fl=5$ and $AP=0.025$

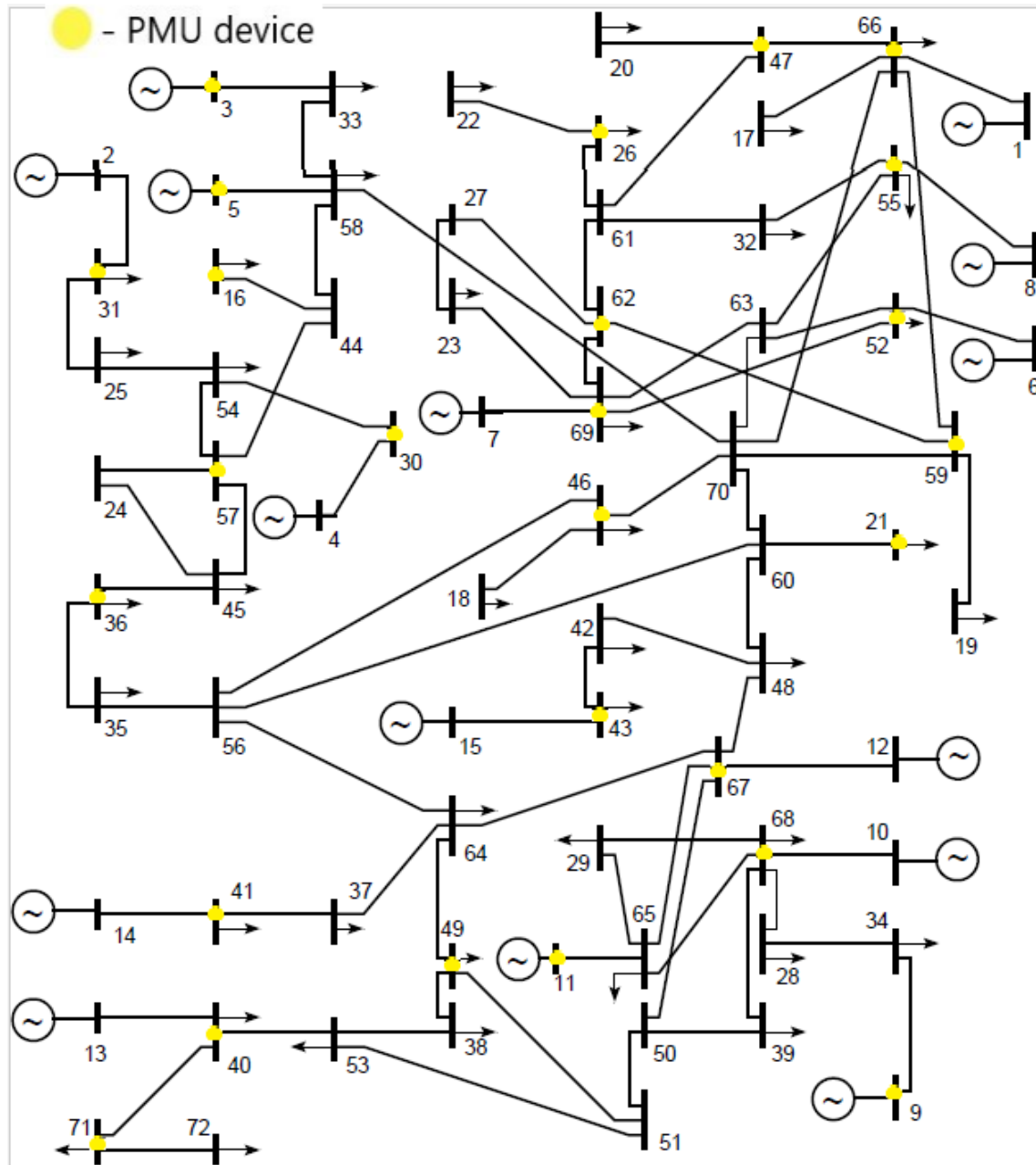


Figure 5.13: Case-1 PMU optimal placement solution - 26 PMUs for practical 72-bus when parameters are tuned to $fl=5$ and $AP=0.025$

Initially, the parameter values $fl=2$ and $AP=0.1$ as proposed by the original researcher that developed the algorithm were evaluated but the algorithm did not converge to the optimal value for test systems IEEE 57-bus (Refer Appendix D) and the practical 72-bus system (Refer Appendix E). This issue is anticipated due to large number of decision variables and constraints involved in our study when compared to the problems tested by the original researcher. As quoted from the original paper on CSA (Askarzadeh, 2016) “Like other optimization techniques, fine tuning of CSA is a problem dependent issue which should be done by trial”. The performance of CSA with varying parameters in the range specified above (Abdelaziz and Fathy, 2017) were studied. Also, for checking parameter values beyond the given range above, the CSA was run with different permutations and combinations of (a) AP values 0, 0.1 and 0.5 with that of (b) $fl = 0, 0.5$ and 2. But for all these parameter value combinations, the sub-optimal solutions were found for the Case 1: topological observability constrained OPP studies. The parameter setting process was done by trial and error so as to match the optimal number result obtained using the dominant global optimization technique BILP results for achieving Case 1. For smaller IEEE 14-bus and 30-bus systems, any of these values were giving the optimal number of PMUs. For IEEE 57-bus and practical 72-bus systems, the variations in AP and fl gave performances as shown in Fig. 5.11. Consequently, for our application of OPP problem for all the test systems, the best recommended values for tuned parameters are $AP=0.025$ and $fl=5$ are noted in Table 5.1. The optimal solutions 17 and 26 are obtained for IEEE 57-bus and the practical 72-bus systems respectively, after this parameter tuning as shown in Fig.s 5.12 and 5.13.

Another popular metaheuristic method PSO has been explored for application for OPP. The tuned parameters specified under the discrete PSO in literature (Del Valle et al., 2008) was examined in this study for the Case 1 OPP studies. The algorithm implementation was verified with respect to obtaining OPP results with respect to IEEE 14-bus and IEEE 57-bus systems with optimal numbers of PMUs 10 and 17 respectively same as in literature (Rather et al., 2013). And for both CSA and PSO, the flock/population size is considered as $2 \times N$ for the OPP studies in the work.

Steps for implementation of CSA

1. *Initialization of adjustable parameters and defining the problem:* The formulation of optimization problem with decision variables corresponding to the test system and defining the constraints to be satisfied. Initialization of parameters of CSA (fl and AP) is done.
2. *Initialize flock of crows with their positions and memories:* $2N \times N$ crows are randomly initialized with position values 0's or 1's as members of the flock. Every $2N$

is a possible solution of the problem and N is the number of decision variables.

$$Crows = \begin{bmatrix} x_1^1 & x_2^1 & \dots & x_d^1 \\ x_1^2 & x_2^2 & \dots & x_d^2 \\ \vdots & \vdots & \vdots & \vdots \\ x_1^{2N} & x_2^{2N} & \dots & x_d^{2N} \end{bmatrix} \quad Memory = \begin{bmatrix} m_1^1 & m_2^1 & \dots & m_d^1 \\ m_1^2 & m_2^2 & \dots & m_d^2 \\ \vdots & \vdots & \vdots & \vdots \\ m_1^{2N} & m_2^{2N} & \dots & m_d^{2N} \end{bmatrix} \quad (5.20)$$

Memory of every crow is initialized with an assumption that crows have hidden their foods at their initial positions.

3. *Determine the value of the objective function:* For every N crows, the quality of its positions tested by checking the objective function.
4. *Updating new positions for the crows:* Crows finds new hiding places by following another crow using (5.19).
5. *Affirm the feasibility of new positions generated:* If the new position of any of the N crows is found to be feasible in terms of satisfying all the constraints, the respective crow moves to its new feasible position. Otherwise, the remaining crows in the flock continue to stay in their previous positions itself.
6. *Check the objective function of updated positions:* The objective function values for the new positions of every N crows is evaluated.
7. *Update memory:* The crows update their memories as follows:

$$m^{i,iter+1} = \begin{cases} x^{i,iter+1} & ; \text{ if } F(x^{i,iter+1}) \text{ is better than } F(m^{i,iter}), \\ m^{i,iter} & ; \text{ Otherwise.} \end{cases} \quad (5.21)$$

where $F(\cdot)$ denotes the objective function. It is seen that if the F values of the new positions of every N crows is better than the F values of the memorized positions, then that group of N crows update their memory by the newly generated positions.

8. *The termination step:* Steps 4-7 are repeated until $iter$ value reaches $itermax$. When this condition is achieved, the best positions in the memory in terms of their F value is reported as the solution of the optimization problem.

The flowchart for these steps implementation is shown in Fig. 5.14.

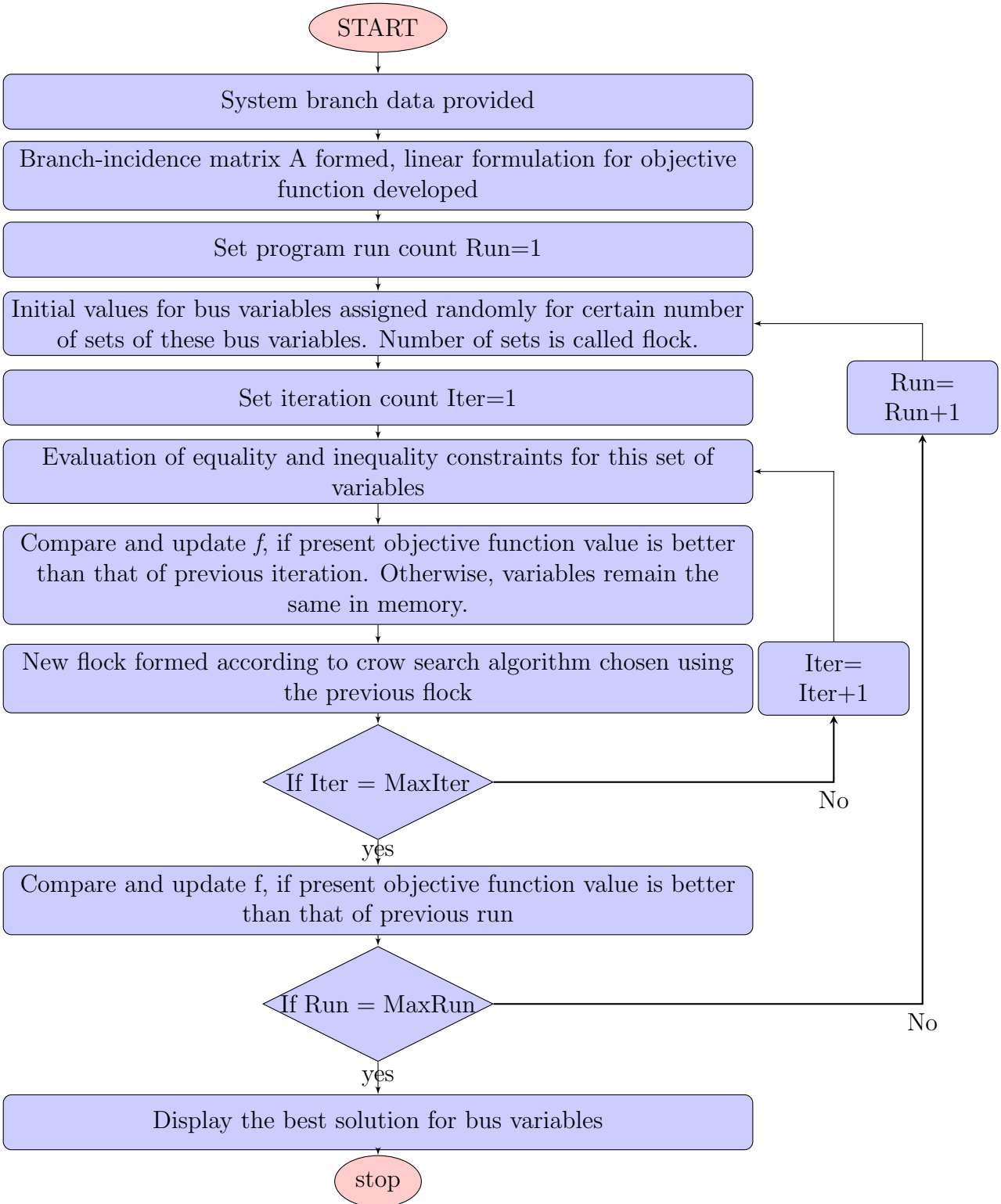


Figure 5.14: General flow of CSA used to solve optimal placement of PMU

5.6 Results and Discussions

Firstly, the CSA implementation code which was developed in MATLAB[®] R2020a has been tested on one of the benchmark constrained engineering problem Gear train design problem. The aim of this problem being minimizing expenditure of gear ratio of gear train with the formulation as follows:

$$\text{Min. } f(x) = \left(\frac{1}{6.931} - \frac{x_3 x_4}{x_1 x_4} \right)^2 \quad (5.22)$$

subject to boundary constraints given as

$$12 \leq x_i \leq 60 \quad (5.23)$$

The program developed was able to find the best solution as expected by the original author of CSA for gear train design problem. That is, the best solution provided the values x_1, x_2, x_3, x_4 and minimized objective function f are 49, 19, 16, 43 and 2.7×10^{12} respectively. For this, the parameter value used for the CSA are $fl = 2$ and $AP = 0.1$ as used by the original author itself. This helped in verifying that the program of CSA is equivalent to the original algorithm as intended by the author who devised it.

Further, the CSA has been implemented on MATLAB[®] R2020a platform and MATPOWER 6.0 package (Zimmerman and Murillo-Sanchez, 2016) for the OPP studies. For the comparison studies, PSO method is also implemented in the same platform and package. Both the programs are run for a maximum of 15 program runs and for a maximum of 200 iterations. The parameters settings for both these methods are indicated in Table 5.1. The tool *intlinprog* is used for BILP (Biswal and Mathur, 2015). Now, the case studies are carried out using the test systems IEEE 14-bus, IEEE 30-bus, IEEE 57-bus and 72-bus practical equivalent system of Indian southern region power grid (Moger and Dhadbanjan, 2015). Refer Appendices B-E for the corresponding system details.

Table 5.2: Number of phasor measurement units (PMUs) with the location solutions for Cases 1 results using Crow search algorithm (CSA), particle swarm optimization (PSO) and Binary integer linear programming (BILP)

System Network	Case 1 using CSA Optimal No. of PMUs (Computational time noted in brackets)	PMU locations (SORI index provided in brackets)	Case 1 using PSO Optimal No. of PMUs (Computational time noted in brackets)	PMU locations (SORI index provided in brackets)	Case 1 using BILP Optimal No. of PMUs (Computational time noted in brackets)	PMU locations (SORI index provided in brackets)
IEEE 14-bus	4 (1.11s)	2,7,10,13 (16)	4 (1.23s)	2,6,7,9 (19)	4 (0.03s)	2,8,10,13 (14)
IEEE 30-bus	10 (3.53s)	2,4,6,10,11,12, 15,18,25,30 (48)	10 (6.96s)	1,2,6,10,11,12, 18,24,26,30 (43)	10 (0.03s)	1,7,8,10,11,12, 19,23,26,30 (35)
IEEE 57-bus	17 (24.87s)	3,6,12,15,19,22, 25,26,29,32,36,38, 41,46,51,54,57 (69)	17 (90.70s)	1,4,7,9,20,22, 25,27,32,36,39,41, 44,46,49,51,53 (67)	17 (0.11s)	2,6,12,15,19,22, 25,27,32,36,38,41, 46,50,52,55,57 (67)
Practical 72-bus	26 (1039.66s)	3,5,9,11,16,21,26, 30,31,36,40,41,43, 46,47,49,52,55,57, 59,62,66,67,68,69,71 (96)	26 (3546.11s)	4,7,9,18,20,23,26, 31,33,35,40,41,43, 44,49,52,55,57,58, 60,65,66,67,68,71 (92)	26 (0.04s)	3,5,6,7,9,11, 16,18,19,20,21, 24,26,27,30,31,35, 40,41,43,49,55,66, 67,68,72 (78)

5.6.1 Comparison studies for validating proposed method for OPP studies

The preliminary results for OPP with Topological observability (Case 1) studies are performed using CSA, PSO and BILP (Refer Table 5.2). Here, it is observed that optimal number of PMUs obtained for Case 1 are same by using any of CSA, PSO and BILP for all the 4 test systems studied. For comparison with literature, BILP results for the standard IEEE 14, IEEE 30 and IEEE 57-bus systems are 4,10 and 17 (Gou, 2008a) same as that obtained using CSA here as noted in Table 5.2.

Performance Evaluation of Results of OPP Studies

A. System Observability Redundancy Index (SORI):

Now, to decide the superiority among the various possible solutions with the same optimal number of PMUs, a performance indicator System Observability Redundancy Index (SORI) is used (Biswal and Mathur, 2015; Dua et al., 2008). Firstly, the number of PMUs which are able to observe each i^{th} bus in the system is calculated and called as bus observability index BOI_i , with respect to an OPP solution location set. Then, the summation of the bus observability indices of all N buses is calculated and the sum is called as SORI.

$$SORI = \sum_{i=1}^N BOI_i \quad (5.24)$$

For example, if a six-bus system is considered as shown in Fig. 5.15. It can be inferred that atleast two PMUs are necessary for ensuring an observable system. Taking two possible optimum location sets as illustrated in Fig. 5.15 (a) and (b) respectively. Achieving larger SORI gives the benefit that a comparatively greater region of the system shall continue to be observable even at the occurrence of a PMU failure (Dua et al., 2008). For example, in Fig. 5.15 (a), one PMU outage at bus 2 will cause 2 buses namely 1 and 3 to become unobservable, as against one PMU outage at bus 1 will cause 3 buses namely 1, 2 and 6 to become unobservable in Fig. 5.15 (b).

Maximum SORI implies maximizing the observability redundancy of the system. The placement of PMUs in IEEE 30-bus system (Refer Appendix B) and their corresponding SORI indices according to the solution sets obtained by CSA, PSO and BILP methods are shown in Figs 5.16a, 5.16b and 5.16c respectively. CSA proved to be advantageous as SORI for CSA solutions are higher than that of BILP solutions. But, another point to be noted is that BILP method provides only one

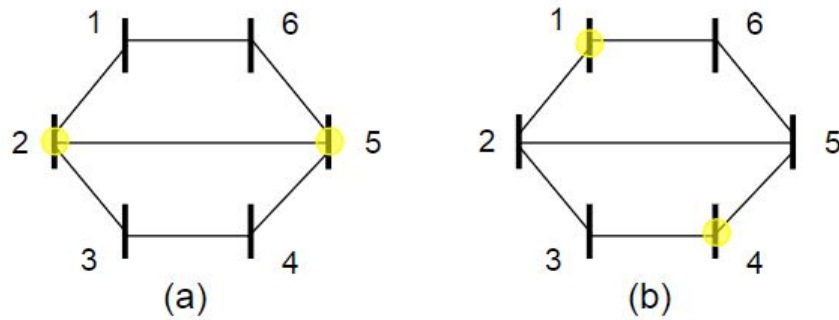


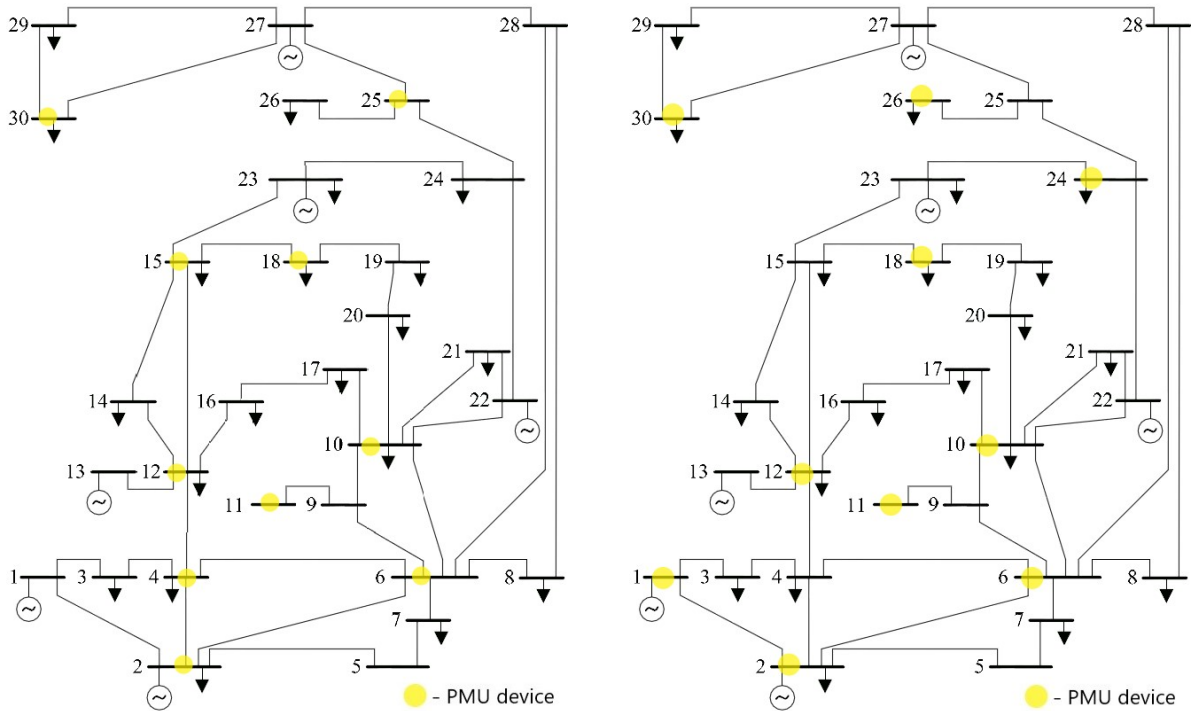
Figure 5.15: System observability redundancy index (SORI) is (a) 8 (b) 6

solution set for each optimal point obtained. While comparing CSA and PSO (Refer Table 5.2) except for IEEE 14-bus system, for all other test systems CSA is superior as SORI for CSA solution is higher than that that of PSO solutions. For instance in case of the practical 72-bus system, the Case 1 optimal solution 26 is obtained by all 3 methods, but their SORI indices are 96, 92 and 78 for CSA, PSO and BILP methods respectively. The higher SORI is mostly attributed to the non greedy nature which increasingly diversifies the solution of CSA. “CSA is not a greedy algorithm since if a crow generates a new position which is not better than its current position, it will move to the new position” (Askarzadeh, 2016). Non-greedy algorithms can increase the diversity of generated solutions. On the other hand, PSO is a greedy algorithm.

B. Computational Time:

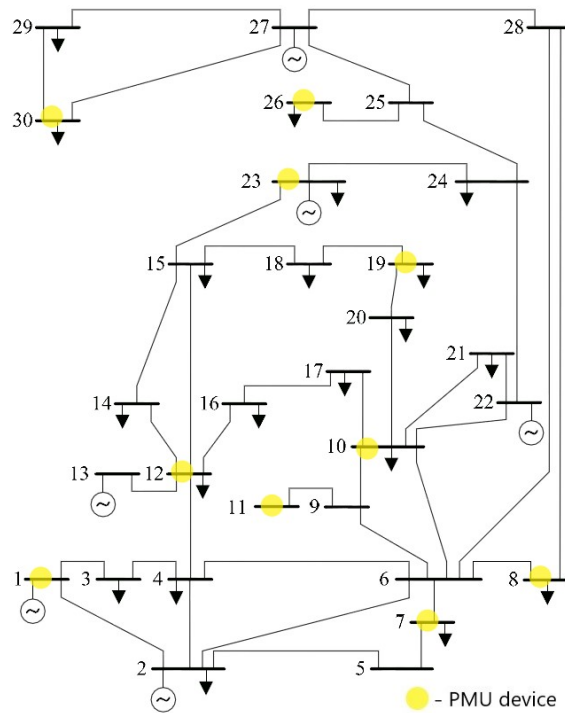
The computational time of BILP method is the least with the computation taking only fraction of second and less than 1 s as seen in Table 5.2. On the other hand, the computational time taken by PSO and CSA are larger and the range can be seen in the Table 5.2. But, the computational time of CSA is significantly less when compared to the meta-heuristic method PSO especially for larger test systems. That is, for the practical 72-bus test system, the time taken by CSA and PSO for arriving at the global solution are 1040 s and 3547 s respectively. The time taken by PSO is almost three times that of CSA. Therefore, CSA outperforms PSO in both SORI index and computational time. So after these preliminary comparison studies, all the security constrained optimal placement of PMUs are carried out (See Tables 5.3-5.25).

It was observed that the major advantage of using the CSA method is that it provides multiple solution sets for every optimal point obtained as noted in Tables 5.5 - 5.25. For example, IEEE 14-bus system multiple solutions are shown in Fig. 5.17. The multiple solution sets correspond to alternative solutions for placement of PMUs, while the number of PMUs required remains the same and is optimal. This provides better options for



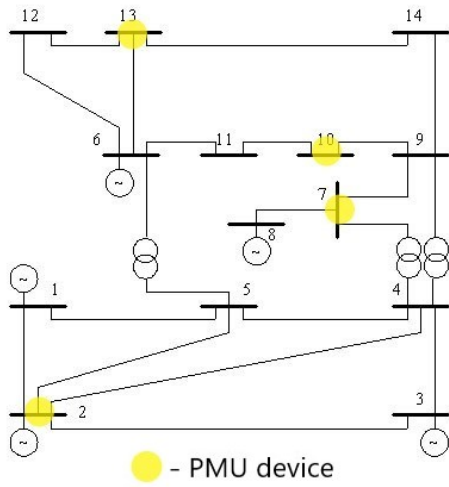
(a) Using proposed CSA method: SORI=48

(b) Using PSO method: SORI=43

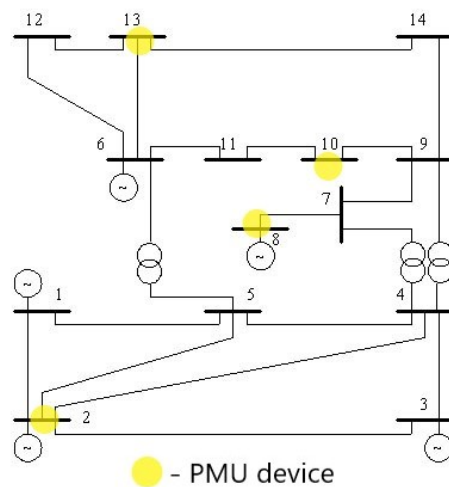


(c) Using BILP method: SORI=35

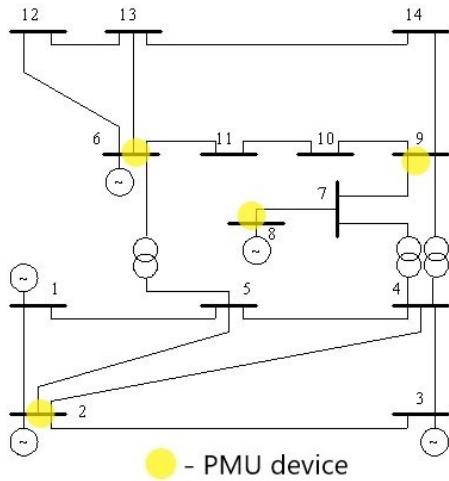
Figure 5.16: Different locations of phasor measurement units (PMUs) in IEEE 30-bus system for Case 1 - topological observability obtained by using methods: (a) Crow search algorithm (CSA) (b) Particle swarm optimization (PSO) and (c) Binary integer linear programming (BILP). Optimal number of PMUs is 10 in all methods. Set of common/similar nodes in all methods is (10, 11, 12, 30). (Note: System observability redundancy index (SORI))



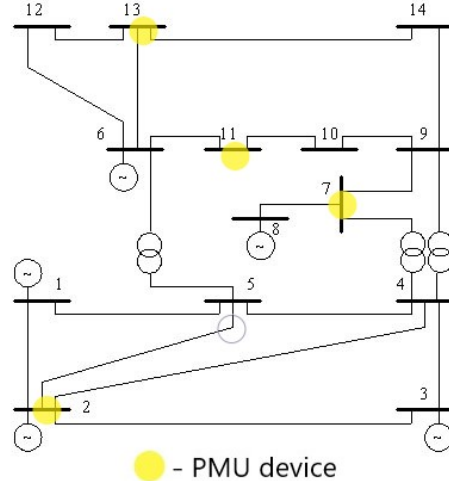
(a) PMUs at 2,7,10 & 13: SORI=16



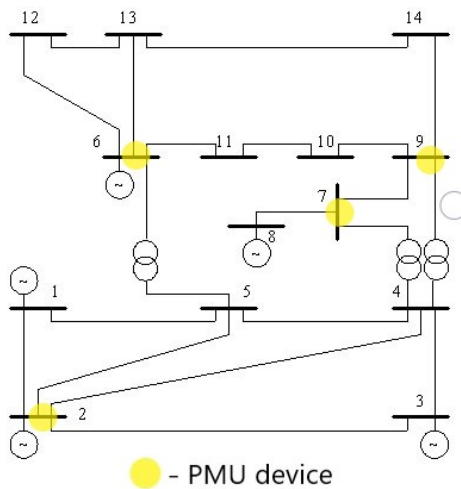
(b) PMUs at 2,8,10 & 13: SORI=14



(c) PMUs at 2,6,8 & 9: SORI=17



(d) PMUs at 2,7,11 & 13: SORI=16



(e) PMUs at 2,6,7 & 9: SORI=19

Figure 5.17: Multiple solutions for placement of phasor measurement units (PMUs) in IEEE 14-bus system for Case 1 using Crow search algorithm (CSA) method . Optimal number of PMUs is 4 in all the sub figures. Only common/similar node in all methods is 2. (Note: System observability redundancy index (SORI))

Table 5.3: Optimized number of phasor measurement units (PMUs) obtained using the proposed Crow search algorithm method

Constraint considered	14-bus	30-bus	57-bus	72-bus
Case 1: Topological Observability	4	10	17	26
Case 1 with ZIB	3	7	12	15
Case 2: Numerical Observability	4	10	17	27
Case 2 with ZIB	4	10	17	27
Case 1 & Single PMU loss	9	21	25	58
Case 1 & Single PMU loss with ZIB	7	15	25	34
Case 2 & Single PMU loss	9	21	33	58
Case 2 & Single PMU loss with ZIB	7	15	26	44
Case 1 & Single Line contingency	7	16	28	44
Case 1 & Single Line contingency with ZIB	7	16	29	44
Case 2 & Single Line contingency	9	21	38	58
Case 2 & Single Line contingency with ZIB	7	16	31	46
Case 1 & Measurement channel limit	4	10	17	26
Case 1 & Measurement channel limit with ZIB	3	7	12	15
Case 2 & Measurement channel limit	4	10	17	27
Case 2 & Measurement channel limit with ZIB	4	10	17	27

planning the installation of PMUs in power system based on the different applications desired by power engineers. Due to space constraints, the PMU placement location sets for single line contingency considering ZIB has been not added here.

5.6.2 Application of proposed CSA for various case studies

From the comparison studies, it is evident that Crow search algorithm is an excellent alternative as it provides higher and better SORI index solution set in majority of the cases. So, further case studies for all different contingencies and constraints discussed in Section 5.2 are carried out using the competent CSA approach and noted down carefully in the Table 5.3 for all the case studies. Following are the observations from Table 5.3:

- (a) The largest number obtained among the OPP results (highlighted in bold) could be considered to be the maximum number of PMUs required to satisfy any of the constrained observability discussed in the paper.
- (b) It is observed that zero-injection bus consideration leads to the lower optimal number of PMUs when compared to the cases when ZIBs are not considered.
- (c) The lowest possible optimal number of PMUs were obtained for both scenarios (i) Case 1 with ZIB consideration and (ii) Case 1 with measurement channel limitation and ZIB.

Both the studies based on cases 1 and 2 are carried out, with and without considering ZIB measurements. Following are the observations made based on the results obtained (Refer Table 5.3):

- (a) The optimal number of PMUs required for both Cases 1 and 2 without ZIB measurements are the same for each of the first three systems.
- (b) Additional number of PMUs are required for majority of the cases, to achieve numerical observability when compared to topological observability constrained optimal number. For example, the case 1 and case 2 results without considering ZIB for practical 72-bus system are 26 and 27. Hence, one additional PMU is required to make the system numerically observable.
- (c) It is observed that there is a significant reduction in the number of PMUs required for achieving Case 1: topological observability when ZIB measurements are considered when compared to that without considering ZIB measurements.
- (d) It is observed that under normal operating conditions, the optimal number of PMUs required for achieving Case 2: numerical observability of the system is not improved by using ZIB measurements. While if any contingencies like single PMU loss or single line loss is considered, then the optimal number of PMUs required for Case 2: numerical observability is reduced significantly by inclusion of ZIB measurements.

Table 5.4: Computational time (in seconds) for obtaining the global optimized number of phasor measurement units (PMUs) using the proposed Crow search algorithm method

Constraint considered	14-bus	30-bus	57-bus	72-bus
Case 1: Topological Observability	1.1s	3.5s	24.9s	1039.7s
Case 1 with zero injection bus (ZIB)	1.2s	3.0s	53.4s	249.2s
Case 2: Numerical Observability	13.2s	177.6s	12265.4s	3351.5s
Case 2 with ZIB	57.2s	1280.7s	690.5s	4777.5s
Case 1 & Single PMU loss	1.9s	4156.1s	37050.2s	45.8s
Case 1 & Single PMU loss with ZIB	1.4s	153.3s	37050.1s	34.0s
Case 2 & Single PMU loss	110.8s	1993.8s	33792.5s	304241.8s
Case 2 & Single PMU loss with ZIB	92.8s	18747.5s	33792.5s	88241.0s
Case 1 & Single Line contingency	2.2s	1061.6s	1672.1s	1059.6s
Case 1 & Single Line contingency with ZIB	2.2s	1059.7s	285.8s	1059.6s
Case 2 & Single Line contingency	792.4s	9588.1s	106448.8s	265462.3s
Case 2 & Single Line contingency with ZIB	791.8s	13727.4s	203010.8s	265462.3s
Case 1 & Measurement channel limit	1.1s	13.5s	92.8s	502.8s
Case 1 & Measurement channel limit with ZIB	1.2s	3.0s	53.3s	249.2s
Case 2 & Measurement channel limit	13.2s	177.6s	12265.4s	2087.3s
Case 2 & Measurement channel limit with ZIB	57.2s	1280.7s	2943.3s	2068.3s

The computational time (in seconds) to obtain the global optimal solution for these various case studies have been noted as well in Table 5.4. The following observations can be made from this table:

- (a) The time required for obtaining OPP solution in majority of the studies is increasing with increasing in the size of the system under study.
- (b) The time taken for finding the OPP solution for Case 2: numerical observability is around 4 to 700 times that of the time taken to find solution for Case 1: topological observability. This is due to complex constraints in Case 2 involving calculation of measurement Jacobian matrix, rank of matrix, etc.

Tables 5.5 - 5.25 show the corresponding PMU location sets for each optimal number of PMUs obtained with respect to different test systems and constraints.

So, further case studies for the constraints mentioned in Section 5.5.2 are carried out using the competent CSA approach and noted down carefully in the Table 5.3 for all the case studies. Tables 5.5 - 5.25 can be referred for the PMU locations obtained for the OPP solutions. Following observations can be drawn from these table results,

1. The largest number among the OPP results could be considered to be the maximum number of PMUs required to satisfy any of the contingency-constrained observability discussed in the work. As observed in Table 5.3, this is decided by the single line contingency-constrained results as its optimal value greater than all other cases for every test system considered.
2. It is observed that zero-injection bus consideration leads to the lower optimal number of PMUs when compared to the cases when ZIBs are not considered (Refer Table 5.3).
3. The lowest possible optimal number of PMUs are obtained for both scenarios (Refer Table 5.3): (a) case 1 with ZIB consideration and (b) case 1 with measurement channel limitation and ZIB.

Since, in some cases topological observability does not guarantee numerical observability, the CSA method is implemented for the numerical observability constraint as well. Numerical observability is necessary condition to carry out state estimation with the given PMU measurements. Both the studies based on cases 1 and 2 are carried out, with and without considering ZIB measurements (noted in Table 5.3). Following are the observations made based on the results obtained:

1. The optimal number of PMUs required for both Cases 1 and 2 without ZIB measurements are the same for each of the first three systems (Refer Table 5.3).

2. Additional number of PMUs are required for majority of the cases to achieve numerical observability when compared to topological observability constrained optimal number (Refer Table 5.3). For instance, the number of PMUs obtained for case 1 and case 2 without considering ZIB with respect to practical 72-bus system are 26 and 27. Hence, one additional PMU is required to make the system numerically observable. This proves that optimal number of PMUs obtained for topological observability constrained OPP might not guarantee numerical observability of the system. This would imply that it might lead to scarcity of measurements necessary for carrying out state estimation of the system and other applications.
3. There is reduction in the number of PMUs required in order to achieve Case 1 topological observability when zero-injection bus measurements are considered. While the numerical observability results are not affected by the consideration of zero-injection bus measurements (Refer Table 5.3).

Assuming ZIB measurements to be available always, the highest number of PMUs are required for case 2 with single line contingency (Refer highlighted in bold in Table 5.3). Consequently, this would be the maximum number of PMUs required to satisfy any of the scenarios discussed.

Table 5.5: Multiple PMU location solutions for Cases 1 and 2 results- PART I

System Network	Case 1 Optimal No. of PMUs	PMU locations	Case 2 Optimal No. of PMUs	PMU locations
IEEE 14-bus	4 (1.11s)	2,7,10,13 2,6,8,9 2,8,10,13 2,7,11,13 2,6,7,9	4 (13.16s)	2,6,7,9 2,7,11,13 2,7,10,13 2,8,10,13
IEEE 30-bus	10 (3.53s)	2,4,6,10,11,12,15,18,25,30 1,7,8,10,11,12,19,24,25,27 2,4,6,10,11,12,18,24,25,29 1,6,7,9,13,15,17,20,21,25,29 3,5,10,11,12,19,23,26,27,28 1,5,8,9,10,12,18,23,26,30 3,6,7,9,10,12,18,24,26,30 1,7,10,11,12,18,23,26,28,30 2,3,6,9,10,12,15,20,25,29 1,5,6,10,11,12,19,24,25,29 1,5,6,9,10,12,18,24,26,30 2,4,6,10,11,12,18,23,25,30	10 (177.63s)	1,5,6,9,10,12,15,20,25,27 1,5,6,10,11,12,18,24,26,29 1,5,6,10,11,12,19,24,25,29 1,5,8,10,11,12,18,23,25,29 1,5,8,9,10,12,19,24,26,30 3,5,8,10,11,12,19,23,26,30 3,6,7,9,10,12,19,23,26,27

Table 5.6: Multiple PMU location solutions for Cases 1 and 2 results- PART II

System Network	Case 1 Optimal No. of PMUs	PMU locations	Case 2 Optimal No. of PMUs	PMU locations
IEEE 57-bus	17 (92.83s)	3,6,12,15,19,22,25,26,29,32,36,38,41,46,51,54,57 2,6,12,15,19,22,25,27,29,32,36,39,41,45,47,50,54 1,4,8,13,19,22,25,26,29,32,36,39,41,44,47,51,54 1,4,7,9,15,20,24,25,28,32,36,38,39,41,47,51,53 1,4,8,13,19,22,25,27,29,32,36,39,41,45,47,51,54 2,6,12,14,19,22,26,29,30,32,36,41,44,47,50,54,57	17 (8685.00s)	1,4,8,13,20,23,25,27,29,32,36,39,41,44,47,51,54 1,6,10,15,19,22,25,27,32,36,39,41,45,46,49,52,54 1,4,9,19,22,25,26,29,32,36,41,44,46,47,50,53,57 1,4,8,13,19,22,25,27,32,36,41,45,47,51,52,55,57 1,4,9,14,20,23,26,29,30,32,36,41,44,47,50,54,57 1,4,9,20,23,26,29,30,32,36,41,45,46,48,51,54,57 1,4,8,10,20,23,25,26,29,32,36,41,45,46,49,54,57
Practical 72-bus	26 (1039.66s)	3,5,9,11,16,21,26,30,31,36,40,41,43,46,47,49,52, 55,57,59,62,66,67,68,69,71 4,5,6,9,18,22,27,31,33,36,40,41,43,44,47,49,55, 57,59,60,65,66,67,68,69,71	27 (3351.46s)	2,4,5,9,21,26,33,35,40,41,43,44,46,47,49,52,54, 55,57,59,62,65,66,67,68,69,72 3,5,6,11,16,18,20,21,26,27,30,31,34,36,40,41,43, 53,55,57,59,64,66,67,68,69,71 3,7,11,15,18,20,23,26,30,31,34,40,41,44,45,48,49, 52,55,56,58,59,60,66,67,68,71 5,6,13,16,22,27,30,31,33,34,35,38,41,43,45,46,47, 50,55,59,60,65,66,67,68,69,72 2,3,5,6,9,11,19,20,22,25,30,35,40,41,43,44,46,49, 55,57,60,62,66,67,68,69,72

Table 5.7: Multiple PMU location solutions for Case 1 and 2 results considering ZIB- PART I

System Network	Case 1 with ZIB Optimal No. of PMUs	PMU locations	Case 2 with ZIB Optimal No. of PMUs	PMU locations
IEEE 14-bus (ZIB bus 7)	3 (1.17s)	2,6,9	4 (57.18s)	2,6,7,9 2,7,11,13 2,7,10,13 2,8,10,13 2,6,8,9
IEEE 30-bus (ZIB buses: 5,6,9, 11,25,28)	7 (2.97s)	1,2,10,12,19,24,27 3,7,10,12,18,23,27 3,7,10,12,15,19,27 3,5,10,12,18,24,27 2,3,10,12,18,24,29 1,5,10,12,19,24,30 2,4,10,12,18,24,27	10 (1280.74s)	1,5,9,10,12,19,24,25,28,29 1,7,8,10,11,12,15,19,25,27 1,6,7,10,11,12,15,19,25,27 1,2,6,10,11,12,19,24,25,30 1,2,6,10,11,12,15,19,25,27 1,2,6,10,11,12,15,18,25,29 1,6,7,9,10,12,18,24,26,27 2,3,6,10,11,12,18,23,26,27 3,5,6,10,11,12,18,24,25,29 1,7,9,10,12,19,24,26,27,28 1,2,6,9,10,12,18,24,25,27 1,5,8,10,11,12,18,23,25,27 1,2,6,10,11,12,19,24,26,29

Table 5.8: Multiple PMU location solutions for Case 1 and 2 results considering ZIB- PART II

System Network	Case 1 with ZIB Optimal No. of PMUs	PMU locations	Case 2 with ZIB Optimal No. of PMUs	PMU locations
IEEE 57-bus (ZIB buses: 4, 7, 11, 21, 22, 24, 26, 34, 36, 37, 39, 40, 45, 46, 48)	12 (53.35s)	3,12,15,20,25,29,32,36,41,47,51,54 1,9,15,18,25,29,32,38,47,51,54,56 1,9,15,18,23,29,31,32,47,51,54,56 3,12,15,20,25,29,32,41,47,50,54,56 1,10,18,25,29,32,38,41,44,47,51,54 1,9,18,25,29,32,38,45,46,51,53,56	17 (690.52s)	1,4,8,13,19,22,25,27,32,36,41,45,47,51,52,55,57 1,4,9,14,20,23,26,29,30,32,36,41,44,47,50,54,57 1,4,9,20,23,26,29,30,32,36,41,45,46,48,51,54,57
Practical 72-bus (ZIB buses: 24, 26, 27, 44, 45, 46, 47, 50, 51, 56, 57, 58, 59, 60, 61, 62, 63, 67, 70)	15 (249.19s)	3,6,11,13,30,31,34,41,43,49,55,66,68,69,71 4,6,7,11,31,33,34,40,41,43,53,55,66,68,72 11,30,31,33,34,40,41,43,49,52,55,66,68,69,71 4,6,10,31,33,34,40,41,43,53,55,65,66,69,72 3,6,7,9,30,31,38,40,41,43,55,65,66,68,72 6,7,8,30,31,33,34,40,41,43,53,65,66,68,71	27 (4777.48s)	3,6,9,13,19,20,21,26,27,30,31,36,41,43,44,45,46, 49,51,55,58,65,66,67,68,69,72

Table 5.9: Multiple PMU location solutions for Cases 1 and 2 results considering measurement channel limitation- PART I

System Network	Case 1 with measurement channel limitation: Optimal No. of PMUs	PMU locations	Case 2 with measurement channel limitation: Optimal No. of PMUs	PMU locations
IEEE 14-bus	4 (1.1143s)	2,7,10,13 2,6,8,9 2,8,10,13 2,7,11,13 2,6,7,9	4 (13.1601s)	2,6,7,9 2,7,11,13 2,7,10,13 2,8,10,13
IEEE 30-bus	10 (3.5306s)	2,4,6,10,11,12,15,18,25,30 1,7,8,10,11,12,19,24,25,27 2,4,6,10,11,12,18,24,25,29 1,6,7,9,13,15,17,20,21,25,29 3,5,10,11,12,19,23,26,27,28 1,5,8,9,10,12,18,23,26,30 3,6,7,9,10,12,18,24,26,30 1,7,10,11,12,18,23,26,28,30 2,3,6,9,10,12,15,20,25,29 1,5,6,10,11,12,19,24,25,29 1,5,6,9,10,12,18,24,26,30 2,4,6,10,11,12,18,23,25,30	10 (177.6293s)	1,5,6,9,10,12,15,20,25,27 1,5,6,10,11,12,18,24,26,29 1,5,6,10,11,12,19,24,25,29 1,5,8,10,11,12,18,23,25,29 1,5,8,9,10,12,19,24,26,30 3,5,8,10,11,12,19,23,26,30 3,6,7,9,10,12,19,23,26,27

Table 5.10: Multiple PMU location solutions for Cases 1 and 2 results considering measurement channel limitation - PART II

System Network	Case 1 with measurement channel limitation: Optimal No. of PMUs	PMU locations	Case 2 with measurement channel limitation: Optimal No. of PMUs	PMU locations
IEEE 57-bus	17 (92.83s)	2,6,12,15,19,22,25,27,29,32,36,39,41,45,47,50,54 3,6,12,15,19,22,25,26,29,32,36,38,41,46,51,54,57 1,4,8,13,19,22,25,26,29,32,36,39,41,44,47,51,54 1,4,7,9,15,20,24,25,28,32,36,38,39,41,47,51,53 1,4,8,13,19,22,25,27,29,32,36,39,41,45,47,51,54 2,6,12,14,19,22,26,29,30,32,36,41,44,47,50,54,57	17 (12265.44s)	1,4,8,13,20,23,25,27,29,32,36,39,41,44,47,51,54 1,6,10,15,19,22,25,27,32,36,39,41,45,46,49,52,54 1,4,9,19,22,25,26,29,32,36,41,44,46,47,50,53,57 1,4,8,13,19,22,25,27,32,36,41,45,47,51,52,55,57 1,4,9,14,20,23,26,29,30,32,36,41,44,47,50,54,57 1,4,9,20,23,26,29,30,32,36,41,45,46,48,51,54,57 1,4,8,10,20,23,25,26,29,32,36,41,45,46,49,54,57
Practical 72-bus	26 (502.81s)	6,9,18,24,26,27,30,31,33,35,40,41,43,44,47, 49,55,58,59,60,65,66,67,68,69,72 9,22,24,30,31,33,36,40,41,43,44,46,47,49,52, 55,58,59,60,62,65,66,67,68,69,72	27 (2087.34s)	5,6,10,12,16,18,20,22,24,30,31,33,34,35,40,41, 43,49,50,55,59,60,62,65,66,69,72 5,6,10,12,16,18,20,22,24,30,31,33,34,35,40,41, 43,49,50,55,59,60,62,65,66,69,72 5,7,9,11,16,18,22,27,30,31,33,38,40,41,43,45, 47,51,52,55,56,59,60,66,67,68,71 5,6,9,11,13,14,19,22,23,30,31,33,43,44,45,46, 47,53,55,56,60,64,66,67,68,69,72 3,4,5,6,7,9,11,16,18,22,23,31,35,40,41,43,47, 51,53,55,57,59,60,66,67,68,71 3,5,6,9,11,12,13,20,23,26,30,31,38,41,43,44, 45,46,51,55,56,59,60,66,68,69,71 3,4,5,6,10,16,19,26,27,31,34,36,39,40,41,43, 46,47,49,55,57,60,65,66,67,69,71

Table 5.11: Multiple PMU location solutions for Case 1 and 2 results considering measurement channel limitation (4 channels for each PMU) and ZIB- PART I

System Network	Case 1 with measurement channel limitation and ZIB: Optimal No. of PMUs	PMU locations	Case 2 with measurement channel limitation and ZIB: Optimal No. of PMUs	PMU locations
IEEE 14-bus (ZIB bus 7)	3 (1.17s)	2,6,9	4 (57.18s)	2,6,7,9 2,7,11,13 2,7,10,13 2,8,10,13 2,6,8,9
IEEE 30-bus (ZIB buses: 5, 6,9,11, 25,28)	7 (2.9726s)	1,2,10,12,19,24,27 3,7,10,12,18,23,27 3,7,10,12,15,19,27 3,5,10,12,18,24,27 2,3,10,12,18,24,29 1,5,10,12,19,24,30 2,4,10,12,18,24,27	10 (1280.7372s)	1,5,9,10,12,19,24,25,28,29 1,7,8,10,11,12,15,19,25,27 1,6,7,10,11,12,15,19,25,27 1,2,6,10,11,12,19,24,25,30 1,2,6,10,11,12,15,19,25,27 1,2,6,10,11,12,15,18,25,29 1,6,7,9,10,12,18,24,26,27 2,3,6,10,11,12,18,23,26,27 3,5,6,10,11,12,18,24,25,29 1,7,9,10,12,19,24,26,27,28 1,2,6,9,10,12,18,24,25,27 1,5,8,10,11,12,18,23,25,27 1,2,6,10,11,12,19,24,26,29

Table 5.12: Multiple PMU location solutions for Case 1 and 2 results considering measurement channel limitation (4 channels for each PMU) and ZIB - PART II

System Network	Case 1 with measurement channel limitation and ZIB: Optimal No. of PMUs	PMU locations	Case 2 with measurement channel limitation and ZIB: Optimal No. of PMUs	PMU locations
IEEE 57-bus (ZIB buses: 4,7,11,21,22,24,26,34,36,37,39,40,45,46,48)	12 (53.35s)	3,12,15,20,25,29,32,36,41,47,51,54 1,9,15,18,25,29,32,38,47,51,54,56 1,9,15,18,23,29,31,32,47,51,54,56 3,12,15,20,25,29,32,41,47,50,54,56 1,10,18,25,29,32,38,41,44,47,51,54 1,9,18,25,29,32,38,45,46,51,53,56	17 (2943.26s)	2,6,12,13,19,22,25,26,29,32,36,41,44,47,50,54,57
Practical 72-bus (ZIB buses: 24,26,27,44,45,46,47,50,51,56,57,58,59,60,61,62,63,67,70)	15 (249.19s)	3,6,11,13,30,31,34,41,43,49,55,66,68,69,71 4,6,7,11,31,33,34,40,41,43,53,55,66,68,72 11,30,31,33,34,40,41,43,49,52,55,66,68,69,71 4,6,10,31,33,34,40,41,43,53,55,65,66,69,72 3,6,7,9,30,31,38,40,41,43,55,65,66,68,72 6,7,8,30,31,33,34,40,41,43,53,65,66,68,71	27 (2068.31s)	2,3,5,6,9,11,19,20,22,25,30,35,40,41,43,44,46,49,55,57,60,62,66,67,68,69,72

Table 5.13: Multiple PMU location solutions for Cases 1 and 2 results considering single PMU loss- PART I

System Network	Case 1 with Single PMU loss Optimal No. of PMUs	PMU locations	Case 2 with Single PMU loss Optimal No. of PMUs	PMU locations
IEEE 14-bus	9 (1.9331s)	2,3,5,6,7,8,9,10,13 2,3,5,6,7,8,9,11,13 2,4,5,6,7,8,9,11,13 2,3,5,6,7,8,9,10,13 1,2,4,6,7,8,9,10,13 2,3,5,6,7,8,9,11,13 1,2,3,6,7,8,9,11,13 1,2,4,6,7,8,9,10,13 1,2,4,6,7,8,9,10,13 1,2,3,6,7,8,9,10,13 1,2,4,6,7,8,9,10,13 2,3,5,6,7,8,9,10,13 1,2,3,6,7,8,9,10,13 2,4,5,6,7,8,9,11,13 1,2,3,6,7,8,9,11,13	9 (110.7884s)	2,3,5,6,7,8,9,10,13 2,4,5,6,7,8,9,11,13 1,2,4,6,7,8,9,11,13 2,3,5,6,7,8,9,10,13 2,4,5,6,7,8,9,11,13 1,2,3,6,7,8,9,11,13 2,4,5,6,7,8,9,11,13 1,2,4,6,7,8,9,10,13 2,3,5,6,7,8,9,10,13 2,3,5,6,7,8,9,10,13 1,2,3,6,7,8,9,11,13 1,2,3,6,7,8,9,11,13 2,4,5,6,7,8,9,11,13 1,2,4,6,7,8,9,10,13 2,3,5,6,7,8,9,11,13

Table 5.14: Multiple PMU location solutions for Cases 1 and 2 results considering single PMU loss (SPL)- PART II

System Network	Case 1 with SPL: Optimal No. of PMUs	PMU locations	Case 2 with SPL: Optimal No. of PMUs	PMU locations
IEEE 30-bus	21 (4156.1s)	2,3,4,5,6,8,9,10,11,12,13,15,16,19,20,21,24,25,26,27,29	21 (1993.78s)	1,2,3,5,6,8,9,10,11,12,13,15,16,18,19,21,24,25,26,27,29
		2,3,4,5,6,9,10,11,12,13,15,17,18,20,22,24,25,26,27,28,29		1,3,5,6,7,9,10,11,12,13,15,16,18,20,22,23,25,26,27,28,29
		1,2,3,5,6,9,10,11,12,13,15,17,18,19,21,23,25,26,27,28,30		1,3,5,6,7,8,9,10,11,12,13,15,16,18,20,22,23,25,26,27,29
		1,2,3,6,7,9,10,11,12,13,15,17,18,19,21,24,25,26,27,28,29		1,3,5,6,7,8,9,10,11,12,13,15,16,19,20,22,23,25,26,27,30
		1,2,4,6,7,9,10,11,12,13,15,17,18,20,21,23,25,26,27,28,30		1,2,3,6,7,9,10,11,12,13,15,16,18,20,21,24,25,26,27,28,29
		2,3,4,6,7,9,10,11,12,13,15,17,18,20,22,23,25,26,27,28,29		1,2,3,6,7,9,10,11,12,13,15,17,18,19,22,24,25,26,28,29,30
		1,2,4,6,7,8,9,10,11,12,13,15,17,18,20,21,23,25,26,27,30		1,3,5,6,7,9,10,11,12,13,15,16,19,20,21,24,25,26,27,28,30
		1,2,3,5,6,8,9,10,11,12,13,15,16,19,20,21,24,25,26,27,29		1,2,3,6,7,9,10,11,12,13,15,17,18,19,22,23,25,26,28,29,30
		2,3,4,6,7,8,9,10,11,12,13,15,16,19,20,22,24,25,26,27,30		1,3,5,6,7,9,10,11,12,13,15,17,18,20,21,23,25,26,27,28,30
		2,3,4,6,7,8,9,10,11,12,13,15,17,19,20,22,23,25,26,27,29		1,2,3,6,7,8,9,10,11,12,13,15,17,18,20,21,23,25,26,27,30
		1,3,5,6,7,8,9,10,11,12,13,15,17,19,20,22,24,25,26,27,30		1,3,5,6,7,9,10,11,12,13,15,17,19,20,21,24,25,26,27,28,30
		1,2,4,5,6,9,10,11,12,13,15,16,18,19,22,24,25,26,27,28,30		1,3,5,6,7,9,10,11,12,13,15,16,18,20,21,24,25,26,27,28,29
		1,2,4,5,6,8,9,10,11,12,13,15,16,19,20,22,24,25,26,27,30		1,2,3,5,6,9,10,11,12,13,15,16,18,19,22,23,25,26,27,28,29
		1,2,4,5,6,9,10,11,12,13,15,16,19,20,21,23,25,26,27,28,29		1,2,3,5,6,8,9,10,11,12,13,15,17,19,20,21,24,25,26,27,30
		1,2,3,5,6,8,9,10,11,12,13,15,17,19,20,22,23,25,26,29,30		

Table 5.15: Multiple PMU location solutions for Cases 1 and 2 results considering single PMU loss- PART III

System Network	Case 1 with Single PMU loss Optimal No. of PMUs	PMU locations	Case 2 with Single PMU loss Optimal No. of PMUs	PMU locations
IEEE 57-bus	25 (37050.14s)	1,3,6,9,12,14,15,18,20,25,27,29,30,32,33,34,38,41,44,47,50,51,53,54,56	33 (s)	1,2,4,6,9,11,12,15,19,20,22,24,25,27,28,29,30,32,33,35,36,37,38,39,41,44,46,47,50,51,53,54,56
Practical 72-bus	58 (45.84s)	1,2,3,4,5,6,7,8,9,10,11,12,13,14,15,16,17,18,19,20,21,22,23,24,26,27,30,31,33,34,35,38,40,41,42,43,44,45,46,47,50,52,53,54,55,56,58,59,60,61,64,65,66,67,68,69,71,72	58 (304241.79s)	1,2,3,4,5,6,7,8,9,10,11,12,13,14,15,16,17,18,19,20,21,22,23,25,26,30,31,32,33,34,35,37,38,40,41,42,43,44,45,46,47,49,50,52,55,56,57,58,59,60,62,65,66,67,68,69,71,72 1,2,3,4,5,6,7,8,9,10,11,12,13,14,15,16,17,18,19,20,21,22,23,24,26,27,30,31,32,33,34,36,39,40,41,43,44,45,46,47,48,49,52,53,54,55,56,58,59,60,64,65,66,67,68,69,71,72 1,2,3,4,5,6,7,8,9,10,11,12,13,14,15,16,17,18,19,20,21,22,23,26,30,31,33,34,36,38,40,41,42,43,44,45,46,47,50,52,53,54,55,56,57,58,59,60,61,62,64,65,66,67,68,69,71,72 1,2,3,4,5,6,7,8,9,10,11,12,13,14,15,16,17,18,19,20,21,22,24,25,26,27,30,31,33,34,35,36,38,40,41,43,44,45,46,47,48,50,52,53,55,58,59,60,61,62,64,65,66,67,68,69,71,72 1,2,3,4,5,6,7,8,9,10,11,12,13,14,15,16,17,18,19,20,21,22,26,27,30,31,33,34,36,38,40,41,43,44,45,46,47,48,49,50,52,54,55,56,57,58,59,60,61,62,64,65,66,67,68,69,71,72 1,2,3,4,5,6,7,8,9,10,11,12,13,14,15,16,17,18,19,20,21,22,26,27,30,31,33,34,36,39,40,41,43,44,45,46,47,48,49,52,53,54,55,56,57,58,59,60,61,62,64,65,66,67,68,69,71,72

Table 5.16: Multiple PMU location solutions for Cases 1 and 2 results considering single PMU loss- PART III (Contd.)

System Network	Case 2 with Single PMU loss: Optimal No. of PMUs	PMU locations
Practical 72-bus	58 (304241.79s)	<p>1,2,3,4,5,6,7,8,9,10,11,12,13,14,15,16,17,18,19,20,21,22,24,25,26,27,30,31,33,34,35,36,38,40,41,43,44,46,47,48,49,50,52,55,57,58,59,60,61,62,64,65,66,67,68,69,71,72</p> <p>1,2,3,4,5,6,7,8,9,10,11,12,13,14,15,16,17,18,19,20,21,22,23,24,26,30,31,32,33,34,35,36,37,38,40,41,43,44,45,46,47,48,49,50,52,54,55,58,59,62,65,66,67,68,69,71,72</p> <p>1,2,3,4,5,6,7,8,9,10,11,12,13,14,15,16,17,18,19,20,21,22,23,26,27,30,31,33,34,35,39,40,41,42,43,44,45,46,47,49,52,53,54,55,56,57,58,59,60,61,64,65,66,67,68,69,71,72</p> <p>1,2,3,4,5,6,7,8,9,10,11,12,13,14,15,16,17,18,19,20,21,22,23,24,25,26,27,30,31,33,34,36,38,40,41,42,43,44,45,46,47,49,50,52,55,56,58,59,60,61,64,65,66,67,68,69,71,72</p> <p>1,2,3,4,5,6,7,8,9,10,11,12,13,14,15,16,17,18,19,20,21,22,24,25,26,27,30,31,33,34,35,36,37,38,40,41,43,44,46,47,48,49,50,52,55,57,58,59,60,61,62,65,66,67,68,69,71,72</p> <p>1,2,3,4,5,6,7,8,9,10,11,12,13,14,15,16,17,18,19,20,21,22,23,24,25,26,30,31,33,34,35,38,40,41,42,43,44,45,46,47,49,50,52,55,56,58,59,60,61,62,64,65,66,67,68,69,71,72</p> <p>1,2,3,4,5,6,7,8,9,10,11,12,13,14,15,16,17,18,19,20,21,22,23,24,26,30,31,33,34,35,36,39,40,41,43,44,46,47,48,49,52,53,54,55,57,58,59,60,61,62,64,65,66,67,68,69,71,72</p> <p>1,2,3,4,5,6,7,8,9,10,11,12,13,14,15,16,17,18,19,20,21,22,24,25,26,27,30,31,33,34,35,36,40,41,43,44,46,47,48,49,50,52,53,55,57,58,59,60,61,62,64,65,66,67,68,69,71,72</p>

Table 5.17: Multiple PMU location solutions for Case 1 and 2 results considering Single PMU loss and ZIB- PART I

System Network	Case 1 with Single PMU loss and ZIB Optimal No. of PMUs	PMU locations	Case 2 with single PMU loss and ZIB Optimal No. of PMUs	PMU locations
IEEE 14-bus (ZIB)	7 (1.4241s)	1,2,4,6,9,10,13 1,2,4,6,9,11,13 2,4,5,6,9,10,13 2,4,5,6,9,11,13	7 (92.7739s) bus 7)	2,4,5,6,9,10,13 1,2,4,6,9,10,13 2,4,5,6,9,11,13
IEEE 30-bus (ZIB buses: 5, 6,9,11, 25,28)	15 (153.34s)	2,3,4,7,10,12,13,15,16,18,19,21,24,27,29 1,3,5,7,10,12,13,15,16,18,20,22,24,27,29 2,3,4,7,10,12,13,15,17,18,20,21,24,27,29 1,2,3,5,10,12,13,15,17,18,19,22,24,27,30 1,2,3,5,10,12,13,15,17,18,20,22,24,27,30 1,2,4,5,10,12,13,15,16,18,20,21,24,27,29 1,2,4,7,10,12,13,15,17,19,20,22,24,27,29 1,2,3,5,10,12,13,15,17,18,20,21,24,27,29 2,3,4,5,10,12,13,15,16,18,19,22,24,27,30 2,3,4,7,10,12,13,15,17,18,19,22,24,27,29 2,3,4,7,10,12,13,15,17,18,19,21,24,27,29 1,3,5,7,10,12,13,15,17,19,20,22,24,27,30 1,2,4,5,10,12,13,15,16,19,20,21,24,27,30	15 (18747.50s)	1,4,5,7,10,12,13,15,17,18,20,22,24,27,29 1,2,4,5,10,12,13,15,16,19,20,22,24,27,29 1,3,5,7,10,12,13,15,17,18,19,22,24,27,29 3,4,5,7,10,12,13,15,17,19,20,22,24,27,30 2,3,4,5,10,12,13,15,17,19,20,22,24,27,30 3,4,5,7,10,12,13,15,16,18,20,22,24,27,29 1,3,5,7,10,12,13,15,17,19,20,22,24,27,29 1,2,4,5,10,12,13,15,16,18,19,22,24,27,29

Table 5.18: Multiple PMU location solutions for Case 1 and 2 results considering Single PMU loss and ZIB- PART II

System Network	Case 1 with Single PMU loss and ZIB Optimal No. of PMUs	PMU locations	Case 2 with single PMU loss and ZIB Optimal No. of PMUs	PMU locations
IEEE 57-bus (ZIB buses: 4, 7,11,21,22, 24,26,34,36, 37,39,40, 45,46,48)	25 (37050.14s)	1,3,6,9,12,14,15,18,20,25,27,29, 30,32,33,34,38,41,44,47,50,51,53, 54,56	26 (33792.52s)	1,2,6,9,12,18,19,23,28,29,30,31,32,33,35,38,41,44, 45,46,47,50,51,53,54,56 1,3,6,9,10,12,14,19,20,25,27,29,30,32,33,35,41,44, 45,47,49,50,52,54,55,56 1,3,6,9,12,19,20,25,28,29,30,32,33,34,38,42,43,44, 45,46,47,50,51,53,54,56 1,3,6,9,10,12,14,19,20,24,28,29,30,31,32,33,35,41, 44,45,47,49,50,53,54,56 1,2,6,9,12,18,20,25,27,29,31,32,33,34,38,41,44,45, 46,47,50,51,52,54,55,56 1,3,6,9,12,15,18,20,25,27,29,31,32,33,34,38,42,43, 44,46,47,50,51,53,54,56 1,3,6,9,12,14,15,19,20,24,27,29,30,31,32,33,35,41, 44,47,48,50,51,53,54,56
Practical 72-bus (ZIB buses: 24, 26,27,44,45, 46,47,50,51, 56,57,58,59, 60,61,62,63, 67,70)	34 (33.99s)	1,2,3,4,6,7,8,9,10,11,13,14,15,17, 30,31,33,34,37,40,41,43,48, 49,52,53,54,55,65,66,68,69,71,72 1,2,3,4,6,7,8,9,10,11,13,14,15,17,25, 30,31,33,34,38,40,41,42,43, 52,53,55,64,65,66,68,69,71,72 1,2,3,4,6,7,8,9,10,11,13,14,15,17,25, 30,31,33,34,38,40,41,43, 48,49,52,55,64,65,66,68,69,71,72	44 (88240.97s)	1,2,3,4,6,7,8,9,10,11,13,14,15,17,21,22,30,31,33, 34,40,41,43,44,45,46,47,48,49,50,52,53,54,55, 56,58,59,64,65,66,68,69,71,72 1,2,3,4,6,7,8,9,10,11,13,14,15,17,21,22,30,31,33,34, 40,41,43,44,45,46,47,48,49,50,52,53,54,55,56,58,59, 64,65,66,68,69,71,72 1,2,3,4,5,6,7,8,9,10,11,12,13,14,15,17,18,19,20,21,25, 26,30,31,33,34,35,37,40,41,43,44,48,49,52,53,55,56, 65,66,68,69,71,72

Table 5.19: Multiple PMU location solutions for Case 1 and 2 results considering Single PMU loss and ZIB- PART II (Contd.)

System Network	Case 1 with Single PMU loss and ZIB Optimal No. of PMUs	PMU locations	Case 2 with single PMU loss and ZIB Optimal No. of PMUs	PMU locations
Practical 72-bus (ZIB buses: 24, 26,27,44,45, 46,47,50,51, 56,57,58,59, 60,61,62,63, 67,70)	34 (33.99s)	1,2,3,4,6,7,8,9,10,11,13,14,15,17,30, 31,33,34,37,38,40,41,42,43, 52,53,54,55,65,66,68,69,71,72 1,2,3,4,6,7,8,9,10,11,13,14,15,17,30, 31,33,34,38,40,41,42,43,49,52,54,55, 64,65,66,68,69,71,72 1,2,3,4,6,7,8,9,10,11,13,14,15,17,30, 31,33,34,37,38,40,41,42,43, 49,52,54,55,65,66,68,69,71,72 1,2,3,4,6,7,8,9,10,11,13,14,15,17,25,30, 31,33,34,37,40,41,43, 48,49,52,53,55,65,66,68,69,71,72 1,2,3,4,6,7,8,9,10,11,13,14,15,17,30, 31,33,34,37,38,40,41,43, 48,49,52,54,55,65,66,68,69,71,72 1,2,3,4,6,7,8,9,10,11,13,14,15,17,25,30, 31,33,34,37,38,40,41, 42,43,49,52,55,65,66,68,69,71,72 1,2,3,4,6,7,8,9,10,11,13,14,15,17,30, 31,33,34,38,40,41,43, 48,49,52,54,55,64,65,66,68,69,71,72	44 (88240.97s)	1,2,3,4,5,6,7,8,9,10,11,13,14,15,16,17,19,25,26,30,31, 33,34,35,36,37,38,39,40,41,43,46,47,48,49,52,55,60, 65,66,68,69,71,72 1,2,3,4,6,7,8,9,10,11,13,14,15,16,17,19,20,22,25,30, 31,33,34,35,37,40,41,42,43,46,49,52,53,55,56,58,60, 65,66,67,68,69,71,72 1,2,3,4,5,6,7,8,9,10,11,13,14,15,17,19,20,21,25,26,30, 31,33,34,36,37,38,40,41,43,44,45,46,48,49,52,55, 65,66,67,68,69,71,72 1,2,3,4,5,6,7,8,9,10,11,13,14,15,16,17,18,21,25,26,30, 31,33,34,36,39,40,41,43,47,48,49,52,53,55,56,59, 64,65,66,68,69,71,72 1,2,3,4,6,7,8,9,10,11,12,13,14,15,16,17,18,20,26,30, 31,33,34,38,40,41,43,45,48,52,53,54,55,56,58,59, 60,64,65,66,68,69,71,72 1,2,3,4,5,6,7,8,9,10,11,13,14,15,17,18,21,25,26,30, 31,33,34,35,38,40,41,43,44,47,48,49,52,55,56,59, 64,65,66,67,68,69,71,72 1,2,3,4,6,7,8,9,10,11,13,14,15,16,17,19,21,26,30, 31,33,34,37,38,39,40,41,42,43,45,46,47,49,52,54,55, 56,58,65,66,68,69,71,72

Table 5.20: Multiple PMU location solutions for Case 1 and 2 results considering Single PMU loss and ZIB- PART II (Contd.)

System Network	Case 1 with Single PMU loss and ZIB Optimal No. of PMUs	PMU locations	Case 2 with single PMU loss and ZIB Optimal No. of PMUs	PMU locations
Practical 72-bus (ZIB buses: 24, 26,27,44,45,46, 47,50,51,56,57, 58,59,60,61,62, 63,67,70)	34 (33.99s)	1,2,3,4,6,7,8,9,10,11,13,14,15,17,25,30, 31,33,34,40,41,43, 48,49,52,53,55,64,65,66,68,69,71,72 1,2,3,4,6,7,8,9,10,11,13,14,15,17,25, 30,31,33,34,38,40,41,42,43, 52,53,55,64,65,66,68,69,71,72 1,2,3,4,6,7,8,9,10,11,13,14,15,17,30, 31,33,34,38,40,41,43, 48,52,53,54,55,64,65,66,68,69,71,72 1,2,3,4,6,7,8,9,10,11,13,14,15,17,30, 31,33,34,40,41,42,43, 49,52,53,54,55,64,65,66,68,69,71,72	44 (88240.97s)	1,2,3,4,6,7,8,9,10,11,12,13,14,15,16,17,20,21,26, 30,31,33,34,35,36,37,38,40,41,43,46,48,52,53,54, 55,58,59,65,66,68,69,71,72

Table 5.21: Multiple PMU location solutions for Cases 1 and 2 results considering single line contingency- PART I

System Network	Case 1 with Single line contingency Optimal No. of PMUs	PMU locations	Case 2 with Single line contingency Optimal No. of PMUs	PMU locations
IEEE 14-bus	7 (2.25s)	1,3,6,8,9,11,13 1,3,6,8,9,10,13	9 (792.40s)	1,2,3,6,7,8,9,10,13 2,3,5,6,7,8,9,11,13 1,2,4,6,7,8,9,10,13 1,2,3,6,7,8,9,11,13 2,4,5,6,7,8,9,10,13 2,3,5,6,7,8,9,10,13 1,2,4,6,7,8,9,11,13 2,4,5,6,7,8,9,11,13
IEEE 30-bus	16 (1061.59s)	2,3,7,8,10,11,12,13,15,17,19,21,24,26,27,29 2,3,7,8,10,11,13,14,16,18,20,22,23,26,27,29 2,3,7,8,10,11,12,13,15,16,19,22,23,26,27,29 2,3,7,8,10,11,12,13,15,17,19,22,23,26,27,30 2,3,7,8,10,11,13,14,15,16,19,22,23,26,27,30	21 (9588.14s)	1,2,3,6,7,9,10,11,12,13,15,17,19,20,22,23,25,26,28,29,30 1,3,5,6,7,9,10,11,12,13,15,16,18,19,21,23,25,26,28,29,30 1,3,5,6,7,8,9,10,11,12,13,15,17,18,20,22,24,25,26,29,30 1,2,3,6,7,9,10,11,12,13,15,17,18,20,21,23,25,26,27,28,29 1,2,3,5,6,8,9,10,11,12,13,15,17,19,20,21,23,25,26,29,30 1,3,5,6,7,8,9,10,11,12,13,15,17,18,20,22,24,25,26,27,29 1,3,5,6,7,9,10,11,12,13,15,17,18,20,21,24,25,26,28,29,30 1,3,5,6,7,9,10,11,12,13,15,16,19,20,21,24,25,26,28,29,30 1,3,5,6,7,9,10,11,12,13,15,17,18,19,22,23,25,26,28,29,30 1,2,3,6,7,9,10,11,12,13,15,16,18,20,21,23,25,26,27,28,29 1,3,5,6,7,9,10,11,12,13,15,16,19,20,21,24,25,26,27,28,30 1,3,5,6,7,9,10,11,12,13,15,17,18,19,22,23,25,26,27,28,29 1,3,5,6,7,8,9,10,11,12,13,15,17,19,20,22,24,25,26,27,30 1,2,3,5,6,9,10,11,12,13,15,16,19,20,21,23,25,26,27,28,30

Table 5.22: Multiple PMU location solutions for Cases 1 and 2 results considering single line contingency- PART II

System Network	Case 1 with Single line contingency Optimal No. of PMUs	PMU locations	Case 2 with Single line contingency Optimal No. of PMUs	PMU locations
IEEE 57-bus	28 (1672.11s)	1,2,4,6,7,9,12,15,19,21,23,25,26, 28,31,33,34,36,39,42,43,44,46, 47,49,51,52,54,56 1,3,5,8,11,12,15,18,20,22,24,25, 27,29,31,33,34,36,39,41,44,46,48, 50,51,53,55,56	38 (106448.79s)	1,3,4,6,9,12,15,18,19,21,22,24,25,26,28,29,30,31, 32,33,34,36,37,38,41,43,44,45,46,47,49,50,51, 53,54,55,56,57 1,3,4,6,9,12,14,15,18,20,21,22,24,25,26,28,29,31,32, 33,35,36,39,40,41,42,43,44,45,47,48,49,50,51,53,54, 56,57 1,2,3,4,6,8,11,12,13,19,20,22,24,25,26,27,29,30,32,33, 34,35,37,38,39,40,42,44,45,46,47,50,51,52,54,55,56 1,3,4,6,9,11,12,14,15,17,18,19,20,22,23,24,27,28,29,30, 31,32,33,35,36,38,39,40,41,44,47,48,50,51,53,54,56,57
Practical 72-bus	44 (1059.59s)	1,2,3,4,5,6,7,8,9,10,11,12,13,14,15, 16,17,18,19,20,21,22,23,24,29,31, 34,36,37,38,39,42,48,51,54,55,56,58, 61,62,63,68,71,72 1,2,3,4,5,6,7,8,9,10,11,12,13,14,15,16,17, 18,19,20,21,22,27,28,29,31,33,35,37,40,42, 45,49,50,53,54,55,57,60,61,68,69,70,72	58 (s)	1,2,3,4,5,6,7,8,9,10,11,12,13,14,15,16,17,18,19,20, 21,22,23,24,26,30,31,32,33,34,36,38,40,41,43,44,45, 46,47,48,50,52,53,54,55,56,58,59,60,62,64,65,66,67, 68,69,71,72

Table 5.23: Multiple PMU location solutions for Cases 1 and 2 results considering single line contingency- PART II (Contd.)

System Network	Case 1 with Single line contingency	PMU locations
Practical 72-bus	44 (1059.59s)	1,2,3,4,5,6,7,8,9,10,11,12,13,14,15,16,17,18,19,20,21,22,25,27,28,29,30,32,33,35,37,38,39,40,42,45,46,51,57,61,67,69,70,72 1,2,3,4,5,6,7,8,9,10,11,12,13,14,15,16,17,18,19,20,21,22,24,26,27,28,29,31,32,36,37,38,39,40,43,48,51,54,56,58,66,69,70,72 1,2,3,4,5,6,7,8,9,10,11,12,13,14,15,16,17,18,19,20,21,22,27,28,29,31,32,35,37,39,42,45,49,53,54,57,58,61,64,67,69,70,71,72 1,2,3,4,5,6,7,8,9,10,11,12,13,14,15,16,17,18,19,20,21,22,23,24,28,29,31,36,38,39,41,42,51,54,55,56,58,60,61,62,64,69,71,72

Table 5.24: Multiple PMU location solutions for Case 1 and 2 results considering Single line contingency and ZIB- PART I

System Network	Case 1 with Single line contingency and ZIB: Optimal No. of PMUs	PMU locations	Case 2 with single line contingency & ZIB: Optimal No. of PMUs	PMU locations
IEEE 14-bus (ZIB bus 7)	7 (2.19s)	1,3,6,8,9,11,13 1,3,6,8,9,10,13	7 (791.84ss)	1,2,4,6,9,10,13 2,4,5,6,9,10,13 2,4,5,6,9,11,13 1,2,4,6,9,11,13
IEEE 30-bus (ZIB buses: 5,6,9,11,25,28)	16 (1059.77s)	2,3,7,8,10,11,12,13,15,17,19,21,24,26,27,29 2,3,7,8,10,11,13,14,16,18,20,22,23,26,27,29 2,3,7,8,10,11,12,13,15,16,19,22,23,26,27,29 2,3,7,8,10,11,12,13,15,17,19,22,23,26,27,30 2,3,7,8,10,11,13,14,15,16,19,22,23,26,27,30	16 (13727.41s)	1,2,4,5,7,10,12,13,15,16,18,19,22,24,27,30 1,2,4,5,10,12,13,15,17,18,19,21,23,24,27,29 2,3,4,5,10,12,13,15,16,18,20,22,23,25,27,29 1,2,4,7,10,12,13,15,17,19,20,21,24,25,29,30 2,3,4,7,10,12,13,15,17,19,20,22,24,27,29,30

Table 5.25: Multiple PMU location solutions for Case 1 and 2 results considering Single line contingency and ZIB- PART II

System Network	Case 1 with Single line contingency and ZIB: Optimal No. of PMUs	PMU locations	Case 2 with single line contingency and ZIB: Optimal No. of PMUs	PMU locations
IEEE 57-bus (ZIB buses: 4,7,11,21,22,24,26,34,36,37,39,40,45,46,48)	29 (285.84s)	1,3,4,6,7,10,12,14,19,21,22,24,25,27,29,31,33,34,36,38,39,41,43,45,47,50,53,55,56 1,3,5,8,11,12,15,18,20,21,23,25,26,27,29,31,33,34,36,39,41,44,46,48,50,51,53,55,56	31 (203010.78s)	1,2,3,6,7,10,12,15,19,20,25,28,29,30,32,33,34,39,41,43,45,46,47,49,50,51,52,54,55,56,57,3,7,9,11,12,13,15,16,17,18,19,24,26,27,29,30,31,32,33,34,38,39,41,42,45,46,47,50,51,53,54
Practical 72-bus (ZIB buses: 24,26,27,44,45,46,47,50,51,56,57,58,59,60,61,62,63,67,70)	44 (1059.59s)	1,2,3,4,5,6,7,8,9,10,11,12,13,14,15,16,17,18,19,20,21,22,27,28,29,31,33,35,37,40,42,45,49,50,53,54,55,57,60,61,68,69,70,72 1,2,3,4,5,6,7,8,9,10,11,12,13,14,15,16,17,18,19,20,21,22,24,25,27,28,29,36,37,39,42,48,49,51,53,54,55,56,58,61,66,69,71,72 1,2,3,4,5,6,7,8,9,10,11,12,13,14,15,16,17,18,19,20,21,22,25,27,28,29,30,32,33,35,37,38,39,40,42,45,46,51,57,61,67,69,70,72 1,2,3,4,5,6,7,8,9,10,11,12,13,14,15,16,17,18,19,20,21,22,24,26,27,28,29,31,32,36,37,38,39,40,43,48,51,54,56,58,66,69,70,72 1,2,3,4,5,6,7,8,9,10,11,12,13,14,15,16,17,18,19,20,21,22,27,28,29,31,32,35,37,39,42,45,49,53,54,57,58,61,64,67,69,70,71,72 1,2,3,4,5,6,7,8,9,10,11,12,13,14,15,16,17,18,19,20,21,22,23,24,28,29,31,36,38,39,41,42,51,54,55,56,58,60,61,62,64,69,71,72	46 (265462.33s)	1,2,3,4,6,7,8,9,10,11,13,14,15,17,20,21,22,30,31,32,33,34,36,37,38,39,40,41,42,43,44,45,46,48,49,52,54,55,58,59,65,66,68,69,71,72

5.6.3 Limitations of the proposed method

Although the proposed CSA method was successful in obtaining global solution and alternative placement solution sets for the same, the following points could be considered as its drawbacks:

- The computational time may be a hindrance if the method is intended to be used for an online application (Refer Table 5.4). Here, the application is for the planning stage in power system monitoring, therefore, the computational time is not of major concern.
- The tuning of the parameters would take a significant amount of time for trial and error method so as to make it suitable for providing global solution to a particular application with larger number of decision variables.

5.7 Summary

A sincere attempt to summarize the developments in the research area of optimal placement of PMUs (OPP) in power network during the past two decades has been made. There is discussion on the mathematical formulations of OPP with descriptions of objective functions and constraints. Topological, numerical, stochastic and probabilistic observabilities are discussed. Scenario of topological observability in presence of DC lines is included. Security related constraints such as PMU loss, line outages, controlled islanding, voltage stability, small-signal stability and fault tolerance consideration are described. Limitation of measurement channels of PMU devices is also discussed. The various methods: conventional mathematical, heuristic, meta-heuristic and hybrid methods discussed in literature are noted.

Implementation of recently developed nature-inspired algorithm, crow search algorithm, has been taken up and its comparison is made with respect to the results obtained with the dominant binary integer linear programming (BILP) method as well as particle swarm optimization (PSO) for an OPP problem. It is found that CSA is capable of producing global optimal solutions for the OPP problem with with location sets having an equivalent or better system observability redundancy index than that of the BILP and PSO methods. Further, two major scenarios are considered where topological observability and numerical observability of the system need to be achieved, along with many other additional constraints. As the sole system monitor, state estimator plays an important role in the security of power system operations. OPP with numerical observability ensures reliable state estimation. Contingency-constrained observability of system also comes under security constraint. Thereby, the OPP studies carried out ensured the security of the power system network. The many alternative solutions are obtained with the help of CSA

method which will help planning power engineers to set up a monitoring measurement system according to need of the system under consideration. The results of the analysis show that the maximum number of PMUs required to satisfy any of the constrained observability criteria discussed in the paper, is decided by the optimal number results of numerical observability with single line contingency.

Chapter 6

Conclusion and Future Scope

6.1 Summary

The application of ISCKF for forecasting-aided state estimation during normal load variations has been explored. It is performed utilizing the hybrid measurements from both field devices: RTUs and PMUs. The ISCKF method has the Newton-Gauss iterative method embedded into square-root CKF to improve its performance and stability. Consequently, ISCKF removes the risk of losing positive definiteness of the error covariance matrix in each update, which can cause the CKF to cease operating. The simulation results show that the proposed ISCKF outperforms the CKF by significant improvement in accuracy of forecasting-aided state estimation. This is evaluated with the help of mean of absolute errors, absolute phase error percentage and absolute voltage error percentage. The online real-time application feasibility is demonstrated with respect to the two different sized test systems IEEE 30-bus and NRPG 246-bus systems.

Dynamic system modelling and state estimation is necessary for optimal control of complicated systems. Beside the noise rejection capability, an estimator uses the state space model of a system to provide information about the states of the system which are in some cases immeasurable. In this study, the mathematical state space modelling is utilized for dynamic state estimation using non-linear Kalman Filters. Preliminary studies are carried out for speed estimation process of an induction motor using the existing Extended, Unscented and Cubature Kalman filter versions. The simulation results of this section shows the capability of the proposed approaches to estimate the speed optimally even with the added noisy measurements. Further, classical model of the synchronous generator are used to model single machine infinite bus system and then large multi-machine power systems (such as IEEE 3-Generator 9-Bus and 19-Generator 42-Bus test systems). Iterated square-root cubature Kalman filter (ISCKF) based state observer design is proposed for the dynamic state estimation of rotor angle and speed of synchronous machines in power systems. Theoretically, ISCKF approach eliminates the hazardous sit-

uation of the loss of positive definiteness of error covariance matrix in each update step which can stop the UKF and CKF from running continuously. Through the simulation studies carried out during a three-phase short circuit fault, the performance comparison of ISCKF is carried out with the existing methods such as EKF, UKF and CKF. It is clearly evident that the accuracy of state estimations is improved greatly when compared to that of EKF, UKF and CKF. At the measurement data rate of 250 samples per second, the estimation time per iteration is within the time 4 ms, i.e., before the next set of measurements arrives. Therefore, it can be implemented for online dynamic state estimation for synchronous machines in a power system. For smaller systems such as SMIB and IEEE 9-bus systems, higher sampling rate of 1000 samples per second for measurement data, further improves the accuracy of estimation.

A novel major event detection method has been proposed which uses probability densities and dynamic thresholding technique to identify major faults efficiently. On proper selection of hyper parameters, the detections occur within 40 ms, The method has been elaborately presented. As the sampling rate of PMUs increase this delay in detection will decrease proportionally. Fast and precise detection of events with data point location is achieved. The proposed framework incorporates differing thresholds for each substation depending on nominal operating characteristics of that particular Substation. It is also visualize which region in a large system has the largest, 2nd largest, 3rd largest, ... n^{th} largest fault using probabilistic model. The method constantly learns nominal system noise hence eliminating false positives even in a very high noise environment. Multiple layers of refinement for obtaining high level of abstraction in event detection. It is observed that robust detection is provided even on selection of absurd hyper-parameter values. Weighted detection feature gives a weighted probabilistic intensity of an event compared to other events occurring in the system hence giving a better insight of the system stability. For comparison studies with event detection methods used by National Renewable Research Laboratory (NREL) in a power system based on Synchrophasor data (frequency and RPAD signals) are carried out on the same dataset of the Northern region of India during cyclone Amphan. To make the conclusion as derived by NREL, intersection of events detected by two or more methods have been classified as event. And their corresponding timestamps are noted as well. This approach is used to detect large faults in power systems. The analysis successfully detects the major line trip fault in the first dataset and the oscillation fault in the second dataset as shown in the plots and tables. Since a window length of 10 seconds is used for all the implementation of the methods, the time at which a fault is detected might have an error margin of ± 10 seconds. Another limitation of the existing NREL method observed is that the methods are sensitive to data pre-processing of RPAD signal calculated from PMU data in some cases.

Optimization problem of minimizing the cost of placing phasor measurement units to

make a power system observable is studied by conducting a thorough survey of the state-of-the-art methods. To solve this problem, a recently developed nature-inspired algorithm, crow search algorithm has been implemented and its results are compared with respect to the results obtained with the dominant binary integer linear programming (BILP) method as well as particle swarm optimization (PSO). It is found that CSA is capable of producing global optimal solutions for the optimal placement of PMUs (OPP) problem with location sets having an equivalent or better system observability redundancy index than that of the BILP and PSO methods. Further, two major scenarios are considered where topological observability and numerical observability of the system need to be achieved, along with many other additional constraints. As the sole system monitor, state estimator plays an important role in the security of power system operations. Optimal placement of PMUs (OPP) with numerical observability ensures reliable state estimation. Contingency-constrained observability of system also comes under security constraint. Thereby the OPP studies carried out ensured the security of the power system network.

6.2 Conclusions

1. The proposed ISCKF outperforms the CKF by significant improvement in accuracy of forecasting-aided state estimation. during normal load variations has been explored. It is performed utilizing the hybrid measurements from both field devices: RTUs and PMUs.
2. Iterated square-root cubature Kalman filter (ISCKF) based state observer design is proposed for the dynamic state estimation of rotor angle and speed of synchronous machines in power systems. Through the simulation studies carried out during a three-phase short circuit fault, the performance of ISCKF is accuracy of state estimations is improved greatly when compared to the existing methods such as EKF, UKF and CKF.
3. Fast and precise detection of events with data point location is achieved within 40ms. It is a data-driven approach utilizing PMU signal data. The proposed framework incorporates differing thresholds for each substation depending on nominal operating characteristics of that particular Substation.
4. Many alternative solutions are obtained with the help of CSA method which will help planning power engineers to set up a monitoring measurement system according to need of the system under consideration. The results of the analysis show that the maximum number of PMUs required to satisfy any of the constrained observability criteria discussed in the paper, is decided by the optimal number results of numerical observability constraints with single line contingency.

6.3 Future Scope

1. Some of the future works which could be explored for getting improved FASE results using Kalman filter based approaches are Nonlinear–linear square-root cubature Kalman filtering (NL-CKF), Huber Second-order Smooth Variable Structure Predictive Filter (HSO-SVSPF) and QR-factorized cubature Kalman filter (QR-CKF). The suggestions are implementations for the improved state filtering step for better accuracy and computational time.
2. In the dynamic state estimation studies for power systems, it is suggested that test cases should be carried out against model uncertainty and cyber attacks (Qi et al., 2018) for modern power systems. For unbalanced systems and symmetrical fault conditions can be explored as further research with computers having good parallel processing capabilities.
3. For future work, the simulation studies could be carried out to study if the method could differentiate disturbances caused by cyber attacks, component failures and sensor data.
4. Optimization problem with aim for probabilistic and stochastic observabilities of the power system could be considered using the proposed crow search algorithm. OPP can be explored for the different objective functions as discussed in the literature survey.

Appendix A

Comparison Methods

A1. Binary Integer Linear Programming

The BILP algorithm is the dominant optimization algorithm for solving the OPP problem but it gives only one solution point [Theodorakatos et al. \(2020\)](#). The tool *intlinprog* uses a linear programming (LP)-based branch-and-bound algorithm to tackle BILP problems [Mathworks \(2020\)](#). The approach seeks for an optimum solution by solving a series of LP-relaxation problems, in which weaker constraint $0 \leq x \leq 1$ are evaluated instead of the binary integer requirement on the variables. The algorithm

- (i) Seeks for a binary integer feasible solution
- (ii) Updates the best binary integer feasible point found so far as the search tree grows
- (iii) Verifies that no better integer feasible solution is possible by solving a series of LP problems.

The branch-and-bound method:

Branching: The algorithm creates a search tree (See Fig. [6.1](#)) by repeatedly adding constraints to the problem, that is, "branching." At a branching stage, the algorithm selects a variable x_j whose current value is not an integer and adds the constraint $x_j = 0$ to form one branch and the constraint $x_j = 1$ to form the other branch. This process can be represented by a binary tree, in which the nodes represent the added constraints. The Fig. [6.1](#) illustrates a complete binary tree for a problem that has three variables x_1 , x_2 and x_3 . Note that, in general, the order of the variables going down the levels in the tree is not the usual order of their subscripts.

Deciding Whether to Branch: At each node, the algorithm solves an LP-relaxation problem using the constraints at that node and decides whether to branch or to move to another node depending on the outcome. There are three possibilities:

- a. If the LP-relaxation problem at the present node is not feasible or its optimal value is greater than that of the best integer point, the algorithm removes the node from the tree, after which it does not search any branches below that node. The algorithm then moves to a new node according to the method Best-node search strategy, which chooses

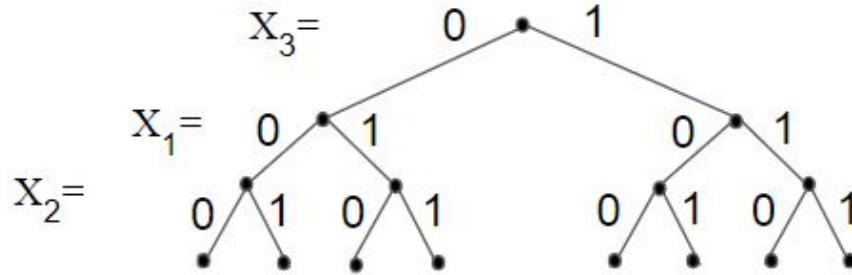


Figure 6.1: BILP logic using branch and bound algorithm

the node with lowest bound on the objective function:

b. If the algorithm finds a new feasible integer point with lower objective value than that of the best integer point, it updates the current best integer point and moves to the next node.

c. If the LP-relaxation problem is optimal but not integer and the optimal objective value of the LP relaxation problem is less than the best integer point, the algorithm branches according to the method 'maxinfeas' which chooses the variable with the maximum integer infeasibility (the variable whose value is closest to 0.5)

Bounds: The solution to the LP-relaxation problem provides a lower bound for the binary integer programming problem. If the solution to the LP-relaxation problem is already a binary integer vector, it provides an upper bound for the binary integer programming problem. As the search tree grows more nodes, the algorithm updates the lower and upper bounds on the objective function, using the bounds obtained in the bounding step. The bound on the objective value serves as the threshold to cut off unnecessary branches.

A2. Particle Swarm Optimization

Particle Swarm Optimization was proposed by [Kennedy and Eberhart \(1995\)](#) drawing inspiration from the behavior of flocking birds, collectively searching for necessary food sources. As mentioned in the original paper, scientists in this field have inferred that a flock of birds that travels in a group can benefit from the experience of all other birds. That is, instead of a single bird flying in search of food randomly, all birds in the flock can share their discovery and assist the whole group to arrive at the best source. In PSO, search agents called as particles are each made up of a set of 3-dimensional vectors: the particle's current position, its previous best position and its velocity. Also, each bird within the flock is assumed to have knowledge of the global best position achieved by its immediate neighborhood during the search process. The resultant velocity is then bounded between a maximum and minimum value using [\(6.3\)](#). With that understanding,

the position update for each particle i is given as follows:

$$x_i^{k+1} = x_i^k + v_i^{k+1} \quad (6.1)$$

where k is the present iteration; v_i^{k+1} denotes the velocity of particle i at iteration $k + 1$ determined by:

$$v_i^{k+1} = \omega \cdot v_i^k + A_1 \cdot (r_1^k \cdot (p_i^k - x_i^k)) + A_2 \cdot (r_2^k \cdot (g_i^k - x_i^k)) \quad (6.2)$$

$$-v_{max} < v_i^{k+1} < v_{max} \quad (6.3)$$

where ω is inertial weight varied from 0.4 to 0.9 through iterations, p_i^k denotes the previous best position of particle i (referred as personal best of i), while g_i^k stand for the present global best position within the whole swarm of particles [Poli et al. (2007)]. Furthermore, r_1^k and r_2^k each denote a d-dimensional vector made up of random numbers in range of $[0, 1]$, while the values A_1 and A_2 are known as cognitive and social parameters, respectively. While we can simulate the movement of a flock, it can understood that each bird would assist in arriving at the optimal solution in a high-dimensional solution space and the best solution found by the flock is the best solution in the space.

For binary discrete search space, the authors have adapted the PSO to search in binary spaces [Kennedy and Eberhart (1995)], by applying a sigmoid transformation to the velocity component (6.4) to limit the velocities into a range $[0, 1]$, and force the component values of the locations of particles to be 0's or 1's. The equation for updating positions (6.1) is then replaced by (6.5).

$$sigmoid(v_i^{k+1}) = \frac{1}{1 + \exp(-v_i^{k+1})} \quad (6.4)$$

$$x_i^{k+1} = \begin{cases} 1 & ; \text{if rand} < \text{sigmoid} (v_i^{k+1}); \\ 0 & ; \text{Otherwise .} \end{cases} \quad (6.5)$$

This is a heuristic solution and we often find that the solution found by PSO is quite close to the global optimal.

A3. Extended Kalman Filter

Extended Kalman filter is a non-linear extension of Kalman filter [Simon, 2006; Welch and Bishop, 2006; Shih and Huang, 2002]. It is also possible to use linearization method explained in Section 1.5.2 for a non-linear system and apply linear Kalman filter for state estimation. Nevertheless, the main goal of this section is to develop a non-linear estimation method based on Kalman filter. In the following section, the equations of

discrete-time Extended Kalman filter are derived. Considering a discretized dynamic system, the system model can be written as (Simon, 2006)

$$\begin{aligned}
 x_k &= f_{k-1}(x_{k-1}, u_{k-1}, w_{k-1}) \\
 y_k &= h_k(x_k, v_k) \\
 w_k &\sim (0, Q_k) \\
 v_k &\sim (0, R_k)
 \end{aligned} \tag{6.6}$$

In this equation, x_k represents the state vector, u_k is the control input vector, f is the non-linear function of the states and inputs, y_k is the output vector, w_k and v_k are the process and measurement noise, Q_k and R_k are the process and measurement noise covariance, and k is the time step for the discrete model. By performing a Taylor series expansion of the state equation around $x_{k-1} = \hat{x}_{k-1}^+$ and $w_{k-1} = 0$, Equation 6.6 can be written as (Simon, 2006)

$$\begin{aligned}
 x_k &= f_{k-1}(\hat{x}_{k-1}^+, u_{k-1}, 0) + \left. \frac{\partial f_{k-1}}{\partial x} \right|_{\hat{x}_{k-1}^+} (x_{k-1} - \hat{x}_{k-1}^+) + \left. \frac{\partial f_{k-1}}{\partial w} \right|_{\hat{x}_{k-1}^+} w_{k-1} \\
 &= f_{k-1}(\hat{x}_{k-1}^+, u_{k-1}, 0) + F_{k-1}(x_{k-1} - \hat{x}_{k-1}^+) + L_{k-1}w_{k-1} \\
 &= F_{k-1}x_{k-1} + [f_{k-1}(\hat{x}_{k-1}^+, u_{k-1}, 0) - F_{k-1}\hat{x}_{k-1}^+] + L_{k-1}w_{k-1} \\
 &= F_{k-1}x_{k-1} + \tilde{u}_{k-1} + \tilde{w}_{k-1}
 \end{aligned} \tag{6.7}$$

The definitions of F_{k-1} and L_{k-1} are presented in Equation (1.50). The known input signal \tilde{u}_k and the noise signal \tilde{w}_k are also expressed by the following equation.

$$\begin{aligned}
 \tilde{u}_k &= f_k(\hat{x}_k^+, u_k, 0) - F_k\hat{x}_k^+ \\
 \tilde{w}_k &= (0, L_k Q_k L_k^T)
 \end{aligned} \tag{6.8}$$

The measurement equation linearized around $x_k = \hat{x}_k^-$ and $v_k = 0$ is presented below.

$$\begin{aligned}
 y_k &= h_k(\hat{x}_k^-, 0) + \left. \frac{\partial h_k}{\partial x} \right|_{\hat{x}_k^-} (x_k - \hat{x}_k^-) + \left. \frac{\partial h_k}{\partial v} \right|_{\hat{x}_k^-} v_k \\
 &= h_k(\hat{x}_k^-, 0) + H_k(x_k - \hat{x}_k^-) + M_k v_k \\
 &= H_k x_k + [h_k(\hat{x}_k^-, 0) - H_k \hat{x}_k^-] + M_k v_k \\
 &= H_k x_k + z_{k-1} + \tilde{v}_k
 \end{aligned} \tag{6.9}$$

H_k and M_k are defined by Equation (1.52) and the known signal z_k and the noise signal \tilde{v}_k are defined as follows.

$$\begin{aligned}
 z_k &= h_k(\hat{x}_k^-, 0) - H_k \hat{x}_k^- \\
 \tilde{v}_k &\sim (0, M_k R_k M_k^T)
 \end{aligned} \tag{6.10}$$

Using the time and measurement update Equations (1.50) and (1.52) for linear Kalman filter and equations derived for EKF up to this point, the discrete-time EKF for a non-linear system presented in Equation (1.49) can be summarized as follows (Simon, 2006;

Welch and Bishop, 2006):

1. The filter is initialized as follows:

$$\begin{aligned}\hat{x}_0^+ &= E(x_0) \\ P_0^+ &= E \left[(x_0 - \hat{x}_0^+) (x_0 - \hat{x}_0^+)^T \right]\end{aligned}\quad (6.11)$$

2. Partial derivative matrices of the system equation are derived using the following equation.

$$\begin{aligned}F_{k-1} &= \left. \frac{\partial f_{k-1}}{\partial x} \right|_{\hat{x}_{k-1}^+} \\ L_{k-1} &= \left. \frac{\partial f_{k-1}}{\partial w} \right|_{\hat{x}_{k-1}^+}\end{aligned}\quad (6.12)$$

3. Time update equations of EKF are as follows:

$$\begin{aligned}P_k^- &= F_{k-1} P_{k-1}^+ F_{k-1}^T + L_{k-1} Q_{k-1} L_{k-1}^T \\ \hat{x}_k^- &= f_{k-1}(\hat{x}_{k-1}^+, u_{k-1}, 0)\end{aligned}\quad (6.13)$$

4. Partial derivative matrices of the output equation are obtained by,

$$\begin{aligned}H_k &= \left. \frac{\partial h_k}{\partial x} \right|_{\hat{x}_k^-} \\ M_k &= \left. \frac{\partial h_k}{\partial v} \right|_{\hat{x}_k^-}\end{aligned}\quad (6.14)$$

5. The final step is the measurement update for which the related equations are as follows:

$$\begin{aligned}K_k &= P_k^- H_k^T (H_k P_k^- H_k^T + M_k R_k M_k^T)^{-1} \\ \hat{x}_k^+ &= \hat{x}_k^- + K_k [y_k - h_k(\hat{x}_k^-, 0)] \\ P_k^+ &= (I - K_k H_k) P_k^-\end{aligned}\quad (6.15)$$

In the above expressions, \hat{x}_k^- is a priori state estimate at step k based on the knowledge of the process prior to this step, \hat{x}_k^+ is a posteriori state estimate at step k based on the measurement y_k and P_k^- is the a priori and a posteriori estimate error covariance, F_{k-1} is the Jacobian matrix of f with respect to x , and K_k is the Kalman gain that minimizes the error covariance.

Features of EKF

One of the interesting and unique features of EKF is its ability for online parameter estimation. In other words, the state vector of the system can be augmented to the parameters of the system and they become updated in each iteration. This capability has a great value for systems with slow changing parameters during operational conditions. An example for this physical phenomenon is an electrical machine in different operating conditions. The main parameters of the machine like rotor and stator resistances are

influenced by the frequency and the temperature of the machine.

However, as EKF linearizes the system equations around each state estimation and deploys only the first order term of Taylor series, in systems with high degree of non-linearity, it might not capture the whole non-linearity of the system, and the mean and covariance of the estimated states are occasionally different from the real states. This problem may lead us to use UKF which approximates mean and covariance of states up to third order.

A4. Unscented Kalman Filter

The basis of the unscented transformation is that "it is easier to approximate a probability distribution than it is to approximate an arbitrary non-linear function or transformation" (Julier et al., 2000). It is worth to investigate how mean and covariance propagate in non-linear equations to understand better the idea of unscented transformation. Consider the following non-linear functions (Simon, 2006)

$$\begin{aligned}y_1 &= r \cos \theta \\y_2 &= r \sin \theta\end{aligned}\tag{6.16}$$

Which is a standard polar to rectangular transformation. This coordinate transformation can be generally written as follows:

$$y = h(x)\tag{6.17}$$

In this equation, y is the two-element function of $h(x)$ and the two-element vector x is defined as

$$x = \begin{bmatrix} r \\ \theta \end{bmatrix}\tag{6.18}$$

Suppose that x_1 and x_2 are random variables defined as

$$\begin{aligned}x_1 &\sim (1, \sigma_r) \\x_2 &\sim (\pi/2, \sigma_\theta)\end{aligned}\tag{6.19}$$

Performing a first order linearization of Equation (1.60) and taking the expected value of both sides results in

$$\begin{aligned}\bar{y} &= E[h(x)] \\&\approx E \left[h(\bar{x}) + \frac{\partial h}{\partial x} \Big|_{\bar{x}} (x - \bar{x}) \right] \\&= h(\bar{x}) + \frac{\partial h}{\partial x} \Big|_{\bar{x}} E(x - \bar{x}) \\&= h(\bar{x}) \\&= \begin{bmatrix} 0 \\ 1 \end{bmatrix}\end{aligned}\tag{6.20}$$

For more accurate evaluation of the mean through a non-linear system, r and θ can be expressed as

$$\begin{aligned} r &= \bar{r} + \tilde{r} \\ \theta &= \bar{\theta} + \tilde{\theta} \end{aligned} \quad (6.21)$$

Which \tilde{r} and $\tilde{\theta}$ are the deviations of r and θ from their means. A thorough analysis of the mean of y_1 can be written as follows (Simon, 2006):

$$\begin{aligned} \bar{y}_1 &= E(r \cos \theta) \\ &= E[(\bar{r} + \tilde{r}) \cos(\bar{\theta} + \tilde{\theta})] \\ &= E[(\bar{r} + \tilde{r})(\cos \bar{\theta} \cos \tilde{\theta} - \sin \bar{\theta} \sin \tilde{\theta})] \end{aligned} \quad (6.22)$$

By performing the multiplication, keeping in mind that \tilde{r} and $\tilde{\theta}$ are independent with symmetric probability density functions (pdf), the expected value of y_1 is equal to

$$\bar{y}_1 = \bar{r} \cos \bar{\theta} = 0 \quad (6.23)$$

The first order approximation of \bar{y}_1 is confirmed by Equation (1.63). For \bar{y}_2 it can be written as (Simon, 2006)

$$\begin{aligned} \bar{y}_2 &= E(r \sin \theta) \\ &= E[(\bar{r} + \tilde{r}) \sin(\bar{\theta} + \tilde{\theta})] \\ &= E[(\bar{r} + \tilde{r})(\sin \bar{\theta} \cos \tilde{\theta} + \cos \bar{\theta} \sin \tilde{\theta})] \end{aligned} \quad (6.24)$$

As $E[\tilde{r}]$, (6.24) is simplified as follows:

$$\begin{aligned} \bar{y}_2 &= \bar{r} \sin \bar{\theta} E(\cos \tilde{\theta}) \\ &= E(\cos \tilde{\theta}) \end{aligned} \quad (6.25)$$

Without assuming the distribution for $\tilde{\theta}$, it is not possible to simplify this expression further. If $\tilde{\theta}$ is uniformly distributed between $\pm\theta_m$, the mean of y_2 is

$$\bar{y}_2 = E(\cos \tilde{\theta}) \quad (6.26)$$

$$= \frac{\sin \theta_m}{\theta_m} \quad (6.27)$$

The mean calculated from (6.26) is less than 1, which is different from the mean calculated in (6.24). This difference can be seen in the following figure which is a plot of 300 randomly generated r and θ values, in which \tilde{r} is uniformly distributed between ± 0.01 , and $\tilde{\theta}$ is uniformly distributed between ± 0.35 radians (Simon, 2006).

Now it is more obvious why the mean calculation in (6.26) is not accurate; it is a first

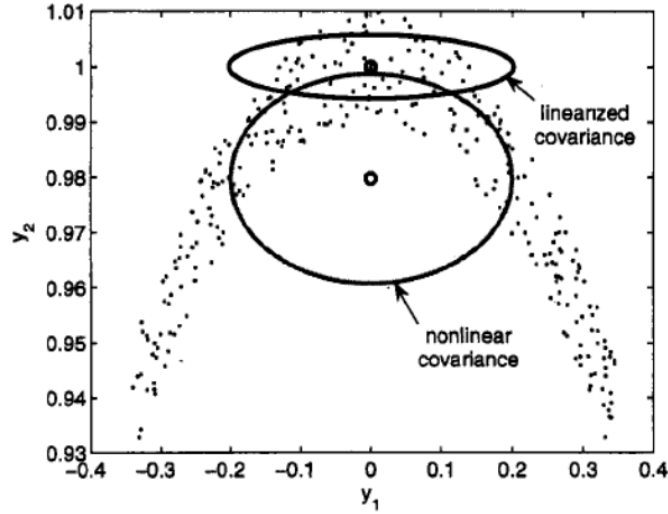


Figure 6.2: linearized and non-linear mean and covariance of 300 randomly generated points [9]

order approximation and as the considered system in (6.6) is highly non-linear, a major discrepancy exists between linearized and non-linear mean. The same analysis can be done for variance of the nonlinear system to show the difference between linearized and non-linear covariance. A comparison of the non-linear and linearized mean and covariance of 300 randomly generated points propagated through the non-linear system is presented in Fig.1.8. It has been shown in (Simon, 2006) that the unscented transformation has the ability to propagate mean and covariance of states of a system through non-linear dynamic model while capturing their non-linearity up to the third order. The unscented transformation procedure is as follows:

1. An n -element vector x with known mean \bar{x} and covariance P is considered. The aim is to estimate the mean and covariance of $y = h(x)$ denoted as \bar{y}_u and P_u .
2. $2n$ sigma point vectors $x^{(i)}$ is formed as follows:

$$\begin{aligned}
 x^{(i)} &= \bar{x} + \tilde{x}^{(i)} & i &= 1, \dots, 2n \\
 \tilde{x}^{(i)} &= (\sqrt{nP})_i^T & i &= 1, \dots, n \\
 \tilde{x}^{(n+i)} &= -(\sqrt{nP})_i^T & i &= 1, \dots, n
 \end{aligned} \tag{6.28}$$

Where \sqrt{nP} is the matrix square root of nP such that $(\sqrt{nP})^T \sqrt{nP} = nP$ and $(\sqrt{nP}_{k-1})^T$ is the i^{th} row of the matrix.

3. The sigma points are transformed as follows:

$$y^{(i)} = h(x^{(i)}) \quad i = 1, \dots, 2n \tag{6.29}$$

4. The mean and covariance of y are approximated as follows:

$$\begin{aligned} \bar{y}_u &= \frac{1}{2n} \sum_{i=1}^{2n} y^{(i)} \\ P_u &= \frac{1}{2n} \sum_{i=1}^{2n} (y^{(i)} - \bar{y}_u) (y^{(i)} - \bar{y}_u)^T \end{aligned} \quad (6.30)$$

The results of the mean and covariance propagation of the 300 randomly generated points through the non-linear system presented in Equation (1.49) using unscented, linearized and non-linear transformation are presented in Figure 1.9. This figure shows clearly the difference between EKF and UKF in terms of mean and covariance propagation through a non-linear system. The center point is the non-linear and unscented mean which are the same, while the upper point is the linearized mean which has a considerable discrepancy from the true one. The unscented and exact non-linear covariances have almost the same shape; in contrast, the linearized covariance has a totally different shape. Using

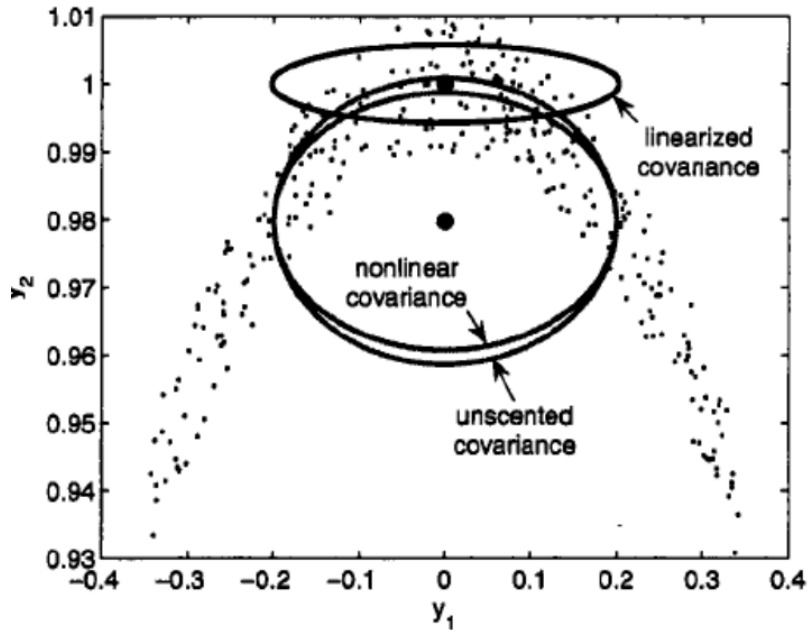


Figure 6.3: The comparison among exact, linearized, and unscented mean and covariance of 300 randomly generated points (Simon, 2006)

the unscented transform hitherto introduced, the Unscented Kalman filter steps can be expressed as follows:

1. The filter is initialized as follows (Simon, 2006):

$$\begin{aligned} \hat{x}_0^+ &= E(x_0) \\ P_0^+ &= E \left[(x_0 - \hat{x}_0^+) (x_0 - \hat{x}_0^+)^T \right] \end{aligned} \quad (6.31)$$

The mean and the covariance of the estimated states at each measurement to the next

one is propagated through the following time update steps.

2. As the current best guess for the mean and covariance of x_k are x_{k-1}^+ and P_{k-1}^+ , sigma points $x_{k-1}^{(i)}$ are derived using the following equations and these sigma points are propagated through the non-linear system from time step $(k-1)$ to (k) .

$$\begin{aligned} x^{(i)} &= \bar{x} + \tilde{x}^{(i)} & i &= 1, \dots, 2n \\ \tilde{x}^{(i)} &= (\sqrt{nP})_i^T & i &= 1, \dots, n \\ \tilde{x}^{(n+i)} &= -(\sqrt{nP})_i^T & i &= 1, \dots, n \end{aligned} \quad (6.32)$$

In this equation, \sqrt{nP} is the matrix square root of nP such that $(\sqrt{nP})^T \sqrt{nP} = nP$ and $(\sqrt{nP_{k-1}})^T$ is the i^{th} row of the matrix.

3. In this step using the known non-linear system equation f , $2n$ sigma points created in the previous step are propagated through the system and $\hat{x}_0^{(i)}$ which also is a $2n$ vector is obtained as follows:

$$\hat{x}_k^{(i)} = f(\hat{x}_{k-1}^{(i)}, u_k, t_k) \quad (6.33)$$

4. The a priori state estimate is obtained by combining all the vectors of $\hat{x}_k^{(i)}$ is given by ,

$$\hat{x}_k^- = \frac{1}{2n} \sum_{i=1}^{2n} \hat{x}_k^{(i)} \quad (6.34)$$

5. The a priori estimate for error covariance matrix is derived by,

$$P_k^- = \frac{1}{2n} \sum_{i=1}^{2n} \left(\hat{x}_k^{(i)} - \hat{x}_k^- \right) \left(\hat{x}_k^{(i)} - \hat{x}_k^- \right)^T + Q_{k-1} \quad (6.35)$$

6. The measurement update steps are presented here. The new sigma points are selected based on updated \hat{x}_k^- and P_k^- .

$$\begin{aligned} \hat{x}_k^{(i)} &= \hat{x}_k^- + \tilde{x}^{(i)} & i &= 1, \dots, 2n \\ \tilde{x}^{(i)} &= (\sqrt{nP})_i^T & i &= 1, \dots, n \\ \tilde{x}^{(n+i)} &= -(\sqrt{nP})_i^T & i &= 1, \dots, n \end{aligned} \quad (6.36)$$

7. In this step, the sigma points $\hat{x}_k^{(i)}$ are transformed into $\hat{y}_k^{(i)}$ using the known nonlinear output equation $h(\cdot)$ as follows:

$$\hat{y}_k^{(i)} = h(\hat{x}_k^{(i)}, t_k) \quad (6.37)$$

8. The prediction for measurement at time step k is obtained by,

$$\hat{x}_k = \frac{1}{2n} \sum_{i=1}^{2n} \hat{y}_k^{(i)} \quad (6.38)$$

9. In this step, the covariance of the predicted measurement is calculated.

$$P_y = \frac{1}{2n} \sum_{i=1}^{2n} \left(\hat{y}_k^{(i)} - \hat{y}_k \right) \left(\hat{y}_k^{(i)} - \hat{y}_k \right)^T + R_k \quad (6.39)$$

10. The cross covariance between \hat{x}_k^- and \hat{y}_k is calculated by,

$$P_{xy} = \frac{1}{2n} \sum_{i=1}^{2n} \left(\hat{x}_k^{(i)} - \hat{x}_k^- \right) \left(\hat{y}_k^{(i)} - \hat{y}_k \right)^T \quad (6.40)$$

11. The measurement update of the states estimates of the system calculated in the previous steps is performed using Equation (1.69).

$$\begin{aligned} K_k &= P_{xy} P_y^{-1} \\ \hat{x}_k^+ &= \hat{x}_k^- + K_k (y_k - \hat{y}_k) \\ P_k^+ &= P_k^- - K_k P_y K_k^T \end{aligned} \quad (6.41)$$

Features of UKF

The unscented transformation (UT) ([Haykin, 2004](#)) is developed to address the deficiencies of linearization by providing a more direct and explicit mechanism for transforming mean and covariance information. Based on UT, the UKF is a derivative-free alternative to EKF.

The basic idea of UKF is to choose the sigma-point set to capture a number of low-order moments of the prior density of the states as correctly as possible, and then compute the posterior statistics of the non-linear functions (either state transition functions f or measurement functions h) by UT which approximates the mean and the covariance of the non-linear function by a weighted sum of projected sigma points. In UKF there is no linearization or calculation of Jacobian matrices is needed.

However, for the sigma-points, the mean at the center is highly significant as it carries more weight which is usually negative for high-dimensional systems. Therefore, the UKF is supposed to encounter numerical instability troubles when used in high-dimensional problems.

A5. Cubature Kalman Filter

Making use of the spherical-radial Cubature rule ([Arasaratnam and Haykin, 2009](#)) propose CKF, which possesses an important virtue of mathematical rigour rooted in the third-degree spherical-radial Cubature rule for numerically computing Gaussian-weighted integrals.

The core problem in any nonlinear Kalman filter is to calculate the integral

$\int_{\mathbf{R}^n} \mathbf{f}(\mathbf{x})N(\mathbf{x}; \bar{\mathbf{x}}, \mathbf{P}_x) d\mathbf{x}$ which, in general, it is difficult to find the analytical solution, where $f(x)$ denotes the arbitrary function, $N(\mathbf{x}; \bar{\mathbf{x}}, \mathbf{P}_x)$ denotes the Gaussian pdf. Specifically, an integral of the form $I(\mathbf{f}) = \int_{\mathbf{R}^n} \mathbf{f}(\mathbf{x})e^{-\mathbf{x}^T\mathbf{x}}d\mathbf{x}$ in the Cartesian coordinate system is considered. Let $x = ry$ with $y^T y = I$, where y denotes the direction vector and $r \geq 0$ denotes the radius, so that $x^T x = r^2$ and then the integral $I(f)$ can be rewritten in a spherical-radial coordinate system as follows:

$$I(\mathbf{f}) = \int_0^\infty \int_{U_n} \mathbf{f}(r\mathbf{y})r^{n-1}e^{-r^2}d\sigma(\mathbf{y})dr \quad (6.42)$$

where U_n is the surface of the sphere defined by $U_n = y \in \mathbf{R}^n : y^T y = 1$ and $\sigma(\cdot)$ is the area element on U_n . Thus, the integral is decomposed into spherical integral $S(r)$ and radial integral R , respectively, and approximately represented using numerical integration as follows:

$$\begin{aligned} S(r) &= \int_{U_n} \mathbf{f}(r\mathbf{y})d\sigma(\mathbf{y}) \approx \sum_{i=1}^{L_s} \omega_{s,i} \mathbf{f}(r\mathbf{y}_i) \\ R &= \int_0^\infty S(r)r^{n-1}e^{-r^2}dr \approx \sum_{j=1}^{L_r} \omega_{r,j} S(r_j) \end{aligned} \quad (6.43)$$

where $(y_i, w_{s,i})$ denote the integral points and weights of the spherical integral and L_s denotes the number of integral points. Similarly, $(r_j, w_{r,j})$ denote the integral points and weights of the radial integral, and L_r denotes the number of points. From the third-degree spherical-radial cubature rule used in [12], we obtain that

$$\begin{aligned} S(r) &= \frac{A_n}{2^n} \sum_{i=1}^n [\mathbf{f}(r\xi_i) + \mathbf{f}(-r\xi_i)] \\ R &= \frac{1}{2} \Gamma\left(\frac{n}{2}\right) S\left(\sqrt{\frac{n}{2}}\right) \end{aligned} \quad (6.44)$$

where $A_n = 2\sqrt{\pi^n}/\Gamma(n/2)$ is the surface area of the unit sphere, $\Gamma(z) = \int_0^\infty e^{-t}t^{z-1}dt$ is the Gamma function, and ξ_i denotes the unit vector with the i^{th} element being 1. $S(r)$ is substituted into R , to get

$$I(\mathbf{f}) = \sum_{j=1}^{L_r} \sum_{i=1}^{L_s} \omega_{r,j} \omega_{s,i} \mathbf{f}(r_j \mathbf{y}_i) \quad (6.45)$$

$$= \sum_{j=1}^L \frac{1}{2} \Gamma\left(\frac{n}{2}\right) \sum_{i=1}^n \frac{A_n}{2^n} [\mathbf{f}(r_j \xi_i) + \mathbf{f}(-r_j \xi_i)] \quad (6.46)$$

$$= \frac{\sqrt{\pi^n}}{2^n} \sum_{i=1}^n \left[\mathbf{f}\left(\sqrt{\frac{n}{2}}\xi_i\right) + \mathbf{f}\left(-\sqrt{\frac{n}{2}}\xi_i\right) \right] \quad (6.47)$$

Due to identity equation

$$\begin{aligned} & \int_{\mathbf{R}^n} \mathbf{f}(\mathbf{x}) N(\mathbf{x}; \bar{\mathbf{x}}, \mathbf{P}_x) d\mathbf{x} \\ &= \frac{1}{\sqrt{\pi^n}} \int_{\mathbf{R}^n} \mathbf{f}(\sqrt{2\mathbf{P}_x} \mathbf{x} + \bar{\mathbf{x}}) e^{-\mathbf{x}^T \mathbf{x}} d\mathbf{x} \end{aligned} \quad (6.48)$$

it may be seen that

$$\begin{aligned} & \int_{\mathbf{R}^n} \mathbf{f}(\mathbf{x}) N(\mathbf{x}; \bar{\mathbf{x}}, \mathbf{P}_x) d\mathbf{x} \\ &= \frac{1}{2n} \sum_{i=1}^n [\mathbf{f}(\sqrt{n\mathbf{P}_x} \xi_i + \bar{\mathbf{x}}) + \mathbf{f}(-\sqrt{n\mathbf{P}_x} \xi_i + \bar{\mathbf{x}})]. \end{aligned} \quad (6.49)$$

The calculation process used in the CKF is listed as follows.

Time Update. Evaluate the cubature points $\hat{\mathbf{x}}_{k-1}^{(i)}$.

$$\begin{aligned} \hat{\mathbf{x}}_{k-1}^{(i)} &= \hat{\mathbf{x}}_{k-1}^+ + \sqrt{n\mathbf{P}_{k-1}^+} \xi_i \\ \hat{\mathbf{x}}_{k-1}^{(n+i)} &= \hat{\mathbf{x}}_{k-1}^+ - \sqrt{n\mathbf{P}_{k-1}^+} \xi_i \\ & i = 1, 2, \dots, n. \end{aligned} \quad (6.50)$$

Evaluate the propagated cubature points $\mathbf{X}_k^{(i)}$

$$\mathbf{X}_k^{(i)} = \mathbf{f}(\hat{\mathbf{x}}_{k-1}^{(i)}) \quad (6.51)$$

Estimate the predicted state $\hat{\mathbf{x}}_k^-$.

$$\hat{\mathbf{x}}_k^- = \frac{1}{2n} \sum_{i=1}^{2n} \mathbf{X}_k^{(i)} \quad (6.52)$$

Estimate the predicted error covariance \mathbf{P}_k^- .

$$\mathbf{P}_k^- = \frac{1}{2n} \sum_{i=1}^{2n} (\mathbf{X}_k^{(i)} - \hat{\mathbf{x}}_k^-) (\mathbf{X}_k^{(i)} - \hat{\mathbf{x}}_k^-)^T + \mathbf{Q}_{k-1} \quad (6.53)$$

Measurement Update. Evaluate the cubature points $\hat{\mathbf{x}}_k^{(i)}$

$$\hat{x}_k^{(i)} = \hat{x}_k^- + \sqrt{nP_{k-1}^+} \xi_i \quad (6.54)$$

$$\hat{x}_k^{(n+i)} = \hat{x}_k^- - \sqrt{nP_{k-1}^+} \xi_i \quad (6.55)$$

$$i = 1, 2, \dots, n. \quad (6.56)$$

Evaluate the propagated cubature points $\mathbf{Z}^{(i)}$

$$\mathbf{Z}^{(i)} = h(\hat{\mathbf{x}}_k^{(i)}) \quad (6.57)$$

Estimate the predicted measurement $\hat{\mathbf{z}}_k^-$.

$$\hat{\mathbf{z}}_k^- = \frac{1}{2n} \sum_{i=1}^{2n} \mathbf{z}_k^{(i)} \quad (6.58)$$

Estimate the measurement covariance matrix \mathbf{P}_z

$$\mathbf{P}_z = \frac{1}{2n} \sum_{i=1}^{2n} \left(\mathbf{z}_k^{(i)} - \hat{\mathbf{z}}_k^- \right) \left(\mathbf{z}_k^{(i)} - \hat{\mathbf{z}}_k^- \right)^T + \mathbf{R}_k \quad (6.59)$$

Estimate the cross-covariance matrix \mathbf{P}_{xz} .

$$\mathbf{P}_{xz} = \frac{1}{2n} \sum_{i=1}^{2n} \left(\hat{\mathbf{x}}_k^{(i)} - \hat{\mathbf{x}}_k^- \right) \left(\mathbf{z}_k^{(i)} - \hat{\mathbf{z}}_k^- \right)^T \quad (6.60)$$

Estimate the Kalman gain \mathbf{K}_k .

$$\mathbf{K}_k = \mathbf{P}_{xz} \mathbf{P}_z^{-1} \quad (6.61)$$

Estimate the updated state $\hat{\mathbf{x}}_k^+$.

$$\hat{\mathbf{x}}_k^+ = \hat{\mathbf{x}}_k^- + \mathbf{K}_k (\mathbf{z}_k - \hat{\mathbf{z}}_k^-) \quad (6.62)$$

Estimate the corresponding error covariance \mathbf{P}_k^+ .

$$\mathbf{P}_k^+ = \mathbf{P}_k^- - \mathbf{K}_k \mathbf{P}_z \mathbf{K}_k^T \quad (6.63)$$

From the algorithm we see that $2n$ points are adopted when approximating the Gaussian pdf.

Features of CKF

Making use of the spherical-radial cubature rule, Arasaratnam (Arasaratnam and Haykin, 2009) proposed CKF, which possesses an important virtue of mathematical rigour rooted in the third degree spherical-radial cubature rule for numerically computing Gaussian-weighted integrals. Similar to UKF, CKF is also derivative-free and is easier for application. CKF also uses a weighted set of symmetric points to approximate the Gaussian distribution. But the cubature-point set does not have a stem at the center and thus does not have the numerical instability problem of UKF discussed in Section 6.3.

UKF treats the derivation of the sigma-point set for the prior density and the computation for posterior statistics as two disjoint problems. By contrast, CKF directly derives the cubature-point set to accurately compute the first two-order moments of a non-linear transformation, therefore naturally increasing the accuracy of the numerical estimates for

moment integrals.

A6. Fast Fourier Transform

A Fast Fourier Transform (FFT) considered in the analysis computes the Discrete Fourier transform (DFT) of a time series signal. The DFT is done by transforming the signal from time domain to frequency domain. This is carried out by dividing the time sequence values into various frequency components present in the signal (Negi et al., 2017). This operation is beneficial in many research areas, but deriving it as per the definition is mostly too time-consuming to be practical. However, an FFT quickly computes such transformations by decomposing the DFT matrix into a product of sparse components. The FFT operation consists of dividing an N-points signal into N signals each composed of a single point (all signals are in time domain). Further, an N frequency spectra corresponding to these N signals are derived. Finally, the N spectra are combined to form a single frequency spectrum. The first step of time domain decomposition of a 16-point signal is illustrated in Fig. 6.4. There are Log_2N stages required in this decomposition, for example, a 16-point signal (2^4) requires 4 stages.

$$X(f) = \sum_{i=0}^{i=N-1} x[i]e^{-j2\pi fi/N} \tag{6.64}$$

where, N is no. of samples, x is signal in time domain and X is FFT of x , i.e signal in frequency domain.

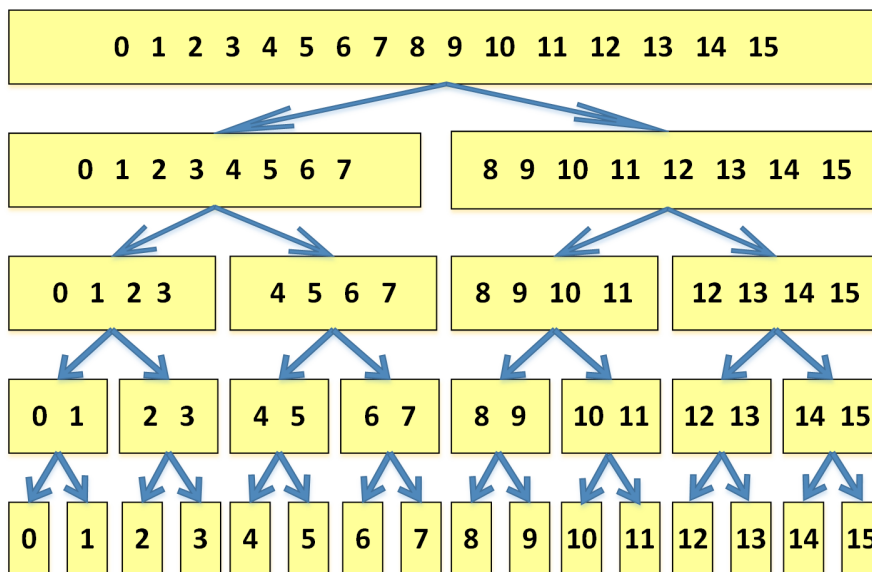


Figure 6.4: Finding N point DFT

Initially, the data is differentiated to remove the DC component and in order to detect

the events in the low frequency range. Differentiating the data does not alter the frequency content and information contained by the signal. In general during the event, frequency is high, hence differentiating the data does not cause problems.

$$Y(f) = \max(X(f)) \quad (6.65)$$

$$f_{event} = \max|Y(f)| \quad (6.66)$$

where, $\mathbf{Y}(\mathbf{f})$ is maximum value from each window and f_{event} is frequency at which event has occurred.

FFT is applied on the data window to gather the strongest frequency component. The maximum amplitude $|Y(f)|$ is stored.

From the plot of all stored values of $|\mathbf{Y}(\mathbf{f})|$, the ones which cross the boundary of 3 standard deviations above mean are flagged as event.

A7. Yule Walker Method

The Yule Walker method depicts the power spectral density (PSD) of a signal which means power of signal at various frequencies. It does so by calculating FFT of autocorrelation function of $x[m]$.

$$R(k) = \sum_{m=-\infty}^{m=\infty} x[m] * x[m - k] \quad (6.67)$$

$$S(f) = \sum_{k=1}^{k=N} R[k]e^{-j2\pi fk} \quad (6.68)$$

MATLAB's built-in function **pyulear** is used to calculate the PSD of a signal. The peak value of PSD in each window length is captured followed by calculations for the mean and standard deviation of peak values. Whichever peak values cross the boundary of 3 standard deviations error band, that particular peak would be considered as an event.

A8. Min-Max Method

In Min-Max method, Minimum and maximum values of magnitude of signal for each window is calculated and saved. Then mean and standard deviation for each window length is calculated and stored. The data point which is above 3 standard deviations from the mean value of the window it belongs, will be classified as events.

$$x_{max} = \max(x[n]) \quad (6.69)$$

$$x_{min} = \min(x[n]) \quad (6.70)$$

$$E_{Min-Max} = x_{max} - x_{min} \quad (6.71)$$

A9. Matrix pencil Method

In the Matrix Pencil Method (Liu et al., 2007), a sum of damped sinusoidal signals to uniformly sampled PMU data is fitted. Mathematically, it is represented as:

$$y(k) = \sum_{i=1}^n R_i Z_i^k \quad (6.72)$$

where $\mathbf{Y}(\mathbf{k})$ is the sum of the product of the complex amplitudes \mathbf{R} and the poles \mathbf{z} . The term \mathbf{n} stands for the number of sinusoids/modes to be estimated.

The damping and frequency estimates of the signal can be extracted from each Z_i .

$$z_i = \exp(-\lambda_i \Delta t); \quad \lambda_i = \sigma_i \pm j\omega_i \quad (6.73)$$

A matrix $[\mathbf{Y}]$ is made from the noisy PMU data $\mathbf{y}(\mathbf{k})$:

$$[\mathbf{Y}] = \begin{bmatrix} y(0) & y(1) & \dots & y(L) \\ y(1) & y(2) & \dots & y(L+1) \\ \dots & \dots & \dots & \dots \\ y(N-L-1) & y(N-L) & \dots & y(N-1) \end{bmatrix} \quad (6.74)$$

The term \mathbf{L} refers to pencil parameter, and \mathbf{N} refers to total number of data points in $\mathbf{y}(\mathbf{k})$. This algorithm uses singular value decomposition (SVD) to get rid of noise in the signal before the estimation process. SVD is applied to $[\mathbf{Y}]$ as shown below:

$$[\mathbf{Y}] = \mathbf{U} \mathbf{M} \mathbf{V}^T \quad (6.75)$$

The matrices \mathbf{U} and \mathbf{V} are unitary matrices. Singular values of \mathbf{Y} are present along diagonal of matrix \mathbf{M} . Further, \mathbf{n} singular values above a certain threshold are used to form the following matrices.

$$[\mathbf{V}'] = [v_1, v_2, v_3, \dots, v_n] \quad (6.76)$$

$$[\mathbf{Y}_1] = \mathbf{U} \mathbf{M}' [\mathbf{V}'_1]^T \quad (6.77)$$

$$[\mathbf{Y}_2] = \mathbf{U} \mathbf{M}' [\mathbf{V}'_2]^T \quad (6.78)$$

where v_1, v_2, \dots, v_n are column vectors, matrix \mathbf{M}' consists of the initial \mathbf{n} columns of \mathbf{M} , $[\mathbf{V}'_1]$ is \mathbf{V} matrix with the last column deleted, and $[\mathbf{V}'_2]$ is \mathbf{V} matrix with the last row

deleted. Using the matrix-pencil method, the matrices from (6.77) and (6.78) can be used to create the following new matrix-pencil definition for noisy data.

$$[Y_1]^+[Y_1] = V_2'^T[V_1'^T]^+ \quad (6.79)$$

The eigenvalues of $[V_2]'^T[V_1]'^T+$ are used to solve for \mathbf{R} from (6.72) and is rewritten in the following format.

$$\begin{bmatrix} y(0) \\ y(1) \\ \vdots \\ y(N-1) \end{bmatrix} = \begin{bmatrix} 1 & 1 & \dots & 1 \\ z_1 & z_2 & \dots & z_n \\ \dots & \dots & \dots & \dots \\ z_1^{N-1} & z_2^{N-1} & \dots & z_n^{N-1} \end{bmatrix} \begin{bmatrix} R_1 \\ R_2 \\ \vdots \\ R_n \end{bmatrix} \quad (6.80)$$

Values for damping and frequency are calculated from the poles \mathbf{z} , while amplitude is computed from \mathbf{R} (Refer 6.73).

Any amplitude crossing the 3 standard deviation mark will be classified as an event.

Appendix B

IEEE 14-bus system:

The single line diagram of the system is shown in the Fig. [6.5](#).

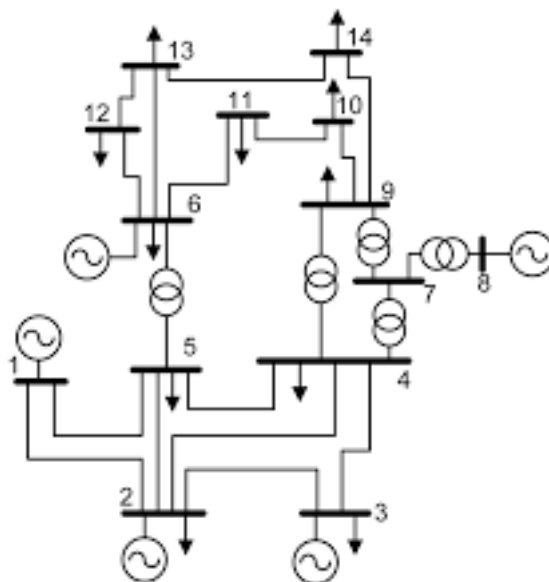


Figure 6.5: Single line diagram of the IEEE 14-bus system

Table 6.1: System information of the IEEE 14-bus system

Number of Generators:	5
Number of Transmission Lines:	20
Number of Shunt Reactors:	1
Number of PQ Loads:	11
P-load (peak, MW):	259.0
Q-load (peak, MVar):	73.5

The system information is given in Table [6.1](#). Branch data of the network system converted from IEEE CDF file from: [\(ARCHIVE, 1993a\)](#) is given in Table [6.2](#).

Table 6.2: Line data of the IEEE 14-bus system

From Bus	To Bus	R (p.u.)	X (p.u.)	B/2 (p.u.)	Rating (MVA)
1	2	0.01938	0.05917	0.0528	100
1	5	0.05403	0.22304	0.0492	100
2	3	0.04699	0.19797	0.0438	100
2	4	0.05811	0.17632	0.034	100
2	5	0.05695	0.17388	0.0346	100
3	4	0.06701	0.17103	0.0128	100
4	5	0.01335	0.04211	0	100
4	7	0	0.20912	0	100
4	9	0	0.55618	0	100
5	6	0	0.25202	0	100
6	11	0.09498	0.1989	0	100
6	12	0.12291	0.25581	0	100
6	13	0.06615	0.13027	0	100
7	8	0	0.17615	0	100
7	9	0	0.11001	0	100
9	10	0.03181	0.0845	0	100
9	14	0.12711	0.27038	0	100
10	11	0.08205	0.19207	0	100
12	13	0.22092	0.19988	0	100
13	14	0.17093	0.34802	0	100

Appendix C

IEEE 30-bus system:

The single line diagram of the system is shown in the Fig. 6.6. The system information is given in Table 6.3. Its branch data is given in Table 6.4 based on data from (O. Alsac, 1974) with branch parameters rounded to nearest 0.01, shunt values divided by 100 and shunt on bus 10 moved to bus 5, load at bus 5 zeroed out.

Table 6.3: System information of the IEEE 30-bus system

Number of Generators:	6
Number of Transmission Lines:	41
Number of Shunt Reactors:	2
Number of PQ Loads:	20
P-load (peak, MW):	189.2
Q-load (peak, MVar):	107.2

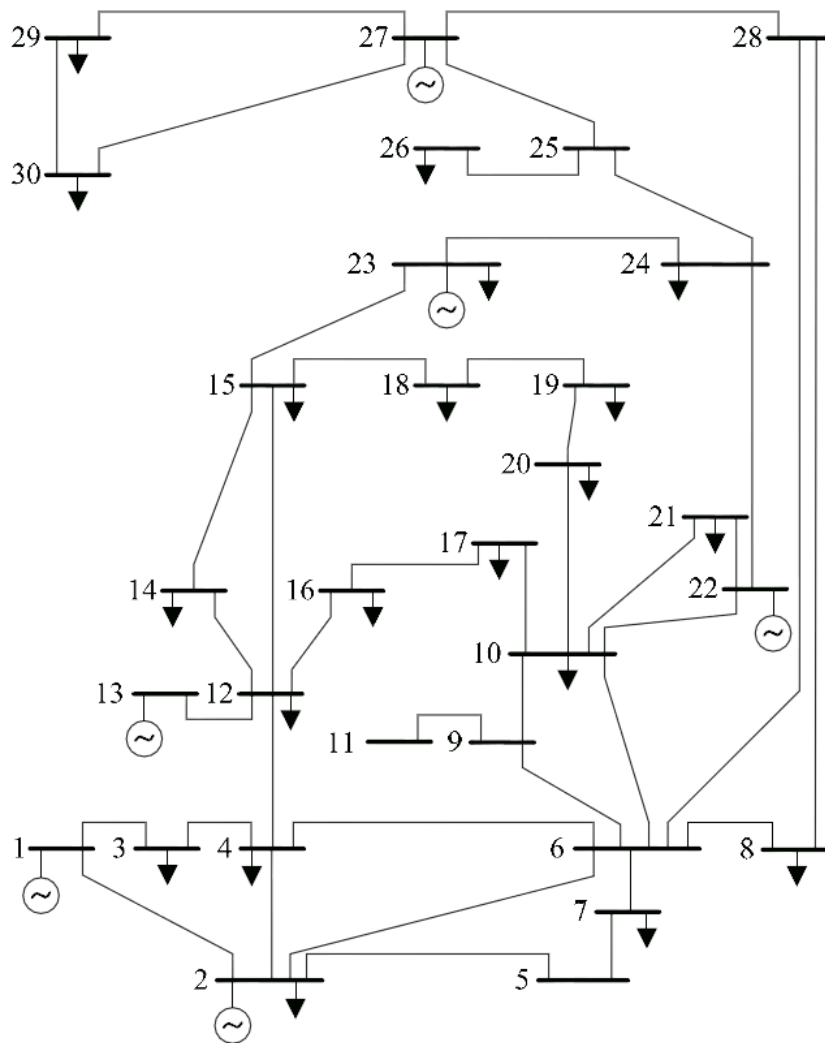


Figure 6.6: Single line diagram of the IEEE 30-bus system

Table 6.4: Line data of the IEEE 30-bus system

From Bus	To Bus	R (p.u.)	X (p.u.)	B/2 (p.u.)	Rating (MVA)
1	2	0.02	0.06	0.03	100
1	3	0.05	0.19	0.02	100
2	4	0.06	0.17	0.02	100
3	4	0.01	0.04	0	100
2	5	0.05	0.2	0.02	100
2	6	0.06	0.18	0.02	100
4	6	0.01	0.04	0	100
5	7	0.05	0.12	0.01	100
6	7	0.03	0.08	0.01	100
6	8	0.01	0.04	0	100
6	9	0	0.21	0	100
6	10	0	0.56	0	100
9	11	0	0.21	0	100
9	10	0	0.11	0	100
4	12	0	0.26	0	100
12	13	0	0.14	0	100
12	14	0.12	0.26	0	100
12	15	0.07	0.13	0	100
12	16	0.09	0.2	0	100
14	15	0.22	0.2	0	100
16	17	0.08	0.19	0	100
15	18	0.11	0.22	0	100
18	19	0.06	0.13	0	100
19	20	0.03	0.07	0	100
10	20	0.09	0.21	0	100
10	17	0.03	0.08	0	100
10	21	0.03	0.07	0	100
10	22	0.07	0.15	0	100
21	22	0.01	0.02	0	100
15	23	0.1	0.2	0	100
22	24	0.12	0.18	0	100
23	24	0.13	0.27	0	100
24	25	0.19	0.33	0	100
25	26	0.25	0.38	0	100
25	27	0.11	0.21	0	100
28	27	0	0.4	0	100
27	29	0.22	0.42	0	100
27	30	0.32	0.6	0	100
29	30	0.24	0.45	0	100
8	28	0.06	0.2	0.02	100
6	28	0.02	0.06	0.01	100

Appendix D

IEEE 57-bus system:

The single line diagram of the system is shown in the Fig. [6.7](#). The system information are given in Table [6.5](#).

Table 6.5: System information of the IEEE 57-bus system

Number of Generators:	7
Number of Transmission Lines:	80
Number of Shunt Reactors:	3
Number of PQ Loads:	42
P-load (peak, MW):	1250.8
Q-load (peak, MVar):	336.4

Branch data of the network system converted from IEEE CDF file from: ([ARCHIVE](#), [1993b](#)) as given in tables [6.6](#) and [6.7](#).

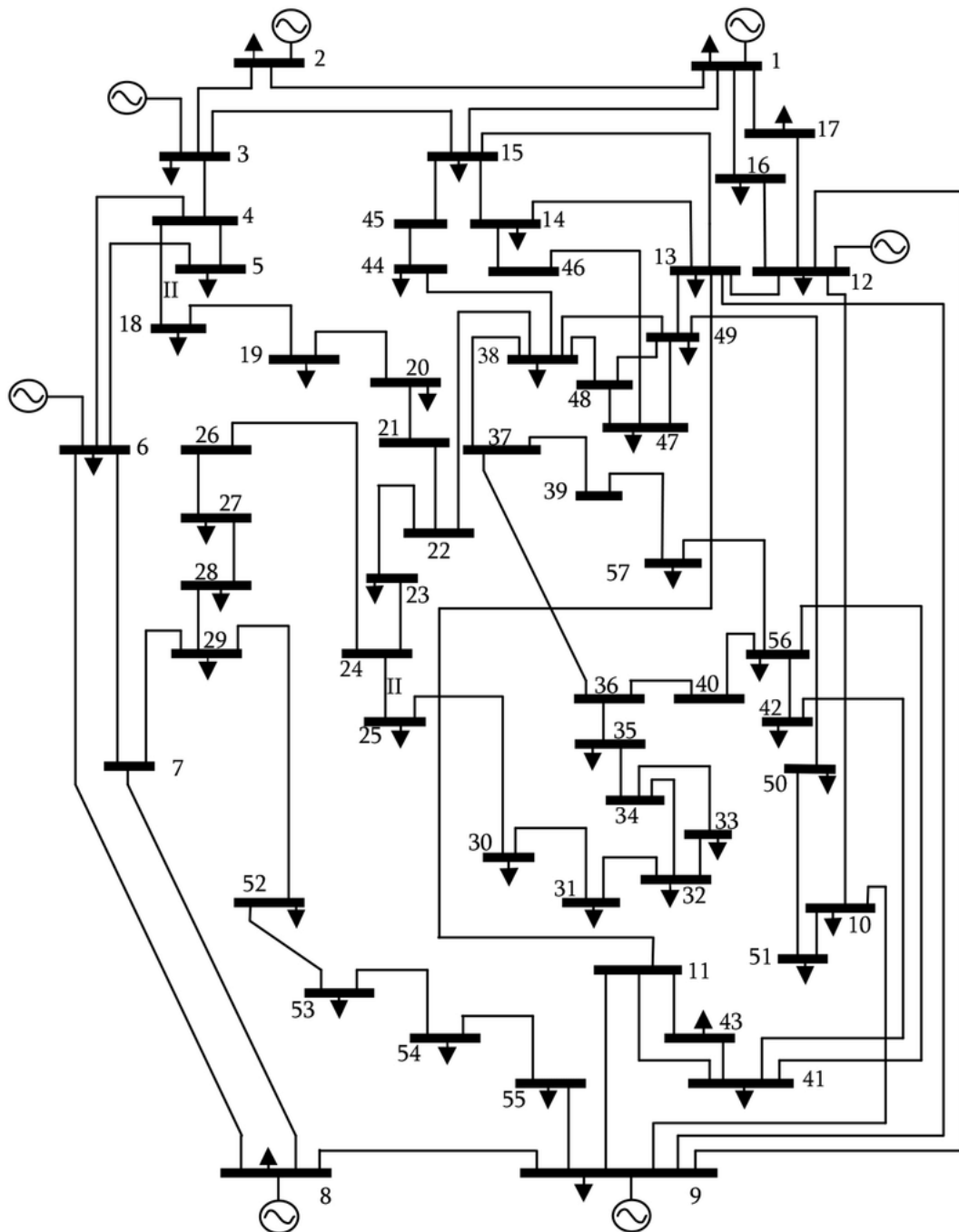


Figure 6.7: Single line diagram of the IEEE 57-bus system

Table 6.6: Line data of the IEEE 57-bus system

From Bus	To Bus	R (p.u.)	X (p.u.)	B/2 (p.u.)	Rating (MVA)
1	2	0.0083	0.028	0.129	100
2	3	0.0298	0.085	0.0818	100
3	4	0.0112	0.0366	0.038	100
4	5	0.0625	0.132	0.0258	100
4	6	0.043	0.148	0.0348	100
6	7	0.02	0.102	0.0276	100
6	8	0.0339	0.173	0.047	100
8	9	0.0099	0.0505	0.0548	100
9	10	0.0369	0.1679	0.044	100
9	11	0.0258	0.0848	0.0218	100
9	12	0.0648	0.295	0.0772	100
9	13	0.0481	0.158	0.0406	100
13	14	0.0132	0.0434	0.011	100
13	15	0.0269	0.0869	0.023	100
1	15	0.0178	0.091	0.0988	100
1	16	0.0454	0.206	0.0546	100
1	17	0.0238	0.108	0.0286	100
3	15	0.0162	0.053	0.0544	100
4	18	0	0.555	0	100
4	18	0	0.43	0	100
5	6	0.0302	0.0641	0.0124	100
7	8	0.0139	0.0712	0.0194	100
10	12	0.0277	0.1262	0.0328	100
11	13	0.0223	0.0732	0.0188	100
12	13	0.0178	0.058	0.0604	100
12	16	0.018	0.0813	0.0216	100
12	17	0.0397	0.179	0.0476	100
14	15	0.0171	0.0547	0.0148	100
18	19	0.461	0.685	0	100
19	20	0.283	0.434	0	100
21	20	0	0.7767	0	100
21	22	0.0736	0.117	0	100
22	23	0.0099	0.0152	0	100
23	24	0.166	0.256	0.0084	100
24	25	0	1.182	0	100
24	25	0	1.23	0	100
24	26	0	0.0473	0	100
26	27	0.165	0.254	0	100
27	28	0.0618	0.0954	0	100
28	29	0.0418	0.0587	0	100
7	29	0	0.0648	0	100
25	30	0.135	0.202	0	100
30	31	0.326	0.497	0	100
31	32	0.507	0.755	0	100

Table 6.7: Line data of the IEEE 57-bus system(Contd.)

From Bus	To Bus	R (p.u.)	X (p.u.)	B/2 (p.u.)	Rating (MVA)
32	33	0.0392	0.036	0	100
34	32	0	0.953	0	100
34	35	0.052	0.078	0.0032	100
35	36	0.043	0.0537	0.0016	100
36	37	0.029	0.0366	0	100
37	38	0.0651	0.1009	0.002	100
37	39	0.0239	0.0379	0	100
36	40	0.03	0.0466	0	100
22	38	0.0192	0.0295	0	100
11	41	0	0.749	0	100
41	42	0.207	0.352	0	100
41	43	0	0.412	0	100
38	44	0.0289	0.0585	0.002	100
15	45	0	0.1042	0	100
14	46	0	0.0735	0	100
46	47	0.023	0.068	0.0032	100
47	48	0.0182	0.0233	0	100
48	49	0.0834	0.129	0.0048	100
49	50	0.0801	0.128	0	100
50	51	0.1386	0.22	0	100
10	51	0	0.0712	0	100
13	49	0	0.191	0	100
29	52	0.1442	0.187	0	100
52	53	0.0762	0.0984	0	100
53	54	0.1878	0.232	0	100
54	55	0.1732	0.2265	0	100
11	43	0	0.153	0	100
44	45	0.0624	0.1242	0.004	100
40	56	0	1.195	0	100
56	41	0.553	0.549	0	100
56	42	0.2125	0.354	0	100
39	57	0	1.355	0	100
57	56	0.174	0.26	0	100
38	49	0.115	0.177	0.003	100
38	48	0.0312	0.0482	0	100
9	55	0	0.1205	0	100

Appendix E

Practical 72-bus test system:

The online and single line diagrams of the system are shown in the Figs. 6.8 and 6.9 respectively. The system information is given in Table 6.8. Its branch data is given in tables 6.9 and 6.10 based on data from (Moger and Dhadbanjan, 2015).

Table 6.8: System information of the Practical 72-bus test system

Number of Generators:	15
Number of Transmission Lines:	85
Number of Shunt Reactors:	17
Number of PQ Loads:	38
P-load (peak, MW):	7494
Q-load (peak, MVar):	3756

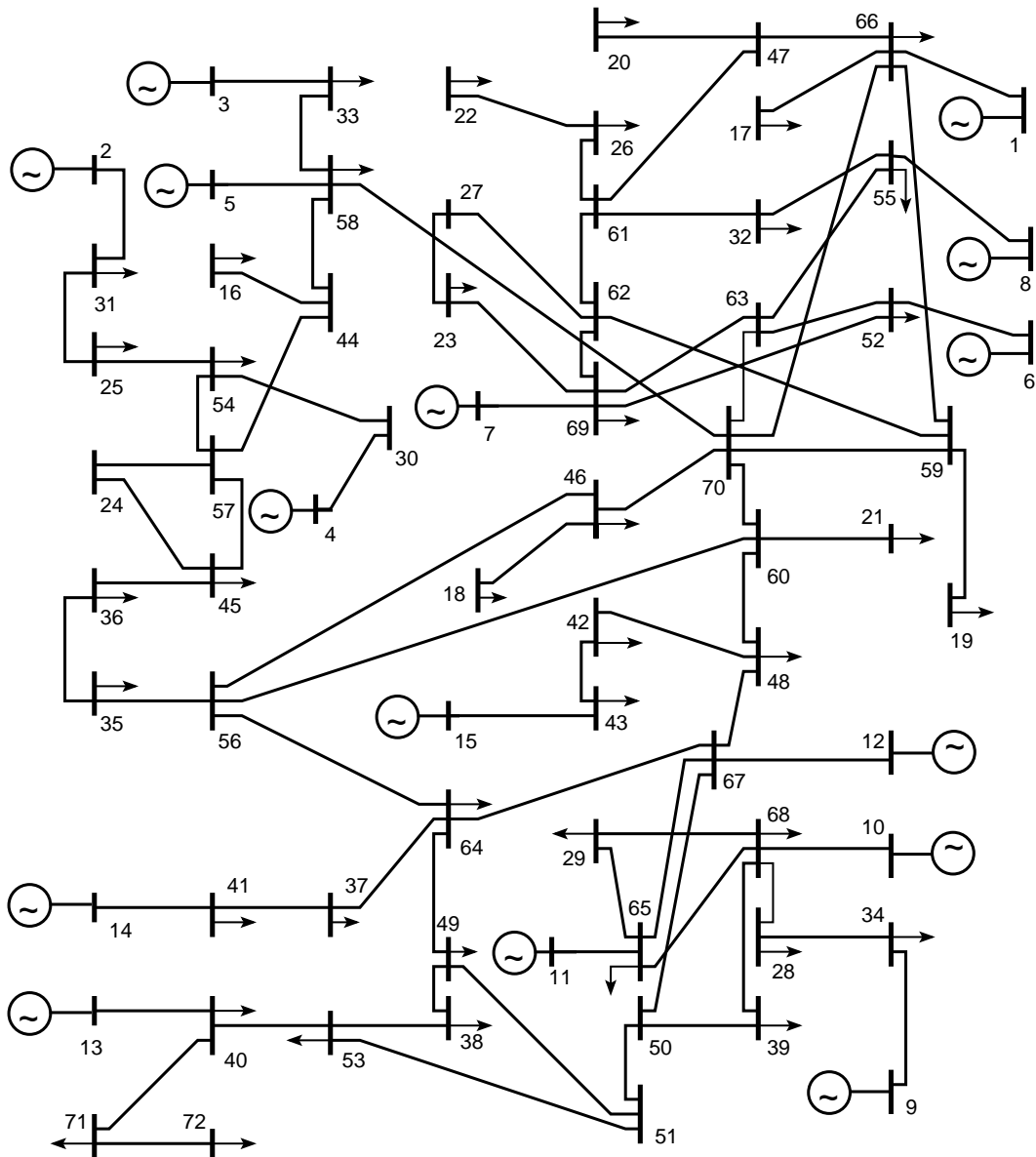


Figure 6.8: Online diagram of the Practical 72-bus test system



Figure 6.9: Geographical map of 72-bus equivalent system of Indian southern region power grid

Table 6.9: Line data of the Practical 72-bus test system

From Bus	To Bus	R (p.u.)	X (p.u.)	B/2 (p.u.)	Rating (MVA)
56	35	0.00063	0.0125	0	100
44	16	0.00198	0.0396	0	100
57	54	0.00198	0.0396	0	100
58	33	0.00198	0.0396	0	100
45	36	0.00125	0.025	0	100
60	21	0.00198	0.03968	0	100
59	19	0.00099	0.01984	0	100
66	17	0.001	0.025	0	100
70	63	0.00099	0.01984	0	100
26	22	0.00198	0.03968	0	100
46	18	0.00198	0.03968	0	100
61	32	0.00198	0.03968	0	100
47	20	0.00198	0.03968	0	100
62	69	0.00198	0.03968	0	100
27	23	0.00198	0.03968	0	100
67	65	0.00099	0.01984	0	100
50	39	0.00099	0.01984	0	100
51	53	0.00099	0.01984	0	100
64	37	0.00099	0.01984	0	100
48	42	0.00099	0.01984	0	100
49	38	0.00099	0.01984	0	100
66	1	0.00033	0.0067	0	100
31	2	0.0007605	0.01521	0	100
33	3	0.00071	0.01403	0	100
30	4	0.00109	0.02182	0	100
58	5	0.0029	0.058	0	100
52	6	0.0006	0.012	0	100
69	7	0.0006	0.012	0	100
55	8	0.0005	0.01	0	100
34	9	0.001275	0.0255	0	100
68	10	0.002645	0.0529	0	100
65	11	0.00063	0.0125	0	100
67	12	0.0007	0.014	0	100
40	13	0.00055	0.0111	0	100
41	14	0.00063	0.0125	0	100
43	15	0.00083	0.01667	0	100
23	69	0.02081	0.1086	0.18308	100
25	54	0.0011	0.0055	0.08328	100
28	68	0.00381	0.01957	0.03622	100

Table 6.10: Line data of the Practical 72-bus test system (Contd.)

From Bus	To Bus	R (p.u.)	X (p.u.)	B/2 (p.u.)	Rating (MVA)
29	68	0.00827	0.04155	0.0692	100
29	65	0.00827	0.04155	0.0692	100
30	54	0.00537	0.06701	0.6574	100
31	25	0.02507	0.12473	0.2096	100
34	28	0.02056	0.10565	0.19522	100
35	36	0.00315	0.01569	0.10548	100
38	53	0.02115	0.10866	0.2007	100
41	37	0.00305	0.01565	0.11568	100
43	42	0.00571	0.02935	0.217360	100
44	57	0.00198	0.02471	0.64608	100
44	58	0.0028	0.02998	0.85398	100
45	24	0.00116	0.01442	0.37688	100
47	61	0.00272	0.0277	0.72462	100
50	51	0.00099	0.01236	1.2887	100
51	49	0.00132	0.01647	0.4226	100
52	69	0.01289	0.07019	0.1086	100
52	63	0.00032	0.00255	0.06816	100
53	40	0.01067	0.05478	0.40488	100
55	32	0.0033	0.01652	0.02776	100
56	60	0.0043	0.0477	1.274	100
56	46	0.00589	0.05995	1.5682	100
56	64	0.00289	0.03603	0.92444	100
57	45	0.00546	0.06794	1.77672	100
57	24	0.0043	0.05352	1.39984	100
58	70	0.00477	0.05103	1.45346	100
59	62	0.00124	0.01544	1.6152	100
60	48	0.00388	0.04834	1.3094	100
61	26	0.00528	0.06588	1.72288	100
62	61	0.00211	0.02625	2.74584	100
62	27	0.00177	0.02203	0.57608	100
63	55	0.00944	0.04808	0.34072	100
64	49	0.00264	0.03294	0.8452	100
66	47	0.00437	0.04445	1.16264	100
66	59	0.00372	0.03931	1.06278	100
66	70	0.00261	0.0278	2.97	100
67	64	0.00145	0.01802	1.87936	100
67	48	0.00297	0.03706	0.95086	100
67	50	0.00099	0.01236	1.2887	100
68	39	0.0132	0.06608	0.11104	100
68	65	0.0008	0.00411	0.00762	100
69	63	0.00787	0.03988	0.28534	100
70	46	0.00569	0.06008	1.58828	100
70	60	0.00272	0.02872	3.03658	100
70	59	0.00245	0.02587	0.69932	100
71	40	0.00396	0.02035	0.03768	100
71	72	0.01371	0.07043	0.13014	100

Appendix F

The parameters of IM used for the data generations are listed in the following table,

Table 6.11: Induction Motor parameters and initial simulation values

Paramters	Values
Rated Power	2.238 kW
Rated Voltage	230 V
Rated Frequency	60 Hz
Rated Speed	1800 rpm
Stator Resistance(R_s)	0.435 Ω/ph
Rotor Resistance(R_r)	0.816 Ω/ph
Stotor leakage Inductance(L_{ls})	0.002 H/ph
Rotor leakage Inductance($L_{lr'}$)	0.002 H/ph
Magnetising Inductance(L_m)	0.06931 H/ph
Initial State	$x_0 = [0; 0; 0; 0; 0]$
Initial error covariance matrix	$P_0 = 10^{-3} \times I$
Process noise covariance	$Q = diag([10^{-6}, 10^{-6}, 10^{-6}, 10^{-6}, 10^{-2}])$
Measurement noise covariance	$R = diag([10^{-3}, 10^{-3}])$

Appendix G

The main parameters of the simulated SMIB system are presented in Table below

Table 6.12: Main parameters of the simulated synchronous generator

Inertia constant in p.u.	H	3
Damping factor in p.u.	D	0
Direct axis transient reactance in p.u.	x'_d	0.2
Mechanical input in p.u.	T_m	1

Appendix H

The main parameters of the simulated synchronous generator models for IEEE 9-bus Test System.

Table 6.13: Main parameters of the simulated synchronous generator models for IEEE 9-bus Test System

D_1, D_2, D_3	Damping factor p.u.	0, 0, 0
H_1, H_2, H_3	Inertia constant p.u.	23, 6.4, 3.01
$x'_{d1}, x'_{d2}, x'_{d3}$	Direct axis transient reactance p.u.	0.0608, 0.1198, 0.1813
T_{m1}, T_{m2}, T_{m3}	Mechanical input p.u.	0.7164, 1.63, 0.85
P_{base}	System base power	100 MVA
V_1, V_2, V_3, V_4	Bus voltages p.u.	$1\angle 0, 1.025\angle 9.28, 1.025\angle 4.66, 1.0258\angle -2.22$
V_5, V_6, V_7, V_8, V_9	Bus voltages p.u.	$0.995\angle -3.99, 1.012\angle -3.69, 1.025\angle 3.72, 1.015\angle 0.73, 1.0323\angle 1.97$

Appendix I

The 19-generator 42-bus test system is simulated using "case19l" and "s_simu" script files in Power System toolbox version 2 (Sauer et al., 2017) and MATLAB to generate the data for state estimation.

Table 6.14: Bus data of the 19-generator 42-bus test system (Part I)

Bus No.	Voltage magnitude (p.u.)	Voltage angle (deg.)	P_{gen} (p.u.)	Q_{gen} (p.u.)	P_{load} (p.u.)	Q_{load} (p.u.)	G shunt (p.u.)	B shunt (p.u.)	Bus type	$Q_{gen_{max}}$ (p.u.)	$Q_{gen_{min}}$ (p.u.)	V rated (kV)	V_{max} (p.u.)	V_{min} (p.u.)
1	1.0490	0.0000	28.3794	23.2983	0.0000	0.0000	0.00	0.00	1	25.00	-10.00	20.00	1.1	0.9
2	1.0490	28.1220	121.0406	62.9955	0.0000	0.0000	0.00	0.00	2	73.20	-35.00	20.00	1.1	0.9
3	1.0490	-57.8509	110.1829	70.1339	0.0000	0.0000	0.00	0.00	2	72.00	0.00	20.00	1.1	0.9
4	1.0490	-98.8765	74.7150	55.1440	0.0000	0.0000	0.00	0.00	2	93.75	-10.00	20.00	1.1	0.9
5	1.0490	-63.8096	68.3083	75.4348	0.0000	0.0000	0.00	0.00	2	78.00	0.00	20.00	1.1	0.9
6	1.0490	8.9660	127.0900	52.5457	0.0000	0.0000	0.00	0.00	2	101.80	-10.00	20.00	1.1	0.9
7	1.0490	16.2350	19.6897	9.1951	0.0000	0.0000	0.00	0.00	2	25.00	-10.00	20.00	1.1	0.9
8	1.0490	-15.9550	22.6313	10.5317	0.0000	0.0000	0.00	0.00	2	25.00	-10.00	20.00	1.1	0.9
9	1.0300	22.6917	12.2000	-0.5245	0.0000	0.0000	0.00	0.00	2	7.00	-5.00	20.00	1.1	0.9
10	1.0400	-7.8713	16.8000	0.9749	0.0000	0.0000	0.00	0.00	2	16.00	0.00	20.00	1.1	0.9
11	1.0490	-56.2245	27.0400	12.2507	0.0000	0.0000	0.00	0.00	2	34.00	-10.00	20.00	1.1	0.9
12	1.0490	-58.4070	5.6000	4.0002	0.0000	0.0000	0.00	0.00	2	16.00	-10.00	20.00	1.1	0.9
13	1.0490	25.3923	6.0300	4.4545	0.0000	0.0000	0.00	0.00	2	10.00	-10.00	20.00	1.1	0.9
14	1.0490	-55.9158	12.7300	4.9559	0.0000	0.0000	0.00	0.00	2	6.00	-10.00	20.00	1.1	0.9
15	1.0490	5.7456	6.6800	5.0596	0.0000	0.0000	0.00	0.00	2	8.00	-10.00	20.00	1.1	0.9
16	1.0490	7.4830	9.4000	4.7339	0.0000	0.0000	0.00	0.00	2	16.00	-10.00	20.00	1.1	0.9
17	1.0490	-2.3803	11.4100	37.4331	0.0000	0.0000	0.00	0.00	2	40.00	0.00	20.00	1.1	0.9
18	1.0490	-86.8303	25.4000	7.0974	0.0000	0.0000	0.00	0.00	2	7.50	-10.00	20.00	1.1	0.9
19	1.0490	-87.8436	21.7700	6.1294	0.0000	0.0000	0.00	0.00	2	7.25	-10.00	20.00	1.1	0.9
20	1.0049	-62.0468	0.0000	0.0000	105.0300	60.0000	0.00	0.00	3	0.00	0.00	500.00	1.1	0.9
21	0.9957	21.4671	0.0000	0.0000	107.0400	48.0000	0.00	0.00	3	0.00	500.00	1.1	0.9	
22	0.9928	-66.8173	0.0000	0.0000	97.1000	40.0000	0.00	10.00	3	0.00	0.00	500.00	1.1	0.9
23	1.0430	15.5132	0.0000	0.0000	11.6800	4.0000	0.00	0.00	3	0.00	0.00	500.00	1.1	0.9
24	1.0421	-16.7853	0.0000	0.0000	41.5300	15.0000	0.00	10.00	3	0.00	0.00	230.00	1.1	0.9
25	1.0098	2.7673	0.0000	0.0000	80.8300	45.0000	0.00	0.00	3	0.00	0.00	500.00	1.1	0.9
26	1.0060	-3.0830	0.0000	0.0000	80.8300	35.0000	0.00	15.00	3	0.00	0.00	500.00	1.1	0.9
27	1.0050	-105.2786	0.0000	0.0000	97.0600	40.0000	0.00	59.00	3	0.00	0.00	500.00	1.1	0.9
28	1.0086	-102.1152	0.0000	0.0000	87.0600	32.0000	0.00	0.00	3	0.00	0.00	500.00	1.1	0.9

Table 6.15: Bus data of the 19-generator 42-bus test system (Part II)

Bus No.	Voltage magnitude (p.u.)	Voltage angle (deg.)	P_{gen} (p.u.)	Q_{gen} (p.u.)	P_{load} (p.u.)	Q_{load} (p.u.)	G shunt (p.u.)	B shunt (p.u.)	Bus type	$Q_{gen_{max}}$ (p.u.)	$Q_{gen_{min}}$ (p.u.)	V rated (kV)	V_{max} (p.u.)	V_{min} (p.u.)
29	1.0243	-59.0441	0.0000	0.0000	0.0000	0.0000	0.00	0.00	3	0.00	0.00	20.00	1.1	0.9
30	1.0226	-60.4863	0.0000	0.0000	0.0000	0.0000	0.00	0.00	3	0.00	0.00	20.00	1.1	0.9
31	1.0153	23.1674	0.0000	0.0000	0.0000	0.0000	0.00	0.00	3	0.00	0.00	20.00	1.1	0.9
32	1.0243	-59.6333	0.0000	0.0000	0.0000	0.0000	0.00	0.00	3	0.00	0.00	20.00	1.1	0.9
33	1.0235	3.8774	0.0000	0.0000	0.0000	0.0000	0.00	0.00	3	0.00	0.00	20.00	1.1	0.9
34	1.0215	4.3326	0.0000	0.0000	0.0000	0.0000	0.00	0.00	3	0.00	0.00	20.00	1.1	0.9
35	1.0310	-2.6429	0.0000	0.0000	0.0000	0.0000	0.00	0.00	3	0.00	0.00	20.00	1.1	0.9
36	1.0171	-95.0157	0.0000	0.0000	0.0000	0.0000	0.00	0.00	3	0.00	0.00	20.00	1.1	0.9
37	1.0275	-92.4547	0.0000	0.0000	0.0000	0.0000	0.00	0.00	3	0.00	0.00	20.00	1.1	0.9
38	1.0347	18.7511	0.0000	0.0000	0.0000	0.0000	0.00	0.00	3	0.00	0.00	20.00	1.1	0.9
39	1.0378	-13.2266	0.0000	0.0000	0.0000	0.0000	0.00	0.00	3	0.00	0.00	20.00	1.1	0.9
40	0.9654	-55.4078	0.0000	0.0000	0.0000	0.0000	0.00	0.00	3	0.00	0.00	230.00	1.1	0.9
41	1.0312	10.2218	0.0000	0.0000	0.0000	0.0000	0.00	0.00	3	0.00	0.00	230.00	1.1	0.9
42	1.0146	-1.0369	0.0000	0.0000	0.0000	0.0000	0.00	0.00	3	0.00	0.00	230.00	1.1	0.9

Table 6.16: Line data of the 19-generator 42-bus test system

From Bus	To Bus	R (p.u.)	X (p.u.)	line charging (p.u.)	tap ratio
30	12	0.00007	0.00700	0.00000	0.0
11	29	0.00010	0.00200	0.00000	0.0
27	28	0.00010	0.00075	0.04000	0.0
13	31	0.00060	0.00730	0.00000	0.0
32	14	0.00007	0.00550	0.00000	0.0
22	27	0.00350	0.02460	0.29200	0.0
41	24	0.00850	0.09950	0.50000	0.0
24	40	0.00920	0.10900	0.50000	0.0
33	15	0.00008	0.00530	0.00000	0.0
34	16	0.00007	0.00630	0.00000	0.0
25	26	0.00025	0.00282	0.01800	0.0
25	26	0.00030	0.00279	0.00900	0.0
25	23	0.00190	0.01550	0.09520	0.0
42	24	0.00800	0.08400	0.33400	0.0
35	17	0.00002	0.00050	0.00000	0.0
26	21	0.00190	0.02100	0.22000	0.0
26	22	0.00300	0.01880	0.01800	0.0
36	18	0.00007	0.00600	0.00000	0.0
37	19	0.00007	0.00400	0.00000	0.0
28	20	0.00200	0.01550	0.03200	0.0
38	9	0.00007	0.00600	0.00000	0.0
39	10	0.00007	0.00600	0.00000	0.0
20	40	0.00000	0.02000	0.00000	1.0
20	29	0.00000	0.00200	0.00000	1.0
20	30	0.00000	0.00500	0.00000	1.0
20	3	0.00000	0.00070	0.00000	1.0
21	2	0.00000	0.00100	0.00000	1.0
21	31	0.00000	0.00500	0.00000	1.0
22	32	0.00000	0.01000	0.00000	1.0
22	5	0.00000	0.00080	0.00000	1.0
23	38	0.00000	0.00500	0.00000	1.0
23	41	0.00000	0.02000	0.00000	1.0
24	39	0.00000	0.00400	0.00000	1.0
25	33	0.00000	0.00300	0.00000	1.0
25	34	0.00000	0.00300	0.00000	1.0
25	6	0.00000	0.00090	0.00000	1.0
25	42	0.00000	0.02000	0.00000	1.0
26	35	0.00000	0.00070	0.00000	1.0
26	1	0.00000	0.00200	0.00000	1.0
28	36	0.00000	0.00500	0.00000	1.0
28	37	0.00000	0.00800	0.00000	1.0
28	4	0.00000	0.00080	0.00000	1.0
23	7	0.00000	0.00070	0.00000	1.0
24	8	0.00000	0.00070	0.00000	1.0

Table 6.17: System information of the 19-generator 42-bus test system

Bus No.	Base MVA	leakage reactance	R_a (p.u.)	x_d (p.u.)	x'_d (p.u.)	x''_d (p.u.)	x_q (p.u.)	x'_q (p.u.)	x''_q (p.u.)	T'_{q0} (s)	T''_{q0} (s)	H (s)	d_0 (p.u.)		
1	3000	0	0	0	0.25	0	0	0	0	0	0	0	0	4.00	2.0
2	12000	0	0	0	0.25	0	0	0	0	0	0	0	0	4.17	2.0
3	13000	0	0	0	0.37	0	0	0	0	0	0	0	0	4.23	2.0
4	9000	0	0	0	0.25	0	0	0	0	0	0	0	0	4.44	2.0
5	8000	0	0	0	0.25	0	0	0	0	0	0	0	0	4.38	2.0
6	13000	0	0	0	0.37	0	0	0	0	0	0	0	0	4.62	2.0
7	2000	0	0	0	0.25	0	0	0	0	0	0	0	0	2.50	2.0
8	6000	0	0	0	0.25	0	0	0	0	0	0	0	0	2.67	2.0
9	2392	0	0	0	0.25	0	0	0	0	0	0	0	0	4.11	2.0
10	1982	0	0	0	0.25	0	0	0	0	0	0	0	0	2.88	2.0
11	3118	0	0	0	0.25	0	0	0	0	0	0	0	0	3.83	2.0
12	640	0	0	0	0.25	0	0	0	0	0	0	0	0	3.23	2.0
13	880	0	0	0	0.25	0	0	0	0	0	0	0	0	5.10	2.0
14	1500	0	0	0	0.25	0	0	0	0	0	0	0	0	5.36	2.0
15	737	0	0	0	0.25	0	0	0	0	0	0	0	0	5.40	2.0
16	1137	0	0	0	0.25	0	0	0	0	0	0	0	0	2.98	2.0
17	2208	0	0	0	0.37	0	0	0	0	0	0	0	0	4.82	2.0
18	3004	0	0	0	0.25	0	0	0	0	0	0	0	0	5.16	2.0
19	2500	0	0	0	0.25	0	0	0	0	0	0	0	0	3.80	2.0

Appendix J

Measurement Uncertainties used in the simulation of state estimation is given below

Table 6.18: Measurement types and corresponding standard uncertainties (Asprou et al., 2013; Sharma et al., 2014)

Measurement type	Power Injection in p.u.	Power Flow in p.u.	Voltage in p.u.	Angle rad.
Conventional	0.01	0.01	0.006
Synchrophasor	0.001	0.001	0.0006	0.018

Bibliography

- Abbasy, N. H. and Ismail, H. M. (2009). A unified approach for the optimal pmu location for power system state estimation. *IEEE Transactions on power systems*, 24(2):806–813.
- Abdelaziz, A. Y. and Fathy, A. (2017). A novel approach based on crow search algorithm for optimal selection of conductor size in radial distribution networks. *Engineering Science and Technology, an International Journal*, 20(2):391–402.
- Abdelkader, M., Selim, A., Kamel, S., and Jurado, F. (2019). Optimal placement of phasor measurement units for state estimation of electrical power systems. In *2019 21st International Middle East Power Systems Conference (MEPCON)*, pages 1048–1052. IEEE.
- Abur, A. and Exposito, A. G. (2004). *Power system state estimation: theory and implementation*. CRC press.
- Ahmed, M. M. and Imran, K. (2019). An optimal pmu placement against n-1 contingency of pmu using integer linear programming approach. In *2019 International Conference on Applied and Engineering Mathematics (ICAEM)*, pages 127–132. IEEE.
- Ahmed, S. S. and Brameller, A. (1991). New algorithm for diakoptical static state estimation. In *IEE Proceedings C (Generation, Transmission and Distribution)*, volume 138, pages 185–192. IET.
- Akhlaghi, S., Zhou, N., and Huang, Z. (2016). A multi-step adaptive interpolation approach to mitigating the impact of nonlinearity on dynamic state estimation. *IEEE Transactions on Smart Grid*, 9(4):3102–3111.
- Al-Mohammed, A., Abido, M. A., and Mansour, M. (2011). Optimal pmu placement for power system observability using differential evolution. In *Intelligent Systems Design and Applications (ISDA), 2011 11th International Conference on*, pages 277–282. IEEE.
- Albuquerque, R. J. and Paucar, V. L. (2013). Evaluation of the pmus measurement channels availability for observability analysis. *IEEE Transactions on Power Systems*, 28(3):2536–2544.

- Allen, A., Santoso, S., and Muljadi, E. (2013). Algorithm for screening phasor measurement unit data for power system events and categories and common characteristics for events seen in phasor measurement unit relative phase-angle differences and frequency signals.
- Allen, A., Singh, M., Muljadi, E., and Santoso, S. (2014). Pmu data event detection: A user guide for power engineers. Technical report, National Renewable Energy Lab.(NREL), Golden, CO (United States).
- Allen, A., Singh, M., Muljadi, E., and Santoso, S. (2021). Northern region-grid event report for may 2020, (available: <https://posoco.in/grid-disturbancesincidence/grid-disturbances-incidences-2020-21/>). Technical report, Grid disturbances incidences 2020-2021- NLDC (National Load Dispatch Centre).
- Almasabi, S. and Mitra, J. (2018). Multistage optimal pmu placement considering substation infrastructure. *IEEE Transactions on Industry Applications*, 54(6):6519–6528.
- Almasabi, S. and Mitra, J. (2019). A fault-tolerance based approach to optimal pmu placement. *IEEE Transactions on Smart Grid*, 10(6):6070–6079.
- Almunif, A. and Fan, L. (2020). Optimal pmu placement for modeling power grid observability with mathematical programming methods. *International Transactions on Electrical Energy Systems*, 30(2):e12182.
- Aminifar, F., Fotuhi-Firuzabad, M., and Safdarian, A. (2013a). Optimal pmu placement based on probabilistic cost/benefit analysis. *IEEE Transactions on Power Systems*, 28(1):566–567.
- Aminifar, F., Fotuhi-Firuzabad, M., Safdarian, A., Davoudi, A., and Shahidehpour, M. (2014a). Synchrophasor measurement technology in power systems: Panorama and state-of-the-art. *IEEE Access*, 2:1607–1628.
- Aminifar, F., Fotuhi-Firuzabad, M., Safdarian, A., and Shahidehpour, M. (2013b). Observability of hybrid ac/dc power systems with variable-cost pmus. *IEEE transactions on power delivery*, 29(1):345–352.
- Aminifar, F., Fotuhi-Firuzabad, M., Shahidehpour, M., and Khodaei, A. (2010a). Probabilistic multistage pmu placement in electric power systems. *IEEE Transactions on Power Delivery*, 26(2):841–849.
- Aminifar, F., Khodaei, A., Fotuhi-Firuzabad, M., and Shahidehpour, M. (2009a). Contingency-constrained pmu placement in power networks. *IEEE Transactions on Power Systems*, 25(1):516–523.

- Aminifar, F., Khodaei, A., Fotuhi-Firuzabad, M., and Shahidehpour, M. (2010b). Contingency-constrained pmu placement in power networks. *IEEE Transactions on Power Systems*, 25(1):516–523.
- Aminifar, F., Lucas, C., Khodaei, A., and Fotuhi-Firuzabad, M. (2009b). Optimal placement of phasor measurement units using immunity genetic algorithm. *IEEE Transactions on Power delivery*, 24(3):1014–1020.
- Aminifar, F., Shahidehpour, M., Fotuhi-Firuzabad, M., and Kamalinia, S. (2014b). Power system dynamic state estimation with synchronized phasor measurements. *IEEE Transactions on Instrumentation and Measurement*, 63(2):352–363.
- Antonova, G., Paduraru, S., Naccarino, J., and Price, E. (2011). Wide-area awareness: Smarter power grid monitoring and analysis. In *PacWorld Conference*.
- Arasaratnam, I. and Haykin, S. (2009). Cubature kalman filters. *IEEE Transactions on automatic control*, 54(6):1254–1269.
- ARCHIVE, U. (1993a). “ieee 14 bus test case- common data format (ieee14cdf.txt)”, <http://www.ee.washington.edu/research/pstca/>.
- ARCHIVE, U. (1993b). “ieee 57 bus test case- common data format (ieee57cdf.txt)”, <http://www.ee.washington.edu/research/pstca/>.
- Arpanahi, M. K., Alhelou, H. H., and Siano, P. (2019). A novel multiobjective opp for power system small signal stability assessment considering wams uncertainties. *IEEE Transactions on Industrial Informatics*, 16(5):3039–3050.
- Asgari, A. and Firouzjah, K. G. (2018). Optimal pmu placement for power system observability considering network expansion andn- 1 contingencies. *IET Generation, Transmission & Distribution*, 12(18):4216–4224.
- Askarzadeh, A. (2016). A novel metaheuristic method for solving constrained engineering optimization problems: crow search algorithm. *Computers & Structures*, 169:1–12.
- Asprou, M., Kyriakides, E., and Albu, M. (2013). The effect of variable weights in a wls state estimator considering instrument transformer uncertainties. *IEEE Transactions on Instrumentation and Measurement*, 63(6):1484–1495.
- Atkinson, D. J., Acarnley, P. P., and Finch, J. W. (1991). Observers for induction motor state and parameter estimation. *IEEE Transactions on industry applications*, 27(6):1119–1127.

- Azizi, S., Dobakhshari, A. S., Sarmadi, S. A. N., and Ranjbar, A. M. (2012). Optimal pmu placement by an equivalent linear formulation for exhaustive search. *IEEE Transactions on Smart Grid*, 3(1):174–182.
- Azizi, S., Gharehpetian, G. B., and Dobakhshari, A. S. (2013). Optimal integration of phasor measurement units in power systems considering conventional measurements. *IEEE Transactions on Smart Grid*, 4(2):1113–1121.
- Azizi, S., Salehi Dobakhshari, A., Nezam Sarmadi, S., Ranjbar, A., and Gharehpetian, G. (2014). Optimal multi-stage pmu placement in electric power systems using boolean algebra. *International Transactions on Electrical Energy Systems*, 24(4):562–577.
- Babu, R., Raj, S., and Bhattacharyya, B. (2020). Weak bus-constrained pmu placement for complete observability of a connected power network considering voltage stability indices. *Protection and Control of Modern Power Systems*, 5(1):28.
- Bagchi, A., Clements, K., Davis, P., and Maurais, F. (1994). A comparison of algorithms for least absolute value state estimation electric power networks. In *Proceedings of IEEE International Symposium on Circuits and Systems-ISCAS'94*, volume 6, pages 53–56. IEEE.
- Bahgat, A., Sakr, M., and El-Shafei, A. (1989). Two level dynamic state estimator for electric power systems based on nonlinear transformation. In *IEE Proceedings C-Generation, Transmission and Distribution*, volume 136, pages 15–23. IET.
- Barut, M., Bogosyan, S., and Gokasan, M. (2005). Speed sensorless direct torque control of imms with rotor resistance estimation. *Energy Conversion and Management*, 46(3):335–349.
- Barut, M., Bogosyan, S., and Gokasan, M. (2007). Switching ekf technique for rotor and stator resistance estimation in speed sensorless control of imms. *Energy Conversion and Management*, 48(12):3120–3134.
- Beides, H. M. and Heydt, G. T. (1991). Dynamic state estimation of power system harmonics using kalman filter methodology. *IEEE Transactions on Power Delivery*, 6(4):1663–1670.
- Beni, G. and Wang, J. (1993). Swarm intelligence in cellular robotic systems. In *Robots and biological systems: towards a new bionics?*, pages 703–712. Springer.
- Bhattacharyya, S. (1978). Observer design for linear systems with unknown inputs. *IEEE transactions on Automatic Control*, 23(3):483–484.

- bin Mohd Nasir, M. N., Sabo, A., and Wahab, N. I. A. (2019). A review on synchrophasor technology for power system monitoring. In *2019 IEEE Student Conference on Research and Development (SCOReD)*, pages 58–62. IEEE.
- Biswal, A. and Mathur, H. (2015). Optimized pmu stationing for wide area monitoring of power grid. *Procedia Technology*, 21:2–7.
- Biswal, M., Brahma, S. M., and Cao, H. (2016). Supervisory protection and automated event diagnosis using pmu data. *IEEE Transactions on power delivery*, 31(4):1855–1863.
- Bogosyan, S., Barut, M., and Gokasan, M. (2007). Braided extended kalman filters for sensorless estimation in induction motors at high-low/zero speed. *IET Control Theory & Applications*, 1(4):987–998.
- Bozorg-Haddad and Omid (2018). *Advanced optimization by nature-inspired algorithms*. Springer.
- Buitrago, J. and Asfour, S. (2017). Short-term forecasting of electric loads using non-linear autoregressive artificial neural networks with exogenous vector inputs. *Energies*, 10(1):40.
- Chakrabarti, S. and Kyriakides, E. (2008). Optimal placement of phasor measurement units for power system observability. *IEEE Transactions on power systems*, 23(3):1433–1440.
- Chakrabarti, S., Kyriakides, E., Bi, T., Cai, D., and Terzija, V. (2008). Measurements get together. *IEEE Power and Energy Magazine*, 7(1):41–49.
- Chakrabarti, S., Kyriakides, E., and Eliades, D. G. (2009). Placement of synchronized measurements for power system observability. *IEEE Transactions on Power Delivery*, 24(1):12–19.
- Charalampidis, A. C. and Papavassilopoulos, G. P. (2009). Comparison of standard and modified recursive state estimation techniques for nonlinear systems. In *2009 17th Mediterranean Conference on Control and Automation*, pages 132–138. IEEE.
- Chen, J. and Abur, A. (2008). Enhanced topology error processing via optimal measurement design. *IEEE Transactions on power systems*, 23(3):845–852.
- Cho, K.-S., Shin, J.-R., and Hyun, S. H. (2001). Optimal placement of phasor measurement units with gps receiver. In *2001 IEEE Power Engineering Society Winter Meeting. Conference Proceedings (Cat. No. 01CH37194)*, volume 1, pages 258–262. IEEE.

- Chouhan, D. and Jaiswal, V. (2016). A literature review on optimal placement of pmu and voltage stability. *Indian Journal of Science and Technology*, 9(47).
- Committee, P. S. R. et al. (2011). C37. 118.1-2011: Ieee standard for synchrophasor measurements for power systems. *IEEE Standard Association*.
- Corporation, P. S. O. (2013). “synchrophasors initiatives in india”, https://posoco.in/download/synchrophasors-initiative-in-india_june-2012/.
- Costa, A. S., Albuquerque, A., and Bez, D. (2013). An estimation fusion method for including phasor measurements into power system real-time modeling. *IEEE Transactions on Power Systems*, 28(2):1910–1920.
- Da Silva, A. L., Do Coutto Filho, M., and De Queiroz, J. (1983). State forecasting in electric power systems. In *IEE Proceedings C (Generation, Transmission and Distribution)*, volume 130, pages 237–244. IET.
- Dahal, O. P. and Brahma, S. M. (2012). Preliminary work to classify the disturbance events recorded by phasor measurement units. In *2012 IEEE Power and Energy Society General Meeting*, pages 1–8. IEEE.
- Dahal, O. P., Brahma, S. M., and Cao, H. (2013). Comprehensive clustering of disturbance events recorded by phasor measurement units. *IEEE Transactions on Power Delivery*, 29(3):1390–1397.
- de Andrade, L. C. M., Oleskovicz, M., Santos, A. Q., Coury, D. V., and Fernandes, R. A. S. (2014). Very short-term load forecasting based on narx recurrent neural networks. In *2014 IEEE PES General Meeting— Conference & Exposition*, pages 1–5. IEEE.
- Del Angel, A., Geurts, P., Ernst, D., Glavic, M., and Wehenkel, L. (2007). Estimation of rotor angles of synchronous machines using artificial neural networks and local pmu-based quantities. *Neurocomputing*, 70(16-18):2668–2678.
- Del Valle, Y., Venayagamoorthy, G. K., Mohagheghi, S., Hernandez, J.-C., and Harley, R. G. (2008). Particle swarm optimization: basic concepts, variants and applications in power systems. *IEEE Transactions on evolutionary computation*, 12(2):171–195.
- DeRusso, P. M., Desrochers, A. A., Roy, R. J., and Close, C. M. (1997). *State variables for engineers*. John Wiley & Sons, Inc.
- Dopazo, J., Klitin, O., Stagg, G., and Van Slyck, L. (1970). State calculation of power systems from line flow measurements. *IEEE transactions on power Apparatus and Systems*, (7):1698–1708.

- Dopazo, J., Klitin, O., and Vanslyck, L. (1972). State calculation of power systems from line flow measurements, part ii. *IEEE Transactions on Power Apparatus and Systems*, (1):145–151.
- Dua, D., Dambhare, S., Gajbhiye, R. K., and Soman, S. (2008). Optimal multistage scheduling of pmu placement: An ilp approach. *IEEE Transactions on Power delivery*, 23(4):1812–1820.
- Dubey, R., Muro, J. C., and Popov, M. (2018). Cost effective wide area measurement systems for smart power network. *IEEE Power and Energy Technology Systems Journal*.
- Durgaprasad, G. and Thakur, S. (1998). Robust dynamic state estimation of power systems based on m-estimation and realistic modeling of system dynamics. *IEEE Transactions on Power Systems*, 13(4):1331–1336.
- El-Ela, A. A. A. (1992). Fast and accurate technique for power system state estimation. In *IEE Proceedings C (Generation, Transmission and Distribution)*, volume 139, pages 7–12. IET.
- El-Shimy, M. (2015). Dynamic security of interconnected electric power systems. *LAP Lambert Academic Publishing*.
- Emami, R. and Abur, A. (2010). Robust measurement design by placing synchronized phasor measurements on network branches. *IEEE Transactions on power systems*, 25(1):38–43.
- Falcao, D. M., Wu, F. F., and Murphy, L. (1995). Parallel and distributed state estimation. *IEEE Transactions on Power Systems*, 10(2):724–730.
- Fan, L. (2015). Least squares estimation and kalman filter based dynamic state and parameter estimation. In *2015 IEEE Power & Energy Society General Meeting*, pages 1–5. IEEE.
- Fausto, F., Reyna-Orta, A., Cuevas, E., Andrade, Á. G., and Perez-Cisneros, M. (2020). From ants to whales: metaheuristics for all tastes. *Artificial Intelligence Review*, 53(1):753–810.
- Ferreira, I. and Barbosa, F. M. (1994). A square root filter algorithm for dynamic state estimation of electric power systems. In *Proceedings of MELECON'94. Mediterranean Electrotechnical Conference*, pages 877–880. IEEE.
- Gajjar, G. and Soman, S. (2014). Auto detection of power system events using wide area frequency measurements. In *2014 Eighteenth National Power Systems Conference (NPSC)*, pages 1–6. IEEE.

- Gao, W. and Wang, S. (2010). On-line dynamic state estimation of power systems. In *North American Power Symposium 2010*, pages 1–6. IEEE.
- Garcia, t. A., Monticelli, A., and Abreu, P. (1979). Fast decoupled state estimation and bad data processing. *IEEE Transactions on Power Apparatus and Systems*, (5):1645–1652.
- Ge, Y., Flueck, A. J., Kim, D.-K., Ahn, J.-B., Lee, J.-D., and Kwon, D.-Y. (2015). Power system real-time event detection and associated data archival reduction based on synchrophasors. *IEEE Transactions on Smart Grid*, 6(4):2088–2097.
- Ghaffarzadeh, N., Parpaei, M., and Tayar, M. Z. (2015). A fast fault location method based on detecting the minimum number of phasor measurement units using a novel adaptive binary differential evolution optimization algorithm. *International Transactions on Electrical Energy Systems*, 25(11):2933–2947.
- Ghahremani, E. and Kamwa, I. (2011a). Dynamic state estimation in power system by applying the extended kalman filter with unknown inputs to phasor measurements. *IEEE Transactions on Power Systems*, 26(4):2556–2566.
- Ghahremani, E. and Kamwa, I. (2011b). Dynamic state estimation in power system by applying the extended kalman filter with unknown inputs to phasor measurements. *IEEE Transactions on Power Systems*, 26(4):2556–2566.
- Ghahremani, E. and Kamwa, I. (2011c). Online state estimation of a synchronous generator using unscented kalman filter from phasor measurements units. *IEEE Transactions on Energy Conversion*, 26(4):1099–1108.
- Gholami, A. and Srivastava, A. K. (2021). Comparative analysis of ml techniques for data-driven anomaly detection, classification and localization in distribution system. In *2020 52nd North American Power Symposium (NAPS)*, pages 1–6. IEEE.
- Glover, J. D. and Sarma, M. S. (2011). Thomas overbye-power system analysis and design. *Peto izdanje, Cengage Learning*.
- Göl, M. (2018). A decentralization method for hybrid state estimators. *IEEE Transactions on Power Systems*, 33(2):2070–2077.
- Göl, M. and Abur, A. (2015a). A fast decoupled state estimator for systems measured by pmus. *IEEE Transactions on Power Systems*, 30(5):2766–2771.
- Göl, M. and Abur, A. (2015b). A hybrid state estimator for systems with limited number of pmus. *IEEE Transactions on Power Systems*, 30(3):1511–1517.

- Golshan, M. E. H., Dolatabadi, S. H. H., and Tabatabaei, S. M. (2018). Determining minimum number and optimal placement of pmus for fault observability in one-terminal algorithms. *IET Generation, Transmission & Distribution*, 12(21):5789–5797.
- Gomez-Exposito, A. and Abur, A. (2004). *Power system state estimation: theory and implementation*. CRC press.
- Gopakumar, P., Chandra, G. S., Reddy, M. J. B., and Mohanta, D. K. (2013). Optimal placement of pmus for the smart grid implementation in indian power grid—a case study. *Frontiers in Energy*, 7(3):358–372.
- Gou, B. (2008a). Generalized integer linear programming formulation for optimal pmu placement. *IEEE transactions on Power Systems*, 23(3):1099–1104.
- Gou, B. (2008b). Optimal placement of pmus by integer linear programming. *IEEE Transactions on Power Systems*, 23(3):1525–1526.
- Gu, C. and Jirutitijaroen, P. (2015). Dynamic state estimation under communication failure using kriging based bus load forecasting. *IEEE Transactions on Power Systems*, 30(6):2831–2840.
- Guo, X.-C., Liao, C.-S., and Chu, C.-C. (2020). Enhanced optimal pmu placements with limited observability propagations. *IEEE Access*, 8:22515–22524.
- Guo, Y., Wu, W., Zhang, B., and Sun, H. (2013). An efficient state estimation algorithm considering zero injection constraints. *IEEE Transactions on Power Systems*, 28(3):2651–2659.
- Gupta, D. K. and Pandey, R. (2014). Grid stabilization with pmu signals—a survey. In *Power Systems Conference (NPSC), 2014 Eighteenth National*, pages 1–6. IEEE.
- Habiballah, I. and Quintana, V. (1991). Fast-decoupled rectangular co-ordinate state estimation with efficient data structure management. In *IEE Proceedings C (Generation, Transmission and Distribution)*, volume 138, pages 462–468. IET.
- Hammad, M. A., Jereb, B., Rosi, B., and Dragan, D. (2020). Methods and models for electric load forecasting: a comprehensive review. *Logistics, Supply Chain, Sustainability and Global Challenges*, 11(1):51–76.
- Hargrave, P. (1989). A tutorial introduction to kalman filtering. In *IEE colloquium on Kalman filters: introduction, applications and future developments*, pages 1–1. IET.

- Hassanzadeh, M. and Evrenosoglu, C. Y. (2011). A regression analysis based state transition model for power system dynamic state estimation. In *2011 North American Power Symposium*, pages 1–5. IEEE.
- Haykin, S. (2004). *Kalman filtering and neural networks*, volume 47. John Wiley & Sons.
- Hinkkanen, M., Leppanen, V.-M., and Luomi, J. (2005). Flux observer enhanced with low-frequency signal injection allowing sensorless zero-frequency operation of induction motors. *IEEE Transactions on Industry Applications*, 41(1):52–59.
- Holten, L., Gjelsvik, A., Aam, S., Wu, F. F., and Liu, W.-H. (1988). Comparison of different methods for state estimation. *IEEE Transactions on Power Systems*, 3(4):1798–1806.
- Holtz, J. (2002). Sensorless control of induction motor drives. *Proceedings of the IEEE*, 90(8):1359–1394.
- Horisberger, H., Richard, J., and Rossier, C. (1976). A fast decoupled static state-estimator for electric power systems. *IEEE Transactions on Power Apparatus and Systems*, 95(1):208–215.
- Huang, L., Sun, Y., Xu, J., Gao, W., Zhang, J., and Wu, Z. (2013a). Optimal pmu placement considering controlled islanding of power system. *IEEE Transactions on Power Systems*, 29(2):742–755.
- Huang, M., Wei, Z., and Lin, Y. (2022). Forecasting-aided state estimation based on deep learning for hybrid ac/dc distribution systems. *Applied Energy*, 306:118119.
- Huang, Y., Li, S., Li, J., Hou, W., Zhang, Y., and Yang, K. (2019). A multi-objective model for pmu placement considering redundancy in the presence of line outages. In *2019 IEEE 3rd Conference on Energy Internet and Energy System Integration (EI2)*, pages 960–965. IEEE.
- Huang, Z., Du, P., Kosterev, D., and Yang, S. (2013b). Generator dynamic model validation and parameter calibration using phasor measurements at the point of connection. *IEEE transactions on power systems*, 28(2):1939–1949.
- Huang, Z., Schneider, K., and Nieplocha, J. (2007). Feasibility studies of applying kalman filter techniques to power system dynamic state estimation. In *2007 International Power Engineering Conference (IPEC 2007)*, pages 376–382. IEEE.
- Hyndman, R. J., Koehler, A. B., Snyder, R. D., and Grose, S. (2002). A state space framework for automatic forecasting using exponential smoothing methods. *International Journal of forecasting*, 18(3):439–454.

- IITK, P. S. L. (2020). “246 bus reduced nrpg system data (nrpg-data.pdf)”, [https://www.iitk.ac.in/eeold/facilities/research_labs/power_system/NRPG – DATA.pdf](https://www.iitk.ac.in/eeold/facilities/research_labs/power_system/NRPG-DATA.pdf).
- Ilas, C., Bettini, A., Ferraris, L., Griva, G., and Profumo, F. (1994). Comparison of different schemes without shaft sensors for field oriented control drives. In *Proceedings of IECON'94-20th Annual Conference of IEEE Industrial Electronics*, volume 3, pages 1579–1588. IEEE.
- Jafarzadeh, S., Lascu, C., and Fadali, M. S. (2011). State estimation of induction motor drives using the unscented kalman filter. *IEEE Transactions on Industrial Electronics*, 59(11):4207–4216.
- Jain, A. and Shivakumar, N. (2008). Impact of pmu in dynamic state estimation of power systems. In *2008 40th North American Power Symposium*, pages 1–8. IEEE.
- Jelodar, M. T. and Fini, A. S. (2016). Probabilistic pmu placement considering topological change in high voltage substations. *International Journal of Electrical Power & Energy Systems*, 82:303–313.
- Jiang, W., Vittal, V., and Heydt, G. T. (2007). A distributed state estimator utilizing synchronized phasor measurements. *IEEE Transactions on Power Systems*, 22(2):563–571.
- Ju, Y., Wu, W., Ge, F., Ma, K., Lin, Y., and Ye, L. (2018). Fast decoupled state estimation for distribution networks considering branch ampere measurements. *IEEE Transactions on Smart Grid*, 9(6):6338–6347.
- Julier, S., Uhlmann, J., and Durrant-Whyte, H. F. (2000). A new method for the nonlinear transformation of means and covariances in filters and estimators. *IEEE Transactions on automatic control*, 45(3):477–482.
- Kalman, R. E. et al. (1960). A new approach to linear filtering and prediction problems [j]. *Journal of basic Engineering*, 82(1):35–45.
- Karimi, E., Ebrahimi, A., and Tavakoli, M. R. (2019). How optimal pmu placement can mitigate cascading outages blackouts? *International Transactions on Electrical Energy Systems*, 29(6):e12015.
- Kavasseri, R. and Srinivasan, S. K. (2010). Joint optimal placement of pmu and conventional measurements in power systems. In *Proceedings of 2010 IEEE International Symposium on Circuits and Systems*, pages 3449–3452. IEEE.

- Kavasseri, R. and Srinivasan, S. K. (2011). Joint placement of phasor and conventional power flow measurements for fault observability of power systems. *IET generation, transmission & distribution*, 5(10):1019–1024.
- Kazempour, F. and Poshtkouhi, S. (2012). Power system state estimation: methods, implementation and evaluation. In *2012 25th IEEE Canadian Conference on Electrical and Computer Engineering (CCECE)*, pages 1–4. IEEE.
- Kekatos, V., Giannakis, G. B., and Wollenberg, B. (2012). Optimal placement of phasor measurement units via convex relaxation. *IEEE Transactions on power systems*, 27(3):1521–1530.
- Kennedy, J. and Eberhart, R. (1995). Particle swarm optimization. In *Proceedings of ICNN'95-International Conference on Neural Networks*, volume 4, pages 1942–1948. IEEE.
- Keyhani, A. and Abur, A. (1985). Comparative study of polar and cartesian co-ordinate algorithms for power-system state-estimation problems. In *IEE Proceedings C (Generation, Transmission and Distribution)*, volume 132, pages 132–138. IET.
- Khajeh, K. G., Bashar, E., Rad, A. M., and Gharehpetian, G. B. (2017). Integrated model considering effects of zero injection buses and conventional measurements on optimal pmu placement. *IEEE Transactions on Smart Grid*, 8(2):1006–1013.
- Khosravi, M., Banejad, M., and Shandiz, H. T. (2016). Forecast aided measurements data synchronisation in robust power system state estimation. *IET Generation, Transmission & Distribution*, 10(10):2379–2388.
- Kim, T. and Wright, S. J. (2018). Pmu placement for line outage identification via multinomial logistic regression. *IEEE Transactions on Smart Grid*, 9(1):122–131.
- Kokai, Y., Masuda, F., Horiike, S., and Sekine, Y. (1998). Recent development in open systems for ems/scada. *International Journal of Electrical Power & Energy Systems*, 20(2):111–123.
- Korkali, M. and Abur, A. (2009). Placement of pmus with channel limits. In *2009 IEEE power & energy society general meeting*, pages 1–4. IEEE.
- Korkali, M. and Abur, A. (2010). Impact of network sparsity on strategic placement of phasor measurement units with fixed channel capacity. In *Proceedings of 2010 IEEE International Symposium on Circuits and Systems*, pages 3445–3448. IEEE.

- Korres, G. and Manousakis, N. (2012). State estimation and observability analysis for phasor measurement unit measured systems. *IET generation, transmission & distribution*, 6(9):902–913.
- Korres, G. N., Manousakis, N. M., Xygkis, T. C., and Löfberg, J. (2015). Optimal phasor measurement unit placement for numerical observability in the presence of conventional measurements using semi-definite programming. *IET Generation, Transmission & Distribution*, 9(15):2427–2436.
- Koutsoukis, N. C., Manousakis, N. M., Georgilakis, P. S., and Korres, G. N. (2013). Numerical observability method for optimal phasor measurement units placement using recursive tabu search method. *IET Generation, Transmission & Distribution*, 7(4):347–356.
- Kumar, S., Tyagi, B., Kumar, V., and Chohan, S. (2018). Incremental pmu placement considering reliability of power system network using analytical hierarchical process. *IET Generation, Transmission & Distribution*, 12(16):3900–3909.
- Kundur, P., Paserba, J., Ajarapu, V., Andersson, G., Bose, A., Canizares, C., Hatziargyriou, N., Hill, D., Stankovic, A., Taylor, C., et al. (2004). Definition and classification of power system stability. *IEEE transactions on Power Systems*, 19(2):1387–1401.
- Kusljevic, M. D. K. and Poljak, P. D. (2011). Simultaneous reactive-power and frequency estimations using simple recursive wls algorithm and adaptive filtering. *IEEE Transactions on Instrumentation and Measurement*, 60(12):3860–3867.
- Laouid, A. A., Rezaoui, M. M., Kouzou, A., and Mohammedi, R. D. (2019). Optimal pmus placement using hybrid pso-gsa algorithm. In *2019 4th International Conference on Power Electronics and their Applications (ICPEA)*, pages 1–5. IEEE.
- Larson, R. E., Tinney, W. F., and Peschon, J. (1970). State estimation in power systems part i: Theory and feasibility. *IEEE Transactions on Power Apparatus and Systems*, (3):345–352.
- Leite, A. V., Araújo, R. E., and Freitas, D. (2004). Full and reduced order extended kalman filter for speed estimation in induction motor drives: A comparative study. In *2004 IEEE 35th Annual Power Electronics Specialists Conference (IEEE Cat. No. 04CH37551)*, volume 3, pages 2293–2299. IEEE.
- Li, H. and Li, W. (2009). Estimation and forecasting of dynamic state estimation in power systems. In *2009 International Conference on Sustainable Power Generation and Supply*, pages 1–6. IEEE.

- Li, Q., Cui, T., Weng, Y., Negi, R., Franchetti, F., and Ilic, M. D. (2013). An information-theoretic approach to pmu placement in electric power systems. *IEEE Transactions on Smart Grid*, 4(1):446–456.
- Li, Y., Li, J., Qi, J., and Chen, L. (2019). Robust cubature kalman filter for dynamic state estimation of synchronous machines under unknown measurement noise statistics. *IEEE Access*, 7:29139–29148.
- Lin, J.-M., Huang, S.-J., and Shih, K.-R. (2003). Application of sliding surface-enhanced fuzzy control for dynamic state estimation of a power system. *IEEE Transactions on Power Systems*, 18(2):570–577.
- Lin, W.-M. and Teng, J.-H. (1995). State estimation for distribution systems with zero-injection constraints. In *Proceedings of Power Industry Computer Applications Conference*, pages 523–529. IEEE.
- Lin, W.-M. and Teng, J.-H. (1996). Distribution fast decoupled state estimation by measurement pairing. *IEE Proceedings-Generation, Transmission and Distribution*, 143(1):43–48.
- Liu, G., Quintero, J., and Venkatasubramanian, V. M. (2007). Oscillation monitoring system based on wide area synchrophasors in power systems. In *2007 iREP symposium-bulk power system dynamics and control-VII. Revitalizing Operational Reliability*, pages 1–13. IEEE.
- Liu, Y., Singh, A. K., Zhao, J., Meliopoulos, A. S., Pal, B. C., Ariff, M. A. B. M., Van Cutsem, T., Glavic, M., Huang, Z., Kamwa, I., et al. (2021). Dynamic state estimation for power system control and protection. *IEEE Transactions on Power Systems*.
- Lixia, M., Benigni, A., Flammini, A., Muscas, C., Ponci, F., and Monti, A. (2012). A software-only ptp synchronization for power system state estimation with pmus. *IEEE Transactions on Instrumentation and Measurement*, 61(5):1476–1485.
- Lo, K., Ong, P., McColl, R., Moffatt, A., and Sulley, J. (1983). Development of a static state estimator part i: Estimation and bad data suppression. *IEEE Transactions on Power Apparatus and Systems*, (8):2486–2491.
- Lu, C., Wang, Z., Ma, M., Shen, R., and Yu, Y. (2018). An optimal pmu placement with reliable zero injection observation. *IEEE Access*, 6:54417–54426.
- Lu, C., Wang, Z., and Yu, Y. (2017). Optimal pmu placement for pessimistic dynamic vulnerability assessment. *IET Generation, Transmission & Distribution*, 12(10):2231–2237.

- Luenberger, D. G. (1979). *Introduction to dynamic systems: theory, models, and applications*, volume 1. Wiley New York.
- Maalej, I., Abid, D. B. H., Rekik, C., and Derbel, N. (2014). Fuzzy augmented state kalman observer for fault and state estimation. In *2014 IEEE 11th International Multi-Conference on Systems, Signals & Devices (SSD14)*, pages 1–5. IEEE.
- Mafaakher, F., Brameller, A., and Bermudez, J. (1979). Optimum metering design using fast-decoupled estimator. In *Proceedings of the Institution of Electrical Engineers*, volume 126, pages 62–68. IET.
- Mallikarjuna, B., Gopakumar, P., Reddy, M. J. B., and Mohanta, D. (2016). A case study on optimal phasor measurement unit placement for emerging indian national smart grid. In *Signal Processing, Communication, Power and Embedded System (SCOPEs), 2016 International Conference on*, pages 1956–1960. IEEE.
- Mandal, J., Sinha, A., and Roy, L. (1995). Incorporating nonlinearities of measurement function in power system dynamic state estimation. *IEE Proceedings-Generation, Transmission and Distribution*, 142(3):289–296.
- Mandich, M., Xia, T., and Sun, K. (2019). Optimal pmu placement using stochastic methods. In *2019 IEEE Power & Energy Society General Meeting (PESGM)*, pages 1–5. IEEE.
- Manoharan, H., Srikrishna, S., Sivarajan, G., and Manoharan, A. (2018). Economical placement of pmus considering observability and voltage stability using binary coded ant lion optimization. *International Transactions on Electrical Energy Systems*, 28(9):e2591.
- Manousakis, N. M. and Korres, G. N. (2019). Optimal allocation of phasor measurement units considering various contingencies and measurement redundancy. *IEEE Transactions on Instrumentation and Measurement*, 69(6):3403–3411.
- Manousakis, N. M., Korres, G. N., and Georgilakis, P. S. (2012). Taxonomy of pmu placement methodologies. *IEEE Transactions on Power Systems*, 27(2):1070–1077.
- Marihart, D. J. (2001). Communications technology guidelines for ems/scada systems. *IEEE Transactions on Power Delivery*, 16(2):181–188.
- Marin, F., Garcia-Lagos, F., Joya, G., and Sandoval, F. (2003). Genetic algorithms for optimal placement of phasor measurement units in electrical networks. *Electronics Letters*, 39(19):1403–1405.

- Martin, K. (2008). Exploring the iee standard c37. 118-2005. In *2008 IEEE Power and Energy Society General Meeting—Conversion and Delivery of Electrical Energy in the 21st Century*, pages 1–1. IEEE.
- Martin, K., Brunello, G., Adamiak, M., Antonova, G., Begovic, M., Benmouyal, G., Bui, P., Falk, H., Gharpure, V., Goldstein, A., et al. (2014). An overview of the iee standard c37. 118.2—synchrophasor data transfer for power systems. *IEEE Transactions on Smart Grid*, 5(4):1980–1984.
- Martin, K. E. (2013). Synchrophasor standards and guides for the smart grid. In *2013 IEEE Power & Energy Society General Meeting*, pages 1–5. IEEE.
- Martin, K. E. (2015). Synchrophasor measurements under the iee standard c37. 118.1-2011 with amendment c37. 118.1 a. *IEEE Transactions on Power Delivery*, 30(3):1514–1522.
- Martin, K. E. and Carroll, J. R. (2008). Phasing in the technology. *IEEE Power and Energy Magazine*, 6(5):24–33.
- Mathworks (2020). Matlab documentation (version 2020a). Available online: <https://in.mathworks.com/help/releases/R2020a/optim/ug/intlinprog.html> (accessed on 7 July 2022).
- Mazhari, S. M., Monsef, H., Lesani, H., and Fereidunian, A. (2013). A multi-objective pmu placement method considering measurement redundancy and observability value under contingencies. *IEEE Transactions on Power Systems*, 28(3):2136–2146.
- McGee, L. A. and Schmidt, S. F. (1985). Discovery of the kalman filter as a practical tool for aerospace and industry.
- Miljanić, Z., Djurović, I., and Vujošević, I. (2012). Optimal placement of pmus with limited number of channels. *Electric Power Systems Research*, 90:93–98.
- Milosevic, B. and Begovic, M. (2003). Nondominated sorting genetic algorithm for optimal phasor measurement placement. *IEEE Transactions on Power Systems*, 18(1):69–75.
- Mishra, C., Jones, K. D., Pal, A., and Centeno, V. A. (2016). Binary particle swarm optimisation-based optimal substation coverage algorithm for phasor measurement unit installations in practical systems. *IET Generation, Transmission & Distribution*, 10(2):555–562.
- Moger, T. and Dhadbanjan, T. (2015). A novel index for identification of weak nodes for reactive compensation to improve voltage stability. *IET Generation, Transmission & Distribution*, 9(14):1826–1834.

- Mohanta, D. K., Murthy, C., and Sinha Roy, D. (2016). A brief review of phasor measurement units as sensors for smart grid. *Electric Power Components and Systems*, 44(4):411–425.
- Mohanty, K. B. and Patra, A. (2005). Flux and speed estimation in decoupled induction motor drive using kalman filter.
- Molina-Moreno, I., Medina, A., Cisneros-Magaña, R., and Anaya-Lara, O. (2018). A methodology for transient state estimation based on numerical derivatives, optimal monitoring, and filtered measurements. *IEEE Transactions on Power Delivery*, 33(4):1527–1535.
- Monticelli, A. (1999). Fast decoupled state estimator. In *State Estimation in Electric Power Systems*, pages 313–342. Springer.
- Monticelli, A. (2000). Electric power system state estimation. *Proceedings of the IEEE*, 88(2):262–282.
- Monticelli, A., Garcia, A., and Slutsker, I. (1992). Handling discardable measurements in power system state estimation. *IEEE transactions on power systems*, 7(3):1333–1340.
- Monticelli, A. and Wu, F. F. (1985). A method that combines internal state estimation and external network modeling. *IEEE transactions on power apparatus and systems*, (1):91–103.
- Müller, H. H. and Castro, C. A. (2016). Genetic algorithm-based phasor measurement unit placement method considering observability and security criteria. *IET Generation, Transmission & Distribution*, 10(1):270–280.
- Munoz, A., Sánchez-Ubeda, E. F., Cruz, A., and Marín, J. (2010). Short-term forecasting in power systems: a guided tour. In *Handbook of power systems II*, pages 129–160. Springer.
- Murty, P. (2017). *Power systems analysis*. Butterworth-Heinemann.
- Muthu-Manivannan, K., Benner, C. L., Xu, P., and Russell, B. D. (2013). Electrical power system event detection and anticipation. US Patent 8,457,910.
- Naess, E. (2004). "configurable middleware-level intrusion detection for embedded systems", <https://www.researchgate.net/publication/4147368>.
- Nazari-Heris, M. and Mohammadi-Ivatloo, B. (2015). Application of heuristic algorithms to optimal pmu placement in electric power systems: An updated review. *Renewable and Sustainable Energy Reviews*, 50:214–228.

- Negi, S. S., Kishor, N., Uhlen, K., and Negi, R. (2017). Event detection and its signal characterization in pmu data stream. *IEEE Transactions on Industrial Informatics*, 13(6):3108–3118.
- Nejati, M., Amjady, N., and Zareipour, H. (2012). A new stochastic search technique combined with scenario approach for dynamic state estimation of power systems. *IEEE Transactions on Power Systems*, 27(4):2093–2105.
- Netto, M. and Mili, L. (2018). A robust data-driven koopman kalman filter for power systems dynamic state estimation. *IEEE Transactions on Power Systems*, 33(6):7228–7237.
- Nikkhah, S., Aghaei, J., Safarinejadian, B., and Norouzi, M.-A. (2017). Contingency constrained phasor measurement units placement with n- k redundancy criterion: a robust optimisation approach. *IET Science, Measurement & Technology*, 12(2):151–160.
- Nimbalkar, N. U. and Joshi, P. M. (2019). Optimal pmu placement using ilp and aco: A comparative study. In *2019 Global Conference for Advancement in Technology (GCAT)*, pages 1–4. IEEE.
- Nuqui, R. F. and Phadke, A. G. (2005). Phasor measurement unit placement techniques for complete and incomplete observability. *IEEE Transactions on Power Delivery*, 20(4):2381–2388.
- Nuthalapati, S. (2019). *Power system grid operation using synchrophasor technology*. Springer.
- O. Alsac, B. S. (1974). Optimal load flow with steady state security. *IEEE Transactions on Power Apparatus and Systems*, 93(3):745–751.
- Okon, T. and Wilkosz, K. (2010). Comparison of weighted-least-squares power system state estimation in polar and rectangular coordinate systems. In *2010 9th International Conference on Environment and Electrical Engineering*, pages 140–143. IEEE.
- Okumus, H. and Nuroglu, F. M. (2018). Event detection and classification algorithm using wide area measurement systems. In *2018 IEEE International Conference on Smart Energy Grid Engineering (SEGE)*, pages 230–233. IEEE.
- Pal, A., Mishra, C., Vullikanti, A. K. S., and Ravi, S. (2017). General optimal substation coverage algorithm for phasor measurement unit placement in practical systems. *IET Generation, Transmission & Distribution*, 11(2):347–353.

- Pan, P., Sharma, M. K., Ghose, T., and Mohanta, D. (2018). Synchrophasor based concurrent swing and state estimation of synchronous generator. In *2018 Technologies for Smart-City Energy Security and Power (ICSESP)*, pages 1–5. IEEE.
- Parpaei, M., Ghaffarzadeh, N., and Tayar, M. Z. (2017). Rational random walk-based optimal placement of phasor measurement units to enhance the initializing and guiding the optimization processes. *International Transactions on Electrical Energy Systems*, 27(7):e2323.
- Pau, M., Pegoraro, P. A., and Sulis, S. (2013). Efficient branch-current-based distribution system state estimation including synchronized measurements. *IEEE Transactions on Instrumentation and Measurement*, 62(9):2419–2429.
- Peng, J., Sun, Y., and Wang, H. (2006). Optimal pmu placement for full network observability using tabu search algorithm. *International Journal of Electrical Power & Energy Systems*, 28(4):223–231.
- Peng, L. and Fan, Z. (2007). Research on a modified ekf for speed estimation in induction motor drives. In *Proceeding of IEEE International Conference on Integration Technology*, pages 432–436.
- Phadke, A. G. and Tianshu, B. (2018). Phasor measurement units, wams, and their applications in protection and control of power systems. *Journal of Modern Power Systems and Clean Energy*, 6(4):619–629.
- Poli, R., Kennedy, J., and Blackwell, T. (2007). Particle swarm optimization. *Swarm intelligence*, 1(1):33–57.
- Pourramezan, R., Seyedi, Y., Karimi, H., Zhu, G., and Mont-Briant, M. (2017). Design of an advanced phasor data concentrator for monitoring of distributed energy resources in smart microgrids. *IEEE Transactions on Industrial Informatics*, 13(6):3027–3036.
- powerWorld ver22 (2021). power world corporation, Champaign, IL, USA.
- Prasad, S. and Kumar, D. M. V. (2018a). Robust meter placement for active distribution state estimation using a new multi-objective optimisation model. *IET Science, Measurement & Technology*, 12(8):1047–1057.
- Prasad, S. and Kumar, D. V. (2018b). Trade-offs in pmu and ied deployment for active distribution state estimation using multi-objective evolutionary algorithm. *IEEE Transactions on Instrumentation and Measurement*.

- Qi, J., Taha, A. F., and Wang, J. (2018). Comparing kalman filters and observers for power system dynamic state estimation with model uncertainty and malicious cyber attacks. *IEEE Access*, 6:77155–77168.
- Rahman, N. H. and Zobaa, A. F. (2016). Optimal pmu placement using topology transformation method in power systems. *Journal of advanced research*, 7(5):625–634.
- Rakpenthai, C., Premrudeepreechacharn, S., Uatrongjit, S., and Watson, N. R. (2007). An optimal pmu placement method against measurement loss and branch outage. *IEEE transactions on power delivery*, 22(1):101–107.
- Ran, C.-J. and Deng, Z.-L. (2008). Two average weighted measurement fusion kalman filtering algorithms in sensor networks. In *2008 7th World Congress on Intelligent Control and Automation*, pages 2387–2391. IEEE.
- Rao, N. and Roy, L. (1983). A cartesian coordinate algorithm for power system state estimation. *IEEE transactions on power apparatus and systems*, (5):1070–1082.
- Rao, N. and Tripathy, S. (1979). A variable step size decoupled state estimator. *IEEE Transactions on Power Apparatus and Systems*, (2):436–443.
- Rashidi, M. and Farjah, E. (2016a). Les based framework for transient instability prediction and mitigation using pmu data. *IET Generation, Transmission & Distribution*, 10(14):3431–3440.
- Rashidi, M. and Farjah, E. (2016b). Lyapunov exponent-based optimal pmu placement approach with application to transient stability assessment. *IET Science, Measurement & Technology*, 10(5):492–497.
- Rasmussen, J. and Jorgensen, P. (2006). Synchronized phasor measurements of a power system event in eastern denmark. *IEEE Transactions on Power Systems*, 21(1):278–284.
- Rather, Z. H., Chen, Z., Thøgersen, P., and Lund, P. (2016). Pragmatic approach for multistage phasor measurement unit placement: a case study of the danish power system and inputs from practical experience. *International Transactions on Electrical Energy Systems*, 26(12):2532–2551.
- Rather, Z. H., Chen, Z., Thøgersen, P., Lund, P., and Kirby, B. (2014). Realistic approach for phasor measurement unit placement: Consideration of practical hidden costs. *IEEE Transactions on Power Delivery*, 30(1):3–15.
- Rather, Z. H., Liu, C., Chen, Z., and Thøgersen, P. (2013). Optimal pmu placement by improved particle swarm optimization. In *2013 IEEE Innovative Smart Grid Technologies-Asia (ISGT Asia)*, pages 1–6. IEEE.

- Rincon, P. (2005). Science/nature— crows and jays top bird iq scale. *BBC News*.
- Roger, W. C. (2005). Statistical method and apparatus for monitoring parameters in an electric power distribution system. Canadian Patent 2,508,965.
- Rosalina, K. M. et al. (2019). Economic study of a power network for observability analysis using optimal arrangement of pmus and dulrs. In *2019 2nd International Conference on Power and Embedded Drive Control (ICPEDC)*, pages 432–436. IEEE.
- Rousseaux, P., Mallieu, D., Van Cutsem, T., and Ribbens-Pavella, M. (1988). Dynamic state prediction and hierarchical filtering for power system state estimation. *Automatica*, 24(5):595–618.
- Roy, L. and Mohammed, T. (1997). Fast super decoupled state estimator for power systems. *IEEE transactions on power systems*, 12(4):1597–1603.
- Saarinen, K., Mousavi, M., Stoupis, J., and McGowan, J. (2019). Systems and methods for power line event zone identification. US Patent 10,324,132.
- Saleh, A. A., Adail, A. S., and Wadoud, A. A. (2017). Optimal phasor measurement units placement for full observability of power system using improved particle swarm optimisation. *IET Generation, Transmission & Distribution*, 11(7):1794–1800.
- Samuelsson, O., Hemmingsson, M., Nielsen, A. H., Pedersen, K. O. H., and Rasmussen, J. (2006). Monitoring of power system events at transmission and distribution level. *IEEE Transactions on Power Systems*, 21(2):1007–1008.
- Sauer, P. W., Pai, M., and Chow, J. H. (2017). Power system toolbox.
- Schinkel, M., Heemels, W., and Juloski, A. L. (2003). State estimation for systems with varying sampling rate. In *42nd IEEE International Conference on Decision and Control (IEEE Cat. No. 03CH37475)*, volume 1, pages 391–392. IEEE.
- Sharma, A., Srivastava, S. C., and Chakrabarti, S. (2014). An iterative multiarea state estimation approach using area slack bus adjustment. *IEEE Systems Journal*, 10(1):69–77.
- Sharma, A., Srivastava, S. C., and Chakrabarti, S. (2017). A cubature kalman filter based power system dynamic state estimator. *IEEE Transactions on Instrumentation and Measurement*, 66(8):2036–2045.
- Sharma, C. and Tyagi, B. (2015). Ranking of phasor measurement units based on control strategy for small-signal stability. *International Transactions on Electrical Energy Systems*, 25(10):2359–2375.

- Shi, J., Foggo, B., Kong, X., Cheng, Y., Yu, N., and Yamashita, K. (2020). Online event detection in synchrophasor data with graph signal processing. In *2020 IEEE International Conference on Communications, Control, and Computing Technologies for Smart Grids (SmartGridComm)*, pages 1–7. IEEE.
- Shi, K., Chan, T., Wong, Y., and Ho, S. (2002). Speed estimation of an induction motor drive using an optimized extended kalman filter. *IEEE Transactions on Industrial Electronics*, 49(1):124–133.
- Shih, K.-R. and Huang, S.-J. (2002). Application of a robust algorithm for dynamic state estimation of a power system. *IEEE Transactions on Power Systems*, 17(1):141–147.
- Shivakumar, N. and Jain, A. (2008). A review of power system dynamic state estimation techniques. In *2008 Joint International Conference on Power System Technology and IEEE Power India Conference*, pages 1–6. IEEE.
- Simon, D. (2006). *Optimal state estimation: Kalman, H infinity, and nonlinear approaches*. John Wiley & Sons.
- Singh, A. P., Kumar, G. H., Paik, S. S., and Roy, D. S. (2019). Storage and analysis of synchrophasor data for event detection in indian power system using hadoop ecosystem. In *Data and Communication Networks*, pages 291–304. Springer.
- Singh, S. P. and Singh, S. P. (2017). Optimal cost wide area measurement system incorporating communication infrastructure. *IET Generation, Transmission & Distribution*, 11(11):2814–2821.
- Sinha, A. and Mondal, J. (1999). Dynamic state estimator using ann based bus load prediction. *IEEE Transactions on Power Systems*, 14(4):1219–1225.
- Sinha, A., Roy, L., and Srivastava, H. (1994). A decoupled second order state estimator for ac-dc power systems. *IEEE transactions on power systems*, 9(3):1485–1493.
- Sodhi, R., Srivastava, S., and Singh, S. (2009). Optimal pmu placement to ensure system observability under contingencies. In *Power & Energy Society General Meeting, 2009. PES'09. IEEE*, pages 1–6. IEEE.
- Sodhi, R., Srivastava, S., and Singh, S. (2010). Phasor-assisted hybrid state estimator. *Electric Power Components and Systems*, 38(5):533–544.
- Sodhi, R., Srivastava, S., and Singh, S. (2011). Multi-criteria decision-making approach for multi-stage optimal placement of phasor measurement units. *IET Generation, Transmission & Distribution*, 5(2):181–190.

- Staines, C. S., Caruana, C., Asher, G. M., and Sumner, M. (2006). Sensorless control of induction machines at zero and low frequency using zero sequence currents. *IEEE Transactions on Industrial Electronics*, 53(1):195–206.
- Sun, L., Chen, T., Chen, X., Ho, W. K., Ling, K.-V., Tseng, K.-J., and Amaratunga, G. A. (2018). Optimum placement of phasor measurement units in power systems. *IEEE Transactions on Instrumentation and Measurement*, (99):1–9.
- Suresh, P. (2016). Regular paper a robust wide-area measurement system for southern region of indian power grid using binary cuckoo search (bcs): A case study. *J. Electrical Systems*, 12(1):45–67.
- Tarif, T., Ladjici, A. A., Amrane, Y., and Chabane, Y. (2019). Multi-objective optimal pmus placement for online assessment of small-signal stability. *International Transactions on Electrical Energy Systems*, 29(11):e12117.
- Tebianian, H. and Jeyasurya, B. (2013). Dynamic state estimation in power systems using kalman filters. In *2013 IEEE Electrical Power & Energy Conference*, pages 1–5. IEEE.
- Terzija, V., Valverde, G., Cai, D., Regulski, P., Madani, V., Fitch, J., Skok, S., Begovic, M. M., and Phadke, A. (2010). Wide area monitoring, protection, and control of future electric power networks. *IEEE*.
- Theodorakatos, N. P., Lytras, M., and Babu, R. (2020). Towards smart energy grids: A box-constrained nonlinear underdetermined model for power system observability using recursive quadratic programming. *Energies*, 13(7):1724.
- Theodorakatos, N. P., Manousakis, N. M., and Korres, G. N. (2015). A sequential quadratic programming method for contingency-constrained phasor measurement unit placement. *International Transactions on Electrical Energy Systems*, 25(12):3185–3211.
- Thorp, J., Phadke, A., and Karimi, K. (1985). Real time voltage-phasor measurement for static state estimation. *IEEE Transactions on Power Apparatus and Systems*, (11):3098–3106.
- Tian, G., Zhou, Q., Birari, R., Qi, J., and Qu, Z. (2020). A hybrid-learning algorithm for online dynamic state estimation in multimachine power systems. *IEEE transactions on neural networks and learning systems*, 31(12):5497–5508.
- Tripathy, P., Srivastava, S. C., and Singh, S. N. (2009). A divide-by-difference-filter based algorithm for estimation of generator rotor angle utilizing synchrophasor measurements. *IEEE Transactions on Instrumentation and Measurement*, 59(6):1562–1570.

- Tungadio, D., Numbi, B., Siti, M., and Jimoh, A. A. (2015). Particle swarm optimization for power system state estimation. *Neurocomputing*, 148:175–180.
- Tungadio, D. H., Jordaan, J. A., and Siti, M. W. (2016). Power system state estimation solution using modified models of pso algorithm: Comparative study. *Measurement*, 92:508–523.
- Valverde, G., Chakrabarti, S., Kyriakides, E., and Terzija, V. (2010). A constrained formulation for hybrid state estimation. *IEEE Transactions on Power Systems*, 26(3):1102–1109.
- Valverde, G. and Terzija, V. (2010). Unscented kalman filter for power system dynamic state estimation. *IET generation, transmission & distribution*, 5(1):29–37.
- Vanfretti, L., Chow, J. H., Sarawgi, S., and Fardanesh, B. (2011). A phasor-data-based state estimator incorporating phase bias correction. *IEEE Transactions on Power Systems*, 26(1):111–119.
- Velázquez, S. C., Palomares, R. A., and Segura, A. N. (2004). Speed estimation for an induction motor using the extended kalman filter. In *14th International Conference on Electronics, Communications and Computers, 2004. CONIELECOMP 2004.*, pages 63–68. IEEE.
- Venkateswaran, V. B. and Kala, V. S. C. (2012). Observability analysis and optimal placement of pmu using differential evolution algorithm. In *Emerging Trends in Electrical Engineering and Energy Management (ICETEEEM), 2012 International Conference on*, pages 205–209. IEEE.
- Wang, C., Wu, P., and Deng, Y. (2015a). Modified iterated square-root cubature kalman filter for non-cooperative space target tracking. *International Journal of Engineering and Applied Sciences*, 2(11):73–77.
- Wang, J. and Quintana, V. (1984). A decoupled orthogonal row processing algorithm for power system state estimation. *IEEE transactions on power apparatus and systems*, (8):2337–2344.
- Wang, S., Feng, J., and Chi, K. T. (2015b). Novel cubature kalman filtering for systems involving nonlinear states and linear measurements. *AEU-International Journal of Electronics and Communications*, 69(1):314–320.
- Wang, S., Gao, W., and Meliopoulos, A. S. (2011). An alternative method for power system dynamic state estimation based on unscented transform. *IEEE transactions on power systems*, 27(2):942–950.

- Wang, W., He, L., Markham, P., Qi, H., Liu, Y., Cao, Q. C., and Tolbert, L. M. (2014). Multiple event detection and recognition through sparse unmixing for high-resolution situational awareness in power grid. *IEEE Transactions on Smart Grid*, 5(4):1654–1664.
- Wang, W., Yin, H., Chen, C., Till, A., Yao, W., Deng, X., and Liu, Y. (2020). Frequency disturbance event detection based on synchrophasors and deep learning. *IEEE Transactions on Smart Grid*, 11(4):3593–3605.
- Welch, G. and Bishop, G. (2006). An introduction to the kalman filter (tr95-041). *Department of Computer Science, University of North Carolina at Chapel Hill, Chapel Hill, NC*, pages 27599–3175.
- Wu, F. (1988). Real-time network security monitoring, assessment and optimization. *International Journal of Electrical Power & Energy Systems*, 10(2):83–100.
- Wu, Z., Du, X., Gu, W., Liu, Y., Ling, P., Liu, J., and Fang, C. (2018). Optimal pmu placement considering load loss and relaying in distribution networks. *IEEE Access*.
- Xie, L., Chen, Y., and Kumar, P. (2014). Dimensionality reduction of synchrophasor data for early event detection: Linearized analysis. *IEEE Transactions on Power Systems*, 29(6):2784–2794.
- Xie, L., Choi, D.-H., Kar, S., and Poor, H. V. (2012). Fully distributed state estimation for wide-area monitoring systems. *IEEE Transactions on Smart Grid*, 3(3):1154–1169.
- Xu, B. and Abur, A. (2004). Observability analysis and measurement placement for systems with pmus. In *IEEE PES Power Systems Conference and Exposition, 2004.*, pages 943–946. IEEE.
- Yang, X.-S. and Press, L. (2010). Nature-inspired metaheuristic algorithms second edition.
- Yang, Y., Hu, W., and Min, Y. (2014). Projected unscented kalman filter for dynamic state estimation and bad data detection in power system.
- Yang, Z., Zhong, D., Guo, F., and Zhou, Y. (2007). Gauss-newton iteration based algorithm for passive location by a single observer. *Systems Engineering and Electronics*, 29(12):2006–2009.
- Yuill, W., Edwards, A., Chowdhury, S., and Chowdhury, S. (2011). Optimal pmu placement: A comprehensive literature review. In *Power and Energy Society General Meeting, 2011 IEEE*, pages 1–8. IEEE.

- Zaborszky, J., Prasad, K., and Whang, K.-w. (1981). Stabilizing control in emergencies part: 2. control by local feedback. *IEEE Transactions on Power Apparatus and Systems*, (5):2381–2389.
- Zaky, M., Khater, M., Yasin, H., and Shokralla, S. (2008). Review of different speed estimation schemes for sensorless induction motor drives. *Journal of electrical engineering*, 8(2):39–39.
- Zhang, C., Jia, Y., Xu, Z., Lai, L. L., and Wong, K. P. (2017). Optimal pmu placement considering state estimation uncertainty and voltage controllability. *IET Generation, Transmission & Distribution*, 11(18):4465–4475.
- Zhao, J., Gómez-Expósito, A., Netto, M., Mili, L., Abur, A., Terzija, V., Kamwa, I., Pal, B., Singh, A. K., Qi, J., et al. (2019). Power system dynamic state estimation: Motivations, definitions, methodologies, and future work. *IEEE Transactions on Power Systems*, 34(4):3188–3198.
- Zhao, J. and Mili, L. (2018). Power system robust decentralized dynamic state estimation based on multiple hypothesis testing. *IEEE Transactions on Power Systems*, 33(4):4553–4562.
- Zhao, J., Netto, M., Huang, Z., Yu, S. S., Gomez-Exposito, A., Wang, S., Kamwa, I., Akhlaghi, S., Mili, L., Terzija, V., et al. (2020). Roles of dynamic state estimation in power system modeling, monitoring and operation. *IEEE Transactions on Power Systems*, 36(3):2462–2472.
- Zhao, L. and Abur, A. (2005). Multi area state estimation using synchronized phasor measurements. *IEEE Transactions on Power Systems*, 20(2):611–617.
- Zhao, Y., Yuan, P., Ai, Q., and Lv, T. (2015). Optimal pmu placement considering topology constraints. *International Journal of Electrical Power & Energy Systems*, 73:240–248.
- Zhou, N., Meng, D., Huang, Z., and Welch, G. (2014). Dynamic state estimation of a synchronous machine using pmu data: A comparative study. *IEEE Transactions on Smart Grid*, 6(1):450–460.
- Zhou, N., Meng, D., and Lu, S. (2013). Estimation of the dynamic states of synchronous machines using an extended particle filter. *IEEE Transactions on Power Systems*, 28(4):4152–4161.
- Zhuang, F. and Balasubramanian, R. (1985). A transformation-decoupled estimator for power system state estimation. *IEEE transactions on power apparatus and systems*, (7):1738–1744.

Zimmerman, R. and Murillo-Sanchez, C. (2016). Matpower (version 6.0)[software]. *Zenodo*. Available online: <https://matpower.org/download/> (accessed on 22 April 2022).

Technical Publications

Patent:

1. Tukaram Moger, **Teena Johnson**, et al. "Method and System for Major Event Detection in a Power System", Indian Patent, Application No.202241012056 A1., 29th Sept 2022. (**Granted**)

Journals:

1. **Teena Johnson** and Tukaram Moger, "Security-Constrained Optimal Placement of PMUs using Crow Search Algorithm", Applied Soft Computing - Elsevier Journal, vol. 128, pp. 109472, August 2022. (**Published**)
2. **Teena Johnson** and Tukaram Moger, "A critical review of methods for optimal placement of phasor measurement units", International Transactions on Electrical Energy Systems, vol. 31, no.3, pp. e12698, Nov 2020. (**Published**)
3. **Teena Johnson**, Sofia Banu and Tukaram Moger, "Dynamic State Estimation of Synchronous Machines using Iterated Square-root Cubature Kalman Filter and Synchrophasor Measurements", Journal of Electronics and Electrical Engineering, pp.8-8, June 2023. (**Published**)
4. **Teena Johnson**, Sofia Banu and Tukaram Moger, "Forecasting-aided State Estimation in Power Systems during Normal Load Variations using Iterated Square-root Cubature Kalman Filter", Journal of Electronics and Electrical Engineering. (**Under Review**)

Conferences:

1. Tukaram Moger, **Teena Johnson**, Thukaram Dhadbanjan, "Significance of reactive power loss and its application to system voltage stability," 2018 IEEMA Engineer Infinite Conference (eTechNxT), New Delhi, 2018, pp. 1-6. (**Published**)
2. Sofia Banu, **Teena Johnson** and Tukaram Moger, "A Comparative Study of Bayesian based filters for Dynamic State Estimation in Power Systems", IEEE International Power and Renewable Energy Conference 2021, pp. 1-6 Sept 2021. (**Published**)
3. **Teena Johnson**, Tukaram Moger, et al, "Case Studies of Event Detection for Indian Power System using Signal Processing Methods", Australian Universities Power Engineering Conference (AUPEC 2021), pp. 1-6, Sept 2021. (**Published**)

4. Sofia Banu, **Teena Johnson** and Tukaram Moger, "A Comparative Analysis of Speed Estimation of Induction Motor Drive using Non-linear Kalman Filters", Australian Universities Power Engineering Conference (AUPEC 2021), pp. 1-6, Sept 2021. (**Published**)
5. **Teena Johnson** and Tukaram Moger, "Latest Trends in Electromechanical Dynamic State Estimation for Electric Power Grid", IEEE 2022 International Conference of Emerging Technologies (INCET), pp. 1-6, May 2022. (**Published**)
6. **Teena Johnson** and Tukaram Moger, "Review of Advancements in Forecasting-aided State Estimation based on Kalman Filter Approach for Voltage Profile of Power Systems", 2nd IEEE International Conference on Emerging Frontiers in Electrical and Electronic Technologies (ICEFEET- 2022), pp. 1-6, June 2022. (**Published**)
7. **Teena Johnson** and Tukaram Moger, "Latest Trends in Event Detection Techniques in Power Systems", 7th Students' Conference on Engineering and Systems, July 2022. (**Published**)